

NSWCDD/MP-96/38

Naval Sea Systems Command



**PROCEEDINGS OF THE
REVERBERATION CHAMBER AND ANECHOIC
CHAMBER OPERATORS GROUP MEETING,
5 - 7 DECEMBER 1995**

MARCH 1996

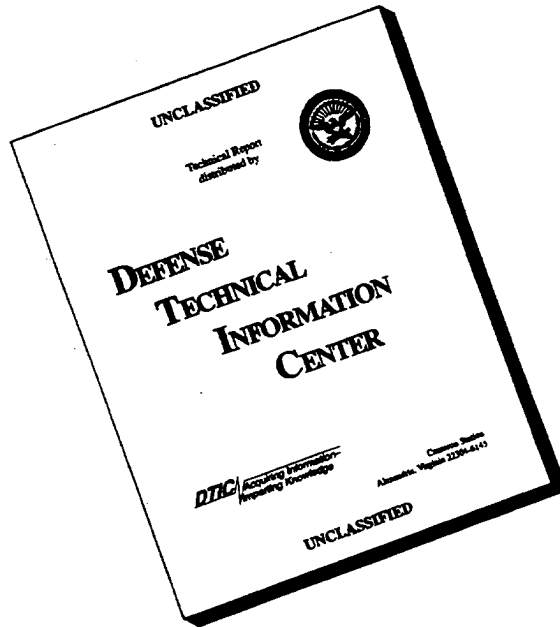
Approved for public release; distribution is unlimited.

19960501 304

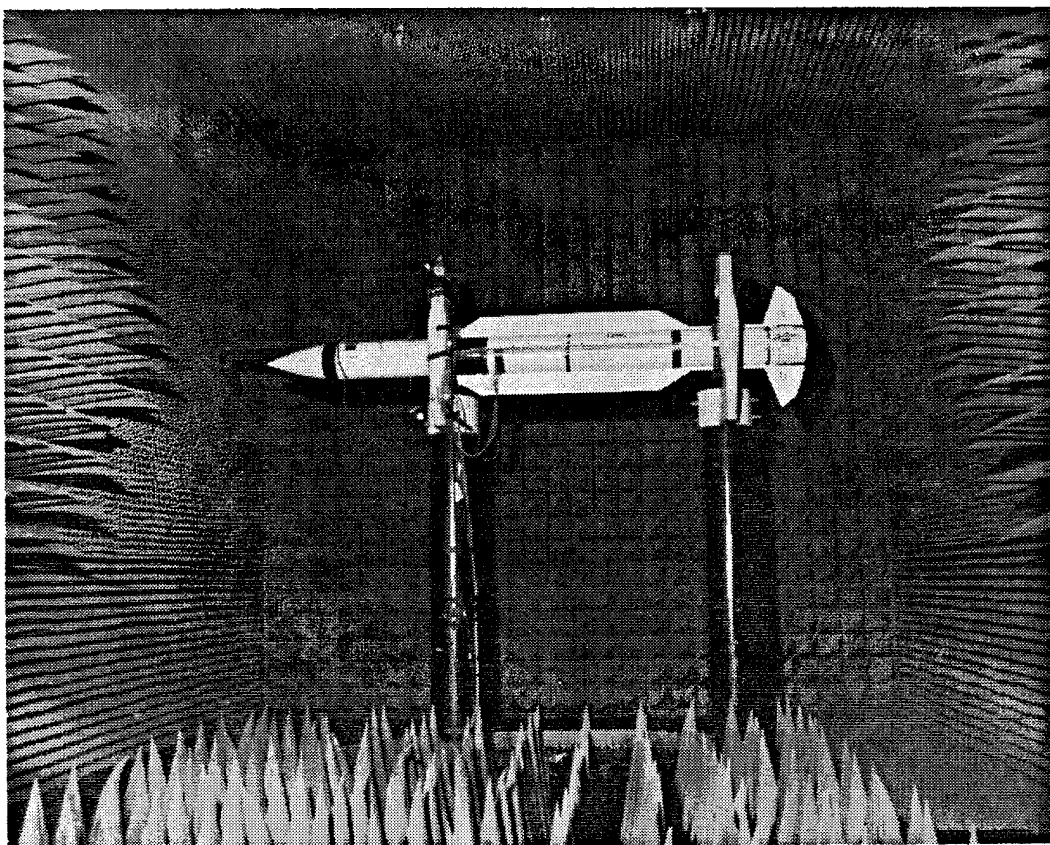


**SPONSORED BY:
NAVAL SURFACE WARFARE CENTER
DAHLGREN DIVISION
DAHLGREN, VA 22448-5100**

DISCLAIMER NOTICE



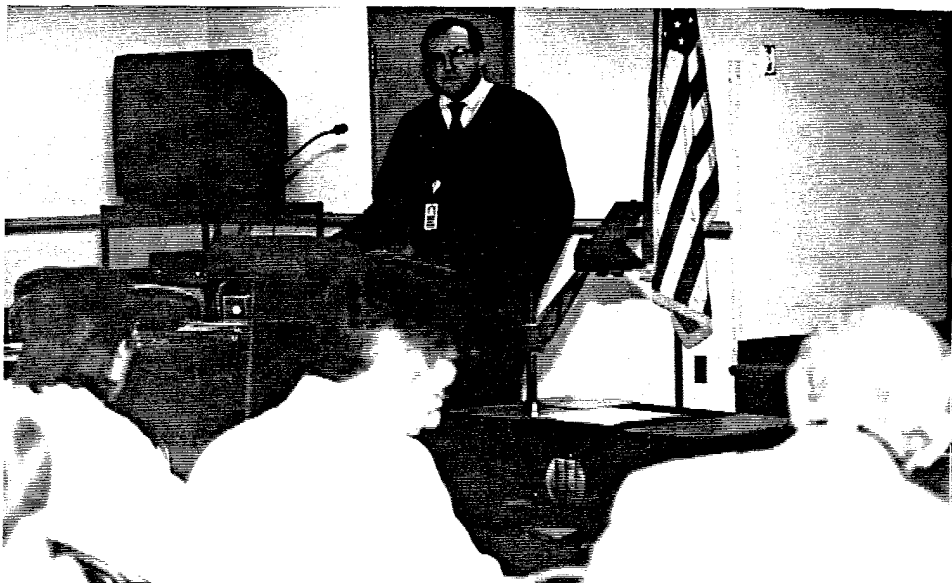
THIS DOCUMENT IS BEST
QUALITY AVAILABLE. THE
COPY FURNISHED TO DTIC
CONTAINED A SIGNIFICANT
NUMBER OF PAGES WHICH DO
NOT REPRODUCE LEGIBLY.





SHIP DEFENSE SYSTEMS DEPARTMENT

NAVAL SEA SYSTEMS COMMAND



PREFACE

A meeting of the Anechoic Chamber and Reverberation Chamber Users Group was held at the Naval Surface Warfare Center, Dahlgren Division from 5 through 7 December. The meeting was hosted by the Electromagnetics Effects Branch (F52) and was chaired by Mike Hatfield. Topics ranging from "Electromagnetic Compatibility Testing of Electric Cars" to "Radio Frequency (RF) Coupling to Commercial Aircraft Avionics" were presented. The meeting was attended by more than 85 people representing both government and industry. There were 15 visitors from overseas representing Sweden, Italy, Australia and the United Kingdom.

A workshop on reverberation chambers also was held on Monday December 4th. It was attended by 50 people including 13 overseas visitors.

The next meeting of the Users Group is scheduled to be held at the National Institute of Standards and Technology in Boulder Colorado in the Spring of 1997.

William P. Lucado, Head, Systems Electromagnetic Effects Branch and Leonard Fontenot, Head, Electromagnetic Effects Division, wish to thank the authors of the papers contained in this proceedings for their contributions. Their participation made the Users Group meeting an overwhelming success.



THOMAS C. PENDERGRAFT, Head
Ship Defense Systems Department





ELECTROMAGNETIC EFFECTS DIVISION

NAVAL SEA SYSTEMS COMMAND



**REVERBERATION CHAMBER AND ANECHOIC CHAMBER
OPERATORS GROUP MEETING**

PROGRAM

MONDAY, DECEMBER 4, 1995

<u>TIME</u>	<u>TOPIC</u>	<u>SPEAKER</u>
0800-0900	WORKSHOP REGISTRATION	
0900-1700	REVERBERATION CHAMBER WORKSHOP	HATFIELD/FREYER/ JOHNSON/SLOCUM/ROAN

TUESDAY, DECEMBER 5, 1995

0730-0830	REGISTRATION	
0830-0840	WELCOME	L. FONTENOT
0840-0900	OVERVIEW OF NSWCDD	T. PENDERGRAFT
0900-0930	BREAK	
0930-1000	EMC/EMI MODELING TECHNIQUES AND TOOLS (p. 1)	BRUCE ARCHAMBEAULT (SETH CORPORATION)
1000-1030	ELECTROMAGNETIC ENVIRON- MENTAL EFFECTS TEST BRANCH, REDSTONE TECHNICAL TEST CENTER (p. 23)	DAVID B. ELKINS (REDSTONE TECHNICAL TEST CENTER)
1100-1130	THREE DIMENSIONAL COMPUTATIONAL MODELS OF ANECHOIC AND SEMIANECHOIC CHAMBERS' PERFORMANCES (p. 49)	DALE STEFFEN (ELECTRO MAGNETIC APPLICATIONS, INC.)
1130-1300	LUNCH	
1330-1400	STATISTICAL ANALYSIS OF ELECTROMAGNETIC FIELDS IN USE IN ELECTROMAGNETIC COMPATIBILITY (EMC) (p. 75)	DR. PAOLO CORONA (INSTITUTO UNIVERS- ITARIO NAVALE)
1400-1430	AN INTEGRATED RF SIGNAL SOURCE FOR IMMUNITY TESTING IN ABSORBER LINED SHIELD ROOMS (p. 85)	POUL ANDERSEN (CHRYSLER CORPORATION)
1430-1500	STANDARD SPHERICAL DIPOLE EMI/EMC SOURCE REPEATABILITY AND CONSISTENCY (p. 91)	BRUCE ARCHAMBEAULT (SETH CORPORATION)
1500-1530	BREAK	

**REVERBERATION CHAMBER AND ANECHOIC CHAMBER
OPERATORS GROUP MEETING**

PROGRAM (CONTINUED)

<u>TIME</u>	<u>TOPIC</u>	<u>SPEAKER</u>
1530-1600	A LOW-COST COMPREHENSIVE METHODOLOGY FOR EME EFFECTS ASSESSMENT OF CRITICAL SYSTEMS (p. 107)	DR. CELESTE BELCASTRO (NASA Langley Research Center)
1600-1630	LARGE AIRCRAFT CAVITY PUMPING AND COMMERCIAL GPS SUSCEPTIBILITY EVALUATION (p. 135)	DR. JANE M. LEHR (PHILLIPS LABORATORY)
1630-1700	GPS RCVR TESTING USING GPS SIMULATOR IN AN ANECHOIC CHAMBER (p. 161)	DR. MAQSOOD MOHD (SVERDRUP TECH- NOLOGY / EGLIN AFB)

WEDNESDAY, DECEMBER 6, 1995

0800-0830	EMC TEST PERFORMED ON AN EXPERIMENTAL ELECTRIC VEHICLE (p. 181)	HARRY GAUL (MOTOROLA)
0830-0900	CALIBRATION OF FULLY ANECHOIC ROOMS AND CORRELATION WITH OATS MEASUREMENTS (p. 195)	ROGER MCCONNELL AND CLARK VITEK (CKC LABORATORIES, INC.)
0930-1000	BREAK	
1000-1030	TRANSMISSION CROSS SECTION OF APERTURES MEASURED BY USE OF A NESTED MSC (p. 211)	PETER LANGREN (NATION- AL DEFENCE RESEARCH ESTABLISHMENT)
1030-1100	TIME DOMAIN CHARACTERIZATION OF MODE-STIRRED CHAMBERS (p. 223)	GARY T. ROAN (NAVAL RESEARCH LABORATORY)
1100-1130	HERO SUSCEPTIBILITY OF CSA MK 2 SYSTEM: COMPARATIVE RESULTS OBTAINED FROM MODE-STIRRED CHAMBER AND GROUND PLANE TEST FACILITIES (p. 249)	PETER VOURAS (EG&G)
1130-1300	LUNCH	
1300-1330	STEPPED-FREQUENCY METHOD- OLOGY FOR OBTAINING FASTER DATA RATES IN REVERBERATION CHAMBERS OPERATED WITHOUT A MECHANICAL MODE STIRRER (p. 277)	DR. J. P. QUINE (ROME LABORATORIES / GRIFFISS AFB)

**REVERBERATION CHAMBER AND ANECHOIC CHAMBER
OPERATORS GROUP MEETING**

PROGRAM (CONTINUED)

<u>TIME</u>	<u>TOPIC</u>	<u>SPEAKER</u>
1330-1400	COMPARISON OF BOEING 757 ELECTROMAGNETIC CAVITY CHARACTERIZATION DATA USING BAND LIMITED WHITE GAUSSIAN NOISE, CW WITH MECHANICAL MODE-MIXING, AND CW FREQUENCY STEP EXCITATIONS (p. 285)	DR. GUSTAV FREYER (NORTHEAST CONSORTIUM FOR ELECTRICAL ENGINEERING)
1400-1430	FREQUENCY CHARACTERIZATION OF REVERBERATION CHAMBERS (p. 293)	MICHAEL HATFIELD (NSWCDD)
1430-1500	MODE-STIRRED CHAMBER SHIELDING EFFECTIVENESS MEASUREMENTS VERSUS ANECHOIC CHAMBER MEASUREMENTS: A COMPARISON OF RESULTS (p. 315)	MICHAEL JESSEE (COMPUTER SCIENCES CORPORATION)
1500-1530	BREAK	
1530-1600	TESTING OF MICROWAVE SHIELDING GASKETS AND COVER PANELS-- RECENT WORK AT ROME LABORATORIES (p. 327)	DR. J. P. QUINE (ROME LABORATORIES / GRIFFISS AFB)
1600-1630	EMV TESTING OF AIRCRAFT: A COMPARISON OF THE MODE-STIRRED AND STANDARD METHODS (p. 343)	DIANE KEMPF (NAVAL AIR WARFARE CENTER AD)
1630-1700	RF COUPLING MEASUREMENTS ON PASSENGER AIRCRAFT AVIONICS EXPOSED TO CAVITY-MODE EXCITATION (p. 375)	D. MARK JOHNSON (COMPUTER SCIENCES CORPORATION)
1830-2230	DINNER	

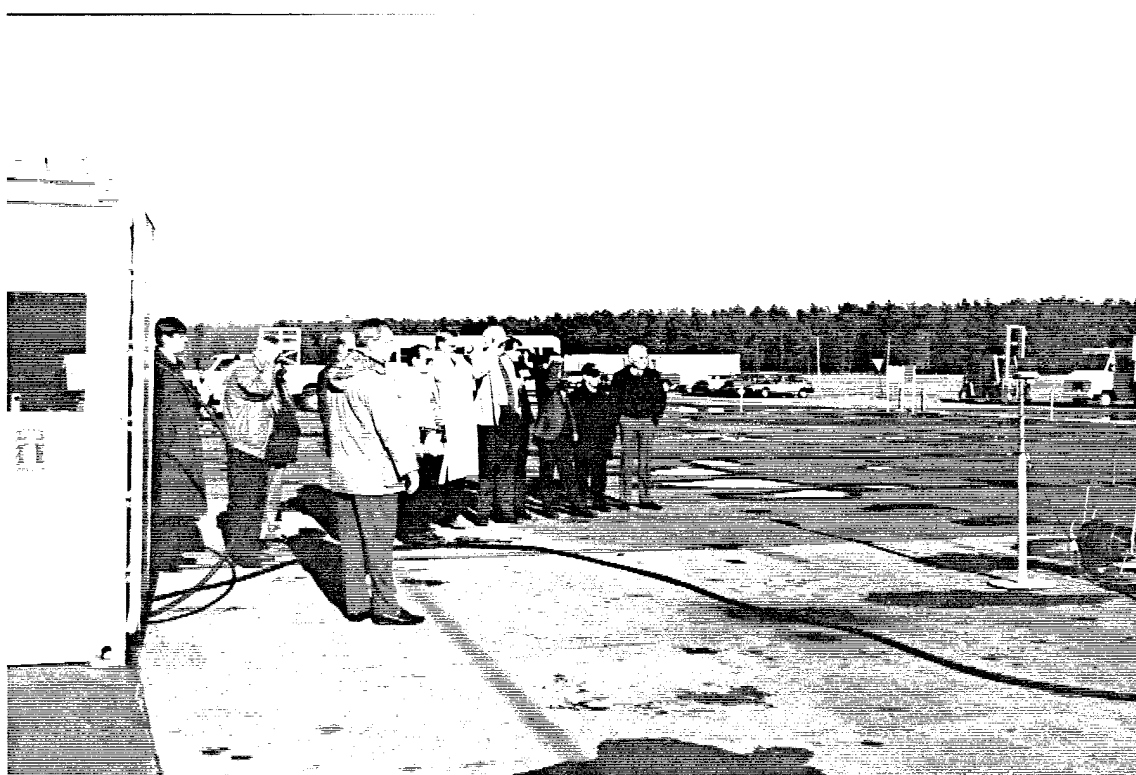
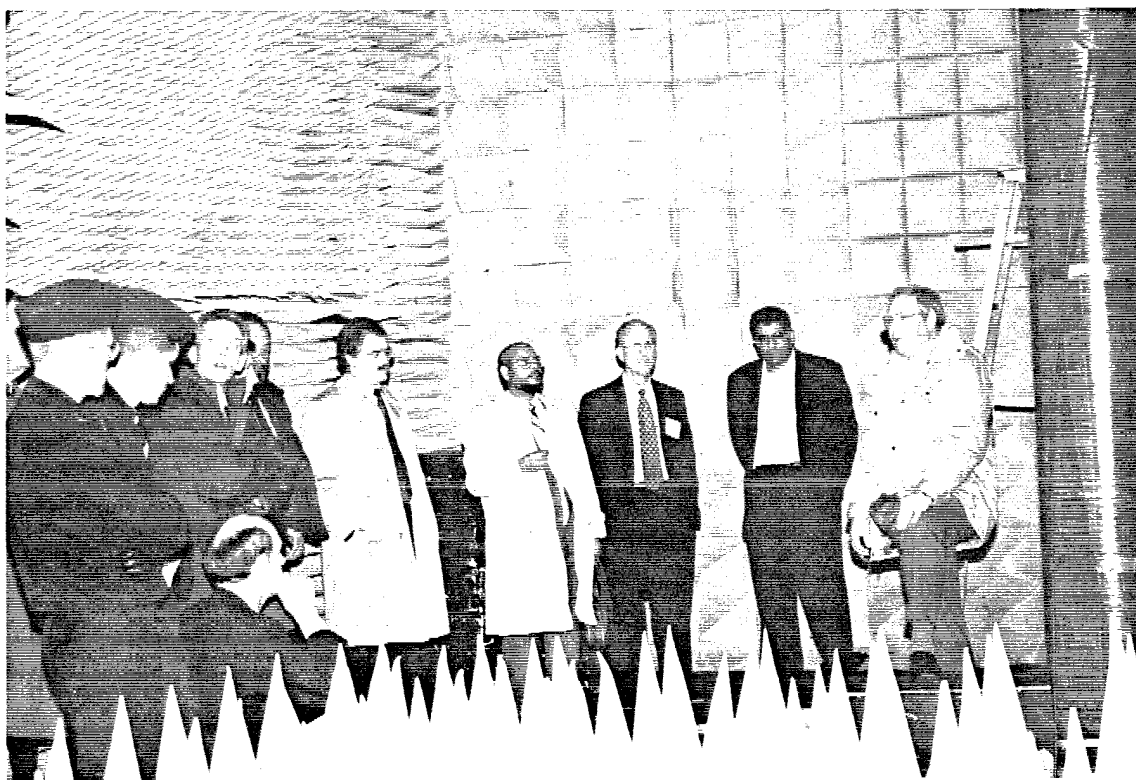
THURSDAY, DECEMBER 7, 1995

0800-0830	RADIATED EMISSIONS TESTS ON BIOMEDICAL TELEMETRY TRANSMITTER DEVICES (p. 385)	RICHARD S. LARA (U.S. ARMY RESEARCH LABORATORY)
0830-0900	EMI: A SILENT THREAT TO THE COMBAT CASUALTY CARE MEDICAL ELECTRONIC SYSTEMS (p. 395)	DR. MAQSOOD MOHD (SVERDRUP TECHNOLOGY / EGLIN AFB)
0900-0930	BREAK	

**REVERBERATION CHAMBER AND ANECHOIC CHAMBER
OPERATORS GROUP MEETING**

PROGRAM (CONTINUED)

<u>TIME</u>	<u>TOPIC</u>	<u>SPEAKER</u>
0930-1000	EM EVALUATION OF PHILLIPS LABORATORY'S REVERBERATION CHAMBER (p. 411)	LT. ERIC JOHNSON (USAF / PHILLIPS LABORATORY)
1000-1030	U.S. ARMY ELECTROMAGNETIC ANALYSIS FACILITY, WHITE SANDS MISSILE RANGE, NM (p. 425)	RICHARD S. LARA (U.S. ARMY RESEARCH LABORATORY)
1030-1100	MOBILE MICROWAVE TEST FACILITY (p. 429)	ANTHONY A. ZANTE (TITAN BETA)
1100-1200	DISCUSS PLANS FOR FUTURE MEETING. END OF TECHNICAL SESSIONS. --MEETING ADJOURNS--	
1200-1330	LUNCH	
1330-1600	FACILITY TOURS/ DEMONSTRATIONS	





**MR. BRUCE ARCHAMBEAULT
SETH CORPORATION**

EMC/EMI Modeling Techniques and Tools

Bruce Archambeault

SETH Corporation
110 Sunray Drive
Johnstown, Pa 15905
814-255-4417

email: arch@sethcorp.com



SETH Corporation

Why Model???

- Eliminate
 - Out of Context Equations
 - Out of Context Graphs
 - Rules of Thumb
- Reduce Cost
 - Being ‘Safe’ Costs Money
- Reduce Trial-and-Error Approach
- Quicker Project Completion



SETH Corporation

Modeling is Here NOW

- Can't Do Everything
- CAD Files have too Much Unnecessary Information
- Identify the Problems
 - Test Configuration Important
 - Break Problem into Most Likely Problem Areas
 - Multiple Models likely to be Needed for Entire System



SETH Corporation

What Can be done with Modeling??

- Radiated Emissions
- Radiated Immunity/Susceptibility
- Coupling Between systems & Between System components



SETH Corporation

Examples of Likely Problems

- Effect of Air Vent Hole Size, Material Thickness
- Proximity of 'Hot' CPU Heatsink to Air Vent
- Effect of Slot Length Variation
 - How Close To Place Screws, Gaskets, Etc...
- Need to Filter or Shield External Cables
- Effect of Decoupling Capacitors
- Shielding Effectiveness



SETH Corporation

Know the Tools !!

- Could You Build a Radio Without Knowing How to Use a Soldering Iron and Screwdriver?
- Need a Basic Understanding of How the Tool Works
 - FDTD
 - MOM
 - FEM
- Understand the Tool's Limits
 - GIGO
- Beware of Advertising Hype
 - Great Color Displays.... But Where's the Beef?



SETH Corporation

Popular Modeling Techniques and Tools

- Don't Need Ph.D. To Use Them
- Codes Are Available In Many Forms
 - Free From Universities
 - User Beware
 - Purchase From Vendors
 - User Beware
- User Should Understand Basic Techniques and Their Limitations
- Each Technique Has Areas Where It Excels and Areas Where Limitations Apply
- Different Modeling Tasks Require Different Techniques



SETH Corporation

Before You Can Apply the Model You Must Identify...

- Radiator
- Coupling Mechanism
- EMI Source



SETH Corporation

Radiator

- Most Common Cause of EMI Radiator is Common Mode Signals on Data Cables
 - Unintentional Signals
 - RF Voltage Between Cable and EUT Shield
 - Creates 'Funny' Dipole Antenna
 - Wires/Cables Increase Radiation Efficiency of EUT Dramatically
- Direct Radiation Through Slots Air Vents, Etc..



SETH Corporation

Understanding the Coupling Mechanism

- EM Fields within Shielded Box Couple Onto the Connector Pins
- EMI 'Noise' on Reference (Ground) Plane Coupled Directly to Connector Reference Pins
- Excessively Fast Signal Rise Time Coupled Intentionally to the Pins



SETH Corporation

The EMI/EMC Source

- Identify the Highest Frequency
 - Highest Energy Source in the EUT
- Any Signal With a Fast Rise Time is a Potential Source
- IC Heatsinks are an Appreciable Source
- Long Buss Runs With Fast Signals are a Potential Source



SETH Corporation

Popular Modeling Techniques

- Method of Moments
- Finite Difference Time Domain
- Finite Element Method
- Others



SETH Corporation

Method of Moments (MoM) (BEM)

- One Frequency at a Time
- Break Problem Into Wire Segments
- Identify Source
 - Voltage
 - E Field
- Identify RF Currents on All Segments and Patches
- Find E Field From Each Current Element



SETH Corporation

Finite Difference Time Domain

- Time Domain - FFT- Range of Frequencies
- Grid All Computational Spare
- Identify Grid Type
 - Metal
 - Air
 - Other
- Solve E and H in Leap Frog Fashion



SETH Corporation

Finite Element Method (FEM)

- Usually One Frequency at a Time
- Grid All of Computerized Space
- Non-Rectangular Grid Allows Easy Curve Fitting
- Identify Material of Every Element
- Solve for E/H
- Boundary Conditions
- Closed Structures Best



SETH Corporation

Other Methods -In General- Not General Enough

- Direct Solutions
- Integral Methods
- TLM
- Specialized Techniques
- Combination Techniques



SETH Corporation

Modeling Software Available from Vendors Today

- Buyer Beware
 - Know What You Need
 - Understand What They Offer
 - Standard Problems
- Everything is Available
 - From Maxwell's Equations Solvers
 - To Out-of-Context Equations Applied to Impressive Graphics
- Standard Modeling Problems Useful
 - IEEE/EMC Symposium 1994/1995



SETH Corporation

Summary

- Modeling on Real-World Problems is Available Now
- Eliminate Guess Work Over Design and Costly Delays
- Break Product Design Into Most Likely Problem Areas
- Identify
 - Radiator
 - Coupling Mechanism
 - EMI Source
- Software is Available from a Wide Variety of Vendors
 - Understand How It Works
 - Know What You Want/Need
 - Be Sure It Is More Than Impressive Graphics
 - Consider the Standard Problems to Help Evaluate Tools



SETH Corporation

EMITTM

EMI Toolbox for Modeling

- Multiple Modeling Techniques Available
- Easy-to-Use Preprocessor
 - Create Models Graphically
- Easy-to-Use Postprocessor
 - display output data in a number of formats
- Method of Moments (MoM)
- Full Wave Solver - 3d
- Finite-Difference Time-Domain (FDTD)
 - Full Wave Solver
 - 3d
 - 2d

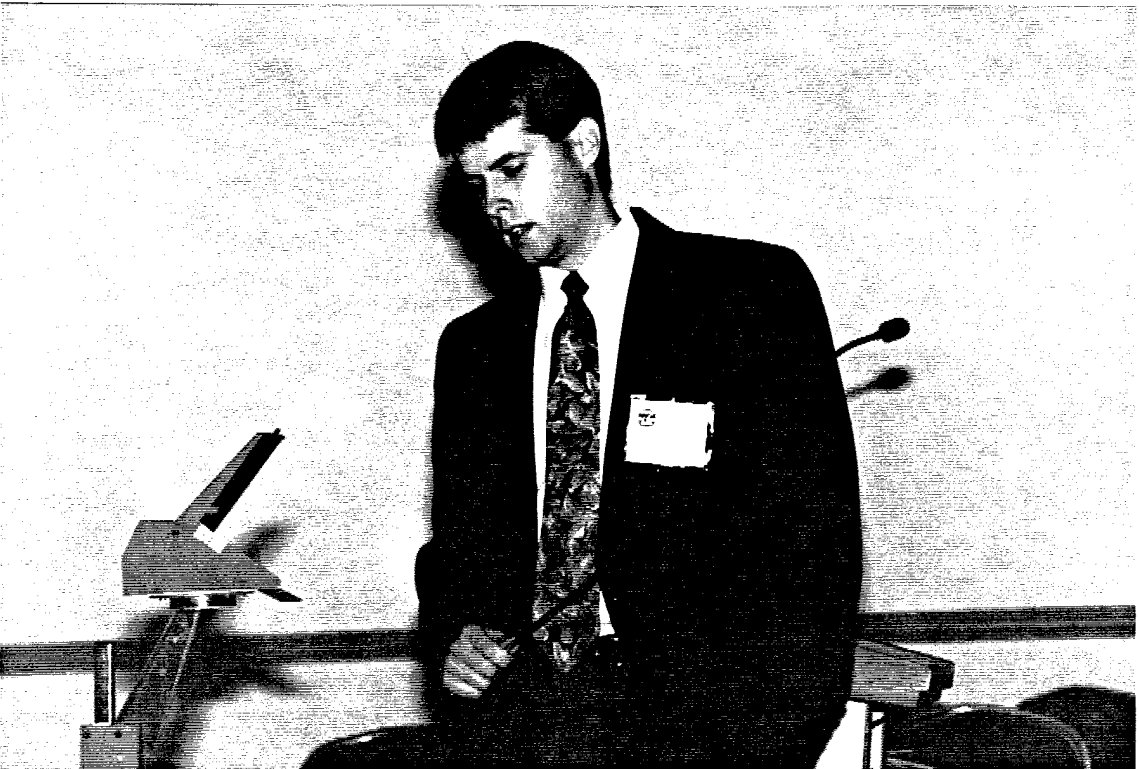


SETH Corporation





**MR. DAVID ELKINS
REDSTONE TECHNICAL TEST CENTER**

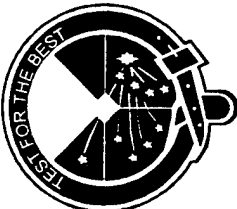




Electromagnetic Environmental Effects Test Branch

Redstone Technical Test Center
David Elkins

Summary

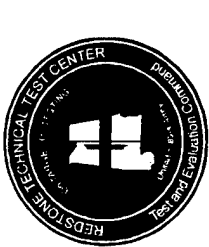


- E3 Test Branch Overview
 - MIL-STD-461D
 - EMR
 - Transient Testing
- Anechoic Chamber Overview
- REES

EMI/EMC Test Lab



- MIL-STD-461D Lab
- EMR System Level Testing
 - EMRO
 - EMRH
- Hazardous/Nonhazardous Lightning Facility
- Electrostatic Discharge



MIL-STD-461D



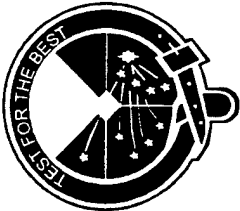
- Four shielded test rooms
 - Two house data collection equipment
 - Two house test equipment
- Carnell Labs EMI Analog Receiver
- HP 8566B Spectrum Analyzer
- Array of antennas, probes, and supporting equipment

EMR Test Lab



- Three large test areas for conducting EMR testing.
- 200 V/m for small items such as missiles and rockets
- 100 V/m for large items such as Bradley, MLRS etc.
- 100 kHz - 18 GHz

Lightning



- Hazardous Lightning Facility
 - Testing of explosive items (Pershing, MLRS, Hellfire, TOW etc.)
- Near and Direct Effects
- Testing per MIL-STD-1757
- Non - Hazardous Facility
 - Instrumented lightning test of non-explosive items

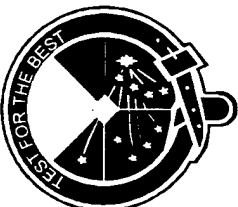
ESD



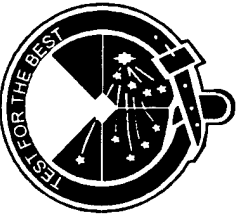
- Helicopter Level ESD
 - 300 kV discharge
 - Instrumented testing
 - Hazardous test items
- Personnel ESD
 - 25 kV discharge
 - Instrumented testing

Instrumentation

- E-field Measuring equipment
- Pulse Code Modulation Telemetry packages specially designed for each item under test
- Real time monitoring of key parameters during test conduct
- Data collection, analysis, and storage



Data Acquisition

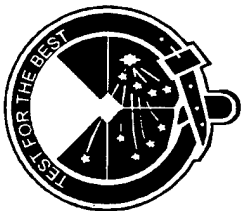


- AUTOTEST

- In-house developed Windows based program to control test apparatus
- Adaptable to the needs of each individual test
- Allows one operator to control EMR test as well as monitoring critical test parameters in real time

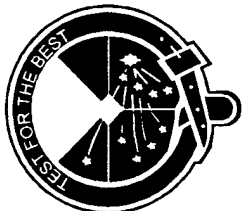


Transient Data Analysis



- HP 54510 Digital Oscilloscopes
- PC Controlled Data Storage
- Critical Cable Current Measurements
- B-dot Measurements

Anechoic Chamber



- Radar Cross Section
 - HP 8530 Network Analyzer
 - Scientific Atlanta Positioner/Controller
- Threat Identifier Verification
 - HP FASS (Frequency Agile Signal Simulator)
 - Non-Cooperative Target Recognition
- System Level Emission Measurements



Anechoic Chamber Cont'd

- Radar Environment Emulation System(REEES)
- High Peak Power EMRO Environment Generation

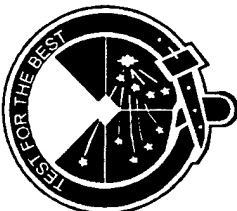
Anechoic Chamber



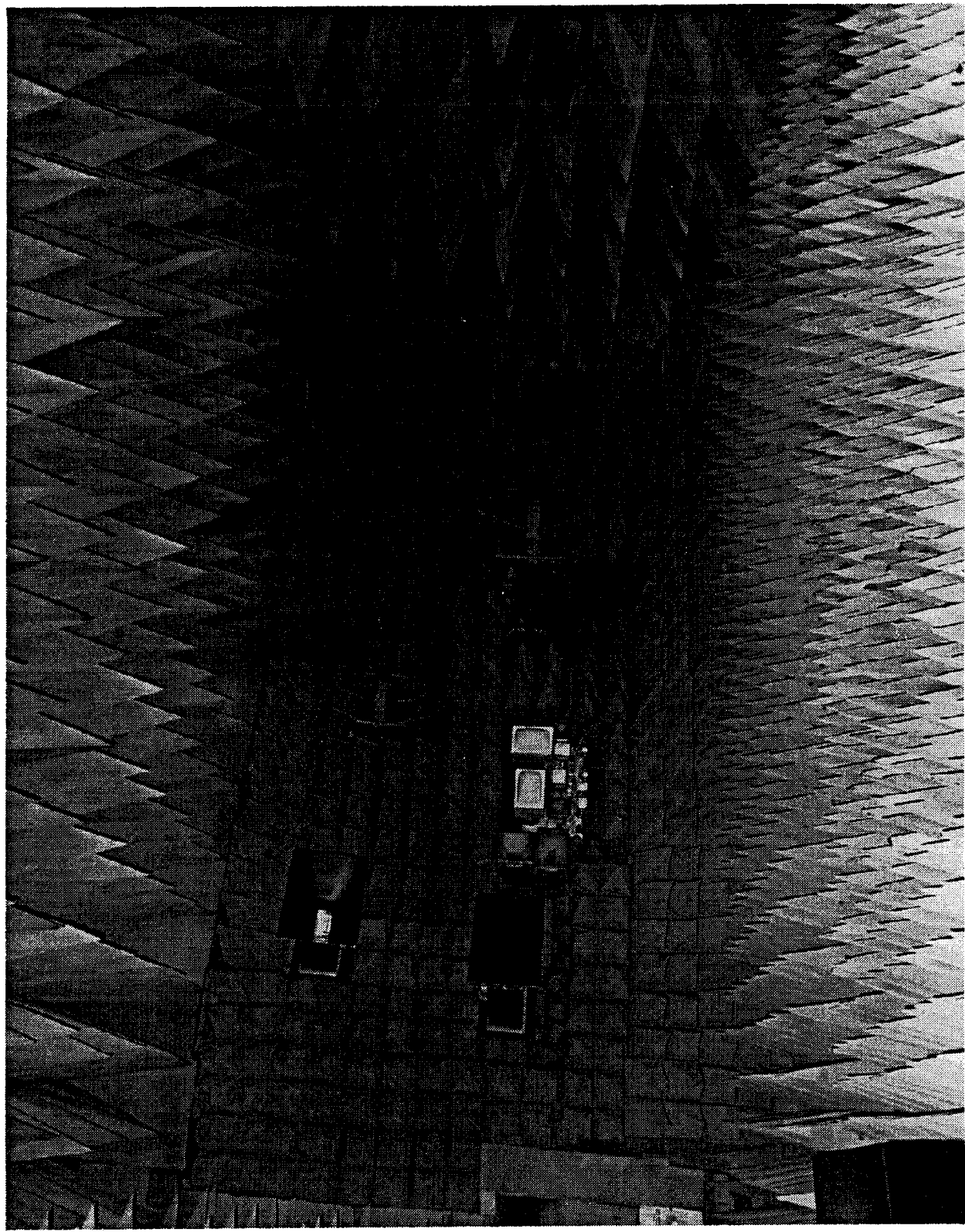
- Physical Characteristics

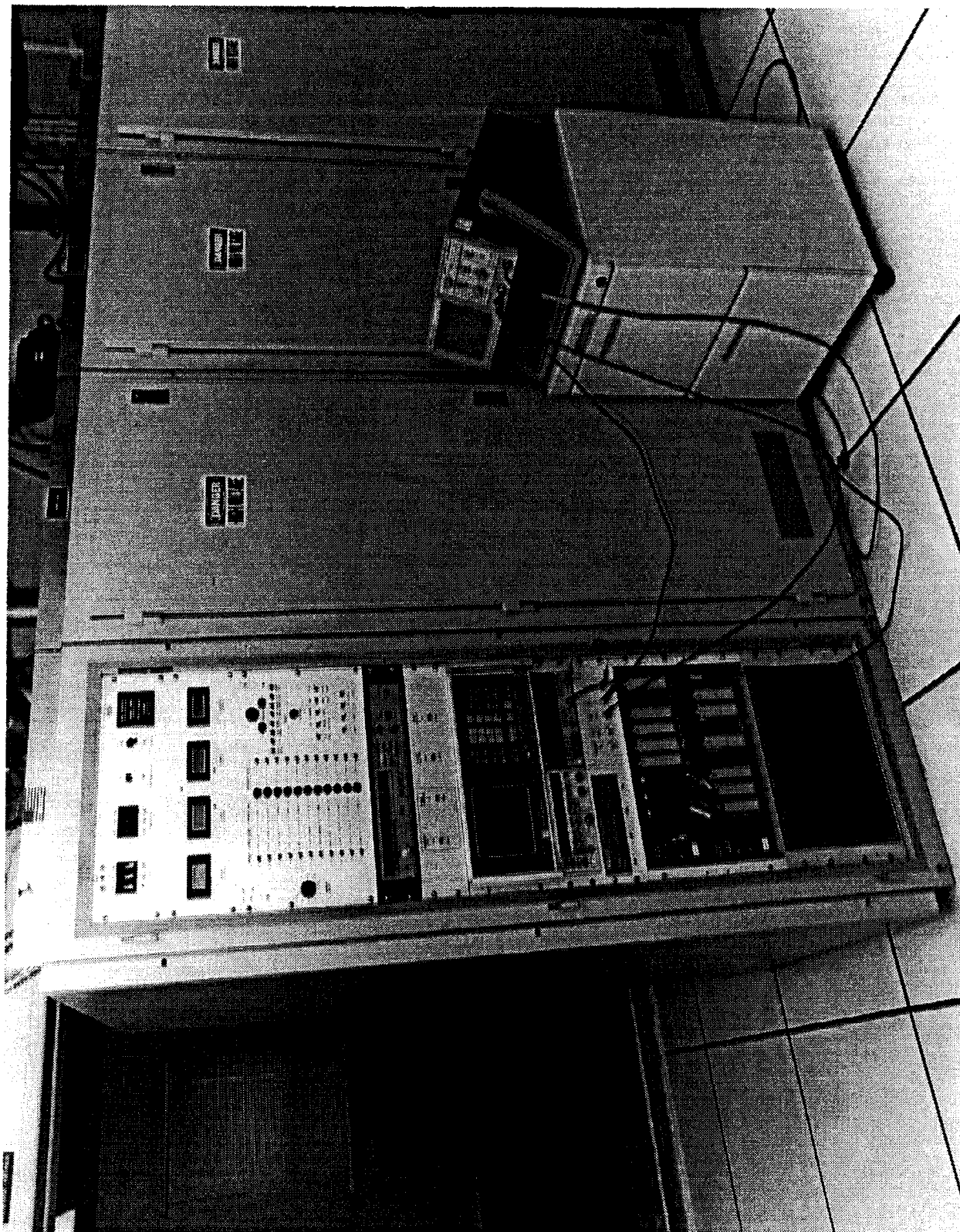
- Dimensions
- 100 dB Shielding Effectiveness
- 100 MHz - 40 GHz
- 18 ft diameter turntable
- Large removable access doors
- 2 small personnel/equipment doors
- 5 ton overhead crane

REES



- Eleven Specific Frequency Bands
- 1500 - 6000 V/m Peak E-field at center of turntable
- System Requirements developed from friendly/hostile emitter databases





REES Frequency Band Requirements



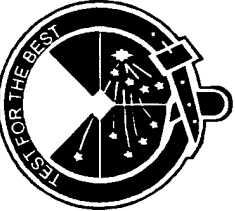
<u>Frequency Band (MHz)</u>	<u>E-field</u>
UHF	1500
L-band (low)	2200
L-band (high)	5000
S-band (low)	2500
S-band (high)	5000
C-band (low)	2300
C-band (high)	4600
X-band	2100
Ku-band	2000
K-band	850
Ka-band	1400

REES Output Capabilities



<u>Frequency Band(MHz)</u>	<u>Output Power</u>	<u>E-field(V/m)</u>
750-1000	200 kW	1700
1220-1350	650 kW	3600
1250-1310	1600kW	6500
2900-3100	840 kW	3600
3000	2100kW	6000
5400-5800	230 kW	2400
5400-5800	830 kW	4400
8500-9600	350 kW	2600
14800-15200	200 kW	1720
24250	35 kW	840
35050	200 kW	1200

Pulse Characteristics



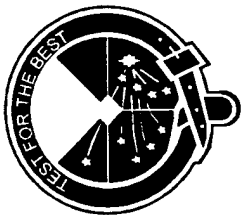
<u>Frequency Band (MHz)</u>	<u>Pulse Width (usec)</u>	<u>Maximum Duty Cycle</u>
UHF	1-4	.001
L-band (low)	1-4	.001
L-band (high)	1-4	.001
S-band (low)	1-2	.001
S-band (high)	1-4	.0009
C-band (low)	0.5-3	.001
C-band (high)	0.5-2	.001
X-band	0.5-3	.001
Ku-band	0.1-0.35	.001
K-band	0.1	.0003
Ka-band	0.1	.0003

Thermal Testing



- Concern - Thermal heating effects on the anechoic material
Instrumentation - Max. temp strips, thermometers, and an infrared pyrometer
- Test Set-up
 - Placed instrumented material at center of turntable
 - Instrumented other cones nearby the antennas and on the side, back walls, and floor
- Operated the transmitter on high for six minutes and then checked temperatures
- Scanned the entire chamber with the infrared pyrometer for any hot spots.
- Results - No significant heating above ambient detected

Shielding Effectiveness



- Existing wall in anechoic chamber had to be modified to mount antennas and allow penetration of conductors
- Carnell Labs Analog Receiver and HP Signal Source with EMCO Ridged Horns
- Measured from 200 MHz to 20 GHz
- Worst case number was 95 dB



Calibration and Acceptance Test



- HP Peak Power Analyzer with Standard Gain Horns and Gore Low-loss cable
- Attenuators, cables, couplers, connectors, etc. calibrated on the HP8510 Network Analyzer
- Measured E-field strengths at test item location

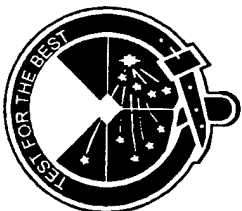
Future Issues

- Map the E-fields in the entire anechoic chamber
- Develop a permanent E-field monitoring system

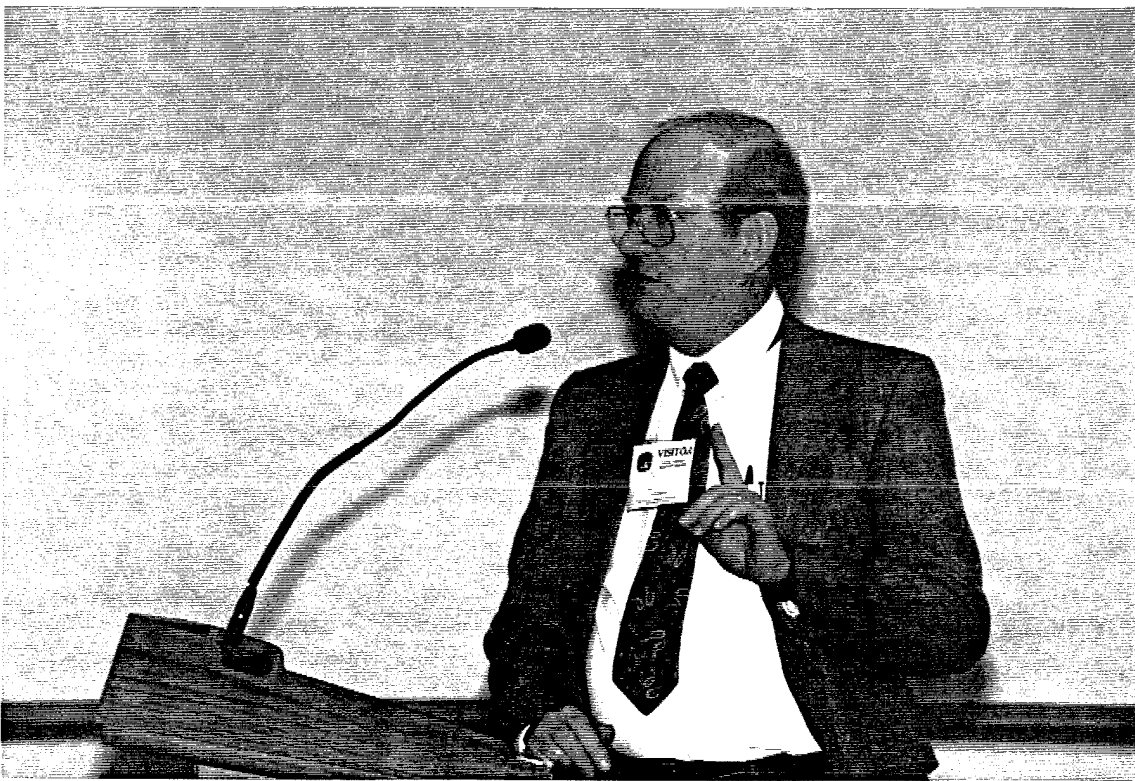


Future Planned Testing

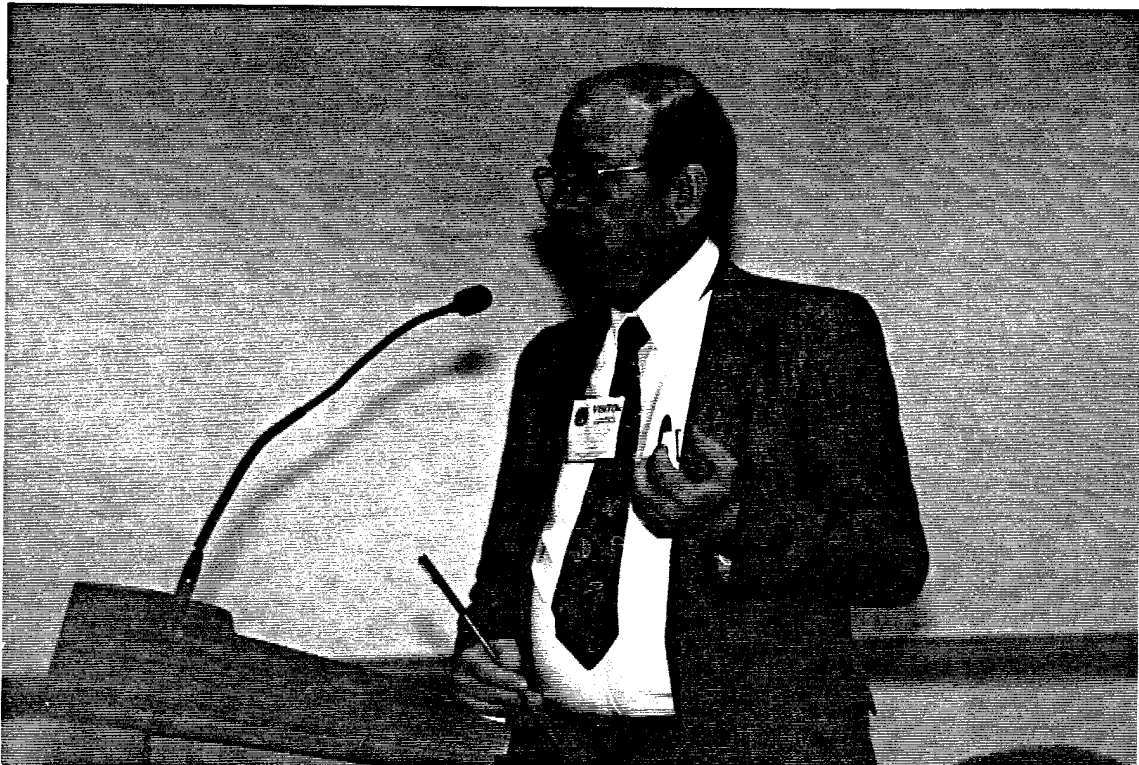
- First test was on the Longbow Missile System
- Other tests planned on MLRS, Javelin, TOW







**MR. DALE STEFFEN
ELECTRO MAGNETIC APPLICATIONS, INC.**





Electro Magnetic Applications, Inc.

7655 West Mississippi Avenue, Suite 300, Lakewood, CO 80226-4332, P.O. Box 260263, Denver, CO 80260-070, (303) 980-0770, Fax: (303) 980-0836

**THREE DIMENSIONAL COMPUTATIONAL MODELS OF
ANECHOIC AND SEMIANECHOIC CHAMBERS' PERFORMANCES**

by

Paul McKenna

presented by

Dale A. Steffen

presented at

REVERBERATION CHAMBER AND ANECHOIC CHAMBER

OPERATORS GROUP MEETING

5-7 DECEMBER 1995

This work has been supported by the Lehman Chambers Program of Paul E. Lehman, Inc. as part of the Ben Franklin Partnership Program of the Commonwealth of Pennsylvania

Absorber Lined Chambers Are Useful as EMC Immunity and Emissions Test Fixtures

- Chamber Figure of Merit for Emissions Testing
 - Normalized Site Attenuation (NSA) relative to that of an Ideal Open Area Test Site (OATS) :
(± 4 dB from 30MHz - 1GHz)
 - Site Attenuation, A:

$$A = \frac{V_I}{V_R}$$

where V_I = indicated signal generator voltage

V_R = received voltage

$$\Lambda(\text{dB}) = -20 \log f_m + 48.92 + \Lambda F_R (\text{dB/m})$$

$$+ \Lambda F_T (\text{dB/m}) - E_D^{Mn} (\text{dB} \cdot \mu\text{V/m})$$

(Smith, A.A.,In, R.F. German & J.B. Pate, Calculation of Site Attenuation from Antenna Factors, IEEE Trans. EMC, Vol EMC-24, No.3,Aug. 1992, pp. 301-316)

Chamber Figure of Merit for Emissions Testing (cont'd)

- Normalized Site Attenuation:
$$\text{NSA}(\text{dB}) = A(\text{dB}) - \Lambda F_k - \Lambda F_r$$
- Chamber must meet at 5 transmit antenna locations, 2 transmit antenna heights, with receive antenna located either 3 m or 10 m away. Receive antenna is scanned in height from 1m - 4m, V_R^{max} is used.
- Both horizontal and vertical polarizations are required.
- NSA is an absolute standard since E_D^{max} can be calculated analytically for an ideal OATIS
- Any deviations from the theoretical result are due to imperfections in absorber performance relative to free space, such as imperfectly damped chamber resonances.

Chamber Figure of Merit for Immunity Testing:

1000 • 4 • 3 (0 - +6 dB, 80 MHz - 1 GHz)

- Transmit antenna is located at a height of 1.5 m, 3 m away from the test surface.
- Test surface is 1.5 m x 1.5 m square, starting .8 m above the floor.
- 16 test points are separated by .5 m intervals
- 12 of the 16 test points must be within +6 dB of the minimum (of the 12)
- This is a relative standard assuming that one can transmit enough power to achieve the minimum required field strength at the test surface (3 - 6 V/m)
- Free space dipole deviation $\leq .5$ dB, radiation zone term only

Choices of Computational Methods

- Quasi-Optical/Ray Tracing Methods
- Frequency Domain Method of Moments
- Integral Equation Techniques (Frequency Domain)
- Time Domain/Frequency Domain Finite Difference Solution

Considerations in the Choice of a Computational Approach

- Method must be broad band
- Method must account for the frequency dependences of the bulk absorber dielectric permittivity and magnetic permeability.
- Method must account for the doubly periodic structure of urethane pyramid and ferrite lattice absorber designs.
- Method must ultimately be capable of characterizing the interaction of fields within a chamber.
 - Both plane wave and non-plane wave types of fields will be present.
 - Consider two limits
 - Absorber is perfect — "plane wave"
 - Absorber is completely imperfect — "chamber modes"
 - Method must be computationally tractable.

Technical Approach

Computational Choice: 3DTDFD

- Time Domain FD is explicit -- no matrix inversions
 - Δt is determined by CFL criterion $\left(\Delta t \leq \frac{\Delta s_{\min}}{c\sqrt{3}} \right)$
 - bandwidth is:
$$f_{\max} = 0.1 \frac{c}{\Delta s_{\max}}$$
 - $\epsilon(\omega), \mu(\omega)$ must be translated to time domain
 - Maximum computational volume is approximately $V = (50\lambda_{\min})^3$ (assuming a supercomputer)
 - Computational volume is swept (in space) each time step, E and H are staggered in space and time according to the Yee scheme
 - Absorber material modeled by "gridding" ϵ, μ
 - Computational volume must be terminated
 - * boundary conditions on the shield are easy ($E_{tan}=0$)
 - * method of treatment of doubly periodic array of absorbing material is problematic if this must be gridded in 3 dimensions
- Primary Difficulties
 - Characterization of doubly periodic array of absorbing material
 - Characterization of $\epsilon(\omega), \mu(\omega)$ in the time domain

Technical Approach

- Solutions
 - Keuster and Holloway developed a methodology for replacing an inhomogeneous doubly periodic region (along with the background medium) material properties with an homogenized material property.
 - (Keuster, E.F. and C.L. Holloway, "A Low Frequency Model for Wedge or Pyramidal Absorber Array: I Theory, II Computed and Measured", Accepted for publication, IEEE Trans. EMC)
 - $[\epsilon_{\text{eff}}] = \begin{bmatrix} \epsilon_t & 0 & 0 \\ 0 & \epsilon_t & 0 \\ 0 & 0 & \epsilon_z \end{bmatrix}$
 - ϵ_z is a direct average
 - $\epsilon_t = \epsilon_0 \left[1 + \delta^2 \frac{2(\epsilon_z - \epsilon_0)}{(1 + \delta^2)\epsilon_0 + (1 - \delta^2)\epsilon_z} \right]$
 - This allows for solutions of the plane wave reflection coefficients for an effectively layered medium using, for example, the Riccati Equation
 - Also allows for direct introduction into the 3DTDFD model.

Technical Approach

- Solutions

- $\epsilon(\omega), \mu(\omega)$ into the time domain

$$D(\omega) = \epsilon(\omega)E(\omega) = \epsilon_0(1 + \chi_e(\omega))E(\omega)$$

- product in frequency domain \rightarrow convolution in time domain
- polarizability $P(\omega) = \epsilon_0\chi_e(\omega)E(\omega)$
- fit $\chi_e(\omega)$ to rational functions in frequency domain. These lead to ordinary differential equations in the time domain. Solve for $P(t)$ and $E(t)$ simultaneously.

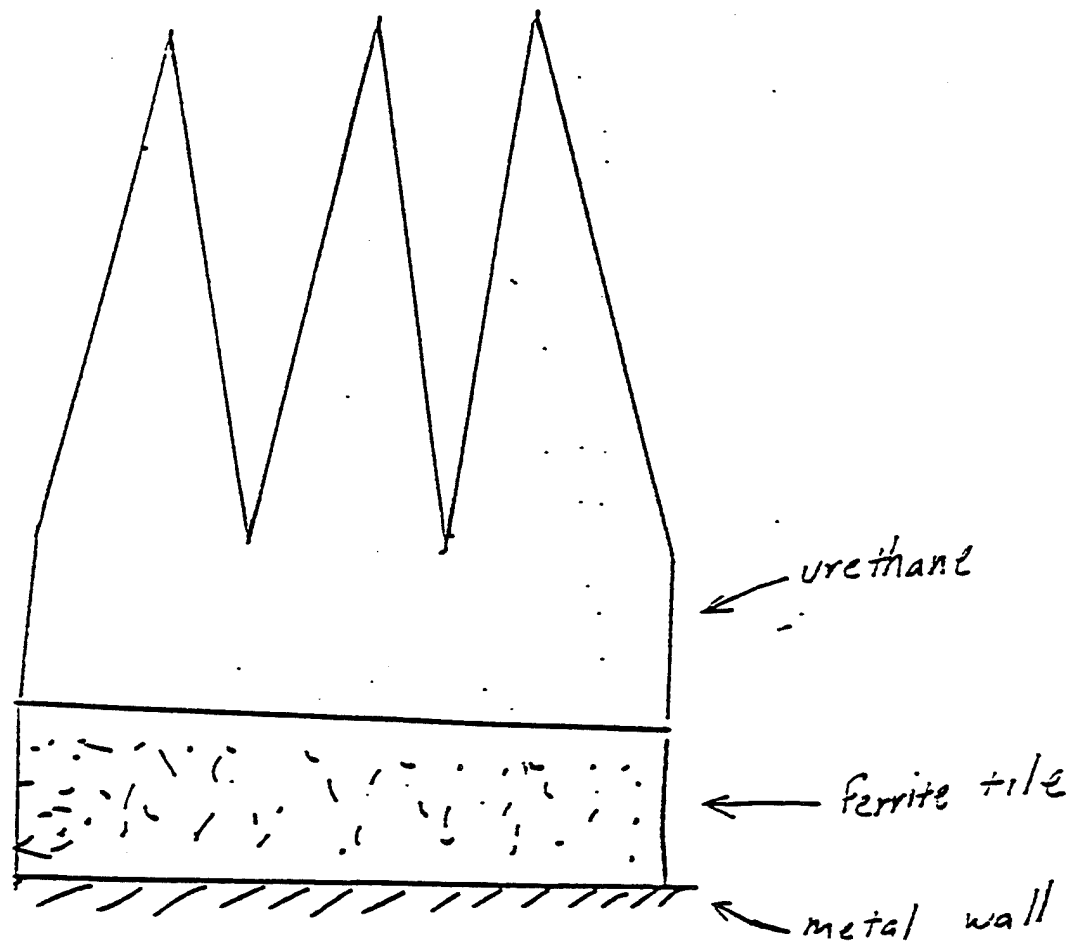


Figure 1 An Example of Pyramidal Absorber-Ferrite Tile Hybrid. σ is the Angle of Incidence for the Plane Wave

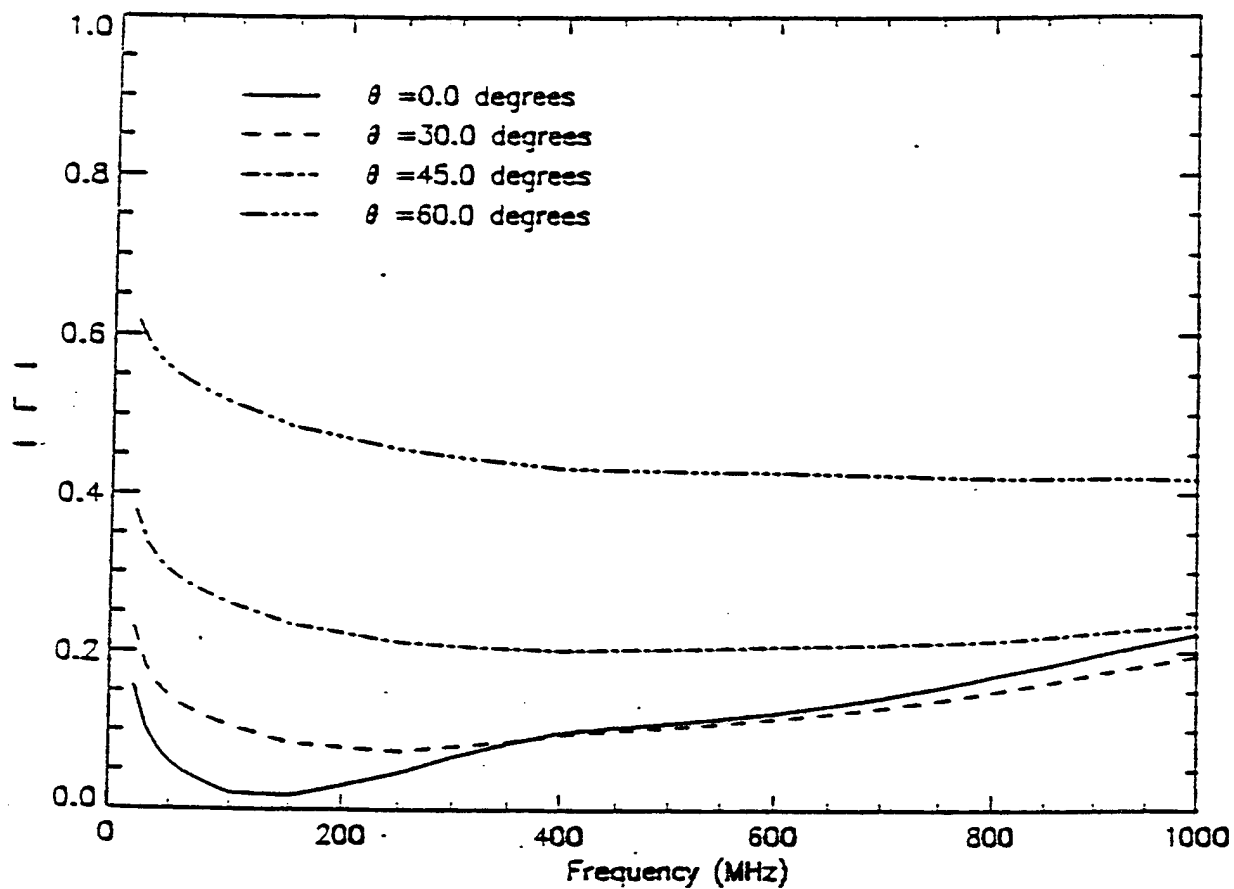


Figure 4 Reflection Coefficient Magnitudes for the Ferrite Tile for Various Angles of Incidence, θ

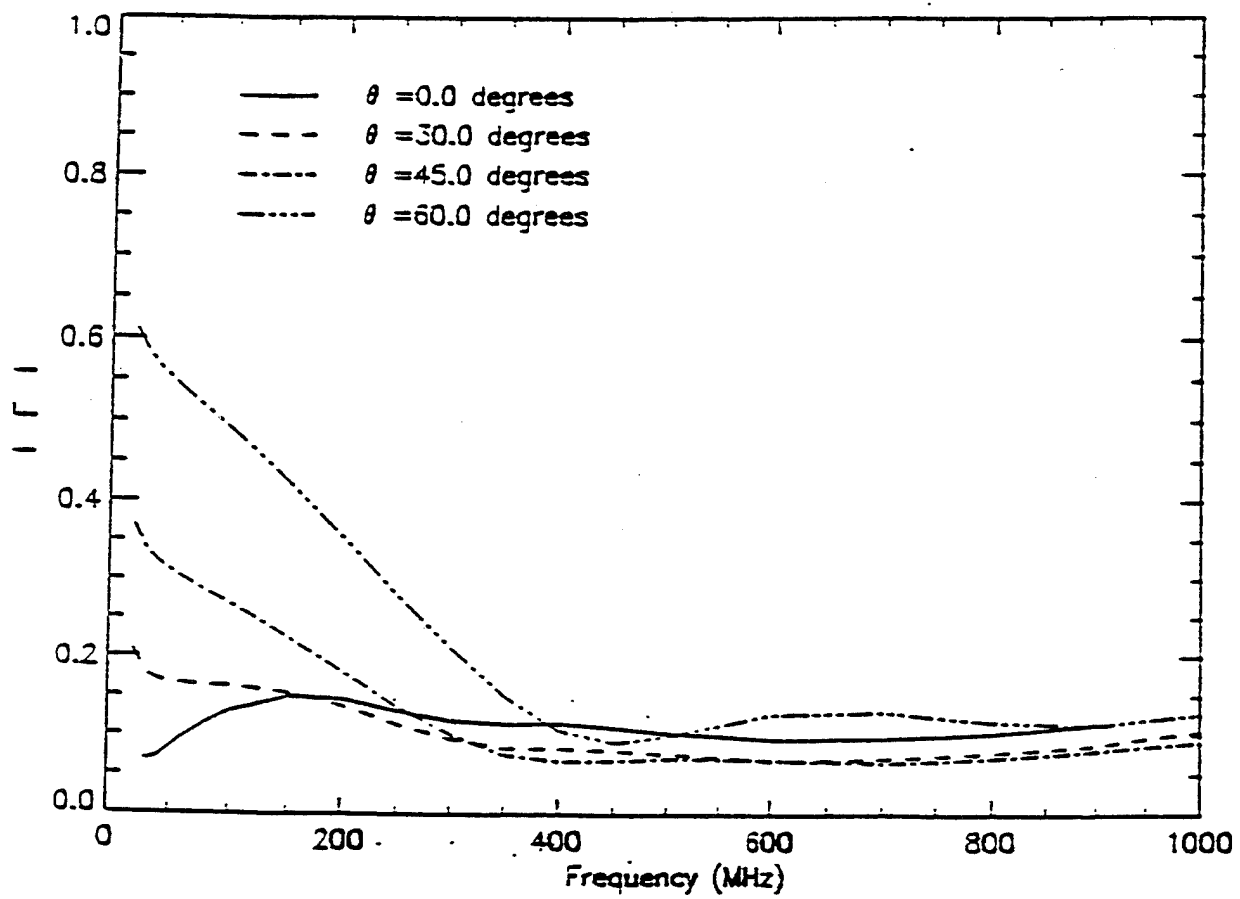


Figure 3 Reflection Coefficient Magnitude for the 24 Inch Pyramid-Ferrite Tile Hybrid for Various Angles of Incidence, θ

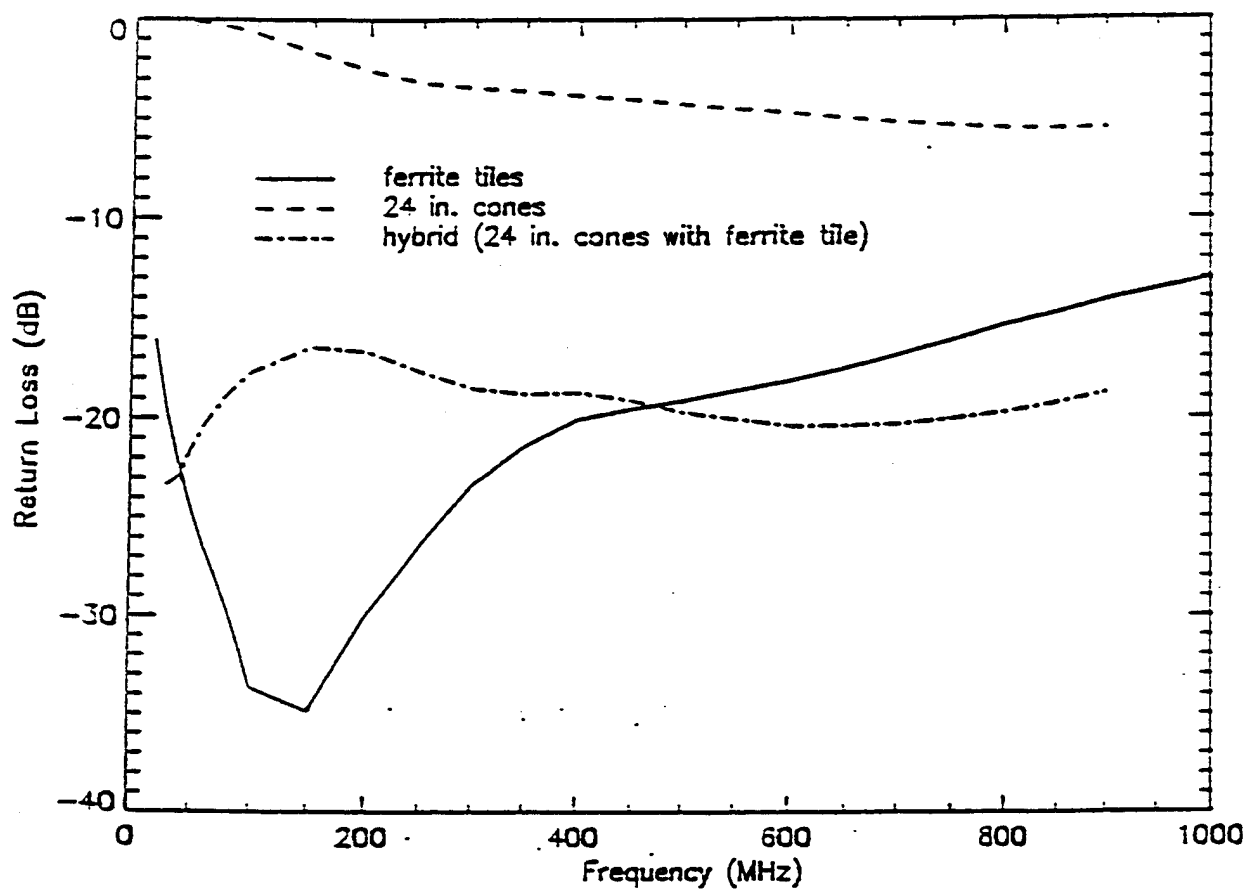
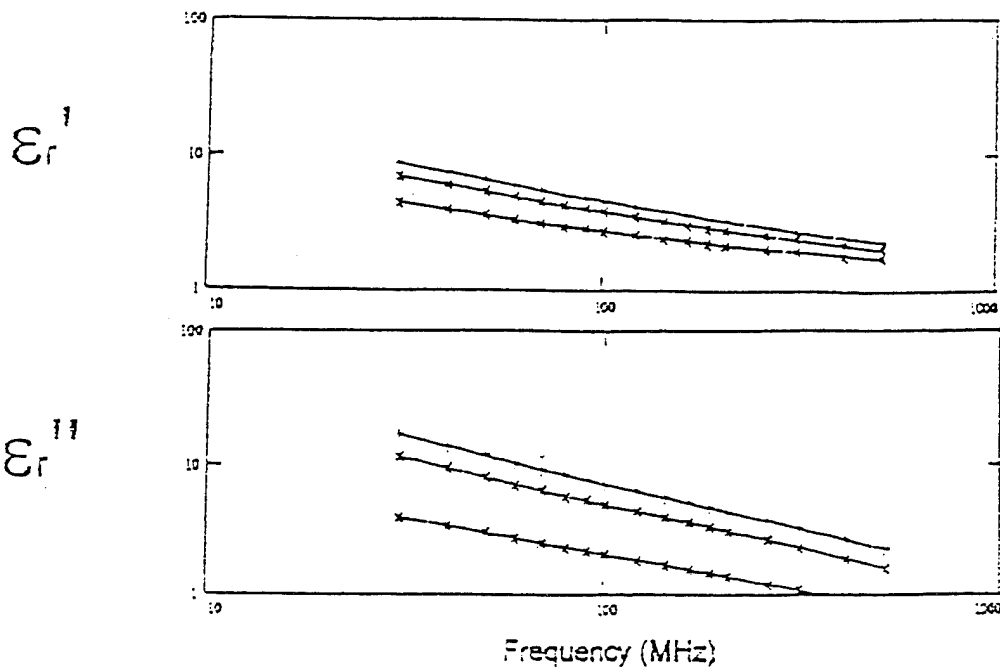


Figure 2 Normal Incidence Return Loss for 24 Inch Pyramids, Ferrite Tiles and a Pyramid-Ferrite Tile Hybrid

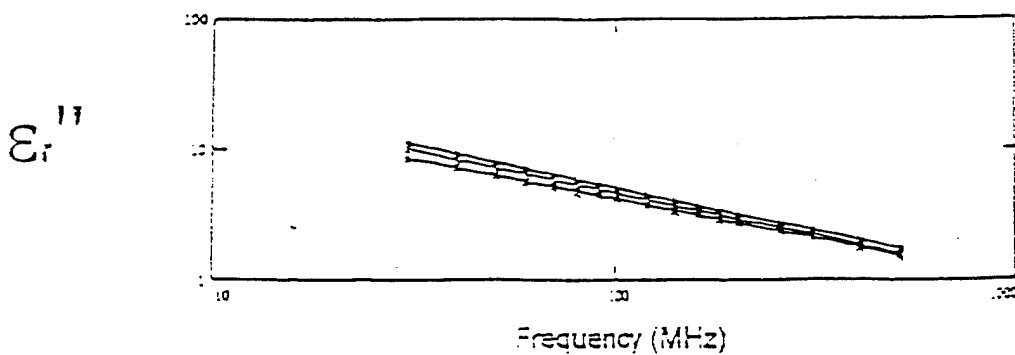
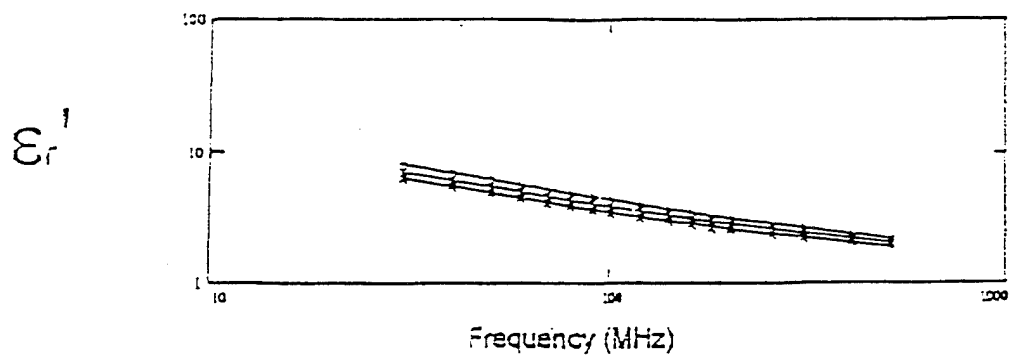
Relative Complex Permittivity of Three Absorber Samples
from the Ceiling of a Semi-anechoic Chamber Ceiling

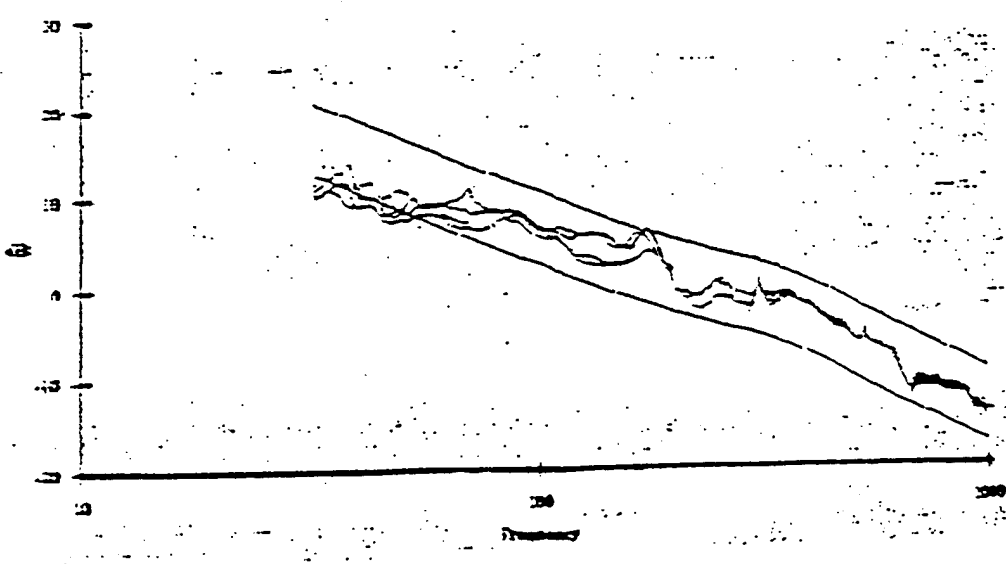
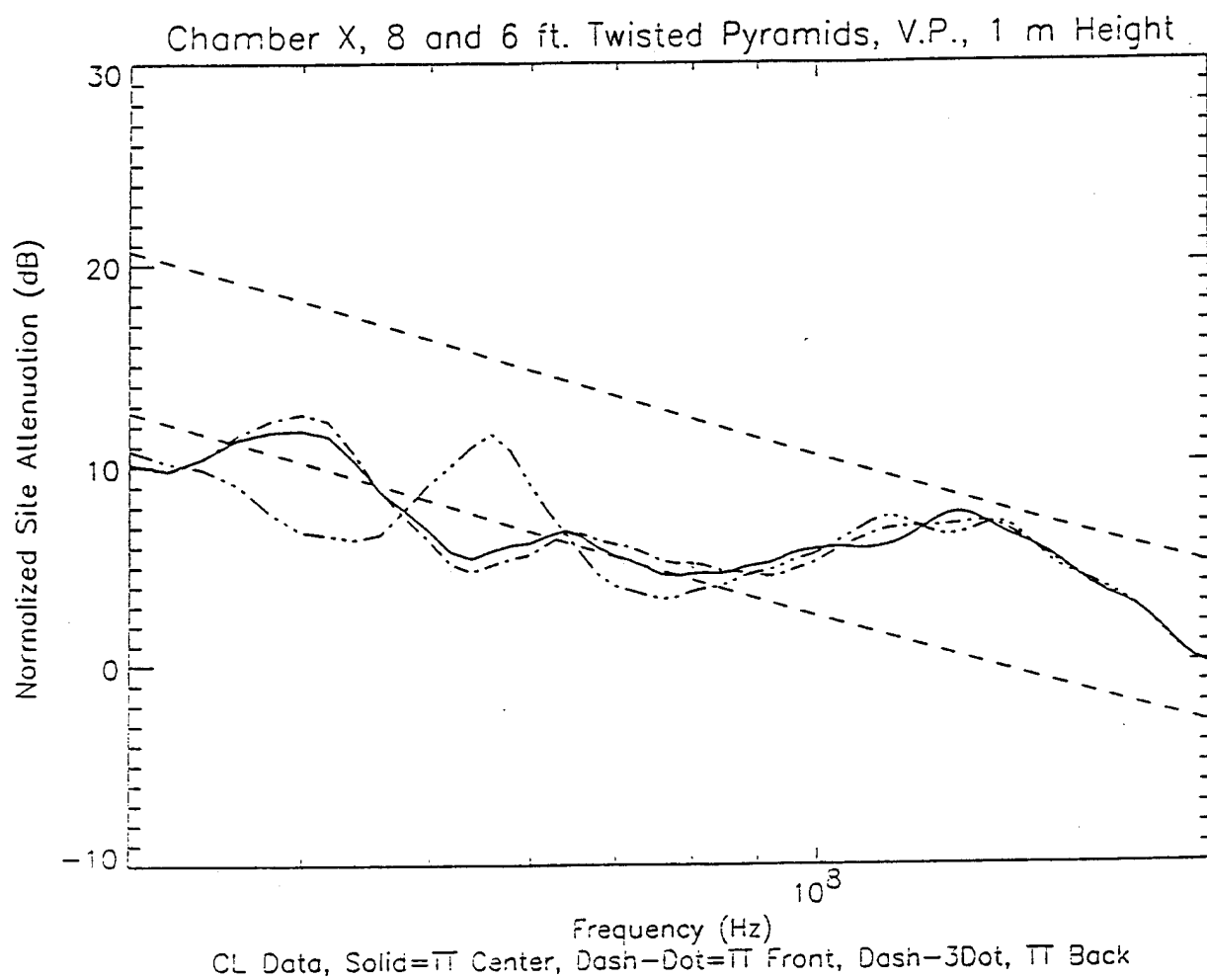
$$(\varepsilon_r = \varepsilon_r' - j\varepsilon_r'')$$

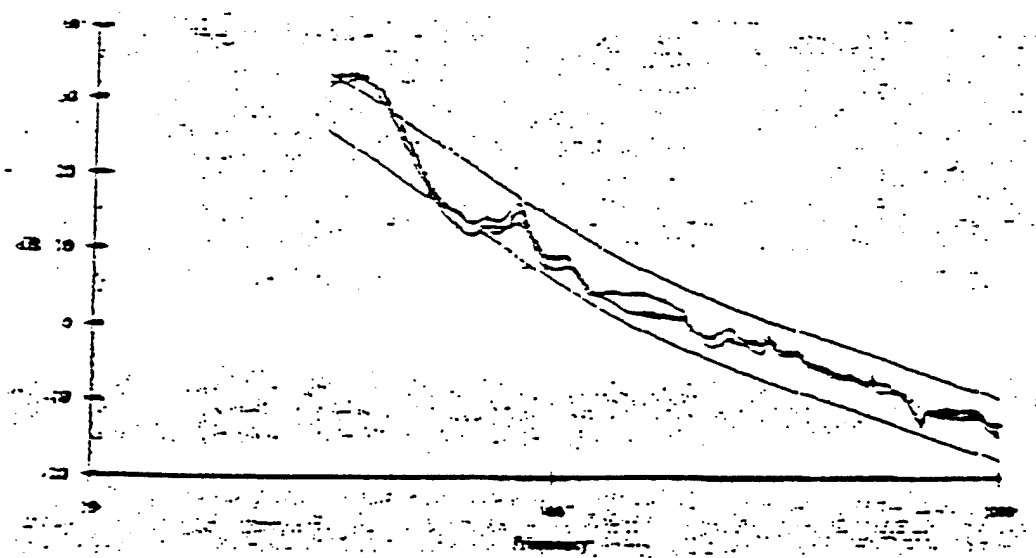
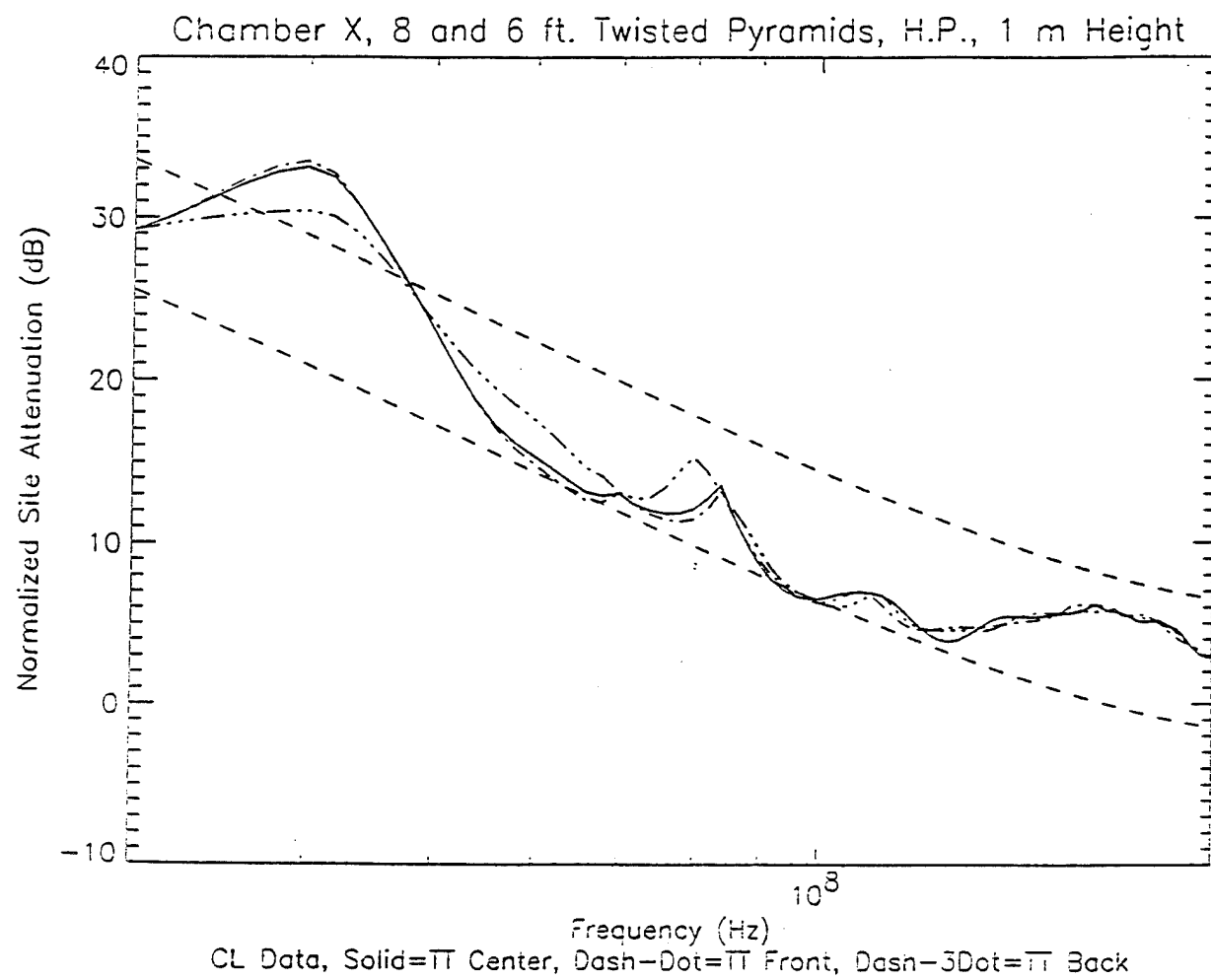


Relative Complex Permittivity of Eight Absorber Samples
from the Walls of a Semi-anechoic Chamber Ceiling

$$(\varepsilon_r = \varepsilon_r' - j\varepsilon_r'')$$







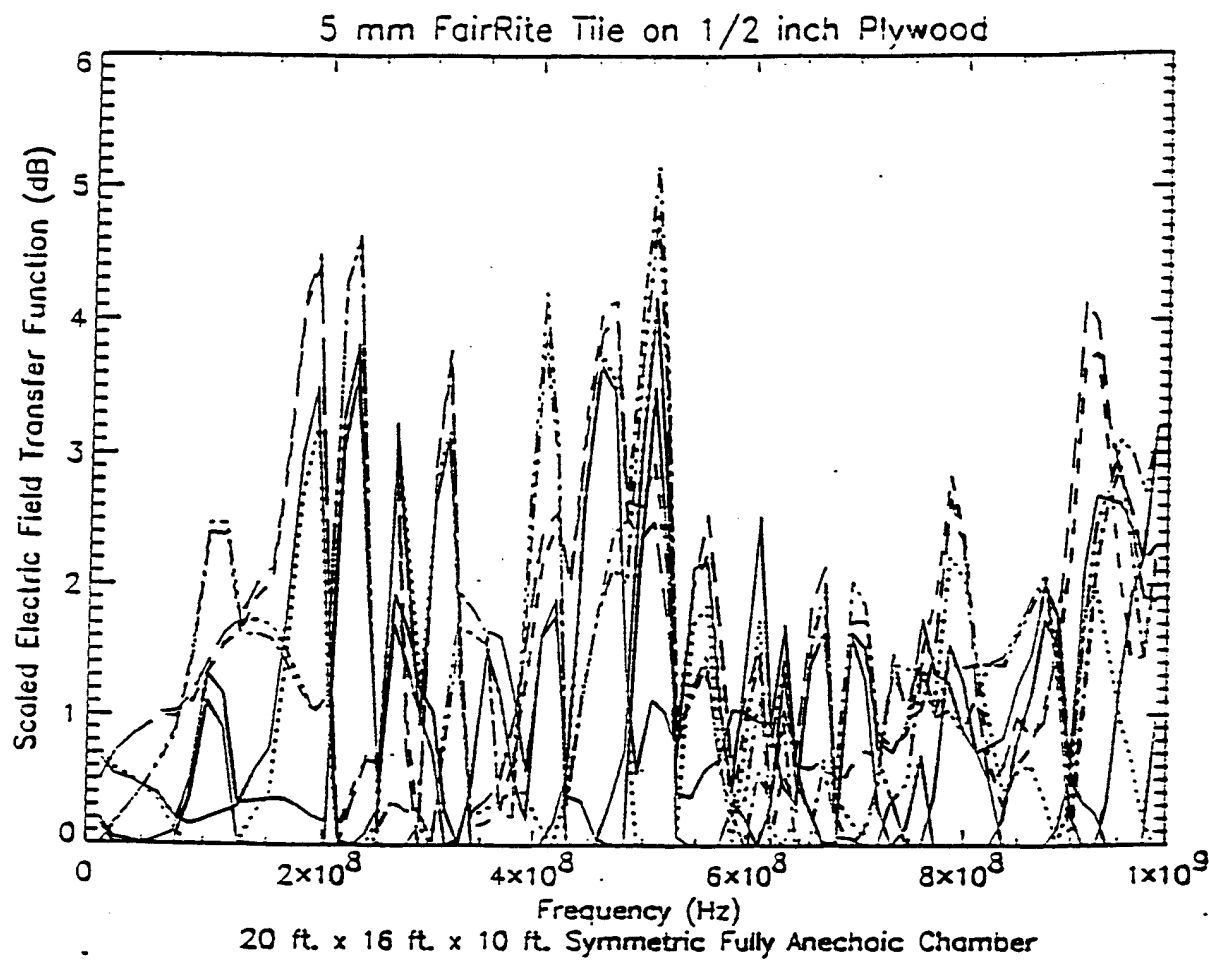
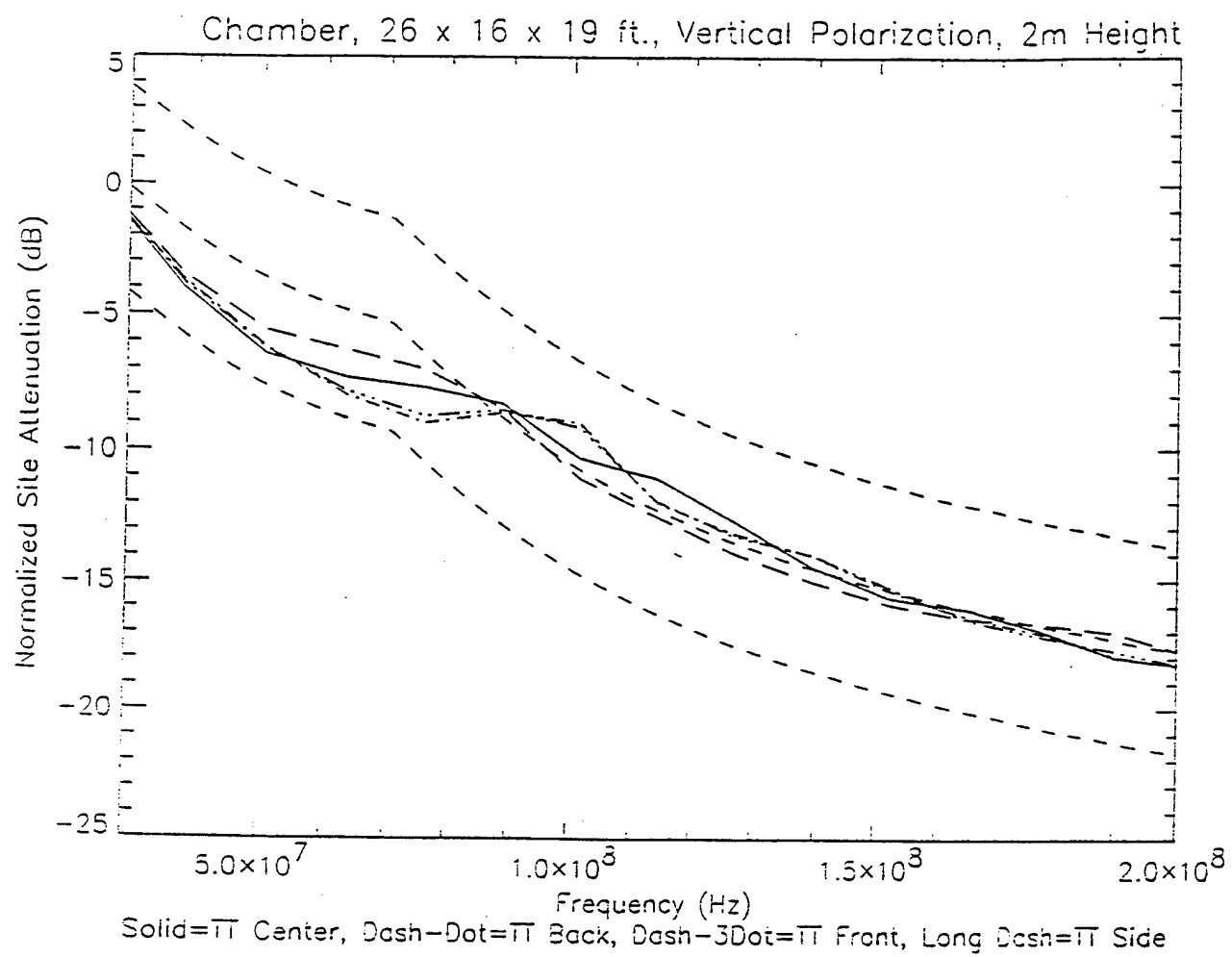
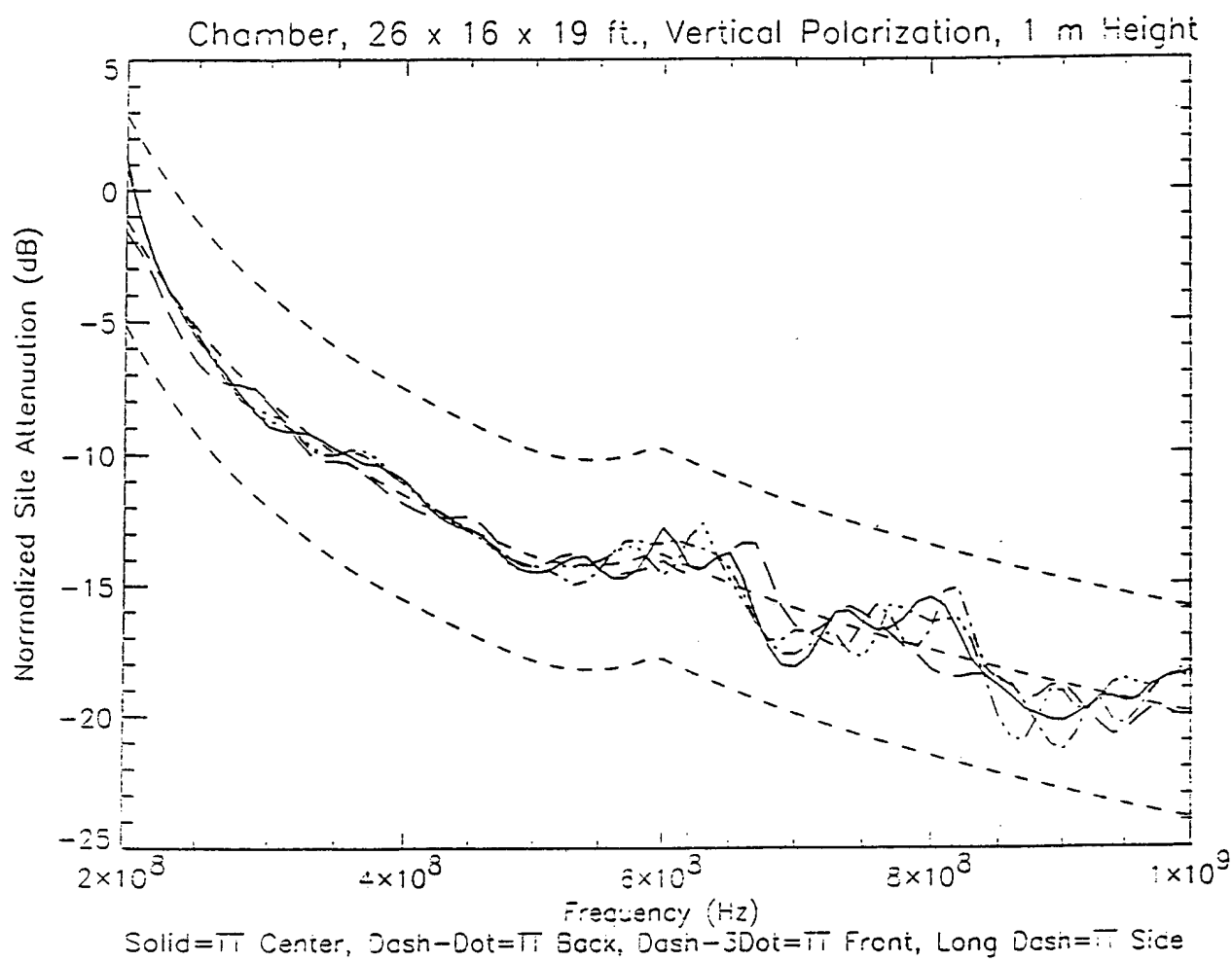
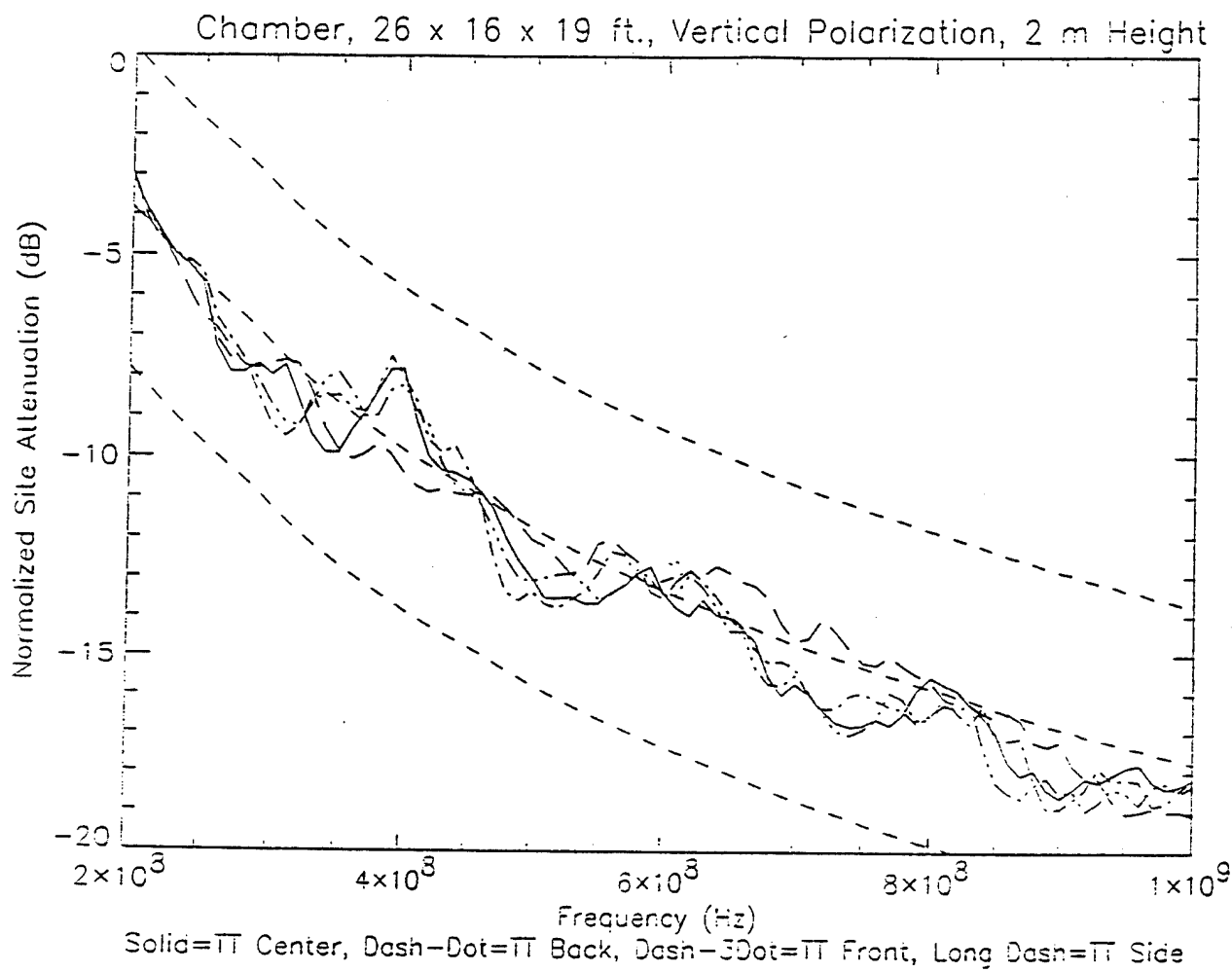
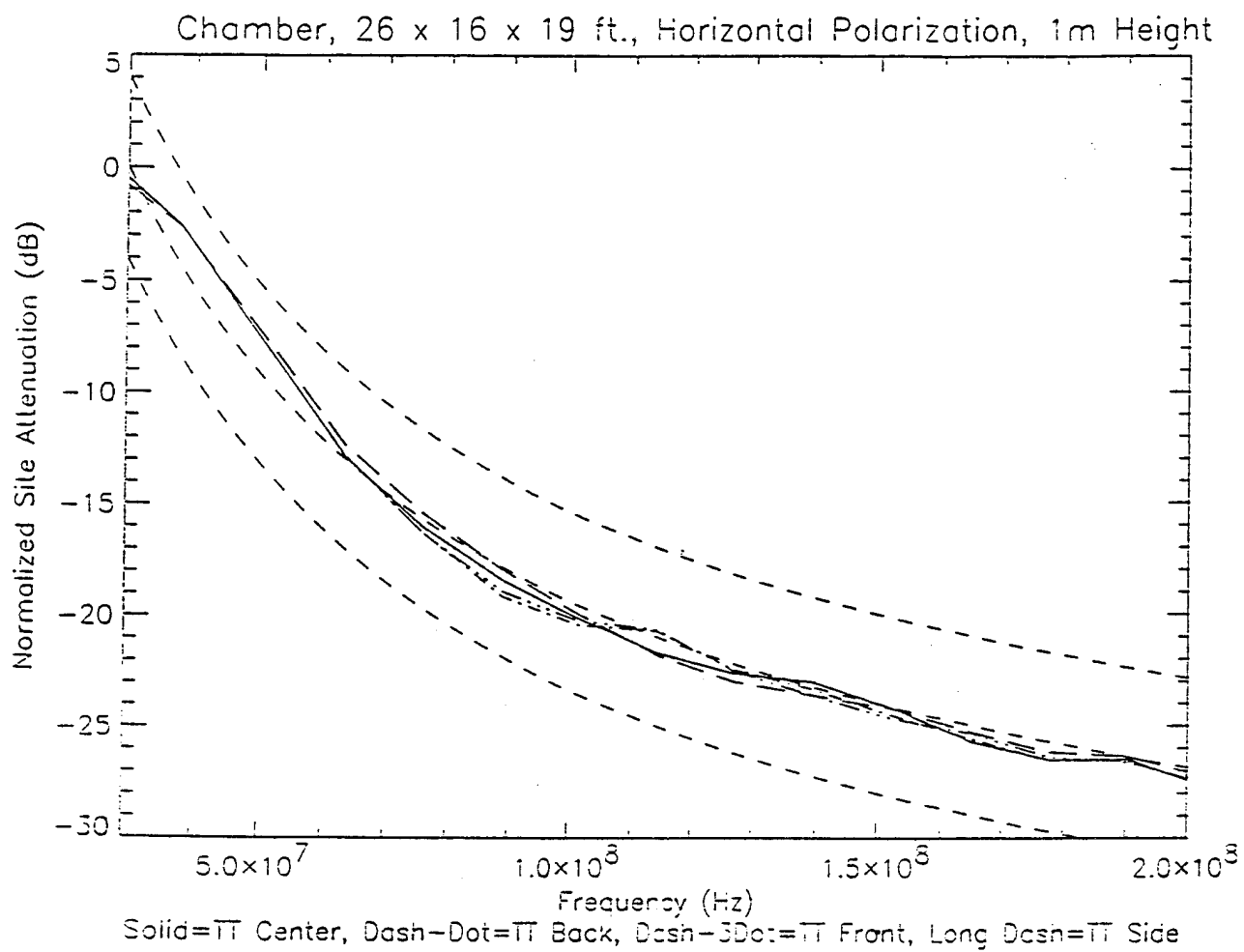


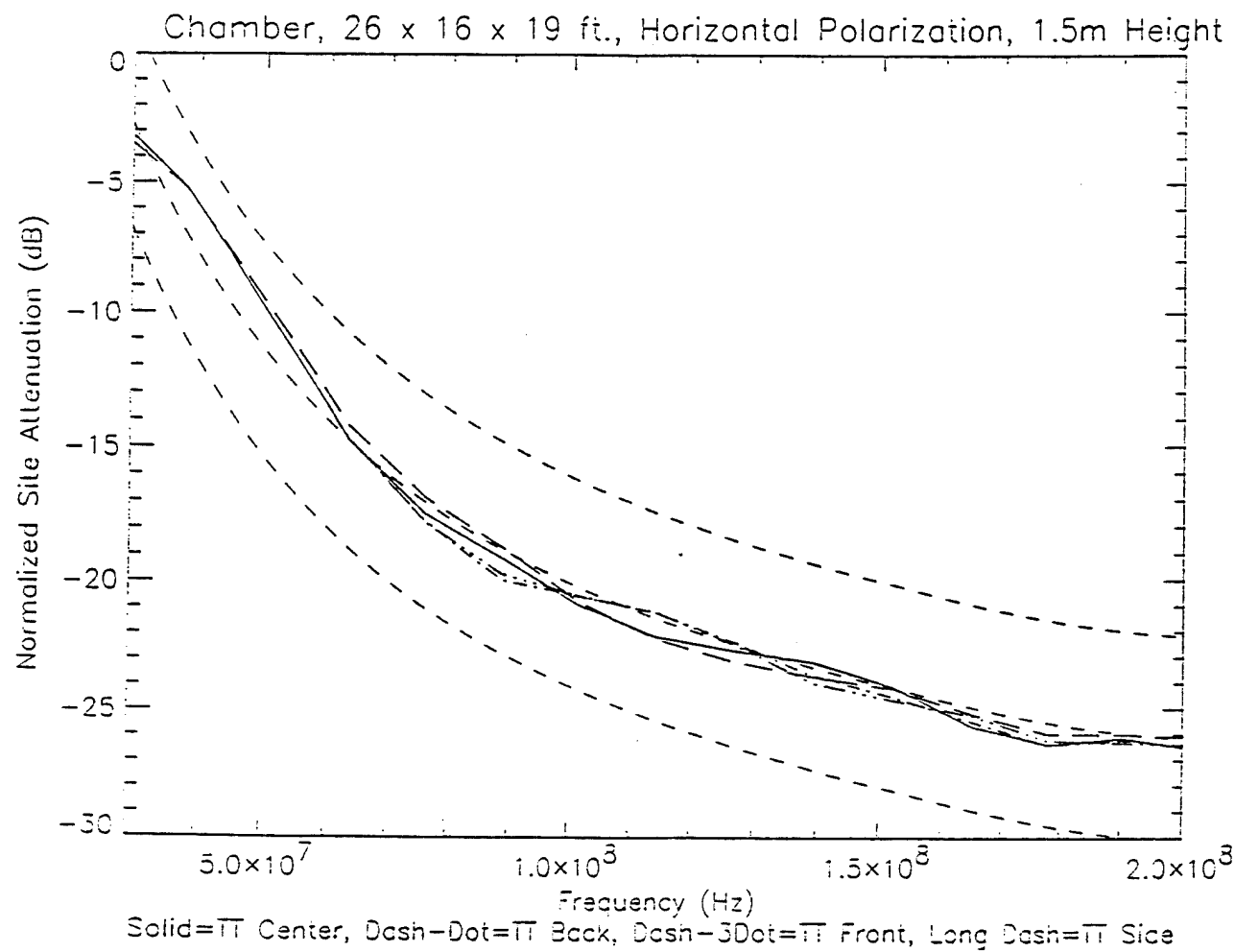
Figure 11 Field Uniformity for a 20'x16'x10' Fully Anechoic Chamber with Ferrite Tile on a 1/2" Thick Dielectric Slab

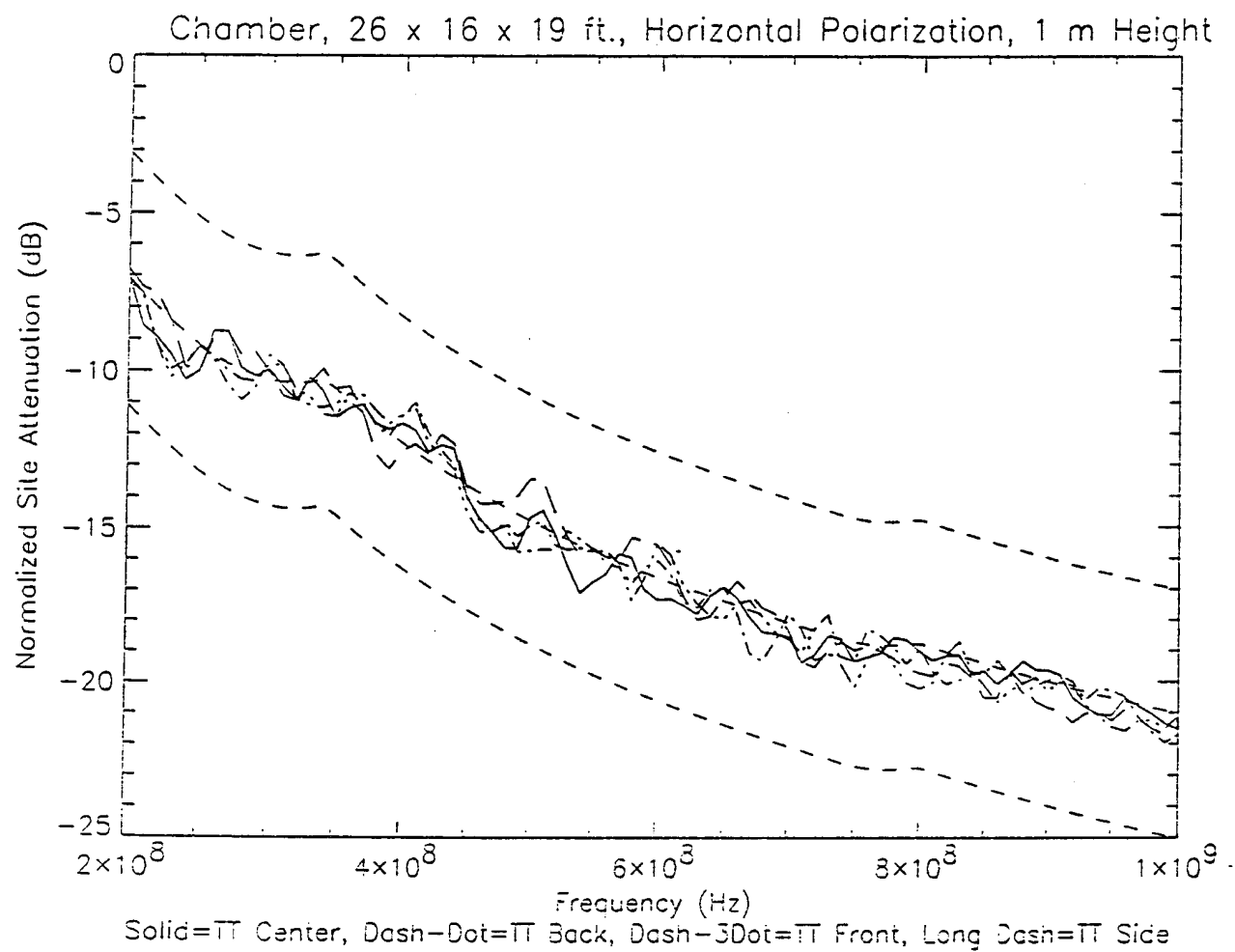


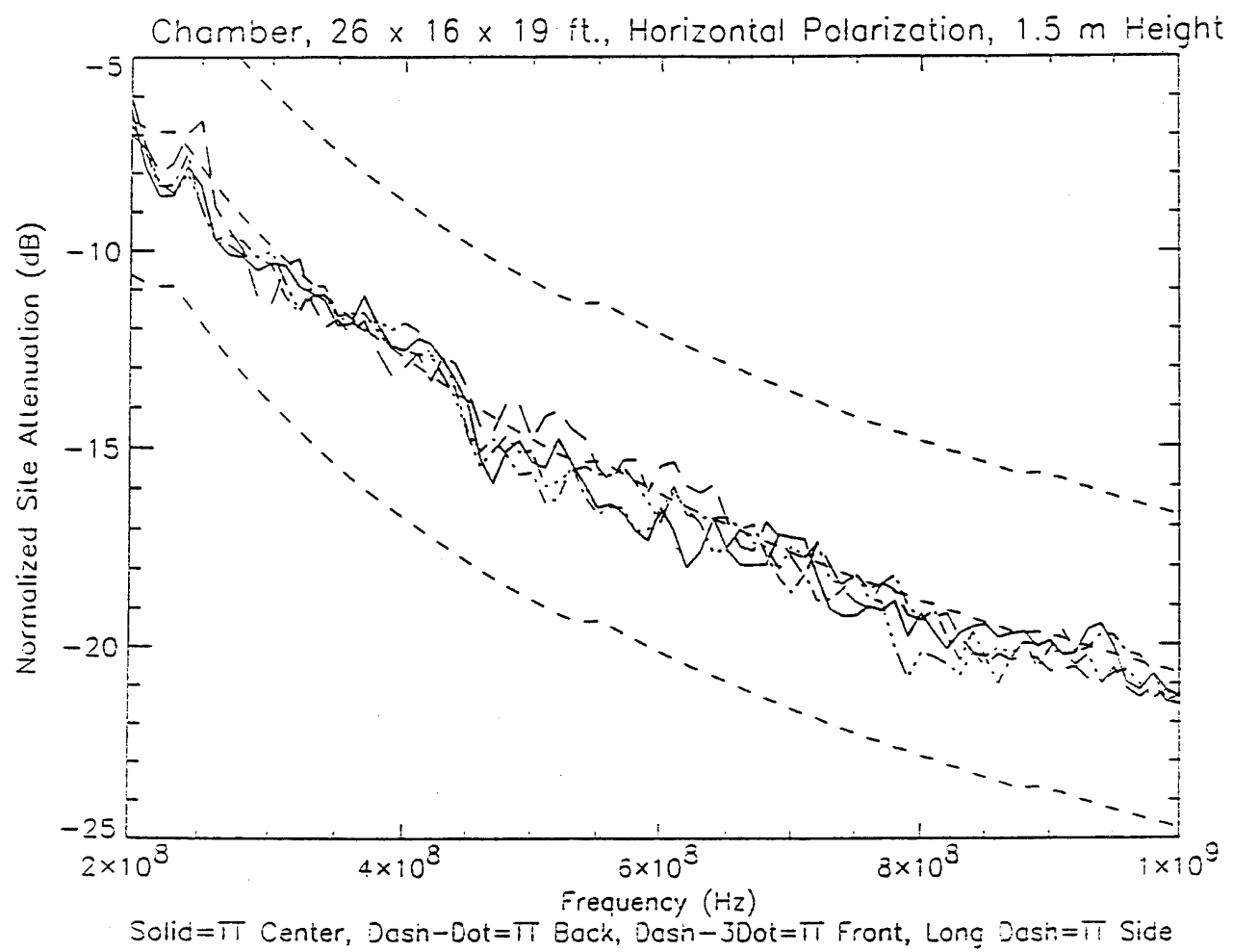
















DR. PAOLO CORONA
INSTITUTO UNIVERSITARIO NAVALE



P. CORONA, G. FERRARA, M. MIGLIACCIO
 ISTITUTO UNIVERSITARIO NAVALE
 Via Acton, 38 - 80133 Naples- ITALY

Statistical Analysis of Electromagnetic Fields in Use in Electromagnetic Compatibility (EMC)

1. SUMMARY

Either in reverberating chambers and in anechoic chambers the field uniformity is considered as a parameter suitable of evaluate the chamber performance. The field uniformity across the quiet zone is often prescribed by standards for the anechoic chambers, and a similar test is usually performed in reverberating chambers.

The field uniformity is perturbed by interference, and such interference can be considered either in terms of waves or resonance, each of these approaches can be, at least in principle, exchanged, but are better suited for specific situations: waves for the free space, approximated by the anechoic chamber, resonance for enclosures, such as reverberating chambers. In both cases field unevenness has to be considered as an unwanted feature, suitable of diagnostic use in reference to the desired condition. Furthermore such uneven fields are usually unstable, if referred to the regular components, and are indicative of reactive, unwanted, behaviour.

Unfortunately, a correct (according the Nyquist rule) sampling procedure cannot usually be performed for two reasons: even at moderate frequencies, the sampling rate (in the space domain) requires a very tight sampling, with a quite large number of samples, on the other hand, the sampling window (again in the space domain) is limited by the scanned area, and is often inadequate for a correct procedure. These referred condition apply to the complete field reconstruction, and this is rarely the case in the EMC, where usually it is enough to know the "over all" behaviour of the electromagnetic field. In this case a statistical analysis of "under sampled samples" can be performed, either in the anechoic chamber and in the reverberating chamber (and quite probably in other situations too).

Purpose of the paper is to present such analysis, applied to data sets obtained in real condition, to compare the statistics, and to extract the related information.

2. Statistical Analysis: Reverberating Chambers

In reverberating chambers the use of statistics as analysis tool is in some sense inherent with the operating process, and the electromagnetic field samples are statistical in their nature; such feature is typical, versus time, in the continuos mode stirred chambers, and is usually performed in the volume or in the "stepped positions" domain, in the step motor operated chambers.

A systematic analysis in order to check statistical hypothesis is necessary and can be performed according the customary statistical procedures. Some care has to be achieved in the sampling and analysis procedure.

Data sampled in the 2mx2mx2m reverberating chamber of the Naval University of Naples, have been checked against the hypothesis Rayleigh distribution.

Normalised bias error and normalised standard error are plotted in fig. 1, for some width (W) of the histogram cells. The best choice appear to be near the 0.4σ width value.

Similarity (against the Rayleigh probability) tests have then been performed with all the three stirrers (S1,S2,S3) in action, results are in fig. 2, and can be compared with the results in fig. 3, relevant to the worst case: i.e. only one stirrer (S1), the less effective, in operation. The comparison allow to consider the performed procedure suitable to characterise the chamber performance, and within the procedure, the autocorrelation function (fig. 2,d and fig. 3,d) as the best sensitive to the diagnosis of the e.m. field in the chamber.

3. Statistical Analysis: Anechoic Chambers

In anechoic chambers the field is typically deterministic. Nevertheless the use of anechoic chambers in the EMC deals mostly with near or reactive fields, considered the distance from the sources in use. On the other hand, it is impossible to obtain the desirable far field condition, considered the operating frequencies, the equipment size, and the remaining operation constraints. As a result, the electromagnetic field presents an uneven behaviour and should be analysed according non conventional features.

E.M. field can be sampled in the measurement area, and, in case of suitable scanning process, presented as in fig. 4. To the sampled field, an interpretation process can be applied. In fig. 5, data pertaining to a longitudinal (from the source) cut are worked out in order to extract the regular (decaying) component, and the oscillating term.

Such analysis gives indication on the general behaviour of the field, but it is worthy to consider the same samples also from the statistical viewpoint, and expressed as probability density function. The related histogram is in fig. 6, and shows some typical features suitable to be analysed according the ordinary statistical procedures. Some questions still are to be examined: 1) the possibility to apply the statistical analysis to the under sampled condition (with reference to the wavelength); 2) the possibility to use the regular component in order to correct (normalise) the oscillating term(s); 3) the hypothesis statistic to be used as a reference.

In any case the approach seems to be of some interest, and processing procedures such as the ones depicted in the previous section, can be proposed.

4. Conclusions

In the most of the procedures in use in EMC, it is unavoidable to consider electromagnetic fields of complex structure. Either in the reverberating chamber and in the anechoic chamber (at shorter than usual distance), field and power are conveyed by reactive fields, these latter are responsible of the coupling with the equipment under test. Statistical analysis can be proposed in both circumstances, and indication are that a common process can be proposed.

The results here referred have been obtained in the frame of the activity carried out at the Naval University of Naples, where mode stirred reverberating chambers were pioneered, in the statistical analysis [1] of them, and in cooperation with ELASIS (FIAT group), in the characterisation of anechoic chambers [2].

- 1] P. Corona, G. Ferrara, M. Migliaccio "Reverberating Chambers as Sources of Statistical Electromagnetic Field", IEEE Electromagnetic Compatibility Trans., Special Issue EMC Research in Italy, submitted
- 2] P. Corona, G. Ferrara, M. Moscariello, A. Izzo, "Automobile Evaluations In Electromagnetic Compatibility." International Conference Advanced Measurement Techniques and sensory Systems for Automotive Applications- ATA - Ancona -June 1995.

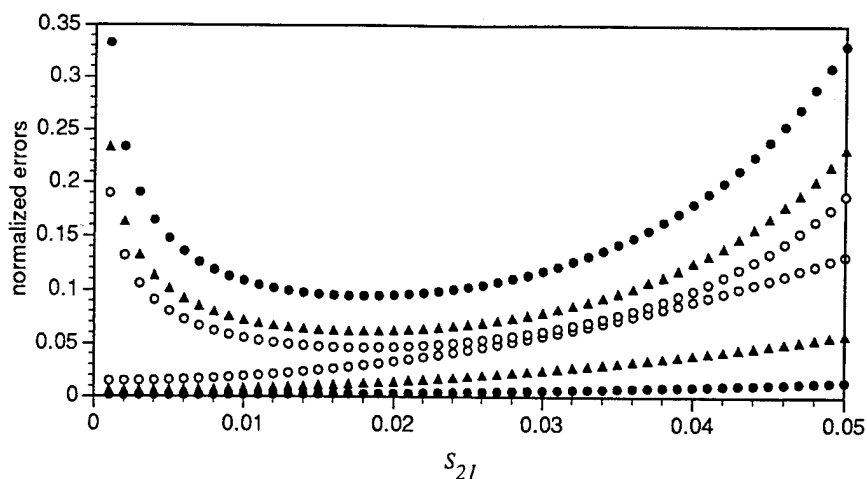


Fig.1: Normalized bias (three lower curves) and normalized standard error (three upper curves) which occur in the construction of the histogram whenever the true pdf is Rayleigh. $N=801$, $\sigma=0.00032$. ● are for $W=0.2\sigma$, ▲ are for $W=0.4\sigma$ and ○ are for $W=0.6\sigma$.

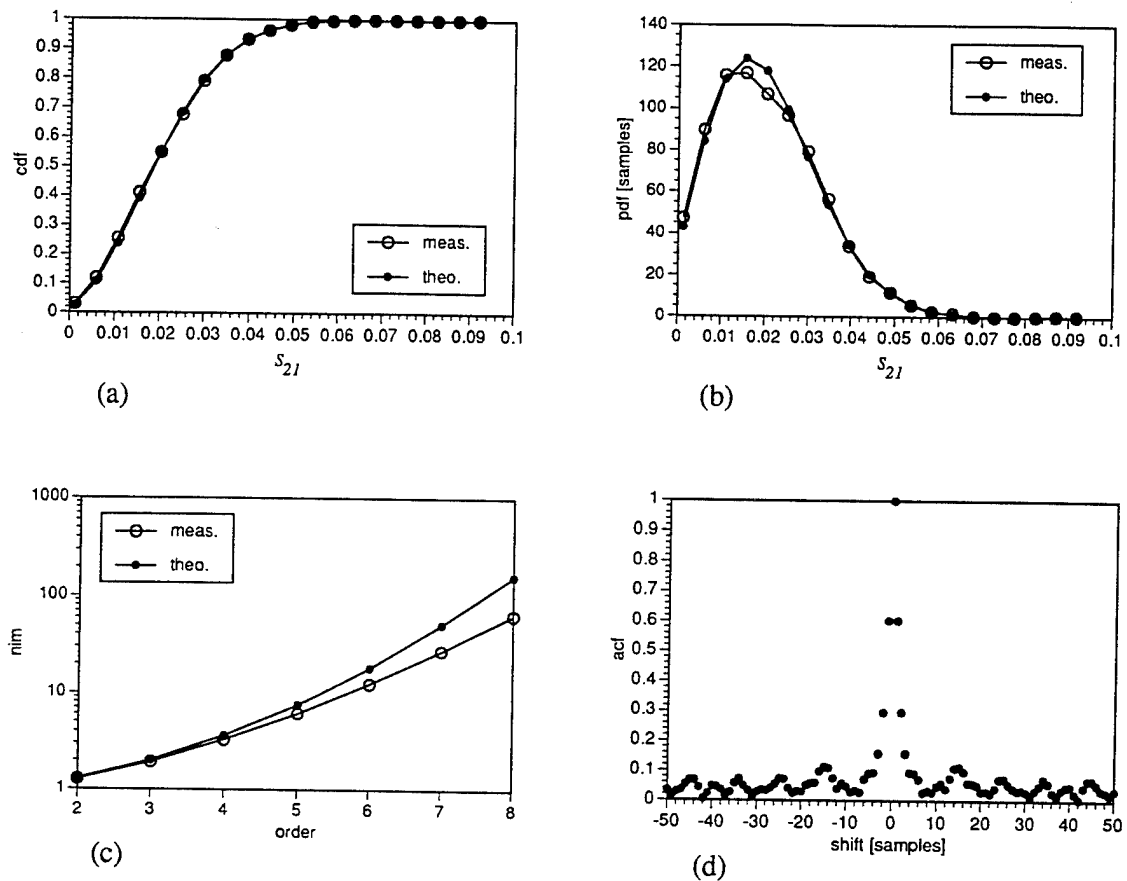


Fig.2: (a) cdf, (b) pdf and (c) nim (semi-logarithmic scale) relevant to the amplitude of the insertion loss. (d) acf of the insertion loss. Case: rotating S1, S2, S3.

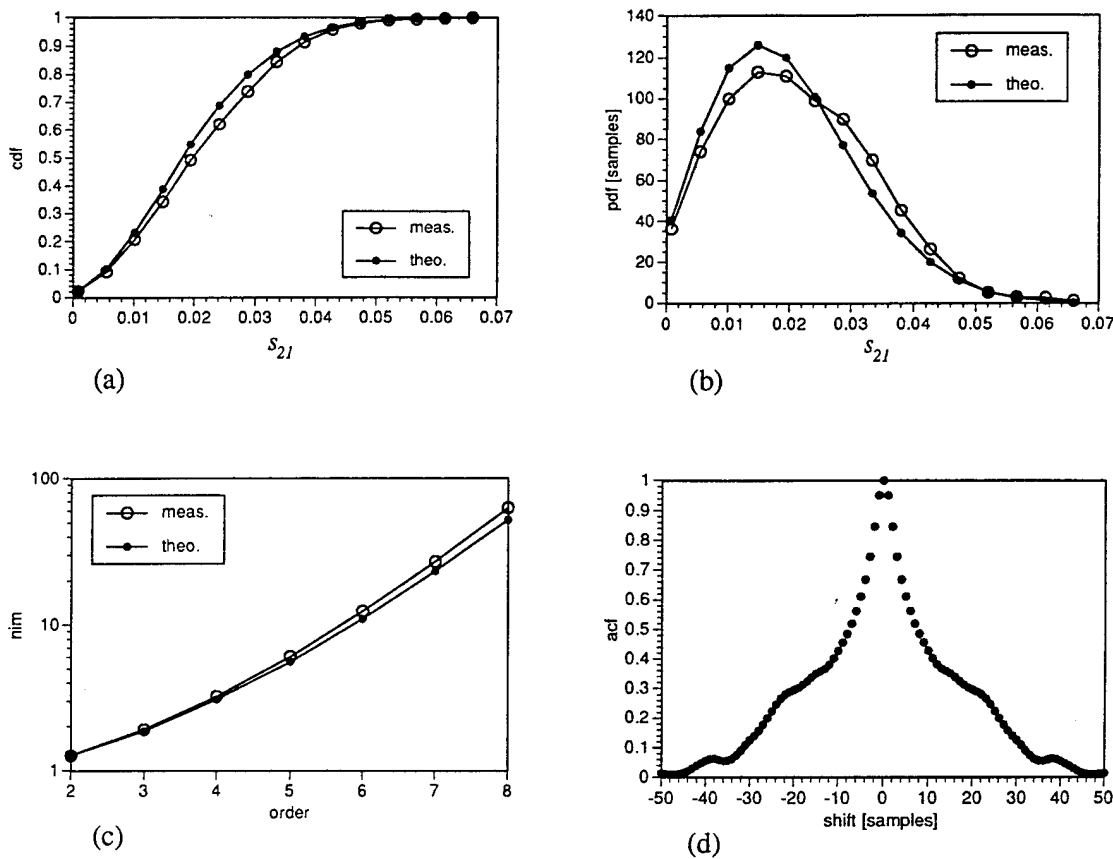


Fig.3: (a) cdf, (b) pdf and (c) nim (semi-logarithmic scale) relevant to the amplitude of the insertion loss. (d) acf of the insertion loss. Case: rotating S1.

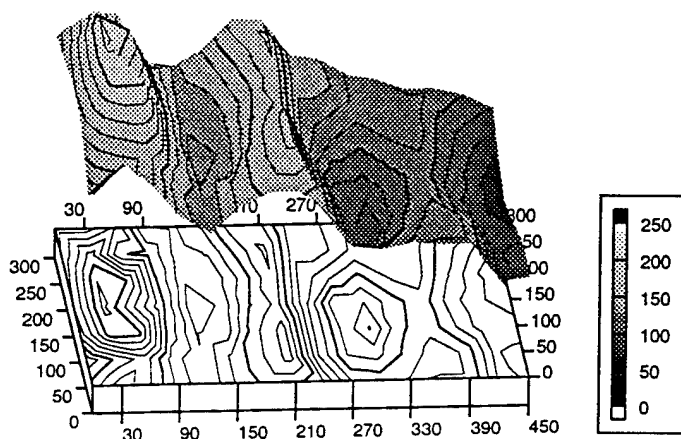


Fig.4: The field levels (V/m) at 100 MHz. Positions are expressed in cm. Source is on the left.

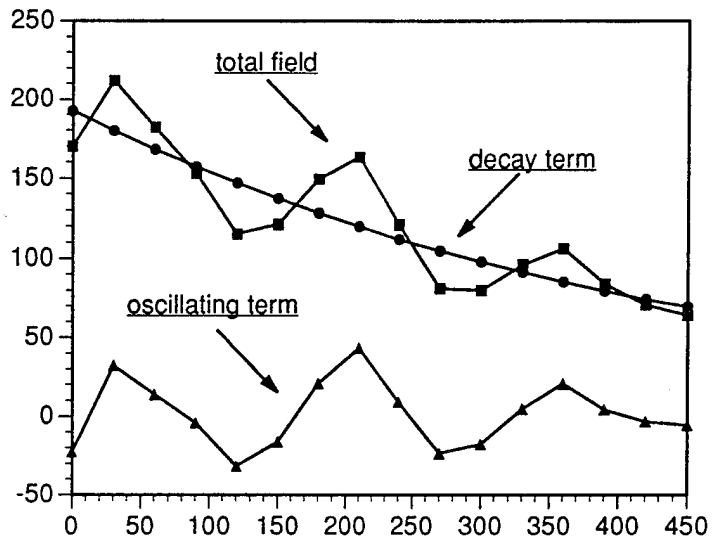


Fig.5: The field levels referred to the fig.4: cut along the antenna boresight line. Decay and oscillating term extraction.

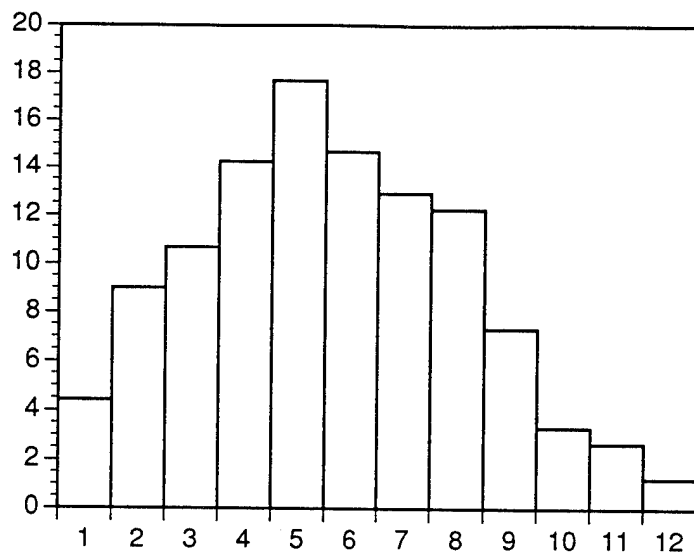
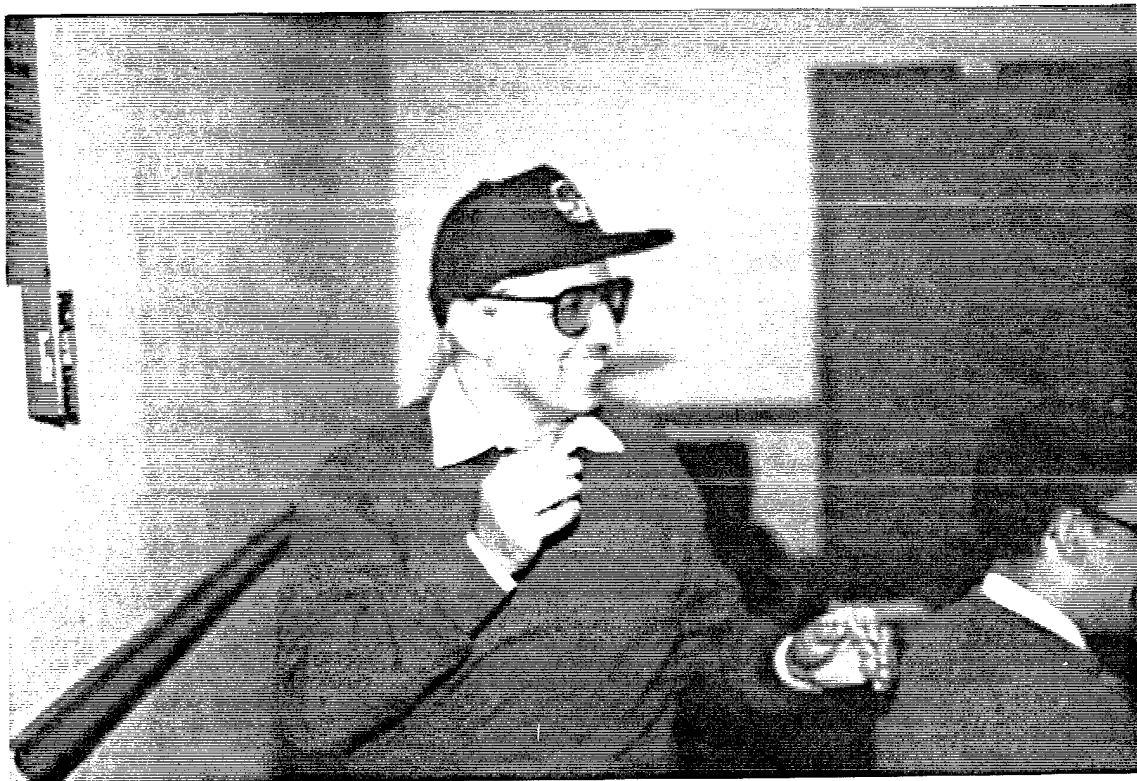


Fig.6: Data of fig. 4 presented according a "statistical" analysis.





**MR. POUL ANDERSEN
CHRYSLER CORPORATION**



An Integrated RF Signal Source for Immunity Testing
in Absorber lined Shield Rooms

Poul Andersen
Chrysler Corp
Vehicle Engineering
November 29, 1995

The Chrysler EMC Facility includes capability for vehicle and module testing. Part of the Chrysler facility is a 10 m absorber lined chamber called the Vehicle Anechoic Test Chamber or VATC. The overall dimensions of the VATC are 90 feet long by 64 feet wide and 46 feet high. The VATC is a double horn configuration. The VATC has two levels. The upper test level and the lower level for the turntable structure and drive mechanism, the dynamometer mechanisms, the antenna floor drive mechanism, etc.

In addition to being able to perform all of the required automotive vehicle tests, a design goal was to minimize the operator intervention to run tests.

The VATC is designed for both emissions and immunity testing. The frequency range for emissions is 30 to 1000 MHz. For immunity, the range of the VATC is 30 MHz to 18 GHz. The primary function of the VATC is testing vehicles. The turntable has a capacity of 10,000 lbs.

The facility includes capability for testing up to 30 MHz in a TEM Cell.

Utility provisions include cooling air, engine exhaust suction, compressed air, 60 Hz power at 120V and 208 V single phase and 480 V three phase.

One design feature of the chamber is a floor drive mechanism that can control the distance between the antenna and the test object. This gives the operator the capability of remotely changing the geometry of the test configuration to optimize the effects of floor bounce.

Emissions measurement is done with a conventional antenna and mast system. Present automotive tests are done at a 3 m antenna height. Capability for scanning from 1 to 4 m has been provided for future considerations.

The primary focus of this presentation is the RF source for immunity testing from 30 MHz to 18 GHz.

The system can be broken into two sections, low and high frequency. For the frequency range of 30 to 200 MHz, a log-periodic antenna is used. The antenna can be remotely controlled for height, polarization, and separation from the DUT. The antenna vertical tilt angle is manually adjusted. By removing screw-in antenna element extensions on the longer elements, the antenna on its mast

and cart assembly, can be removed from the test chamber for maintenance or for reflection free emission measurements.

For 30 to 100 MHz, a nominal 10 kW amplifier, which is shared with the TEM cell, is used. For 100 to 200 MHz, a 2.5 kW amplifier, which is located in a basement area outside, but adjacent to the chamber is used. This amplifier can also be used to generate lower field strengths in the 30 to 100 MHz band as a backup source.

The second segment for high frequencies presented more of a challenge to generate the desired field strengths. The initial design focused on a cart mechanism with a turntable. On the turntable is mounted the antennas for 200 MHz to 18 GHz.

200 - 1000 MHz Horn Antenna

1 - 1.8 GHz	Dual polarization driver with a parabolic reflector
1.8 - 4.4 GHz	Dual polarization driver with a parabolic reflector
4.4 - 8 GHz	Dual polarization driver with a parabolic reflector
8 - 18 GHz	Separate horn antennas for H and V polarization

You will note that the frequency ranges for the bands are a little unusual. This was done to minimize the potential problem of second harmonic output. The 1 - 1.8 amplifier utilizes a single low pass filter to attenuate harmonic energy. In the 1.8 to 4.4 GHz amplifier, two sub-bands are created by coax relays to feed the output energy through separate low pass filters. Provisions have been made, but not implemented, for the output of the 8 - 18 GHz amplifier to be split for similar filtering.

The initial design also mounted 4 microwave amplifiers in a vertical stack in the center of the turntable. This was done to minimize the loss of RF energy between the amplifiers and the antennas. Coaxial cable is used for 1 to 4.4 GHz and waveguide for 4.4 to 18 GHz. Dummy loads for each amplifier, directional couplers and RF switching is also incorporated into the design.

The amplifiers for 200-400 MHz and 400-1000 MHz were located in the basement area outside the chamber along with the previously mentioned 100-200 MHz amplifier.

In the design process, an attenuation budget was established and calculations based on amplifier power output, attenuation and antenna gain indicated that the desired field strengths would be generated. Keep in mind that there are relatively long coaxial cables between the two amplifiers feeding the horn antenna on the antenna cart because of their location and the floor drive mechanism.

During the commissioning process, we quickly learned that we were not achieving the design field strength levels. This was due mainly to incomplete evaluation of floor bounce effects and to a lesser extent, lower antenna gain than expected. Although within the original design expectation, the coax attenuation at 1000 MHz was over 3 dB.

After considerable discussion, two changes were instituted. The 200-400 MHz amplifier was moved into the lower area of the test chamber. This allowed the removal of about 30 feet of coax with the subsequent reduction in attenuation. Along with the relocation, a new larger, lower loss flexible coax was installed in the cable track. The resulting total reduction in attenuation made significant improvements to the available field strength. A further aspect of this change was the relocation of the power measuring dual directional coupler (DDC) to be in proximity to the antenna on the cart. The relocation of the DDC provides power readings that more accurately reflect the power delivered to the antenna and reflected from the antenna because of impedance mismatch.

Two of the original concerns about installing the amplifier in the lower level of the test chamber proved to be inconsequential. The amplifier has shown no indication of being affected by the RF field that leak into the lower level. Although there is risk of a chilled water leak inside the chamber, that is considered to be a manageable risk.

The second and more extensive change was the relocation of the 400-1000 MHz amplifier, which weighs about 800 lbs, to the antenna cart. Before the decision was made to do the relocation, a temporary connection was made and a test run to determine if there would be any coupling to the amplifier, which would now be located in the main region of the test chamber. No negative effects were observed. The amplifier was never returned to its original location. The implementation required the removal of the amplifier rack. The 400-1000 MHz amplifier was mounted on a pedestal. This allowed one of the heavier microwave amplifiers to be mounted on the turntable floor in the pedestal. An attempt was made to distribute the remaining microwave amplifiers to minimize cable lengths and maintain balance of the turntable. The effort has been a success. The cable loss has been reduced by 3 dB and the desired field strengths are achieved at a comfortable amplifier output level.

One aspect of the design that has not been discussed yet is the location of the signal generation and controller functions of the system. The initial thoughts were to locate the signal generator in the control room console. This would allow the operator to view the panel to read frequency, output level, operate control buttons, etc. This concept required a significant length of coaxial cable between the control room and the amplifiers and would have required a booster amplifier in particular for the microwave frequencies.

The design that was built appeared to have some risk. The signal generator was mounted in a shielded rack cabinet on the antenna cart in the chamber. This allowed short coax connections to the microwave amplifiers. The signal is fed to the lower frequency amplifiers through the cable track to the lower area of the chamber. A relay selects a feed to the amplifier now located there. The feed extends out of the chamber to the 100-200 MHz amplifier

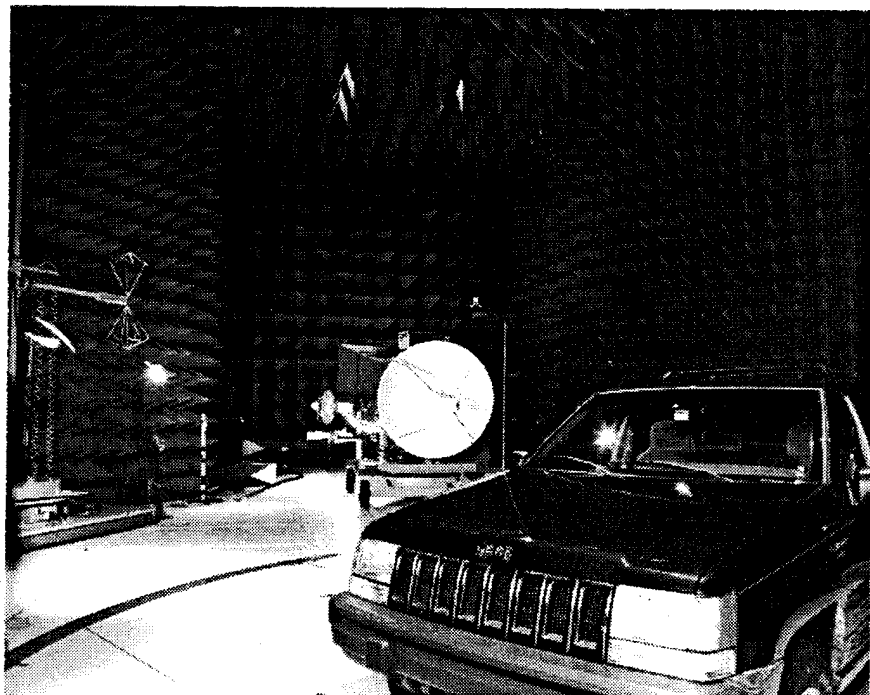
outside the chamber. It then extends a considerable distance of about 200 feet to the 10 kW 30-100 MHz amplifier. The only problem encountered with this extensive and lengthy distribution was some ground loop noise on the feed to the 10 kW amplifier. A 50Ω to 50Ω isolation transformer cured that problem.

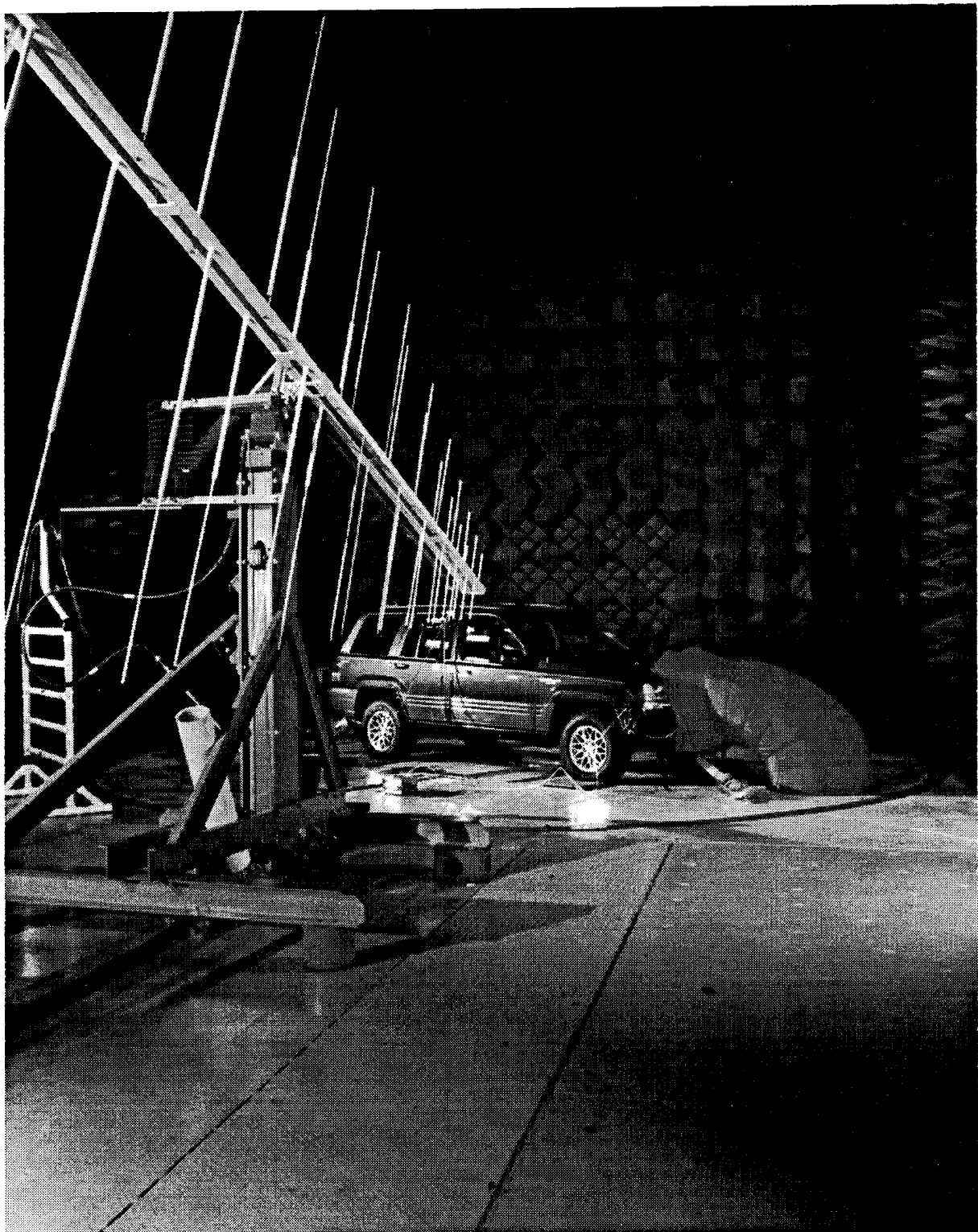
The controls for some amplifier functions and RF paths are interfaced via a VXI instrument. The power meter, some microwave amplifier controls and cart motion control is on the same IEEE 488 bus with the VXI interface. A fiber optic IEEE 488 bus extender is used to link the VXI interface to the test stand controller in the control room console. No special means were required for the IEEE 488 bus even though several of the bus cables are exposed to RF fields in the chamber.

The facility allows for efficient operation over the design frequency range. The antenna cart which weighs about 5000 pounds need never be removed from the chamber. When it is not in use, the floor drive parks it in a garage. A counter balanced frame on which the end wall absorber is mounted is lowered in front of the parked cart making it transparent to the low frequency and emissions testing. There are only two manual changes to perform a complete emissions and immunity test.

1. Location and connection of the emissions antenna cart.
2. Location and connection of the low frequency antenna cart.

Experimentation has shown that the low frequency antenna cart can remain in the chamber (parked off to the side) while high frequency immunity testing is performed.







**MR. BRUCE ARCHAMBEAULT
SETH CORPORATION**

*Standard Spherical
Dipole EMI/EMC
Source Repeatability
and Consistency*

Bruce Archambeault

SETH Corporation
110 Sunray Drive
Johnstown, Pa 15905
814-255-4417
email: arch@sethcorp.com



SETH Corporation

Developed to Satisfy Need

- Physically and Electrically Small E-field Source
- Wide Frequency Range
- Linear Amplitude Variation
- High dynamic Range
- Very Repeatable and Consistant
- Very Accurate E-Field Levels



SETH Corporation

Originally Developed as Joint Project

- NIST
- U.S. Navy
- Digital Equipment Corporation



SETH Corporation

Wide Variety of Uses

- Test Facility Certification
- Comparison between Test Facility Types
- Shielding Performance Tests
- Antenna Calibration
- Field Uniformity Testing



SETH Corporation

Test Facility Certification

- Known Electric Field
- Repeatable and Accurate
- Traceable to NIST
- Daily quick Checkout or Period Careful Calibration
- Comparison between Similar Test Facilities



SETH Corporation

Comparison between Different Test Facility Types

- Anechoic and Reverberation Chambers
- Anechoic Chambers and Open Area Test Sites (OATS)
- GTEM/TEM and OATS
- Shielded Room and Anechoic Chambers



SETH Corporation

Shielding Performance Tests

- Physically small
- Eliminate 'Wire Loop' Sources and Their Problems
- Comparisons between Shielding Options
- Repeatable over Days/Weeks/Months



SETH Corporation

Antenna Calibration

- Manufacturers Provide only Far Field Antenna Factors
- Test Environment Affects Antenna Factors
- Allows Antenna Factors to be found for TRUE Test Environment
- Allows Near Field Antenna Factors to be Determined



SETH Corporation

Field Uniformity Testing

- IEC 801-3 (1000-4-3) Specifies 10 cm maximum Antenna Size
- Eliminates Field Averaging of Larger Antennas
- Use Reciprocity
- Aids in Diagnostic Evaluation When Necessary



SETH Corporation

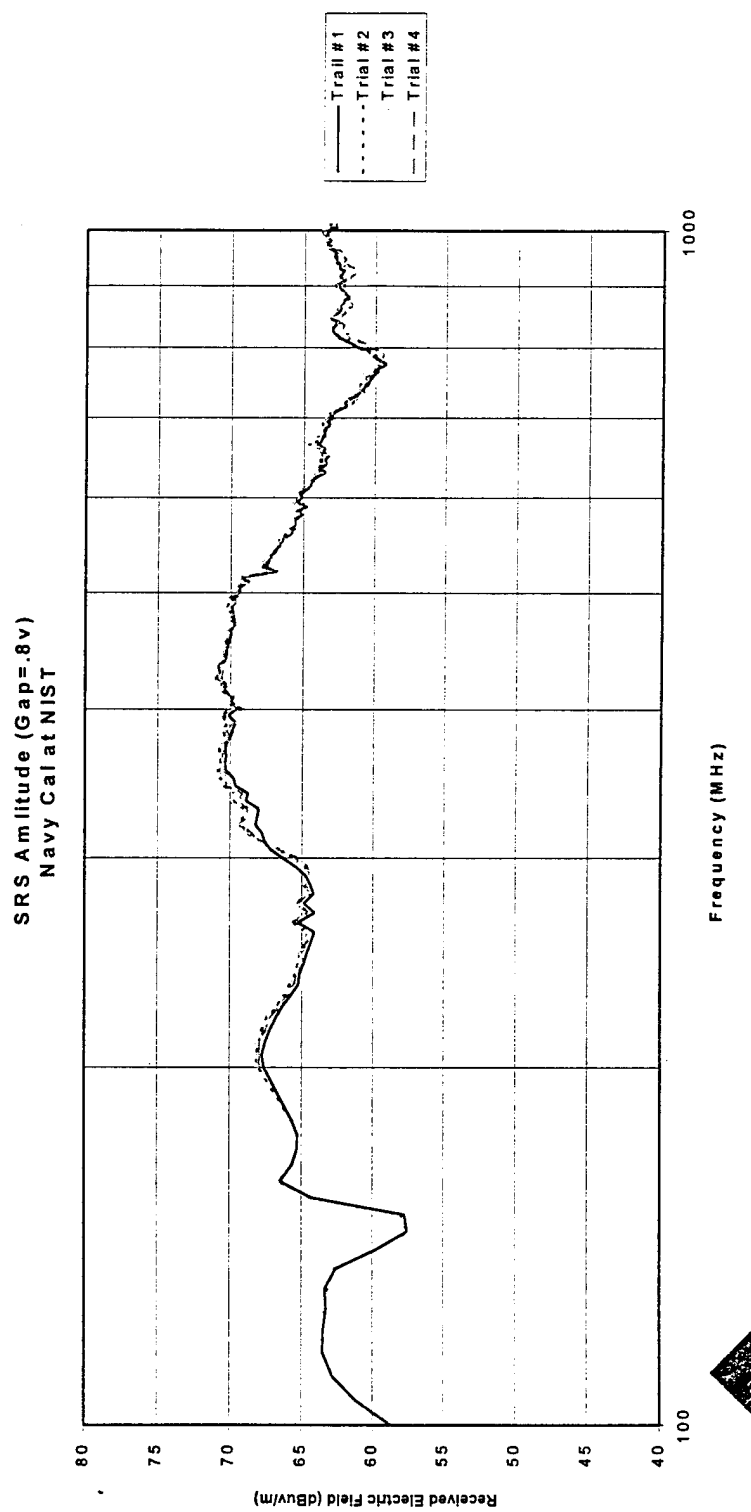
SRS2100 Performance

- Frequency Range
 - 10 MH - 2 GHz
 - 15 KHz - 30 MHz
- Size ---- 10 cm Sphere
- Field Strength
- Multi-Measurement Field Deviation



SETH Corporation

SRS2100 Typical E-Field Strength 2 m Anechoic Room Test

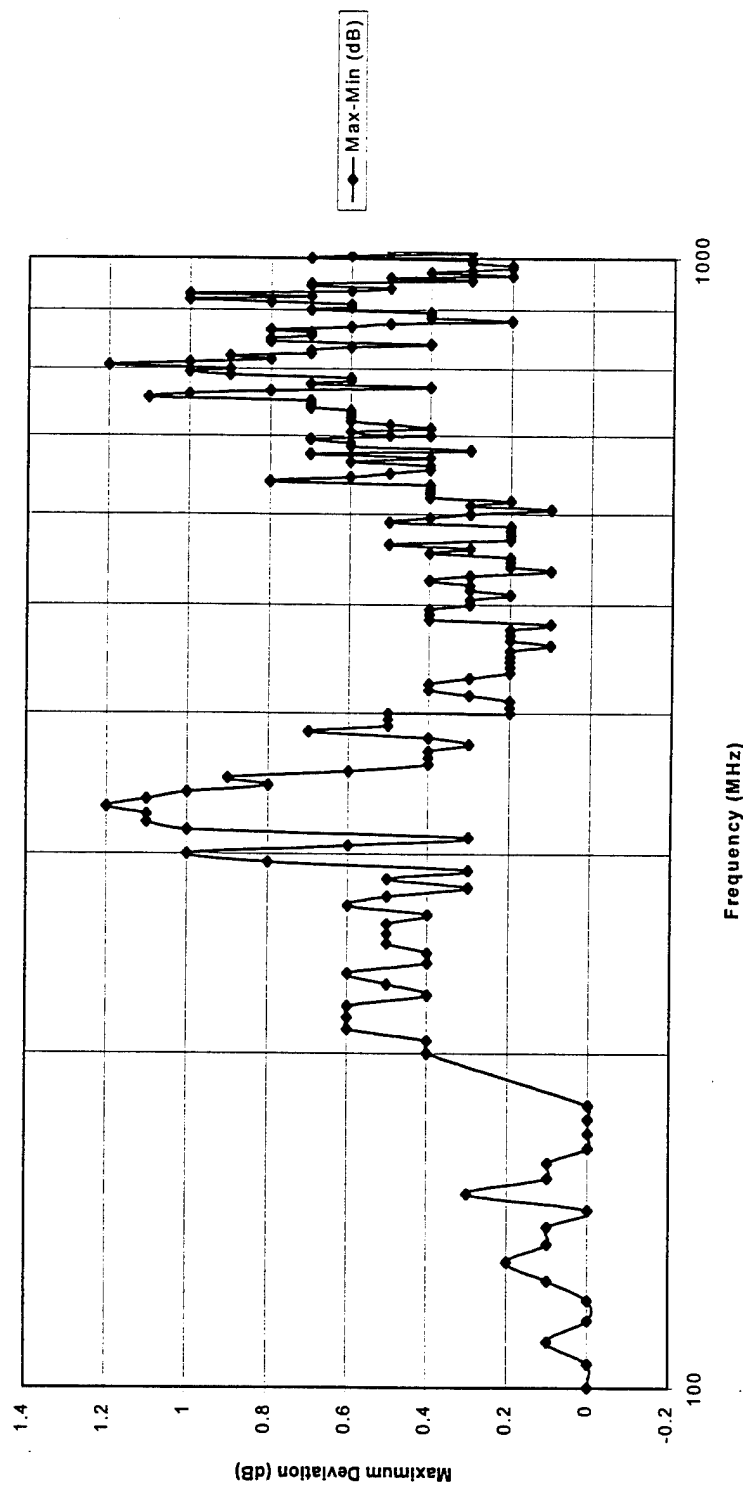


SETH Corporation



Multi-Measurement E-Field Maximum Deviation

SRS NIST Calibration Trial Deviation



SETH Corporation



Summary

- Wide Variety of Uses
- Accurate and Repeatable
- Confidence in Test Results Greatly Increased



SETH Corporation





DR. CELESTE BELCASTRO
NASA Langley Research Center



A Low-Cost Comprehensive Methodology for EME Effects Assessment of Critical Systems

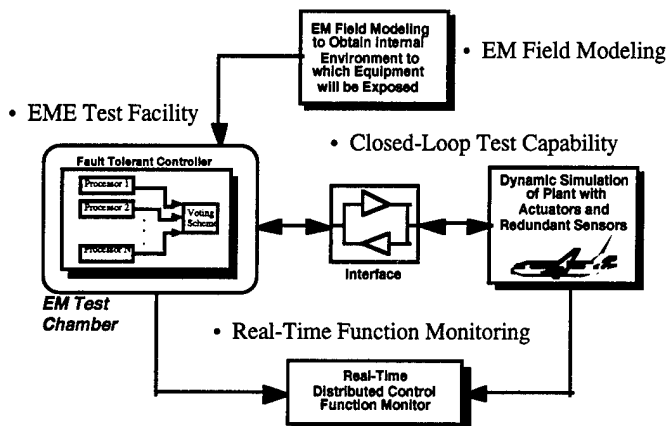
Celeste M. Belcastro, Ph.D.

NASA Langley Research Center
Mail Stop 130
Hampton, VA 23681-0001

Phone: (804) 864-6182
FAX: (804) 864-4234
celeste.m.belcastro@larc.nasa.gov

ABSTRACT

Electromagnetic environment (EME) assessment technology being developed at the NASA Langley Research Center involves electromagnetic (EM) field modeling codes for excitation of large geometric structures over a wide frequency spectrum, validation of these codes using ground tests and flight tests of the B757, a multi-chamber test facility, and a closed-loop test capability with real-time function monitoring of the equipment under test.



The EM field modeling codes under development at NASA Langley will significantly extend the high-frequency capability of available codes for application to large-scale geometries, such as the B757. Using ground tests and flight tests to validate these codes will enhance the confident application of the codes in industry. The test facility at NASA Langley includes three reverberation chambers that could be used during multi-chamber tests of distributed systems. For example, this facility has the capability to perform tests in which a controller that would be in the equipment bay of an aircraft is placed in one chamber and exposed to appropriate fields for that internal environment, and a smart actuator that is connected to the controller is placed in another chamber and exposed to fields that would be appropriate for that external environment. The closed-loop test capability with function monitoring that is currently under development at NASA Langley will enable upsets in the equipment under test to be evaluated in terms of function relative to aircraft dynamics and performance, and to be evaluated dynamically over the entire flight mode of interest. EME tests are typically performed as static open-loop tests at a few operating points in the flight envelope of interest. In addition, by using closed-loop testing, performance of the system during exposure to EM energy can be assessed when the aircraft is experiencing potentially destabilizing atmospheric conditions such as wind gusts, clear air turbulence, and wind shears. This comprehensive methodology will reduce the cost of EME assessment of critical systems by reducing the amount of full-aircraft testing required to demonstrate certification compliance.



Langley Research Center

EME Assessment Methodology

A Low-Cost Comprehensive Methodology for EME Effects Assessment of Critical Systems

Celeste M. Belcastro, Ph.D.
Assessment Technology Branch
Flight Electronics Technology Division

Reverberation Chamber and Anechoic Chamber
Operators Group Meeting
December 5 - 7, 1995



Outline

- Background
 - HIRF Threat to Advanced Aircraft
 - FAA HIRF Certification Requirements
- Objectives
- Approach
- Status and Accomplishments
- Summary and Conclusions



Langley Research Center

EME Assessment Methodology

HIRF Threat to Advanced Aircraft

- Composite Airframe Structures
 - Less Shielding than All Metal
- Flight-Critical Controls
 - Higher Reliability Requirements than Non-Critical Controls
- Digital Control Systems
 - More Sensitive to Transient Signals than Analog
 - Can Cease Correct Operation (Upset) without Component Damage



FAA HIRF Requirements

- FAA Commissioned SAE AE-4R to Develop HIRF Spectrum for Certification (12/88)
- Advisory Circular Draft #16 (8/93)
 - Frequency Range from 10 KHz - 40 GHz
 - Peak and Average Field Strength External to Vehicle
 - » Normal HIRF Environment
 - Peak: 10 - 4500 V/m
 - Average: 10 - 360 V/m
 - » Certification HIRF Environment
 - Peak: 20 - 6800 V/m
 - Average: 20 - 750 V/m
 - » Severe HIRF Environment
 - Peak: 30 - 6680 V/m
 - Average: 30 - 1270 V/m



Objectives

- Develop Methodology for Comprehensive EME Assessment of Critical Digital Systems
 - EME Modeling and Test Facility
 - Evaluation of Functional Integrity of Equipment Under Test During EME Exposure
 - » Impact on Safety and Performance of the Closed-Loop System
 - » Margins Within Which EUT Performance will Allow Functional Integrity of the Closed-Loop System to be Maintained
- Develop Technology for Lower Cost EME Certification Methods
 - Compliance with Stringent FAA and JAA High Intensity Radiated Fields (HIRF) Requirements
 - Reduce Costs by Reducing Required Full-Aircraft Testing
- Transfer Technology to Industry
 - Incorporation into Standards, Handbooks, Industry Practice
 - Certification Credit for EM Methods by FAA and JAA



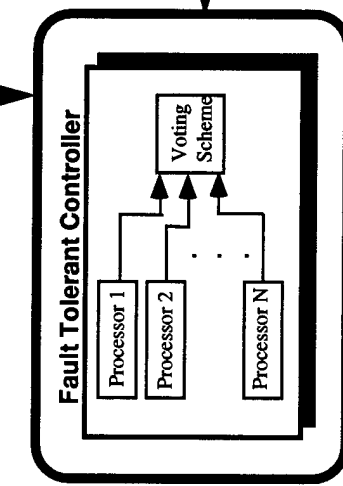
Langley Research Center

EME Assessment Methodology

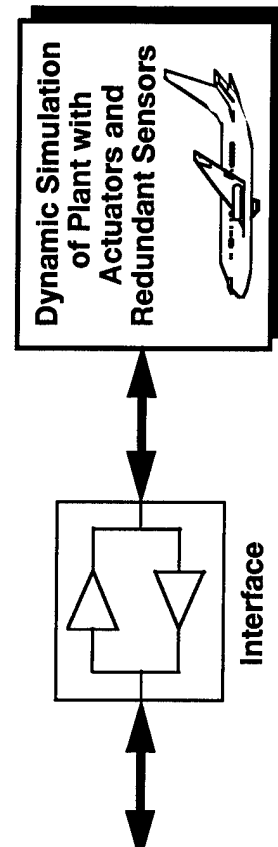
EME Assessment Approach

- EME Test Facility
 - EM Field Modeling to Obtain Internal Environment to which Equipment will be Exposed
- EM Field Modeling

• EME Test Facility



• Closed-Loop Test Capability



EM Test Chamber

• Real-Time Function Monitoring

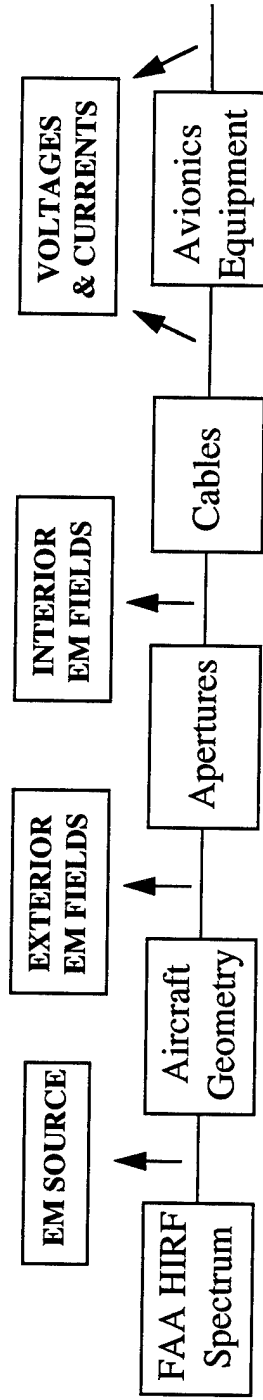


- Closed-Loop Test Capability
- Real-Time Function Monitoring



EM Field Modeling

- Develop EM Software Code Capability to Determine Internal EME Environment for Avionics Testing



- Validate the EM Code Using Empirical Data Obtained from B757 Ground Tests and Flight Tests



EM Field Modeling

Status and Accomplishments

- B757 Computer Model Complete
- B757 Ground Test Complete
 - Phillips Lab Large Electromagnetic System Level Illuminator (LESLI) facility selected for ground tests
 - » Low-level, non-ionizing electromagnetic radiation (300KHz-8GHz) with rhombic, monopole, dipole and horn antennas
- B757 Flight Test Complete
 - Voice of America Flight Tests
 - » Greenville, NC (~60 miles East of Raleigh)
 - » 26 MHz (500KW cw)
 - Wallops Flight Tests
 - » 430 MHz radar ASRF UHF (58 KW, 2microS, 1280 pps)
 - » 172 MHz (1 KW cw)
 - » 2730 MHz radar (optional) ASRF SPANDAR (135KW, 2 microS, 1280 pps)
 - » 5400 MHz radar (optional) FPS-16 Tracking radar (1MW, 1 microS, 640 pps)
- Data Analysis in Progress



Langley Research Center

EME Assessment Methodology

EME Test Facility

- Develop Methodology and Test Techniques for EM Environment Testing
 - Build a Facility that Could be Used as a National Resource
 - » Reverberation Chambers
 - » GTEM Cell
 - » High Frequency and High Power Capabilities



Langley Research Center

EME Assessment Methodology

EME Simulation Test Facility

Status and Accomplishments

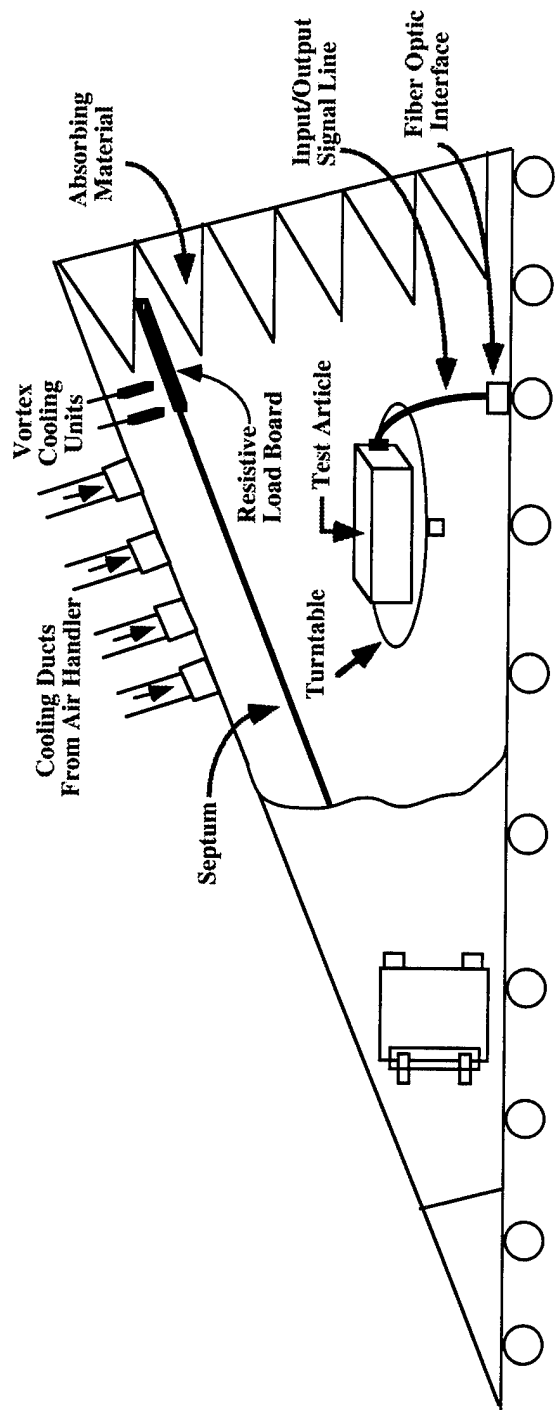
- Design & Construction Complete for Laboratory (EMA, NIST, NSWIC, LaRC)
 - GTEM Cell
 - » Frequency Range of 10 kHz to 4 GHz (18 GHz Planned)
 - » High-Power Excitation Needed for High-Power Field Level
 - » Need to Rotate Equipment Under Test
 - » Well-Understood Field Pattern Analysis Methods
 - 3 Reverberation Chambers
 - » Frequency Range of 10 kHz to 4 GHz (18 GHz Planned)
 - » Resonance Can Produce High-Power Field Levels with Lower Power Excitation
 - » No Need to Rotate Equipment Under Test
 - » Field Pattern Analysis Methods Must be Developed
- Chambers to be NIST Certified by 7/96



Langley Research Center

EME Assessment Methodology

GTEM Cell



- Specifications

- Frequency Range: 10 kHz - 18 GHz
- Test Volume: 1 cu. m.
- 80 dB Shielding



Langley Research Center

EME Assessment Methodology

Reverberation Chambers

Reverberation Chamber A

47ft. x 23ft. x 9.5 ft.
60 modes @ 87 MHz
860 V/m @ 1 GHz

Reverberation Chamber B	Amplifier Room 18 ft. x 24 ft. x 10 ft.	Control Room 18 ft. x 24 ft. x 10 ft.
	Reverberation Chamber C 8.92ft. x 7ft. x 9.5 ft. 60 modes @ 238 MHz 2460 V/m @ 1 GHz	



Langley Research Center

EME Assessment Methodology

Closed-Loop Test Capability

- Develop Test Methodology and Techniques to Enable Closed-Loop Dynamics Over Entire Flight Profile to be Represented During Testing
 - Enclose Equipment Under Test (EUT) Inside Test Chamber
 - Interface EUT to Computer Simulation of Plant Outside Test Chamber
 - Demonstrate on Actual Flight System
 - » Flight Control Computer
 - » Specific Phase of Flight Envelope



Closed-Loop Test Capability

Status and Accomplishments

- Demonstration on Flight Control Computer Near^{ing} Completion (FCC)
 - Quad-Redundant Military FCC (Allied Signal Bendix)
 - » B737 Autoland Control Laws Complete
 - » 1553 Data Bus Drivers In Progress
 - Computer Simulation of Aircraft and Atmosphere
 - » B737 Aircraft, Engines, Sensors, Actuators Complete
 - » Dryden Wind Gust and Turbulence Models Complete
 - Electrical Isolation Achieved via Fiber Optic Interface
 - » Design and Fabrication Complete
 - » EME Susceptibility Testing In Progress
- Contract for Advanced Commercial Flight Control Computer (Honeywell, Phoenix)



Langley Research Center

EME Assessment Methodology

Real-Time Function Monitoring

- Develop Methodology and Techniques for Real-Time Upset Assessment of EUT During Tests to Reduce Post Test Data Processing
 - Sub-System Level Monitoring
 - » Control Law Calculation Errors
 - » Redundancy Management Errors
 - » Input/Output Rate and Range Check Errors
 - Demonstrate on Real Flight System
 - » Quad Redundant Military Flight Control Computer
 - » Landing Phase of Flight Envelope



Langley Research Center

EME Assessment Methodology

Real-Time Function Monitoring *Status and Accomplishments*

- Design of Algorithms Complete for Detecting Malfunctions in Control Law Calculations of a Quad-Redundant Computer
 - Simulation of Detector for Quad-Redundant B737 Longitudinal Autoland in Heavy Clear-Air Turbulence Complete
 - Published as Ph.D. Dissertation (Drexel University)
- Implementation of Algorithms in the Laboratory for Application to the Bendix Quad Flight Control Computer In Progress
 - Applicability to Fault Tolerance Techniques to be Determined (Honeywell, Phoenix)



Simulation Example

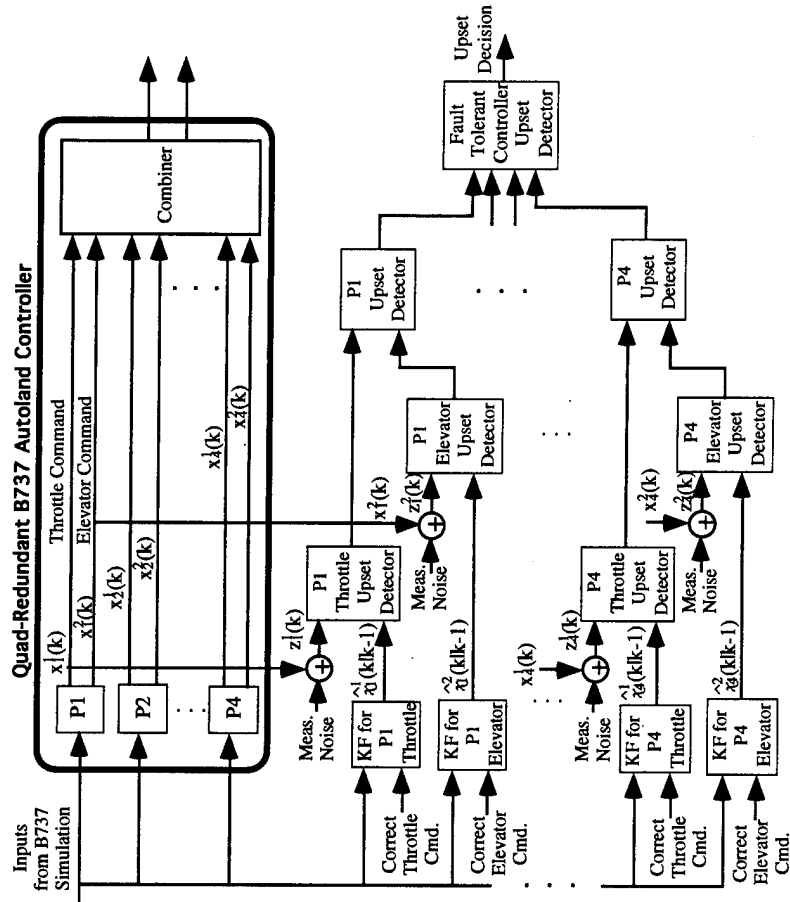
Upset Detection in a Quad-Redundant B737 Autoland Controller

- Longitudinal Control System
 - Throttle Command (Engine Thrust)
 - Elevator Command (Pitch Attitude)
- Heavy Clear Air Turbulence
 - 20 knot winds
 - 6 ft/s gusts
- Glide-Slope Engaged until Flare
 - 50 ms control cycle
 - Divided into 9 Segments for Modeling
- Control Law Calculation Models are Assumed to be Identical for All of the Processors



Simulation Example (cont)

- Conceptual Diagram



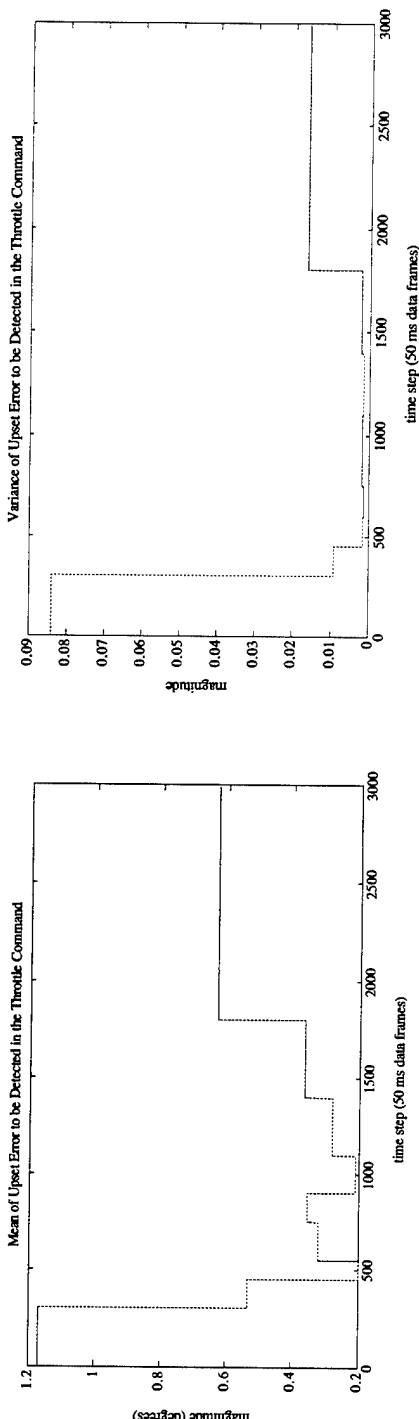


Langley Research Center

EME Assessment Methodology

Simulation Example (cont)

- **Mean and Variance of Upset Error to be Detected in the Throttle Command Calculation**



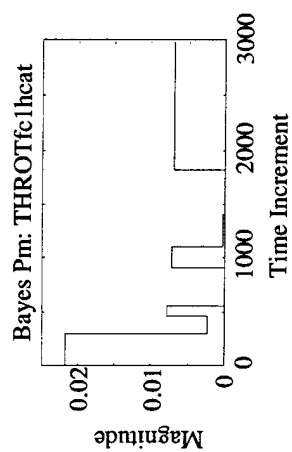
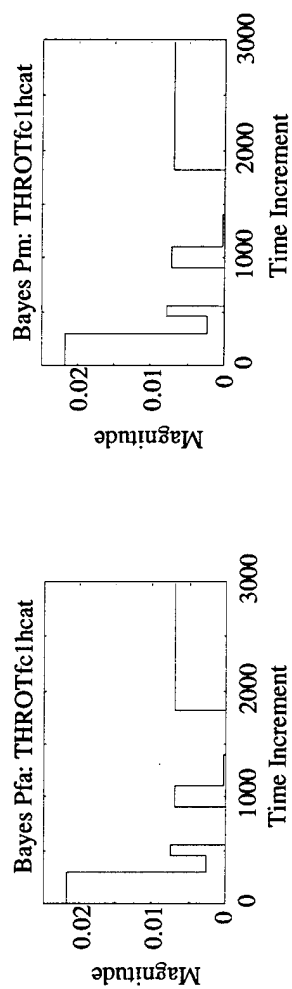
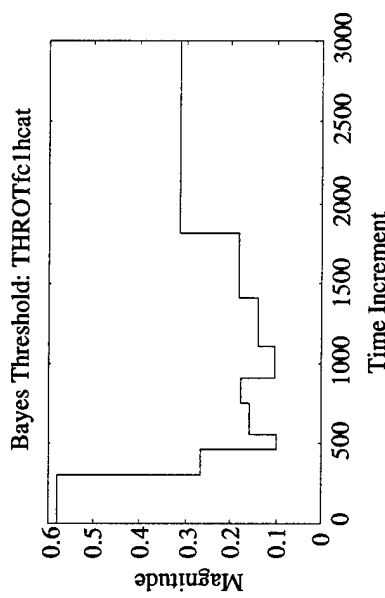


Langley Research Center

EME Assessment Methodology

Simulation Example (cont)

- Throttle Command Calculation Upset Detector (Bayes)



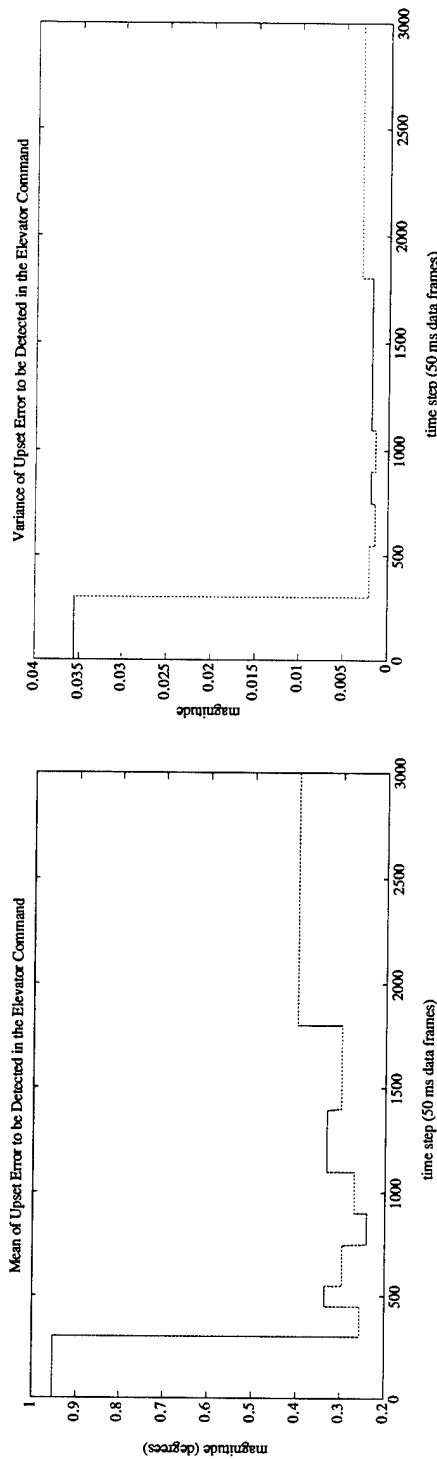
Langley Research Center



EME Assessment Methodology

Simulation Example (cont)

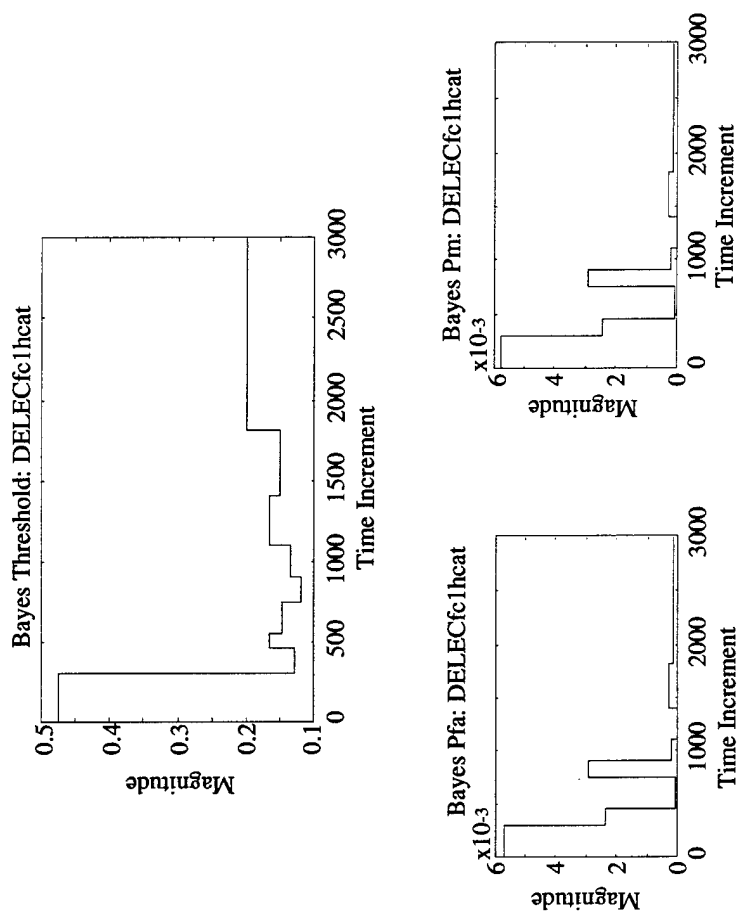
- **Mean and Variance of Upset Error to be Detected in the Elevator Command Calculation**





Simulation Example (cont)

- Elevator Command Calculation Upset Detector (Bayes)



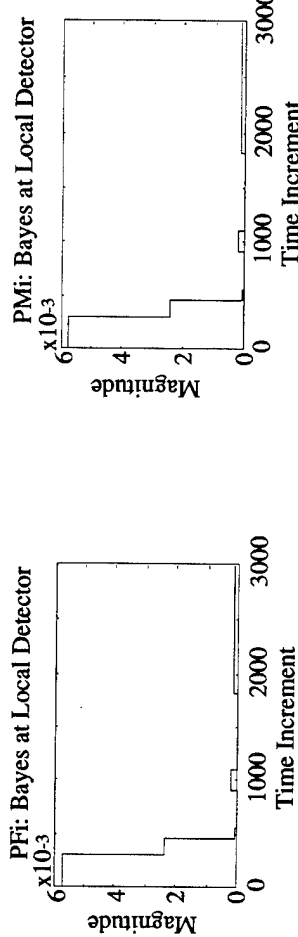


Langley Research Center

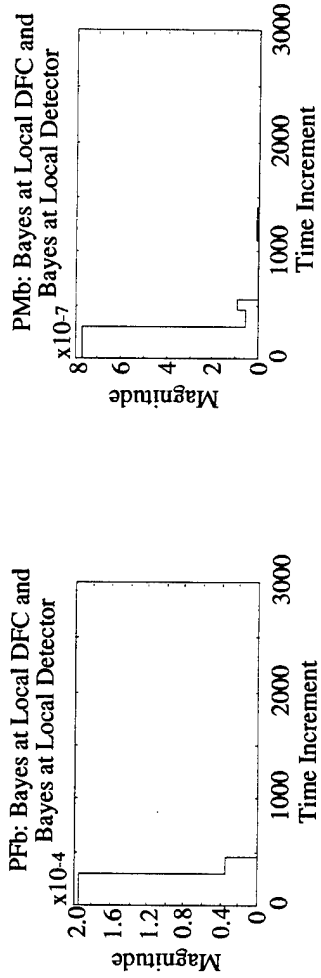
EME Assessment Methodology

Simulation Example (cont)

- Processor Upset Detector (Bayes)



- Fault Tolerant Controller Upset Detector (Bayes)





Langley Research Center

EME Assessment Methodology

Summary and Conclusions

- Described Methodology for Comprehensive EME Assessment for Critical Systems
 - EM Field Modeling
 - EME Test Facility
 - Closed-Loop Test Capability
 - Real-Time Function Monitoring
- Technology Could Potentially Reduce Cost of EME Certification Demonstration
 - Reduce Amount of Full-Aircraft Testing Required to Demonstrate Compliance



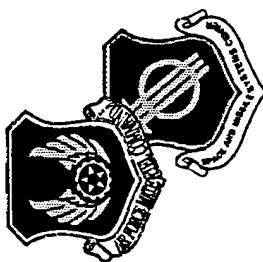


**DR. JANE LEHR
PHILLIPS LABORATORY**





EM EVALUATION OF LARGE AIRCRAFT



LARGE ARCFET CAVITY PUMPING & COMMERCIAL GPS SUSCEPTIBILITY EVALUATION

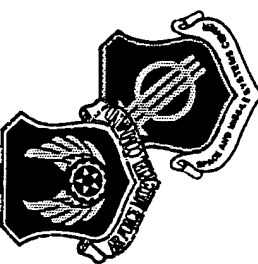
PRESENTED TO

REVERBERATION AND ANECHOIC CHAMBER
OPERATORS GROUP

BRIEFER
DR. JANE M. LEHR

PHILLIPS LABORATORY
ELECTROMAGNETIC EFFECTS DIVISION PL/WSM
5-7 DECEMBER 1995

(6 POINT) BRIEFING TITLE 1 11/3/96

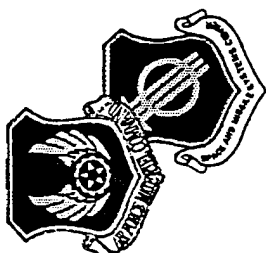


OVERVIEW

- EXPERIMENTAL OBJECTIVES
- EXPERIMENTAL APPROACH
- EMPTAC GEOMETRY
- COUPLING SENSORS
- CAVITY Q
- FIELD UNIFORMITY
- COMPARISONS OF EXPERIMENTAL RESULTS
- EXPERIMENTAL SET- UP FOR GPS VULNERABILITY ASSESSMENT
- GARMIN-150 SUSCEPTIBILITIES



EXPERIMENTAL OBJECTIVES



- Investigate feasibility of subsystem testing using pumping of arctf cavity and noise modulated frequency stirring.
- Perform functionality tests of commercial GPS RxS using frequency stirring

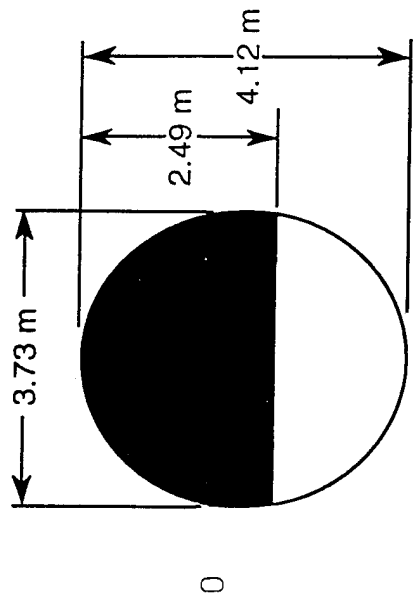


EXPERIMENTAL APPROACH

- **LARGE AIRCRAFT**
 - Determine cavity Q.
 - illuminate exterior with monochromatic fields and measure coupling to various subsystems test points.
 - Measure coupling to same test points under noise-modulated cavity pumping.
 - Measure coupling with noise-modulated external illumination for intermediate comparison
 - Average monochromatic data over noise BW for comparison with noise-modulated data.
- **GPS VULNERABILITY ASSESSMENT**
 - Determine EM susceptibilities of GPS Garmin-150 and Apollo Units

EMPTAC GEOMETRY

- Cross section of EMPTAC fuselage is shown at right – shaded area is cavity used in experiment.
- Also shown is outline of one of fifteen windows, which form a major loss mechanism for cavity above resonance frequency of about 300 MHz.
- Length of cavity is 17.6 m. Volume is 131 m³ and wall area is 216 m².

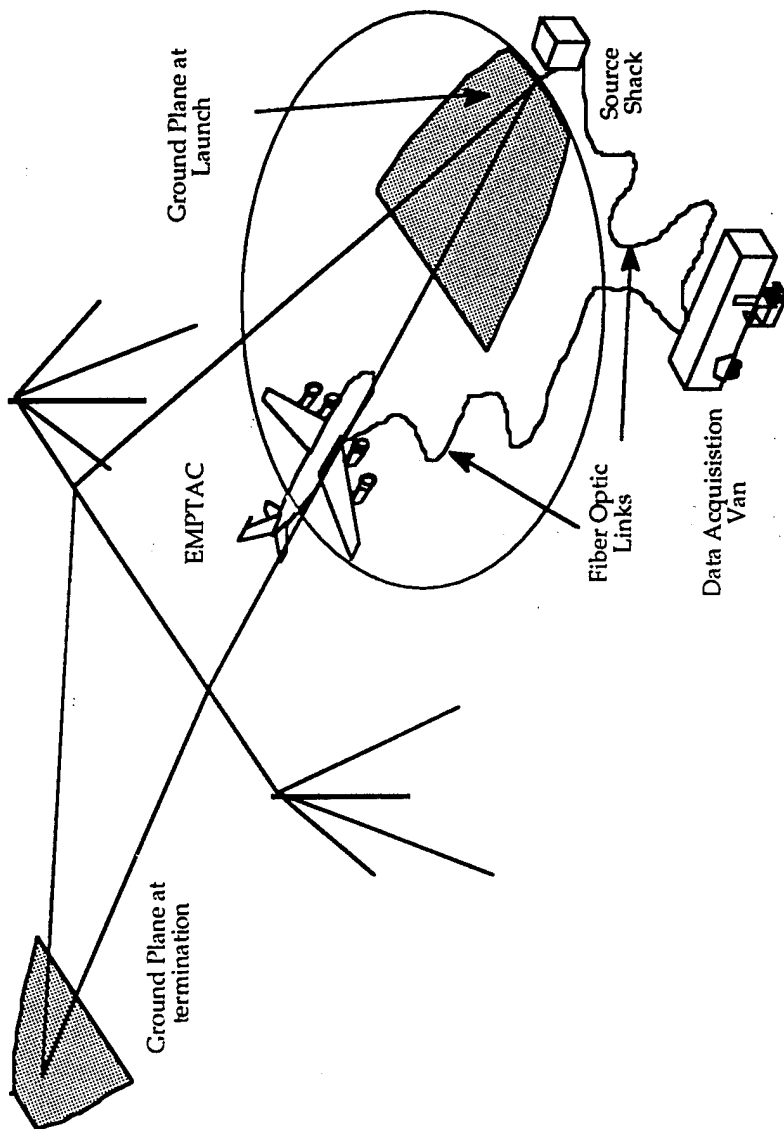


COUPLING SENSORS

- External surface field
- Internal surface and free field
- Wire and cable currents
- Voltage probes in Flight Control Computer
- Two GPS units
 - Antenna ports
 - Voltage probe
 - External and internal field probes



The Rhombic Antenna at the LESLI Facility

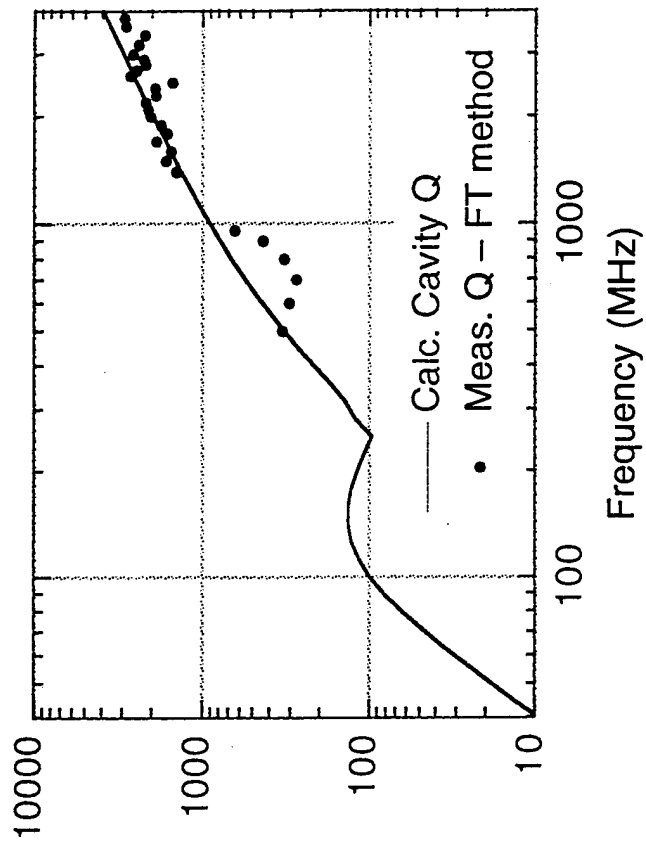


CAVITY Q

- It is desired that Q be high enough to establish relatively uniform, high-amplitude fields in the cavity. Values of several hundred to several thousand should be sufficient.
- Q was calculated using volume given on earlier slide and various loss mechanisms.
 - Principal loss mechanisms were long cables at low frequencies and cabin windows at high frequencies.
 - Losses to walls, dielectrics, and slot apertures were also included.
 - Results are shown on next slide.

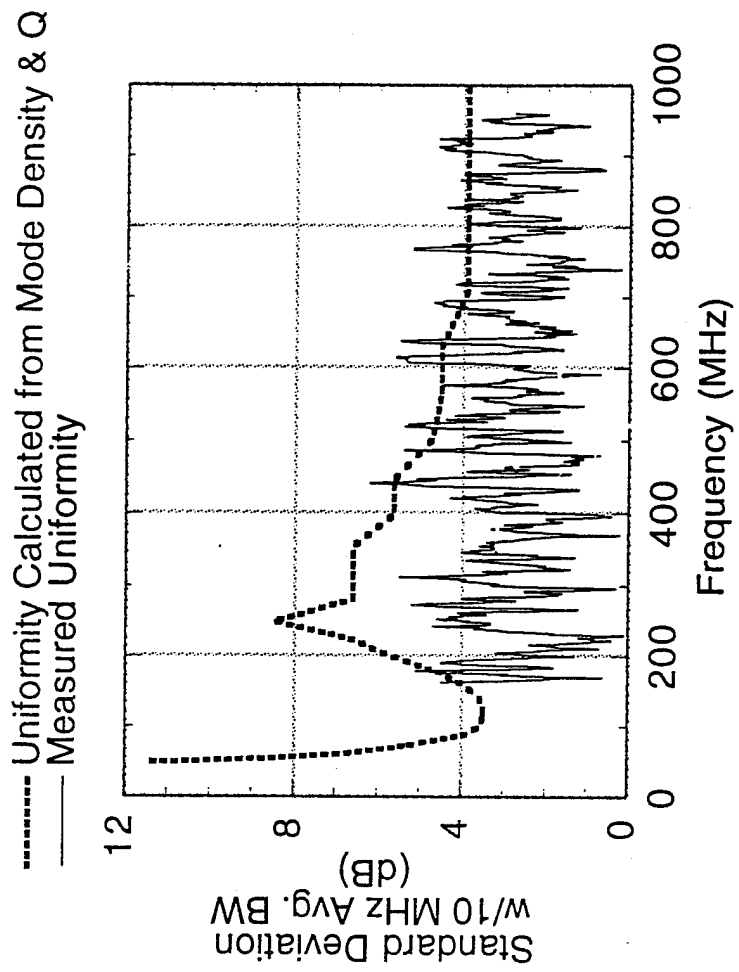
CAVITY Q, cont'd.

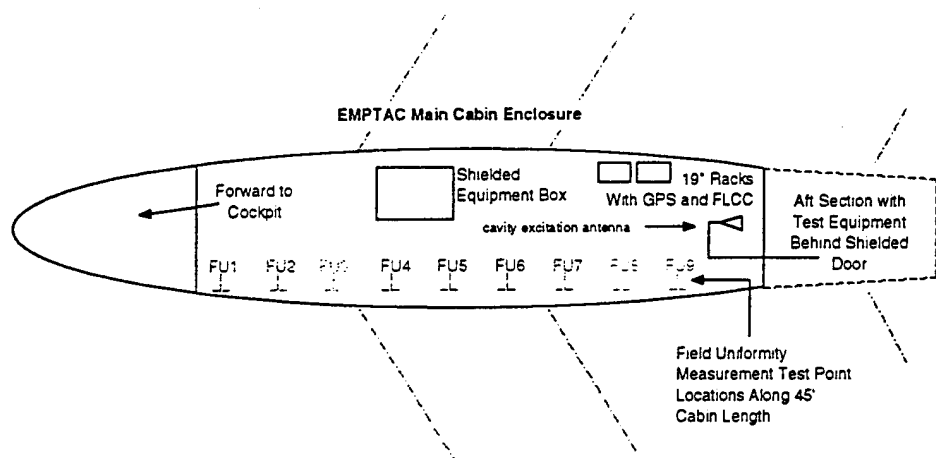
- The Q, calculated as described in the previous slide, is shown by the solid line.
- The Q was measured by observing the fall time of fields in the cavity. These results are shown by the dots.



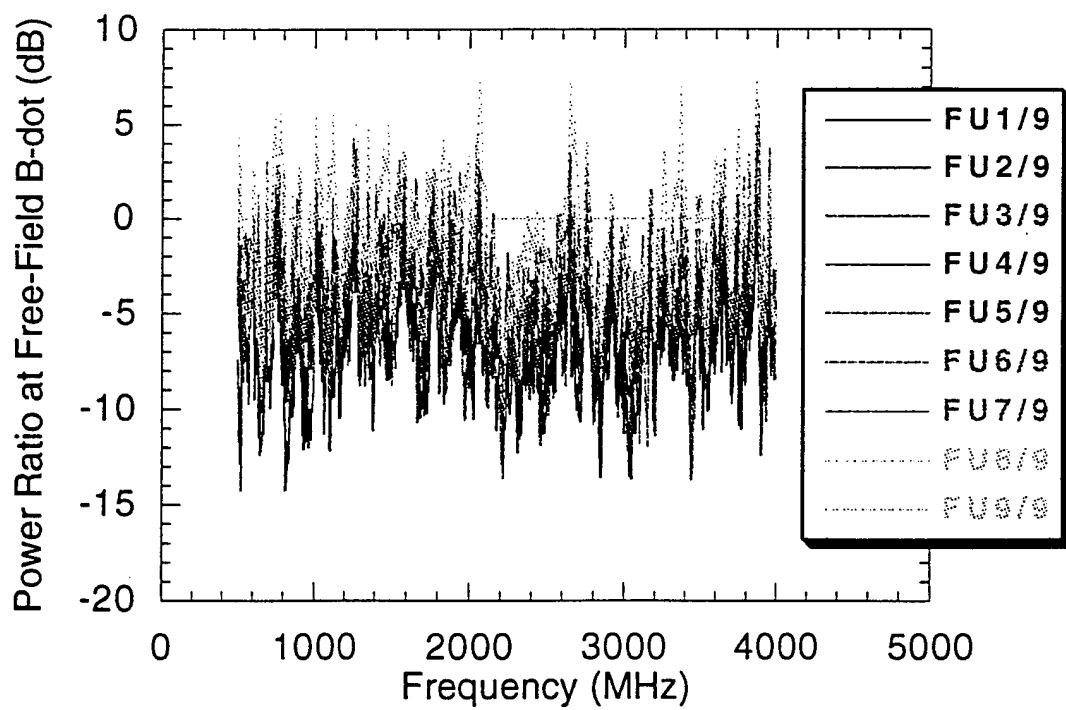
FIELD UNIFORMITY

- The uniformity was calculated from the predicted Q , the theoretical mode density for the EMPTAC cavity, and the uniformity for a high Q (mode broadening $<$ mode spacing) cavity.
- The uniformity was also obtained from measurements of the cavity field at different locations. The data were averaged over a 10 MHz window and the standard deviation taken of the averaged values in different locations.



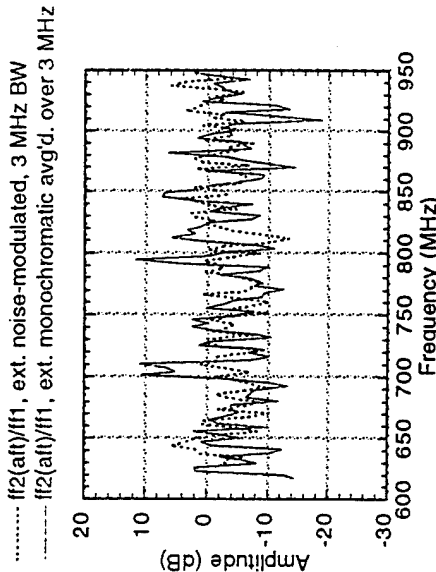
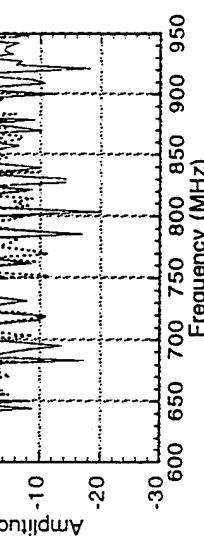
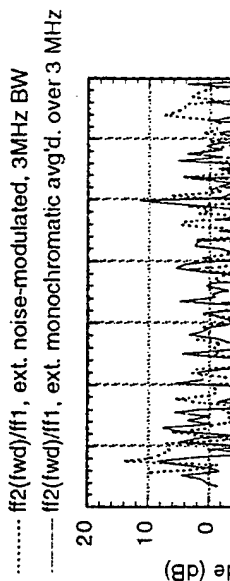


**EMPTAC Field Uniformity Data;
Power Measurements Relative to Position 9**



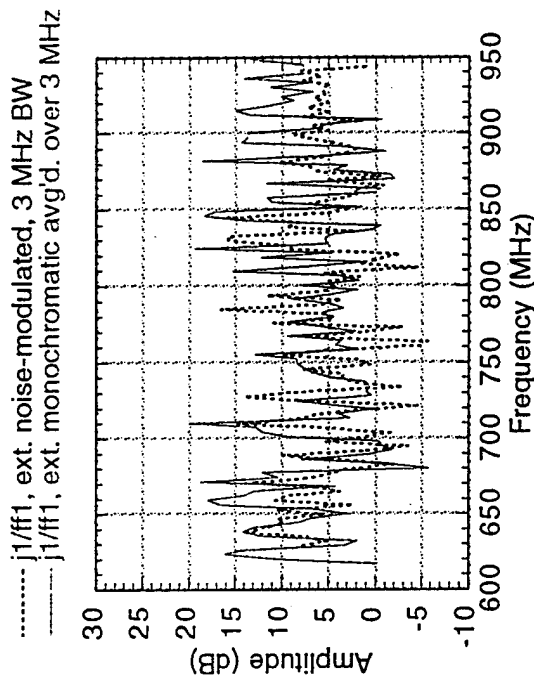
COMPARISONS – INTERNAL FIELD

- Comparisons of the field measurements at the forward and aft areas of the cavity (normalized to the field sensor in the center of the cavity) are shown at the right.
 - Noise modulation was over a 3 MHz bandwidth.
 - Monochromatic data were numerically averaged over 3 MHz.
 - Comparison is good; indicates no change in field structure with noise modulation.
 - Noise data has smaller peak-to-null range than averaged monochromatic data; may indicate averaging process not fully understood.



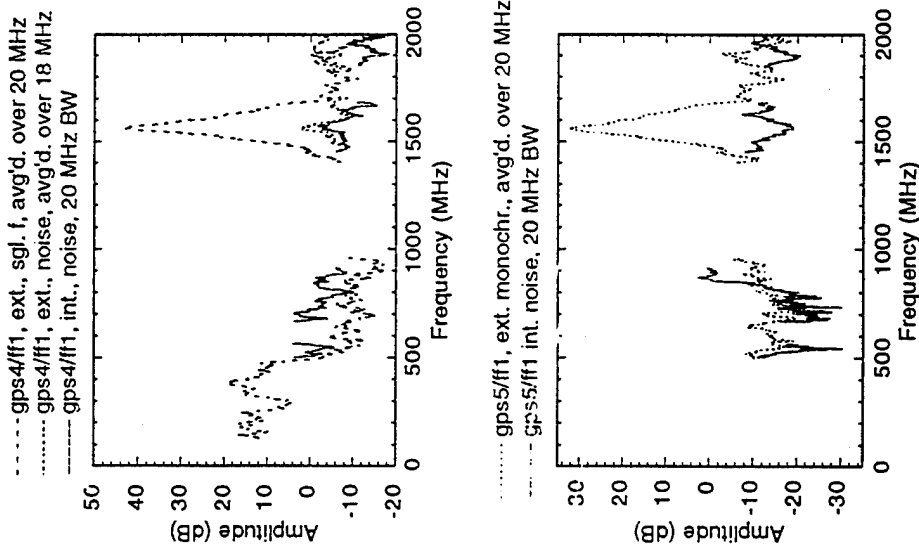
COMPARISONS -INTERNAL FIELDS, cont'd.

- Comparison of internal surface field under external monochromatic and noise-modulated illumination



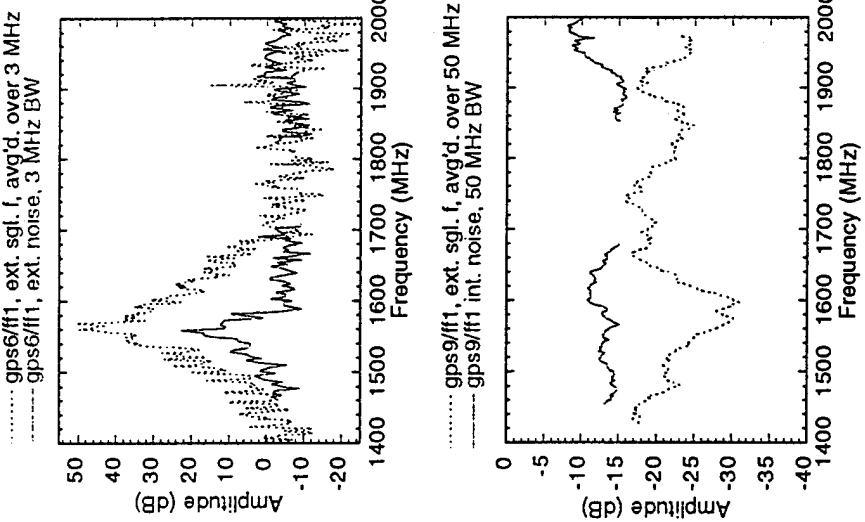
COMPARISONS – GPS ANTENNA LINE

- The forward (gps4) and reverse (gps5) signals coupled on the antenna line of one of the GPS units are shown at right.
- The coupling for external monochromatic illumination, external noise-modulated illumination, and internal noise-modulated cavity pumping compare well outside the GPS operating band.
- The in-band data compare poorly between the monochromatic and noise-modulated cases. Either the coupling is very different, or the antenna became disconnected in the course of the experiment.



COMPARISONS – GPS ANTENNA PORT

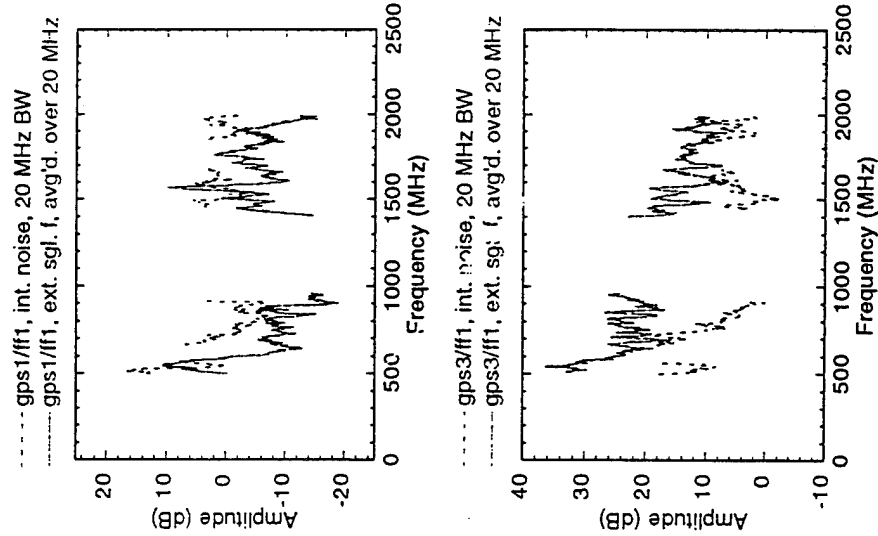
- The output of the antenna line, disconnected from the GPS port, is shown at right for external monochromatic and noise-modulated illumination. Again, either the coupling is different, or the antenna connection was poor in the noise-modulated case.



- The coupling to the GPS antenna port with the antenna disconnected is shown at right. The comparison is fair to poor.

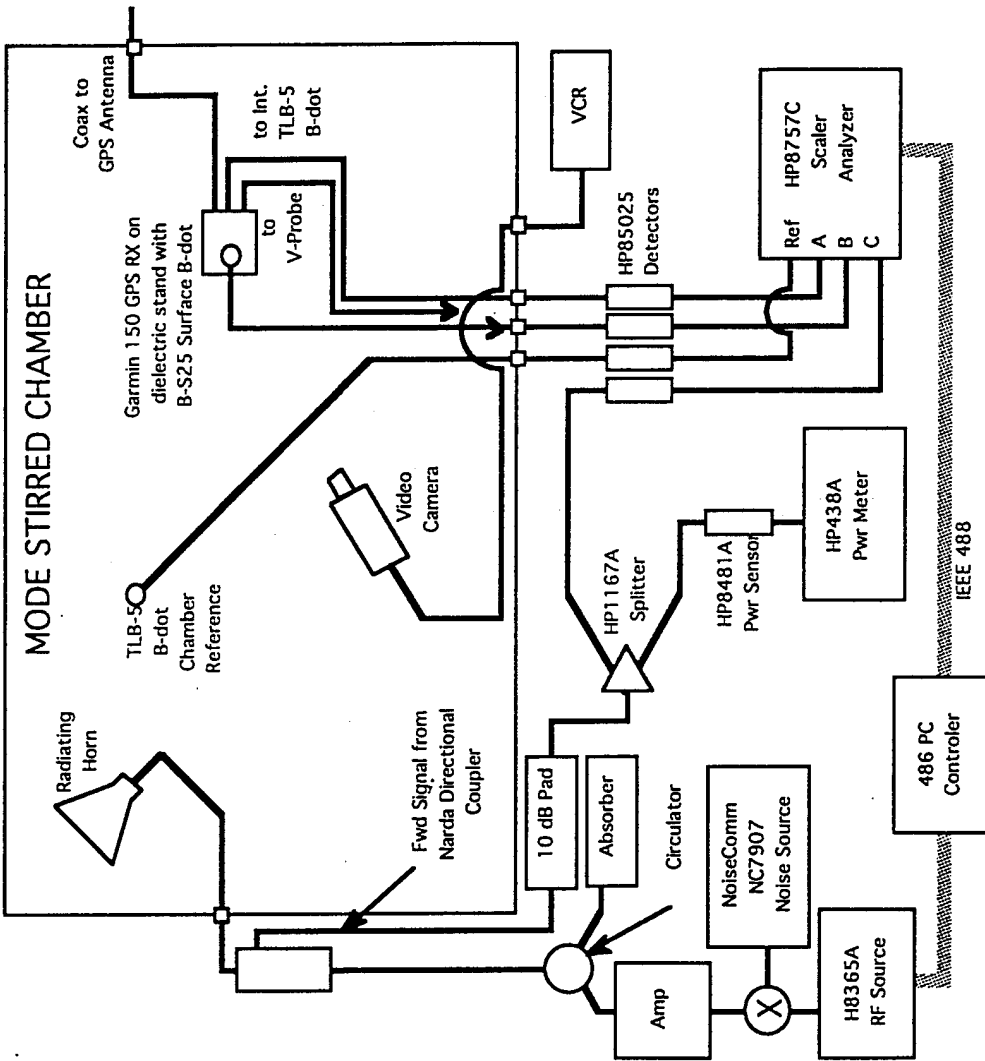
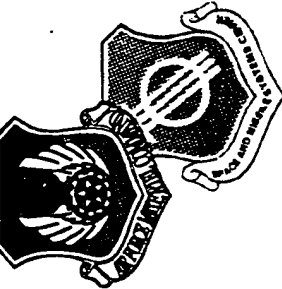
COMPARISONS – OTHER GPS TEST POINTS

- In the plot at right, good agreement is seen between external monochromatic and internal noise-modulated coupling to a field sensor inside one of the GPS units.

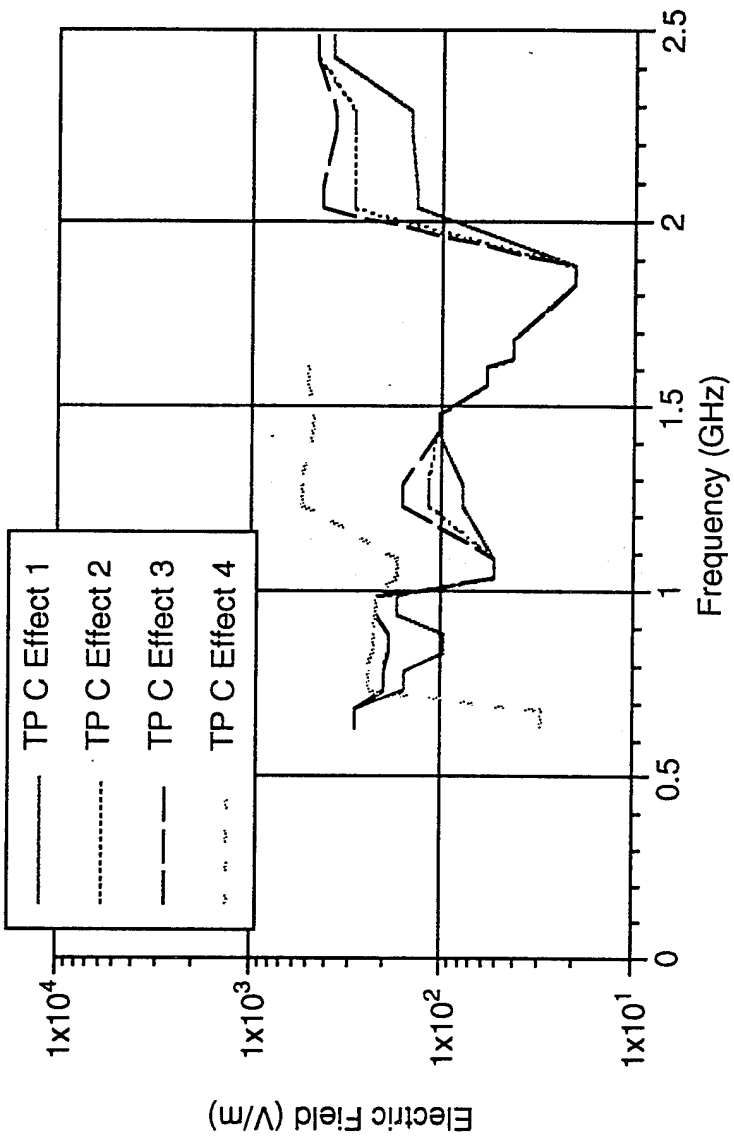


- A voltage probe inside one of the GPS units shows fair agreement between external monochromatic and internal noise-modulated coupling in the plot at right.

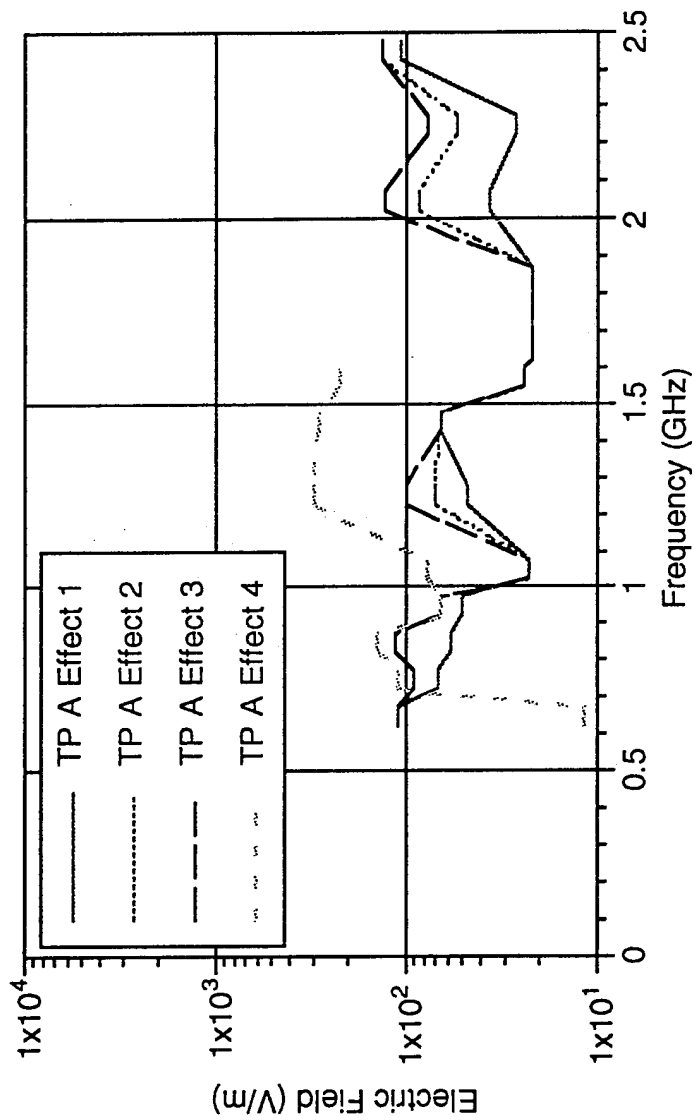
The Mode-Stirred Chamber Layout



Electric Field at GPS Receiver for Effects

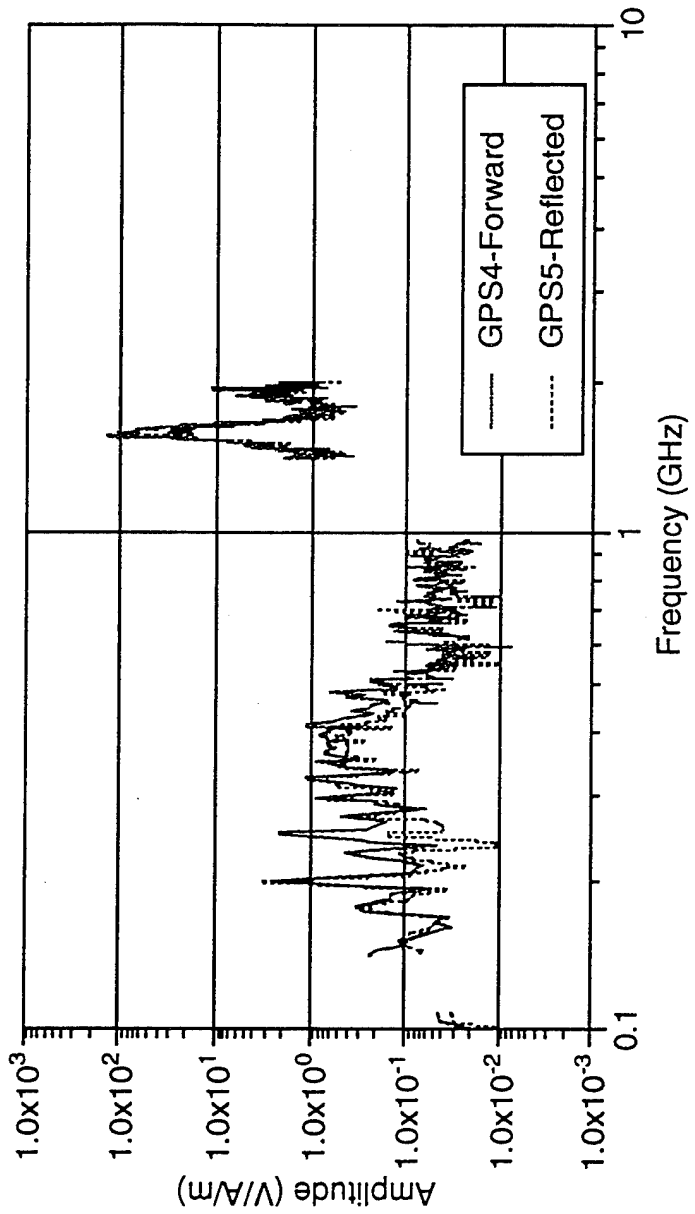


Electric Field Inside GPS for Effects



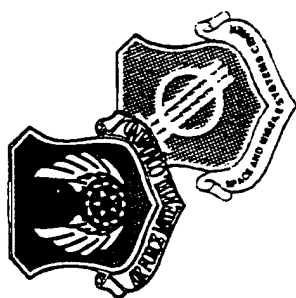
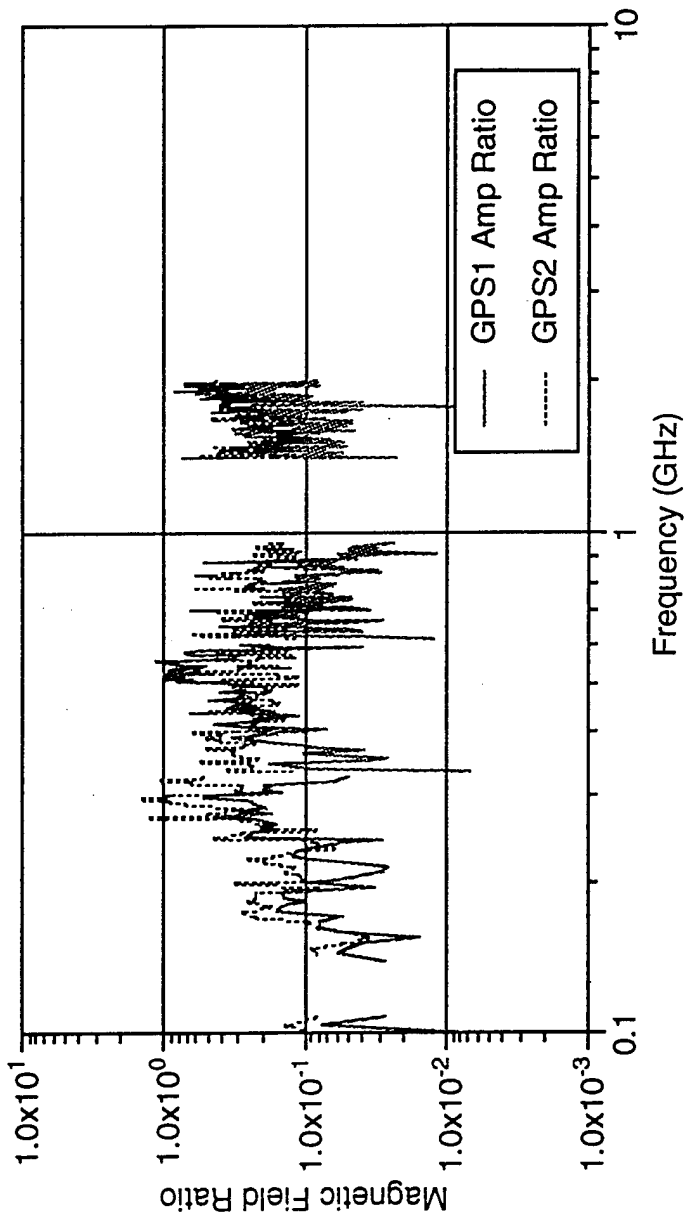


Normalized GPS Forward (GPS4) and Reflected (GPS5) Voltages

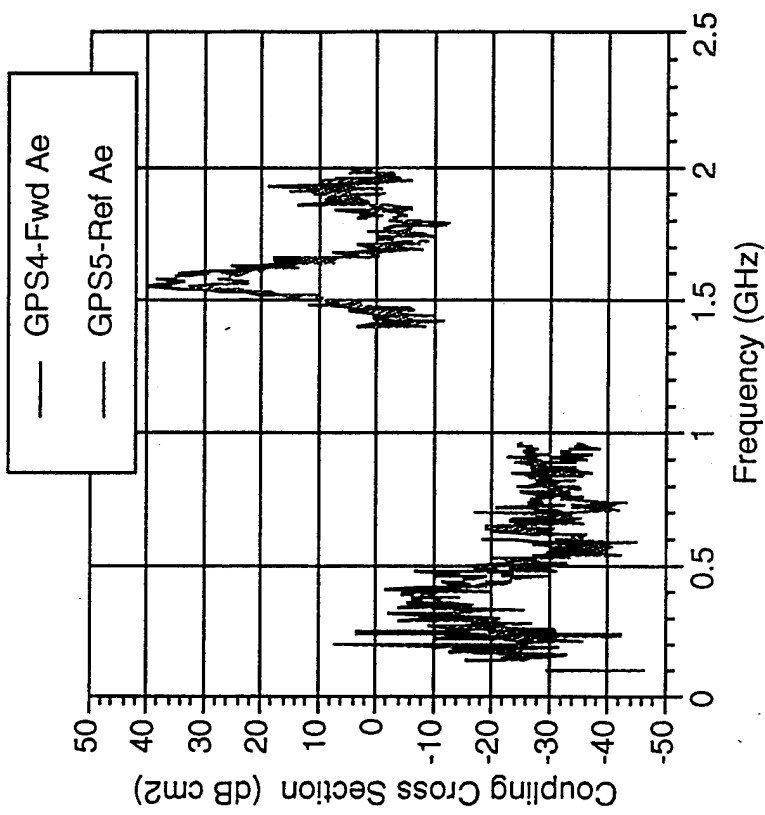




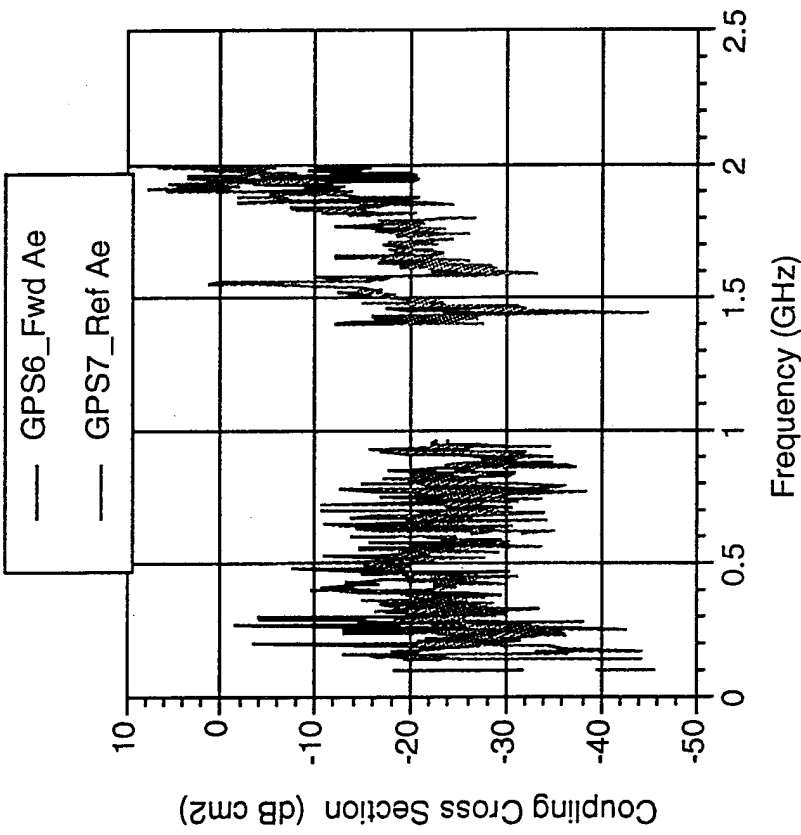
Normalized GPS Receiver Magnetic Field Ratios Inside (GPS1) and Outside (GPS2) the Receiver



Normalized GPS Forward (GPS4) and
Reflected (GPS5) Cross Sections
(Garmin)

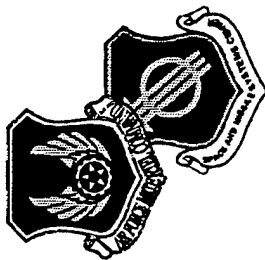


Normalized GPS Forward (GPS6) and
Reflected (GPS7) Cross Sections
(Apollo)





CONCLUSIONS



- Aircraft hull shielding was determined to be 20 dB.
- EMPTAC Cargo cavity does not provide the lossless medium for optimal mode stir chamber.
- Field uniformity for both external and internal illumination was determined.
- Comparison of measured coupling under several configurations were achieved.
- Good agreement among measurements were obtained.
- GPS Garmin-150 susceptible at in-band and out-of-band frequencies.
- Encouraging results for performing effects and EMI/EMC experiments using the Aircraft as a reverberation chamber.





**DR. MAQSOOD MOHD
SVERDRUP TECHNOLOGY**



GPS RCVR Testing Using GPS Simulator in an Anechoic Chamber

By:

**Maqsood A. Mohd, PhD, NCE, Sverdrup Technology
Charles Steadman and Carolyn Coleman, 46TW/TSWW
Eglin AFB, FL 32542**

**5 December, Tuesday, 1995
Reverberation and Anechoic Chamber Operators
Group Meeting, NSWCDD, Dahlgren, VA**

Outline

- What is GPS?
- Why Simulate GPS?
- How to Simulate GPS?
- Details of GPS Testing
- Summary

What is GPS?

- GPS is Global Positioning System
- GPS uses satellites and computers
- Position is computed based on distance from satellites
- Four measurements are needed for exact position
- Distance depends on satellite accuracy (atomic clocks)
- Position calculations require precise location of satellites

What is GPS? (cont.)

- GPS satellite orbits are predictable
- GPS satellites transmit pseudo random code for timing and data message
- Data message includes orbit location, system health and errors
- GPS errors due to ionospheric and atmospheric delays
- Satellite clocks, multipath, receiver clock errors

What is GPS? (cont.)

- Satellite configuration introduce errors
- The PN code matches satellite signal to the receiver signal unambiguously
- The PN code allows one frequency usage by all satellites
- The PN code makes it possible the use of low power signal receiver, and small antennas
- Differential GPS concept eliminates almost all standard errors

Why Simulate GPS?

- GPS simulation has inherently all the advantages of any modeling and simulation
- To test and evaluate the GPS receiver performance
- Control parameters, satellite positions, and configurations

Why Simulate GPS? (cont.)

- Test under past, present, or future Almanac
- Test for any location (Lat., Long. Altitude)
- Test for different power levels
- Ability to introduce interfering signals
- Ability to introduce jamming signals

How to Simulate GPS?

Parameters to be considered:

- Low Dynamics
- High Dynamics
- Accuracy (RMS over 1 minute), Pseudo Range, Pseudo Range Rate, and Delta-Pseudo Range
- Clock Stability
- Output Power at L₁ and L₂

How to Simulate GPS?

Parameters to be considered (cont.):

- C/A and P Code
- Spurious and Harmonic Content
- Power, Size, Weight, Form-Factor, Number of Channels
- Built-in-Test
- Differential Capability

Details of GPS Testing

Simulator Test Objectives:

1. Establish the basic performance of the GPS simulator

Power output at L₁ and L₂

What scenarios can be generated?

so that the RCVR under test can be exercised thoroughly

2. Accurately quantify GPS power levels at each location inside the chamber at L₁ and L₂
3. Quantitatively determine the interference signal levels at various locations inside the chamber

Details of GPS Testing (Cont.)

RCVR Test Objectives:

1. Exercise the RCVR thoroughly at a known surveyed point
2. Exercise the RCVR thoroughly inside the anechoic chamber with pristine GPS signal environment.
Determine the RCVR performance quantitatively
3. Repeat step 2 with known interfering signals inside the chamber

Basic Performance of the Simulator

- Pure tone at L_1 , injected into the transmission line
- The gain of the patch antenna determined
- Measurements on top of the ceiling and inside the chamber
- Problems on top of the ceiling
- Farfield measurements matched manufacturer data
- Polarization was also investigated
- Inside the chamber a healthy signal was registered on the spectrum analyzer

Basic Performance of the Simulator (cont.)

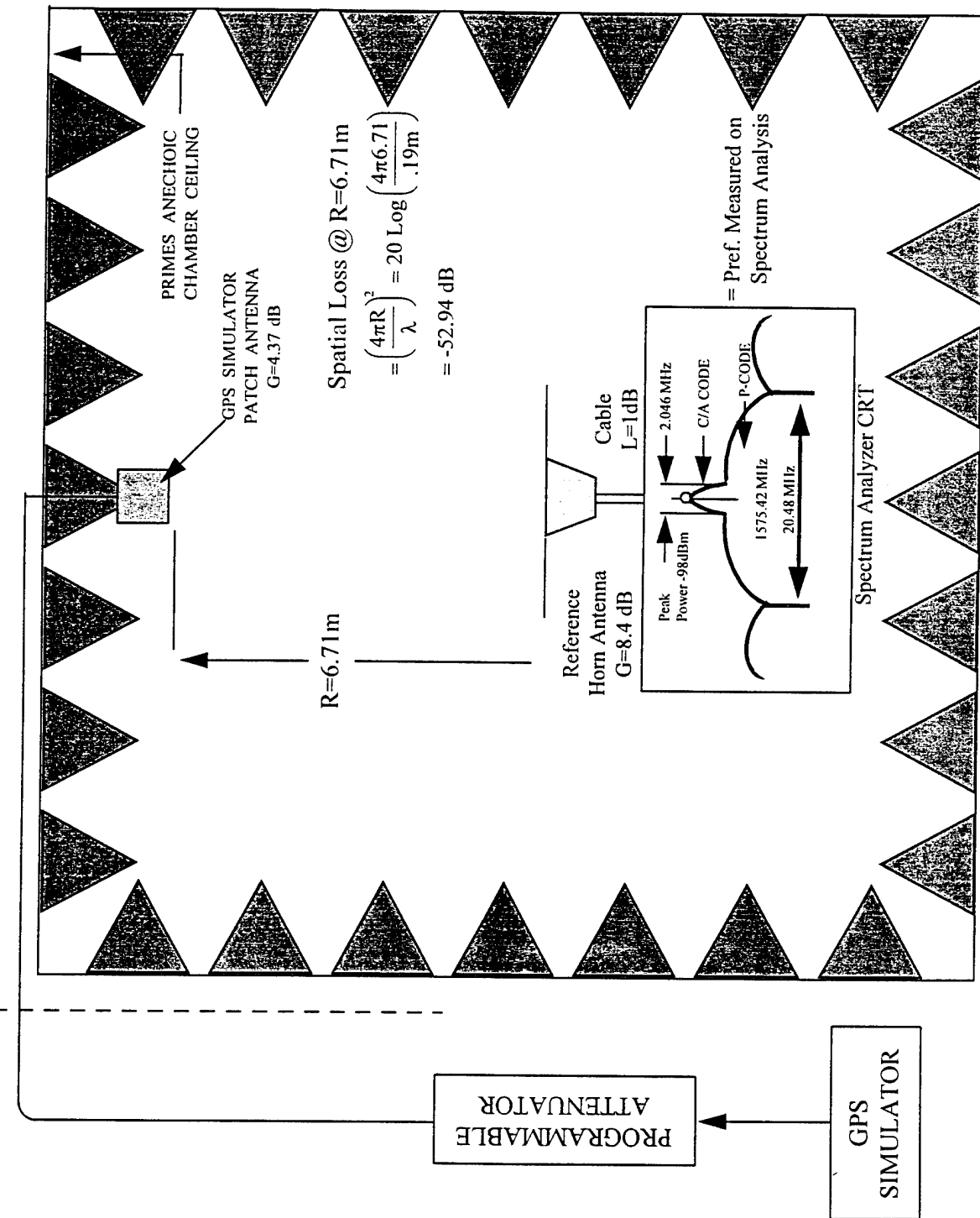
- Initiated the simulator
- Selected a scenario
- Downloaded the Almanac for a reference point
- Simulated a scenario based on the Almanac
- Scenario includes date and time
- Set up the RCVR inside the chamber

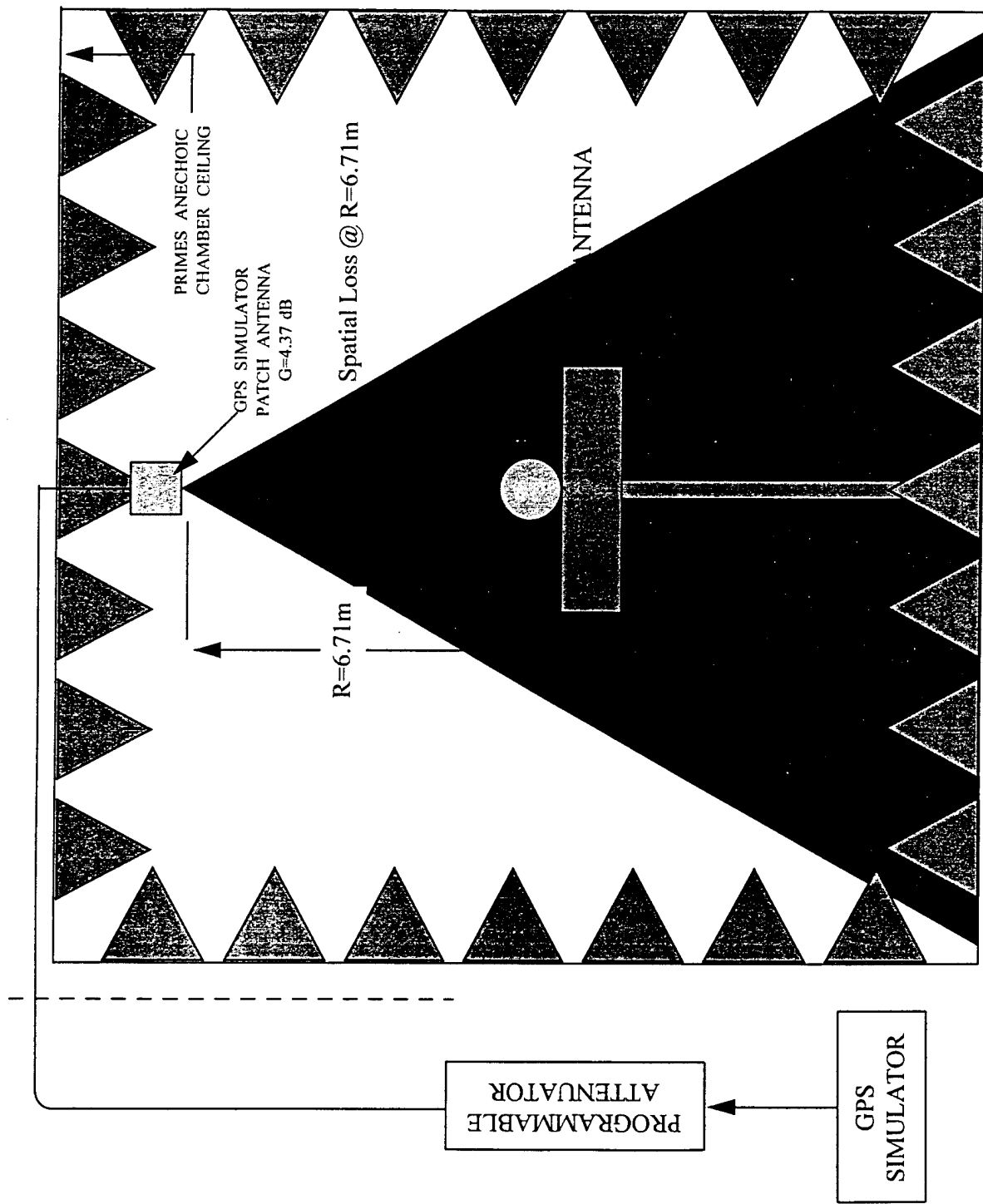
Basic Performance of the Simulator (cont.)

- Watch the performance of the RCVR
- Determine the acquisition time, the satellites used to converge to a solution, and time for the first solution
- Determine the performance for P/Y code and C/A code
- Determine the impact of interfering signals
- Simulator output power was varied

Basic Performance of the Simulator (cont.)

- With generic Spec-an equipment signal not measurable
- Interference source was activated
- Geometry (location and height) of the emitting antenna was varied
- Performance of the GPS RCVR was analyzed with the simulator operational





Summary

- GPS is ubiquitous in every geolocation application
 - Low power
 - Spreading modulation signals
- Significant learning experience
 - Simulation
 - Testing
- Follow-up efforts





**MR. HARRY GAUL
MOTOROLA**



EMC TEST PERFORMED ON AN EXPERIMENTAL ELECTRIC VEHICLE

Harry W. Gaul, Motorola 602-441-5321

Tom Huettl, Motorola 602-413-2518

Chuck Powers, Motorola 512-891-4594

Presented at the Reverberation Chamber and Anechoic Chamber Operators Group Meeting at the Naval Surface Warfare Center Dahlgren Division (NSWCDD), Dahlgren, Virginia, December 5-7, 1995.

ABSTRACT

Although this paper does not specifically address anechoic or reverberation chamber testing, the Electromagnetic Compatibility (EMC) tests performed on an experimental electric vehicle should prove extremely interesting to the EMC community. The experimental electric vehicle platform uses an electric converted 1993 Dodge Dakota pickup truck. The vehicle is powered by a Motorola designed ac controller which converts the DC power from twenty-four 12 VDC deep cycle lead acid batteries to three phase AC power. This vehicle is utilized as a semiconductor evaluation test vehicle with a particular emphasis on evaluating the performance of microprocessors in a harsh automotive environment. EMC tests were conducted which included radiated magnetic field and radiated electric field emissions from 9 kHz to 30 MHz. The radiated tests were performed in accordance with the Society of Automotive Engineers (SAE) Draft Standard J551/5. This draft standard specifically addresses the testing of electric vehicles for broadband radiated emissions. Additional tests were performed on the SAE J1850 multiplex communication bus to measure the induced voltage transients.

The test results presented in this paper are for an experimental electric vehicle which has minimal EMC design features and are not to be construed as representative of commercially available electric vehicles.

INTRODUCTION

The California Air Resources Board (CARB) has put into place a number of mandates to encourage use of zero emissions vehicles (ZEV). Indeed in 1998, CARB is requiring that 2% of all vehicles sold in California must be ZEV. This number climbs to 5% in the year 2001 and 10% in the year 2003. The development of electric vehicles presents the vehicle OEMs, their electronic components suppliers, and their semiconductor suppliers with a variety of opportunities for future vehicle designs. It also presents the system designers with an entirely new set of technological hurdles to be overcome, the most formidable of which is the susceptibility to large levels of electromagnetic interference (EMI) as produced by the high power switching electric motors. Using advanced power semiconductors these motors, connected to high voltage, high current battery packs, can have switching times as short as 100 ns.

The electromagnetic fields generated by this high current switching can affect any component in the vehicle, from the engine controller to optional features like an AM radio, CD player, or even critical systems, like ABS. These EMI issues must be overcome in order for electric vehicles to become a practical reality.

BACKGROUND

A cross functional research team was established by the Motorola Semiconductor Products Sector (SPS) to research emerging automotive technologies. One particularly promising technology was identified to be a serial multiplex communication network which would replace complex and costly wiring harnesses in vehicles. A serial multiplex communication network is created by connecting each module or system which must collect, calculate, exchange, or display data to a single serial communication bus.

In order to determine whether the serial communication technology currently available can operate in the EMI intensive environment of an electric vehicle, an SAE J1850 serial communication system was designed, installed, and tested in Motorola's electric vehicle research platform, a 1993 Dodge Dakota pickup truck which has been converted to electric power. The network was designed to be simple enough to be monitored easily but complex enough to ensure that any EMI related problems which might be encountered would quickly become evident. The SAE J1850 allows the use of a single wire bus at 10.7 kbps or a dual wire bus at 41.7 kbps. The 10.7 kbps single wire bus was installed in the electric vehicle platform. The dual wire bus would have been more tolerant of common mode EMI since it is a balanced system. However, the single wire bus was chosen in order to prove that a multiplex system would function in the EMI intensive environment.

A block diagram of the electric vehicle multiplex system is shown in Figure 1. The DC to AC inverter utilizes insulated gate bipolar transistors (IGBTs) which are controlled by using the centered pulse width modulated (PWM), vector control technique. The AC motor control node consists of an MC68HC705V8 connected via the serial peripheral interface (SPI) port to a Motorola MC68332 32-bit micro controller unit (MCU). The MC68332 performs the vector control algorithms which are used to drive the AC induction motor. Noise spikes are created as the IGBTs switch on and off at a rate of 8 kHz. These spikes are the by-product of the rising and falling edges of the IGBTs. The switching edge time is determined by the IGBT capability. In this case the turn on time is 200 ns and the turn off time is 500 ns.

These spikes radiate from the input DC wires and from the output AC wires and then couple onto other wires and components in the system. The radiated levels are so high that the AM radio has never functioned properly in this vehicle! Also, the unshielded J1850 bus wire was found to have common mode spikes induced at levels up to 20 volts!

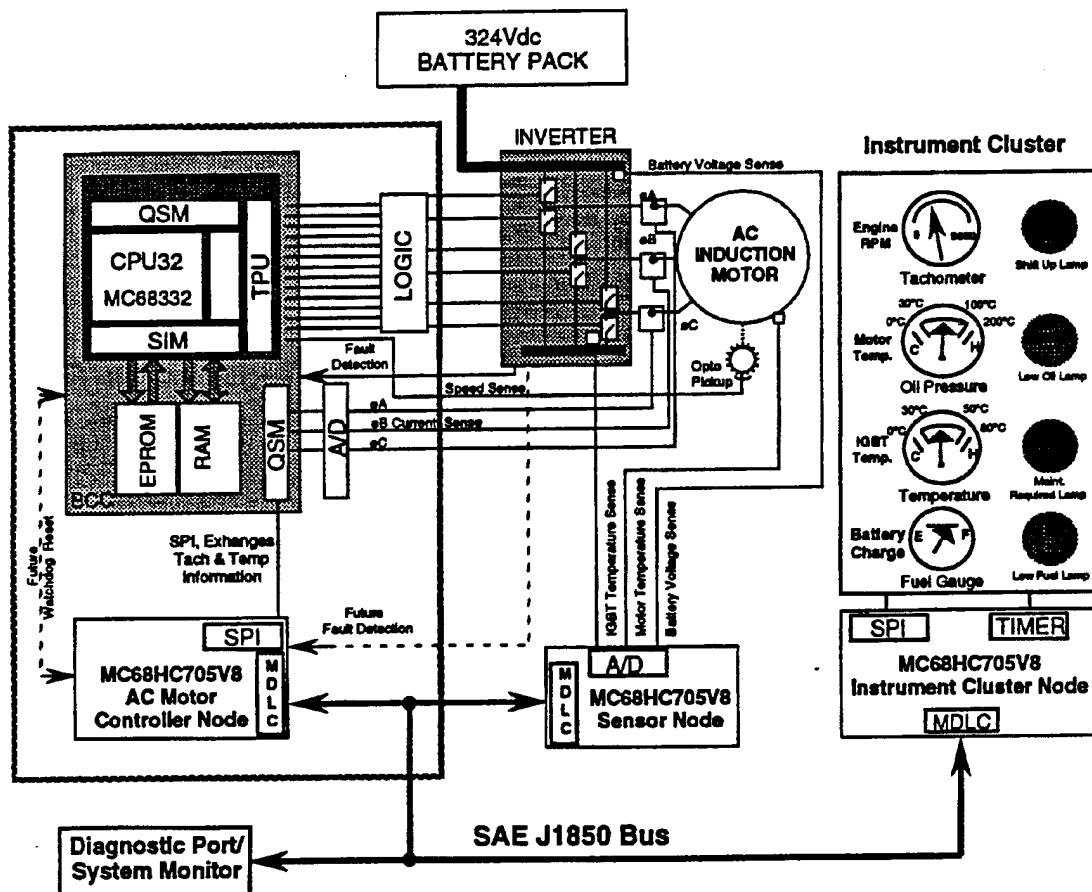


FIGURE 1 - BLOCK DIAGRAM OF THE ELECTRIC VEHICLE MULTIPLEX SYSTEM

Initially the MCU would not function properly due to these high level spikes. The network communication and MCU were able to function properly in the presence of these spikes after using a combination of the design and processing of the MCU, the use of digital filtering in the SAE J1850 communication modules, and the use of opto-isolation between the MCU and the sensing circuits. See Multiplex Reports and 1995 SAE FTTC Paper entitled "Using Existing Multiplex Communication Technology to Implement an Electric Vehicle Communication Network".²

EMC TEST FACILITY

The Motorola GSTG EMC/TEMPEST Facility in Scottsdale, Arizona was used to accurately measure the radiated and conducted EMI in the electric vehicle platform. This facility is accredited by the National Voluntary Laboratory Accreditation Program (NVLAP) as administered by the National Institute of Standards and Technology (NIST) formerly NBS. Within the EMC/TEMPEST Group are 10 EMC personnel who are Certified EMC Engineers and Technicians by the National Association of Radio and Telecommunications Engineers (NARTE).

The EMC tests were performed from May 9 through May 12, 1995. The test chamber used was a double wall, modular constructed, 16 gauge steel shield room manufactured by Rayproof Incorporated. The main chamber measured 9.8 m by 8.6 m by 3.4 m high. Two vestibule type chambers adjoin the main chamber and are used for the instrumentation. Each of the vestibules measured 4.3 m by 3.6 m by 3.4 m high. The floor of the shield room is an exposed steel floor. The main chamber has its first modal frequency at 23 MHz. Thus any radiated field levels measured at 23 MHz could be in error by perhaps \pm 20 dB due to the effects of standing waves. All other modal frequencies are above 30 MHz for the main chamber.

The EMC test instrumentation included a Tektronix TDS684A digital storage oscilloscope (DSO), two Tektronix P6245 active FET oscilloscope probes (1.5 GHz bandwidth), a Singer EMI receiver system, a Singer 94607-1 vertical rod antenna (1 meter), and an Electro Metrics ALP-70 loop antenna (60 cm diameter).

MULTIPLEXED SAE J1850 - CLASS B DATA COMMUNICATION NETWORK INTERFACE BUS

Voltage measurements were made on the multiplexed bus signal and ground lines at the point where they enter the sensor node. The measurements were made with a DSO utilizing various digital sampling rates in order to ascertain whether the DSO was being aliased by the voltage spikes (impulsive signals). The DSO was powered through an isolation transformer to prevent ground loops. The test vehicle was bonded to the shield room floor with a ground strap attached to the point where the return of the accessory 12 VDC battery is grounded to the vehicle chassis. The high voltage battery pack consists of twenty-four 12 VDC car batteries wired in series. The high voltage battery pack is isolated from chassis ground to meet safety regulations. The test vehicle was placed on jack stands in order to simulate the vehicle traveling at 25 mph.

Figure 2 shows a plot of the multiplexed data signal with respect to chassis ground (top trace). With no throttle the signal appears clean. The middle trace shows the multiplexed signal ground measured with respect to chassis ground. The bottom trace is the mathematical difference between the top and middle traces and it represents the differential signal between the data and its signal ground.

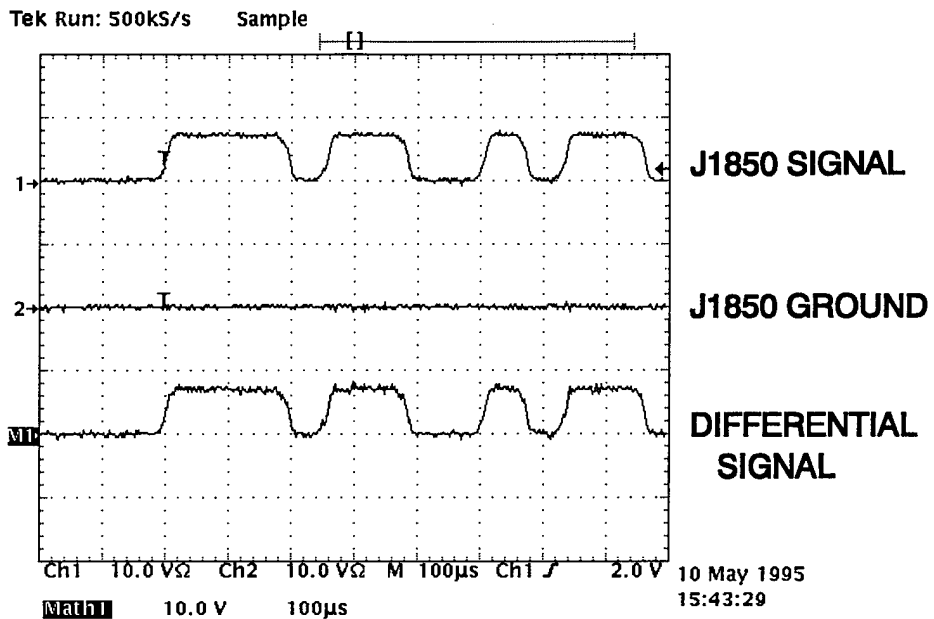


FIGURE 2 - SAE J1850 BUS WITH HIGH VOLTAGE TURNED OFF

Figure 3 is similar to the plot in Figure 2 except that the throttle is depressed and the vehicle's speed is approximately 25 mph. The peak levels of the noise spikes in this plot are inaccurate since the sample rate is only 1 MS/s and the DSO is aliased.

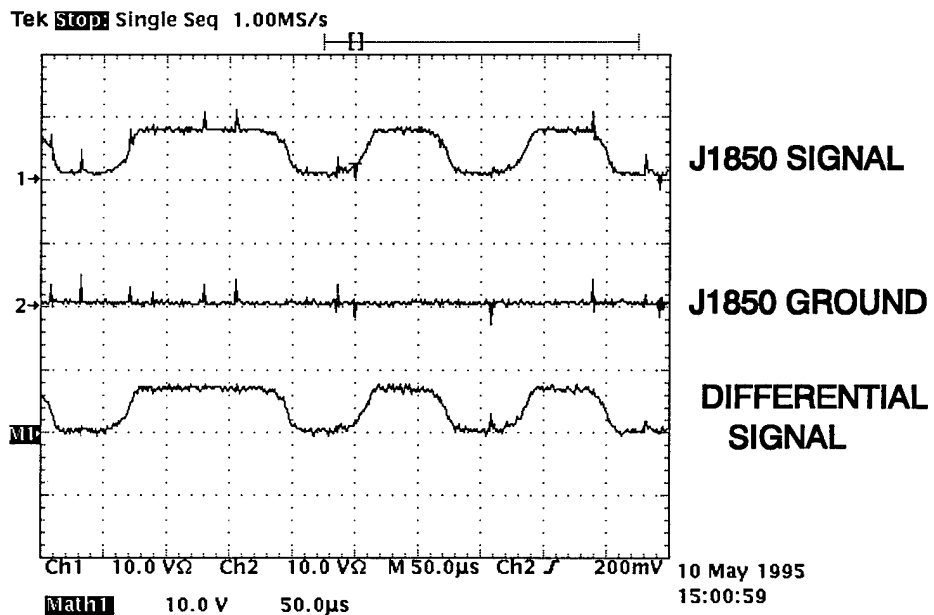


FIGURE 3 - SAE J1850 BUS WITH REAR WHEELS AT 25MPH

Figure 4 is the same as Figure 3 except that DSO sample rate has been increased to 250 MS/s. The DSO is no longer aliased and the levels of the spikes are seen to be up to 20 V peak on the top and middle traces. These traces represent a common mode coupling since each line is measured with respect to chassis ground. The bottom trace in Figure 4 shows that the spikes are much lower in level when measured differentially (i.e. about 6 V peak). The multiplexed data signal and signal ground are not twisted or shielded but they are run side-by-side between the various nodes. If the multiplexed cable was shielded and used a twisted pair then both the common mode and differential mode spikes would be reduced.

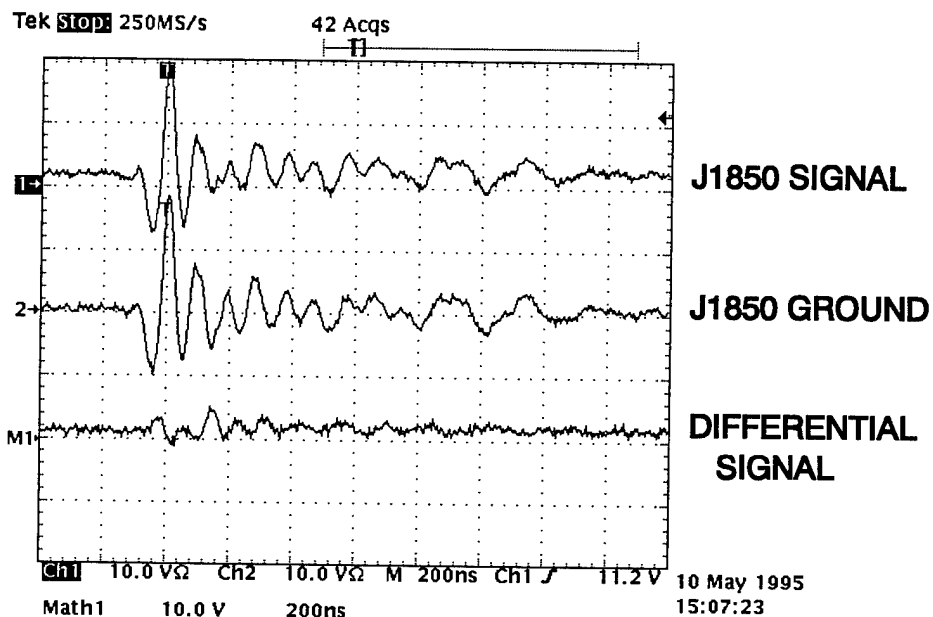


FIGURE 4 - SAE J1850 BUS AT 25 MPH WITH 250 MS/s SAMPLE RATE

RADIATED MAGNETIC FIELD EMISSIONS

The broadband radiated magnetic field emissions were measured in accordance with SAE J551/5 (Draft) Performance Levels and Methods of Measurement of Magnetic and Electric Field Strength from Electric Vehicles, Broadband, 9 kHz to 30 MHz, dated February 2, 1995. The test method involves placing the center of a 60 cm loop antenna a distance of 1 meter above the ground level and 1 meter away from the nearest part of the vehicle. All four sides of the vehicle are measured for magnetic field emissions in all three orthogonal polarizations of the loop antenna with the car elevated on jack stands and the rear wheels spinning at 25 mph.

In accordance with SAE J551/5, the vehicle side with the highest levels is also tested at 10 mph and 40 mph to determine the speed that produces the maximum radiation. A speed of 10 mph and an antenna location at the front of the vehicle was found to give the highest levels as shown in Figure 5. The worst case antenna polarization was determined to be with the loop axis perpendicular to the front face of the vehicle.

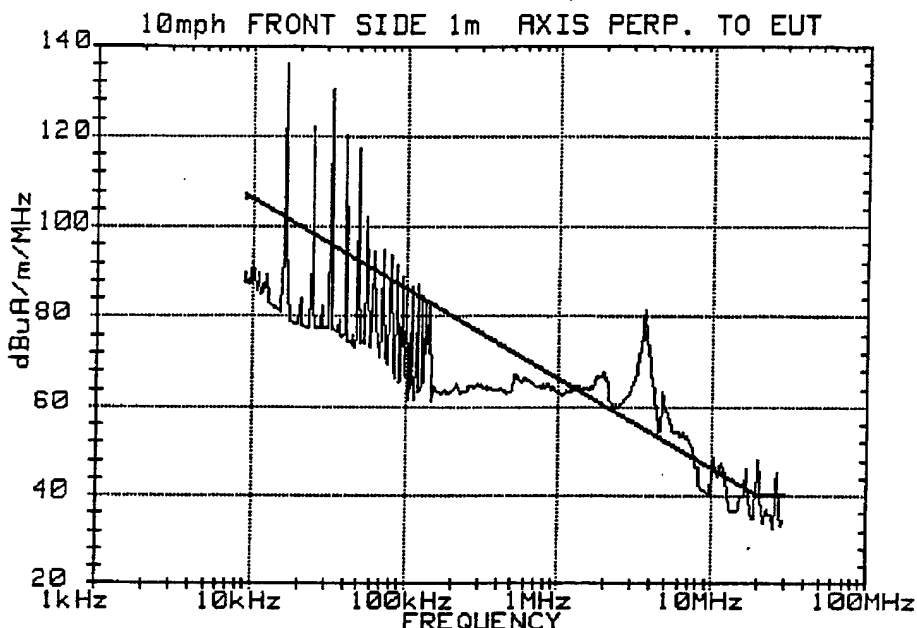


FIGURE 5 - RADIATED MAGNETIC FIELD EMISSIONS AT 10 MPH

The SAE J551/5 document recommends certain receiver bandwidths and minimum scan times. The recommended bandwidths were not available on the Singer receiver system that was used for the testing. The recommended and actual bandwidths and sweep times are shown in Table 1.

TABLE 1 - RECEIVER PARAMETERS USED FOR EMI MEASUREMENTS

Frequency Range (Hz)	SAE J551/5 Bandwidth (Hz)	Actual Bandwidth (Hz)	SAE J551/5 Minimum Scan Time	Actual Scan Time
9k - 50k	200	200	100 ms/kHz	470 ms/kHz
50k - 150k	200	1k	100 ms/kHz	47 ms/kHz
150k - 30M	9k	10k	100 ms/MHz	293 ms/kHz

The minimum scan times of SAE J551/5 are based on a pulse repetition rate (PRF) of 50 Hz for frequencies below 150 kHz and a PRF of 1100 Hz for frequencies above 150 kHz. The actual PRF for the electric vehicle is 8 kHz so the actual scan times used were more than adequate to capture the emissions during the scans.

In retrospect, it probably would have been better to use just one or two bandwidths rather than three for the test. There would have still been adequate sensitivity but the data would look more consistent instead of having "jumps" at the bandwidth changes.

The data and test limit shown in Figure 5 is in broadband units of $\text{dB}\mu\text{A/m/MHz}$. The values can be converted from $\text{dB}\mu\text{A/m/MHz}$ to $\text{dB}\mu\text{A/m/kHz}$ by subtracting 60 dB.

RADIATED ELECTRIC FIELD EMISSIONS

The broadband radiated electric field emissions were also measured in accordance with SAE J551/5 (Draft). The test method involves placing the base of a 1 meter monopole antenna at ground level and 3 meters away from the nearest part of the vehicle. The monopole base is grounded to the metal shield room floor to form a counterpoise. All four sides of the vehicle are measured for electric field emissions with the car elevated on jack stands and the rear wheels spinning at 25 mph.

The maximum electric field emissions were found to occur from the passenger side of the vehicle. These levels are shown in Figure 6. In accordance with SAE J551/5, the vehicle side with the highest levels is also tested at 10 mph and 40 mph to determine the speed that produces the maximum radiation. A speed of 25 mph was found to give the highest levels.

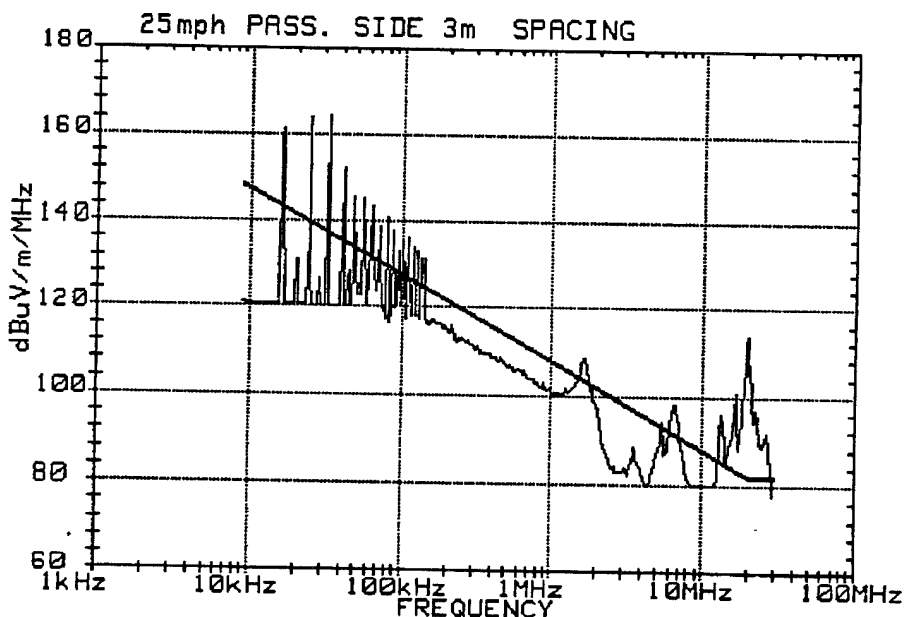


FIGURE 6 - RADIATED ELECTRIC FIELD EMISSIONS AT 25MPH

The receiver bandwidths and scan times were the same as used for the magnetic field radiated emissions tests as previously shown in Table 1. The data and test limits shown in Figure 6 are in broadband units of $\text{dB}\mu\text{V/m/MHz}$. The values can be converted from $\text{dB}\mu\text{V/m/MHz}$ to $\text{dB}\mu\text{V/m/kHz}$ by subtracting 60 dB.

A major concern with the electric field measurements was the potential for saturation of the active rod antenna from the impulsive electric fields emitted by the vehicle. Initial tests were performed with an Eaton 95010-1 active rod antenna. The output of the 95010-1 was fed into a DSO and the output level was determined to be in saturation. Next, a Singer 94607-1 active rod antenna was used because it can tolerate fields up to 20 dB higher than the 95010-1. The 94607-1 output was fed into a DSO and the worst case output level was determined to be about 2 dB below where saturation can occur. A DSO plot of the 94607-1 antenna output is shown in Figure 7.

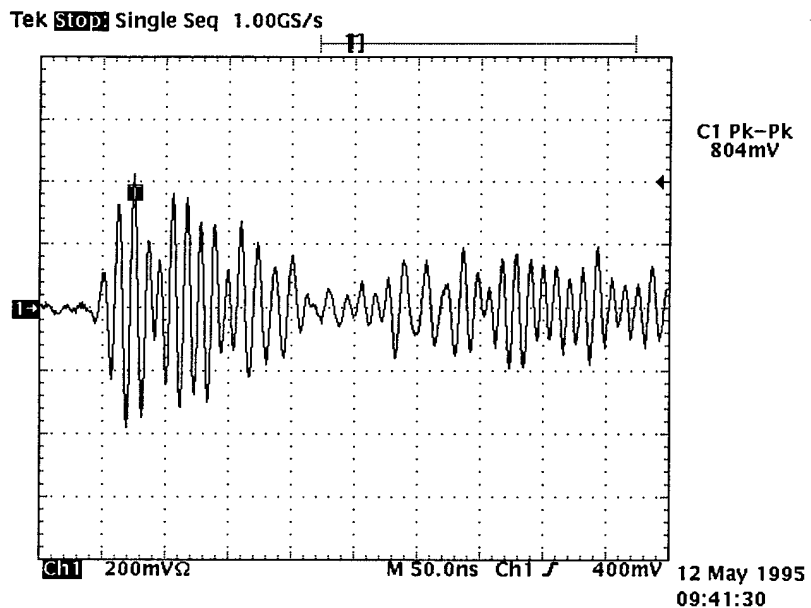


FIGURE 7 - RADIATED ELECTRIC FIELD TIME DOMAIN MEASUREMENT

The resonant frequency of the 94607-1 output is approximately 100 MHz. This is well beyond the 30 MHz upper operating frequency of the antenna. The natural quarter wave resonance for a 1 meter monopole is about 100 MHz. Thus, the electric field impulses from the vehicle are exciting the natural resonance of the monopole antenna. By using signal substitution from a 100 MHz sinewave generator, the saturation level was found to be a level of 20 dBm into the 94607-1 active rod preamp. The output of the preamp is 970 mVpp for a 20 dBm input at 100 MHz. Therefore, as long as the output of the 94607-1 is less than 970 mVpp, then the antenna will not be saturated.

All of the calibrated electric field measurements were made at 3 meters from the vehicle in accordance with SAE J551/5. Additional electric and magnetic field measurements were made with radiation hazard probes to determine location and approximate levels. These probes are very broadband in design and basically measure average rather than peak field strength. A reading of several volts/meter was found to be emanating from the vehicle's radio antenna. The antenna is apparently acting as a re-radiator of electromagnetic energy. It is no wonder that the AM radio has never functioned properly! The highest readings were found in close proximity (i.e. about 20 cm) to the high voltage battery pack where levels were measured up to 0.3 A/m and 300 V/m! The limited amount of time allotted for EMC testing did not permit further investigation into these apparently high levels of electromagnetic radiation.

CONCLUSIONS

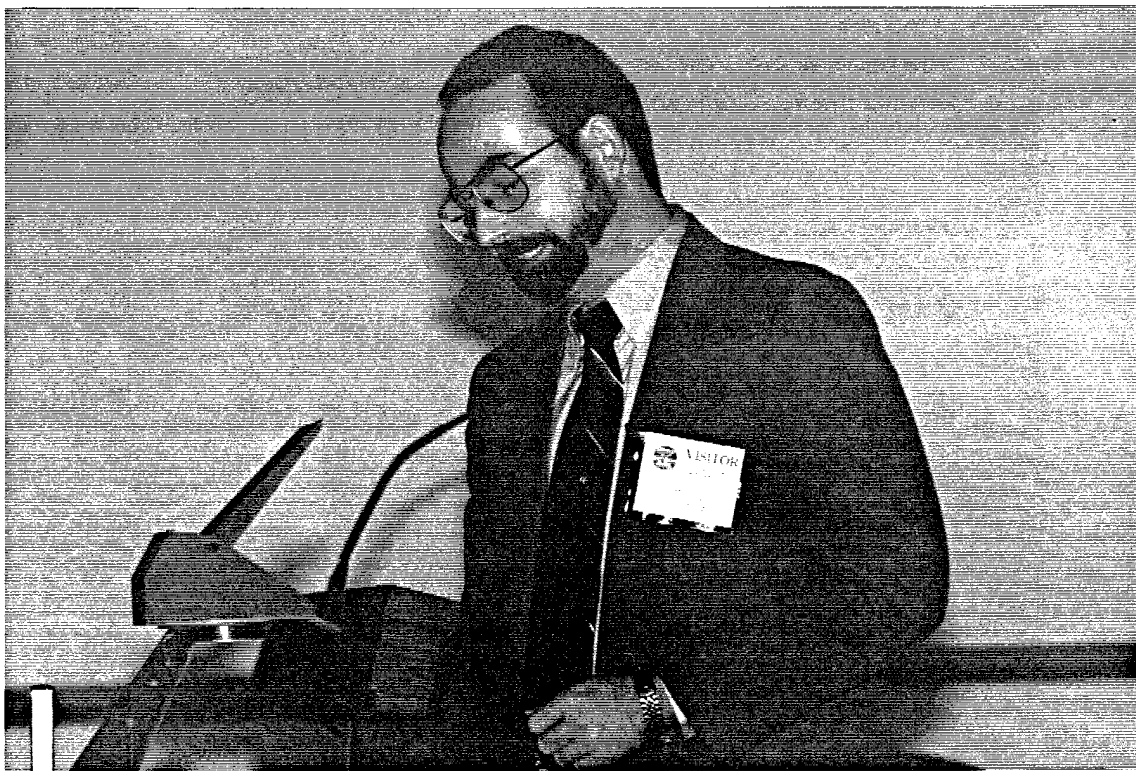
The Motorola electric vehicle platform was found to have substantially high levels of radiated electric and magnetic fields. The levels were up to 34 dB above the SAE J551/5 (Draft) limits. Also, conducted spike levels were measured up to 20 volts peak on the SAE J1850 serial communication bus. The electric vehicle platform was built without EMI control features since this was not a production vehicle and the purpose was to identify next generation semiconductors. The purpose of the multiplex project was to verify whether the serial communication technology currently available can operate in a worst case EMI intensive environment of an electric vehicle. The answer is a qualified "yes" in that isolation and signal filtering were necessary to ensure reliable operation of the MCUs and the multiplexed communication system. However, other vehicle circuits and components (e.g. the AM radio) will require further reduction of the high current/high voltage switching noise of the AC inverter.

Indeed, if one were to install EMI control features to reduce the radiated emissions by 34 dB, then the vehicle would be compliant with SAE J551/5. Moreover, the conducted spike levels on the multiplex bus would also be reduced to 0.4 volts peak or less. Thus compatible operation would be ensured in the vehicle perhaps without the need for extensive signal filtering and isolation. Of course the EMI control measures would increase the cost of the vehicle systems.

Future research work on the Motorola electric vehicle platform will involve installing EMI feed through filters on the input and output power lines of the AC inverter. An EMI shield around the AC inverter will be used to reduce the fields created by the impulsive switching noise. Other modules may utilize EMI shielding techniques to isolate their circuits from the radiated switching noise that is present. The use of balanced circuits and shielded cables would further improve the immunity to the switching noise. These practices and many more will be incorporated in the next generation inverter. The next generation inverter will use the ARROW Module along with the new Advanced Motor Control MCU.

REFERENCES

- [1] SAE J551/5 (Draft), Performance Levels and Methods of Measurement of Magnetic and Electric Field Strength from Electric Vehicles, Broadband, 9 kHz to 30 MHz, 2 February 1995.
- [2] Powers, C., Huettl, T., Using Existing Multiplex Communication Technology to Implement an Electric Vehicle Communication Network, (to be presented at the SAE Future Transportation Technology Conference in Los Angeles, August 1995).
- [3] MIL-STD-461D, Requirements for the Control of Electromagnetic Interference Emissions and Susceptibility, 11 January 1993.
- [4] MIL-STD-462D, Measurement of Electromagnetic Interference Characteristics, 11 January 1993.





**MR. ROGER McCONNELL
AND
MR. CLARK VITEK
CKC LABORATORIES, INC.**



CALIBRATION OF FULLY ANECHOIC ROOMS AND
CORRELATION WITH OATS MEASUREMENTS

Roger A. McConnell & Clark Vitek
CKC Laboratories, Inc.
5473A Cloud's Rest Road
Mariposa, CA. 95338

ABSTRACT

Fully anechoic rooms may gradually replace open area test sites as the preferred type of testing facility for the measurement of radiated emissions. The fully anechoic room offers several advantages over the open area test site: Immunity to high ambient signal levels, the capability of being located in metropolitan areas close to the customer base, more uniform field over a larger area, a reduction in test time since there is no need to scan the receiving antenna in height, and the capability of being used for both emissions and susceptibility testing. Measurements of site attenuation in a fully anechoic room show excellent correlation with the mathematical model for Normalized Site Attenuation in free space. The mathematical model and the measurement results are presented here.

INTRODUCTION

Measurements of Normalized Site Attenuation have been made in a fully anechoic room at a test distance of 3 meters. The measurement procedure used was that defined by ANSI C63.4-1992 for Alternate Test Sites, with the antennas being repositioned to four different locations in both horizontal and vertical polarization. The theoretical free space Normalized Site Attenuation model was developed from the same principles used in the development of the original Normalized Site Attenuation model for Open Area Test Sites. The free space model converges to the Open Area Test Site model when a ground plane is introduced.

Correlation of the measurements with the theoretical model for free space is excellent, demonstrating that the fully anechoic room yields results equivalent to those obtainable on an open area test site.

THE FREE SPACE THEORETICAL MODEL

Open Area Test Sites are required by the FCC to meet the Normalized Site Attenuation standards published in ANSI C63.4-1992. The theoretical model for these standards was developed as an extension of the work presented by Smith, German and Pate [1].

Smith's Equation (18),

$$A = \frac{279.1 \text{ } AF_R \text{ } AF_T}{f_m \text{ } E_D^{\max}} \quad (1)$$

assumes 50 ohm source and load impedances, a velocity of light of 3×10^8 meters per second, a power into the transmitting antenna of 1 picowatt, and that the units of E_D^{\max} are microvolts per meter. A further assumption is that the numeric gain of a resonant dipole is 1.64.

Retaining the 50 ohm source and load impedances, but using the value $c = 2.997925 \times 10^8$, normalizing the power into the transmitting antenna to 1 watt, normalizing the antenna factors to unity, expressing E_D^{\max} in volts, and using the relationship for E_D^{\max} in free space:

$$E_D^{\max} = \frac{\sqrt{30 P G}}{D} \quad (2)$$

Equation (1) becomes:

$$NSA = \frac{39.76 D}{f_m} \quad (3)$$

and in decibel form:

$$NSA_{dB} = 20 \text{ Log } \frac{39.76 D}{f_m} \quad (4)$$

In the above equations D is the distance separating the two antennas, f_m is the frequency of measurement in MHz, G is the numeric gain of a resonant dipole, and P is the power into the transmitting antenna, (1 watt).

An alternate form for NSA yielding precisely the same results is:

$$NSA_{dB} = 20 \text{ Log } \frac{2 \text{ } R_s \text{ } R_L}{R_s + R_L} \frac{\lambda D}{Z_0} \quad (5)$$

where R_S and R_L are the source and load resistances of 50 ohms, λ is the wavelength, D is the distance between the antennas, and Z_0 is the impedance of space, 120π ohms.

Over a ground plane, the distance D becomes an effective distance, D_{eff} , a combination of the direct path from antenna to antenna, and the indirect path reflected from the ground plane, taking into consideration also the phasing between these two paths. The effective distance for horizontal and vertical polarizations respectively is contained in Equations (8) and (13) of [1].

Recognizing that the effective distance D_{eff} converges to the actual distance D as the height above the ground plane increases, a complete equivalency can be shown between the NSA equations for free space and for the open area test site.

Equations (4) or (5) can be used to generate free space NSA values for any test distance desired. Table 1 below gives the free space NSA values at 3 and 10 meters.

THE MEASUREMENT TECHNIQUE

Site attenuation was measured in the same manner as on an open area test site. The feed lines to each antenna were connected together to determine a reference signal level at each measurement frequency. Then the feed lines were connected to the transmitting and receiving antennas, and the signal level from the receiving antenna was measured with a spectrum analyzer. Classical Site Attenuation, CSA, was determined by taking the difference between the reference signal and the spectrum analyzer reading.

In a process completely parallel to that used in ANSI C63.4-1992, Normalized Site Attenuation was computed by subtracting the antenna factors and the mutual coupling correction factor from the measured value of site attenuation:

$$NSA_{\text{meas}} = CSA - AF_T - AF_R - \Delta AF \quad (6)$$

Antenna factors were determined using MININEC, a commercially available numerical analysis program for thin linear antennas. The mutual coupling correction factor, ΔAF , was computed as in the ANSI C63.4-1992 procedure by taking the difference between site attenuation as computed by MININEC and site attenuation for a pair of "isolated dipoles". The isolated dipole is a hypothetical antenna developed in [1] which exhibits the gain, pattern, antenna factor and center impedance of a dipole antenna, but which exhibits no near field effects. Antenna factors and the mutual coupling correction factors are shown in Table 2. As in ANSI C63.4-1992, the mutual coupling correction factors were assumed to be negligible above 180 MHz.

The dimensions of the fully anechoic room did not permit the use of full length resonant dipoles at the lower frequencies. In horizontal polarization a 50 MHz resonant dipole was used from 30 through 50 MHz, after which resonant dipoles were used through 400 MHz. In vertical polarization, an 80 MHz dipole was used from 30 MHz through 80 MHz, after which resonant dipoles were used through 400

MHz. Ferrite baluns having a 1:1 turns ratio were used with the dipole antennas to 1000 MHz. In the MININEC computation of site attenuation, the mismatch loss of the ferrite baluns was accounted for, but otherwise the baluns were assumed to be lossless.

At 500 MHz and above, a resonant dipole was used as the transmitting antenna, and an EMC Biconilog was used as the receiving antenna.

DESCRIPTION OF FULLY ANECHOIC ROOM

The fully anechoic room used to compare to the model for free space site attenuation was constructed in 1994 in Hillsboro, Oregon. The room dimensions (inside surfaces of the metal walls) are 6.0 m x 8.0 m x 3.0 m (w, l, h). All surfaces of the room are then lined with 10 cm square ferrite tiles, Fair-Rite Corporation material #42, 0.5 cm thickness. The EUT test area is a 1.5m diameter turntable, the periphery of which is located 1.0 m from the back wall of the chamber and centered with respect to the side walls. The front edge of the turntable is located 3.0 m from the center of the receive antenna. The back of the receive antenna is a minimum of 1.0 m from the back wall of the chamber. Care was taken in the construction of the facility to ensure that disruptions in the absorber material are limited to the minimum necessary to provide adequate light and cooling. All cooling and light apertures are located in the roof of the structure outside the 3.0 m distance between the EUT area and the receive antenna.

MEASUREMENT RESULTS : FREE SPACE NORMALIZED SITE ATTENUATION OF FULLY ANECHOIC ROOM

Figures 1 and 2 show the results of the Normalized Site Attenuation measurements performed in the above described fully anechoic room. These measurements were performed at four locations which are plotted in Figures 1 and 2 : Horizontal front and center of EUT area at a 1m and 2m transmit height, and Vertical 1m transmit height at front, center, left, and right locations. For all measurements, the receive antenna was fixed at a 1.5m antenna height above the floor (centered in the room width and height) at a 3m test distance.

In general, the results show excellent correlation to the free space NSA values provided by Equation (4), and are within the +/- 4 dB ANSI C63.4 criteria at all frequencies measured except 30 MHz, Vertical polarity.

FREE SPACE TO OPEN FIELD CORRELATION : GENERAL CORRECTION FACTORS BASED ON NSA MODEL

The above experiment suggests that a fully anechoic room can be modeled by the free space NSA provided by Equation (4), and that a facility can be constructed to meet this model within the +/- 4 dB provided by ANSI C63.4 with minor limitations. However, because no free space specification limits exist for directly evaluating measurements made on equipment under test (EUT's) in the fully anechoic facility, correlation to open field measurements is necessary.

Using NSA as an attenuation model, whereby a reading R may be considered as the product (or sum in dB) of a source signal S and its attenuation, NSA can be used to correct readings R made on a sample source signal S, in a full anechoic chamber (FAC) by the following relationships :

$$R_{OATS} (dBuV/m) = S (dBuV/m) - NSA_{OATS} (dB) \quad (\text{open field attenuation model}) \quad (7a)$$

$$R_{FAC} (dBuV/m) = S (dBuV/m) - NSA_{Free\ Space} (dB) \quad (\text{full anechoic attenuation model}) \quad (7b)$$

subtracting equations 7a and 7b yields the following :

$$R_{OATS} (dBuV/m) = R_{FAC} (dBuV/m) + NSA_{Free\ Space} (dB) - NSA_{OATS} (dB) \quad (8)$$

where the subscript OATS represents the open field site, FAC represents the full anechoic chamber, and $NSA_{Free\ Space}$ is provided by Equation (4).

From this relationship, a general free space to open field correction factor, ΔNSA_{FS} can be defined which can be applied to readings made in a fully anechoic chamber to represent equivalent open field readings :

$$\Delta NSA_{FS} = NSA_{Free\ Space} (dB) - NSA_{OATS} (dB) \quad (9)$$

Table 3 provides ΔNSA_{FS} for a 3 m Full Anechoic to 10 m Open Field correlation. The 3 m Full Anechoic NSA values are provided in Table 1, the 10m Open Field NSA values are taken from Table 1 of ANSI C63.4 (1992) for a 1 meter transmit height. Note that the selection of the 1 m transmit antenna height limits the test volume to 1 m in depth by 1.5 m in width by 1.5 m in height, in accordance with paragraph 5.4.6.5 of ANSI C63.4 (1992). This height selection also limits the correlation to the use of broadband antennas which can be brought down to the 1m height and still maintain 0.25 m from the ground plane on the open field site.

FREE SPACE TO OPEN FIELD CORRELATION : EUT MEASUREMENTS

To evaluate the use of the general free space to open field correction factor provided in Equation (9), measurements were performed on a sample EUT table top system (computer, monitor, keyboard, mouse, and modem) in the above described 3.0 m Full Anechoic Chamber and a 10 m Open Field test site that meets the +/- 4 dB criteria to the open field NSA model provided in ANSI C63.4. The results of these measurements are provided in Table 4 for all readings from the EUT within 10 dB of the specification limit. Note that for the free space measurements, all reading were obtained at a fixed 1.5m antenna height, and that for the open field measurements, the scan height was varied from 1 m to 4 m. Table rotation angle was maximized in both tests. The results of Table 4 show that correlation within the bounds of the +/- 4 dB provided for open field site correlation is achievable for a full anechoic chamber to open field correlation by using the general free space to open field correction factors provided by Equation (9) and presented in Table 3 of this paper.

CONCLUSIONS

A theoretical model for the Normalized Site Attenuation (NSA) of a fully anechoic chamber (absorber on all surfaces including the floor) has been developed using the same technique that was used to develop the NSA for open field sites in ANSI C63.4. Further, NSA can be used to develop a general correction factor for representing readings obtained in a full anechoic chamber as their equivalents on the open field site. This is useful because no specification limits presently exist for directly evaluating readings obtained in the fully anechoic chamber. The fully anechoic chamber, when constructed to meet +/- 4 dB to the theoretical free space NSA provided by Equations (4) an (5) above should yield repeatable results when measurements are made at a fixed antenna height. This will yield an improvement in test time over the presently available open field or semi-anechoic facilities, and will allow both emissions and immunity testing (in full accordance with IEC 1000-4-3 field uniformity, 0 to +6.0 dB over a 1.5m x 1.5m plane) to be performed in the same test facility without the need to add or remove absorber material.

TABLE 1
Free Space Normalized Site Attenuation

Frequency, MHz	NSA _{dB} , 3 Meters	NSA _{dB} , 10 Meters
30	11.99	22.45
35	10.65	21.11
40	9.49	19.95
45	8.47	18.93
50	7.55	18.01
60	5.97	16.43
70	4.63	15.09
80	3.47	13.93
90	2.45	12.91
100	1.53	11.99
120	-0.05	10.41
125	-0.41	10.05
140	-1.39	9.07
150	-1.99	8.47
160	-2.55	7.91
175	-3.33	7.13
180	-3.57	6.89
200	-4.49	5.97
250	-6.43	4.03
300	-8.01	2.45
400	-10.51	-0.05
500	-12.45	-1.99
600	-14.03	-3.57
700	-15.37	-4.91
800	-16.53	-6.07
900	-17.55	-7.09
1000	-18.47	-8.01

TABLE 2
Antenna Factors and Mutual Coupling Correction Factors

Frequency, MHz	Antenna Factor	Mutual Coupling Correction Factor
30	16.23(H), 26.09(V)	2.17(H), 1.91(V)
35	13.05(H), 24.21(V)	1.76(H), 1.61(V)
40	9.35(H), 22.38(V)	1.38(H), 1.37(V)
45	5.17(H), 20.55(V)	1.38(H), 1.16(V)
50	3.31(H), 18.66(V)	1.93(H), 0.96(V)
60	5.02(H), 14.48(V)	1.02(H), 0.62(V)
70	5.84(H), 9.61(V)	0.80(H), 0.26(V)
80	6.88	0.62
90	8.01	0.77
100	8.94	0.70
120	10.52	0.29
125	10.87	0.28
140	11.86	0.41
150	12.46	0.40
160	13.02	0.31
175	13.80	0.21
180	14.04	0.23
200	14.96	—
250	16.90	—
300	18.49	—
400	20.99	—
500	21.62(T), 17.3(R)	—
600	24.12(T), 18.1(R)	—
700	25.89(T), 20.0(R)	—
800	27.01(T), 21.4(R)	—
900	27.48(T), 23.5(R)	—
1000	27.33(T), 24.8(R)	—

Notes:

(H): Horizontal, Dipole; (V): Vertical, Dipole

(T): Transmitting Antenna, Dipole; (R): Receiving Antenna, Bilog

**FIGURE 1 : Free Space Normalized Site Attenuation Hillsboro Anechoic Facility :
Vertical 3 Meter Test Distance**

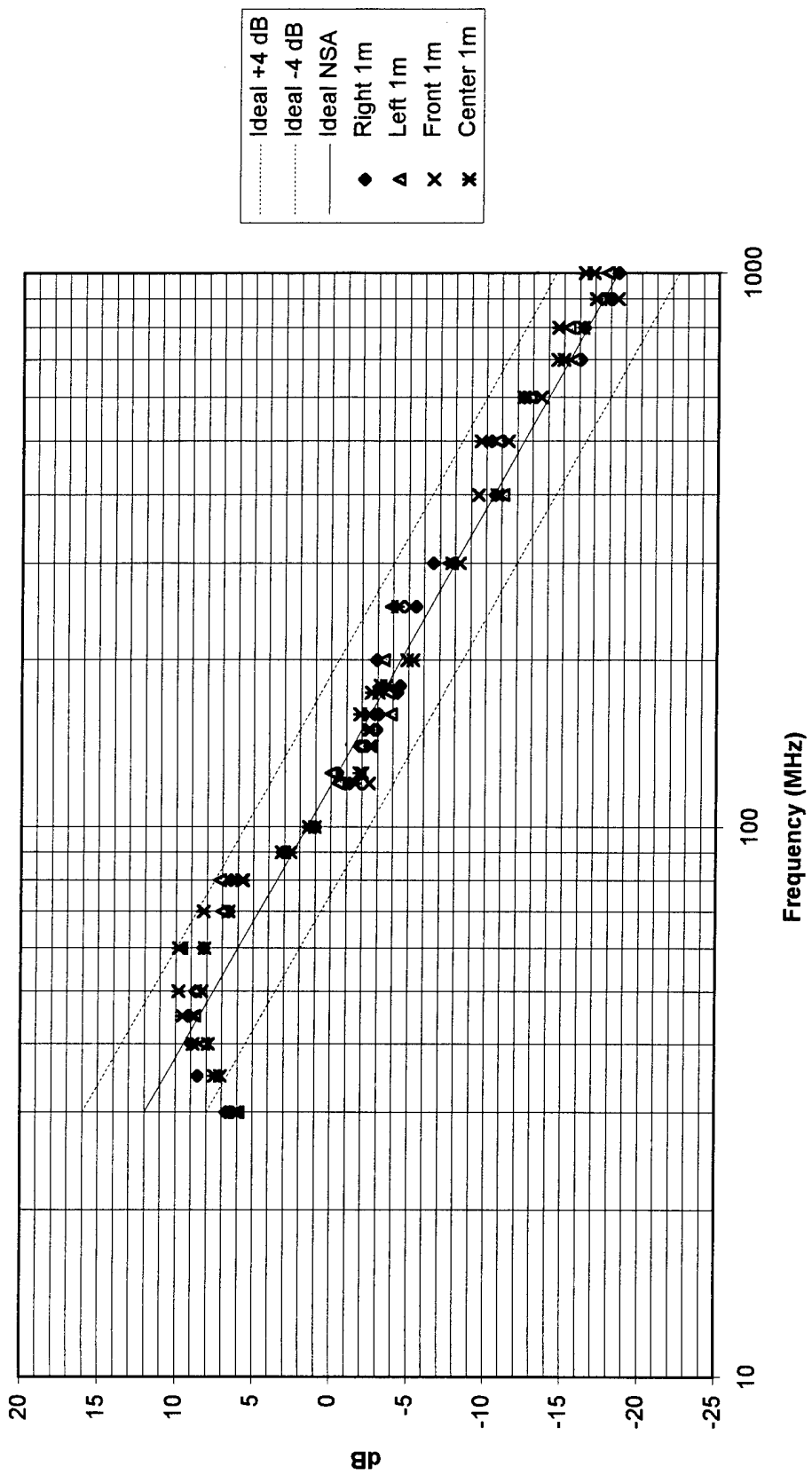


**Figure 2 : Free Space Normalized Site Attenuation Hillsboro Anechoic Facility : Horizontal
3 Meter Test Distance**

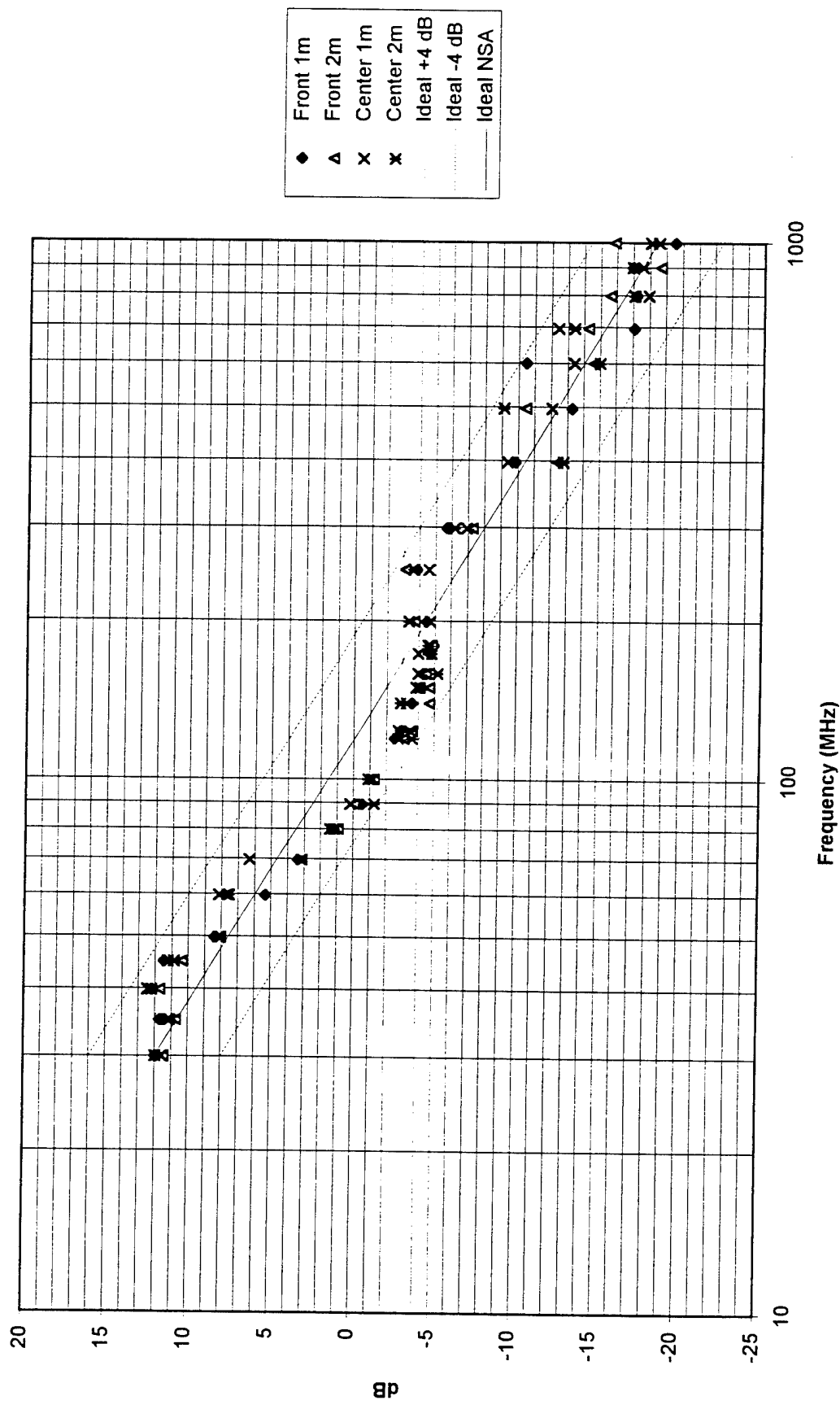


TABLE 3
3 Meter Fully Anechoic to 10 Meter Open Field Correction Factor, $\Delta\text{NSA}_{\text{FS}}$

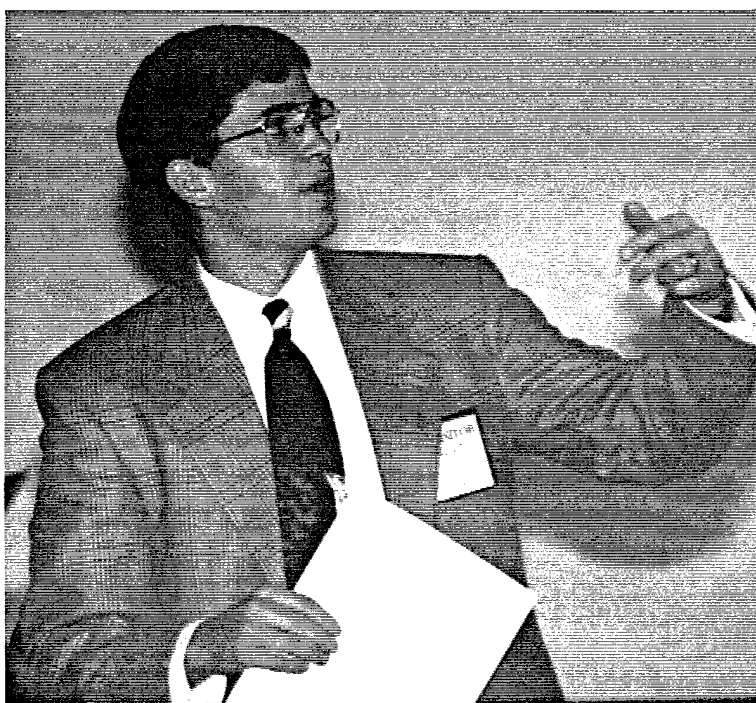
Frequency, MHz	$\Delta\text{NSA}_{\text{FS}}$ Horizontal	$\Delta\text{NSA}_{\text{FS}}$ Vertical
30	-17.81	-4.81
35	-16.45	-4.85
40	-15.41	-4.91
45	-14.43	-4.93
50	-13.58	-4.95
60	-10.87	-4.93
70	-12.03	-4.97
80	-9.83	-5.03
90	-8.95	-5.15
100	-8.16	-5.27
120	-7.05	-5.45
125	-6.81	-5.51
140	-6.19	-5.69
150	-5.89	-5.79
160	-5.65	-5.95
175	-5.32	-6.43
180	-5.27	-6.27
200	-5.09	-6.59
250	-4.83	-6.73
300	-4.71	-6.11
400	-4.61	-5.51
500	-4.55	-5.25
600	-4.53	-5.13
700	-4.57	-5.07
800	-4.53	-4.93
900	-4.75	-4.95
1000	-4.66	-4.87

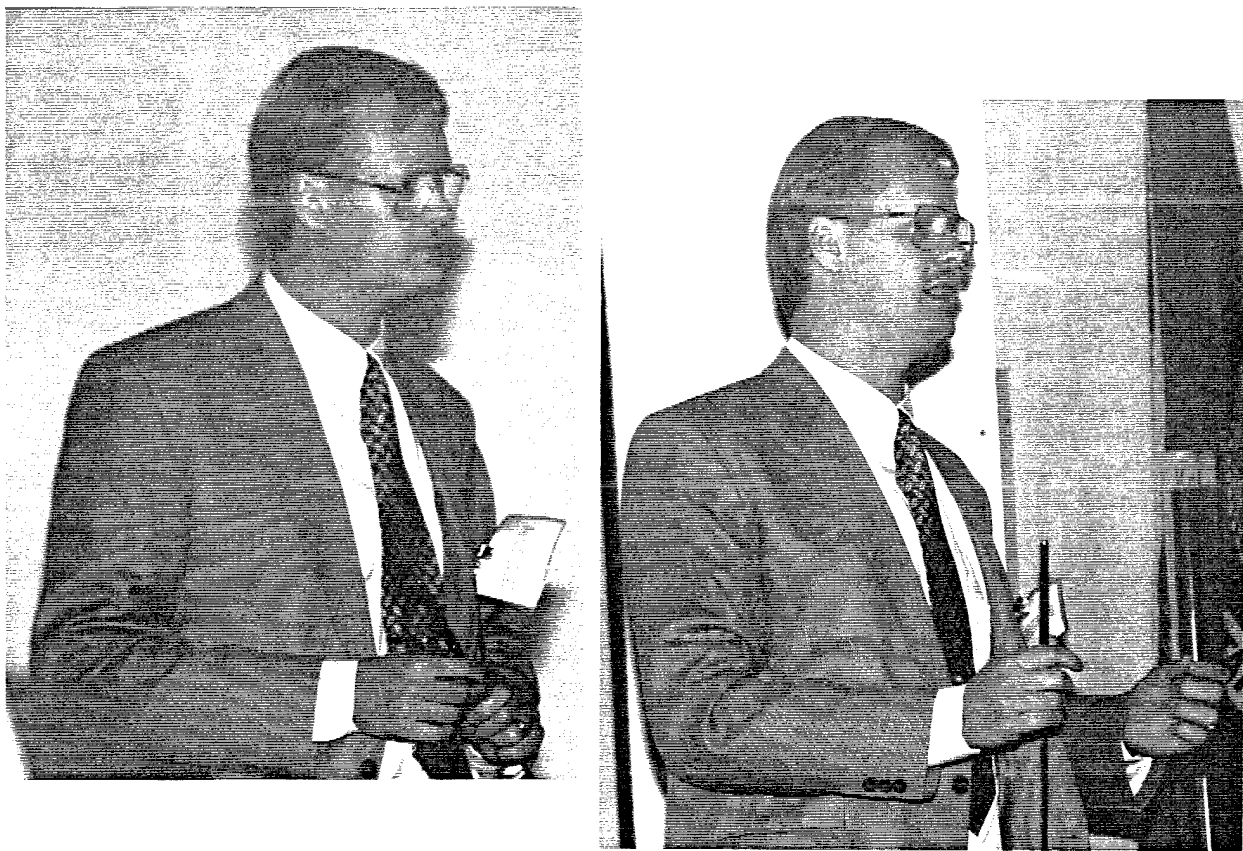
TABLE 4
Sample EUT Correlation : Full Anechoic to OATS incorporating ΔNSA_{FS}

Frequency, MHz	Reading, 3m Full Anechoic including ΔNSA_{FS} (dBuV/m)	Reading, 10m OATS (dBuV/m)
160.0 Horizontal	23.4	22.3
200.0 Horizontal	30.7	29.3
275.0 Horizontal	31.7	31.5
950.0 Horizontal	35	32.6
35.8 Vertical	28.4	24.3
39.5 Vertical	32.7	26
116.4 Vertical	25.7	22.5
875 Vertical	34.5	32.1
900 Vertical	35.2	36.3
987.5 Vertical	33.6	35.3
999.9 Vertical	33.8	31.4

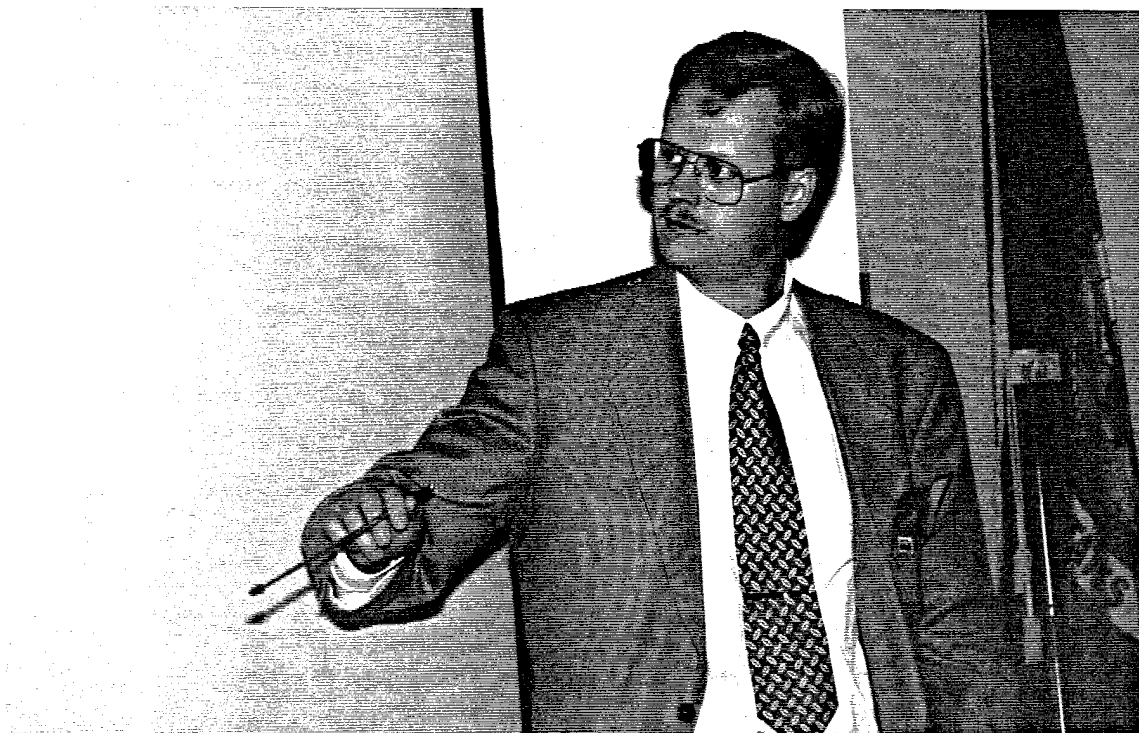
REFERENCES

- [1] Albert A. Smith, Robert F. German and James B. Pate, "Calculations of Site Attenuation from Antenna Factors", IEEE Transactions on Electromagnetic Compatibility, Vol. EMC-24, No. 3, August 1982.
- [2] John Berry, Barry Pate and Alan Knight, "Variations in Mutual Coupling Correction Factors for Resonant Dipoles Used in Site Attenuation Measurements", IEEE 1990 International Symposium on Electromagnetic Compatibility, pages 444-449, August 1990, Washington, D.C.
- [3] Akira Sugiura, "Formulation of Normalized Site Attenuation in Terms of Antenna Impedances", IEEE Transactions on Electromagnetic Compatibility, Vol. EMC-32, No. 4, November 1990.
- [4] Akira Sugiura, Correction Factors for Normalized Site Attenuation", IEEE Transactions on Electromagnetic Compatibility, Vol. EMC-34, No. 4, November 1992.
- [5] Roger A. McConnell, "An Impedance Network Model for Open Field Range Site Attenuation", IEEE 1990 International Symposium on Electromagnetic Compatibility, pages 435-439, August 1990, Washington, D.C.
- [6] Roger A. McConnell, "A Derivation of the Normalized Site Attenuation Mutual Coupling Correction Factor and An Improved Method of Antenna Factor Determination", IEEE 1992 International Symposium on Electromagnetic Compatibility, pages 407-411, August 1992, Anaheim, California.
- [7] J. David Gavenda, "Near Field Corrections to Site Attenuation", IEEE Transactions on Electromagnetic Compatibility, Vol. EMC-36, No. 3, August 1994.
- [8] ANSI C63.4-1992, "American National Standard for Methods of Measurement of Radio-Noise Emissions from Low-Voltage Electrical and Electronic Equipment in the Range of 9 kHz to 40 GHz", ISBN 1-55937-212-5, Copyright 1992 by the Institute of Electrical and Electronics Engineers.





**MR. PETER LANGREN
NATIONAL DEFENCE RESEARCH ESTABLISHMENT**



Transmission Cross Section of Apertures Measured by Use of a Nested MSC

by

Mats Bäckström and Olof Lundén

National Defence Research Establishment, P O Box 1165, S-581 11 Linköping, Sweden

Abstract. Knowledge of the transmission cross section of apertures, σ_a , constitutes an important factor in design and analysis of electrically large shielded structures. The paper presents a rationale of measuring σ_a as well as a method to measure it by use of nested mode stirred chambers. Results of measurements are presented and successfully compared with theoretical predictions.

1. Introduction

In later years a growing attention has been paid to the threat posed by pulsed high power microwaves against the operational reliability of electrical systems, such as cars and aircraft. This has led to an increased need of reliable tools, experimental as well as theoretical, for design, analysis and verification of system immunity against intense microwave radiation.

Numerical modelling has in many cases proved to be an efficient mean to analyse the interaction between electromagnetic fields and real objects /1,2/. However, much development will still be required before numerical methods can be used as an efficient engineering tool when dealing with complex electrically large real objects. This motivates the search for approximate analytical expressions for field penetration and coupling to cables. Also, a merit of analytical expressions is that they often provide a more direct way to physical understanding than numerical methods.

One of the activities of the HPM project at FOA (the National Defence Research Establishment) has been to find and evaluate simple analytical expressions which describe the coupling of microwaves into electronic compartments and onto cables. The study has supported the conclusion that the following expression can be used to estimate the average shielding effectiveness (SE) of compartments that are not electrically small /3,4/:

$$SE = \frac{2\pi \cdot V}{\sigma_a \cdot \lambda \cdot Q} \quad (1)$$

where V is the volume and Q the quality factor for the cavity. The parameter σ_a denotes the (total) aperture transmission cross section, defined by:

$$P_T = \sigma_a \cdot S_{inc} \quad (2)$$

where P_T is the (forward) power transmitted through the aperture and S_{inc} the power density of the incident field. Equation (1) has also been treated in /5,6/.

The usefulness of eq. (1) requires that σ_a can be measured or calculated for real apertures such

as gaskets and seams, and that it essentially does not depend on the characteristics of the cavity backing the aperture. In theory, if certain conditions are fulfilled a critical coupling between aperture and cavity may occur that will increase σ_a to its theoretical maximum value of $3\lambda^2/4\pi$, see /7/. However, it seems likely that σ_a essentially does not depend on the cavity if the aperture is physically small compared to the cavity, provided the Q-value of the cavity is not very high /8/. In general it seems reasonable to assume that critical coupling cannot occur if the shielding effectiveness is good ($> 10-20$ dB), a view similar to the criterion for black-hole condition stated in /6/.

In order to make use of eq. (1) we need to be able to determine σ_a for real geometries. In this paper we show that σ_a can be measured by use of a nested mode-stirred chamber. Obviously σ_a cannot in general be derived from a MIL-STD 285 type of measurement since this just gives a relative (i.e. not absolute) determination of the shielding properties of an aperture. This means that a SE curve resulting from a shielding measurement of that type is not applicable if the same aperture is located on an arbitrary cavity. Moreover, it is in general very difficult to know how to modify the SE data to apply to arbitrary cavity conditions.

The fundamental problem with a MIL-STD 285 type of measurement, even if it is performed by use of a nested MSC, is that the result (in principle) does not only depend on the properties of the aperture itself but also (according to eq. (1)) on the properties of the cavity backing the aperture.

To conclude, we think that our proposed measurement procedure to determine transmission properties of apertures has two important advantages compared to traditional methods. Firstly, the method yields an *absolute* value of the transmission properties of the aperture. Secondly, it gives a result that can easily be used to estimate SE for a given cavity.

2. The FOA nested MSC facility

The facility consists of a two mode-stirred chambers, one located inside the other. Their dimensions are $2.4 \times 2.4 \times 3.6 \text{ m}^3$ and $9.7 \times 4.9 \times 3.0 \text{ m}^3$. The DUT is mounted on a flange located on a wall of the smaller chamber. The DUT consists of an aperture furnished panel with size 35 cm x 35 cm. A HP 8510C network analyzer, controlled by a PC computer and HP-VEE software, is used for the coupling measurements.

The transmitting and receiving antennas are 2 - 18 GHz quadridged WJ horn antennas, with gain varying between 5 and 18 dBi. Typical curves for the antenna impedance mismatch factor, q , defined as in eq. (4) below, are shown in figure 1. The factor q has been derived from

$$q = 1 - |\Gamma|^2, \text{ where } \Gamma \text{ is the measured reflection coefficient.}$$

The frequency range in all measurements presented below has been 2 - 18 GHz, resolved in 201 points.

2.1 Q-values of the chambers

Q-values for the two chambers have been determined according to, cf. /5,9/:

$$Q = \frac{16\pi^2 V}{\lambda^3} \cdot \left(\frac{P_r}{P_T} \right)_{ave} \quad (3)$$

where P_r is the power received by an impedance matched antenna (i.e. $q = 0$ dB is assumed) and P_T is the power injected into the chamber. The average of the quotient between P_r and P_T has been taken over 200 paddle positions at each frequency point. The expression follows from eq. (1) using the following expression for the receiving area, A_e , of the antenna:

$$A_e = \frac{\lambda^2}{4\pi} \cdot G \cdot p \cdot q = \frac{\lambda^2}{8\pi} \quad (4)$$

where the antenna gain, $G=1$, the polarisation mismatch factor, $p=1/2$ and the impedance mismatch factor, $q=1$ (i.e. 0 dB). $G=1$ and $p=1/2$ follows from assuming isotropic conditions to prevail in the chamber. As can be seen in figure 1 the factor q generally deviates less than 1 dB from its ideal value. Applying eq. (3) on measured values from the two chambers gives the Q -values shown in figure 2.

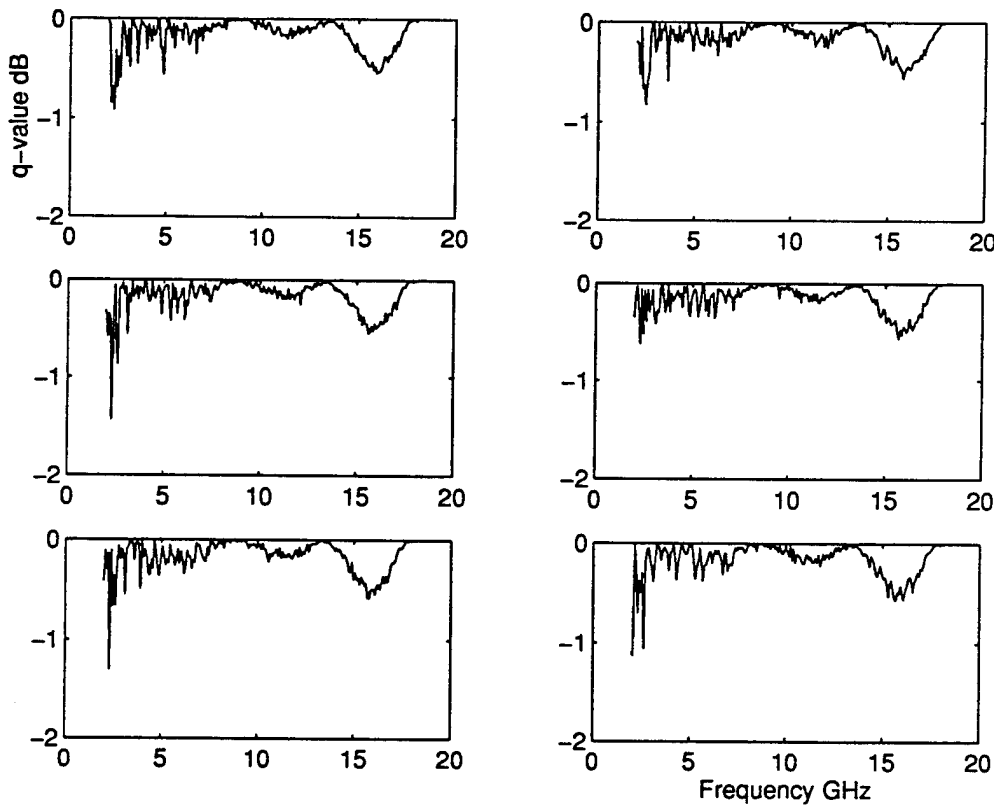


Figure 1. Impedance mismatch factor, q , for the antenna located in the nested (inner) chamber. The figures show q at different paddle positions, 7.2 degrees between each position. The frequency range was 2 to 18 GHz, resolved in 201 points.

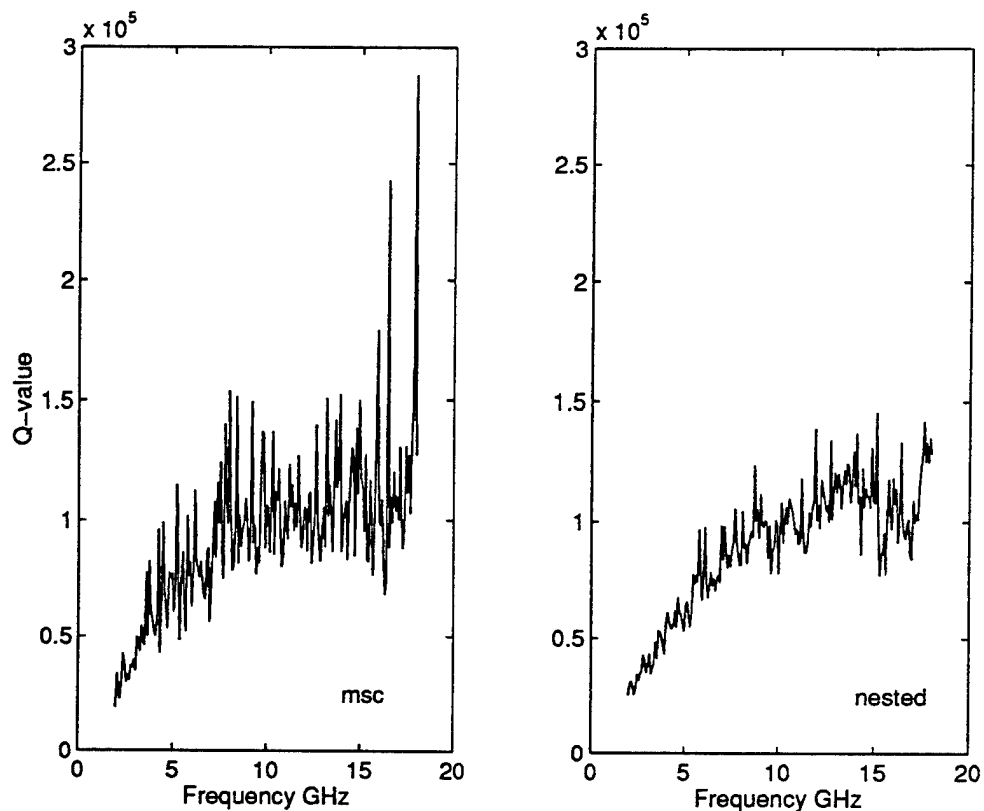


Figure 2. Q-values, between 2 and 18 GHz, for outer chamber, denoted msc (left) and nested chamber, determined from eq. (3). The calculations are based on the average value of 200 paddle positions at each frequency.

3. Results

A necessary requirement for performing measurements of σ_a for realistic apertures is that the isolation between the chambers is good. A measure of the isolation is the shielding effectiveness (SE) defined as the quotient between the average field in the outer chamber and the average field in the nested (inner) chamber when the DUT is replaced by a solid panel. The result of such a measurement is shown in figure 3. In the same figure the isolation is also presented in terms of a total σ_a for all leakage paths between the chambers (the relation between SE and σ_a follows from eq. (1)).

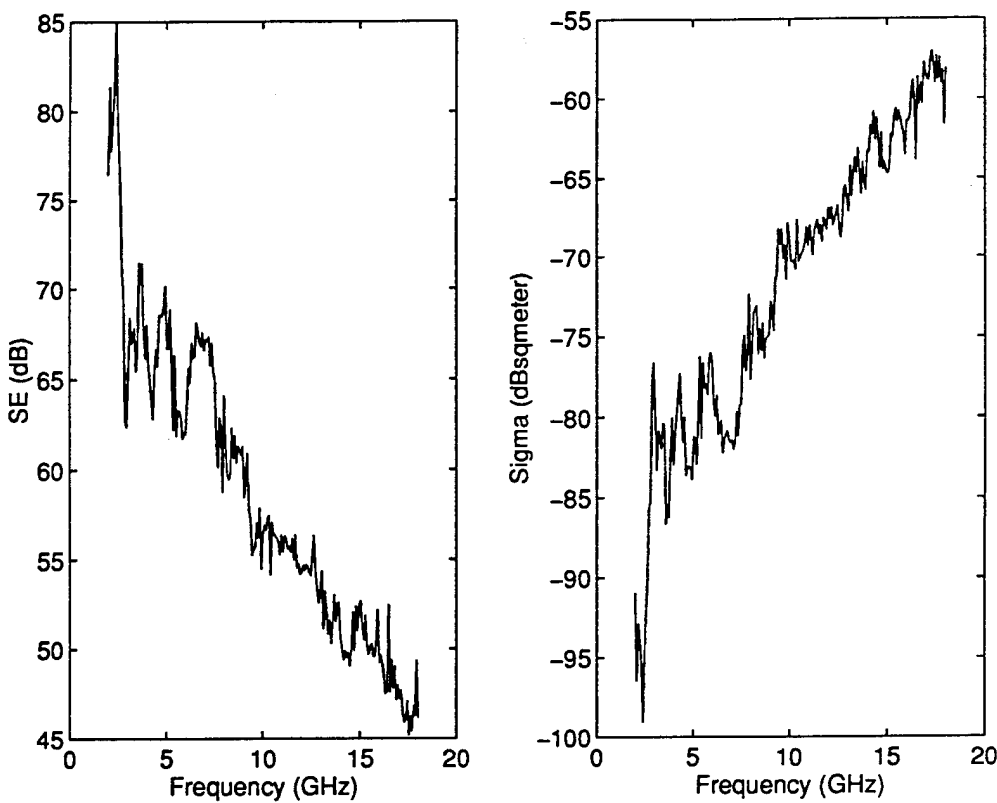


Figure 3. The isolation between the chambers, between 2 and 18 GHz, shown in terms of SE (left) and total transmission cross section, σ_a .

3.1 Power calibration

In order to calculate the transmission cross section, σ_a , from the measured coupling through an aperture one needs, for both chambers, to relate the measured field, i.e. the power received by the antenna, to the power injected into the chamber.

The transmission cross section is achieved from:

$$\sigma_a = \frac{2\pi V}{SE \cdot \lambda \cdot Q} \quad (5)$$

where Q refer to the nested chamber and is calculated according to eq. (3). SE is given by:

$$SE = \frac{(S_{msc})_{ave}}{(S_{nes})_{ave}} = \frac{(P_{r, norm, msc})_{ave}}{(P_{r, norm, nes})_{ave}} = \frac{Cal_{msc}}{Coupl_{nes}} \quad (6)$$

where S is the power density, $P_{r, norm}$ is the received power normalized to the power injected in the outer chamber. $Cal_{msc} = (P_{r, norm, msc})_{ave}$ is the calibration for the outer chamber, i.e. the normalized received average power at each frequency, where the average is taken over 200 paddle positions. $Coupl_{nes} = (P_{r, norm, nes})_{ave}$ is the coupling into the nested chamber, i.e. the normal-

ized received average power at each frequency. The average is a "nested" average, i e for each paddle position in the nested chamber the average is taken over all the paddle positions in the outer chamber, whereafter the final average is calculated based on all paddle positions in the nested chamber. Normally 20x20 paddle positions have been used.

If $(P_r/P_T)_{ave}$ in eq. (3) accordingly is denoted Cal_{nes} (since Q refer to the nested chamber), we finally get for σ_a :

$$\sigma_a = \frac{\lambda^2 \cdot Coupl_{nes}}{8\pi \cdot Cal_{msc} \cdot Cal_{nes}} \quad (7)$$

The calibration curves, Cal_{msc} for the outer chamber and Cal_{nes} for the nested chamber, are shown in figure 4.

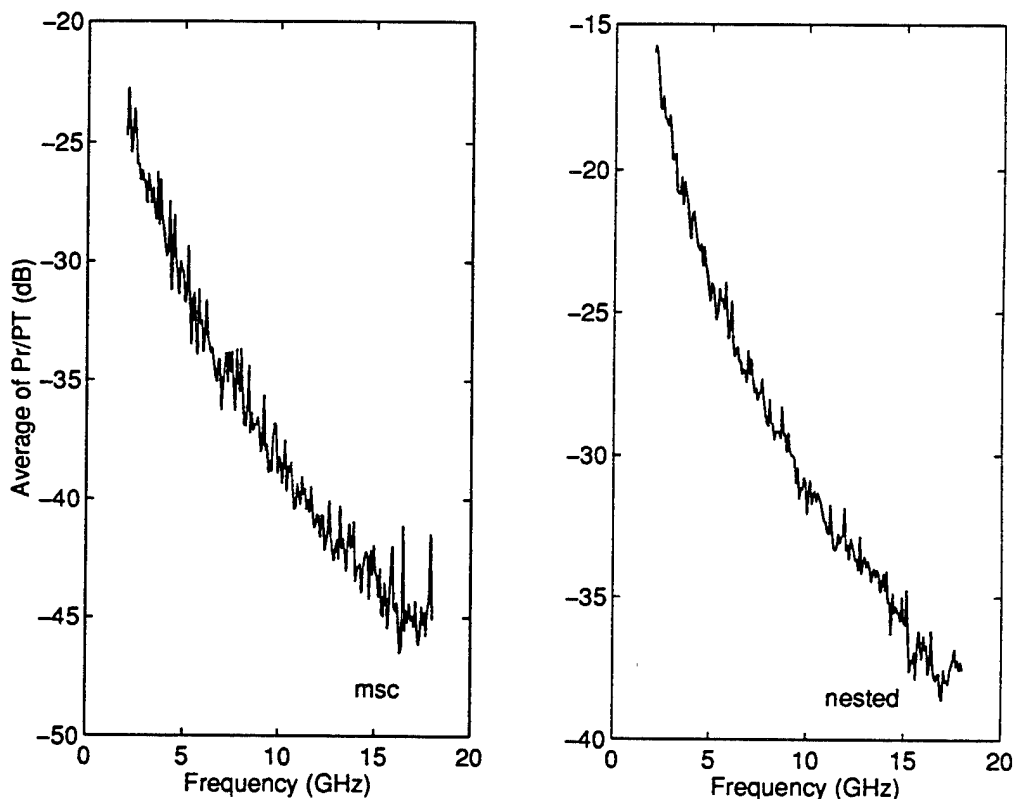


Figure 4. Calibration curves between 2 and 18 GHz for the outer chamber (left) and the nested chamber.

3.2 Measured transmission areas

All results shown below are based on measurements using 20x20 paddle positions.

3.2.1 Circular hole. The measured transmission cross section for a circular hole with a diameter of 20 mm is shown in figure 5. The figure also includes the background level (cf. fig 3) and the exact solution (dashed line) read from a diagram in /10/. In figure 5 the exact solution has been divided by a factor of 4 to correct for the difference between the measured case, where isotropic radiation is falling on the aperture from the outer half-space, and the exact solution,

which represents the case of normal incidence. A reduction factor of 4 is strictly valid only in the high frequency (optical) limit, in the low frequency limit it should instead be $8/3$, see /5/. However, since the correction factor for the resonance region is unknown a factor of 4 has been chosen for the whole frequency interval.

The correction factor consists of two parts. Firstly, a factor of two arises from the fact that all measurements refer to the isotropic field measured in the outer chamber (4π steradians) while the aperture is irradiated only from a half-space (2π steradians). Secondly, a correction is needed in order to take into account the dependence of polarization and angle of incidence.

3.2.2. Penetrated aperture. Figure 6 shows the effect of penetrating the 20 mm circular aperture with a 40 mm metal stick, thickness 2 mm, centrally and symmetrically positioned in the hole. As expected the transmission increases below the first resonance (around 8 GHz) of the hole. The first resonance of the stick is around 3.5 GHz which roughly corresponds to a wavelength equal to twice the length of the stick. It is interesting to note that σ_a at the stick resonance is well above (> 5 dB) the optical level for the hole.

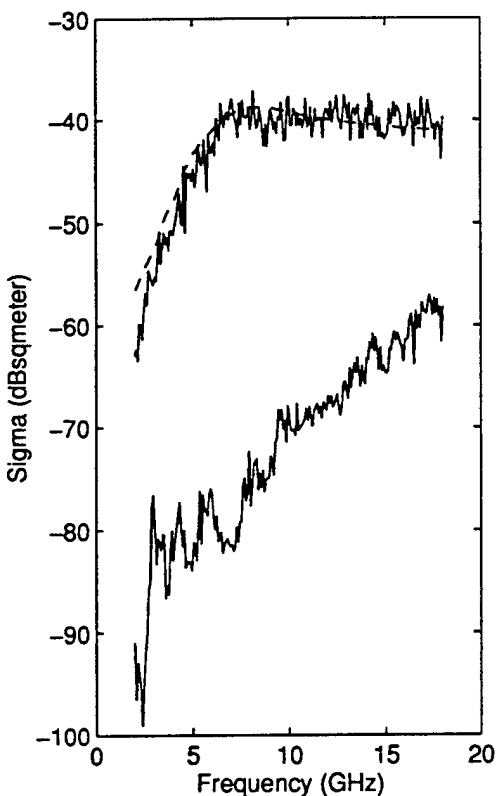


Figure 5. σ_a for a 20 mm circular hole compared with exact solution (dashed curve, see text). Background level is also shown.

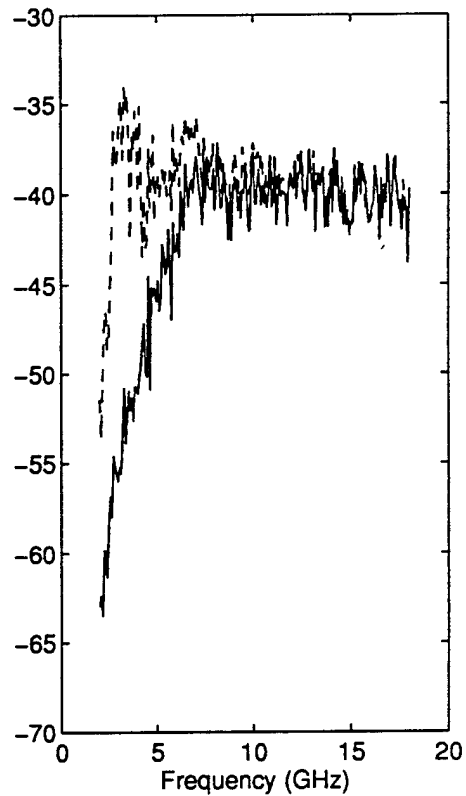


Figure 6. σ_a for 20 mm circular hole and for the same hole penetrated by a 40 mm stick (dashed curve).

3.2.3 Thin slot. In figure 7 the result of a measurement of σ_a of a 30 mm long, 1 mm wide and 2 mm deep slot is shown. Clear resonances are visible at roughly 5, 10 and 15 GHz. The first

resonance corresponds, as expected, to twice the length of the slot. Due to the isotropic conditions the σ_a at each resonance should be equal to approximately $\lambda^2/8\pi$. This can be seen from eq. (4). If the slot impedance is real 4 times as much power is radiated by a non-loaded slot then would be absorbed by a matched load [8]. However, only half of that power will be radiated into the half-space backing the slot. Since our measurements refer to the conditions in the middle of the chamber, cf. paragraph 3.2.1, a further reduction of two is necessary, resulting in a maximum of σ_a at resonance equal to $\lambda^2/8\pi$. This level is included in the figure. As seen in the figure the agreement is better at 5 GHz than at the higher resonances. The reason for that is not yet clear.

3.2.4 Riveted seam. Measurements were done on a panel with a "generic" riveted aircraft seam, put to our disposal by Saab Military Aircraft in Linköping. The 30 cm long seam consists of two plates at one mm distance riveted together by a T-element of width 38 mm, see figure 8. The rivet to rivet distance was 30 mm. There is a roughly 0.1 mm distance between the T-element and the plates, essentially consisting of (non-conductive) paint. The result of the measurement is shown in figure 8. There are clear resonances at 4, 8, 12 and 16 GHz. The same resonance frequencies have also been found in a FDTD-calculation studying the scattering from the same object [11]. In that calculation the resonances were shown to originate from the rivet to rivet distance and also from the thin, 38 mm wide, space between the top of the T-element and the plates.

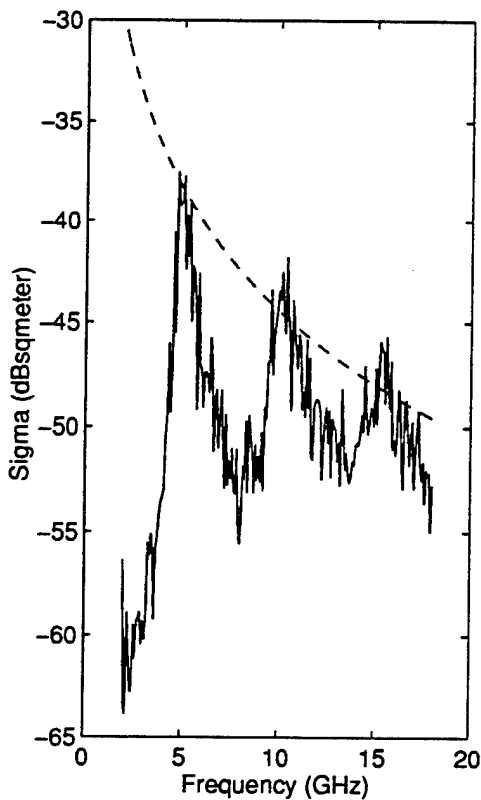


Figure 7. σ_a for the 30x1 mm slot. The dashed line indicates theoretical upper levels at the resonance frequencies.

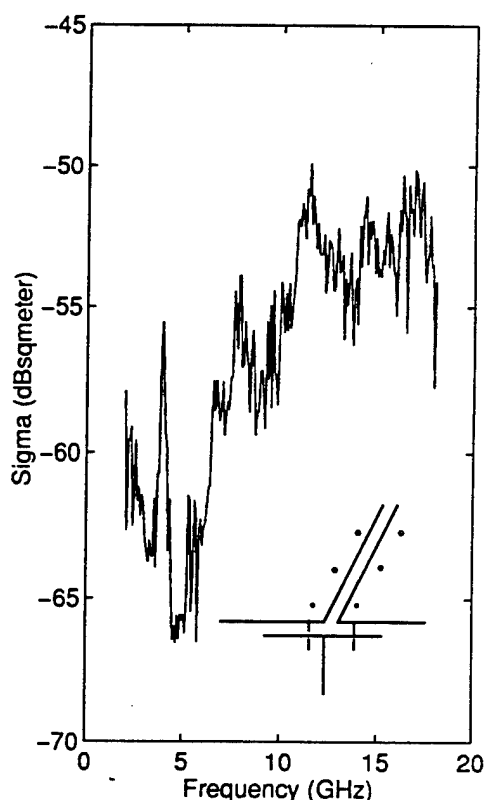


Figure 8. σ_a for the riveted seam.

4. Conclusions and Future Work

We have shown that the transmission cross section of apertures can be measured by use of a nested mode-stirred chamber. Furthermore, since σ_a is an absolute property of the aperture itself, we claim that the transmission cross section is a more appropriate measure of the shielding properties of the aperture than what is obtained in a MIL-STD 285 type of measurement. We will proceed to measure σ_a for different type of apertures, real as well as experimental. One specific item of great interest is corrosion of gaskets and seams.

Since the usefulness of σ_a partly depends on the applicability of equation (1) this expression has to be further evaluated, especially for real structures.

Finally, a more rigid validation against theoretical and numerical results will probably require the possibility to perform excitation of a well controlled polarization and angle of incidence.

5. References

1. Wahlgren B I, Bäckström M G and Perala R A, McKenna P M, "The Use of Finite Difference Electromagnetic Analysis in the Design and Verification of Modern Aircraft", Proc. of the 1989 Int. Conf. on Lightning and Static Electricity, Univ. of Bath, UK, 26 - 28 Sept., 1989.
2. Frennberg H et al., "HIRF-Testing of the SAAB 200 and the JAS 39 Gripen Aircraft", Proc. from EuroEM, Bordeaux, France, 1994.
3. Bäckström M G and Lorén J, "Microwave Coupling into a Slotted Cavity", Proc. of 3rd Int. Conf. on Electromagnetics in Aerospace Applications, Turin, Italy, September 14 - 17, 1993.
4. Bäckström M and Lorén J, "Microwave Coupling into a Slotted Cavity. Additional Results" FOA Report FOA-R--94-00042-3.2--SE, December 1994.
5. Hill D A et al., "Aperture Excitation of Electrically Large, Lossy Cavities", IEEE Trans. on EMC, vol. 36, no. 3, August 1994.
6. Quine J P, "Distortion of Radiation Patterns for Leakage Power Transmitted Through Attenuation Cover Panels and Shielding Gasket-Need for Reverberation Chamber Measurement of Total Leakage Power", 1994 Int. Symp. on EMC, Chicago, pp. 285, 1994.
7. Harrington R F, "Resonant Behaviour of a Small Aperture Backed by a Conducting Body", IEEE Trans. on Antennas and Propagation, vol. AP-30, no. 2, pp. 205, March 1982.
8. Bäckström M, FOA Report FOA-D--95-00186-3.2--SE, October 1995 (in Swedish).
9. Crawford M L and Koepke G H, "Design, Evaluation, and Use of a Reverberation Chamber for Performing Electromagnetic Susceptibility/Vulnerability Measurements", National Bureau of Standards (USA) Technical Note 1092, April 1986.
10. King R W P and Wu T T, "The Scattering and Diffraction of Waves", Harvard University Press, Cambridge, Mass., p 126, 1959.
11. Private communication with Ulf Thibblin, Saab Military Aircraft, Dep TUST, S-581 88 Linköping, Sweden.





**MR. GARY ROAN
NAVAL RESEARCH LABORATORY**



TIME DOMAIN CHARACTERIZATION OF MODE STIRRED CHAMBERS

NSWCDD/MP-96/38

Gary T. Roan
Naval Research Laboratory
Washington, D.C.

REVERBERATION CHAMBER AND ANECHOIC CHAMBER
OPERATORS GROUP MEETING
DECEMBER 5-7, 1995

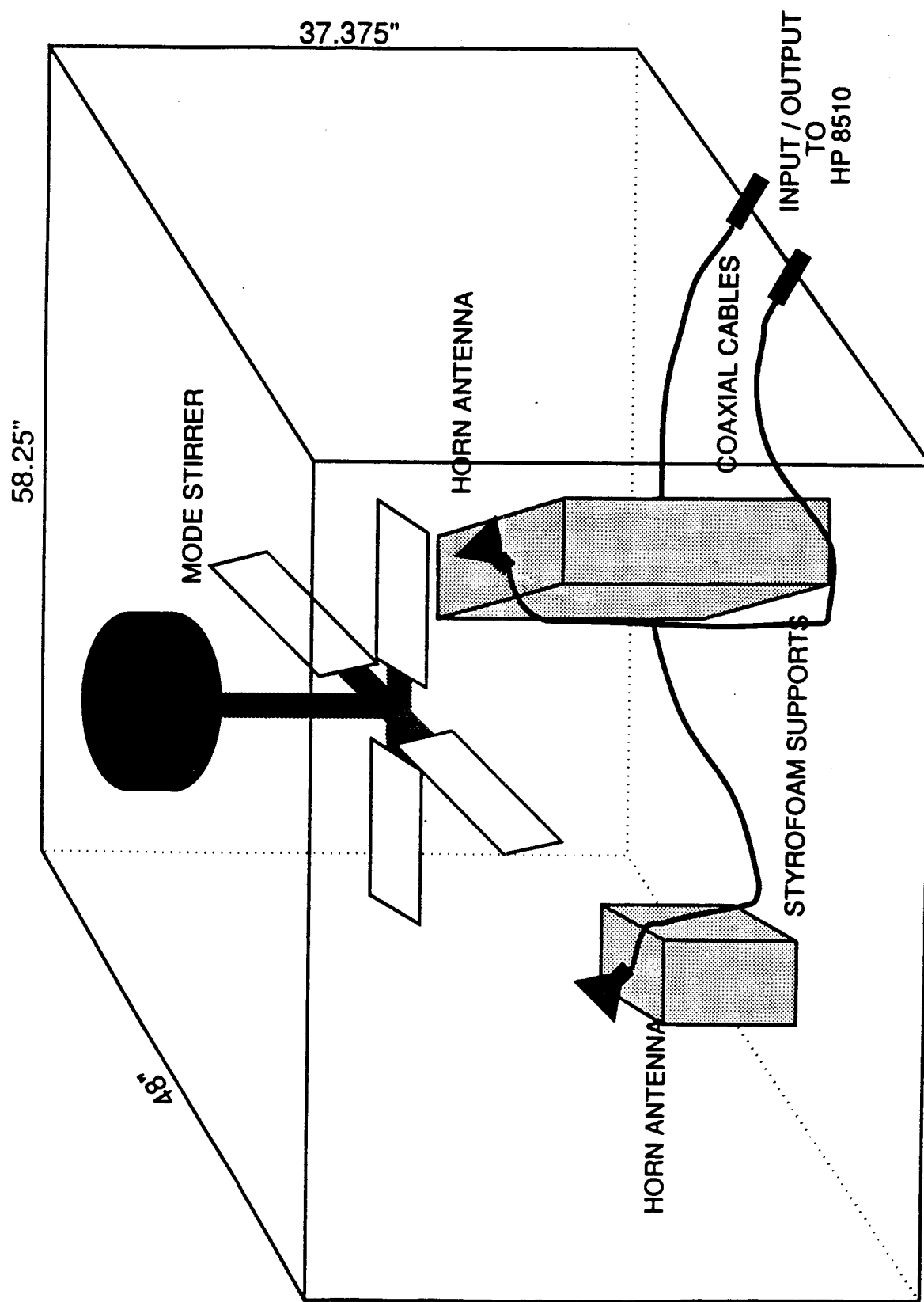
TIME DOMAIN CHARACTERIZATION

OBJECTIVES

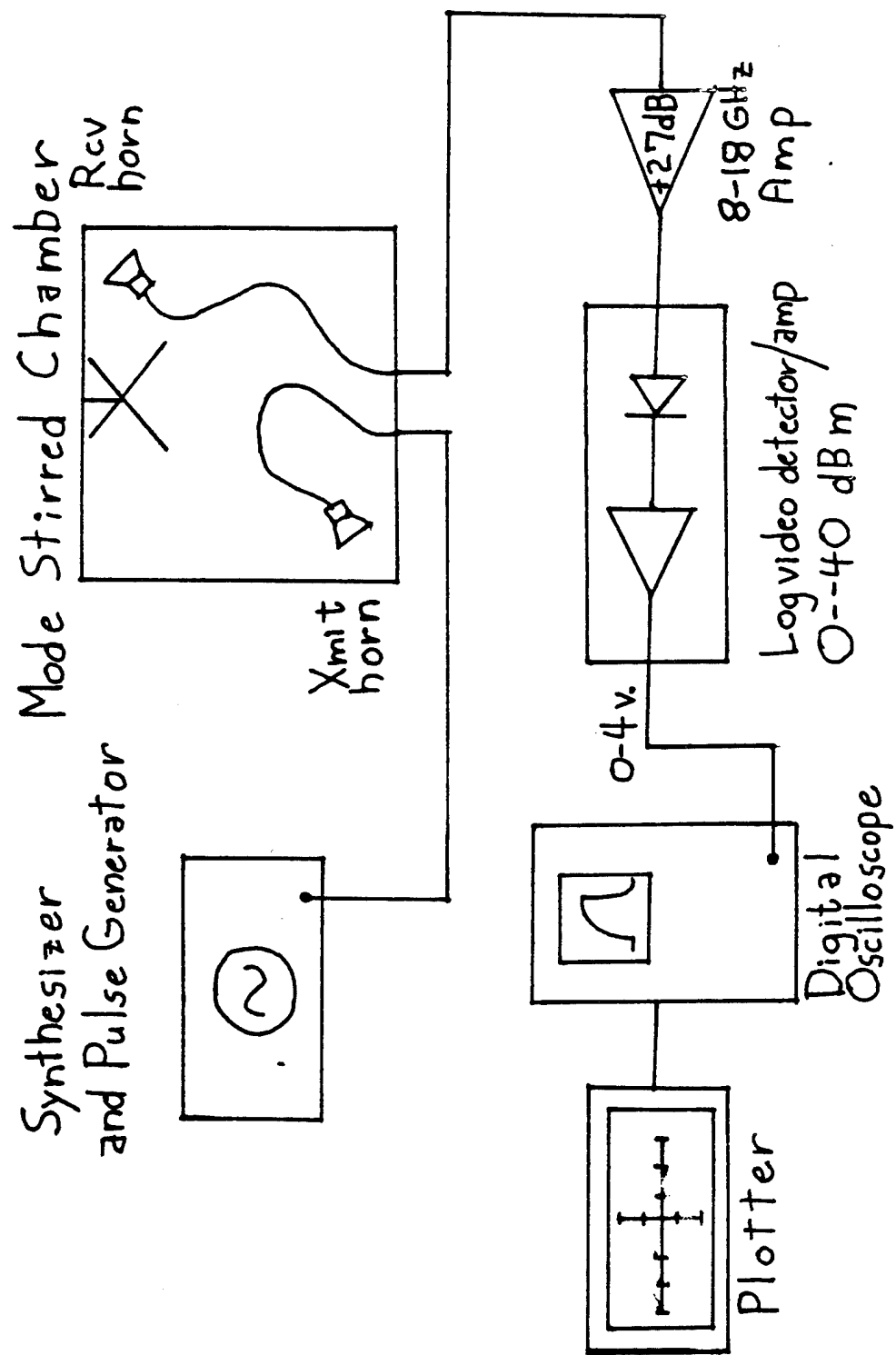
- Compare aluminum and steel chambers
- Minimum pulse width specification
- Effect of chamber loading on field levels
- Effect of loading on rise and fall times

This work was performed in cooperation Mike Hatfield of NSWC,
Dahlgren, Virginia

MODE-STIRRED REVERBERATING CHAMBER

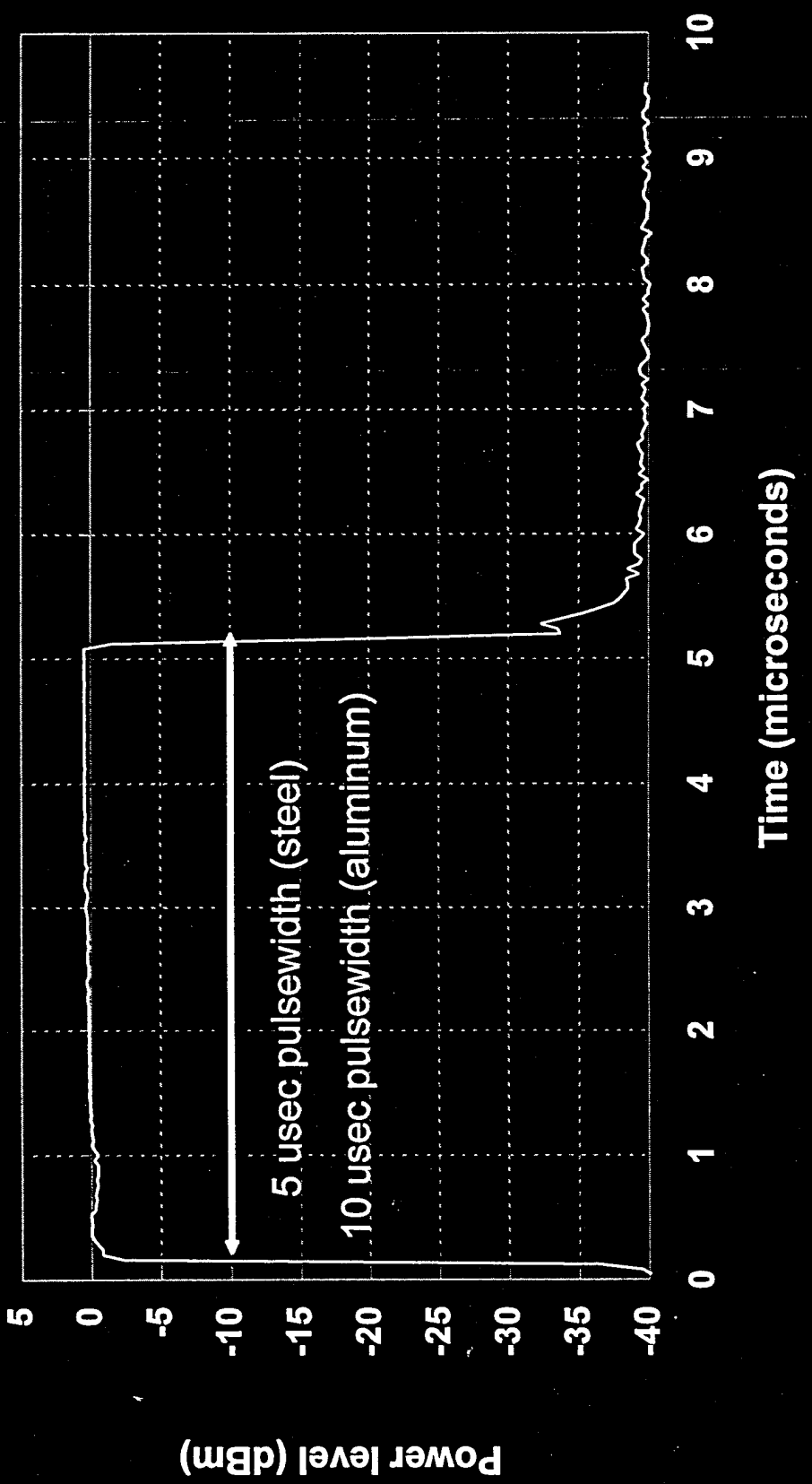


TEST CONFIGURATION FOR PULSE MEASUREMENTS



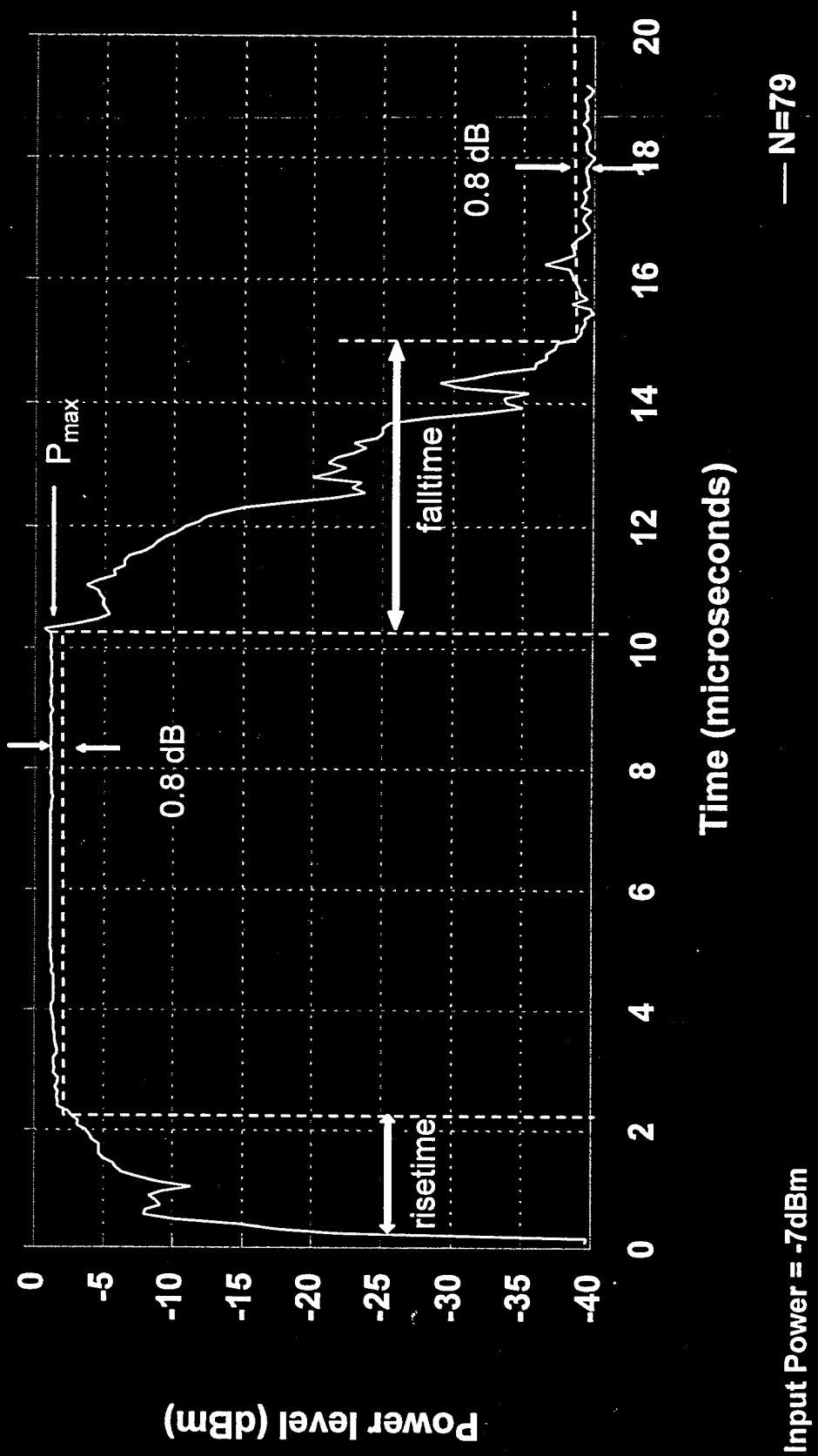
INPUT PULSE LEVEL vs. TIME

5 usec pulse at 9 GHz



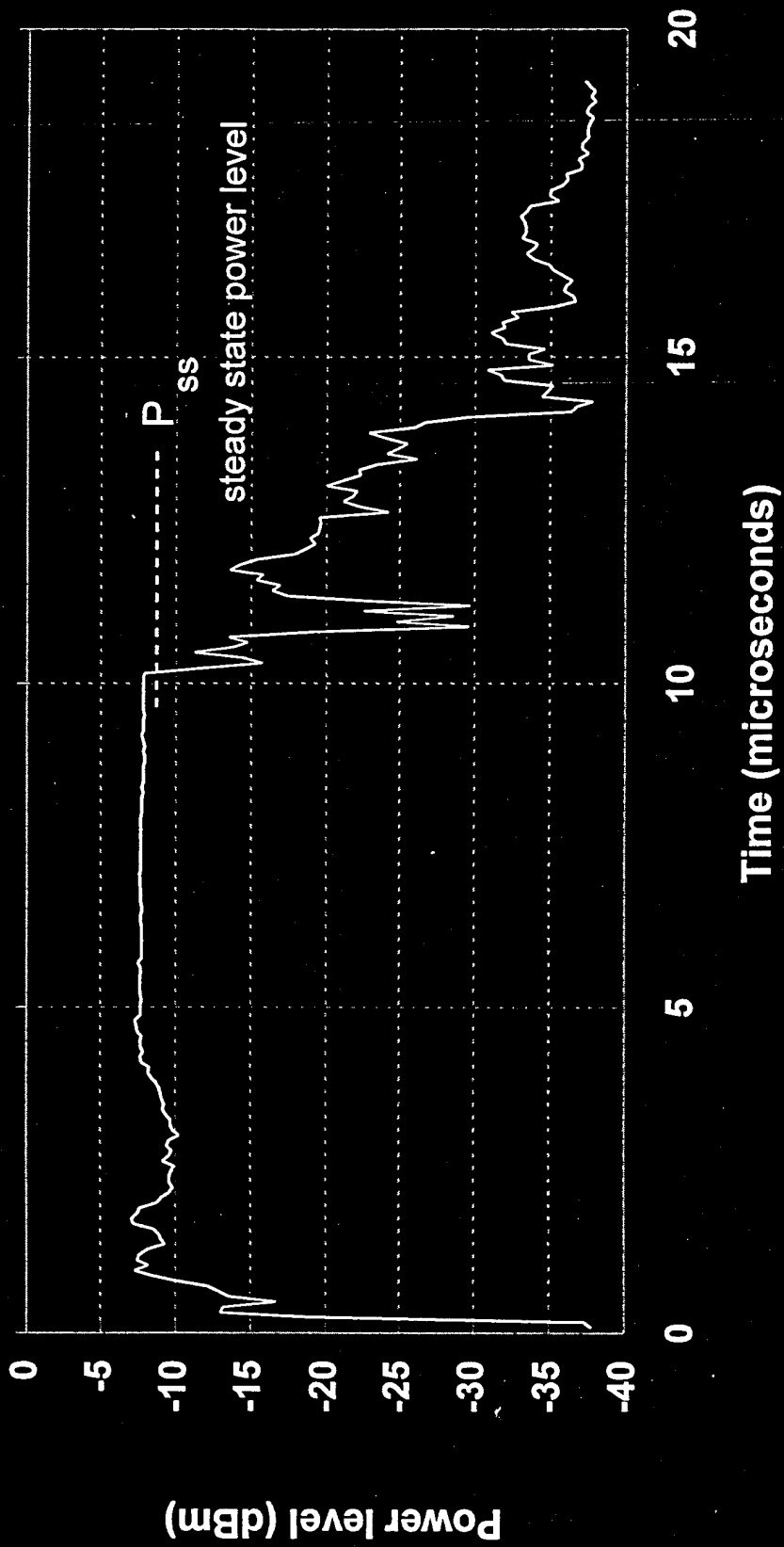
POWER LEVEL vs. TIME

Aluminum chamber at 9 GHz



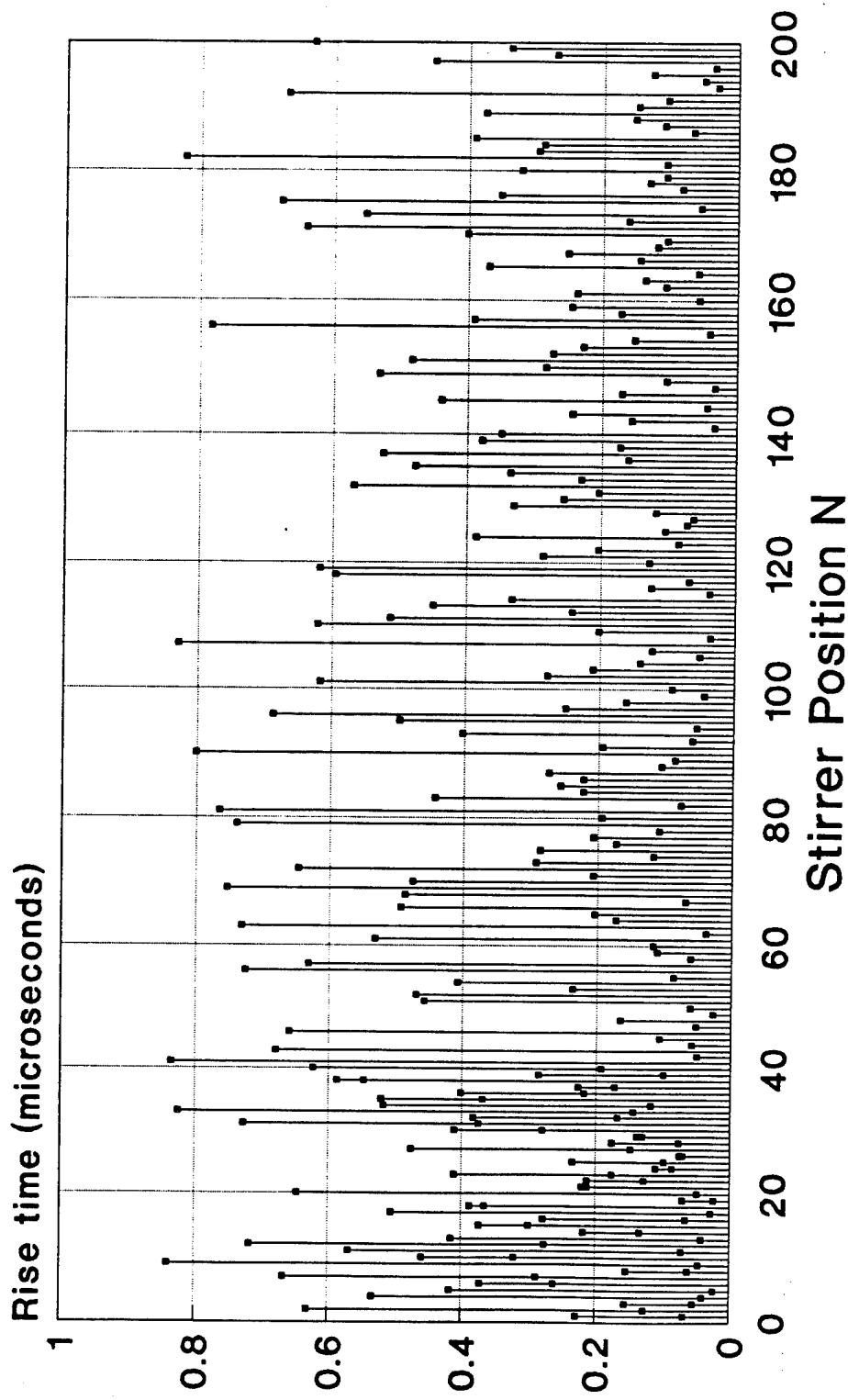
POWER LEVEL vs. TIME

Aluminum chamber at 9 GHz



RISE TIMES

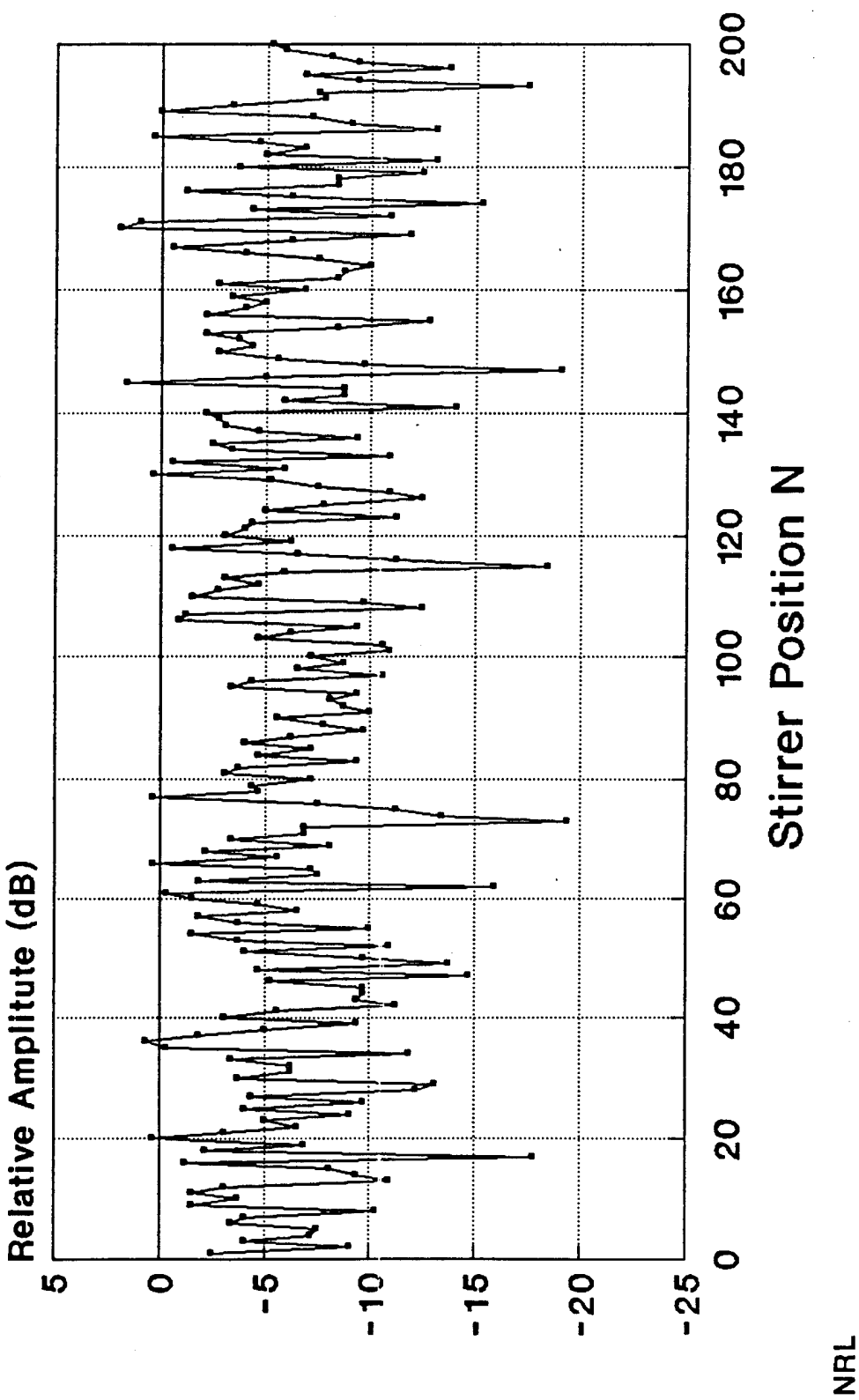
Steel Chamber @ 9 GHz



NRL

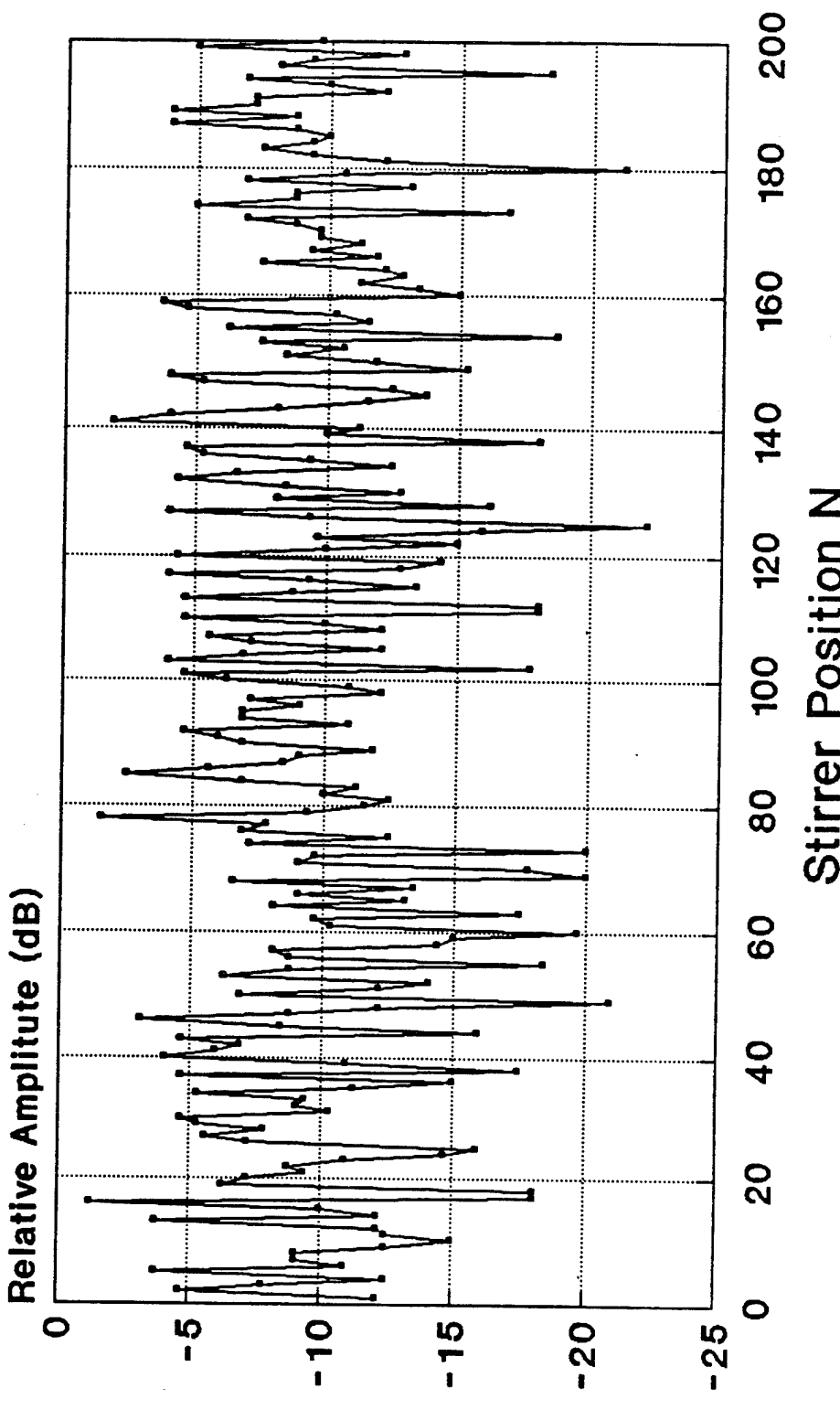
STEADY STATE AMPLITUDE

Steel Chamber @ 8 GHz



STEADY STATE AMPLITUDE

Aluminum Chamber @ 8 GHz

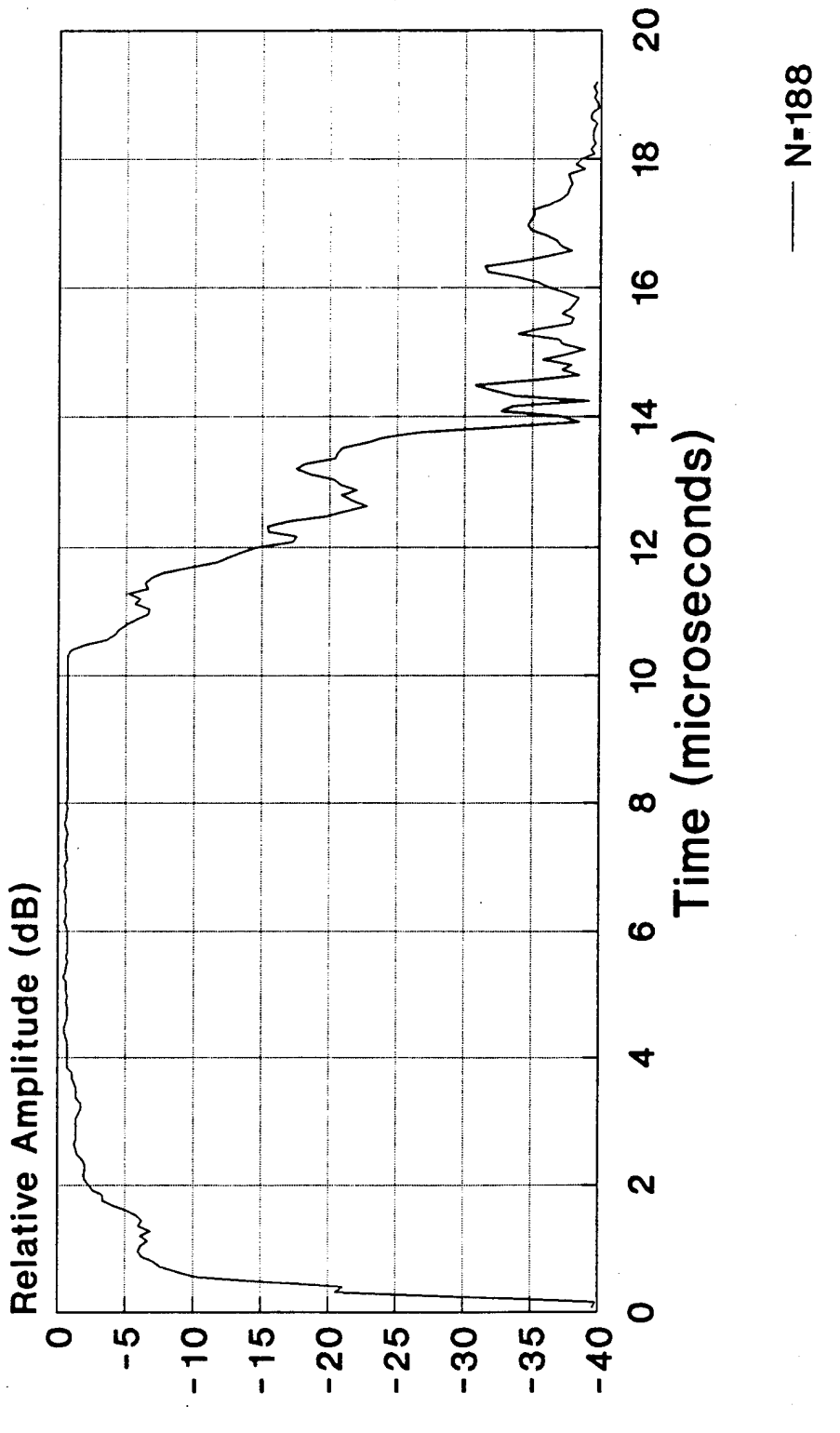


NRL

POWER LEVEL VS. TIME

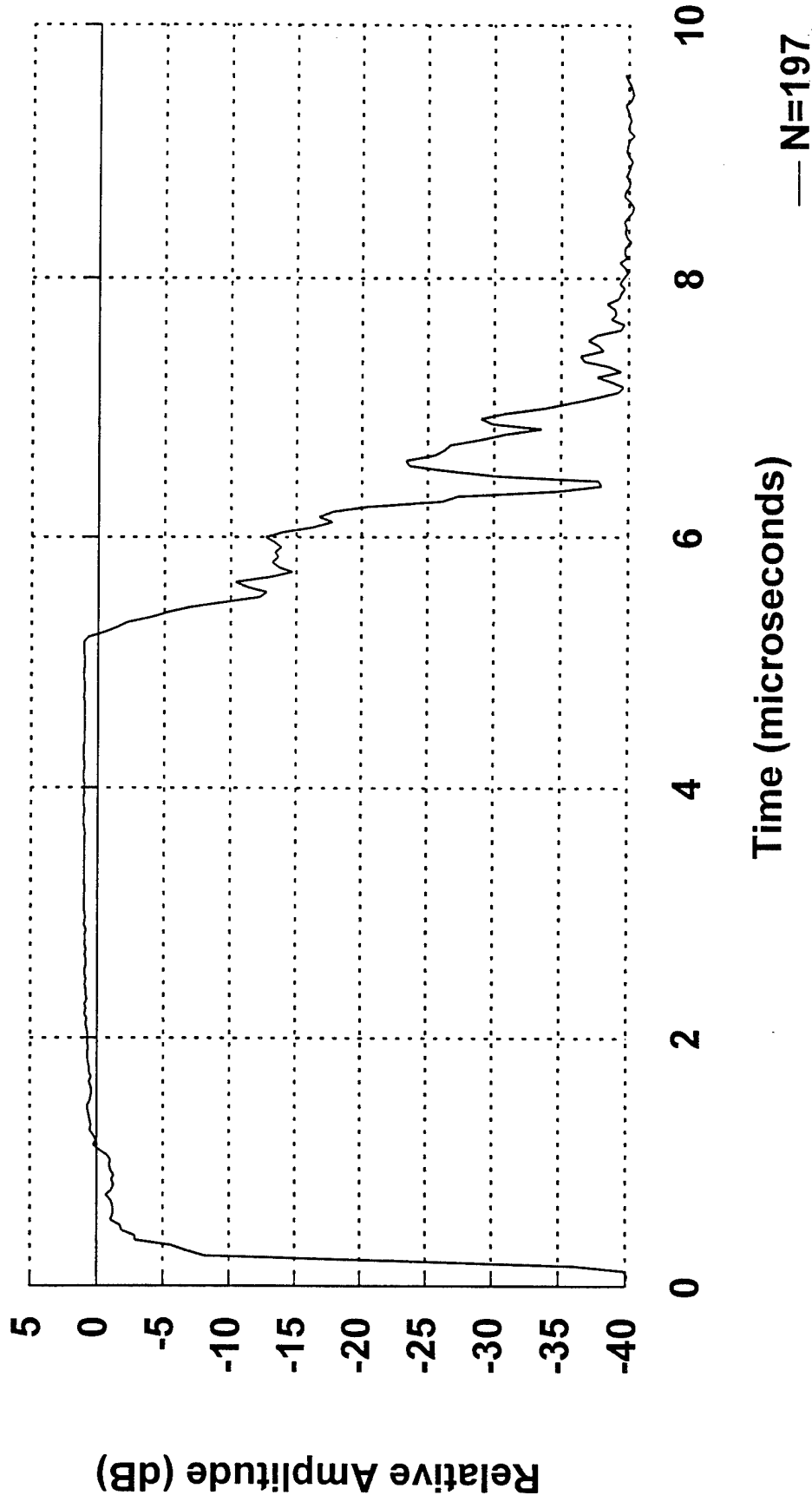
Aluminum chamber at 9 GHz

NSWCDD/MP-96/38



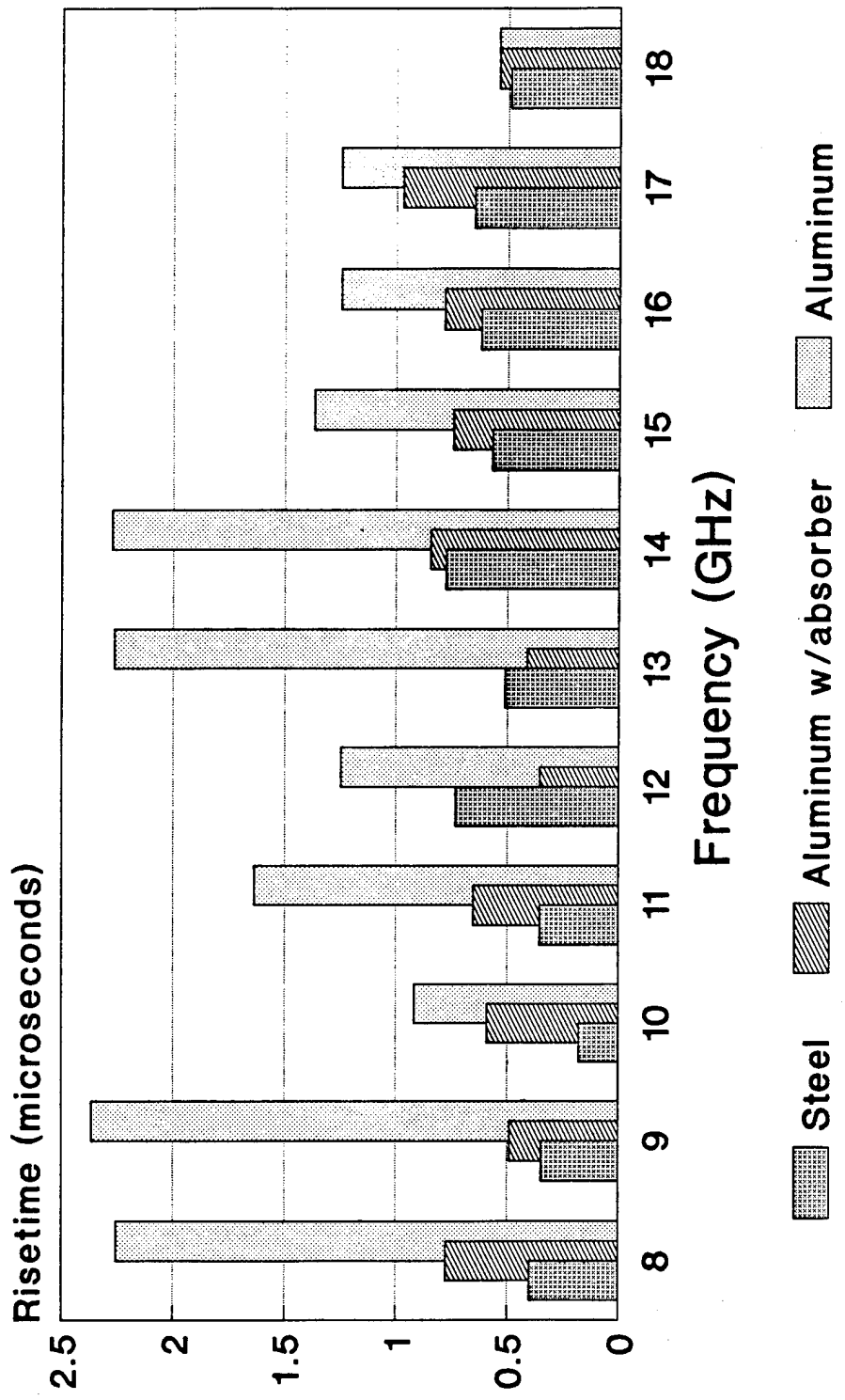
POWER LEVEL vs. TIME

Steel Chamber at 9 GHz



RISE TIME TO MAXIMUM POWER

Aluminum vs. Steel Chamber



Stirrer position for max power level

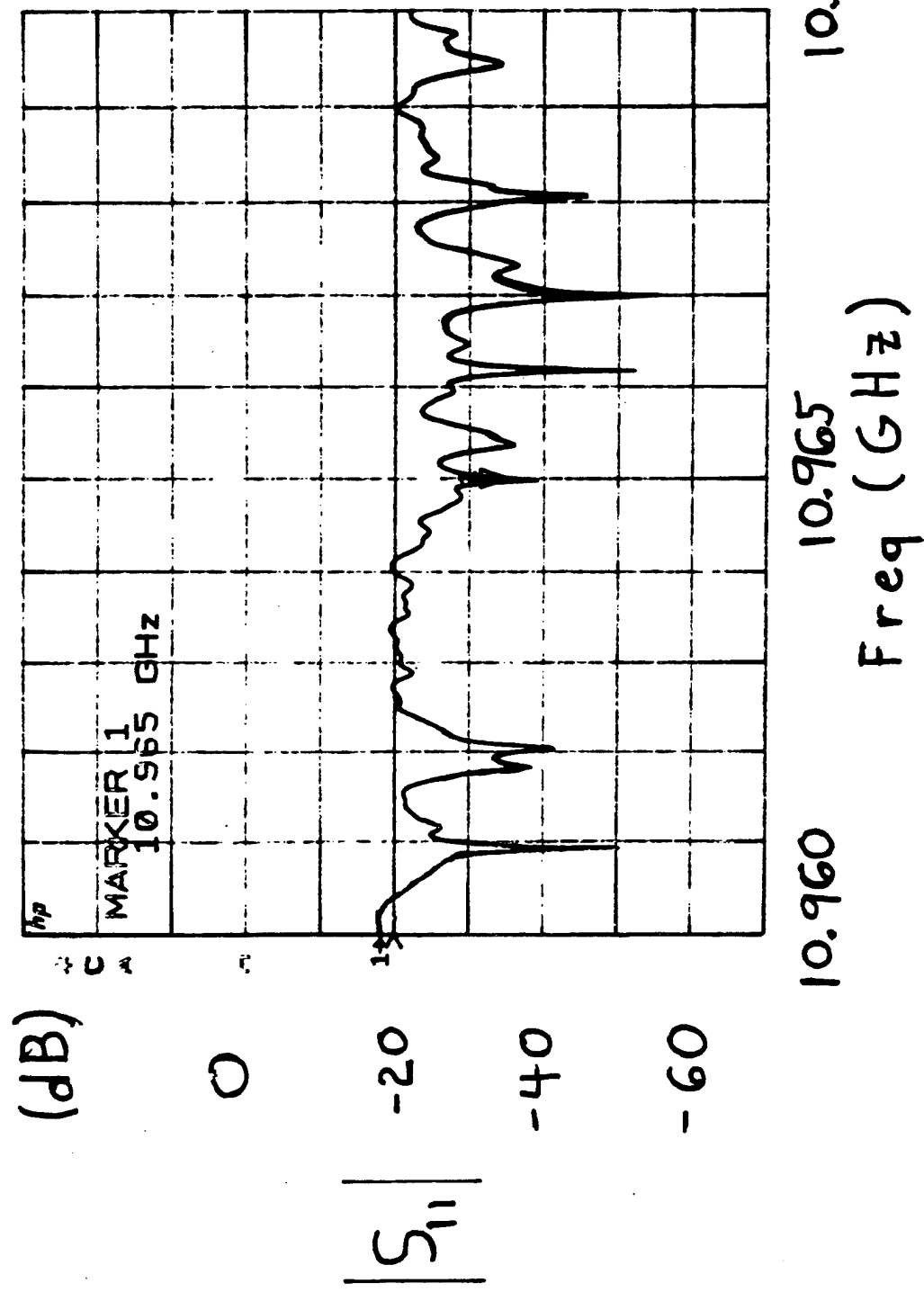
TIME DOMAIN CHARACTERIZATION SUMMARY OF FINDINGS

- Aluminum walls provide a 3x increase in power level and rise time over steel
- Pulse distortion is minimized when the steady state power level is maximized
- Proper mode-stirring is essential to ensure maximum power level for testing

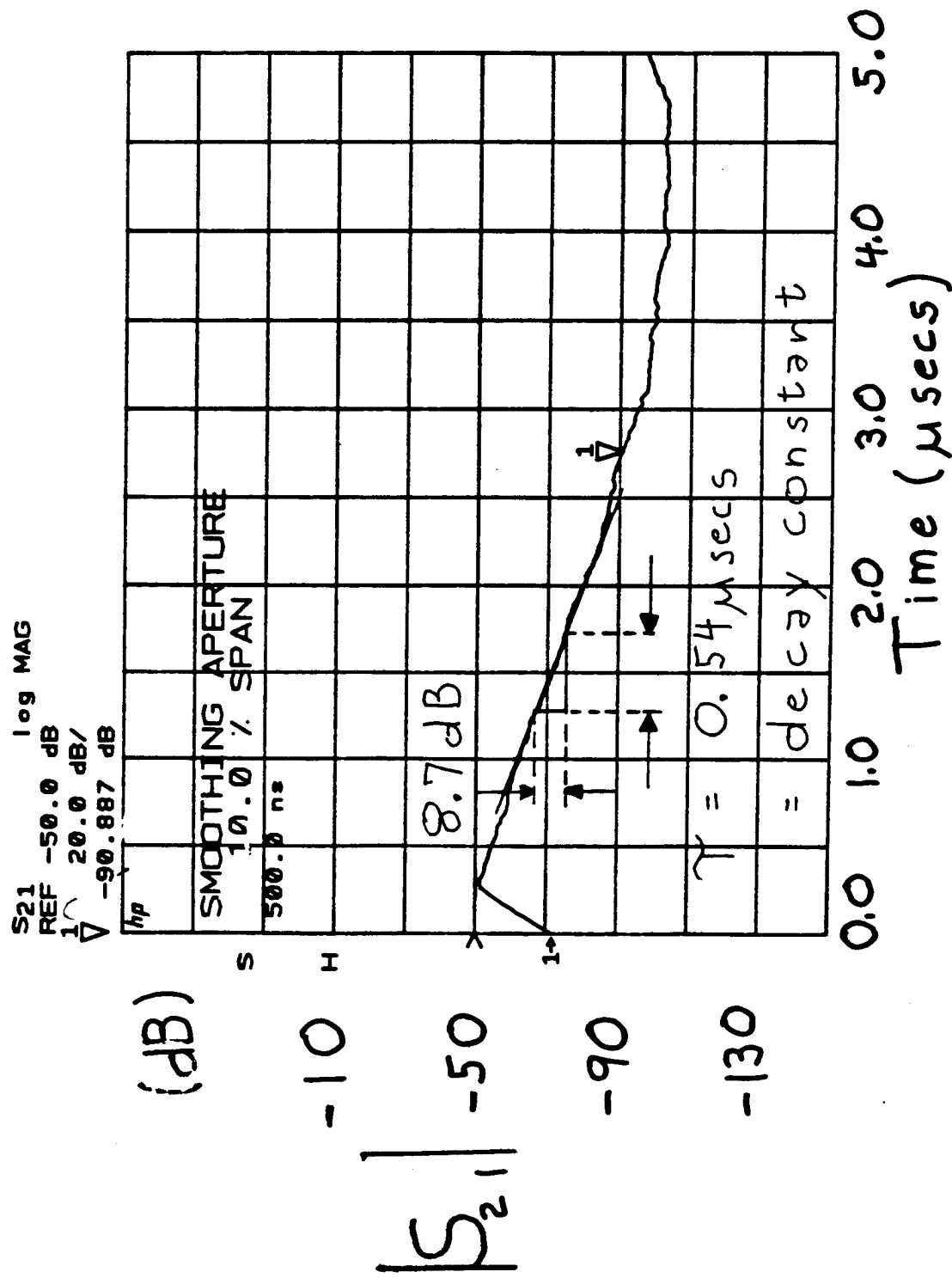
NRL

**MEASUREMENT OF DECAY CONSTANT
USING VECTOR NETWORK ANALYZER**

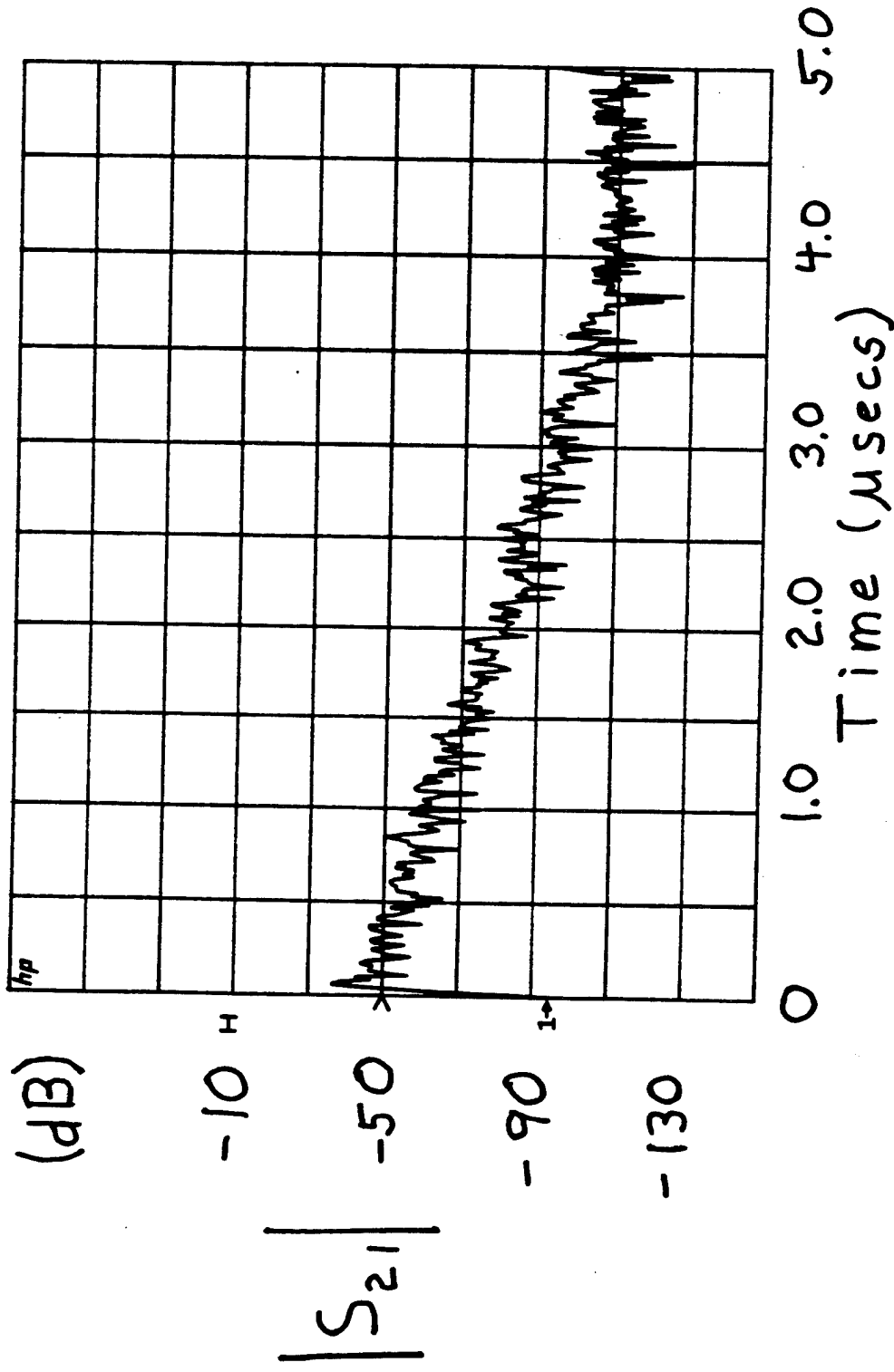
MAGNITUDE OF REFLECTION COEFFICIENT (S_{11})
FROM STEEL CHAMBER IN FREQUENCY DOMAIN



MAGNITUDE OF TRANSMISSION COEFFICIENT FROM STEEL CHAMBER AFTER SMOOTHING

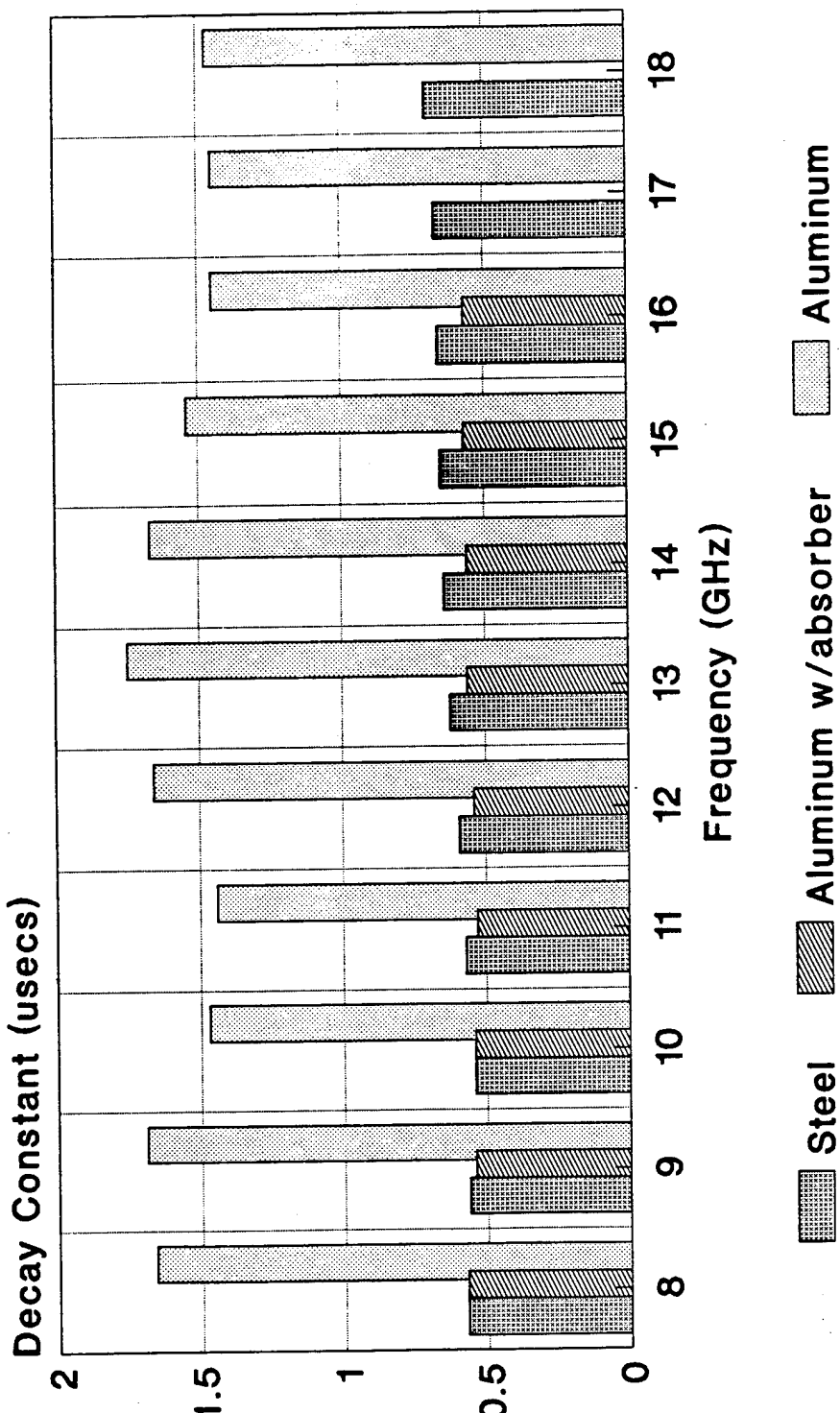


MAGNITUDE OF TRANSMISSION COEFFICIENT (S21)
FROM STEEL CHAMBER IN TIME DOMAIN



Decay Constant

Aluminum vs. Steel Chamber



NRL

Quality Factor Q

$$Q = \omega_0 \frac{\text{Stored energy}}{\text{Power Loss}}$$

$$= \omega_0 \frac{U}{P_L}$$

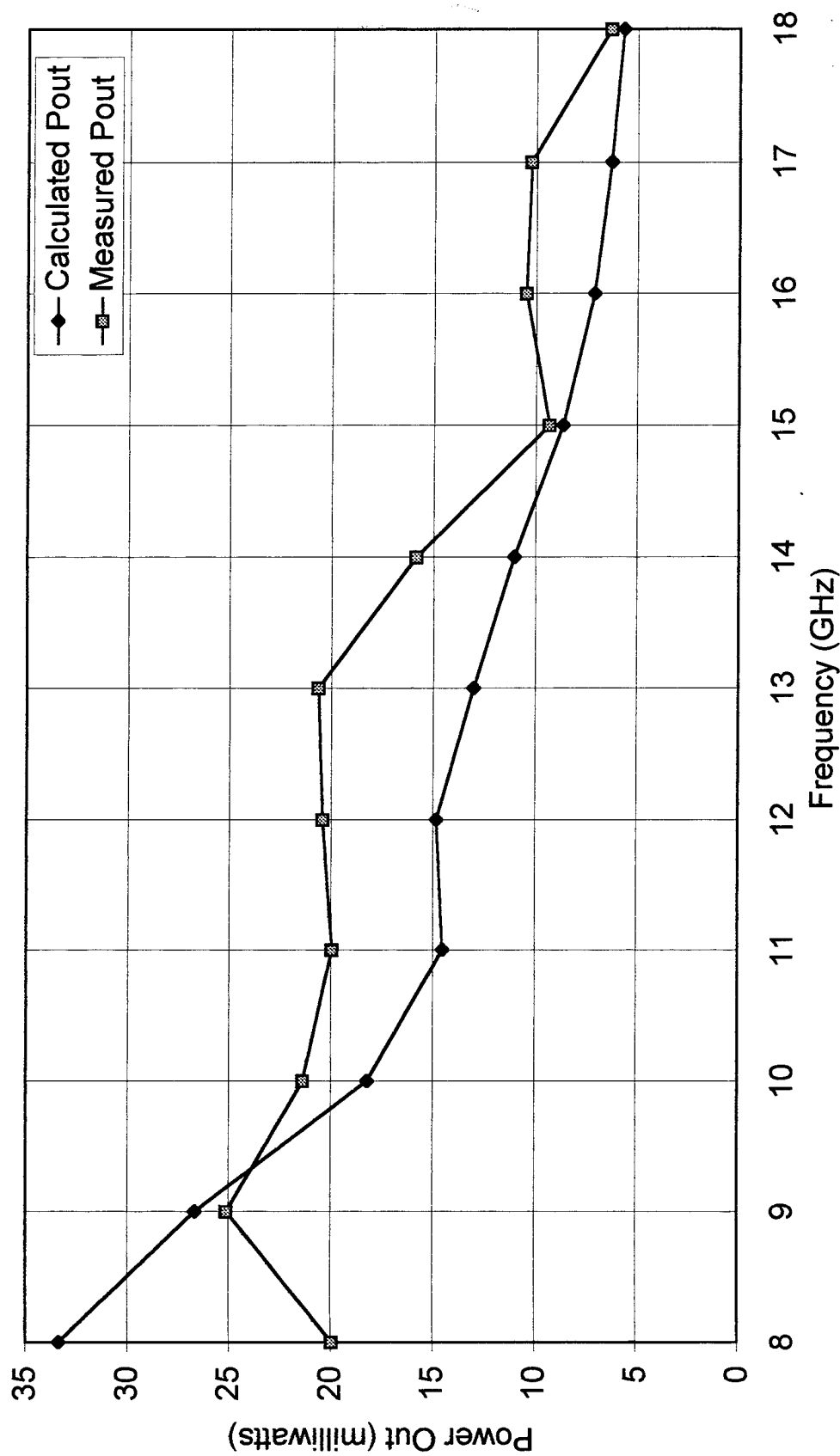
$$= 2 \omega_0 \tau$$

$$\overline{P_{av}} = \frac{U_C}{V} = \frac{2 P_L c}{V} \tau$$

$$A_e = \frac{\lambda^2}{8\pi}$$

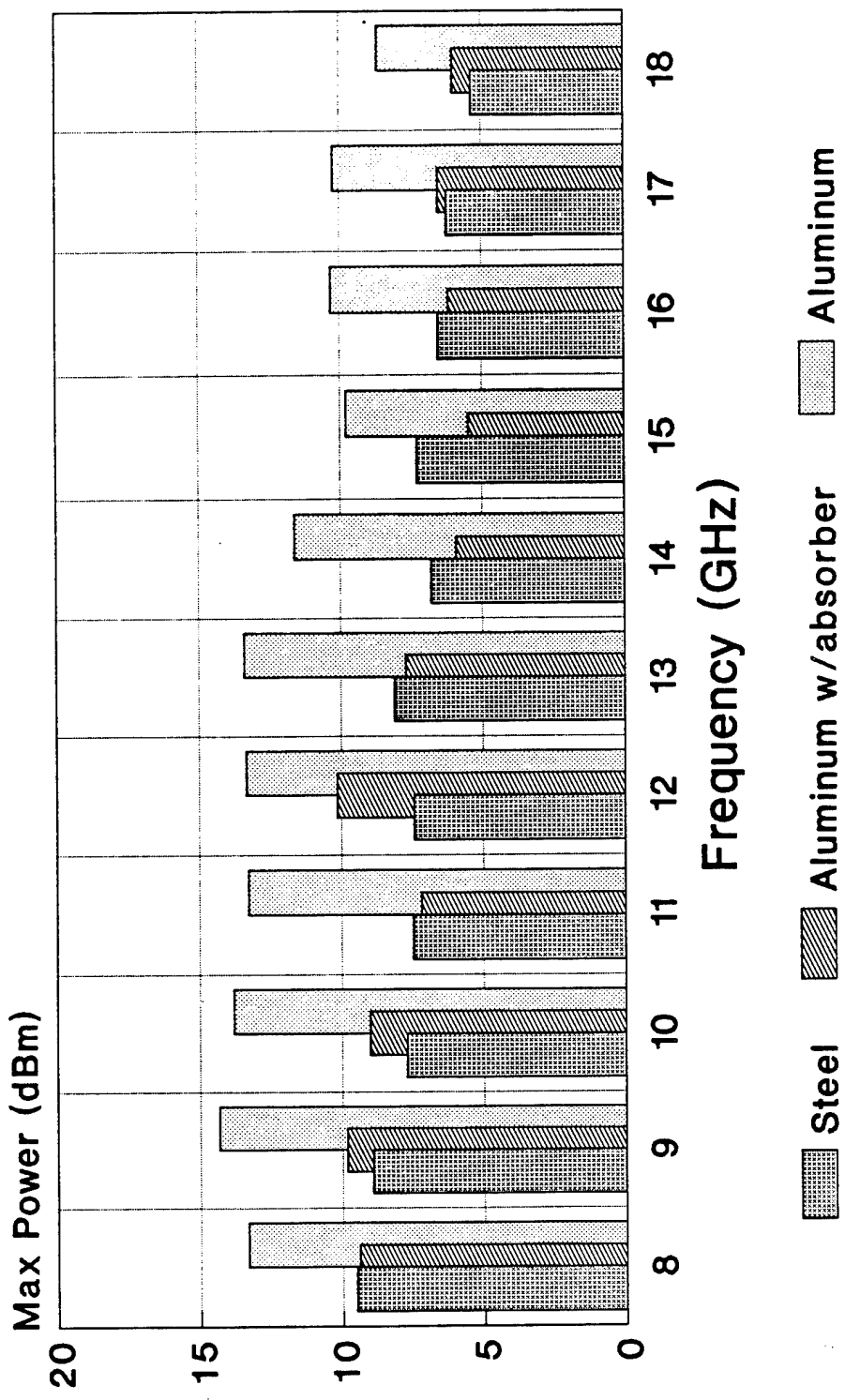
$$\overline{P_{out}} = \frac{c \lambda^2}{4\pi V} \tau P_{in}$$

Comparison of Calculated Power Out of the Aluminum Reverberation Chamber based on Decay Constant to Measured Power Out of Chamber for a One Watt Input Power



MAXIMUM STEADY STATE POWER LEVEL

Aluminum vs. Steel Chamber



Normalized to 1 watt input power

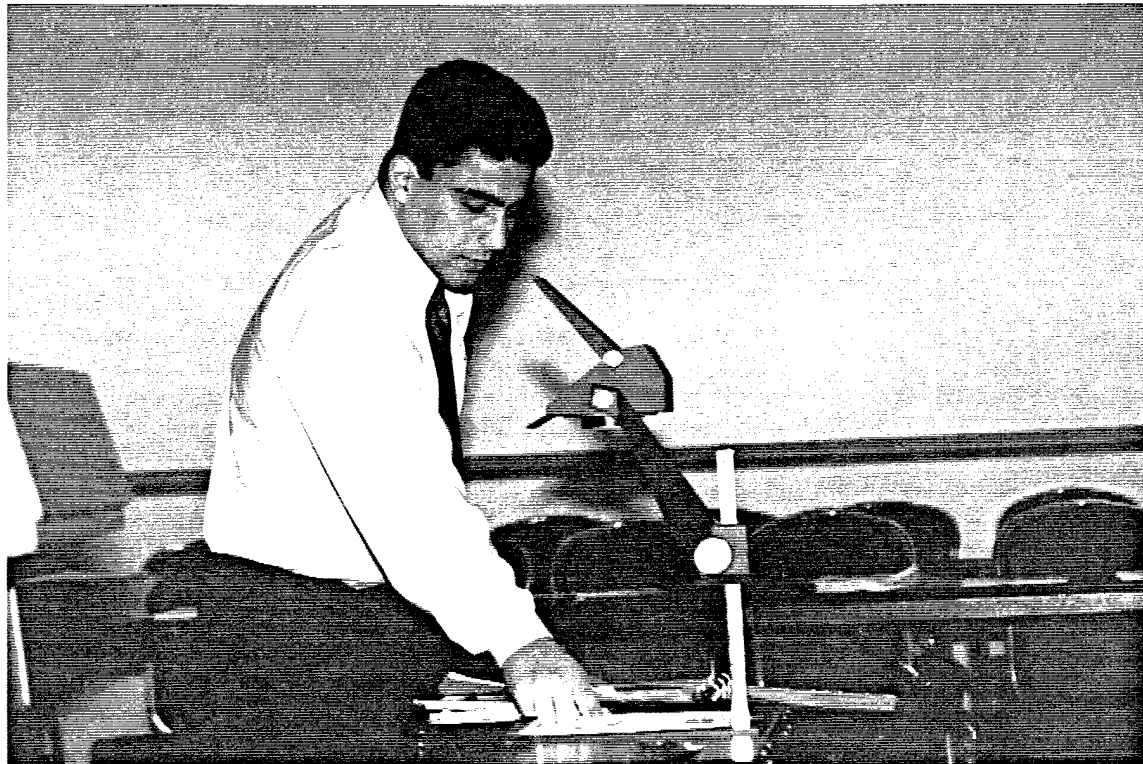
TIME DOMAIN CHARACTERIZATION SUMMARY OF FINDINGS (cont'd)

- The rf power density is proportional to the decay constant
- The decay constant is an accurate gauge of loading by the equipment under test
- Precise decay constant measurements are obtained with a network analyzer





**MR. PETER VOURAS
EG&G**



**HAZARDS OF ELECTROMAGNETIC RADIATION TO ORDNANCE (HERO)
SUSCEPTIBILITY OF COUNTERMEASURES SET ACOUSTIC (CSA) MK 2
SYSTEM: COMPARATIVE RESULTS OBTAINED FROM MODE-STIRRED
CHAMBER AND GROUND PLANE TEST FACILITIES**

Peter Vouras
EG&G

INTRODUCTION

A Countermeasures Set Acoustic (CSA) MK 2 was tested for the Hazards of Electromagnetic Radiation to Ordnance (HERO) on the ground plane at the Naval Surface Warfare Center, Dahlgren Division, and in the mode-stirred chamber. The ground plane is a large steel deck designed to simulate the electromagnetic environment on a ship's flight deck. Figure 1 shows the ground plane test facility with the CSA MK 2. Figure 2 is a closer view of the CSA MK 2. It is a long steel tube with an acoustic device inside and a gas generator on the aft end. The purpose of the test was to measure the ohmic heating in the system electroexplosive devices (EEDs) created by induced currents from the external electromagnetic environment. The EEDs were instrumented with fiber optic sensors which detect the temperature rise of the bridgewires in the EEDs and then the instrumentation system outputs a proportional analog voltage to a strip chart recorder. Figure 3 shows the mode-stirred chamber test configuration. The mode-stirred chamber is a large metal enclosure with highly reflective walls. Electromagnetic energy is transmitted into the chamber from transmitting antennas. Large metallic paddle wheels on the ceiling rotate and change the boundary conditions in the chamber. The result is that the peak of the environment moves through the chamber as if the system under test was being radiated from all possible aspect angles. Figure 4 is a closer view of the CSA MK 2 in the mode-stirred chamber.

EXPECTED CORRELATION BETWEEN GROUND PLANE AND
MODE-STIRRED CHAMBER TEST RESULTS

The directivity, D , of an antenna is a measure of the extent to which an antenna pattern is focused in a given direction in space. It is defined as,¹

$$D = 4\pi \frac{F_{MAX}}{P_{RAD}}, \quad (1)$$

where F_{MAX} is the maximum value of radiation intensity, F , and P_{RAD} is the total power radiated by the antenna. The directivity may be considered as the ratio of the peak radiation intensity to the average radiation intensity. In the mode-stirred chamber, the peak of the electromagnetic field moves through space as the paddle wheels rotate. After one complete revolution of the paddle wheels, every point in the chamber will have seen the peak electromagnetic field.² Therefore, on average, the directivity in the chamber is unity, $D_{MSC} = 1$. For receiving antennas, it is useful to define an effective area, A_e , that represents the "capture area" the antenna presents to an incident plane wave,¹

$$A_e = \frac{P_L}{S_i}, \quad (2)$$

where P_L is the power delivered to the load of the antenna, which is assumed lossless, and S_i is the incident power

density. The following relation exists between the directivity and the effective area of an antenna,¹

$$D = 4\pi \frac{A_e}{\lambda^2}, \quad (3)$$

where λ is the wavelength. Using the above equations, the ratio of the effective area of an antenna on the ground plane to its effective area in the mode-stirred chamber may be written as,

$$\frac{A_{eGP}}{A_{eMSC}} = \frac{\lambda^2 D_{GP}}{4\pi} \frac{4\pi}{\lambda^2 D_{MSC}} = \frac{D_{GP}}{D_{MSC}} = D_{GP}, \quad (4)$$

where D_{GP} is the free space directivity of the antenna. For a lossless antenna, the power gain, G , equals the directivity, D .³ Thus one would expect the susceptibility measurements obtained on the ground plane to be greater than the results in the chamber by the factor G .

CORRECTION MADE NECESSARY BY IMPERFECT ANTENNAS

In a practical antenna, which is not lossless, the gain is not equal to the directivity. Instead, the gain is equal to the directivity times an efficiency factor, η , which takes into account the losses in the antenna,³

$$G = \eta D_{GP}. \quad (5)$$

Thus, assuming the environment in the chamber is perfectly uniform, the measurements obtained on the ground plane should be greater than those in the chamber by the corrected factor,

$$D_{GP} = \frac{G}{\eta}. \quad (6)$$

The gain G is defined as the maximum radiation intensity from the antenna divided by the radiation intensity from a lossless isotropic source with the same power input. If the field in the chamber is not perfectly uniform, than the correlation factor between mode-stirred chamber and ground plane results is simply the ratio of the antenna directivities in each environment, D_{GP}/D_{MSC} .

Another correction is necessary if the antenna is not terminated in a matched load. Then the power coupled out of the environment into the antenna can not be accurately determined by measuring the power dissipated in the antenna load because a portion of the power is being reradiated. The magnitude of the power, P_R , reflected from the antenna terminals is proportional to the square of the current reflection coefficient. This reflected power is,⁴

$$P_R = \gamma^2 \frac{G \lambda^2}{4\pi} S_i, \quad (7)$$

where S_i is the incident power density and γ is the current reflection coefficient. Therefore, one must account for

how efficiently antennas are capable of converting received energy into measurable heat so that the total power coupled out of the chamber environment can be accurately determined. Without this correction, different antennas in the chamber will not appear isotropic.

The effective area of an ideal antenna in the mode-stirred chamber may be determined by rearranging equation (3),

$$A_e = \frac{\lambda^2 D_{MSC}}{4\pi} = \frac{\lambda^2}{4\pi}. \quad (8)$$

Figure 5 graphs the effective area of an ideal antenna in the mode-stirred chamber as a function of frequency. Deviations of a practical antenna from this characteristic will be due to ohmic losses in the antenna and the power reradiated from a mismatched antenna load.

TEST DATA

Figure 6 shows the peak current measured in the mode-stirred chamber in any electroexplosive device and the peak current measured on the ground plane in any electroexplosive device as a function of frequency. The currents are normalized to an arbitrary power level to permit comparisons. The correlation coefficient between the two curves is 0.42. The correlation coefficient, ρ , is a statistical parameter which describes the extent to which two random variables, X and Y, are coupled. If $\rho = 0$, then X and Y are independent. If $\rho = 1$, then if X is high, Y is likely to be high. If $\rho = -1$, then Y is likely to be low when X is high. Figure 7 shows the sum total of the measured currents in all the EEDs for the mode-stirred chamber and the ground plane. The correlation coefficient between these curves is higher, $\rho = 0.77$. The reason is that the sum total of measured currents in the EEDs is a better indicator of the total energy coupled out of the electromagnetic environment by the system than the peak measured current in any one EED.

COUPLING OF ENERGY INTO THE SYSTEM IS A RANDOM PROCESS

The induced current profile in any one EED may have a deterministic form. But, it is a random variable $X(t, \zeta_i)$ which depends on time, t, and the probability of choosing the outcome ζ_i from a sample space, S. Figure 8 shows one such random variable $X(t, \zeta_1)$ where ζ_1 is fixed. It is a graph, or equivalently a statistical realization, of the temperature profile of an EED in the CSA MK 2 system caused by induced currents in the mode-stirred chamber at the frequency 441 MHz. An ensemble of indexed random variables, $X(t_k, \zeta_i)$, where the index, t_k , is successive increments of time constitutes a random process. Figure 9 is the ensemble of all the measured signals in the EEDs at 441 MHz in the mode-stirred chamber. This ensemble represents a random process. The correlation matrix,

$$X = \begin{bmatrix} \rho_{11} & \rho_{12} & \rho_{13} & \rho_{14} \\ \rho_{21} & \rho_{22} & \rho_{23} & \rho_{24} \\ \rho_{31} & \rho_{32} & \rho_{33} & \rho_{34} \\ \rho_{41} & \rho_{42} & \rho_{43} & \rho_{44} \end{bmatrix}, \quad (9)$$

summarizes the coupling between the signals. The diagonal of the matrix will be one and the elements of the matrix

will be the same above and below the diagonal. The correlation coefficient, ρ_{ij} , represents the coupling between the signal, i , and the signal, j , over all time. For the ensemble shown in Figure 9 the correlation matrix is,

$$X = \begin{bmatrix} 1.00 & 0.76 & 0.33 & 0.25 \\ 0.76 & 1.00 & 0.42 & 0.31 \\ 0.33 & 0.42 & 1.00 & 0.39 \\ 0.25 & 0.31 & 0.39 & 1.00 \end{bmatrix}, \quad (10)$$

It is evident that all the signals, except perhaps signal 1 and signal 2, are not well coupled because $\rho_{ij} \neq 1$ when $i \neq j$.

Figure 10 illustrates the internal configuration of components in a typical system such as the CSA MK 2. Each internal wire may be represented by a dipole. The system enclosure comprises a cavity through which electromagnetic energy penetrates. The energy that is incident on the cavity aperture will illuminate the internal dipoles to varying degrees depending on the aspect angle of the transmitting antenna and the orientation of the internal wires. Thus, it is important that all aspect angles be illuminated on the ground plane, not only to find the direction of maximum gain, but also to illuminate all the internal components. At a given frequency, antenna A is a dipole of length l_1 that is terminated in a matched resistive load, R . Antenna B is a dipole of the same length terminated in a mismatched impedance, Z_1 . Therefore, antenna B will reradiate some energy. Antenna C is a dipole of different length, l_2 , and load impedance, Z_2 . At this frequency, antenna A resonates, so it will absorb a greater amount of the internal energy.

Figure 11 shows the decibel spread in magnitude between the lowest current measured in an EED and the highest current measured in an EED at any given frequency in the mode-stirred chamber or on the ground plane. Clearly, some wide ranges are possible, which is to be expected if the signals are loosely coupled. Figure 12 is a graph of the difference in decibels referenced to 1 mA between the test results in the mode-stirred chamber and the test results on the ground plane. The median difference between chamber results and ground plane results is 2.59 dB_{mA} when comparing peak values and 1.96 dB_{mA} when comparing the total currents induced in each environment. Any sources of error are likely due to not illuminating the system from all aspect angles on the ground plane.

STATISTICAL PROPERTIES OF THE COUPLING PROCESS

Because the environment in the mode-stirred chamber is random, the energy coupled into the EEDs is a random process. The properties of this process may be investigated by writing the signals in matrix form where each signal is a row vector and each sequential time sample is a column vector. For example, the first seven time samples in the signal matrix are

$$\begin{bmatrix} & t=1 & t=2 & t=3 & t=4 & t=5 & t=6 & t=7 \\ Signal 1 & 10.39 & 14.69 & 16.43 & 18.00 & 10.39 & 14.69 & 10.39 \\ Signal 2 & 10.00 & 14.14 & 17.32 & 18.70 & 10.00 & 14.14 & 10.00 \\ Signal 3 & 13.47 & 15.55 & 14.75 & 28.04 & 29.10 & 15.55 & 13.47 \\ Signal 4 & 10.73 & 18.59 & 18.59 & 10.73 & 10.73 & 15.17 & 15.17 \end{bmatrix}.$$

If the random process is stationary, then the nature of the randomness in the process does not change with time.⁵

A characteristic of stationary processes is that the mean is constant with time. Figure 13 shows the average of each column in the signal matrix. As is evident, the mean of the ensemble is not very constant. Therefore, the process is not very stationary, which may be expected because the rotating paddle wheels stir the field in the chamber and change the coupling to the system.

Each column in the signal matrix may be thought of as a random variable. Therefore, the correlation coefficient may be computed for every possible pair of time samples. The result is another matrix with approximately 30,000 elements. A few of the elements in this matrix are

	$t=1$	$t=2$	$t=3$	$t=4$	$t=5$	$t=6$	$t=7$
$t=1$	1.00	0.10	-0.76	0.76	0.98	0.84	0.47
$t=2$	0.10	1.00	0.52	-0.56	-0.03	0.57	0.92
$t=3$	-0.76	0.52	1.00	-0.96	-0.82	-0.39	0.18
$t=4$	0.76	-0.56	-0.96	1.00	0.84	0.31	-0.20
$t=5$	0.98	-0.03	-0.82	0.84	1.00	0.74	0.35
$t=6$	0.84	0.57	-0.39	0.31	0.74	1.00	0.80
$t=7$	0.47	0.92	0.18	-0.20	0.35	0.80	1.00

The entry at row 3 and column 7, for example, represents the correlation between the third and seventh time samples, which is very low, 0.18. If the process was stationary, then the diagonals of the matrix would not change drastically. In this case, however, it is evident that the diagonals do change much. For instance, the diagonal {0.10, 0.52, -0.96, 0.84, 0.74, 0.80} almost spans the entire possible range from -1 to 1. Figure 14 is a graph of all the diagonals. It is clear that they span a wide range.

The first row of the matrix represents the correlation of the first time sample of the ensemble with every subsequent time sample. It is graphed in Figure 15. This graph indicates how fast the random process is changing. If successive samples are remaining highly correlated, than the probability of a drastic change in the process during that time interval is very small. As is evident in Figure 15 there are times when the samples are well correlated and then as the paddle wheels rotate they become uncorrelated. Over one complete revolution of the field stirrers, the transition from correlated to uncorrelated samples should be periodic. It is clear in Figure 15 that there is some periodicity. Consider the null at 30 time samples after the origin. It is repeated approximately 30 time samples before the end of the paddle wheel rotation. The correlation at the origin is a maximum because the time increment between the first and the next couple of samples is small. As the paddle wheels return to their original position, one would expect the correlation of the samples to approach a maximum again. Indeed, the correlation at the origin is 1, and the correlation at the last sample is about 0.85.

If the random process has the property that it is ergodic, than the time autocorrelation of one signal should converge to the autocorrelation of the ensemble. The time autocorrelation of one signal is found by calculating the convolution of the signal with a time-reversed version of itself where the last sample becomes the first. Figure 16 shows the time autocorrelation of each signal. Clearly, they do not converge to the autocorrelation of the ensemble and the process is not ergodic.

By taking the fourier transform of the ensemble autocorrelation, one can estimate the power spectrum of the process. This is shown in Figure 17 and again in Figure 18 using decibel notation. The frequency axis of each graph is normalized such that the sampling frequency does not need to be taken into account. To convert the frequency axis to Hertz, divide by π and multiply by the sampling frequency. The largest frequency component of

the ensemble is the power at the origin which is the DC or average power of the process. It is about 10 dB greater than the noise floor. One would expect a large DC power component because the observed signals during the test were steady-state temperatures of the EED bridgewires. The thermal time constant of each bridgewire is of the order of 10 milliseconds and therefore the bridgewire can not respond to rapidly changing stimuli.

The power spectrum of one signal may also be calculated by taking the fourier transform of the signal amplitude squared. This spectrum is shown in Figure 19 and also in Figure 20 using decibels referenced to 1 milliwatt. Again, there is a relatively large DC component. However, this power is buried in the noise floor and can not be measured directly.

There are two parameters which describe the performance of the mode-stirred chamber. The first is the ratio of peak to minimum received power. A lower bound for this ratio may be found by taking the peak power of the ensemble and dividing it by the average power shown in Figure 17, since the minimum received power in each signal can not be seperated from noise. The value obtained is 18.4 dB. If the field stirring in the chamber was complete, than this value should be 20 dB. Since the approximated value is very close to the predicted value it seems that the field in the chamber was well stirred.

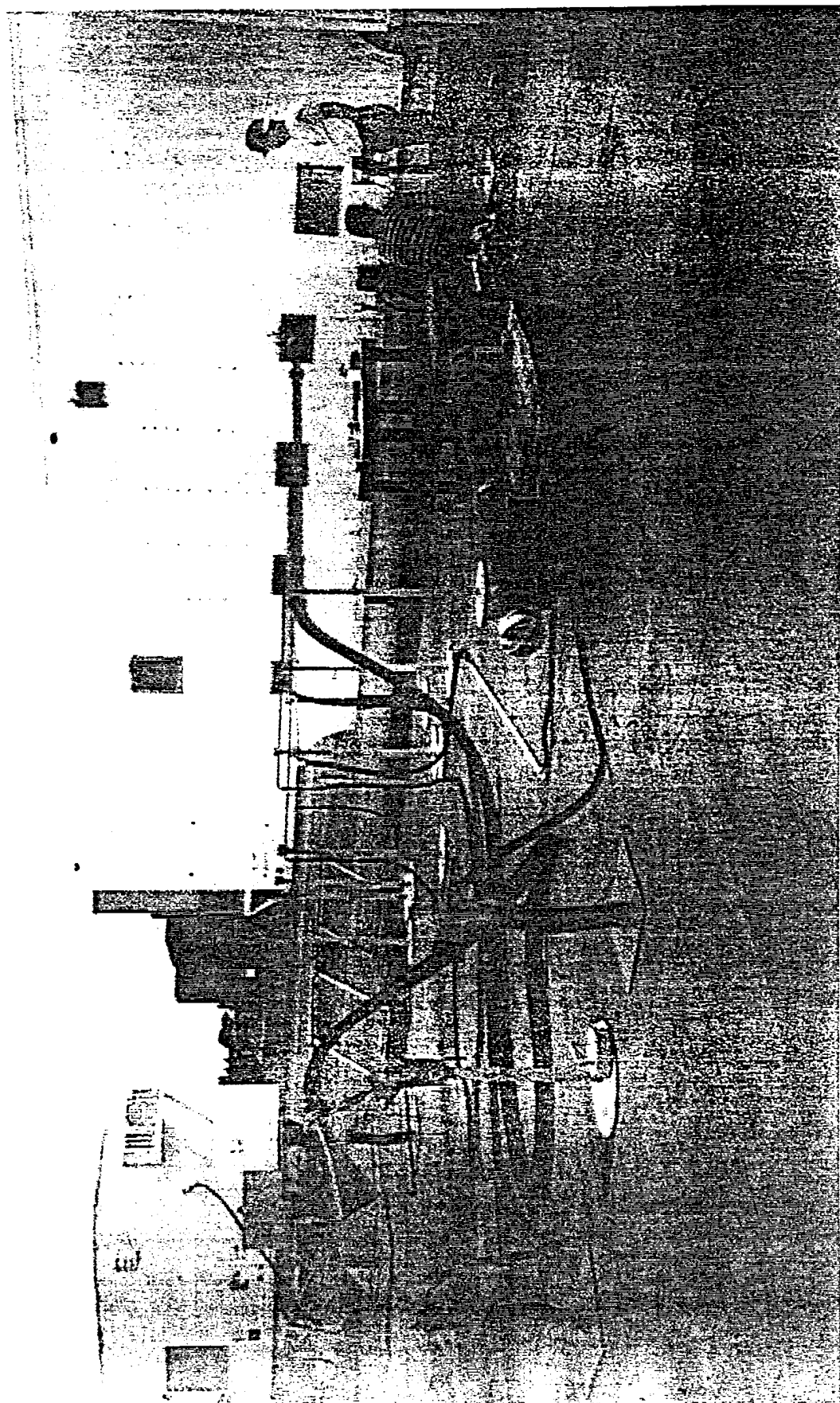
The second parameter of interest is the ratio of peak to average power. This parameter depends on the mode structure and theoretically should be close to 9 dB. Since the mode structure in the chamber will affect each signal independently if the EEDs are loosely coupled, this ratio should be calculated for each signal seperately. The value obtained using the average power for the signal in Figure 19 is 10.2 dB, which is very close to the predicted value. Any error in this figure is likely due to the fact that the power density in the chamber is rapidly changing and the value at the peak signal amplitude was measured manually.

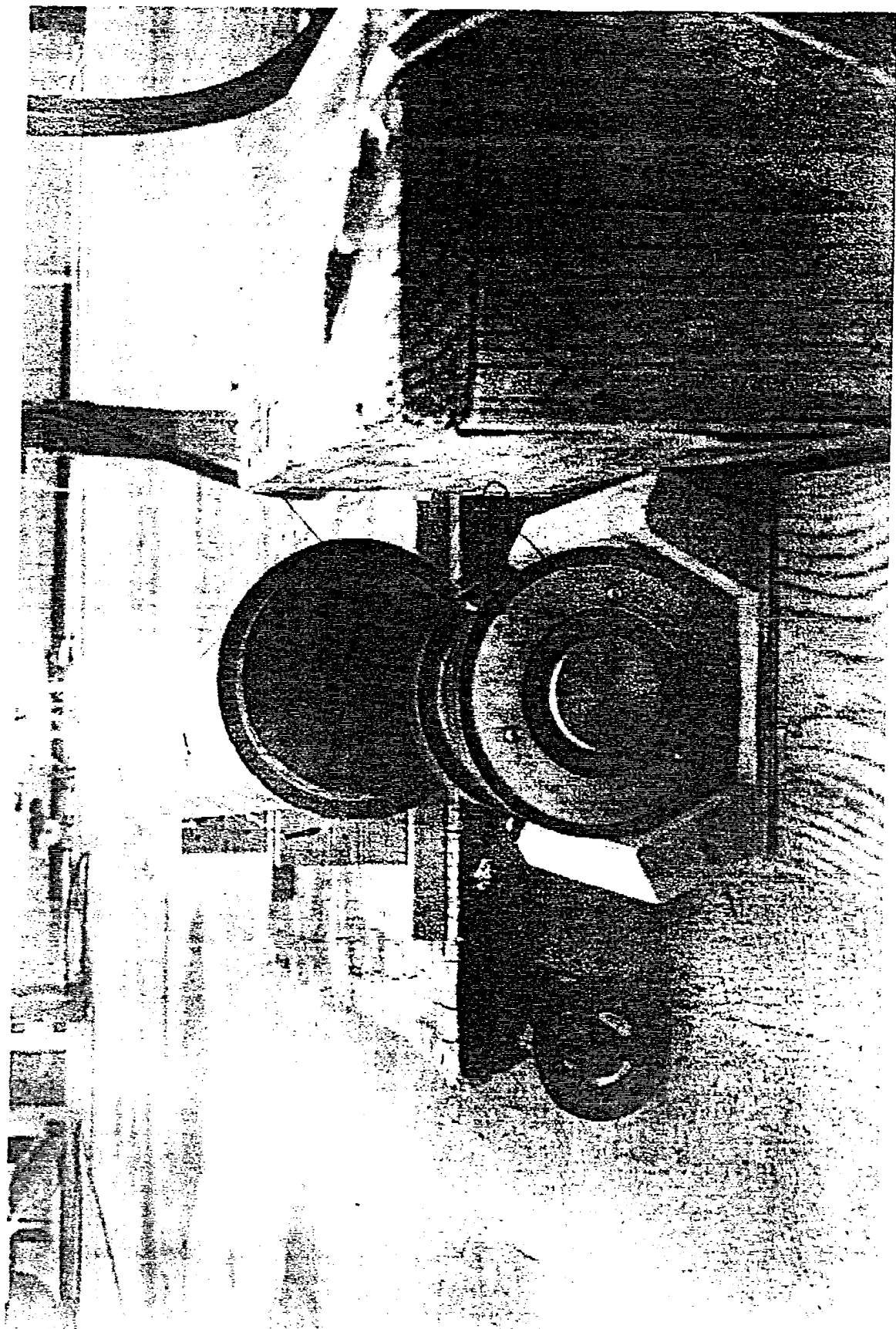
CONCLUSIONS

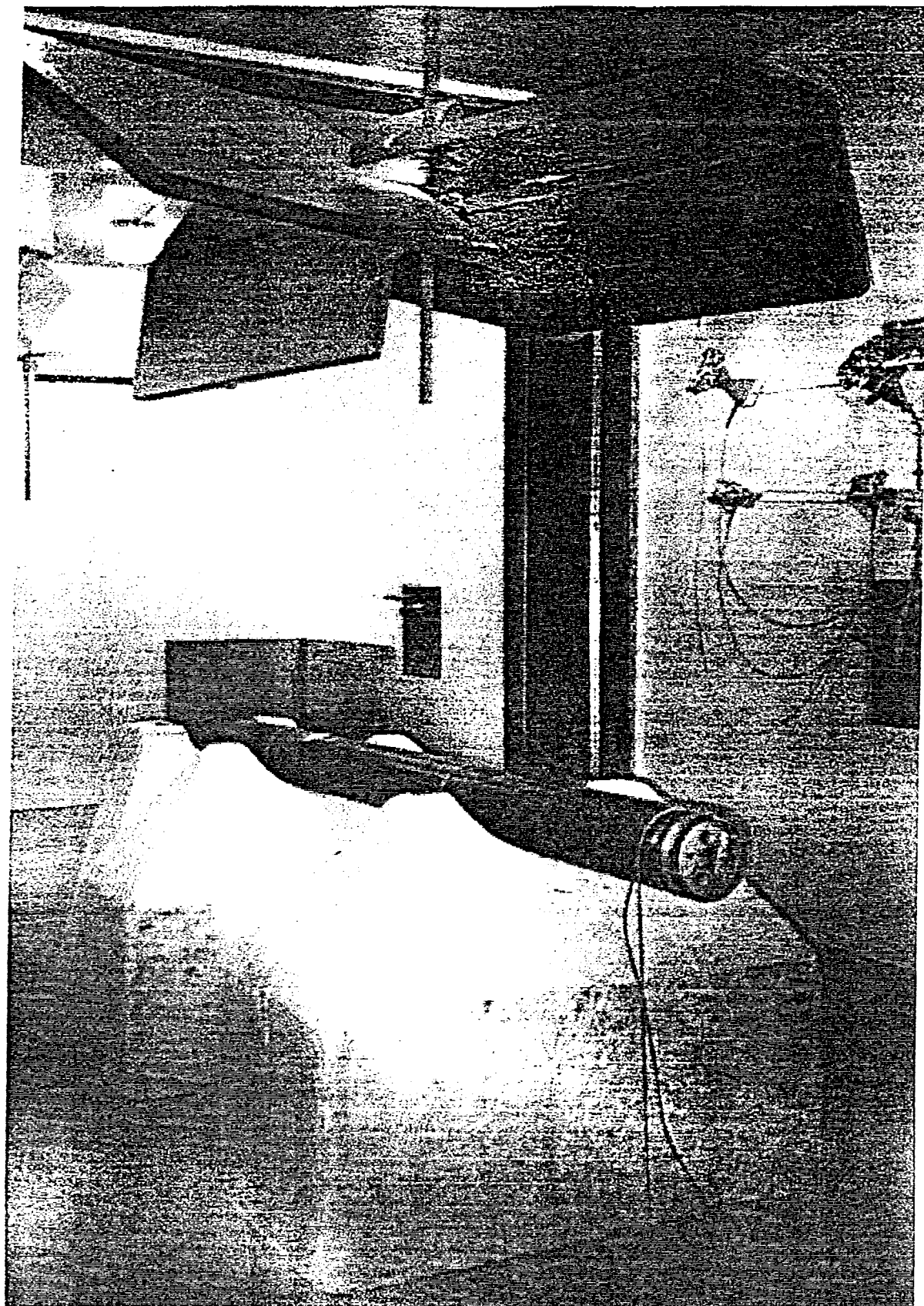
For the CSA system, the mode-stirred chamber provided valuable test results because the results of mode-stirred chamber testing were reliable indicators of the system's performance during an open-field test. The two test facilities, mode-stirred chamber and ground plane, complement each other. Theoretically, the difference between the results obtained from mode-stirred chamber tests and the results from ground plane tests is a factor equal to the open space gain of the antenna. However, this factor must be corrected for practical antennas which are not lossless and which suffer from impedance mismatches between the antenna terminals and the load. To best correlate mode-stirred chamber results with ground plane results it is important that the system be radiated from all possible aspect angles on the ground plane to find the direction of maximum gain and also to illuminate all the internal components.

REFERENCES

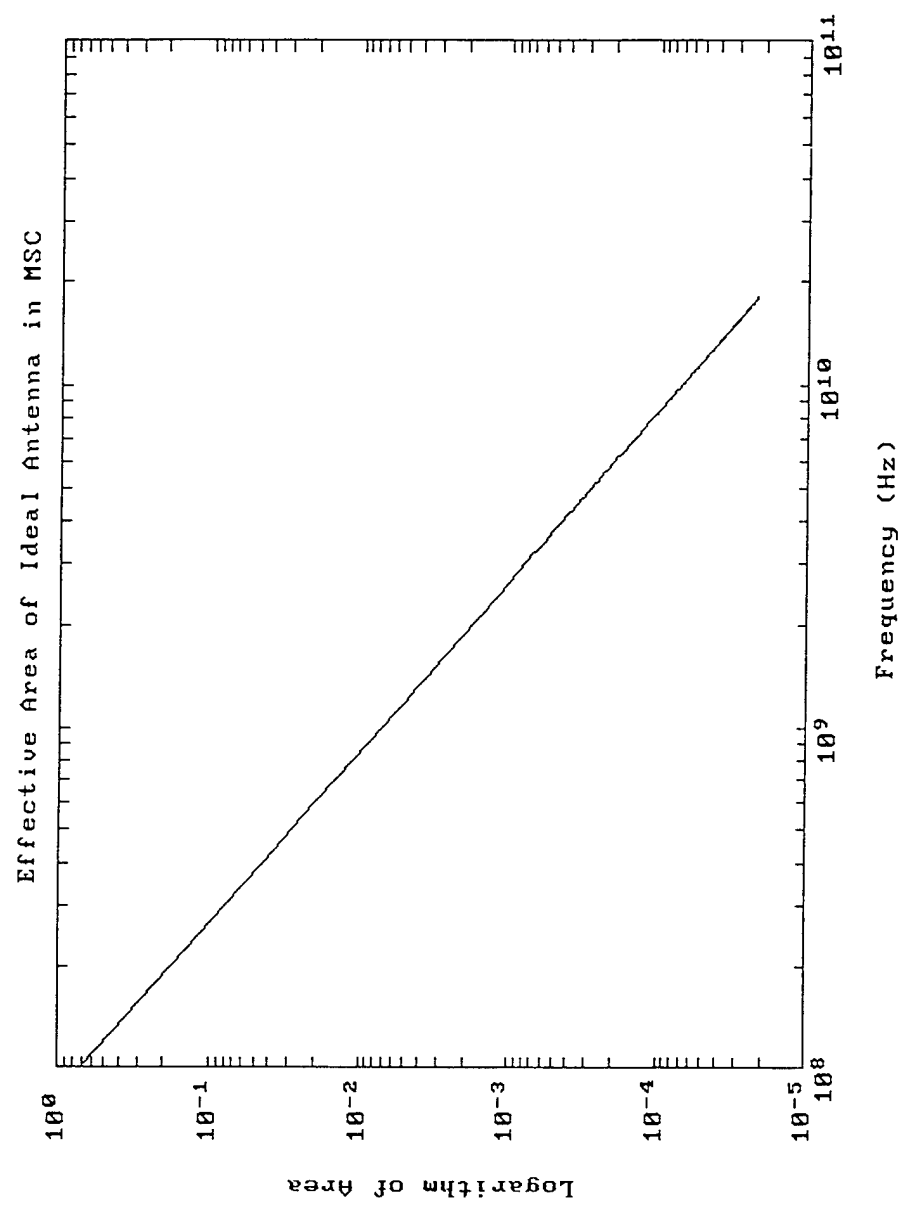
1. Pozar, D. M., Microwave Engineering, Addison-Wesley Publishing Company, 1990.
2. Bean, J.L. and Hall, R.A., "Electromagnetic Susceptibility Measurements Using a Mode-Stirred Chamber", U.S. Naval Surface Weapons Center, Dahlgren, VA.
3. Skolnik, M.I., editor-in-chief, Radar Handbook, McGraw-Hill Book Company, 1970.
4. Peters, L. Jr, "End-Fire Echo Area of Long, Thin Bodies", IRE Transactions on Antennas and Propagation, January 1958.
5. Leon-Garcia, A., Probability and Random Processes for Electrical Engineering, Addison-Wesley Publishing Company, 1994.



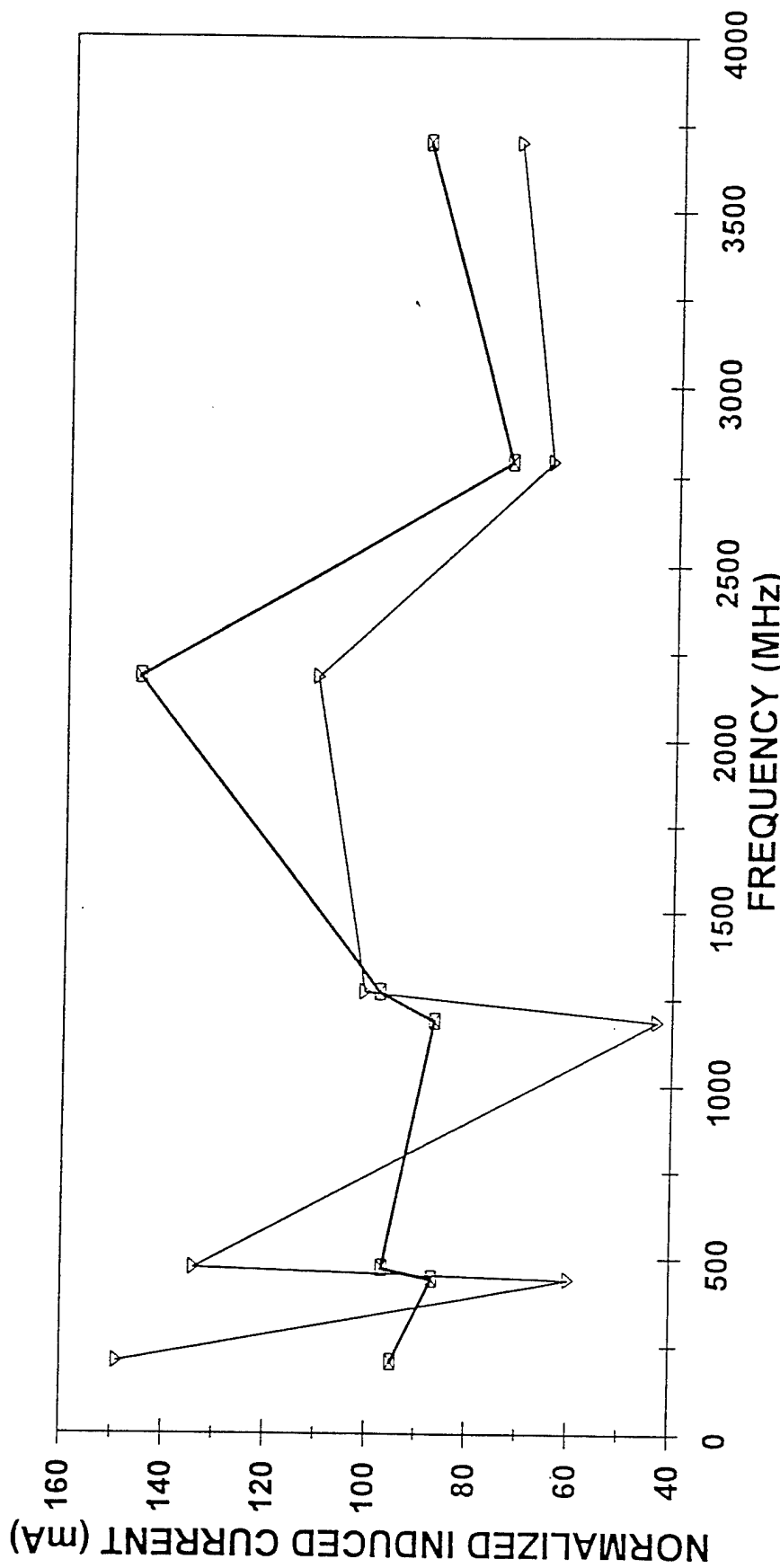




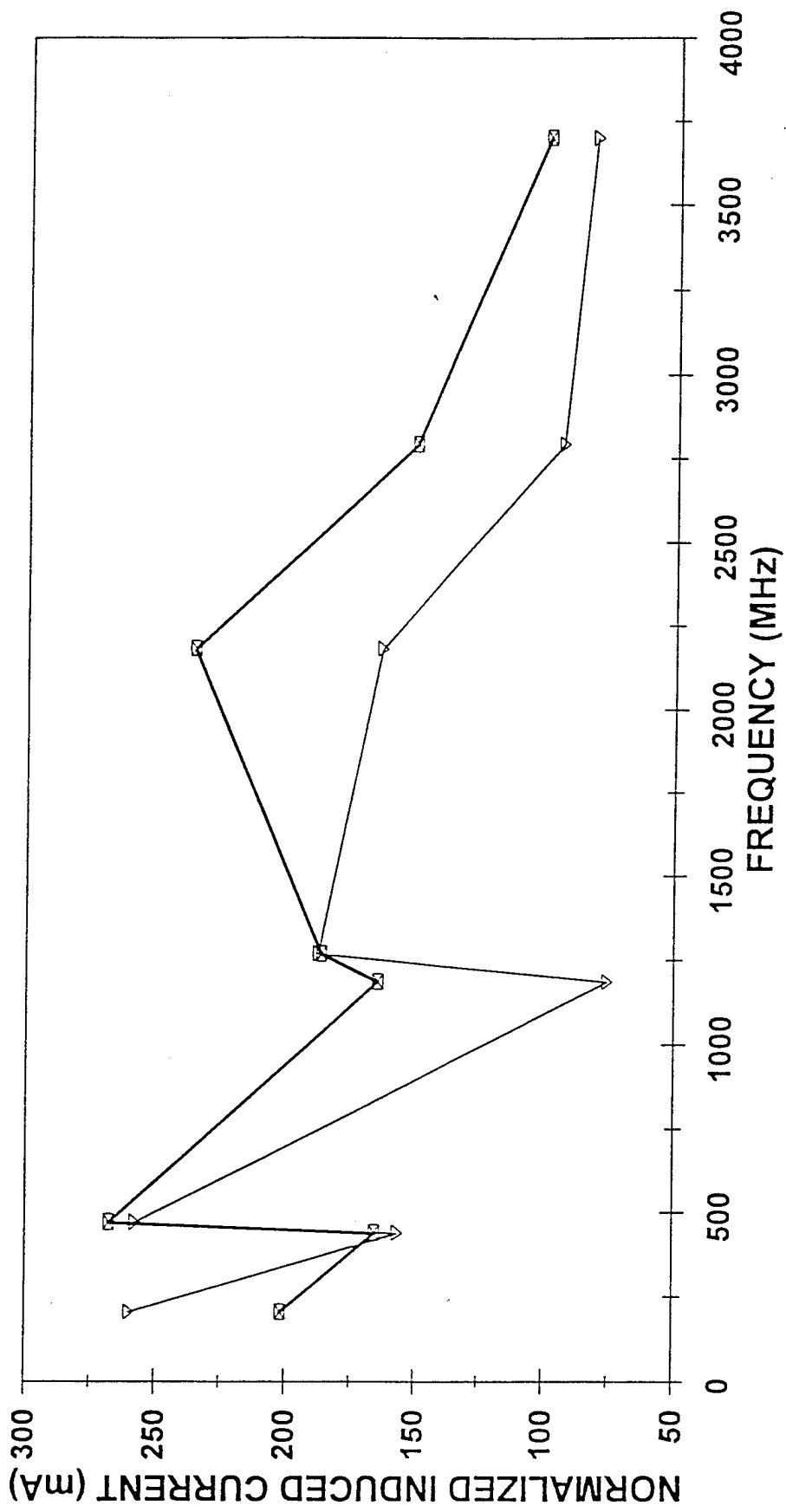




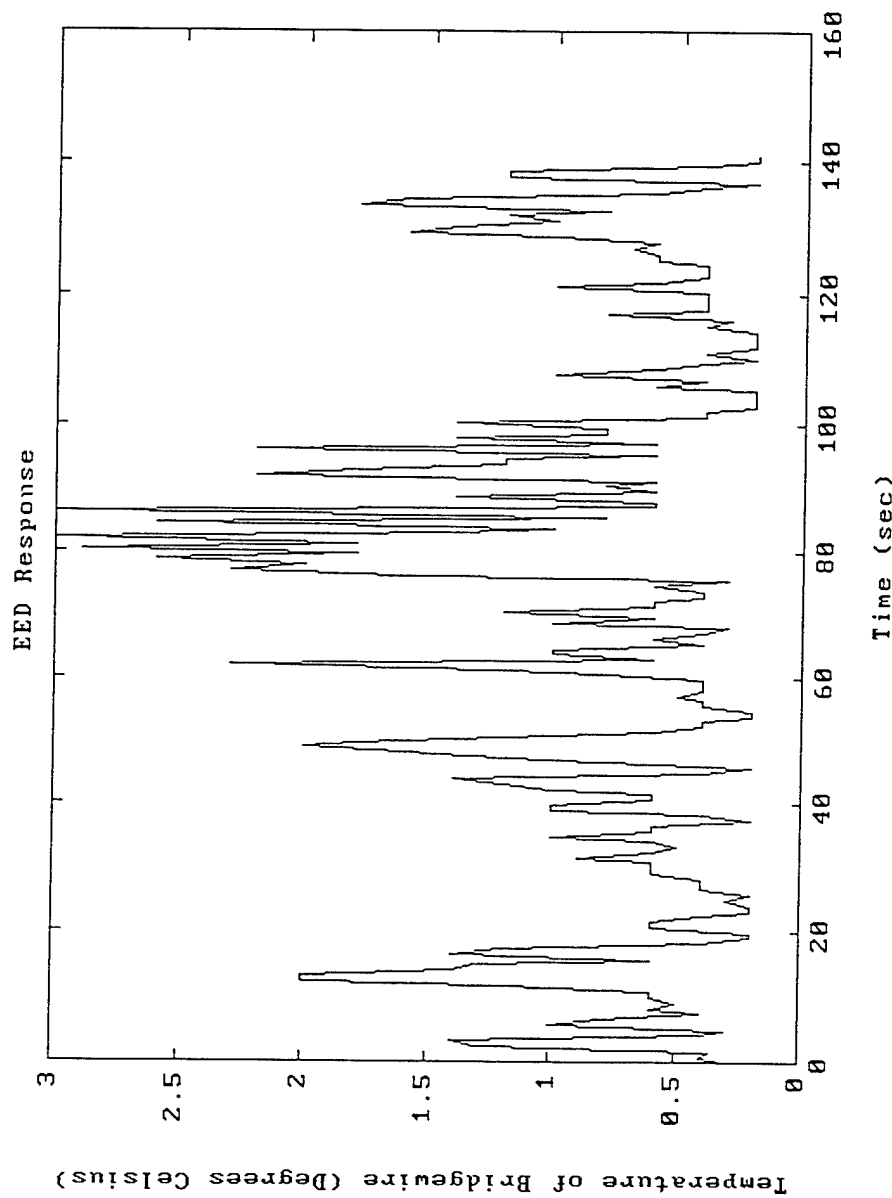
MODE-STIRRED CHAMBER VS GROUND PLANE
CSA MK 2 SYSTEM

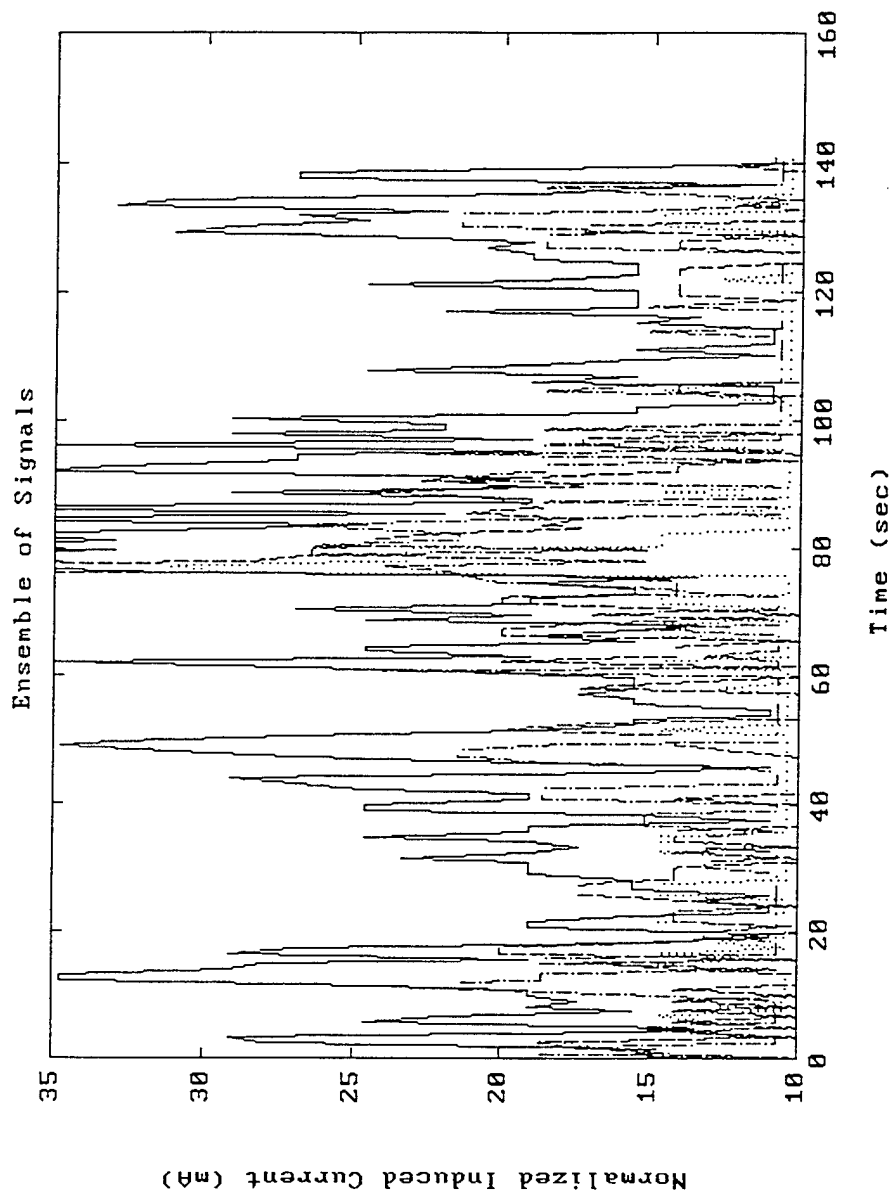


—□— PEAK MEASURED CURRENT IN MSC —△— PEAK MEASURED CURRENT ON GP

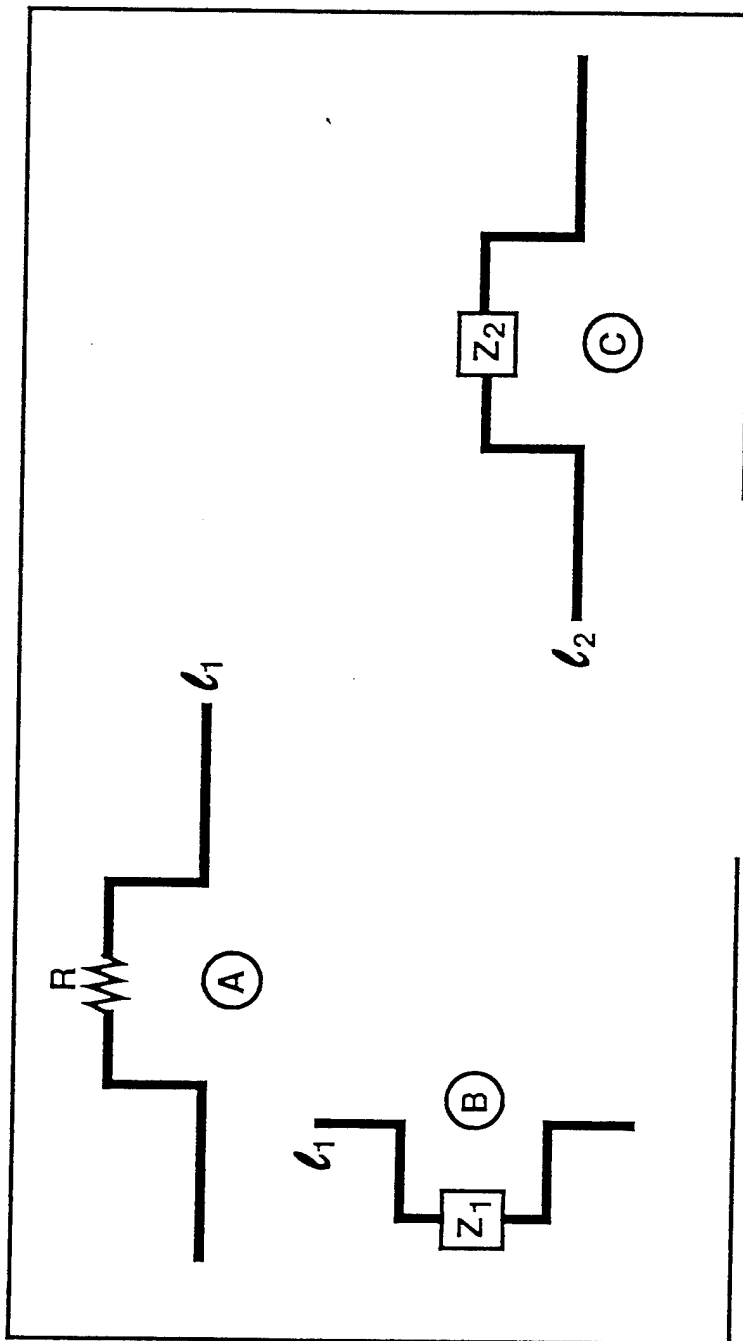
MODE-STIRRED CHAMBER VS GROUND PLANE
CSA MK 2 SYSTEM

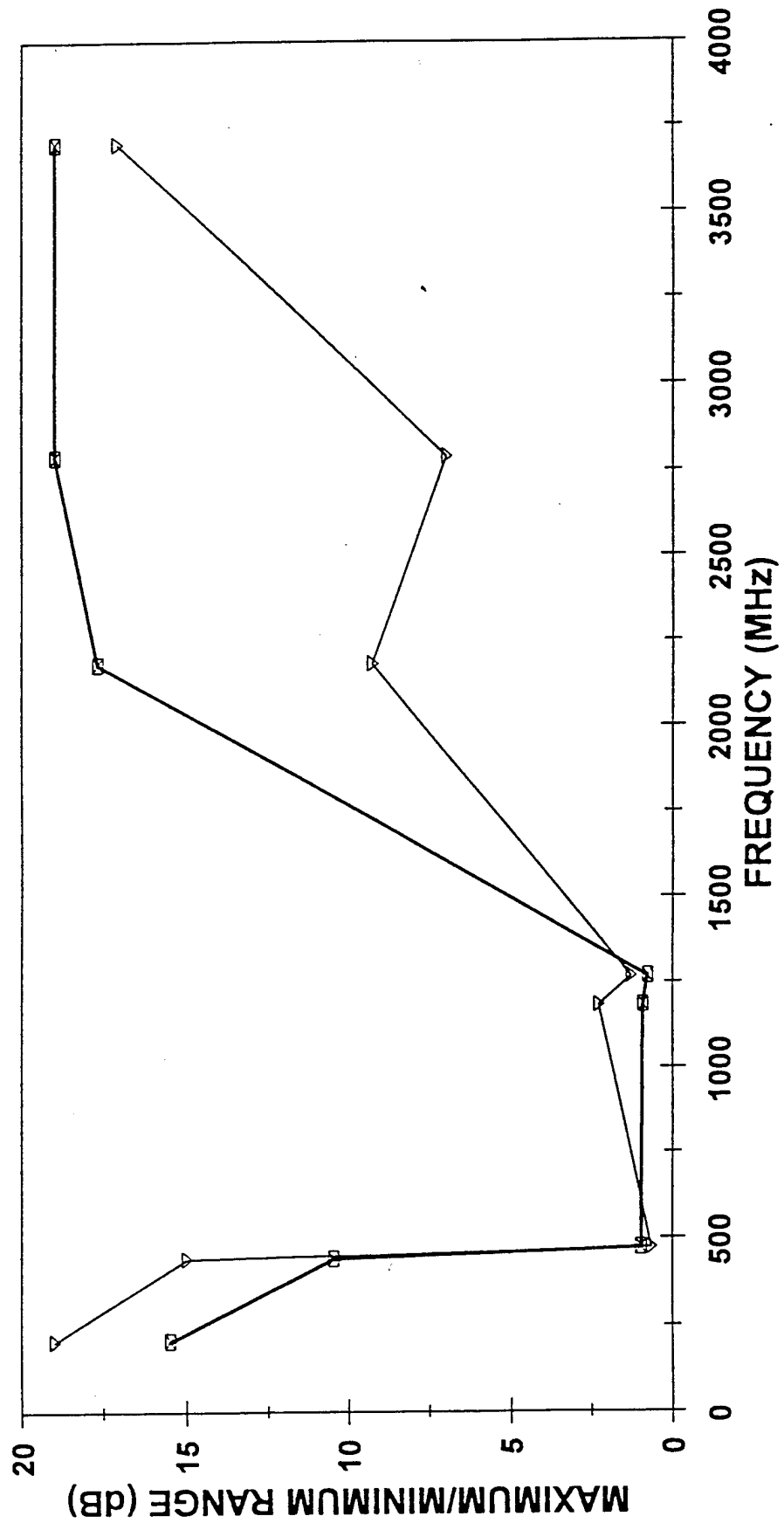
—▽— TOTAL MEASURED CURRENTS IN MSC —■— TOTAL MEASURED CURRENTS ON GP

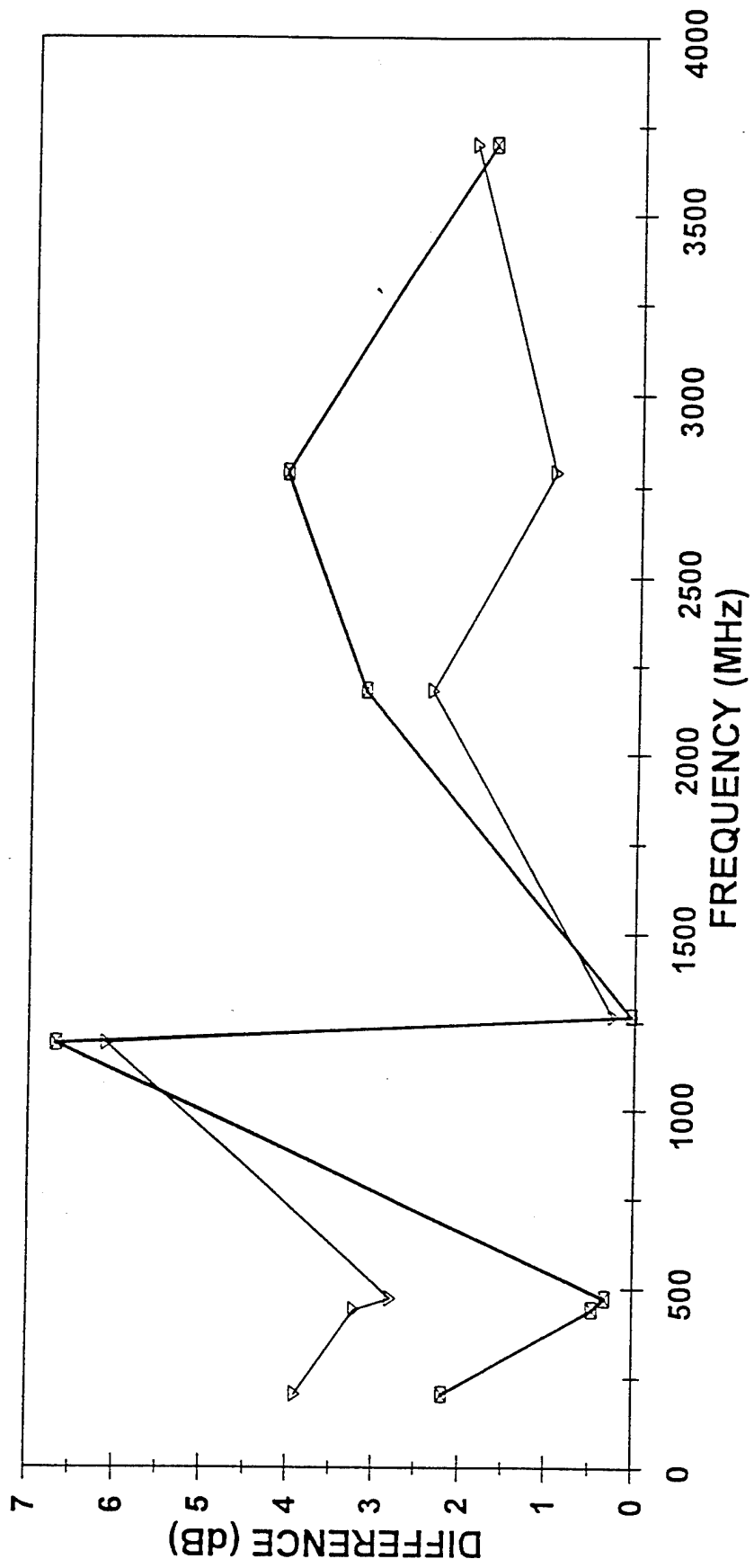




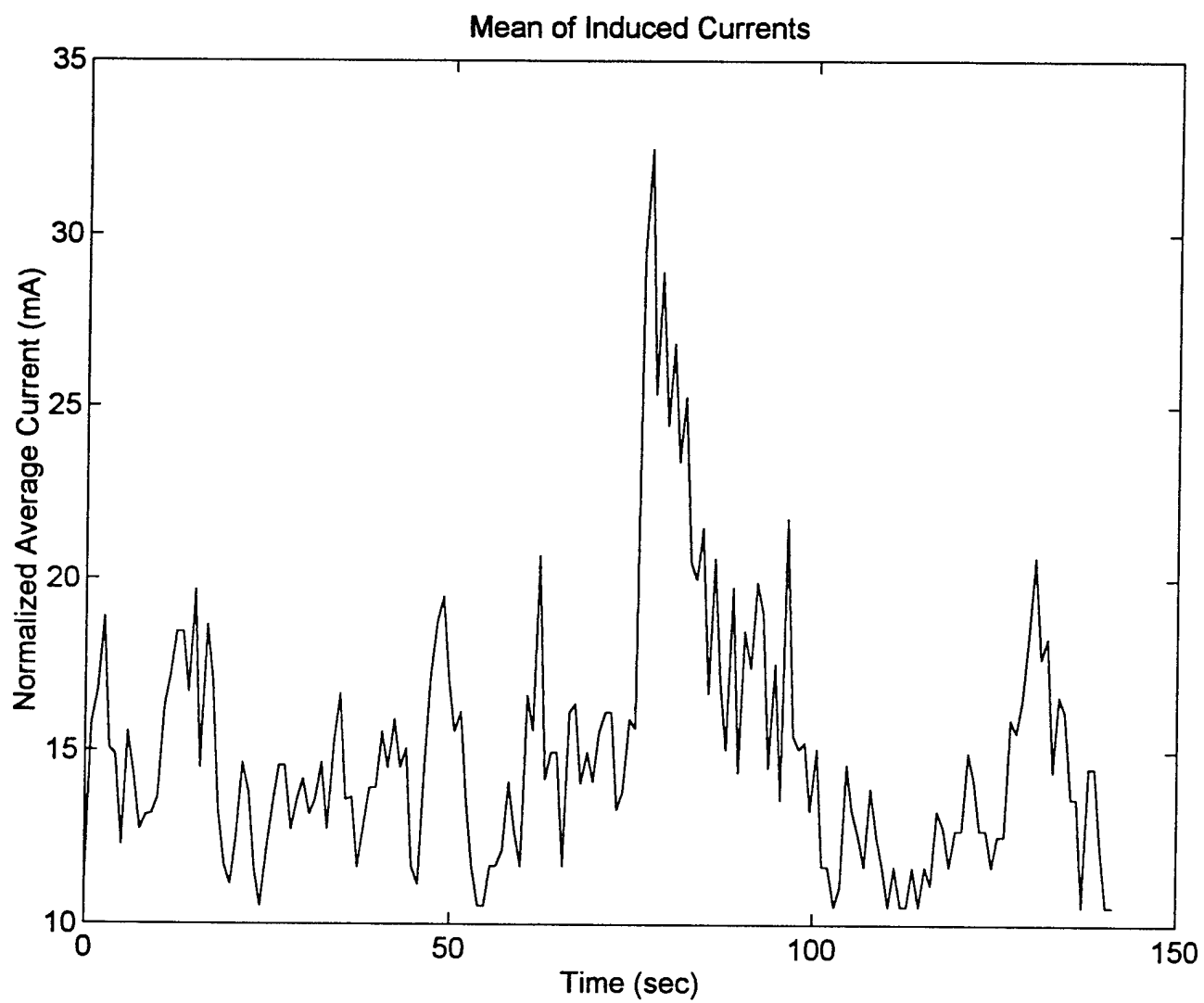
INTERNAL COMPONENTS ACT AS ANTENNA

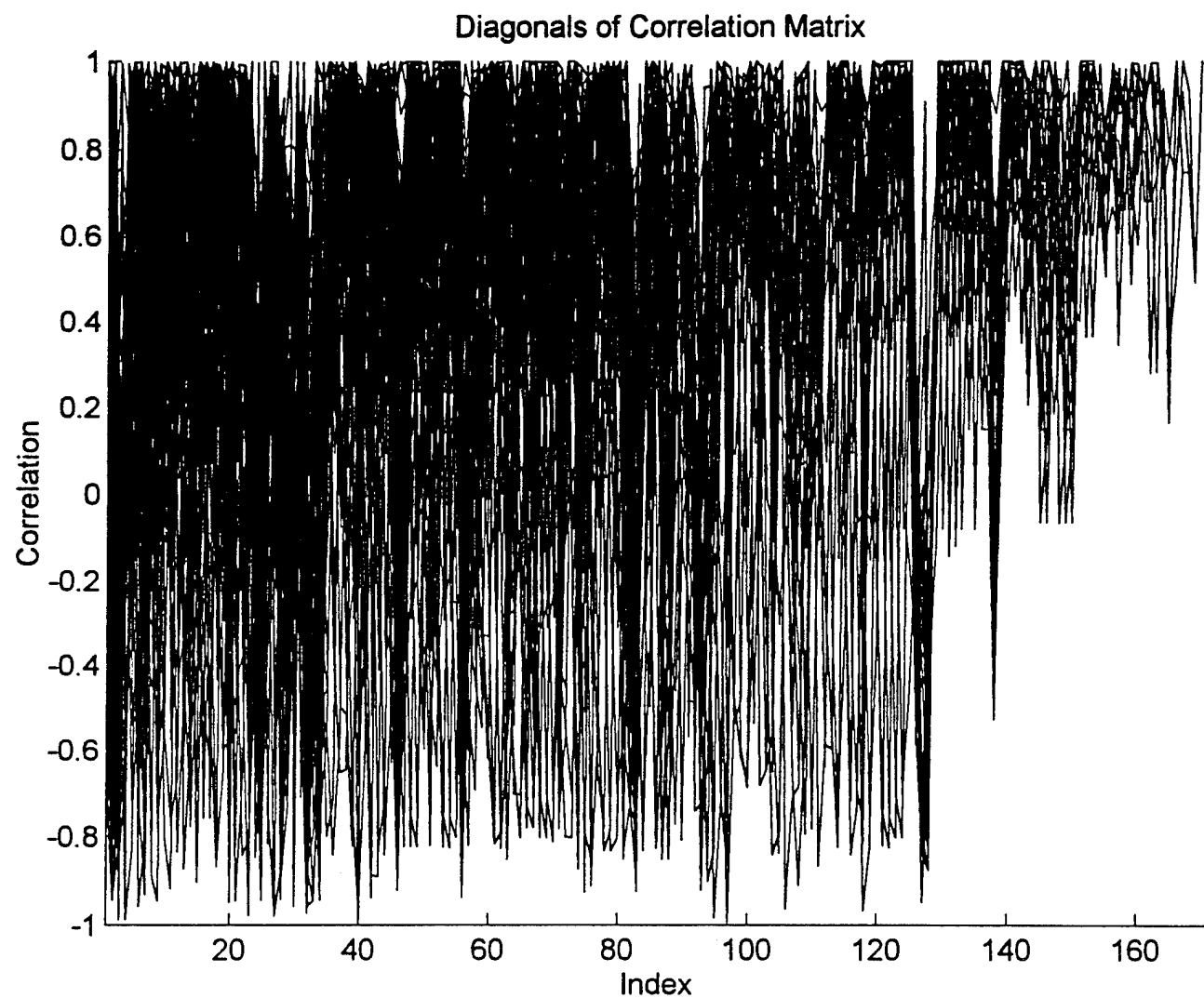


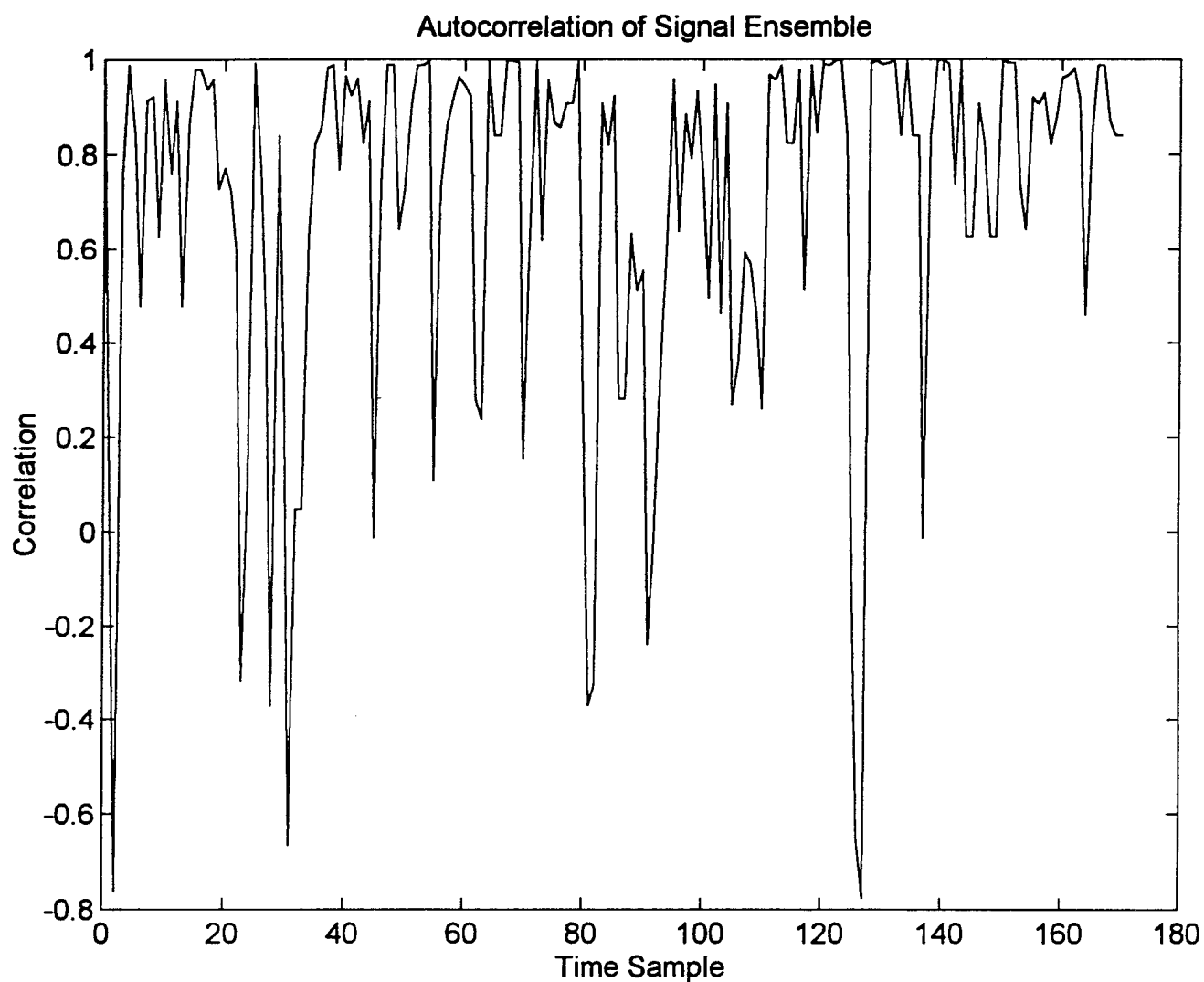
MODE-STIRRED CHAMBER VS GROUND PLANE
CSA MK 2 SYSTEM

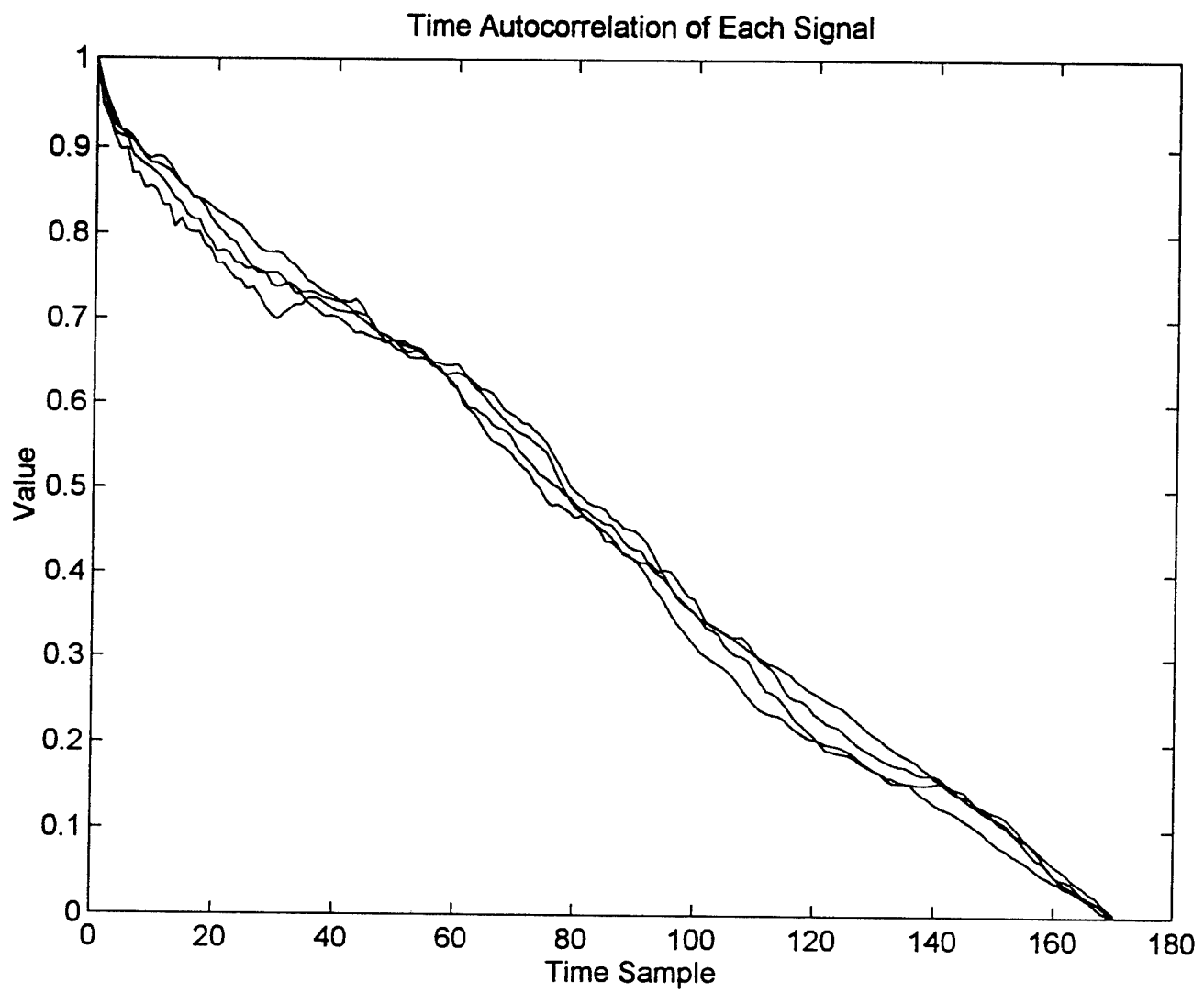
MODE-STIRRED CHAMBER VS GROUND PLANE
CSA MK 2 SYSTEM

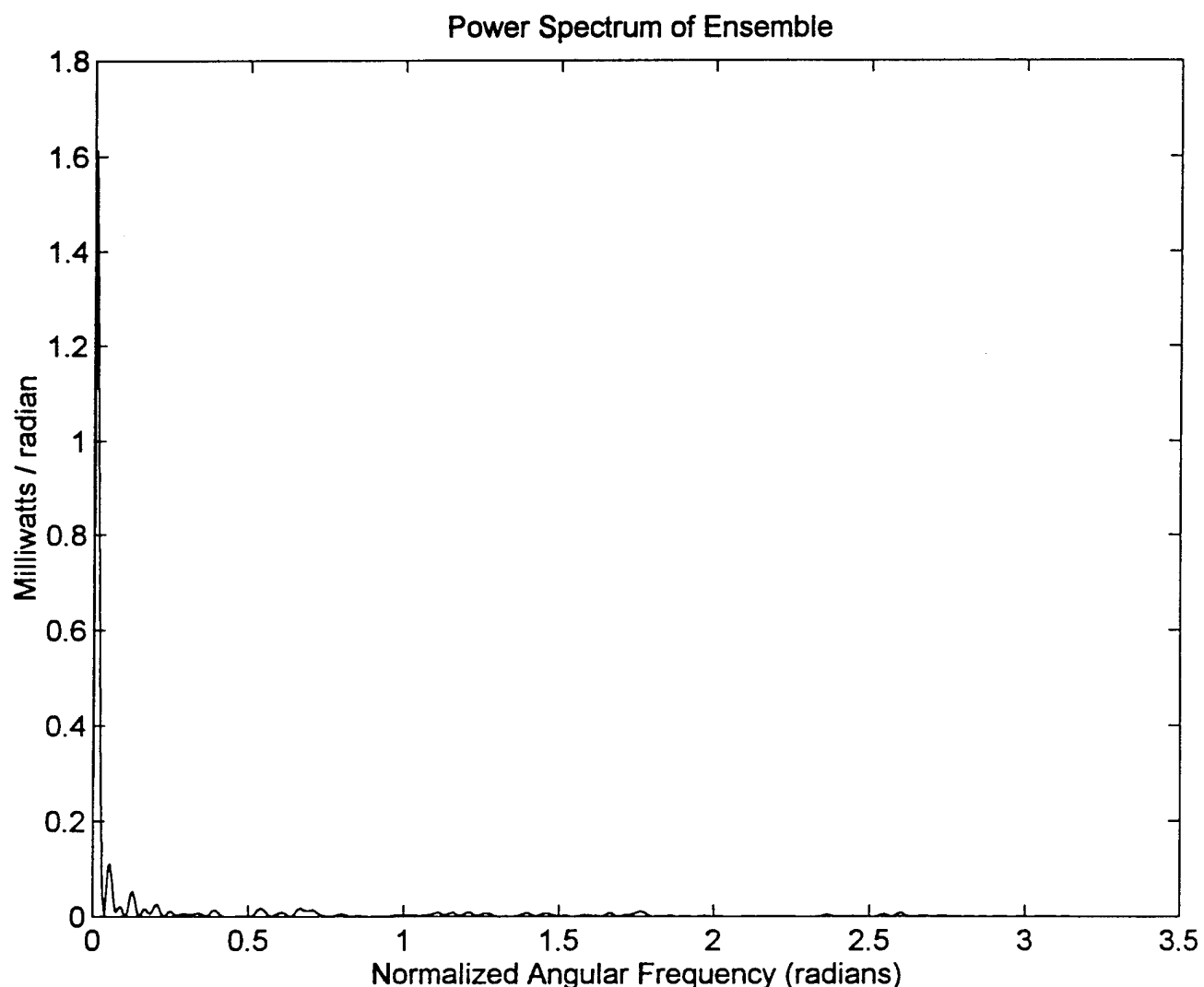
→ DIFFERENCE IN PEAK INDUCED CURRENTS → DIFFERENCE IN TOTAL CURRENTS

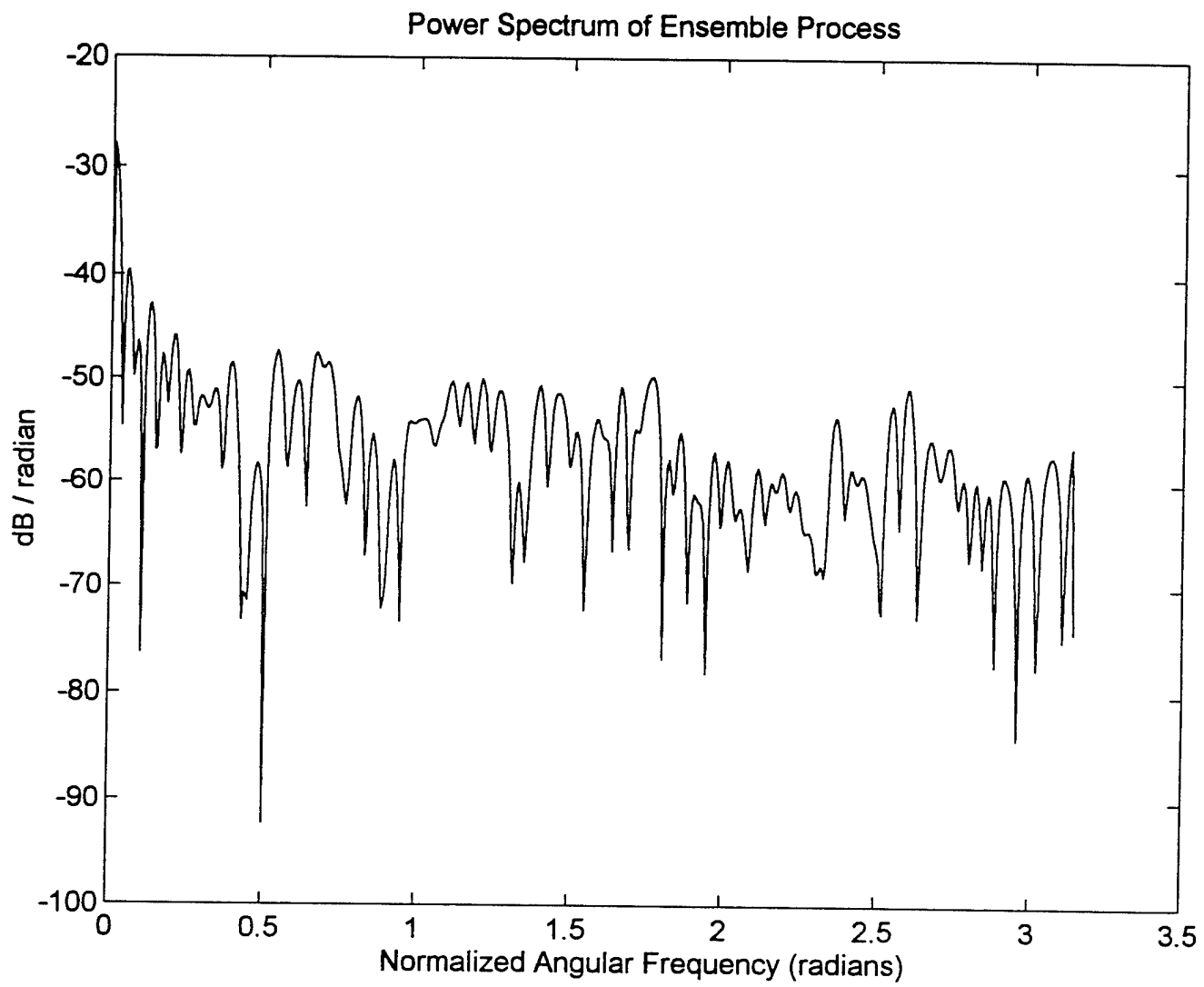


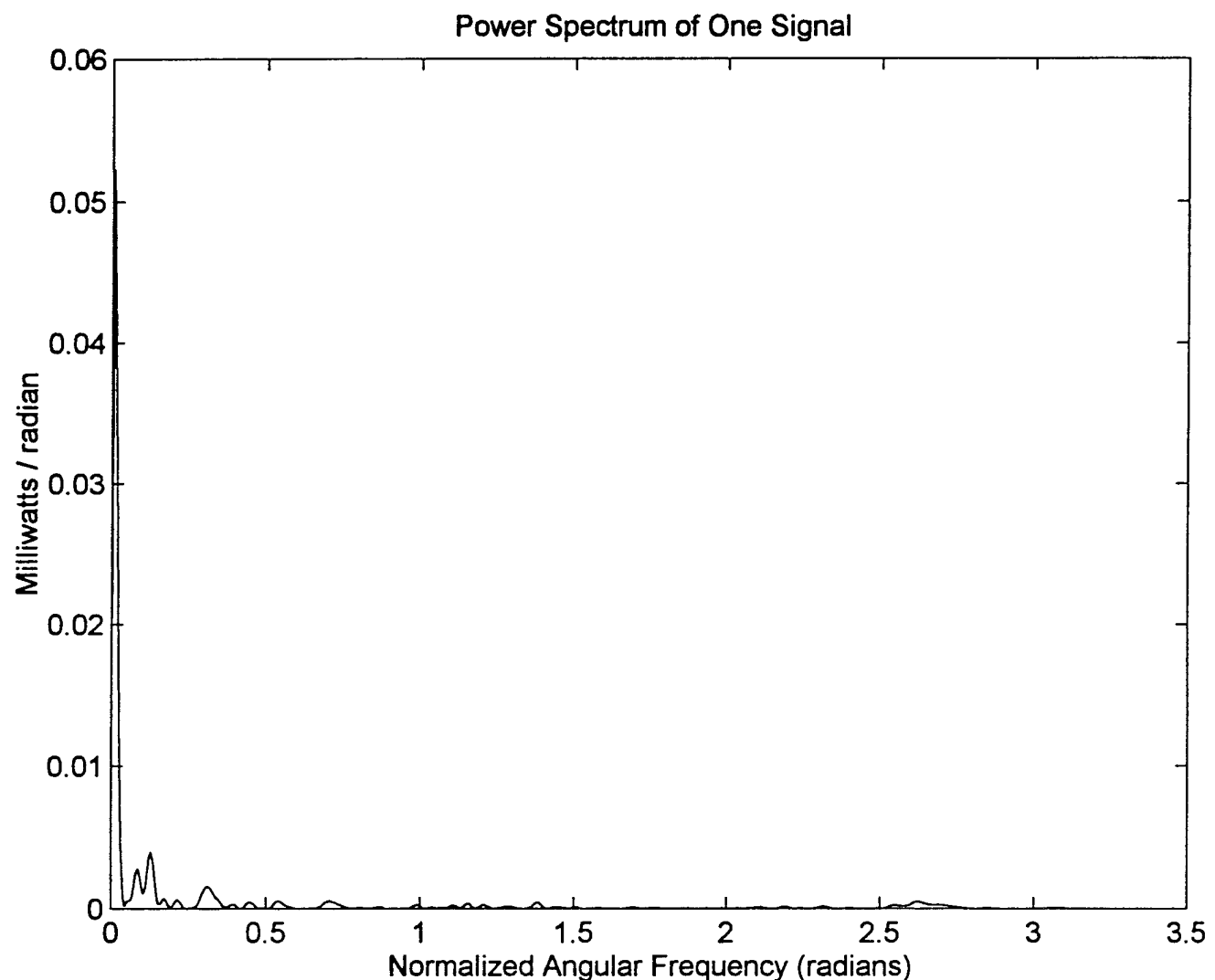


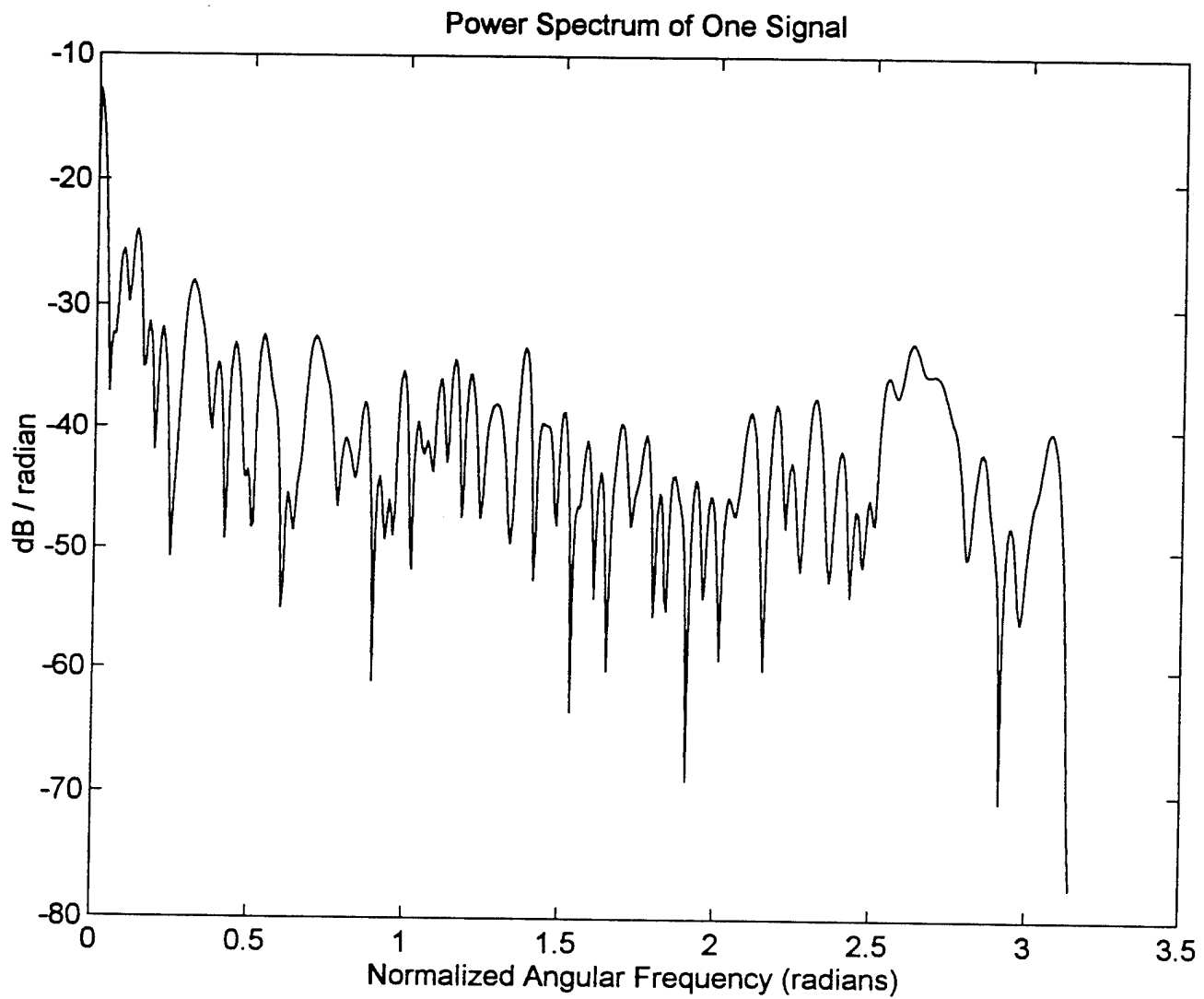
















DR. J. P. QUINE
ROME LABORATORIES



**STEPPED-FREQUENCY METHODOLOGY FOR OBTAINING
FASTER DATA RATES IN REVERBERATION CHAMBERS
OPERATED WITHOUT A MECHANICAL MODE STIRRER***

J.P. Quine
Rome Laboratories
Griffiss AFB, NY, USA

A.J. Pesta
Rome Laboratories
Griffiss AFB, NY, USA

Abstract

A stepped-frequency method is discussed for obtaining faster data rates with a reverberation chamber operated without a mechanical mode stirrer. The conditions for obtaining spatially uniform fields on a time (or frequency) average basis for all three polarizations are reviewed. Computer calculations are presented showing the degree of field uniformity that can be achieved with this stepped-frequency method.

Introduction

Use of a mechanical mode stirrer to obtain a well-stirred field distribution in a reverberation chamber (REVCH) may result in data rates that are slower than desired. On the other hand, data rates in an anechoic chamber can be much faster, but the radiation patterns produced by the equipment under test (EUT) may be too complicated [1] to allow a reliable determination of the total radiated power unless a very large number of measurements are made over the entire spatial extent of the radiation pattern.

Field distributions that are spatially uniform over all polarizations on a time or frequency average basis (hereinafter referred to simply as spatially uniform) can be obtained inside a REVCH, provided certain conditions reviewed below involving chamber size, frequency, and Q are satisfied; and, provided the fields are well stirred either mechanically [2] or by a stepped frequency method. Mechanically stirred reverberation chambers have been employed in the past to measure the total power radiated into all spatial directions and field polarizations by an interference producing EUT located inside the REVCH. Important applications in which total radiated power must be measured is in the evaluation of the shielding effectiveness (SE) provided by cover panels and gaskets [2, 3, 4]. A REVCH can also be employed to produce a spatially uniform field environment for measuring the susceptibility of an EUT to external interference fields arriving at arbitrary angles of incidence and polarization.

It can be seen that if the total radiated power density is spatially uniform throughout the volume of the REVCH with respect to all field polarizations, then the total radiated power (and hence SE as well as susceptibility can be determined from single measurements obtained with arbitrarily positioned and oriented linearly polarized antennas. This is a principal advantage of a REVCH, which can be exploited by means of the stepped-frequency method of fast mode stirring.

Conditions for Obtaining Spatially Uniform Field Distributions Inside a Reverberation Chamber

Spatially uniform fields can be obtained inside a REVCH, provided that a sufficient number of modes, N are excited. More specifically, there must be a sufficient number of modes, NDIS within one dissipation bandwidth, \bar{F}/Q where F is the applied frequency and Q is the loaded Q of the enclosure. In the case of a rectangular enclosure, the total number of modes that have resonance up to frequency F is given by [2]

$$N_{(Total)} = (8\pi/3) (VOL / \lambda^3) \approx VOL / (\lambda/2)^3 \quad (1)$$

* Previously presented at Zurich EMC Symposium, March 7-9, 1995

where λ is the free space wavelength at frequency F . This shows that within a factor of $(\pi/3)$, N is equal to the number of small $(\lambda/2)^3$ volumes that can be fitted into the total volume. Equation (1) is also a good approximation for a non-rectangular enclosure (e.g., an ellipsoid) that is not too "flat", i.e., the smallest dimension must exceed a few wavelengths.

NDIS can be determined by differentiating Eq. (1) with respect to λ . Thus,

$$dN = 8\pi(VOL / \lambda^3)(dF / F) \quad (2)$$

If dN is one, dF is dF_{SEP} the average frequency separation between modes. Thus,

$$dF_{SEP} = (F\lambda^3) / (8\pi VOL) \quad (3)$$

But, NDIS is $dFDIS/dF_{SEP} = (F/Q)/\Delta F_{SEP}$.

$$NDIS = (8\pi / Q)(VOL / \lambda^3) \quad (4)$$

Equation (4) is equivalent to Eq. (22) of [5]. A value of NDIS equal to 0.5 can be taken as the threshold for overlapping modes, and corresponds to one mode on the average within two dissipation bandwidths ($2 F/Q$). The minimum size volume for overlapping modes can be determined by setting $NDIS = 0.5$ in Eq. (4). Thus, for overlapping modes,

$$VOL > Q\lambda^3 / 50.265 = Q\lambda^3 / 50 \quad (5)$$

For smaller volumes than given by condition (5), resonances of individual modes can be expected; in fact, critical coupling with strong field buildup inside the enclosure can occur even for relatively small leakage holes [4].

Based on Eq. (2), five distinct frequency regions can be identified for a shielding enclosure. As a simple example, Figure 1 shows a chart for a cubic enclosure of side $A = 1.0$ meter and $Q = 10,000$. Quasi-static conditions apply for $A/\lambda < 0.1$, and in this case, high and low-impedance shielding effectiveness values based on the ratio of equivalent dipole moments of the shielded and unshielded EUT can be defined which are independent of frequency [4]. For $0.1 < A/\lambda < 0.707$ (lowest mode), a transition region exists in which the quasi-static approximations are inaccurate, and Maxwell's Equations are required. Isolated single-mode resonances occur for A/λ greater than 0.707 and less than 5.8, the threshold for overlapping modes, $NDIS = 0.5$. The lower limit for the quasi-optical region has been arbitrarily set at $NDIS = 50$, based on measurements of the input impedance of feed horns used to excite a REVCH [2, 6]. The feed impedance is approximately the free-space value in the quasi-optical region.

Maximum Size of EUT

The maximum size of EUT that can be tested accurately can be determined by requiring that the Q not be lowered significantly when the EUT is placed inside the chamber. In this connection, the effective absorption aperture $EFFA$ of the EUT is defined as the ratio of the power that is absorbed by the EUT to the effective average power flux that surrounds the EUT. If the $EFFA$ of the EUT is equal to the effective aperture due to wall losses, then the Q is reduced by a factor of 2 relative to the unloaded Q (wall losses only). This corresponds to a 3 dB measurement error if the reduction in Q is not accounted for. This approach has a clear meaning in the case of a gasket or a cover panel that covers an opening at an arbitrary position on an internal wall of the REVCH and is excited from outside the REVCH. The meaning is also clear for any general EUT comprised of an equipment cabinet that is placed inside the REVCH. In the case of a simple cover panel of area A which is greater than about λ^2 (to permit the geometrical optics approximation), the maximum allowable value of $A = A_{MAX}$ can be shown to be on the order of [6]

$$A_{MAX} = 6\pi VOl / \lambda Q \quad (6)$$

It is assumed that the panel is highly reflecting, otherwise the measurement error occurring when $A = A_{MAX}$ would be less than 3 dB. Using $VOl = 187m^3$ (Rome Laboratories chamber), $Q = 100,000$ and $\lambda = 0.1M$ (~ 3.0 GHz), $A_{MAX} = 19"$. These calculations are consistent with the small reductions in Q that were measured when a 10.5"-square wall opening was first covered with a panel and then uncovered. The Q measurements were based on Eq. (2) of [2] which shows that the Q -ratio in this case is simply the ratio of the two receiver power readings.

The Stepped Frequency Method

A computer program [4] based on an accurate modal analysis of an empty rectangular enclosure was employed to study a stepped-frequency method for achieving electronic mode stirring with fast data rates. The analysis employs the TE_{mn} and TM_{mn} modes of a uniform rectangular cylindrical waveguide with perfectly conducting walls. The waveguide has cross-sectional dimensions A and B and length C , and is shorted at both ends by perfectly conducting end walls to form the enclosure. Excitation holes are placed close to one end wall and the TE and TM mode amplitudes excited by an external incident field H_{INC} are determined by employing the hole polarizabilities [7]. The fields of all modes were summed to obtain the total internal fields. Enclosure dissipation was introduced by assuming a small dielectric loss for the medium that fills the otherwise empty enclosure. This assumption maintains degeneracy between TE_{mn} and TM_{mn} mode pairs, and results in a constant Q value for all modes given by $\omega\epsilon/\sigma$ where $\omega = 2\pi f$ and ϵ and σ are the dielectric permittivity and conductivity of the filling medium. It is well known [8] that this approach represents an accurate approximation for an actual enclosure having dissipative walls, for which the modes are not known in simple terms. The accuracy of the computer program was checked by comparing the calculated internal fields with the values calculated on the basis of the black-hole principle (BHP) [4, 6].

As shown in Figure 2, the microwave excitation applied to the REVCH can be in the form of periodic pulses with pulse width $T/2$ and period T . The frequency can be stepped from an initial value, F_0 by a small increment ΔF_P , between successive pulses. The pulse width $T/2$ should be greater than say two or three times the chamber buildup time, T_B equal to $Q/\pi F_0$ and ΔF_P should be equal to the frequency autocorrelation width, $FCOR$. Values of $FCOR$ calculated with the above computer program for the Rome Laboratory chamber ($9.78 \times 5.18 \times 3.69$ meters) [2, 4] range between 50 and 100 KHz for values of F_0 between 2.0 and 8.0 GHz, and for Q values between 10,000 and 100,000. Thus, $FCOR$ is not a strong function of F_0 and Q . Measurements of $FCOR$ for a somewhat smaller chamber show similar results [8].

Figures 3 to 5 show calculated H-field distributions for the Rome Laboratory chamber for a Q -value of 100,000, and dimensions, $A, B, C = 5.18, 3.69, 9.78$ meters, respectively. A rectangular coordinate system has origin at the lower right-hand corner of wall AB with x, y, z along A, B, C, respectively. Excitation holes were placed near wall AB. The enclosure fields were sampled over a rectangular array of 24 probe points (6 along X, and 4 along Y) uniformly distributed over the entire X-Y plane at $Z = 0.7C$.

Figure 3a shows calculated values near 2000.0 MHz of the magnitude-square of H_x , with only an incident H_x field. The data are normalized relative to the incident H-field and, therefore, represent the shielding effectiveness with respect to H_x . The excitation, in this case, is a single 0.200" diameter leakage hole centered in the end wall ($z = 0$), and therefore results in symmetrical field distributions with respect to x (and y). Because the shielding effectiveness is high (on the order of 65 dB), and there are a large number of modes in the bandwidth F/Q , reasonable agreement is obtained between the computer data and the Black-Hole principal [4, 6].* Figure 3b shows the results of averaging over 10

* Black-hole value indicated on Figures refers to the value of magnitude of H - Field = $\sqrt{H_x^2 + H_y^2 + H_z^2}$.

frequencies. Note that very little polarization mixing occurs, H_x being significantly greater than H_y and H_z .

Figure 4a shows calculated data near 2000.0 MHz when the excitation hole is moved to the lower right-hand corner of the back wall, 0.375λ from other walls. The individual frequency plots in this case are unsymmetrical. Note that the average fields are nearly equal for the two hole positions in Figures 3 and 4, showing that average fields are nearly independent of the position of the source. Other calculations with NH equal holes show that internal power density is proportional to NH. These are important characteristics of a good REVCH.

Figures 5a and 5b show data calculated near 2000 MHz with a single 0.200" diameter leakage hole placed on each of the three walls that intersect at the lower right-hand back corner. The distances of the holes from the wall intersections are 0.375λ , and each hole is excited with circular polarization. Figure 5a shows a wide spread in data for internal H_x with only H_x incident. The data show a shifting of maximum and minimum points as the frequency is stepped. Figure 5b shows that internal H_x , H_y , and H_z fields have only about ± 4 dB variation over the 24 probes when averaged over 10 frequencies. Similar results have also been obtained at 4.0, 6.0, and 8.0 GHz.

Conclusions

The computer calculations show that frequency stepping can be an effective means for obtaining nearly spatially uniform fields. The calculations also confirm that the Black-Hole Principle can provide reasonable estimates of the internal fields.

References

- [1] J.P. Quine, A.J. Pesta, J.P. Streeter, E.A. Surowiec, "Distortion of radiation patterns for leakage power transmitted through attenuating cover panels and shielding gaskets - need for reverberation chamber measurement of total leakage power", 1994 IEEE EMC Symposium, Chicago, IL, August 1994
- [2] M.L. Crawford, G.H. Koepke, "Design evaluation and use of a reverberation chamber for performing electromagnetic susceptibility/vulnerability measurements", NBS Technical Note 1092, April 1986
- [3] J.P. Quine, "Characterization and testing of shielding gaskets at microwave frequencies", pp. 306-308, 1993 IEEE EMC Symposium, Dallas, TX, August 1993
- [4] J.P. Quine, "Opening leakage for enclosures at low and high frequencies", pp. 183, 187, 1993 IEEE EMC Symposium, Dallas, TX, August 1993
- [5] R.E. Richardson, "Mode-stirred chamber calibration factor, relaxation time, and scaling laws", IEEE Trans. Instrum. Meas. Vol. IM-34, pp. 573--580, 1985
- [6] J.P. Quine, "Application of the black-hole principle to the estimation of shielding effectiveness to radio frequency energy", pp. 33-35, 1989 IEEE EMC Symposium, Denver, CO, May 1989
- [7] R.E. Collin, "Field theory of guided waves (Second Edition)", IEEE Press, 1991, pp. 358-362
- [8] B. Bovarie, "Mode stirred chamber field statistics: correlation widths", Sandia National laboratory, presented at Reverberation Chamber Users' Group, Group Meeting, Boulder, CO, August 1-2, 1991

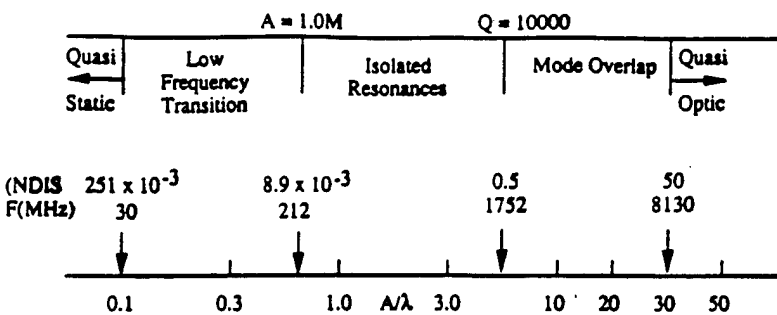


Figure 1 Mode chart for cubic enclosure

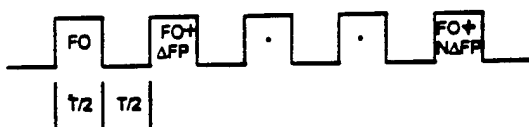
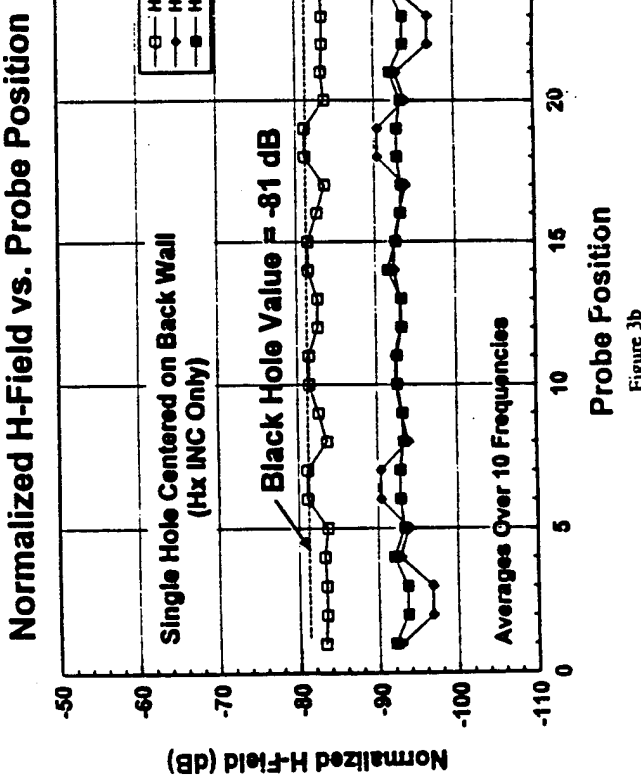
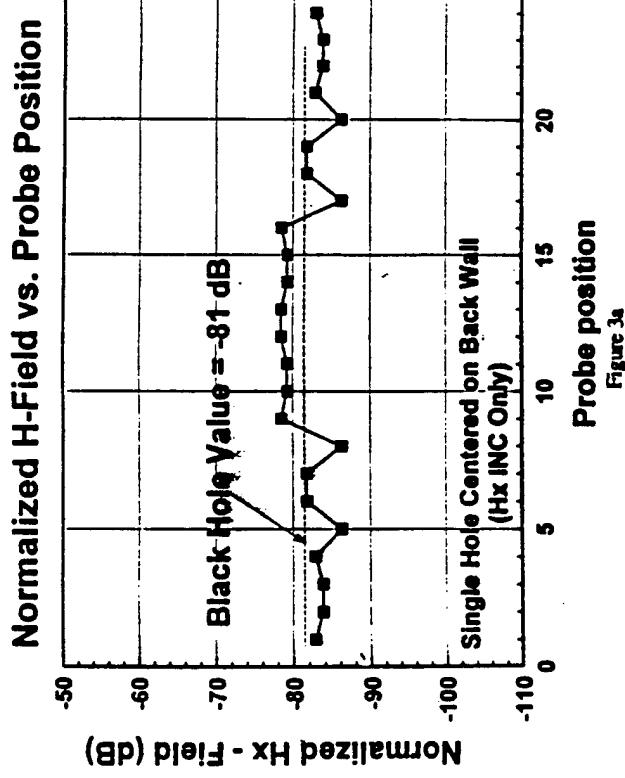
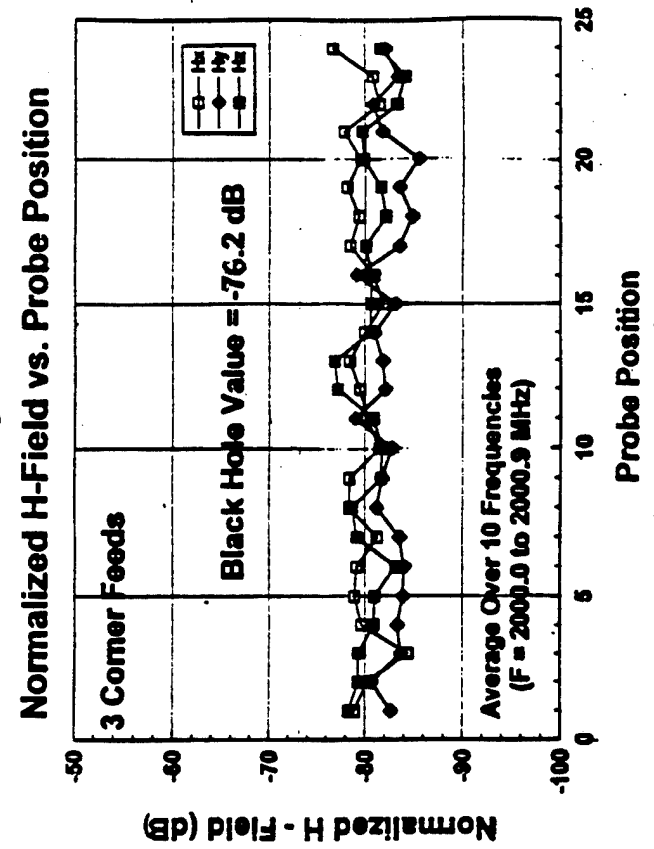
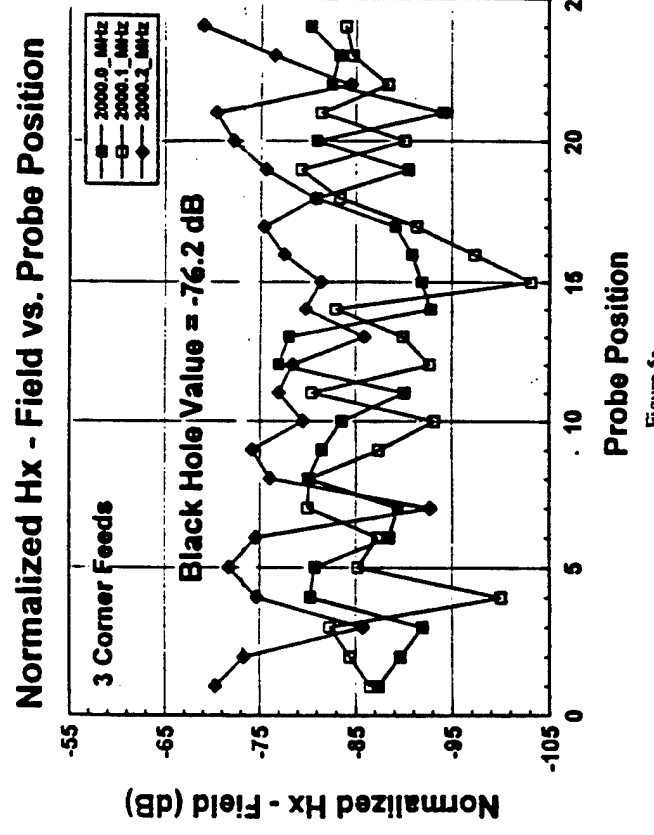
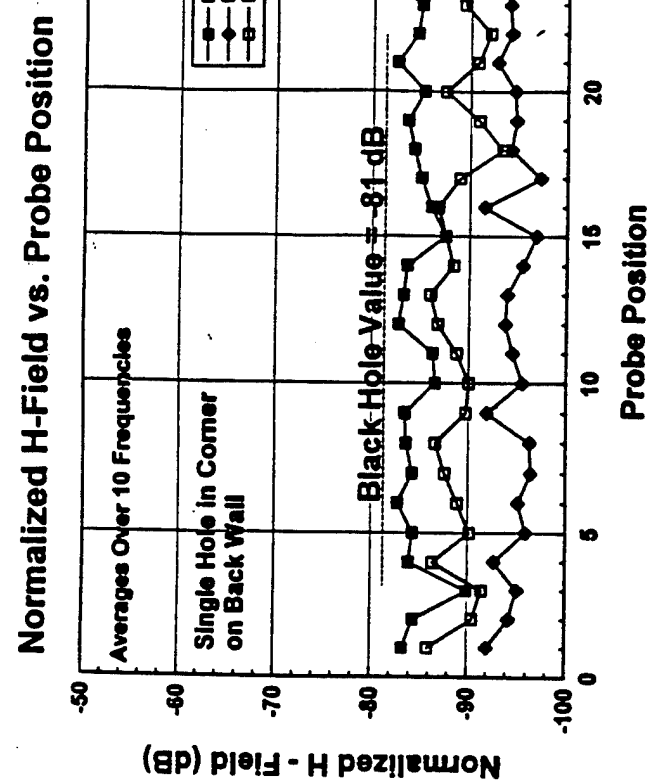
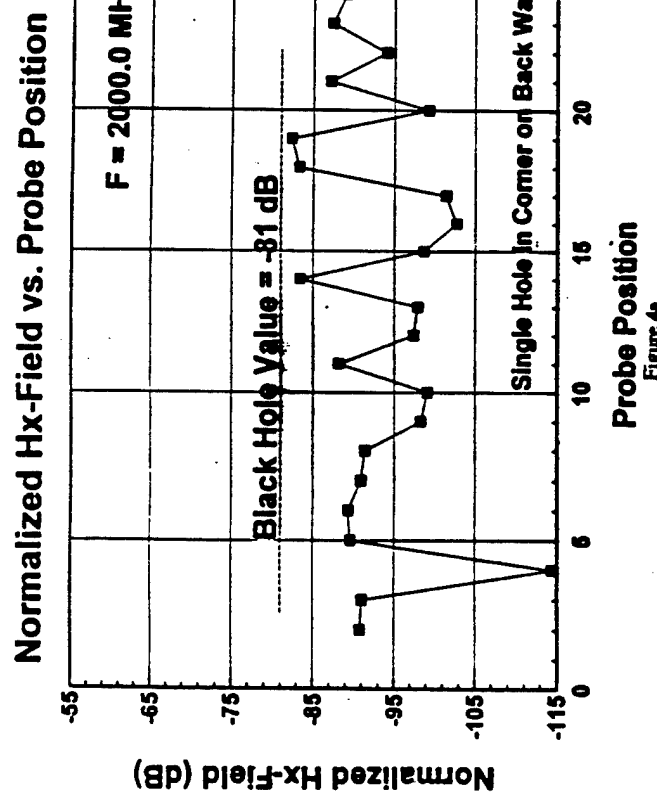
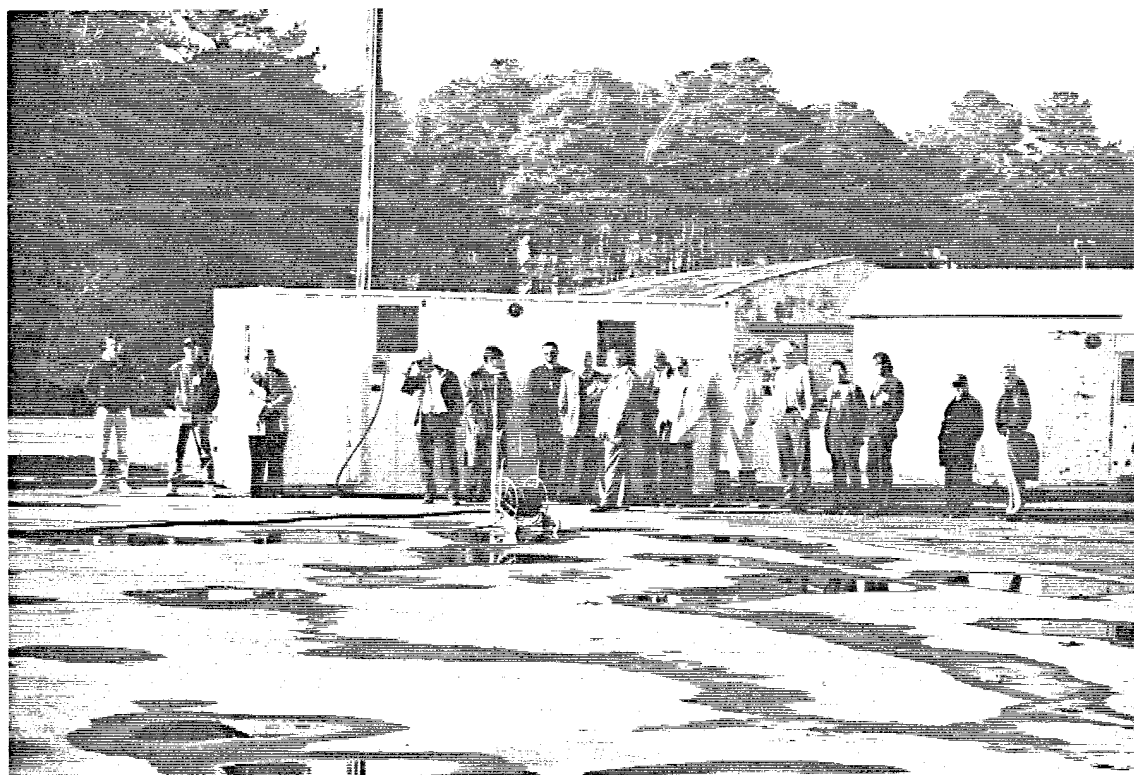


Figure 2 Applied pulses

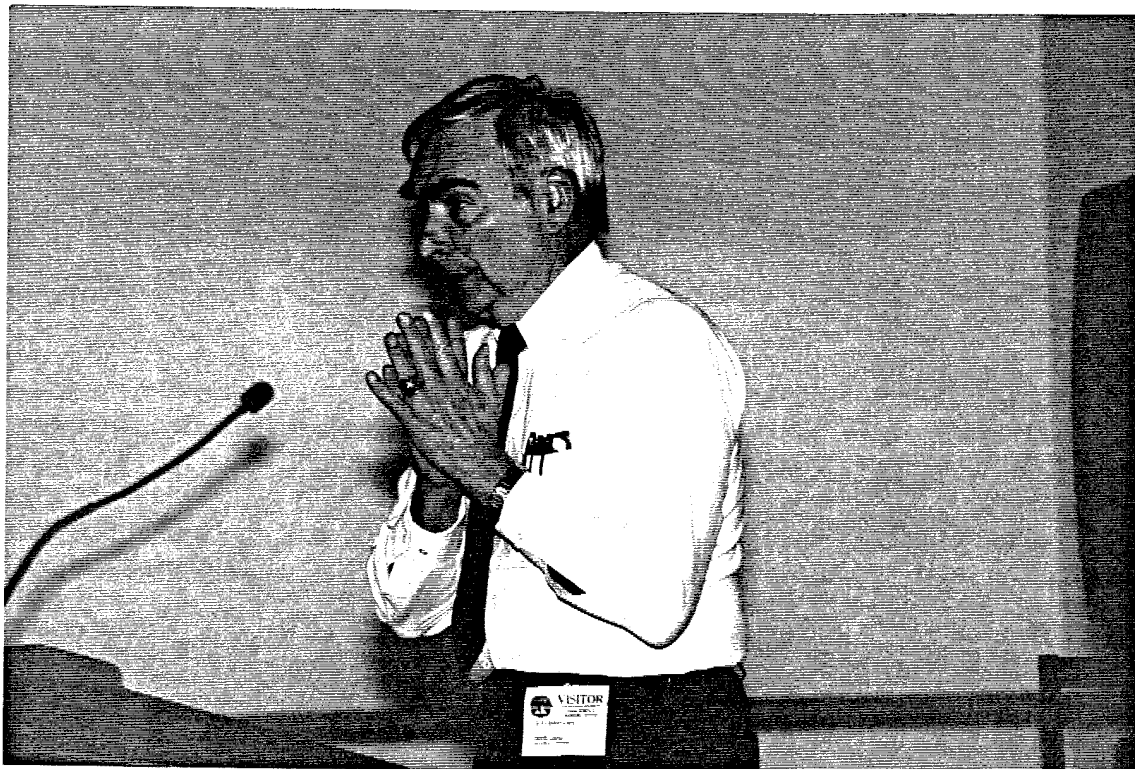








**DR. GUASTAV FREYER
NORTHEAST CONSORTIUM FOR
ELECTRICAL ENGINEERING**



**COMPARISON OF BOEING 757 ELECTROMAGNETIC CAVITY
CHARACTERIZATION DATA USING BAND LIMITED WHITE
GAUSSIAN NOISE, CW WITH MECHANICAL MODE-MIXING,
AND CW FREQUENCY STEP EXCITATIONS**

Gustav J. Freyer
Monument, CO

ABSTRACT

This paper presents a preliminary analysis of a limited data set from tests characterizing the electromagnetic environment in the cavities of an operational, passenger configured Boeing 757. The aircraft cavities were excited using band limited white gaussian noise, swept frequency CW with mechanical mode-mixing, and swept frequency CW without mode-mixing (frequency stepping). The results presented for the passenger cabin show that the electromagnetic environment produced by the band limited white gaussian noise is equivalent to the bandwidth average of the frequency stepping environment. The mode-mixed CW excitation is a statistical upper bound to the other two excitation techniques.

INTRODUCTION

The USAF Phillips Laboratory (PL) and the Naval Surface Warfare Center, Dahlgren Division (NSWCDD) each performed electromagnetic characterization tests on the NASA Langley Research Center (LaRC) Boeing 757. The aircraft was passenger configured and fully operational. The aircraft cavities have quality factors, Q , which vary from less than 100 to greater than 1000 over the frequency interval 0.5 - 6 GHz.

The PL tests were performed at Kirtland AFB, NM using the Band Limited White Gaussian Noise (BLWGN) excitation technique developed by Major T. Loughry of the PL [1]. The BLWGN data presented in this paper were not included in the published report of a portion of the BLWGN data [2]. The NSWDD tests were performed at LaRC, Langley, VA using CW excitation and mechanical mode-mixing. Both tests included CW excitation by frequency stepping (FS) with no mode-mixing.

This paper presents the results of a preliminary analysis of a small portion of the extensive BLWGN and CW test data. A complete analysis of the data is in process [3].

BAND LIMITED WHITE GAUSSIAN NOISE DATA

Figure 1 shows the electromagnetic environment (EME) for internal excitation of one of the several passenger cabin configurations. A configuration consisted of a unique location,

orientation, and polarization of the transmit (TX) and receive (RX) antennas. The TX and RX antennas were broad band horns. The same antennas were used to collect all data for the PL portion of the test.

The BLWGN signal excited the modes existing in the cavity within a 50 MHz bandwidth (BW). No physical changes occurred in the cavity during the collection of data associated with a particular configuration.

Note the structure in the 50 MHz BLWGN data (solid line). There are variations approaching 10 dB over a frequency interval of 100 MHz. This structure has also been observed in other aircraft data.

Figure 1 also shows FS data for the same configuration (dotted line). These data were obtained by stepping a CW signal over the frequency interval 0.5 to 6 GHz. The sampling interval for both data sets was about 3.5 MHz.

As expected the FS data show substantially more structure than the BLWGN data which frequency averages over the modal structure. Calculating a 50 MHz BW running average of the FS data yields a trace identical to the BLWGN data. The BLWGN averages out the narrow, deep minima which are generally not of interest. However, in the averaging process the BLWGN data also miss the peaks. The difference between the FS peaks and the BLWGN average will vary with BW and the intrinsic width of the peak. This difference could be a parameter of interest for immunity testing. The maximum difference shown is about 5 dB which is a consistent maximum from several configurations in the B-757 cockpit and passenger cabin.

CW/MECHANICAL MODE-MIXING DATA

Figure 2 shows CW data with mechanical mode-mixing for a particular cockpit cavity configuration. The TX and RX antennas were dual-ridged horns for all data acquired with CW excitation and mechanical mode-mixing. The data were taken over two bands, 0.8 to 2.9 GHz and 2.75 to 6 GHz. The signal generator was set to dwell at a particular frequency for a period exceeding the tuner rotation time. The data were acquired with a spectrum analyzer in the "max hold" mode. The step size for the low band was 3.5 MHz and 4 MHz for the high band.

The cause of the power density offset (~ 20 dB) between the BLWGN and the CW passenger cabin measurements has not been resolved. However a much smaller offset (~ 5 dB) in the cockpit data suggest that it may be caused, at least in part, by the variation in field uniformity observed in the B-757 passenger cabin.

Figure 3 shows a comparison of several types of data over the frequency interval 1.0 ± 0.1 GHz. The heavy solid line is the

swept CW data from Figure 2. The triangles indicate the peak data from stirring ratio (SR) measurements. These data were obtained by sampling the power density at a discrete frequency as the tuner rotated. Theoretically the swept CW and SR data should be the same. The differences indicate measurement uncertainty.

The light solid line is FS data obtained with 0.65 MHz frequency steps. Measurements obtained with 20 KHz spacing over limited frequency intervals verify the FS data of Figure 4. As indicated by the BLWGN data, the modal structure occurs over frequency intervals of about 2 MHz or greater. The FS data are bounded by the swept CW with mode-mixing. From SR measurements with adequate mode-mixing, the peak-to-average power density ratio is typically in the range 6 - 8 dB with a maximum-to-minimum ratio of greater than 20 dB. The FS data appear to agree with these general observations about the statistical variations in the EME of a complex cavity. These data also indicate the potential problems of interpreting the results obtained with a single FS measurement.

Also shown in Figure 3 is the expected result of using 50 MHz BLWGN (dashed line). These data are calculated from the FS measurement but are representative of an actual BLWGN measurement. The average difference between the simulated BLWGN data and the swept CW with mode-mixing is greater than 5 dB with a maximum difference greater than 10 dB. Again these data indicate the potential problem of interpreting the results obtained with a single BLWGN measurement.

SUMMARY

This paper has presented preliminary results from an extensive data base of cavity EME for an operational, passenger configured B-757.

As expected the data show that the BLWGN EME is equivalent to the FS EME average over the appropriate bandwidth.

The FS data is consistent with the statistical variations in EME in a complex cavity with adequate mode-mixing.

The swept CW with mode-mixing data bounds the FS and BLWGN data.

REFERENCES

1. Loughry, T.A., "Frequency Stirring: An Alternate Approach to Mechanical-Mode-Stirring for the Conduct of Electromagnetic Susceptibility Testing", USAF Phillips Laboratory PL-TR-91-1036, November 1991.
2. Loughry, T.A. and Younger, C.L., "NASA B-757 Cavity Band Limited White Gaussian Noise Tests", USAF Phillips Laboratory Draft Tech Rpt, March 1995.

3. Freyer, G.J., Hatfield, M.O., Loughry, T.A., Dudley, V., and Slocum, M., "Phase III Demonstration Test of the Electromagnetic Reverberation Characteristics of Large Transport Aircraft", Naval Surface Warfare Center, Dahlgren Division, NSWCDD/TR-95/XXX, in process.

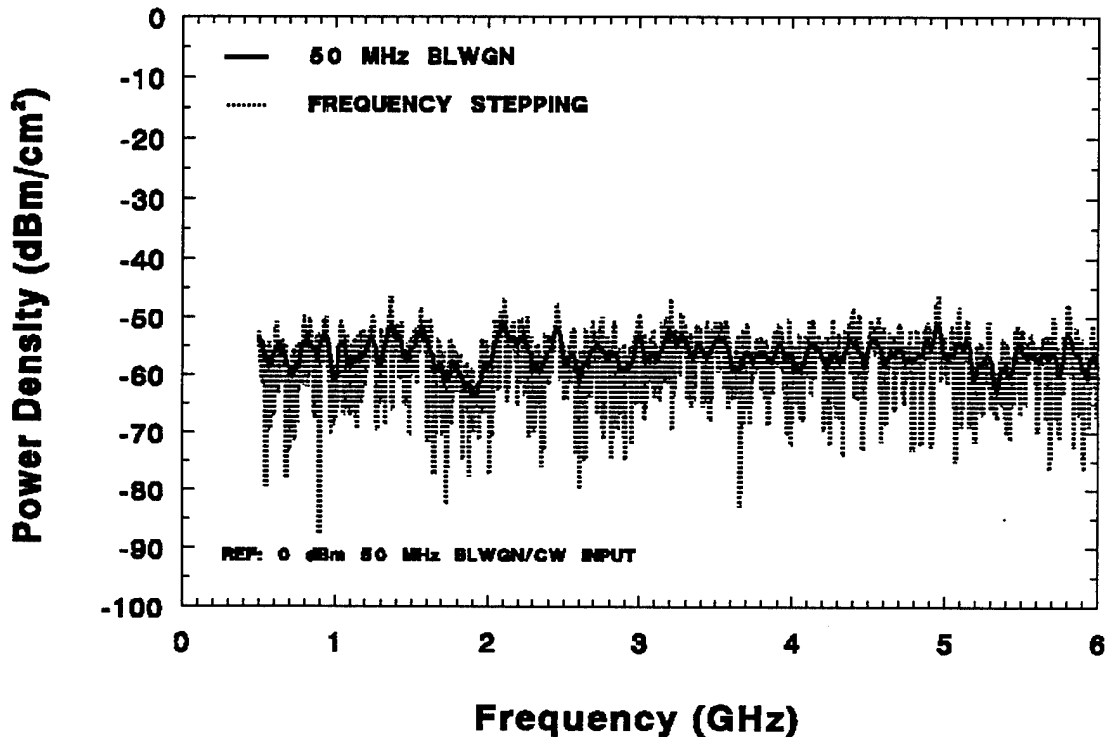


FIGURE 1.B-757 PASSENGER CABIN ELECTROMAGNETIC ENVIRONMENT FROM 50 MHz BLWGN AND STEPPED FREQUENCY CW EXCITATION

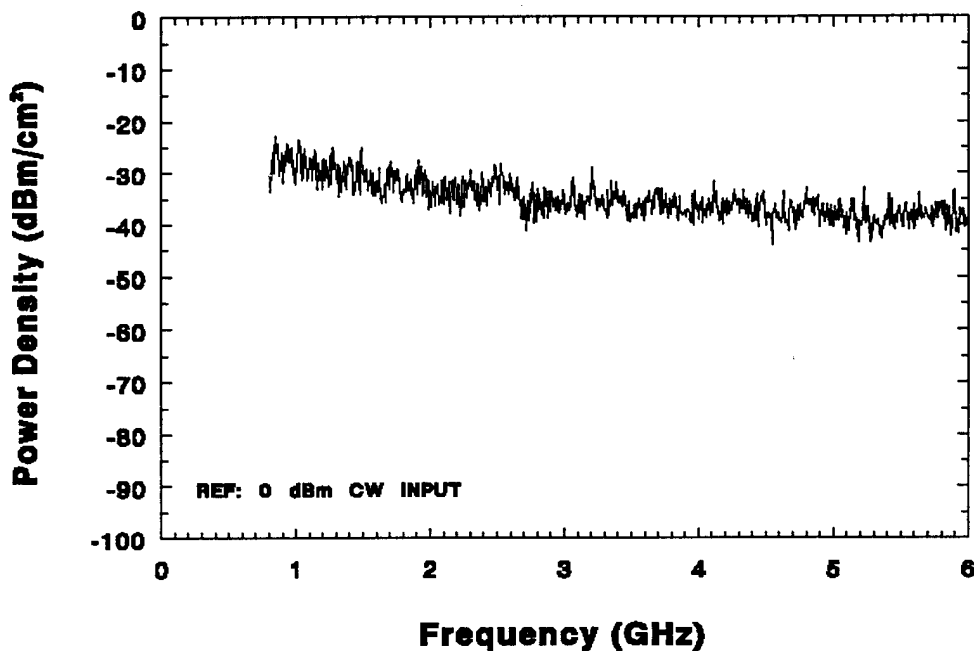


FIGURE 2.B-757 PASSENGER CABIN ELECTROMAGNETIC ENVIRONMENT FROM SWEPT FREQUENCY EXCITATION WITH MODE-MIXING

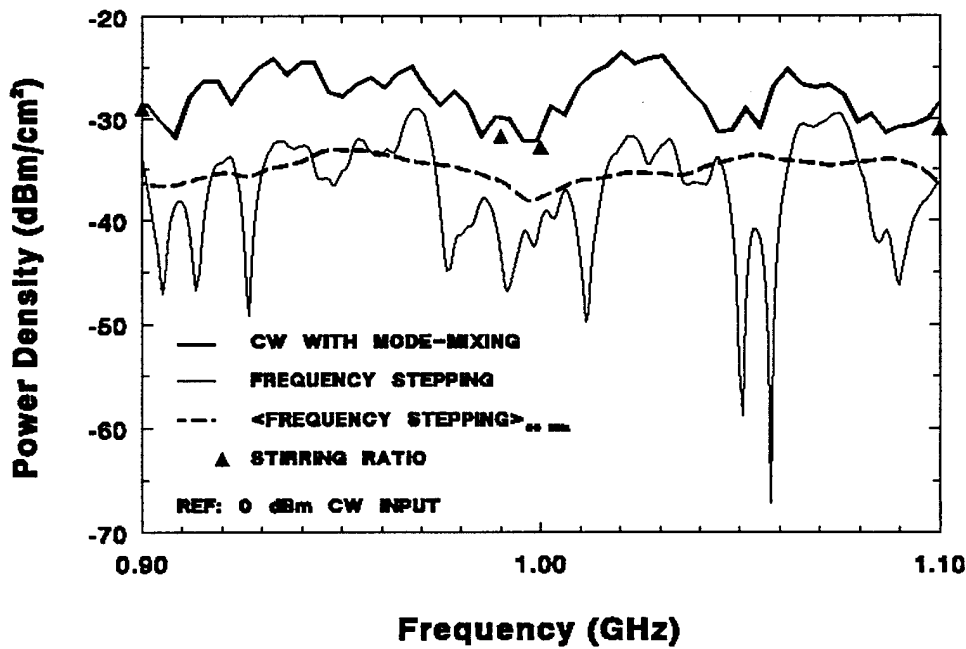
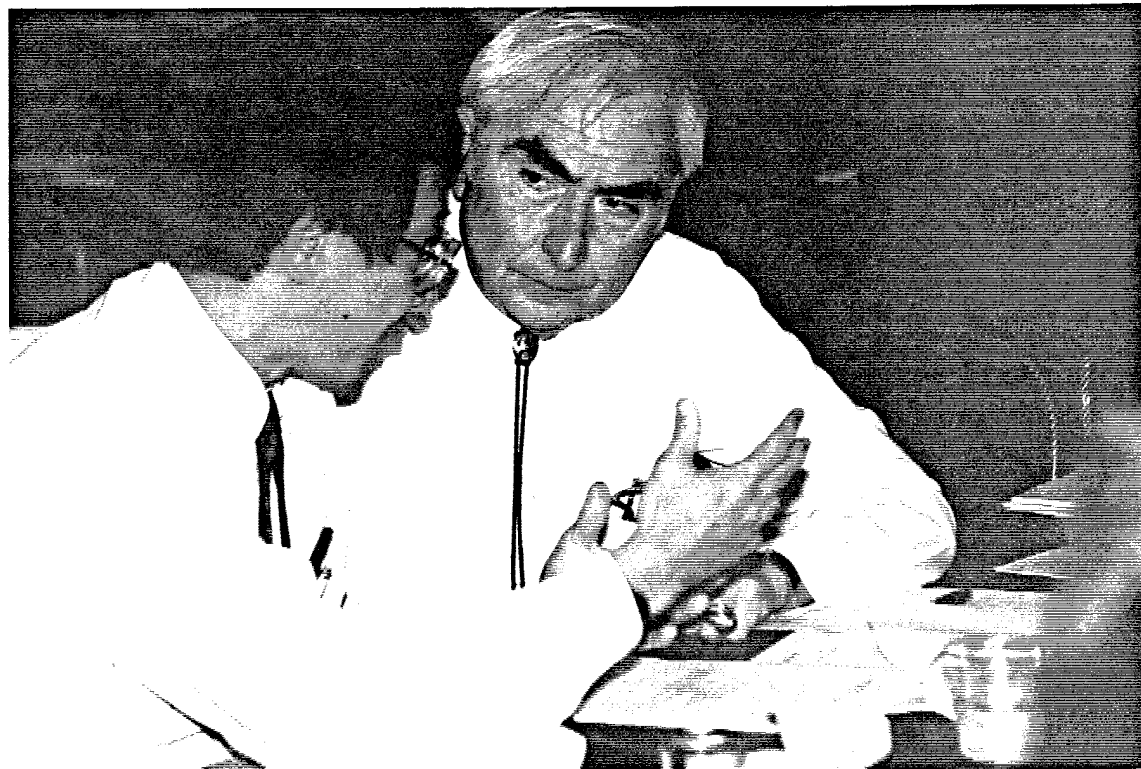
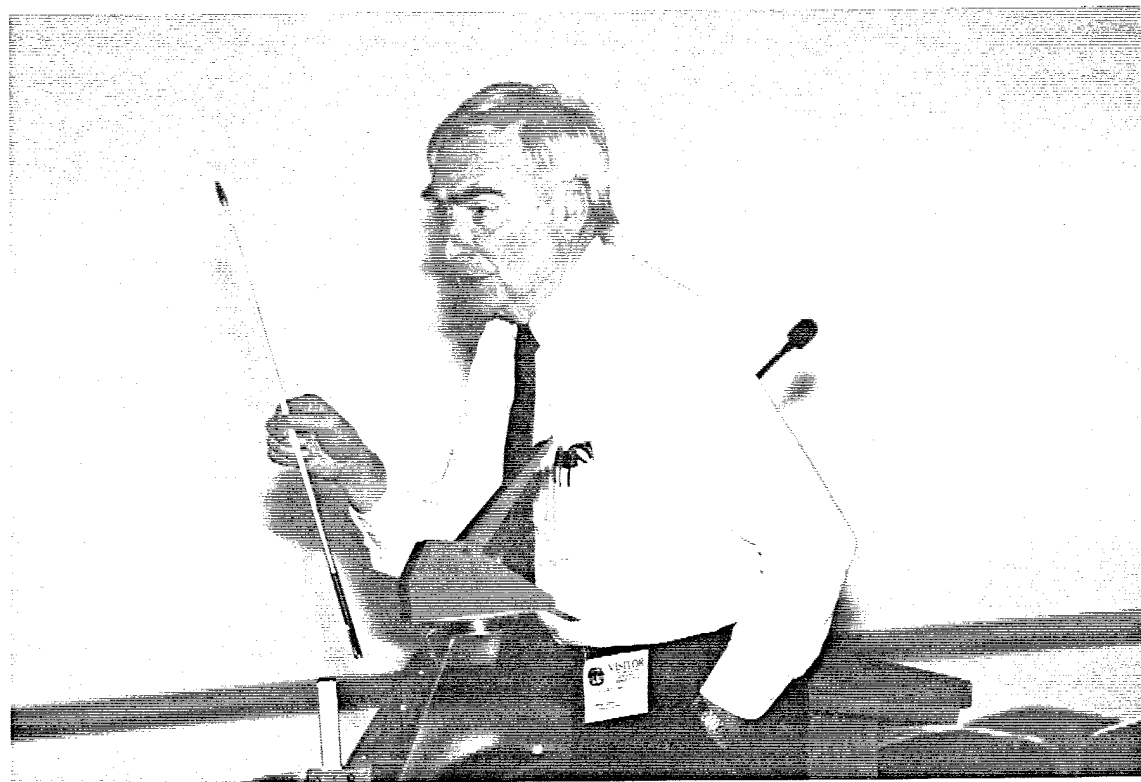
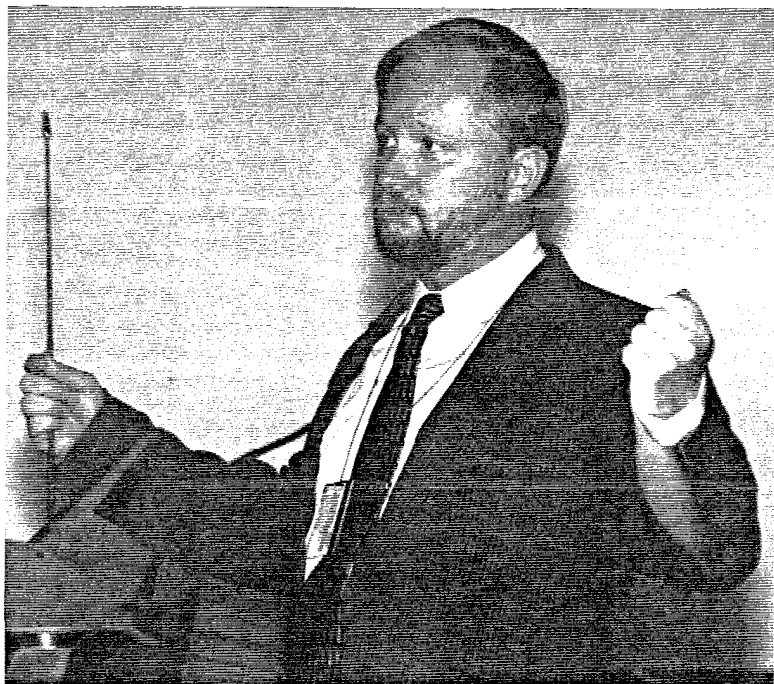


FIGURE 3.COMPARISON OF THREE EXCITATION TECHNIQUES





NAVAL SEA SYSTEMS COMMAND



**MR. MICHAEL HATFIELD
NSWCDD CODE F-52**

FREQUENCY CHARACTERIZATION OF
REVERBERATION CHAMBERSMICHAEL O. HATFIELD
NAVAL SURFACE WARFARE CENTER
DAHLGREN DIVISIONMICHAEL B. SLOCUM
COMPUTER SCIENCES CORPORATION
KING GEORGE, VA

ABSTRACT

A series of measurements to investigate the modal structure of a reverberation chamber were conducted at the Dahlgren Division of the Naval Surface Warfare Center, Dahlgren Virginia. These measurements were Phase I of a project to determine the frequency dependent characteristics of the fields in a reverberation chamber.

Measurements were taken to compare the modal structure excited by both CW and band limited white gaussian noise.

Measurements were also obtained to determine the required step size for collecting field characterization data using discrete frequency data.

The measurements were taken over frequency bands ranging from 1 MHz to 100 MHz using frequency steps from .1 to 100 kHz. The frequency bands selected covered frequencies from below the first chamber resonance to 18 GHz. Each frequency band was evaluated for multiple boundary conditions (i.e. independent positions of the paddle wheel tuner). The data collected were analyzed to determine the width of the peaks that occur within the chamber as a function of frequency. The results of the analysis yielded the uncertainty of obtaining the true peak of the fields in the chamber as a function of the size of frequency and the frequency step.

INTRODUCTION

Use of reverberation chambers to conduct electromagnetic (EM) effects testing is increasing as the technology matures. Inclusion of the test technique into such documents as RTCA DO-160D which covers the testing of aircraft avionics, the FAA HIRF Users Guide for certification of commercial aircraft to High Intensity Radiated Fields, SAEJ551, and GM-9120P has led to many manufacturers and commercial test houses acquiring reverberation chambers.

Recent investigations into the use of band limited white gaussian noise (BLWGN) to excite the modal structure of reverberation chambers [1,2] have yielded some interesting findings. Results of EM effects testing [2] show that BLWGN yielded comparable results to those obtained using CW excitation and mechanical stirring. However, other investigations [3] show large variations in upset levels when utilizing BLWGN. These variations lead to the need for direct comparison of the modal structures excited by CW and BLWGN excitations. The first set of measurements addresses this issue.

Further investigations conducted by the authors and others suggest that the effective electromagnetic test environment for a device under test (DUT) when utilizing BLWGN is affected not only by the bandwidth of the noise as reported in [1], but also by the susceptibility bandwidth of the DUT. The implications of these observations is that the effective electromagnetic test environment is determined by the susceptibility bandwidth of the DUT as well as the field characteristics of the reverberation chamber. Data show that this applies to swept CW excitation as well as BLWGN.

The observations on the role of the DUT in defining the effective test environment indicate the need to understand the electromagnetic environment in a reverberation chamber to a level of detail not currently available. The field characteristics include the statistical distribution of the three field components at an arbitrary location in the chamber. Also required is the chamber uniformity, which is a comparison of the field components for multiple locations within the chamber. Since test results appear to depend on the susceptibility bandwidth of the DUT, the chamber field characteristics must be known as a function of frequency for bandwidths equal to the susceptibility bandwidths of the DUT. The detailed field characteristics described above will require collection of a significant data base. A major factor in determining the size of the data base is the number of frequencies, i.e. the frequency step size, required to adequately characterize the chamber with a reasonable level of uncertainty. As the frequency step size decreases the total number of data points increases and, in the limit, could become unmanageable. Conversely, as the step size increases the expected uncertainty in determining the characteristics of the peak field components also increase. Thus it is necessary to determine an optimum frequency step size before the full characterization measurements can begin. The second set of measurements addresses this issue.

APPROACH

Two sets of data were collected for this report. The first set of data were used to compare the modal structure generated using CW and BLWGN excitation. Data were collected using BLWGN and swept CW illumination of the NSWCDD reverberation chamber at a common center frequency using multiple positions of the paddle wheel tuner.

The second set of data were collected to determine the optimum frequency step to be used to characterize the chamber as a function of frequency. Data were taken over frequency bands ranging from 1 MHz to 100 MHz in width, and using frequency steps from .1 to 100 kHz. Each frequency band was evaluated for multiple boundary conditions (i.e. independent positions of the paddle wheel tuner). The data collected were analyzed to determine the "minimum" width of the peaks that occur within the chamber as a function of frequency.

EXPERIMENTAL PROCEDURE

To compare the modal structure excited by CW and BLWGN, the chamber was configured as shown in Figure 1. The CW mode of excitation was accomplished by disconnecting the noise source input from the mixer. The set-up allowed the excitation mode of the chamber to be changed without effecting the chamber in any other way. The fields in the chamber were monitored using a spectrum analyzer set to the "peak and hold" mode with the resolution bandwidth (RBW) set to 30 kHz. The spectrum analyzer RBW was much less than the noise BW. This allowed the spectrum analyzer to capture the "peak envelope" of the field pattern generated by each excitation method.

For BLWGN excitation, the spectrum analyzer was left in the "peak and hold" mode while multiple sweeps of the spectrum analyzer were collected. The RF synthesizer was set to the frequency of interest and "mixed" with a fixed bandwidth of white gaussian noise as shown in Figure 1. When the rate of change of the peak and hold trace, which was capturing the peak envelope of the rapidly changing noise excitation, had diminished such that no appreciable change occurred the additional sweeps, data collection was stopped.

For CW excitation, the spectrum analyzer was again left in the "peak and hold" mode while a single 200 second sweep of the spectrum analyzer was collected. The RF synthesizer was set to sweep over the interval of interest (equivalent to that generated by the BLWGN) at a rate of 20 milliseconds per sweep.

To determine the optimum frequency step to be used to characterize the chamber as a function of frequency the test set-up was changed as shown in Figure 2. Data were collected by stepping through multiple frequency bands up to 100 MHz in width using frequency steps ranging from .1 to 100 kHz. For each band the synthesizer was stepped through the frequency band while the spectrum analyzer was used as a receiver to measure the amplitude of the signal received at each frequency. The process was repeated for five (5) positions of the paddle wheel tuner.

RESULTS

The data collected to compare the modal structure excited by CW and BLWGN for fixed boundary conditions are shown in Figures 3 - 6. Figure 3 shows the data for 200 +/- 10 MHz and the delta between the two excitation techniques for two different boundary conditions (paddle wheel tuner conditions). As expected the modal structures in Figure 3 vary by as much as 25 dB at some frequencies but the peak values are essentially the same. The two traces in each Figure show that both CW and BLWGN excite the same modal structures. The same characteristics can be seen in Figure 4 for 1000 +/- 10 MHz, Figure 5 for 8000 +/- 10 MHz and Figure 6 for 16000 +/- 10 MHz.

The data collected to define an optimized frequency step as a function of frequency are shown in Figures 7a - 15a.

In order to determine the frequency interval to use in collecting the Phase II data, it was necessary to replot the data normalizing both the peak amplitude of each trace to 0 dBm and the frequency at which the peak occurred to 0 Hz. These plots are shown in Figures 7b - 15b.

Figures 7 - 10 show the data collected at or near 500 MHz. Figure 7a shows the data collected from 500 - 600 MHz using 10 kHz frequency steps. Figure 7b shows that the normalized peak for Figure 7a is approximately 30 kHz wide at the 1/2 dB point. Figure 8a shows the data for 500 - 510 MHz collected using 1 kHz frequency steps. Figure 8b shows that the normalized peak for Figure 8a is again approximately 30 kHz wide. Figures 9 and 10 show the data for 500 - 501 MHz collected using 1 and 0.1 kHz frequency steps respectively. Again the normalized peaks show that the peaks are approximately 30 kHz wide. These data show not only the approximate width of the peaks, they also show that a 1 kHz frequency step is adequate for collecting the data needed. Similar data are shown in Figures 11 - 12 for 1 GHz, Figures 13 - 14 for 4 GHz and Figure 15 for 18 GHz.

CONCLUSIONS

The boundary effects data show that the modal structure which is excited in a reverberation chamber for a fixed boundary condition is the same for both CW and BLWGN excitation methods.

The modal structure data show that below 4 GHz a frequency interval of 25 kHz should detect the peak within .25 dB and a frequency interval of 50 kHz should detect the peak within 1 dB. Data above 4 GHz show that a frequency interval of 25 kHz should detect the peak within 0.2 db and a frequency interval of 50 kHz should detect the peak within 0.4 dB.

ACKNOWLEDGEMENTS

The authors wish to thank Mr. Ben Franklin of the Naval Surface Warfare Center, Dahlgren Division, for supporting this work. The authors also wish to acknowledge Dr. Gustav J. Freyer of Universal Systems Incorporated, Dr. David A. Hill and Mr. Galen Koepke of the National Institute of Standards and Technology, Mr. Truong Nguyen and Mr. Ken Dudley of the National Aeronautics and Space Administration, Ms. Diane Kempf and Mr. Bob Rakoski of the Naval Air Warfare Center for the many useful discussions regarding this topic.

REFERENCES

- [1] Loughry,T.A., Frequency Stirring: An Alternative Approach to Mechanical Mode-Stirring For The Conduct of Electromagnetic Susceptibility Testing, USAF Phillips Laboratory, PL-TR-91-1036, November 1991.
- [2] Crawford,M.L., Loughry,T.A., Hatfield,M.O., and Freyer,G.J., Validation of Band Limited, White Gaussian Noise Excitation of Reverberation Chambers and Verification of Applications to Radiated Susceptibility and Shielding Effectiveness Testing, NIST Technical Note 1375,xxxx, 1995.
- [3] Kempf, D.R., A Comparison of the Isotropic Broadband Susceptibility Test Method and An RS103 Test on An ARC-182 Radio presented at the IEEE International Symposium on EMC, Chicago, IL, August, 1994.

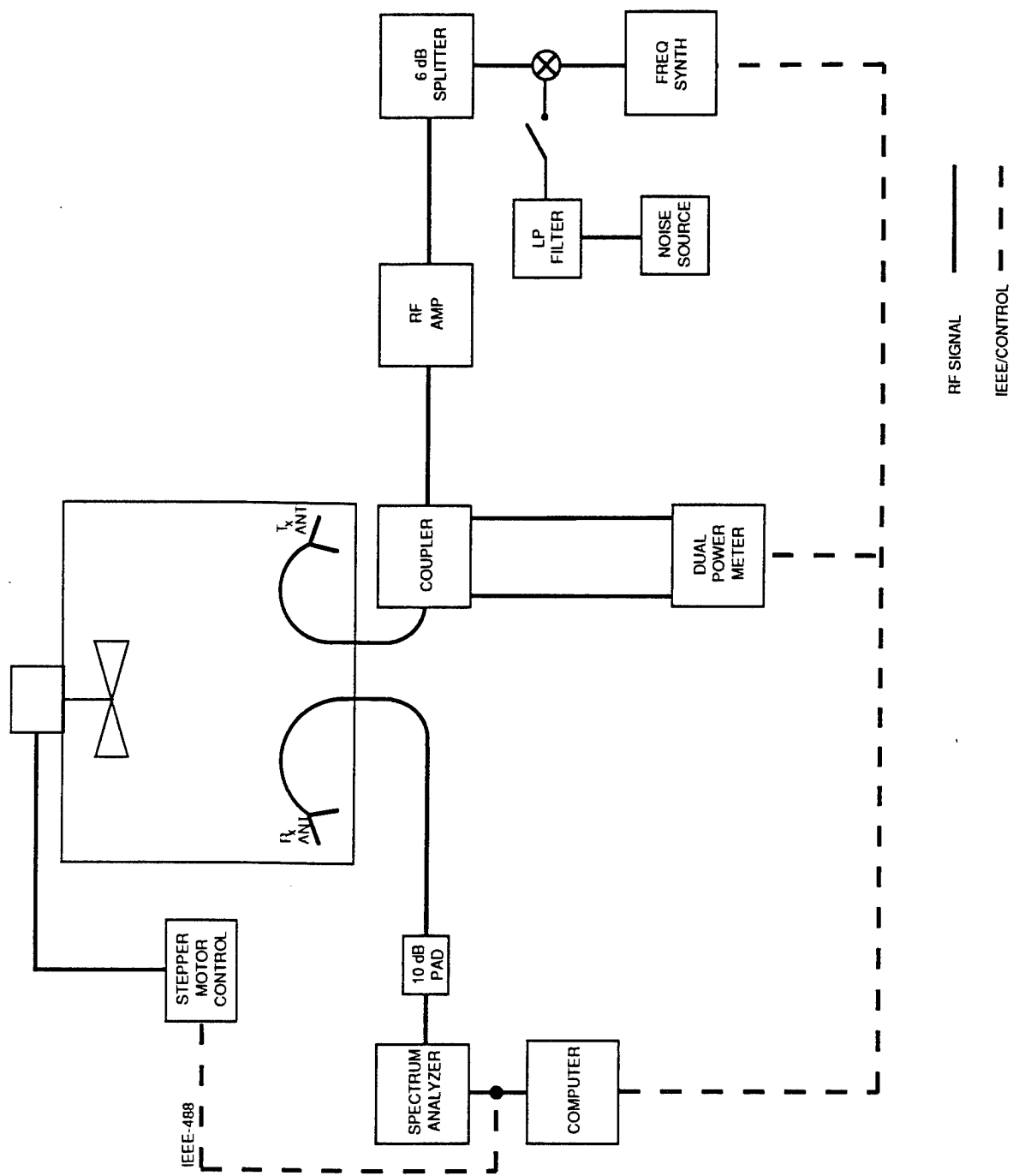


Figure 1. Test Set-up for CW vs BLWGN comparison.

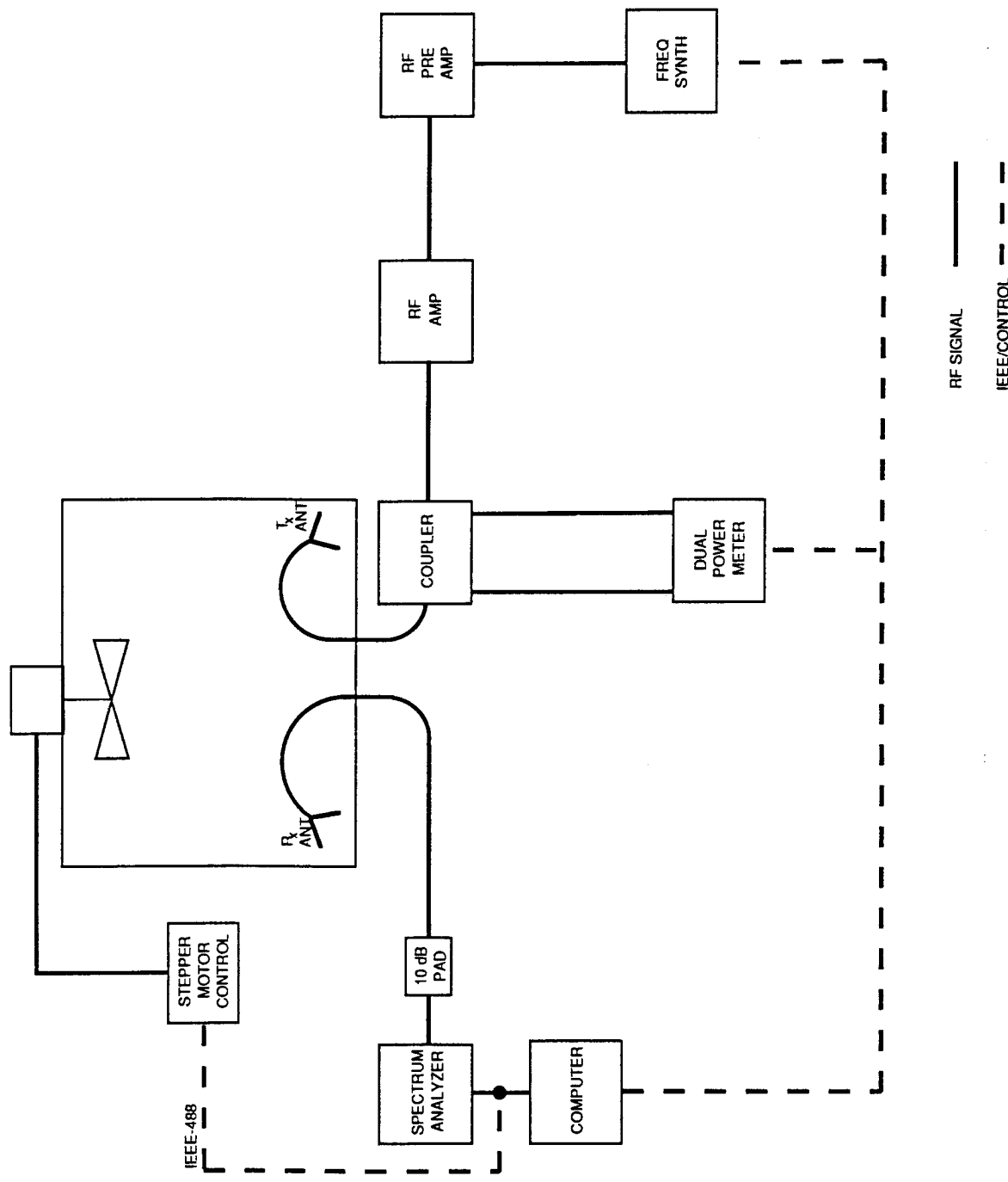


Figure 2. Test Set-up for determining the optimum frequency step.

8154415211 85

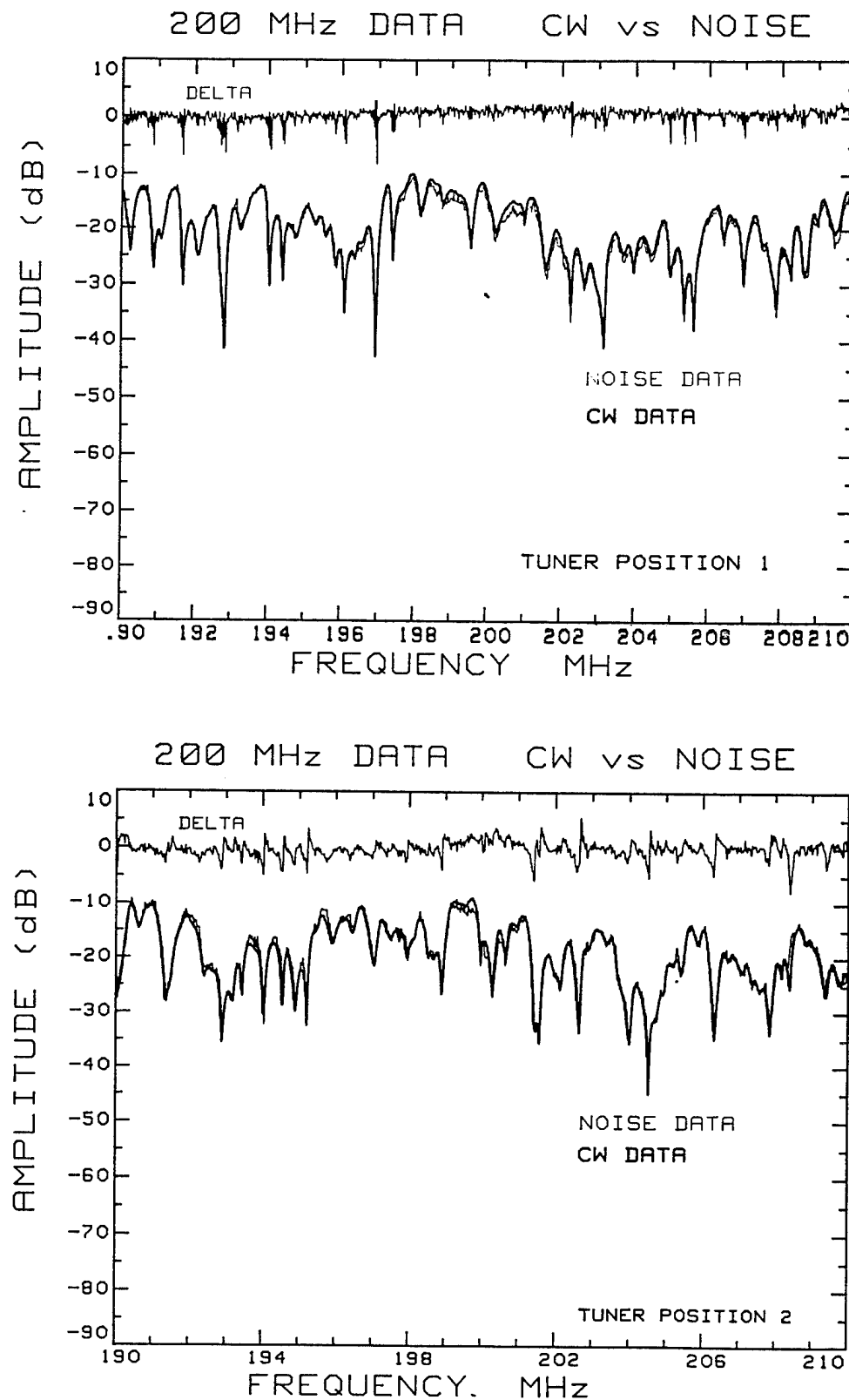


Figure 3. 200 MHz data for CW vs BLWGN comparison.

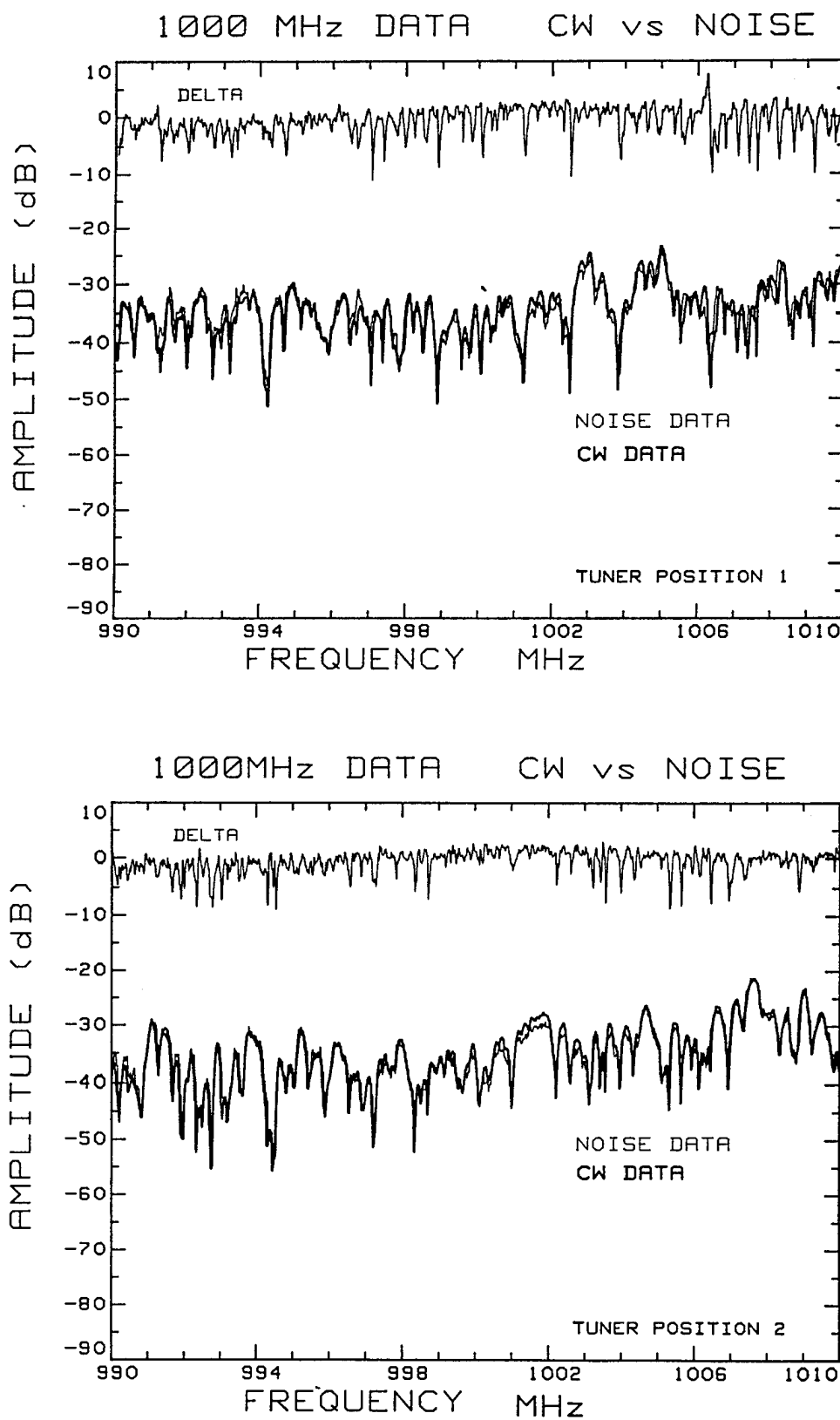


Figure 4. 1000 MHz data for CW vs BLWGN comparison.

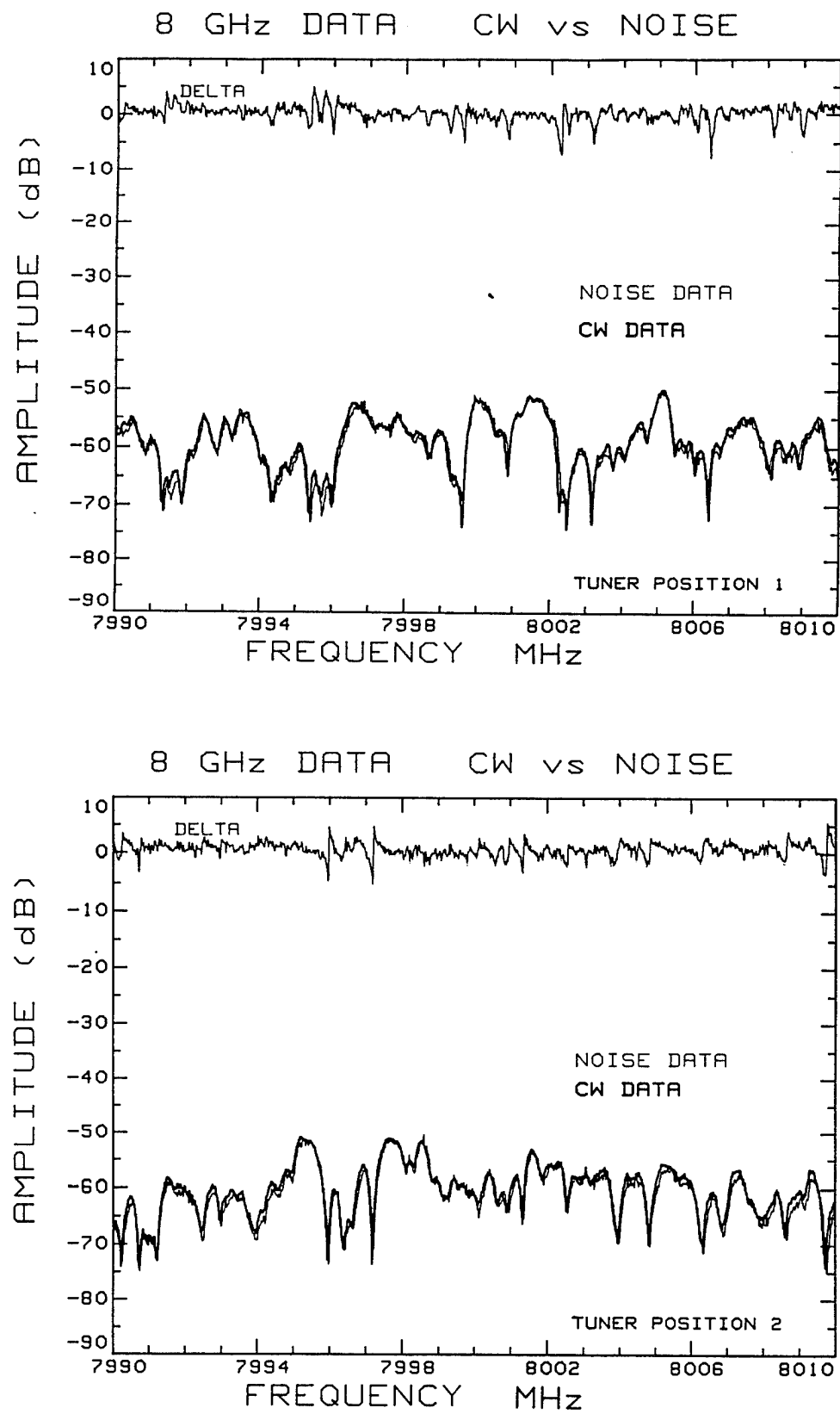


Figure 5. 8 GHz data for CW vs BLWGN comparison.

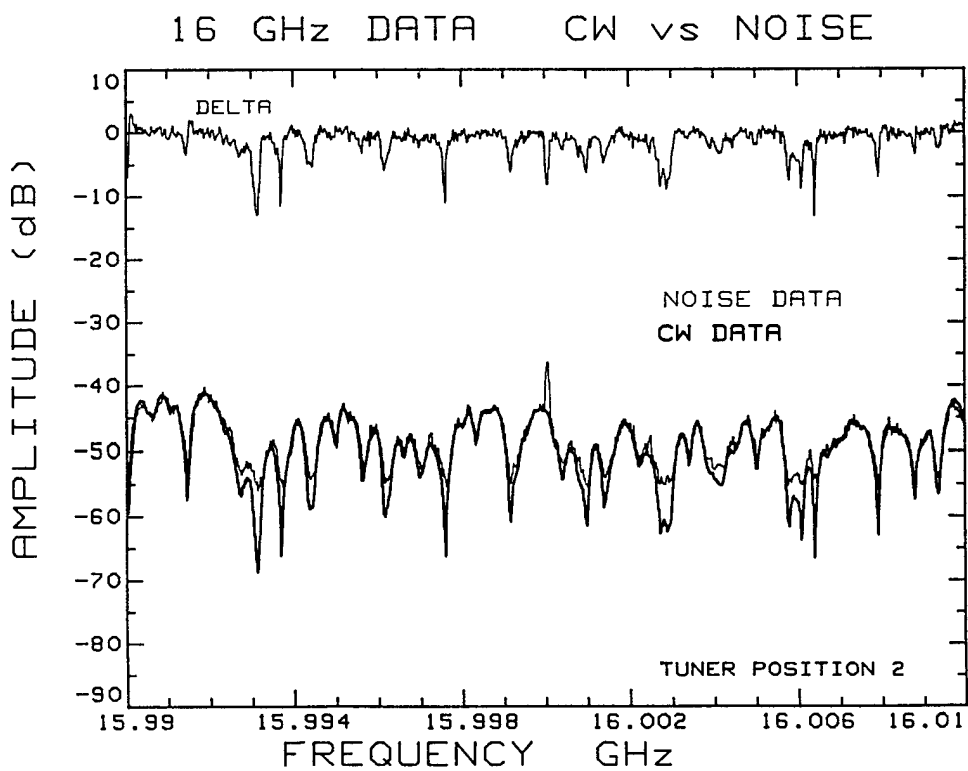
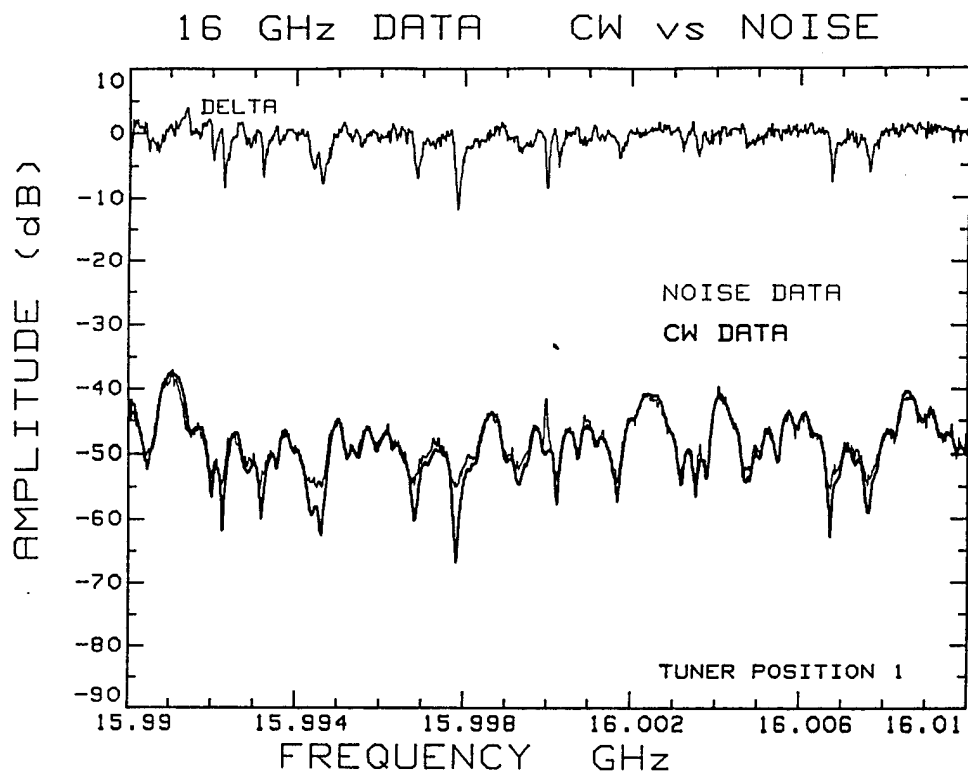


Figure 6. 16 GHz data for CW vs BLWGN comparison.

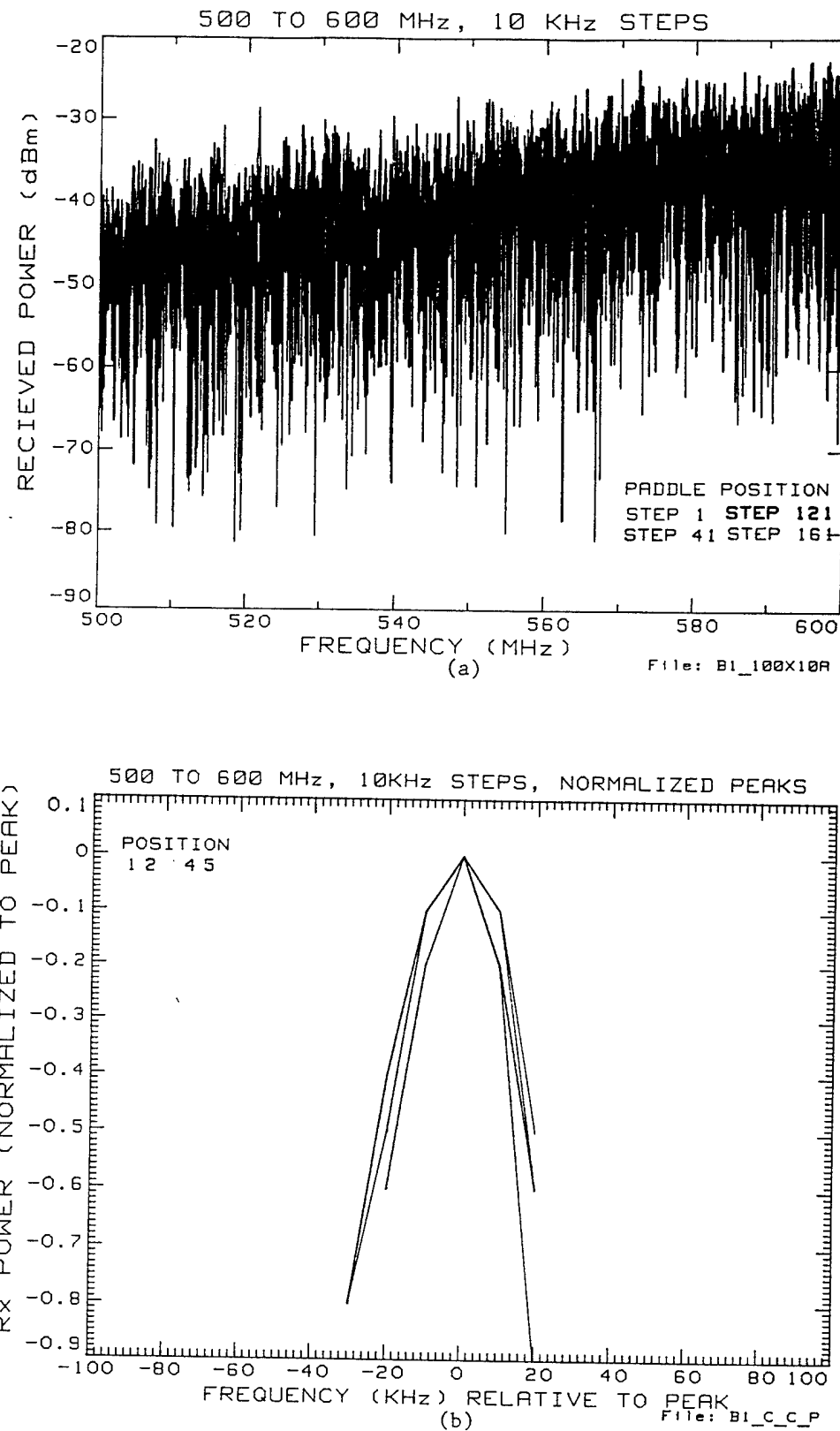


Figure 7. 500 - 600 MHz Frequency Stepping Data.

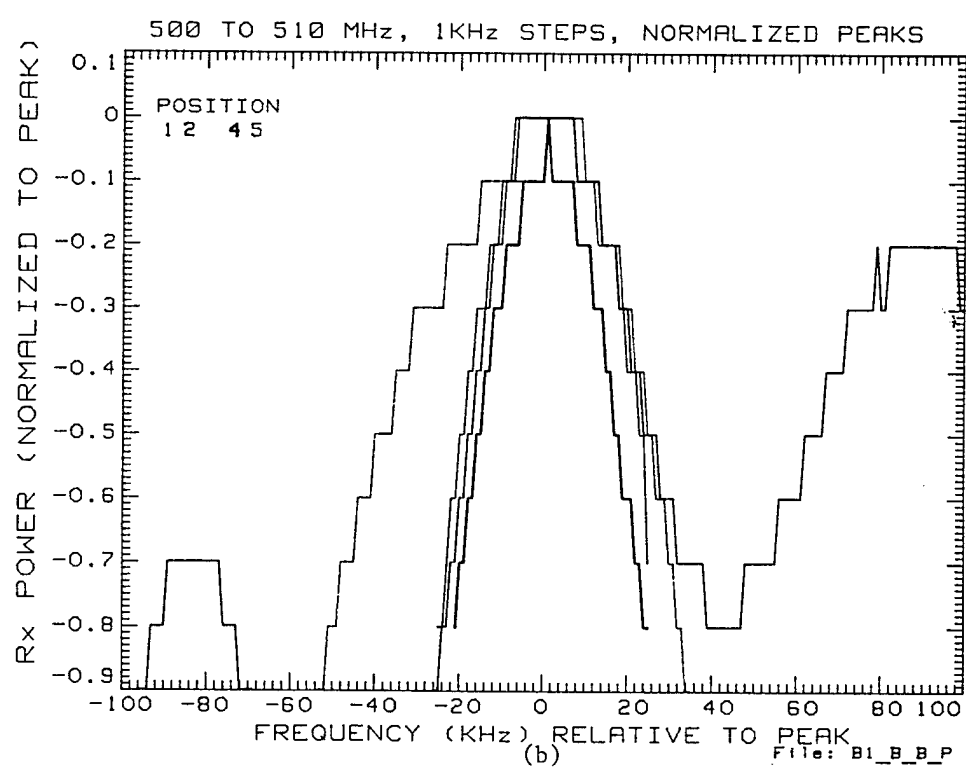
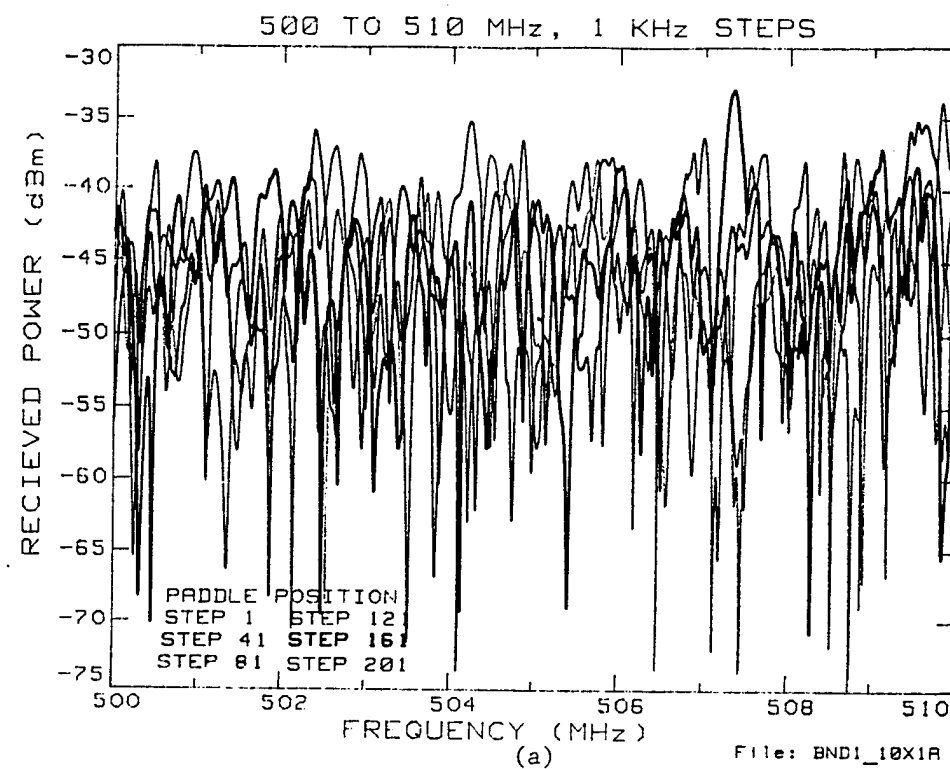


Figure 8. 500 - 510 MHz Frequency Stepping Data.

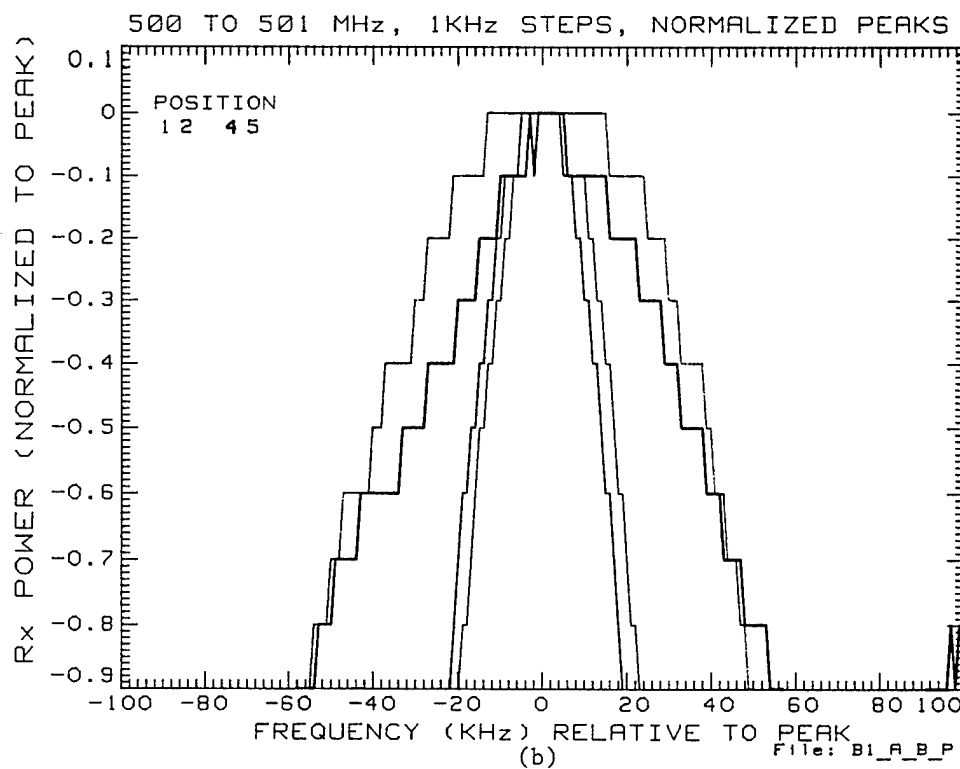
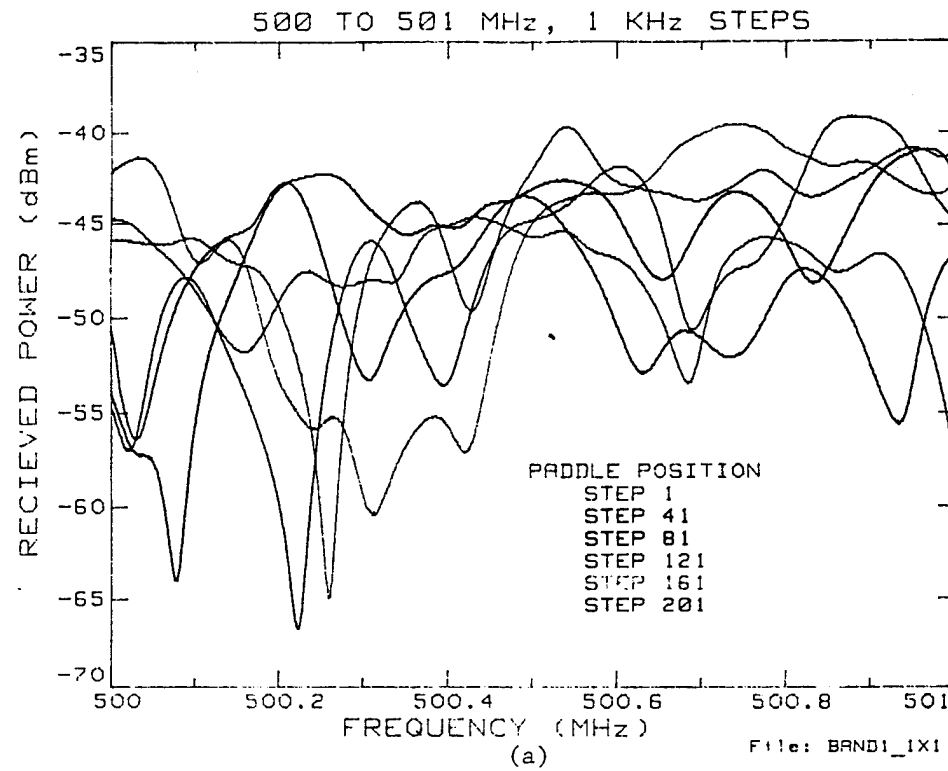


Figure 9. 500 - 501 MHz Frequency Stepping Data.

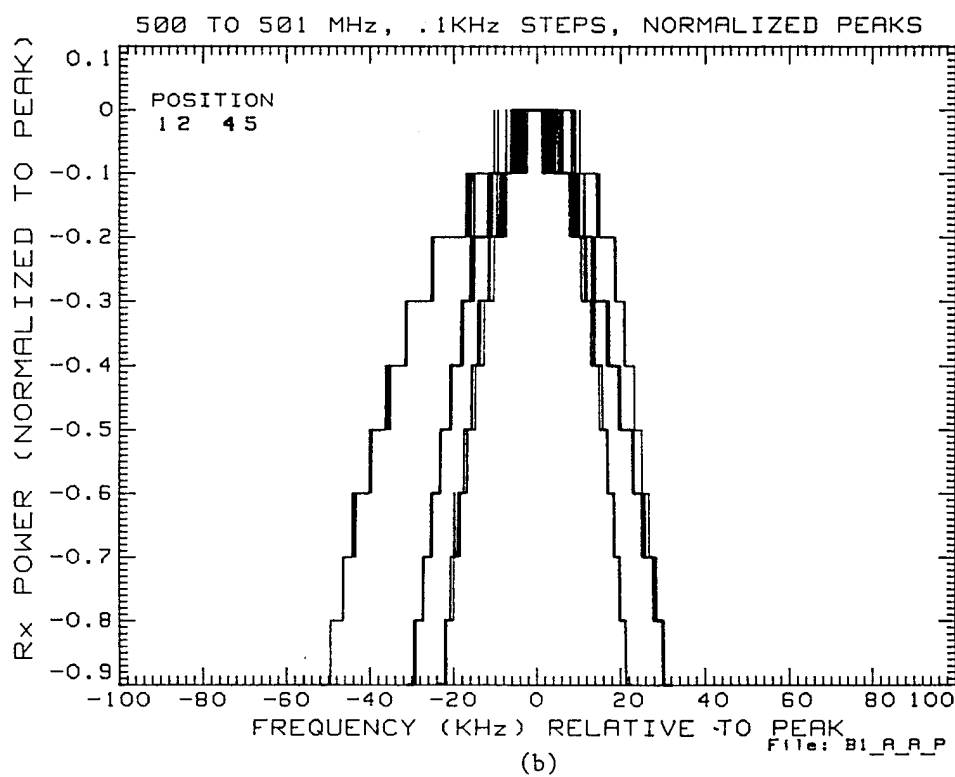
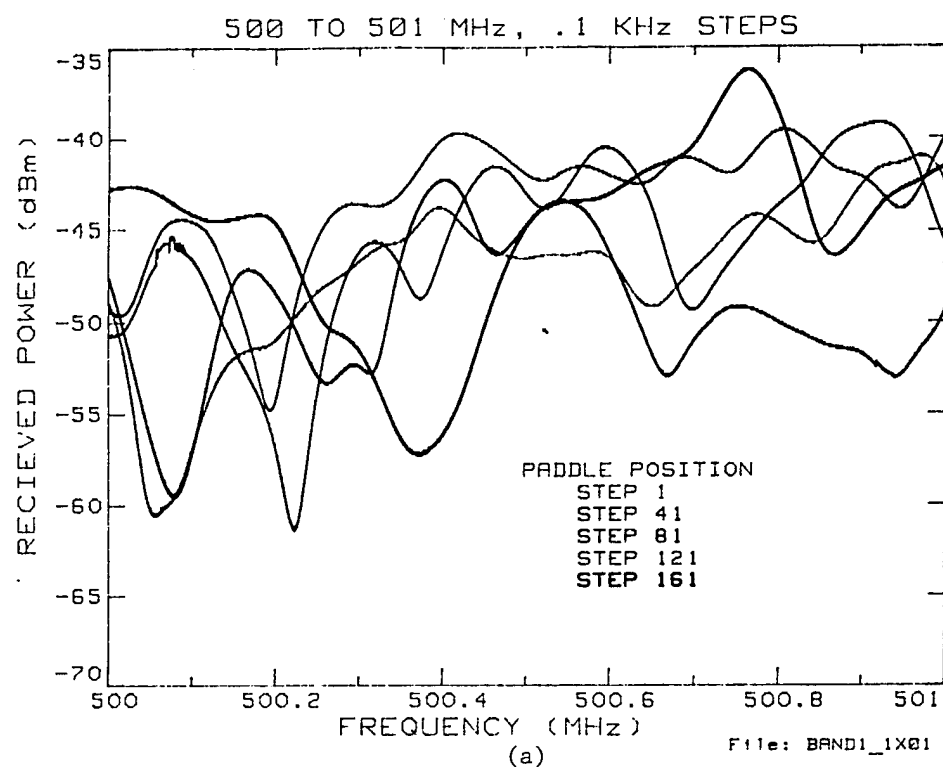


Figure 10. 500 - 501 MHz Frequency Stepping Data.

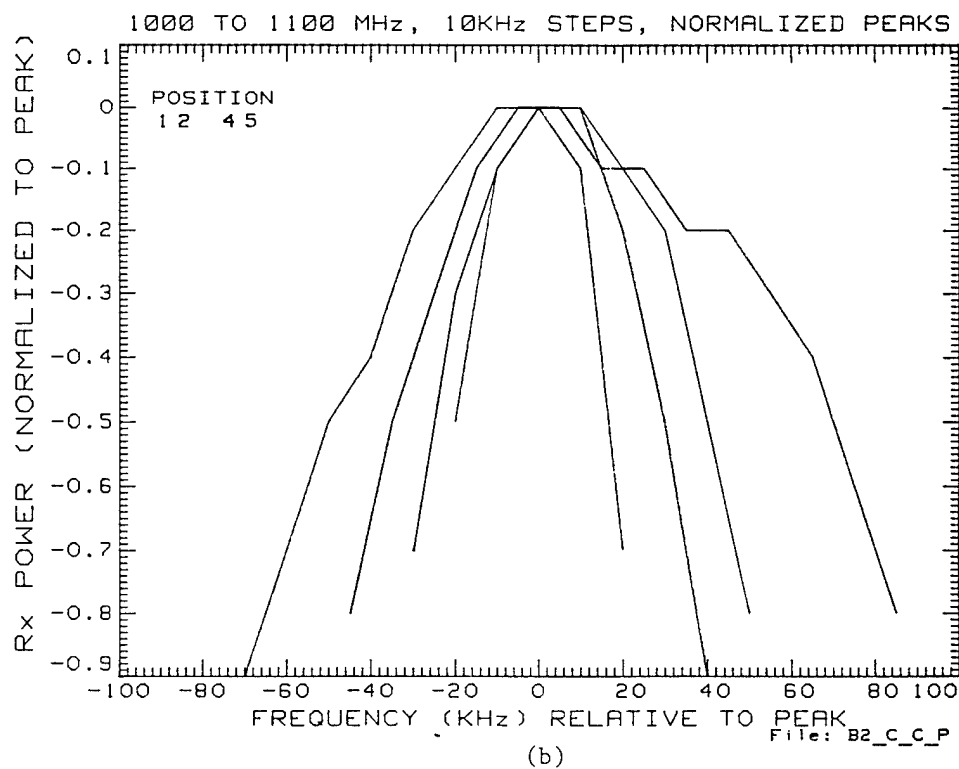
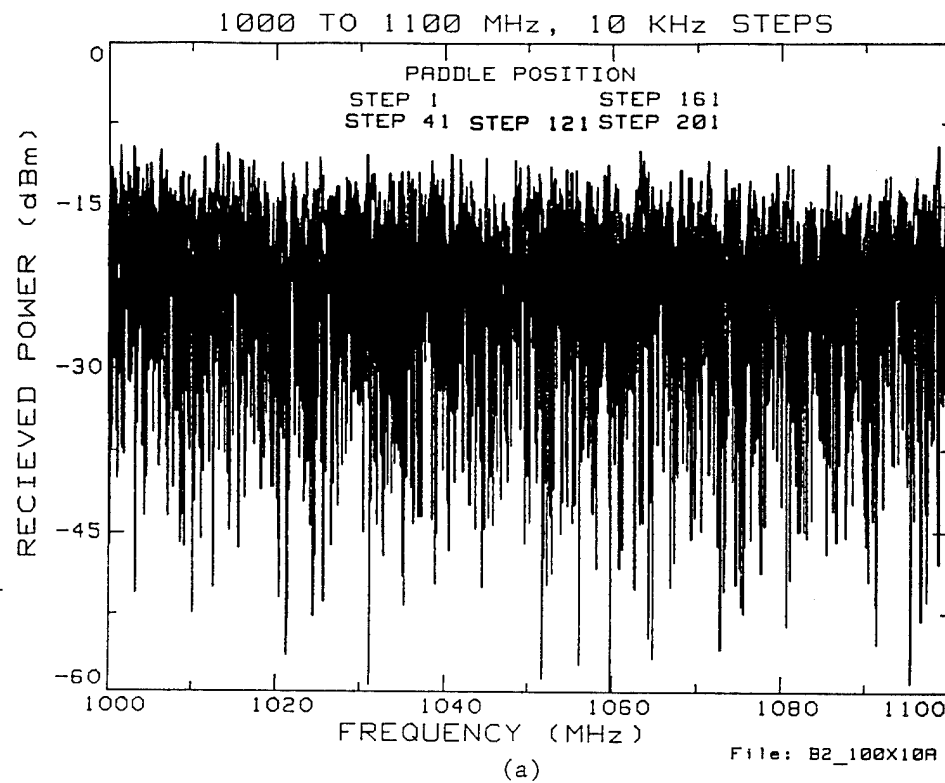


Figure 11. 1000 - 1100 MHz Frequency Stepping Data.

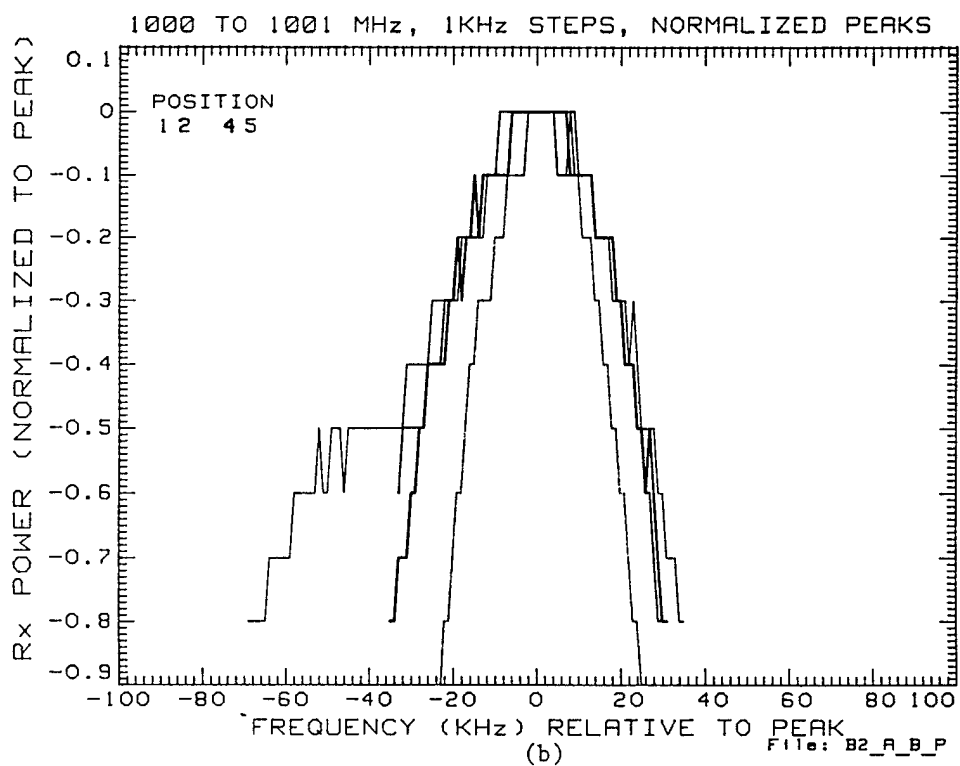
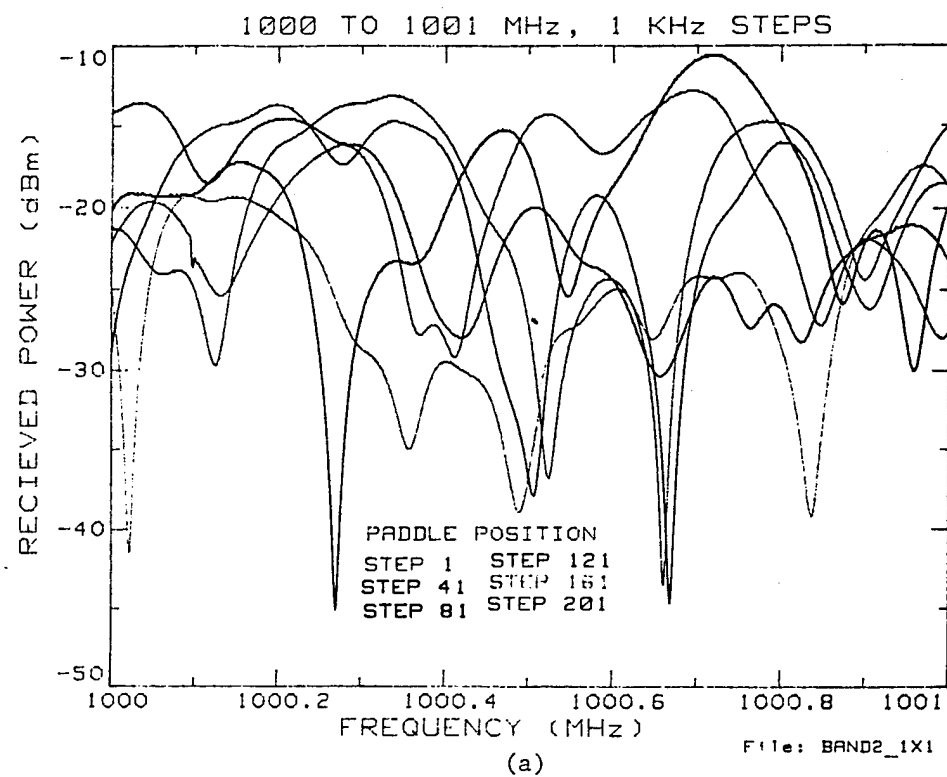


Figure 12. 1000 - 1001 MHz Frequency Stepping Data.

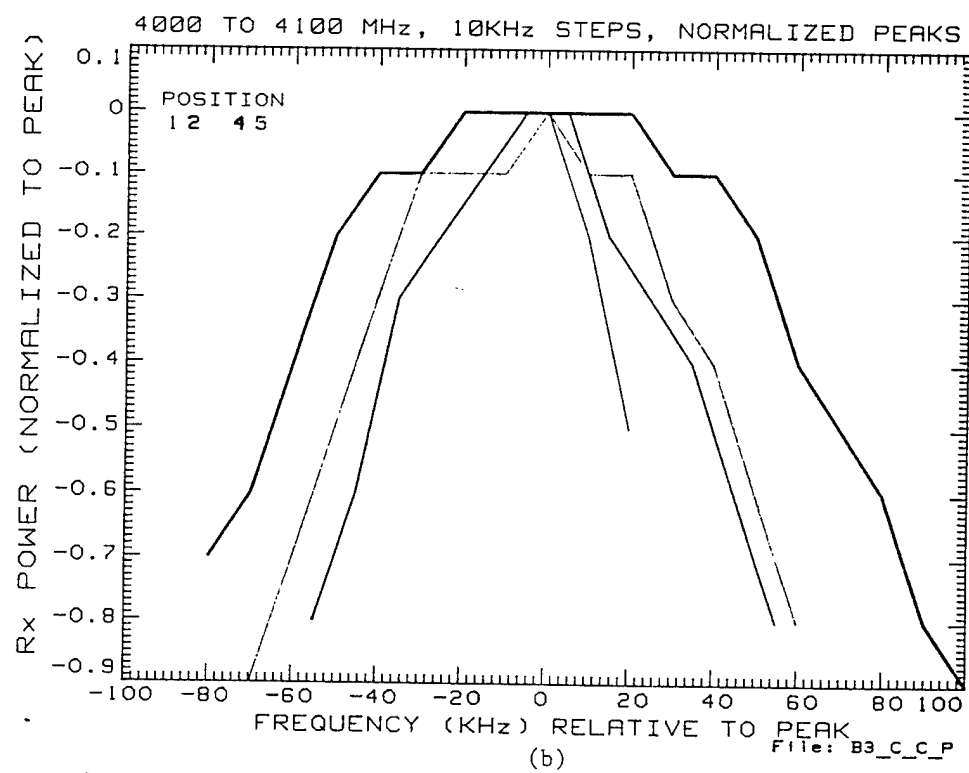
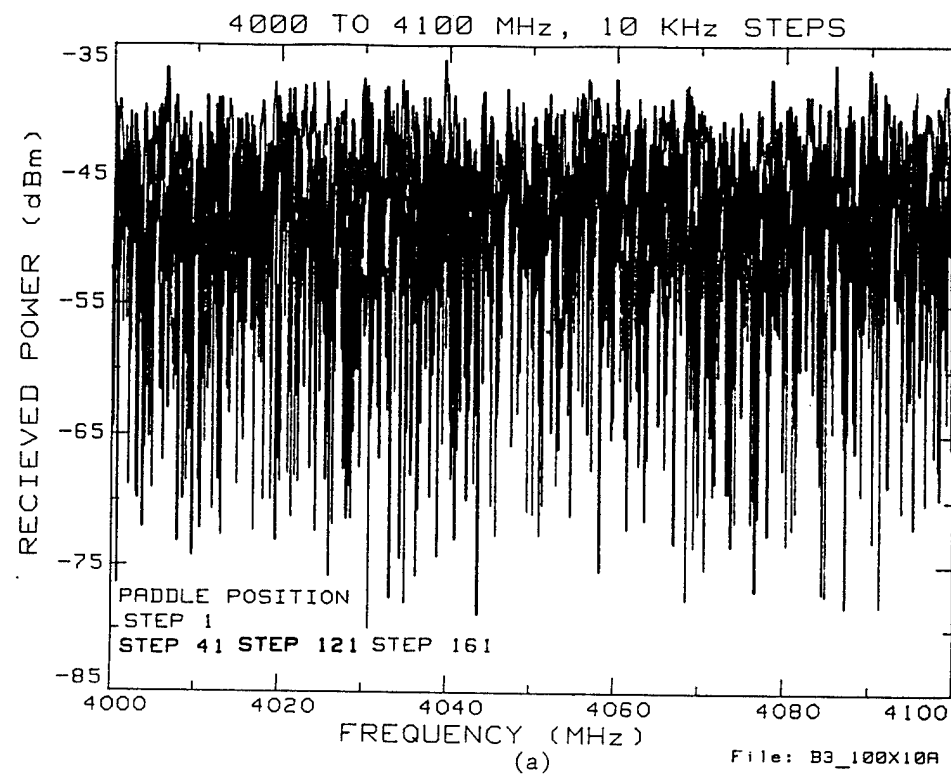


Figure 13. 4000 - 4100 MHz Frequency Stepping Data.

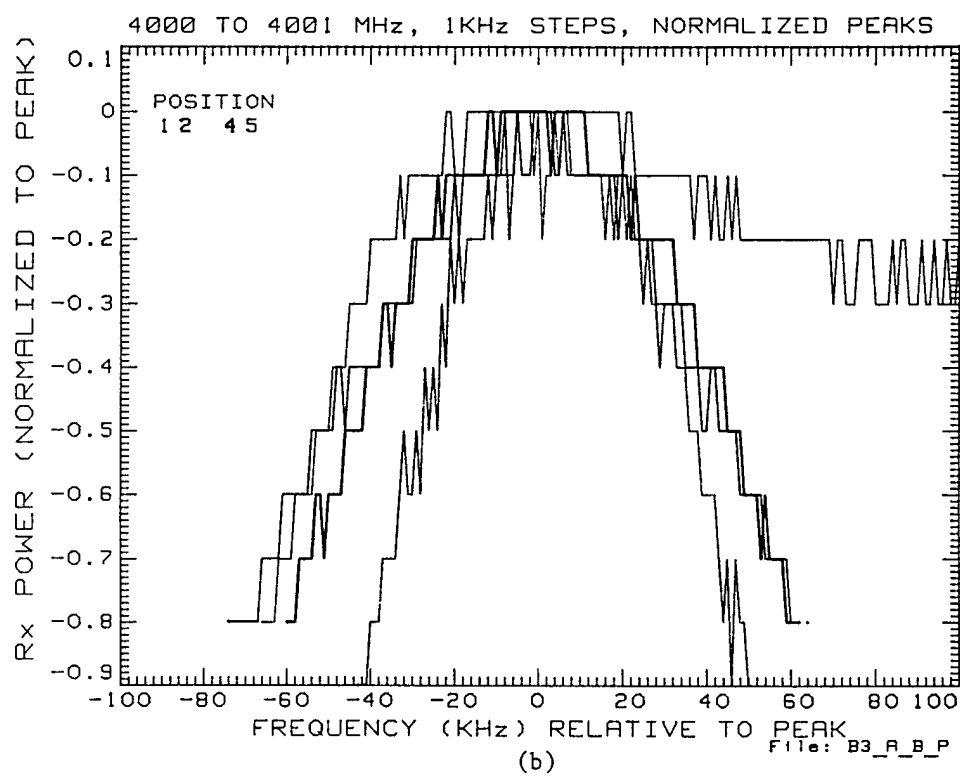
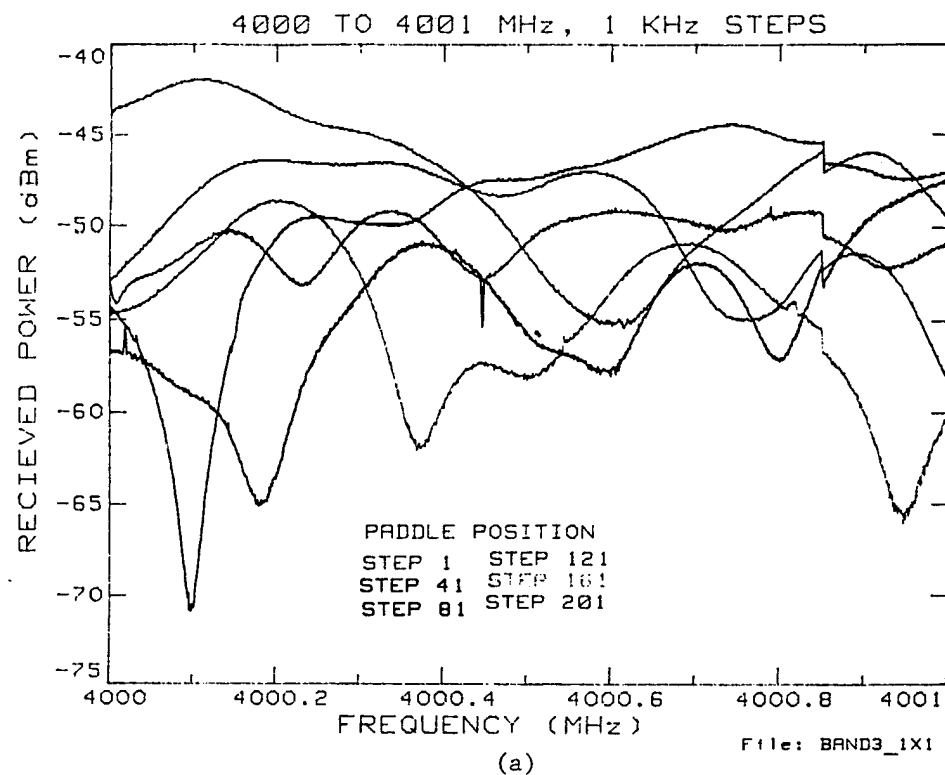


Figure 14. 4000 - 4001 MHz Frequency Stepping Data.

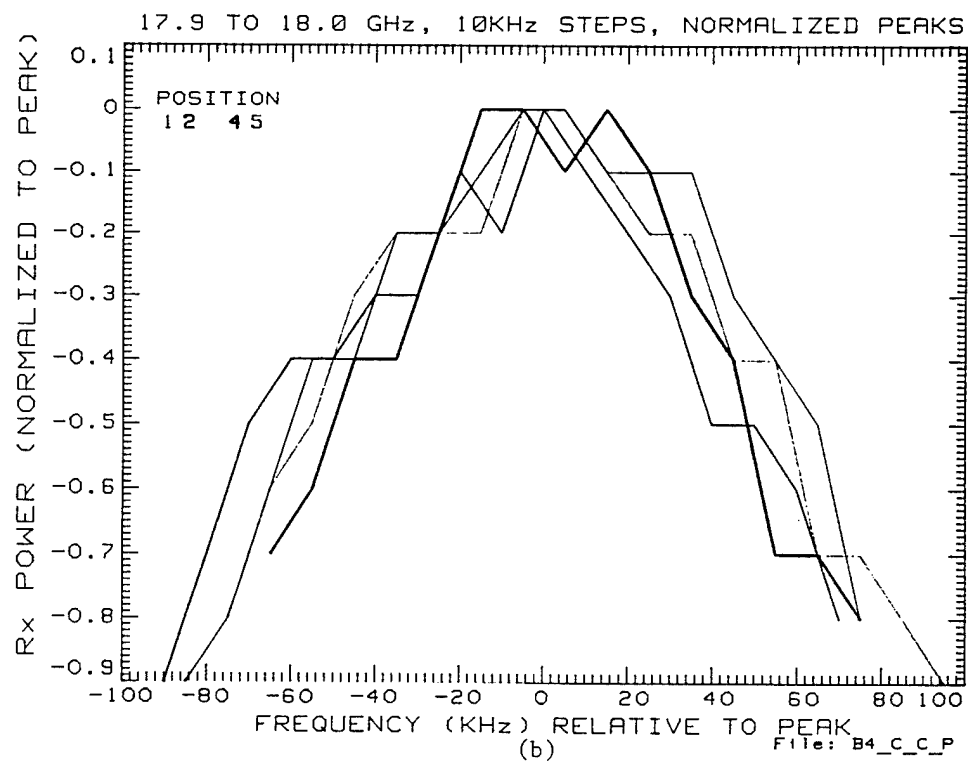
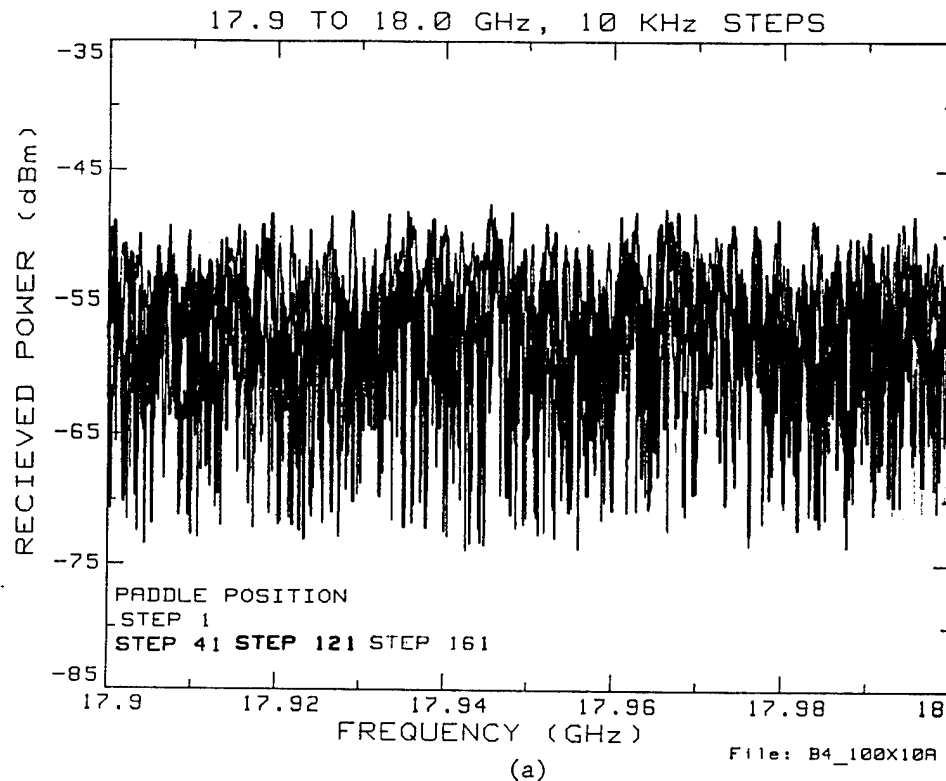
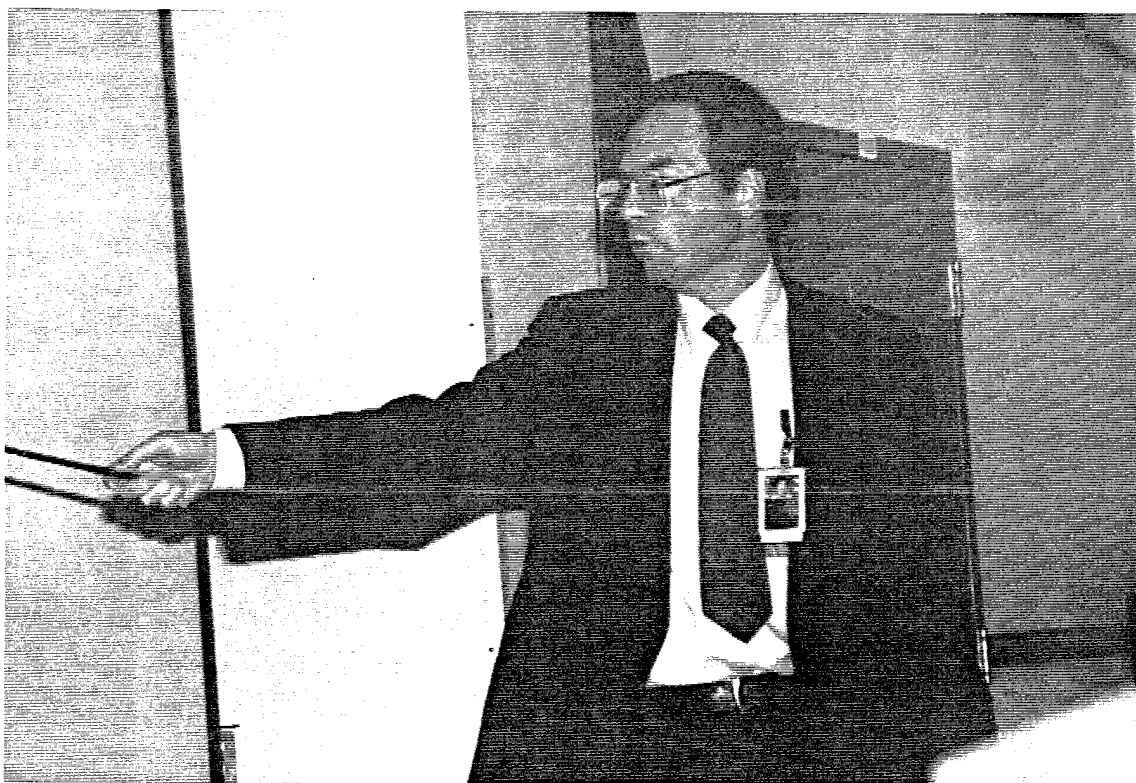
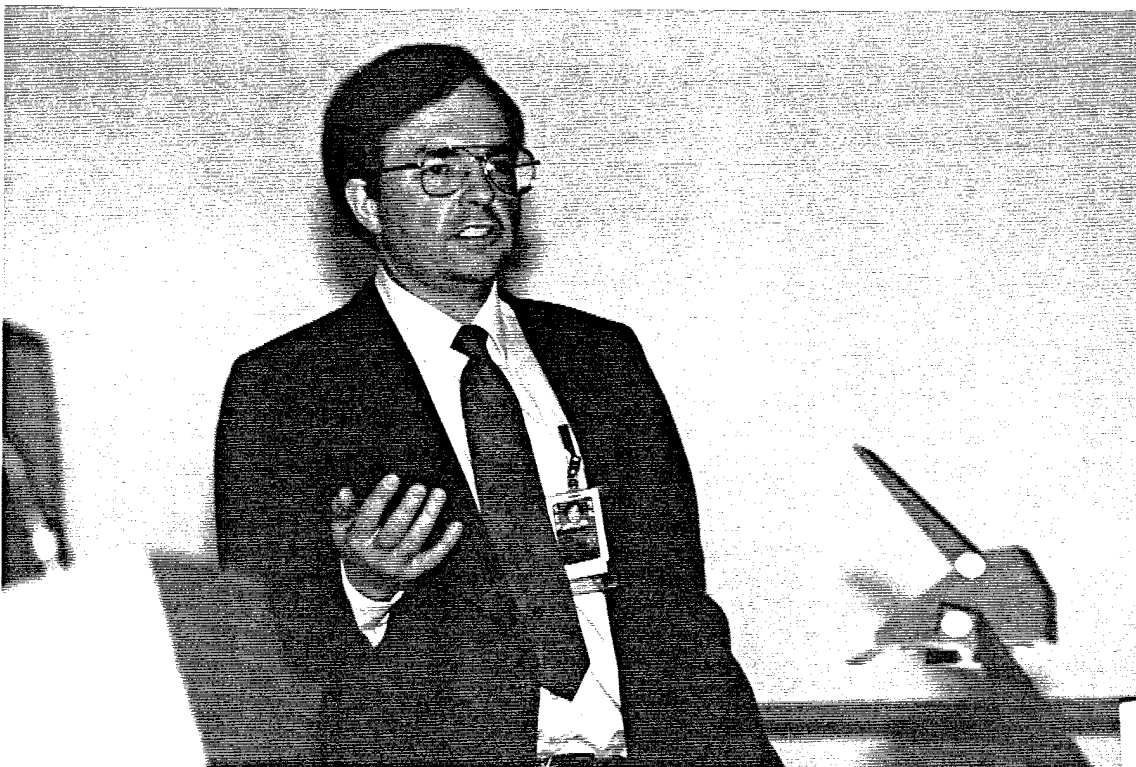


Figure 15. 17.9 - 18 GHz Frequency Stepping Data.





**MR. MICHAEL JESSEE
COMPUTER SCIENCES CORPORATION**



MODE-STIRRED CHAMBER
SHIELDING EFFECTIVENESS MEASUREMENTS
VERSUS
ANECHOIC CHAMBER MEASUREMENTS:
A COMPARISON OF RESULTS

Michael V. Jessee
Computer Sciences Corporation
King George, Virginia

Richard Porter
Naval Surface Warfare Center,
Dahlgren Division
Dahlgren, Virginia

Abstract: This paper represents a continuation of work being performed to determine the feasibility of using Mode-Stirred Chamber (MSC) techniques to measure shielding effectiveness (SE). The results obtained from SE measurements conducted using a generic enclosure assembly (nested chamber) in the Naval Surface Warfare Center, Dahlgren Division (NSWCDD), MSC facility are compared to results obtained from measurements conducted over numerous aspect angles in the NSWCDD Anechoic Chamber facility using the same generic enclosure assembly. The results obtained using MSC techniques are shown to be in general agreement with results obtained in the Anechoic Chamber when the MSC is operated at frequencies where adequate mode mixing and spatial averaging occur (the Reverberation Region) in the enclosure assembly. Discrepancies between the MSC and Anechoic Chamber results for frequencies below the Reverberation Region limit of the enclosure assembly are also discussed.

INTRODUCTION

SE has been measured since the 1950s essentially using one standard technique¹. This technique generally involves using source and measurement antennas placed on opposite sides of a test enclosure wall or test fixture and measuring the intensity of the radiation from the source antenna, at discrete frequencies and positions, which passes through the enclosure/fixture wall to the measurement antenna. This intensity is then compared to measurements made from the source antenna without the enclosure/fixture wall(s) present (the "free-field" measurements) in order to determine the SE. Efforts have been made to improve upon the standard technique by revising measurement procedure and frequency selection². However, resonance characteristics of the enclosure/fixture under test, gain effects resulting from apertures and enclosure structure, polarization of the illuminating field, and nonuniformities in structure illumination have presented problems in acquiring repeatable data with a high degree of confidence. Furthermore, measurements have to be made at numerous antenna positions (and polarizations) around the test enclosure/fixture at a given frequency to adequately characterize the SE. Finally, as fixtures and enclosures which house sensitive electronics become physically smaller, use of traditional methods and equipment may become restricted because of the size of the subject enclosure or fixture, since the accepted standard technique is more adequately suited for room-sized enclosures.

In the past few years, other methods to determine SE have been developed in order to address the deficiencies that were encountered using accepted techniques. One of the methods involves using MSCs. Operated at frequencies where adequate mode mixing and spatial averaging occur (the Reverberation Region), measurements of an enclosure/fixture SE can be made with a high degree of confidence, with the systematic errors associated with previous measurement techniques being minimized. However, at frequencies below the Reverberation Region (which is dependent on the physical dimensions and resonance characteristics of the test enclosure/fixture), measurement of SE using MSC techniques becomes questionable as the number of modes available in the enclosure decreases. The purpose of this paper is to present the results of SE measurements that were conducted on an aluminum/Flectron panel mounted on a generic test enclosure in the NSWCDD MSC, and to compare this data with results that were obtained from SE measurements of the same enclosure assembly in the NSWCDD Anechoic Chamber over several elevation and azimuth angles. Results acquired at frequencies in and below the Reverberation Region of the enclosure will be discussed.

DISCUSSION

Approach

A version of the "nested chamber"³ method was used to measure the shielding effectiveness of the enclosure assembly in both the MSC and the Anechoic Chamber. The following types of measurements were conducted to determine the SE of the enclosure assembly.

- Baseline--Measurements of electromagnetic energy were made in the enclosure assembly with the aluminum/Flectron panel removed from the enclosure. This configuration represents the "unshielded state" of the enclosure assembly.
- Shielding--Measurements of electromagnetic energy were made in the enclosure assembly with the aluminum/Flectron panel installed on the enclosure.

Test Enclosure Assembly Description

The generic enclosure assembly consisted of a 71.1-cm x 55.9-cm aluminum/Flectron panel mounted over the open side of an aluminum enclosure. The panel was mounted to the enclosure via a 76.2-cm x 61.0-cm steel frame and 16 6-32 UNC screws. The resonant frequency of the entire 76.2-cm x 61.0-cm x 30.5-cm enclosure assembly can be approximated as a function of the enclosure assembly dimensions using⁴:

$$f_{res}(m, n, p) = (15000) [(m/a)^2 + (n/b)^2 + (p/d)^2]^{1/2} \text{ MHz.}$$

Setting a=76.2 cm, b=61.0 cm, and d=30.5 cm, and taking the lowest resonant mode of the enclosure to be at m=1, n=1, and p=0, f_{res} of the enclosure assembly is approximately 315 MHz.

The frequency at which the enclosure assembly becomes a reverberating cavity can also be approximately calculated. The number of modes present in a rectangular enclosure as a function of frequency and enclosure dimensions is given by the following⁴:

$$N(f) = (8\pi/3) (a) (b) (d) (f/c)^3 - (a+b+d) (f/c) + 1/2,$$

where $c = 2.998 \times 10^{10}$ cm/s, the speed of light in vacuum. If the minimum number of modes $N_0(f_{rc})$ required for the enclosure assembly to be operating in the Reverberation Region is 60, f_{rc} , the low frequency cutoff for the reverberating cavity, will be approximately 1.15 GHz. Figure 1 shows graphically the number of modes generated in the enclosure assembly [N(f)] as a function of frequency.

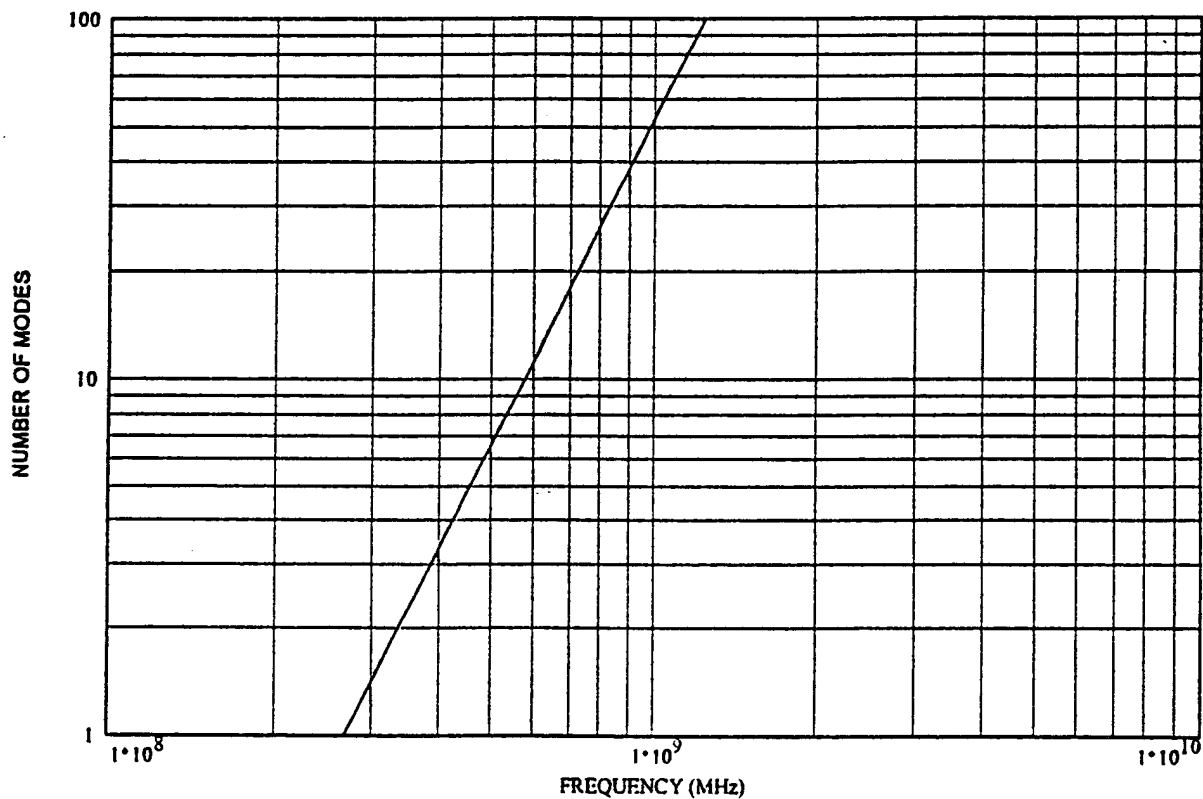


FIGURE 1. NUMBER OF MODES IN THE ALUMINUM/ELECTRON PANEL ENCLOSURE ASSEMBLY AS A FUNCTION OF FREQUENCY

The generic enclosure assembly contained a DC motor-driven paddle wheel tuner and four monopole antennas positioned to cover the volume of the enclosure. The DC motor was operated at a voltage to drive the paddle wheel tuner at a rotation rate of approximately 1 Hz to ensure that data was collected over a complete paddle wheel rotation. Electromagnetic energy penetrating the enclosure was detected by the probes, with the distribution of the antennas and the paddle wheel tuner ensuring that the maximum energy would be detected.

Mode-Stirred Chamber Measurements

The enclosure assembly was positioned in the MSC as shown in Figure 2. The enclosure assembly was placed on a 1-meter-high styrofoam block to isolate the assembly from the MSC floor. Five 0.141-inch-diameter semi-rigid coaxial cables were used to connect the DC motor/paddle wheel tuner assembly and the four probe antennas inside the enclosure assembly to the motor power source and MSC measurement equipment (see Figure 2).

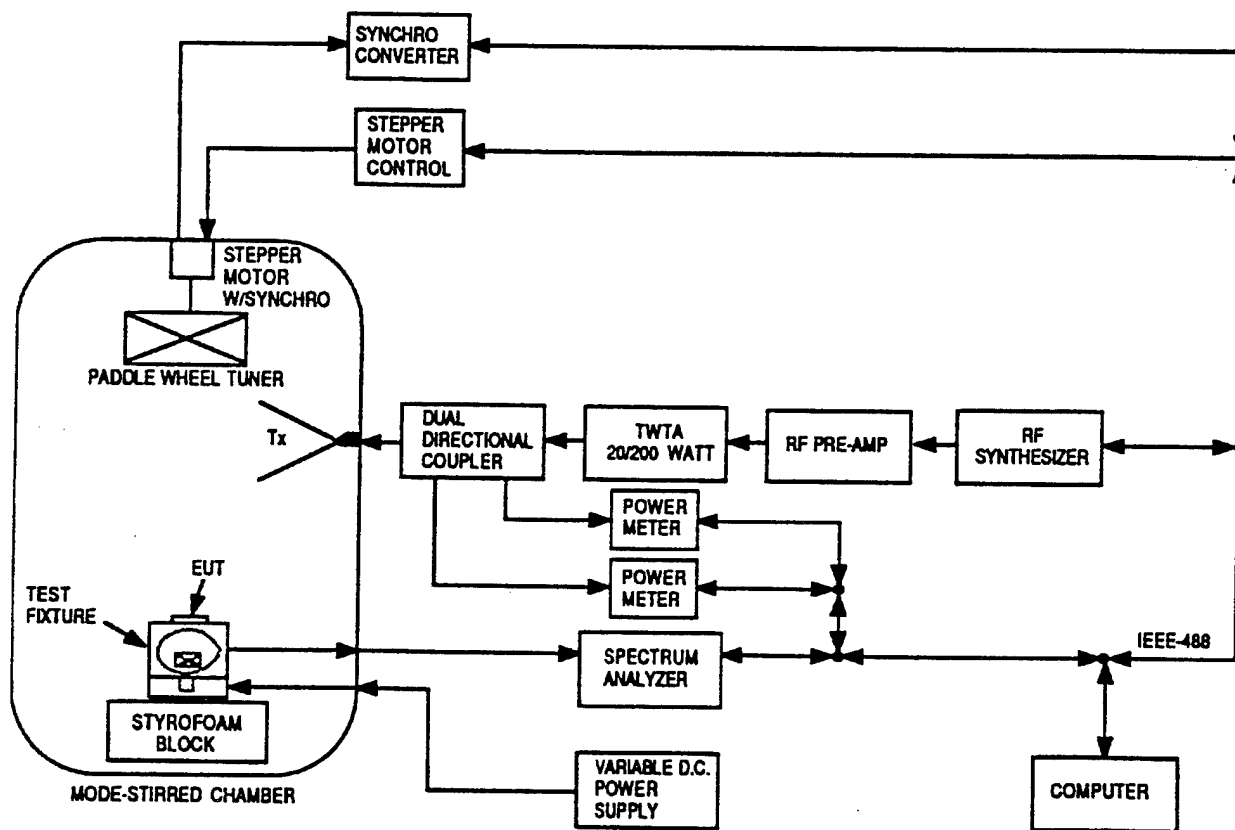


FIGURE 2. BLOCK DIAGRAM OF THE TEST SETUP IN THE MSC

Table 1 specifies the frequency bands and step sizes used to conduct the baseline and SE measurements in the MSC. During the measurements, the large paddle wheel tuners of the MSC were rotated 360° through 200 steps (1.8° per step) per measurement. The dwell time between each step was such that the small paddle wheel tuner inside the enclosure assembly was allowed to complete one revolution, ensuring that the receiver (a spectrum analyzer, operating in the "max hold" mode), detected the maximum received power in each of the four antennas in the assembly.

TABLE 1. MSC TEST FREQUENCY BANDS

Frequency Band (GHz)	Frequency Step (MHz)
0.2 - 1.0	200
1.0 - 2.0	250
2.0 - 4.0	400
4.0 - 10.0	500

Anechoic Chamber Measurements

The enclosure assembly was positioned in the Anechoic Chamber as shown in Figures 3 and 4. The assembly was suspended between two 4.27-meter-high fiberglass pedestals to ensure that the assembly was positioned in the chamber's "quiet zone." The assembly was suspended such that it could be pivoted to discrete elevation angles relative to line-of-sight between the aluminum/Flectron panel of the assembly and the source antenna. The fiberglass pedestals which were used to suspend the enclosure assembly were mounted on the Anechoic Chamber's turntable to allow for rotation of the assembly in azimuthal directions.

Measurements were conducted at two discrete polarizations (vertical and horizontal) of the electromagnetic environment (EME) source antenna and at the following discrete elevation angles relative to line-of-sight between the aluminum/Flectron panel of the assembly and the EME source antenna: 0°, 10°, 20°, 30°, 40°, 60°, 90°, -15°, -30°, and -45°. At each EME polarization and elevation angle, the enclosure assembly was rotated in azimuth, by computer control, from +90° to -90° (relative to the copper-nylon panel/EME source antenna line-of-sight) in 5° steps. The dwell time between each azimuth angle step was determined by the dwell time necessary to collect data from each of the four probe antennas in the enclosure assembly at any given frequency, and the amount of time necessary to step through a specific frequency band. The dwell time necessary for collecting data from each probe antenna was, in turn, determined by the time required for the small paddle wheel tuner inside the enclosure assembly to complete one revolution and to ensure that the spectrum analyzer, operating in the "max hold" mode, detected the maximum received power in each of the four antennas in the assembly.

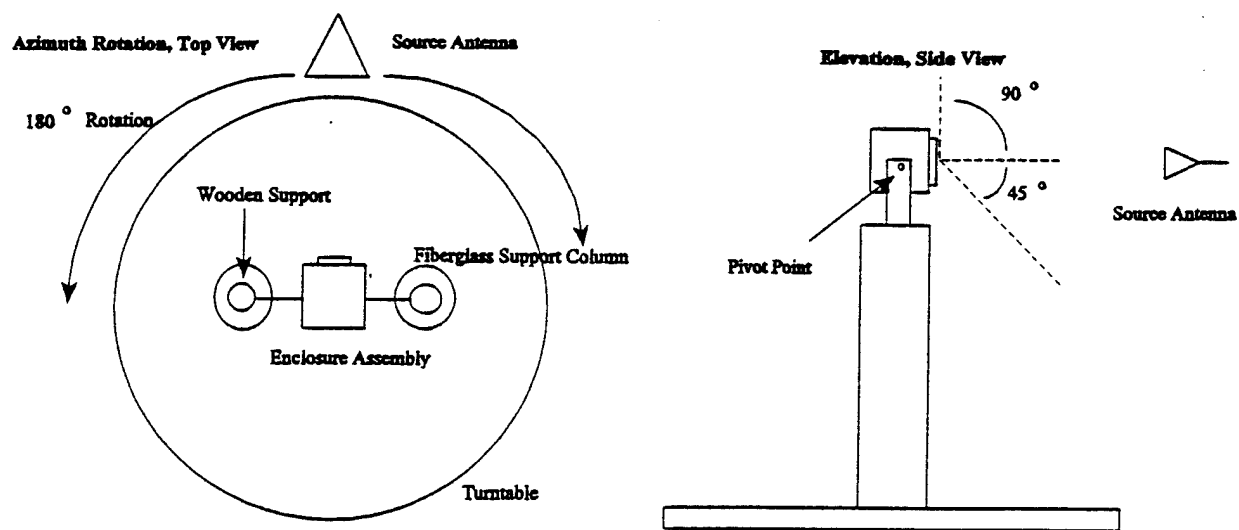


FIGURE 3. ANECHOIC CHAMBER TEST SETUP FOR AZIMUTH AND ELEVATION ROTATIONS

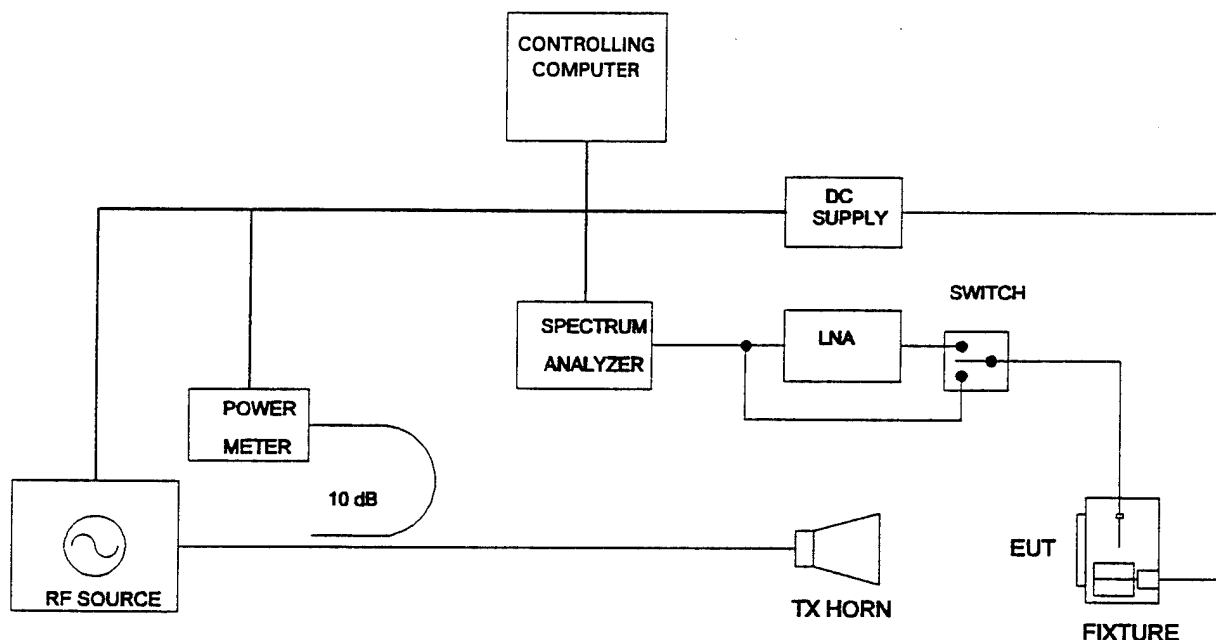


FIGURE 4. BLOCK DIAGRAM OF ANECHOIC CHAMBER EME GENERATING AND DATA MEASUREMENT EQUIPMENT

Table 2 specifies the frequency bands and step sizes used to conduct the baseline and SE measurements in the Anechoic Chamber. Because of time constraints and scheduling conflicts, measurements were not conducted in the 1-4 GHz frequency band.

TABLE 2. ANECHOIC CHAMBER TEST FREQUENCY BANDS

Frequency Band (GHz)	Frequency Step (MHz)
0.2 - 0.3	50
0.3 - 0.5	100
0.5 - 1.0	250
4.0 - 10.0	1000

RESULTS

Figure 5 presents the results of SE measurements made in both the MSC and Anechoic Chamber. SE as a function of frequency was calculated using the standard relation for SE⁵:

$$SE(f) = 10 \log [P(f)_{\max, \text{baseline}} / P(f)_{\max, \text{shield}}].$$

For measurements conducted in the MSC, a set of SE values were calculated corresponding to each individual probe antenna as a function of frequency, where $P(f)_{\max, \text{baseline}}$ and $P(f)_{\max, \text{shield}}$ are the baseline and shielding measurement maximum powers, respectively, coupled into the individual probe antenna at a given frequency over one complete rotation of each large MSC paddle wheel tuner. A set of SE values representing a composite of measurements from the four probe antennas was also calculated, where $P(f)_{\max, \text{baseline}}$ and $P(f)_{\max, \text{shield}}$ are the baseline and shielding measurement maximum powers, respectively, over all four antennas at a given frequency.

For measurements made in the Anechoic Chamber, a set of SE values were calculated corresponding to each individual probe antenna as a function of frequency, where $P(f)_{\max, \text{baseline}}$ and $P(f)_{\max, \text{shield}}$ are the baseline and shielding measurement maximum powers, respectively, coupled into the individual probe antenna at a given frequency over all elevation and azimuth aspect angles, and over both EME polarizations. A set of SE values representing a composite of measurements from the four probe antennas was also calculated, as with the data collected during measurements in the MSC.

At frequencies above the Reverberation Region cutoff (1.15 GHz), the SE measured from any particular enclosure probe, in either the MSC or Anechoic Chamber, is in good agreement with the SE measured from the other probes in the enclosure and with the composite of all probe measurements (Figure 5).

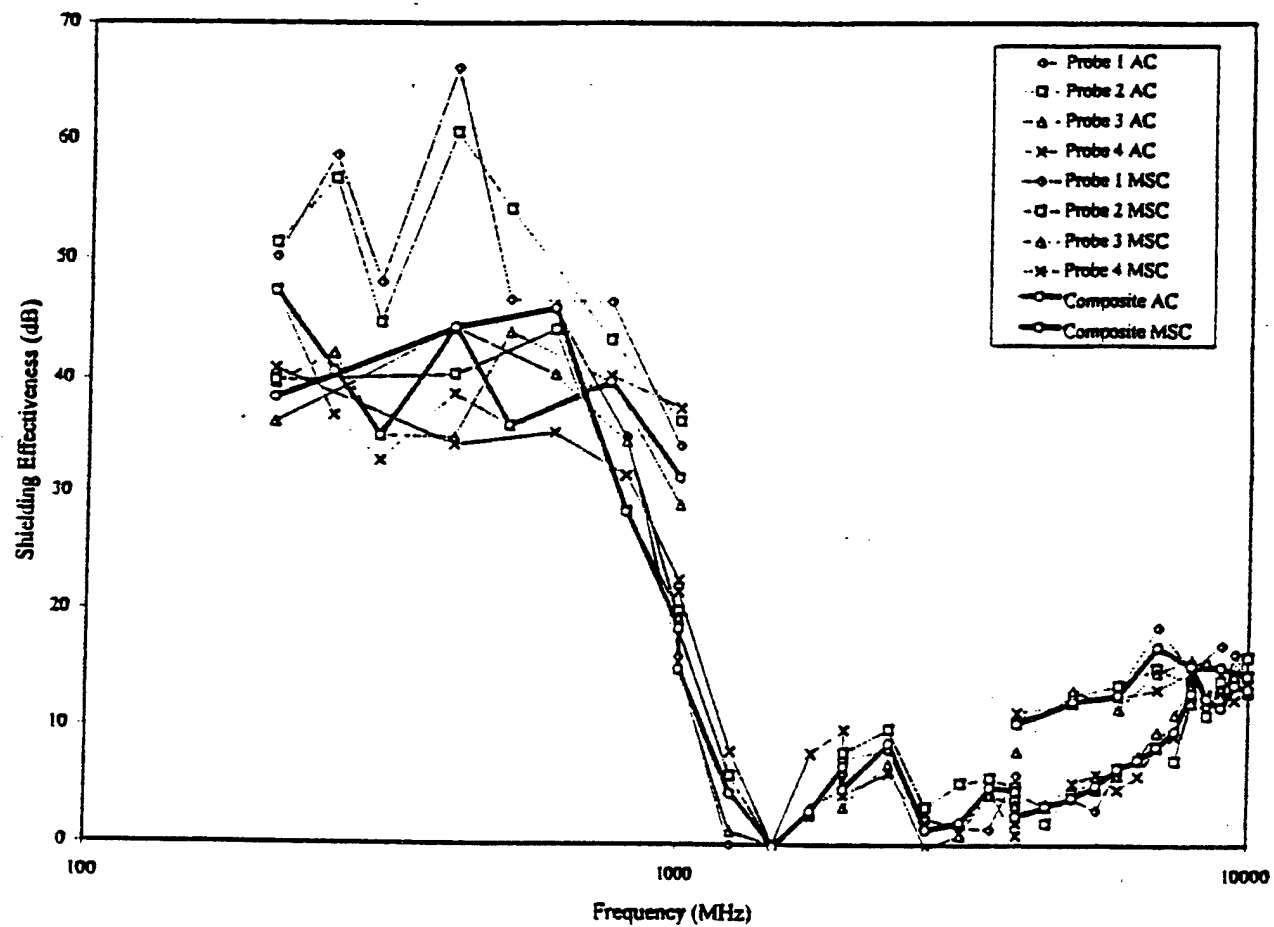


FIGURE 5. COMPARISON OF ALUMINUM/ELECTRON FIXTURE SHIELDING EFFECTIVENESS,
MODE-STIRRED AND ANECHOIC CHAMBERS

Furthermore, the results indicate that the SE measured in the MSC between 4 GHz and 10 GHz is in good agreement (within 6 dB) with the SE measured in the Anechoic Chamber, with the deviation between the SE measured in each chamber decreasing significantly above approximately 8 GHz. The trend in the data also indicates that the SE measured in the MSC should remain consistent with the SE measured in the Anechoic Chamber in the frequency range between the Reverberation Region cutoff and 4 GHz.

At frequencies below the Reverberation Region cutoff, Figure 5 shows that the SE measured from any particular enclosure probe, in either the MSC or Anechoic Chamber, deviates significantly from the SE measured from the other enclosure probes and from the composite of all probe measurements. Furthermore, Figure 5 shows poor agreement between the SE measured in the MSC and SE measured in the Anechoic Chamber; however, comparison of the composite of probe measurements between the two chambers shows a less severe difference in measured SE at a given frequency (approximately 11 dB) than the differences between SE measured from individual probes (over 30 dB). The results at frequencies below the Reverberation Region cutoff indicate that, as the number of available modes contributing to spatial averaging in the enclosure assembly decreases, the differences between the SE measured from each individual probe in the enclosure assembly increase as polarization and directivity effects, which contribute to the standard deviation in the spatial averaging of the fields, become more pronounced. However, it should be noted that polarization and directivity effects, indicated by the differences between the SE values obtained from each individual enclosure assembly probe, are less severe for measurements made in the MSC because the MSC itself was operating in its Reverberation Region, resulting in adequate mode mixing and spatial averaging of the fields external to the enclosure assembly.

An interesting event indicated by the MSC measurements shown in Figure 5 is the apparent decrease of SE to zero at a frequency of approximately 2 GHz. An explanation for the zero SE value is the existence of apertures which resulted from the imperfect bonding of the aluminum/Flectron panel to its mounting frame, and/or the imperfect bonding of the aluminum/Flectron/mounting frame assembly to the enclosure assembly. The dimensions of at least some of these apertures probably were suitable to meet the resonance conditions of the 2-GHz field, resulting in the creation of slot antennas which could reradiate the external field into the enclosure assembly.

CONCLUSION

Measurements of SE using the "nested chamber" approach are accurate and repeatable when the measurements are conducted in the Reverberation Region of the nested chamber. However, below the Reverberation Region cutoff frequency of a nested chamber, uncertainty in SE measurements increases as the number of modes in the nested chamber decreases below the number required for adequate stirring. This decrease in modes results in measurements heavily biased by polarization and directivity effects. The biasing of SE measurements outside the Reverberation Region of a nested chamber is partially offset when measurements are made in an MSC, and the MSC is operated in its Reverberation Region.

BIBLIOGRAPHY

- (1) Department of Defense: MIL-STD-285, Attenuation Measurements for Enclosures, Electromagnetic Shielding, for Electronic Test Purposes, Method of, U.S. Government Printing Office, Washington, D.C., 1956
- (2) Standards Committee of the IEEE Electromagnetic Compatibility Society: IEEE STD 299-1991, IEEE Standard Method for Measuring the Effectiveness of Electromagnetic Shielding Enclosures, Institute of Electrical and Electronics Engineers, Inc., New York, New York, 1991
- (3) Michael O. Hatfield: "Shielding Effectiveness Measurements Using Mode-Stirred Chambers: A Comparison of Two Approaches," IEEE Transactions on Electromagnetic Compatibility, vol. 30, no. 3, p. 232, Aug. 1988
- (4) M. L. Crawford and G. H. Koepke: National Bureau of Standards Technical Note 1092, Design, Evaluation, and Use of a Reverberation Chamber for Performing Electromagnetic Susceptibility/Vulnerability Measurements, U.S. Department of Commerce/National Bureau of Standards, Boulder, Colorado, 1986, p. 2
- (5) Henry W. Ott: Noise Reduction Techniques in Electronic Systems, John Wiley and Sons, Inc., New York, New York, 1976, p. 140





**DR. J. P. QUINE
ROME LABORATORIES**



Testing of Microwave Shielding Gaskets and Cover Panels -
Recent Work at Rome Laboratories

Dr. J.P. Quine*, C. Brown, K. Fisher, J.P. Streeter, A.J. Pesta
Rome Laboratories, Griffiss AFB, NY

1. Introduction

This paper discusses problems associated with the experimental characterization of leakage sources such as gasketed seams and attenuating cover panels by methods that employ a reverberation chamber (REVCH) to measure the total power radiated into the REVCH by the leakage source. The preferred characterization of a leakage source is in terms of the Effective Transmission Area (ETA)[1] defined as the total radiated leakage power (watts) divided by the applied incident microwave flux $EINC^2/\eta_0$ (watts per square meter) where EINC is the incident E-field, and $\eta_0 = 120\pi$ ohms. An absolute value of ETA can be determined by measuring the power received by an antenna that is well matched to free space before being placed inside the REVCH. The use of multiple receiving antennas to obtain spatial averaging may lead to improved performance when used in conjunction with a mode stirrer.

In order to avoid errors that can occur in the measurement of absolute ETA values (e.g. due to uncertainty in Q), it may be advantageous to measure the ETA of an unknown leakage source relative to the known ETA of a standard opening (e.g., a small round hole). The ratio of the two ETA values can then be defined as the Shielding Effectiveness (SE) of the unknown leakage source relative to the standard opening. Thus, in reporting data on SE of a leakage source, the standard opening employed must also be reported. SE, defined in this way is meaningful, and can be viewed as a relative ETA.

The following sources of error in estimating total radiated leakage power can be identified:

- errors caused by incomplete mode stirring
- errors caused by non-uniform transmission over the area (or length) of the leakage source
- errors caused by differences in the coupling into the REVCH between unknown and standard.

* 83 Ash Tree Lane, Schenectady, NY 12309
(518) 785-5439, (518) 387-5442 (fax)

Three dimensional electric field probes were employed to measure the spatial distributions of the three orthogonal components of the electric fields E_x , E_y and E_z . Data was obtained with a total of six probes placed randomly inside the REVCH.

2. Errors in Estimating Total Leakage Power Due to Incomplete Mode Stirring

An expression for the total leakage power radiated into and absorbed inside the REVCH can be derived from the definition of Q . Thus, the total leakage power is given by

$$\text{Power} = \omega \epsilon \frac{(\text{EMAGAVE}^2) \text{ VOL}}{Q} \quad (1)$$

where EMAGAVE^2 is the average of the sum of the component magnitudes $E_x^2 + E_y^2 + E_z^2$ over the volume, VOL, and ϵ is permittivity = 8.854×10^{-12} Farads/meter.

The total leakage power can be estimated if a single electric field component (e.g., E_y) is measured at only a single point, and if it is assumed that complete mode stirring results in exactly uniform fields ($E_x^2 = E_y^2 = E_z^2$) throughout the volume. Then $\text{EMAGAVE}^2 = 3E_y^2$, and

$$\text{Estimated Power} = \frac{3\omega \epsilon (E_y^2) \text{ VOL}}{Q} \quad (2)$$

Defining estimated ETA as Estimated Power/(EINC $^2/\eta_0$), then

$$\text{Estimated ETA} = \left(\frac{6\pi \text{ VOL}}{Q\lambda} \right) \left(\frac{E_y}{\text{EINC}} \right)^2 \quad (3)$$

where we have used $\omega \epsilon \eta_0 = 2\pi/\lambda$.

The power error can be defined as the ratio of estimated to actual power. Thus, from Eqs. (1) and (2),

$$\text{Power Error} = \frac{\text{Estimated}}{\text{Actual}} = \frac{3E_y^2}{\text{EMAGAVE}^2} \quad (4a)$$

Note that by this method, if E_x and E_z are zero and E_y is constant at all points in the volume, then $EMAGAVE = E_y$, and under these extreme conditions, the estimated power based on the assumption of complete mode stirring is three times the actual power. On the other hand, if both E_x and E_y are measured at a single point,

$$\text{Power Error} = \frac{1.5 (E_x^2 + E_y^2)}{EMAGAVE^2} \quad (4b)$$

In this case, if E_x and E_z are zero everywhere and E_y is constant, the estimated power is 1.5 times the actual power. Similarly, if E_x , E_y , and E_z are all measured at only a single point, the power error would be

$$\text{Power Error} = \frac{(E_x^2 + E_y^2 + E_z^2)}{EMAGAVE^2} \quad (4c)$$

Thus, a particular REVCH can be characterized by a set of three-dimensional electric field data obtained from several probes distributed randomly throughout the volume[4,5]. Equations (4) can then provide at least a rough estimate of the error in estimating the total leakage power radiated into the REVCH under actual conditions of incomplete mode stirring.

Alternately, if the "Black-Hole" principle applies [2, 3], and if ETA and $EINC$ are known, the estimated power can also be determined from

$$\text{Estimated Power} = ETA (EINC^2) / \eta_0 \quad (5)$$

The total radiated leakage power can also be calculated, based on an assumed wave impedance of 120π and a gain of $\lambda^2/8\pi$ for a matched receiving antenna in a perfectly isotropic field[4,5]. Thus, if only E_y is measured, the receiving antenna power (RAP) is

$$RAP = (E_y^2 / \eta_0) \left(\frac{\lambda^2}{8\pi} \right), \text{ and} \quad (6)$$

$$E_y^2 = \eta_0 \frac{8\pi}{\lambda^2} (RAP) \quad (7)$$

Substituting this value of E_y^2 into Eq. (2),

$$\text{Estimated Power} = 3\omega\eta_0 \left(\frac{8\pi}{\lambda^2} \right) \left(\frac{\text{VOL}}{Q} \right) \text{RAP}, \quad (8)$$

and since $\omega\eta_0 = 2\pi / \lambda_0$,

$$\text{Estimated Power} = \frac{48\pi^2}{Q} \left(\frac{\text{VOL}}{\lambda^3} \right) \text{RAP}. \quad (9)$$

$$\text{Estimated ETA} = \frac{48\pi^2}{Q} \left(\frac{\text{VOL}}{\lambda^3} \right) \left(\frac{\eta_0}{\text{EINC}^2} \right) \text{RAP} \quad (10)$$

Note that the ratio of estimated values of ETA obtained from Eqs. (3) and (10) is given by

$$\text{Ratio } ((3 / (10)) = \left(\frac{\lambda^2}{8\pi} \right) \left(\frac{\text{Ey}^2}{\eta_0} \right) / \text{RAP} \quad (11)$$

This ratio is seen to be correct by definition, is independent of Q, VOL, and EINC, and depends only on measured EMAGAVE and RAP. If this ratio is not unity, then errors exist in either measured EMAGAVE or RAP, or both. Errors can result from the assumption in Eq. (5) that the average wave impedance is equal to the constant free space value η_0 ; whereas, it is known that the wave impedance varies from point to point. Incomplete mode stirring as well as probe calibration errors can also result in a failure to satisfy Eq. (11).

Results obtained recently at Rome Laboratories with the three-dimensional electric field probes employed inside the 3.69 x 5.18 x 9.78 meter reverberation chamber are consistent with earlier results obtained with this same chamber that are reported in [4]. Thus, Figure 3.8a and Table 3.1 of [4] show mode-stirred data averaged over 100 positions of the mode stirrer. As stated in [4], the data has a spread of ± 9.5 dB at 100 MHz, ± 3.5 dB at 300 MHz, ± 2.5 dB at 1.0 GHz, ± 2.0 dB at 2.0 GHz for the ten probes relative to the value of each component averaged over all probe positions. Since EMAGAVE^2 is nominally equal to $3 \times \text{EYAVE}^2$, the right-hand side of Eq. (2a) becomes $\text{Ey}^2 / (\text{EYAVE})^2$, and the dB error in power estimates are the same as the dB values quoted above for the spread in the field components.

Tables 1a and 1b list data obtained at Rome Laboratories with a 10.5" x 1/8" slot (without a gasket) mounted on a wall of the REVCH as shown in Figs. (1a) and (1b). These experiments

were intended to show the effect of placing a cone-shaped scatterer in front of the slot. The purpose was to scatter the relatively high-gain beam of the slot into more diverse directions, with the hope of increasing the randomness of the fields and reducing the power errors. However, it appears that in this case, the cone provided little, if any, significant advantage.

Tables 2a and 2b shows measured data for a 10.5" x 10.5" open area, without and with the cone scatterer. It is seen that in the case of this somewhat higher gain leakage source, the power errors are somewhat less with the cone scatterer.

The tabulated values of E_x , E_y , E_z , and $EMAG(1)$ in Tables 1 and 2 are in units of volts/meter, and are derived from the values of E_x , E_y , E_z and $EMAG$ measured at each probe at each of 100 mode stirrer positions, and then averaged over all mode stirrer positions. On the other hand, the tabulated values of $EMAG(2)$ are simply the square-root of the sum of the squares of the tabulated values of E_x , E_y , and E_z . Power errors are given for both $EMAG(1)$ and $EMAG(2)$.

3. Errors Caused by Non-Uniform Material and Cross Sectional Dimensions of Cover Panels and Gasketed Seams

The transmitted leakage power can vary significantly in an unknown way from point-to-point over the area of an attenuating cover panel, or along the length of a gasketed seam, as a result of non-uniformities in material composition and cross-sectional dimensions [6]. This can result in relatively small local regions of high or low leakage which can vary by as much as ± 10 dB or more about typical average values of say 30 to 80 dB. The total leakage power for the non-uniform panel or seam can be higher or lower than for the uniform panel or seam, depending on whether the "hot" and "cold" spots lie at points of high or low coupling for radiation into the REVCH. The local coupling at a particular point depends on how the multitude of modes excited inside the REVCH combine at a particular wall point to form local net E and H fields, the ratio E/H being the local radiation admittance at that point. At a fixed frequency and mode stirrer position, the local radiation admittance can be expected to vary significantly even between closely spaced points over the area of the wall of the REVCH. Computer and experimental data were obtained to determine to what degree the effects of the variations in local radiation admittance can be reduced (on a time-averaged basis) by mechanical or stepped-frequency mode stirring.

A "hot spot" at an unknown point along a gasketed seam was modeled by moving a short (1.5" x 1/8") slot horizontally along a 10.5" path on the end wall of the REVCH as shown in the inset. Figure 2a shows stepped frequency computer calculations [3] for E_y^2 at probe point at $x =$

$A/2$, $y = B/2$ and $z = C/2$ in the Rome Laboratories REVCH with mechanical mode stirrer removed. The fields were produced by simulating a slot by two rows of four 0.5"-diameter holes spaced by $\lambda/8$ along the x -direction, with the rows spaced 0.31875λ in the y -direction. Data is shown as a function of the displacement of the hole array center from the center of the end wall at $x = A/2$, $y = B/2$, $z = 0$. For a constant frequency of 2000.0 MHz, $Ey^2/EINC^2$ varies from a maximum of 3.44×10^{-3} to a minimum of 0.1×10^{-3} or a ratio of $34.4 = 15.37$ dB. On the other hand, if Ey^2 is averaged over ten stepped frequencies, the maximum and minimum are 6.18 and 2.22 or a ratio of $2.78 = 4.45$ dB (± 2.25 dB). Figure 2b shows Ey^2 for the same conditions as for Fig. (2a), except that Ey^2 is averaged over 81 probe points spaced $\lambda/16$ over an area = $0.5625\lambda^2$. A reduction of about 1.0 dB in the max/min ratio results. It is believed that these ratios of maximum to minimum values represent an upper bound for an actual gasketed seam having a single hot spot with dimensions that are small compared to λ_0 .

Figure 3a shows experimental stepped-frequency data obtained in the Rome Laboratories REVCH with stationary mechanical mode stirrer. The leakage source is an actual 1.5" x 1/8" slot in a 1/16" thick wall. The slot was moved along a 10.0" line centered on the test fixture on the wall $z = 0$ (see Figure 1), and receiver power was measured using a single horn antenna that responded only to Ey . The data show, as expected, that Ey -squared tends to increase with increasing frequency. The variations are greater than 10 dB at some frequencies. Figure 3b shows similar data obtained with the probe sensors. The variations are less with the (6) probe sensors, implying that perhaps multiple receiving horns may provide an advantage.

4. Comments on Stepped-Frequency Mode Stirring

Extensive data were also obtained using stepped-frequency mode stirring with the mechanical mode stirrer removed from the REVCH. Power errors were similar to those obtained using mechanical mode stirring. It was noted that Q values increased to 90712 and 348356 at 2.0 and 4.0 GHz, respectively. Furthermore, it was found that considerable cross-polarized field, Ex was produced when linearly polarized excitation, Ey was applied to the leakage source.

It can be shown that if empty REVCH has perfectly rectangular geometry and very high Q , then only weak cross-polarized field Ex can be excited anywhere in the REVCH even with the stepped-frequency mode stirring. Instead, measured values of Ex were comparable to the values of Ey and Ez , typically equal to within ± 3 dB with stepped-frequency mode stirring. This can occur if there is a small amount of coupling between TE and TM modes as can be caused by

relatively small deviations from rectangularity. This results in unequal propagation constants β_{TE} and β_{TM} .

The REVCH can be modeled as a rectangular waveguide shorted at each end, with cross-sectional dimensions that are many wavelengths in size, and with a length that is comparable to the cross-sectional dimensions. However, with a very high Q , the effective length can be much greater than the actual length because of the many round-trip reflections that occur during the time for buildup to the steady state fields. The buildup time is $Q/(2\pi f)$, and the effective length (E.L.) is $Q\lambda/2\pi$ which is about 400 meters at 2.06 GHz. Significant cross polarization can be expected to occur if $(\beta_{TE} - \beta_{TM}) \times (E.L.)$ approaches a value of $\pi/2$.

Thus, an analogy exists between a high- Q REVCH with random deviations from rectangularity and a very long circular waveguide with small random deviations from circularity all along its length. If the circular waveguide is excited at one end by linear polarization, the random coupling will cause the fields at a long distance from the source end to be randomly polarized.

References

- [1] J.P. Quine, A.J. Pesta, 1995 IEEE EMC Symposium, August 1995
- [2] J. P. Quine, 1993 IEE EMC Symposium, Dallas, August 1993 (two papers)
- [3] J.P. Quine, A.J. Pesta, IEEE EMC Symposium, Zurich, March 1993 - revised version included in digest of this workshop
- [4] M.L. Crawford, G.H. Koepke, J.M. Ladbury, NBSIR 87-3080, National Bureau of Standards, December 1987
- [5] M.L. Crawford, G.H. Koepke, NBS Technical Note 1092, National Bureau of Standards, April 1986
- [6] J.P. Quine, A.J. Pesta, IEEE EMC Symposium, Chicago, IL, August 1994

11/29/95

TABLE Ia ESTIMATED POWER ERROR (dB) - MECHANICAL MODE STIRRING

10.5" x .125" SLOT WITHOUT CONE (F = 2 GHz)

Probe	Ex	Ey	Ez	Emag (1)	Err X (1)	Err Y (1)	Err Z (1)	Emag (2)	Err X (2)	Err Y (2)	Err Z (2)
1	6.48	6.73	6.01	11.61	-0.38	-0.05	-1.03	11.11	0.03	0.36	-0.63
3	6.32	6.17	5.61	11.05	-0.59	-0.80	-1.63	10.46	-0.19	-0.40	-1.22
4	5.56	6.78	6.23	11.33	-1.71	0.02	-0.72	10.76	-1.30	0.42	-0.31
6	6.66	6.03	6.02	11.38	-0.14	-1.00	-1.02	10.81	0.27	-0.60	-0.61
7	6.39	7.06	7.28	12.49	-0.50	0.37	0.63	11.99	-0.09	0.77	1.04
8	6.47	7.45	6.81	12.47	-0.39	0.83	0.05	11.99	0.02	1.24	0.46
Average	6.31	6.70	6.33	11.72	-0.62	-0.11	-0.62	11.19	-0.21	0.30	-0.21

10.5" X 125" SLOT WITH CONE (F = 2 GHz)

Probe	Ex	Ey	Ez	Emag (1)	Err X (1)	Err Y (1)	Err Z (1)	Emag (2)	Err X (2)	Err Y (2)	Err Z (2)
1	5.92	5.57	5.39	10.29	0.23	-0.30	-0.59	9.75	0.69	0.16	-0.12
3	5.74	5.33	4.70	9.64	-0.04	-0.69	-1.78	9.13	0.42	-0.22	-1.31
4	4.69	5.43	5.29	9.46	-1.80	-0.52	-0.75	8.91	-1.33	-0.06	-0.29
6	5.92	5.24	5.17	9.92	0.23	-0.83	-0.95	9.45	0.69	-0.37	-0.49
7	5.42	5.41	6.52	10.58	-0.54	-0.56	1.06	10.06	-0.08	-0.09	1.53
8	5.15	6.10	5.18	10.05	-0.98	0.49	-0.93	9.52	-0.52	0.95	-0.47
Average	5.47	5.51	5.38	9.99	-0.48	-0.40	-0.66	9.47	-0.02	0.06	-0.19

Emag (1) = Average Magnitudes

Emag (2) = Magnitude (Averages)

E-Field Normalized Relative to 200 V/m Incident on Slot

TABLE I b ESTIMATED POWER ERROR (dB) - MECHANICAL MODE STIRRING

10.5" X .125" SLOT WITHOUT CONE (F = 4 GHz)

Probe	Ex	Ey	Ez	Emag (1)	Err X (1)	Err Y (1)	Err Z (1)	Emag (2)	Err X (2)	Err Y (2)	Err Z (2)
1	6.74	7.26	6.53	12.80	-2.50	-1.86	-2.78	11.86	-1.80	-1.16	-2.08
3	7.89	8.44	8.79	15.87	-1.13	-0.55	-0.20	14.52	-0.43	0.15	0.50
4	7.90	7.66	7.59	14.65	-1.12	-1.39	-1.47	13.37	-0.42	-0.69	-0.77
6	9.45	7.59	7.71	15.49	0.43	-1.47	-1.34	14.37	1.13	-0.77	-0.63
7	8.77	9.47	9.33	17.20	-0.22	0.45	0.32	15.93	0.48	1.15	1.02
8	8.70	10.37	8.81	17.43	-0.29	1.24	-0.18	16.15	0.42	1.94	0.52
Average	8.24	8.47	8.13	15.57	-0.81	-0.60	-0.94	14.37	-0.10	0.10	-0.24

10.5" X .125" SLOT WITH CONE (F = 4 GHz)

Probe	Ex	Ey	Ez	Emag (1)	Err X (1)	Err Y (1)	Err Z (1)	Emag (2)	Err X (2)	Err Y (2)	Err Z (2)
1	6.28	5.72	5.48	10.84	-1.35	-2.16	-2.54	10.11	-0.63	-1.44	-1.81
3	7.05	6.66	6.06	12.42	-0.35	-0.84	-1.66	11.44	0.37	-0.12	-0.94
4	6.14	6.24	6.62	11.98	-1.55	-1.41	-0.90	10.98	-0.83	-0.69	-0.17
6	8.30	6.58	6.97	13.77	1.07	-0.95	-0.45	12.68	1.79	-0.23	0.27
7	7.32	6.92	8.43	14.19	-0.02	-0.51	1.20	13.14	0.70	0.21	1.93
8	6.49	7.60	6.36	13.07	-1.07	0.30	-1.24	11.85	-0.35	1.03	-0.52
Average	6.93	6.62	6.65	12.71	-0.55	-0.93	-0.93	11.70	0.18	-0.21	-0.21

Emag (1) = Average (Magnitudes) Emag (2) = Magnitude (Averages)

E-Field Normalized Relative to 200 V/m Incident on Slot

11/29/95

TABLE 2a ESTIMATED POWER ERROR (dB) - MECHANICAL MODE STIRRING

10.5" x 10.5" SLOT WITHOUT CONE (F = 2 GHz)

Probe	Ex	Ey	Ez	Emag (1)	Err X (1)	Err Y (1)	Err Z (1)	Emag (2)	Err X (2)	Err Y (2)	Err Z (2)
1	51.30	66.72	50.14	101.46	-0.92	1.37	-1.11	97.97	-0.57	1.71	-0.77
3	54.87	59.07	48.87	98.11	-0.33	0.31	-1.34	94.28	0.01	0.65	-0.99
4	50.34	56.13	46.96	92.25	-1.08	-0.13	-1.68	88.83	-0.74	0.21	-1.34
6	53.10	49.79	51.05	93.12	-0.62	-1.18	-0.96	88.91	-0.27	-0.83	-0.61
7	47.41	64.09	54.76	100.54	-1.60	1.02	-0.35	96.72	-1.26	1.36	0.00
8	51.21	72.90	51.08	106.93	-0.93	2.14	-0.95	102.69	-0.59	2.48	-0.61
Average	51.37	61.45	50.48	98.74	-0.91	0.59	-1.07	94.90	-0.57	0.93	-0.72

10.5" X 10.5" SLOT WITH CONE (F = 2 GHz)

Probe	Ex	Ey	Ez	Emag (1)	Err X (1)	Err Y (1)	Err Z (1)	Emag (2)	Err X (2)	Err Y (2)	Err Z (2)
1	47.31	45.49	59.44	92.01	-0.14	-0.48	1.84	88.55	0.20	-0.14	2.18
3	48.50	49.22	47.89	87.10	0.08	0.20	-0.03	84.07	0.42	0.54	0.31
4	43.48	45.79	44.20	80.12	-0.87	-0.42	-0.73	77.08	-0.53	-0.08	-0.39
6	43.33	44.70	45.67	80.51	-0.90	-0.63	-0.45	77.21	-0.58	-0.29	-0.11
7	44.16	44.87	47.33	82.03	-0.74	-0.60	-0.14	78.78	-0.40	-0.26	0.20
8	44.69	42.68	42.09	77.89	-0.64	-1.03	-1.16	74.77	-0.29	-0.69	-0.81
Average	45.25	45.46	47.77	83.28	-0.54	-0.49	-0.11	80.07	-0.20	-0.15	0.23

Emag (1) = Average(Magnitudes) Emag (2) = Magnitude (Averages)

E-Field Normalized Relative to 200 V/m Incident on Slot

11/29/95

TABLE 2b ESTIMATED POWER ERROR (dB) - MECHANICAL MODE STIRRING

10.5" X 10.5" SLOT WITHOUT CONE (F = 4 GHz)

Probe	E _x	E _y	E _z	Emag (1)	Err X (1)	Err Y (1)	Err Z (1)	Emag (2)	Err X (2)	Err Y (2)	Err Z (2)
1	56.52	67.57	53.15	109.85	-2.07	-0.52	-2.60	102.88	-1.48	0.07	-2.01
3	68.97	69.43	61.54	122.81	-0.34	-0.28	-1.33	115.61	0.25	0.31	-0.74
4	64.66	58.74	62.75	114.86	-0.90	-1.73	-1.16	107.58	-0.31	-1.14	-0.57
6	66.51	58.12	67.89	121.01	-0.65	-1.82	-0.47	111.40	-0.06	-1.24	0.11
7	57.74	81.46	72.11	131.95	-1.88	1.11	0.05	123.16	-1.29	1.70	0.64
8	64.77	95.27	71.78	144.70	-0.88	2.47	0.01	135.73	-0.29	3.06	0.60
Average	63.20	71.77	64.87	124.20	-1.12	-0.13	-0.92	116.06	-0.53	0.46	-0.33

10.5" X 10.5" SLOT WITH CONE (F = 4 GHz)

Probe	E _x	E _y	E _z	Emag (1)	Err X (1)	Err Y (1)	Err Z (1)	Emag (2)	Err X (2)	Err Y (2)	Err Z (2)
1	50.93	42.50	47.50	87.12	-1.40	-2.98	-2.01	81.59	-0.81	-2.38	-1.42
3	53.23	68.67	59.73	111.90	-1.02	1.19	-0.02	105.44	-0.43	1.78	0.57
4	57.65	58.30	52.53	103.33	-0.33	-0.23	-1.14	97.37	0.26	0.36	-0.54
6	60.38	53.70	62.74	110.74	0.07	-0.94	0.41	102.30	0.87	-0.35	1.00
7	53.54	56.56	55.97	103.40	-0.97	-0.49	-0.58	95.91	-0.38	0.10	0.01
8	61.39	56.36	52.70	105.68	0.22	-0.52	-1.11	98.60	0.81	0.07	-0.52
Average	56.19	56.02	55.20	103.70	-0.57	-0.66	-0.74	96.87	0.02	-0.07	-0.15

Emag (1) = Average (Magnitudes)

Emag (2) = Magnitude (Averages)

E-Field Normalized Relative to 200 V/m Incident on Slot

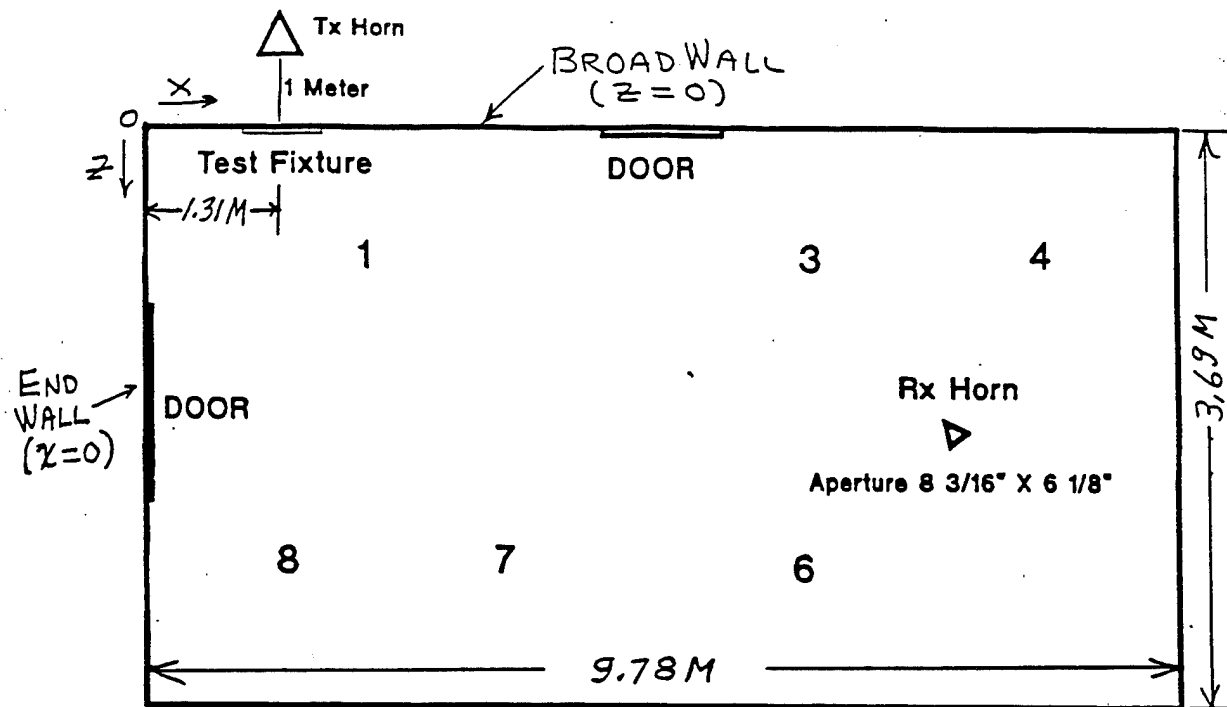


FIG.1a EQUIPMENT LOCATIONS IN REVCH #=Probe

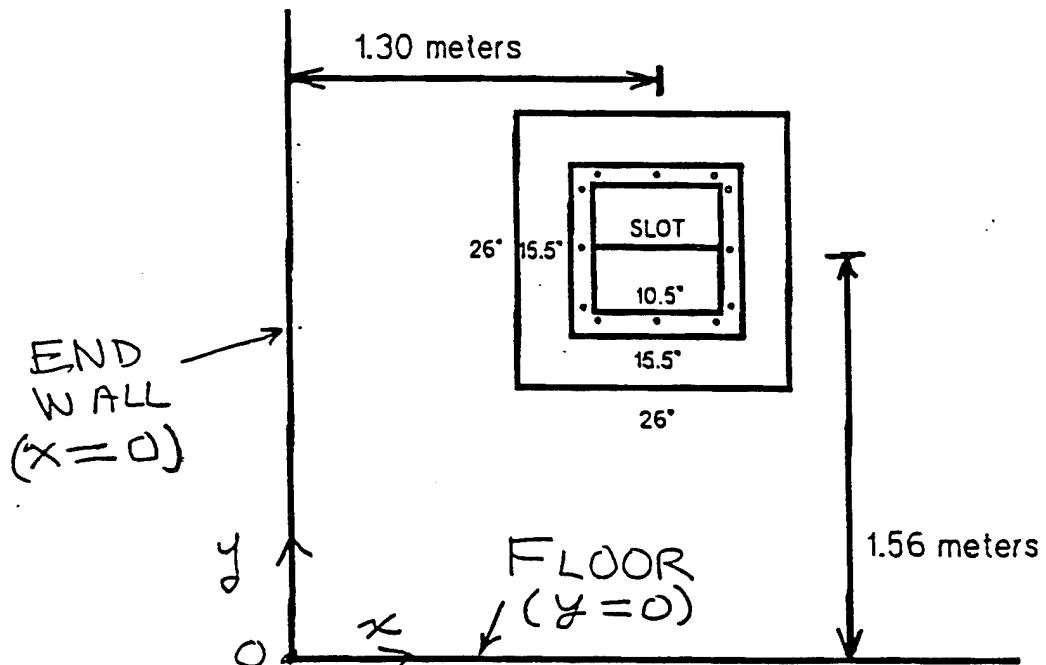
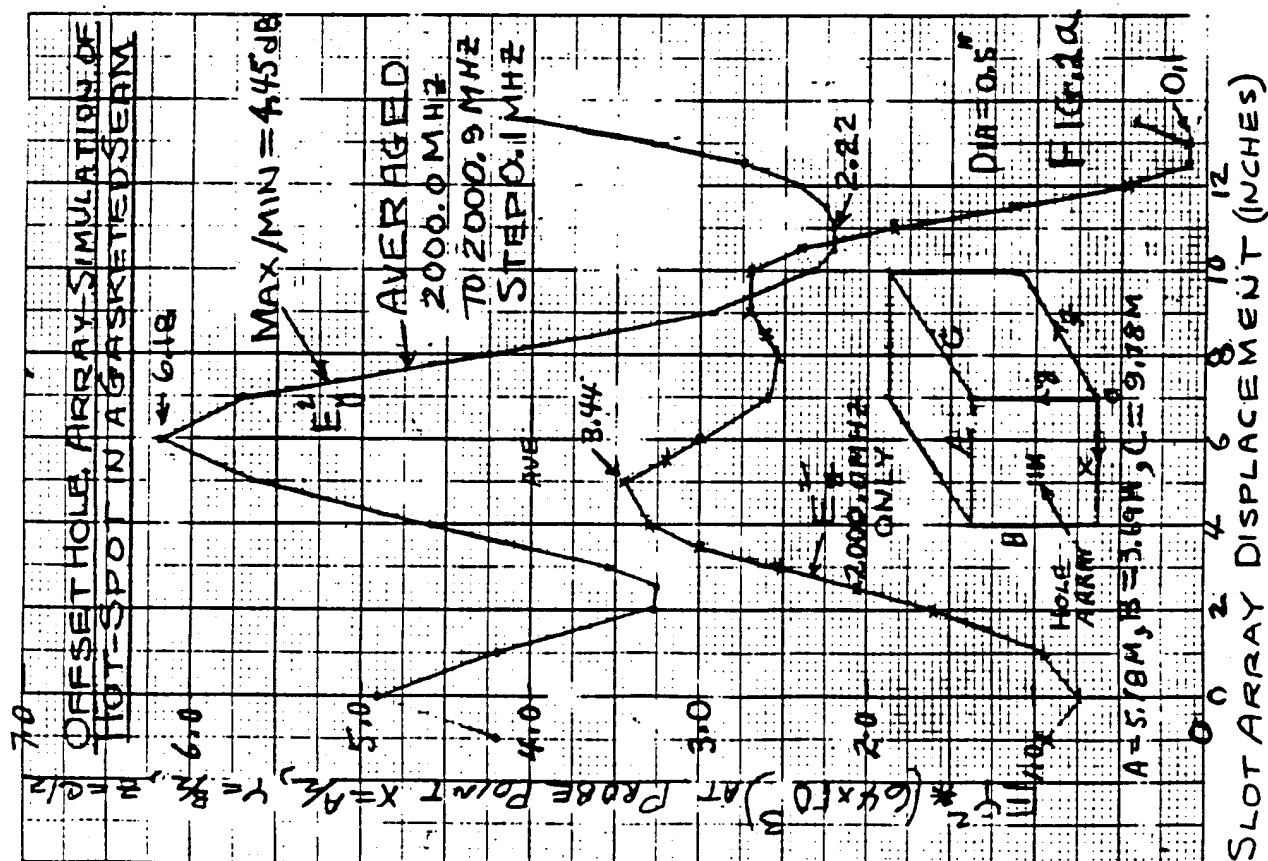
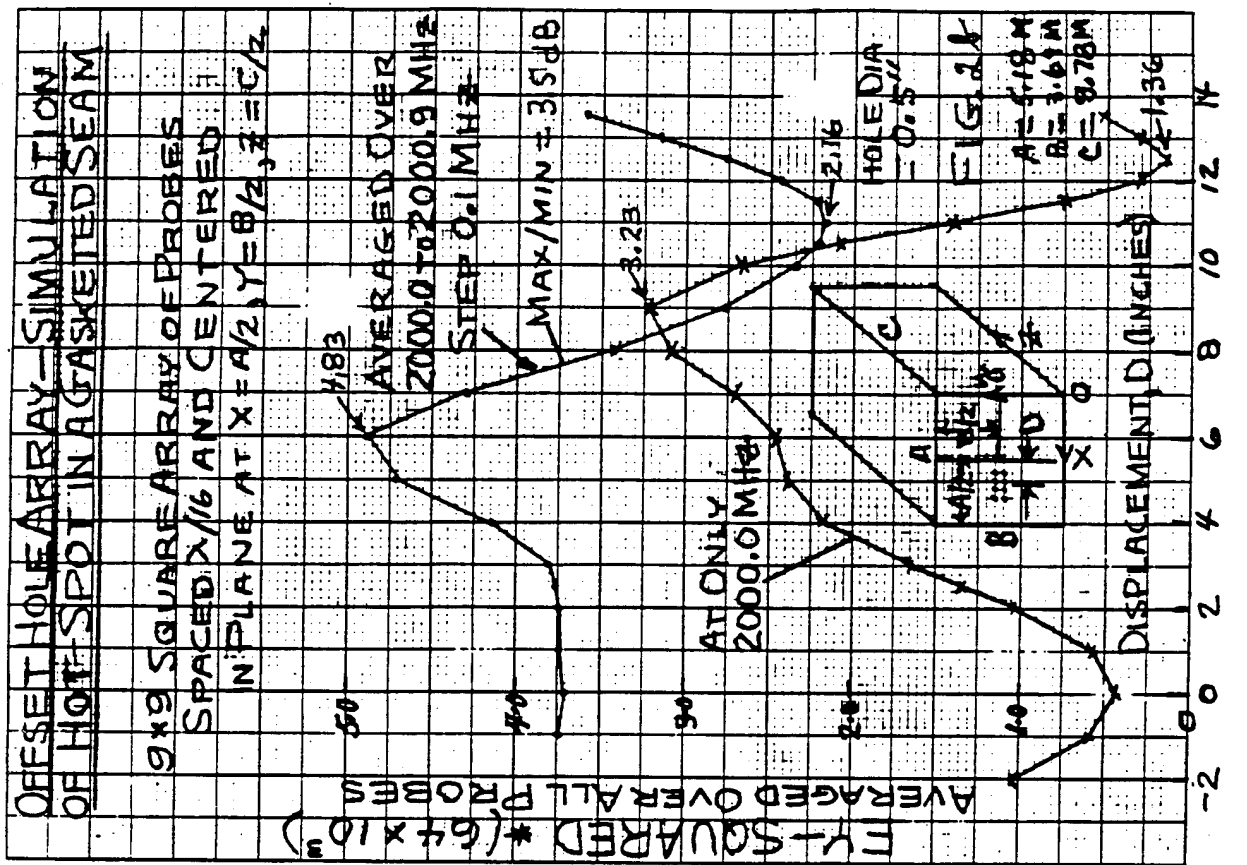


FIG.1b Location of Test Fixture in Chamber Wall

15.5" Mounting Flange is .5" thick with .125" gasket.
Test panel is $1/16''$ thick



EFFECT OF DISPLACING 1.5 x 1/8 Inch SLOT

FREQUENCY STIRRING - 6 MHz ABOUT CENTER FREQUENCY

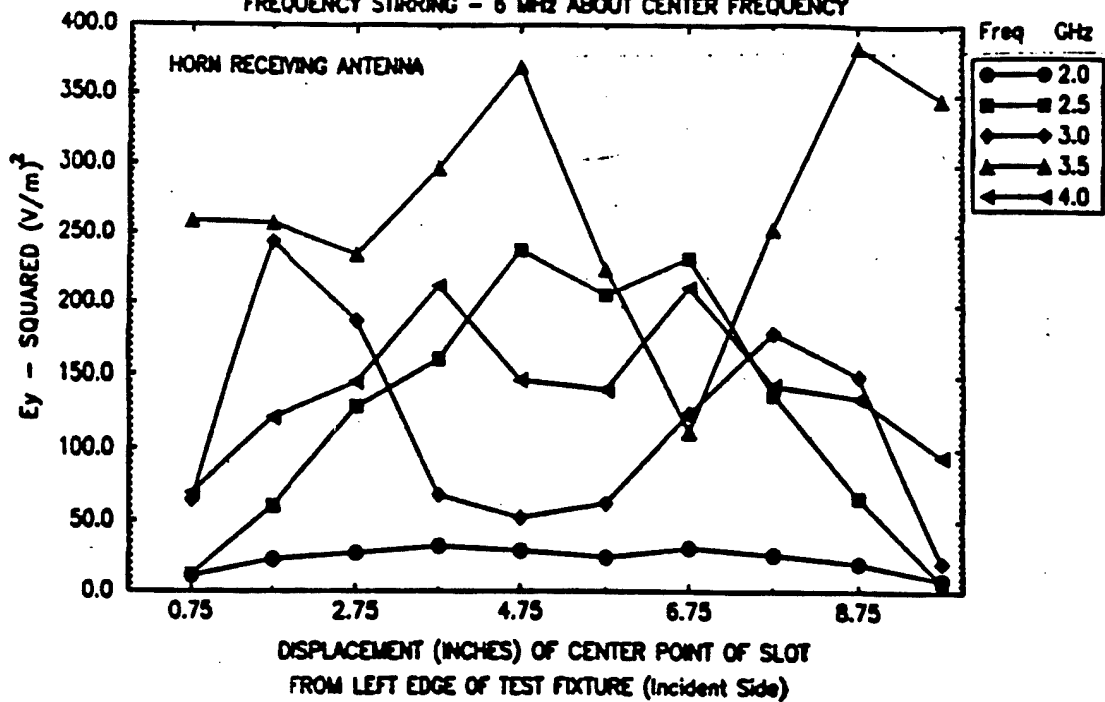


FIGURE 8-A

EFFECT OF DISPLACING 1.5 x 1/8 Inch SLOT

FREQUENCY STIRRING - 6 MHz ABOUT CENTER FREQUENCY

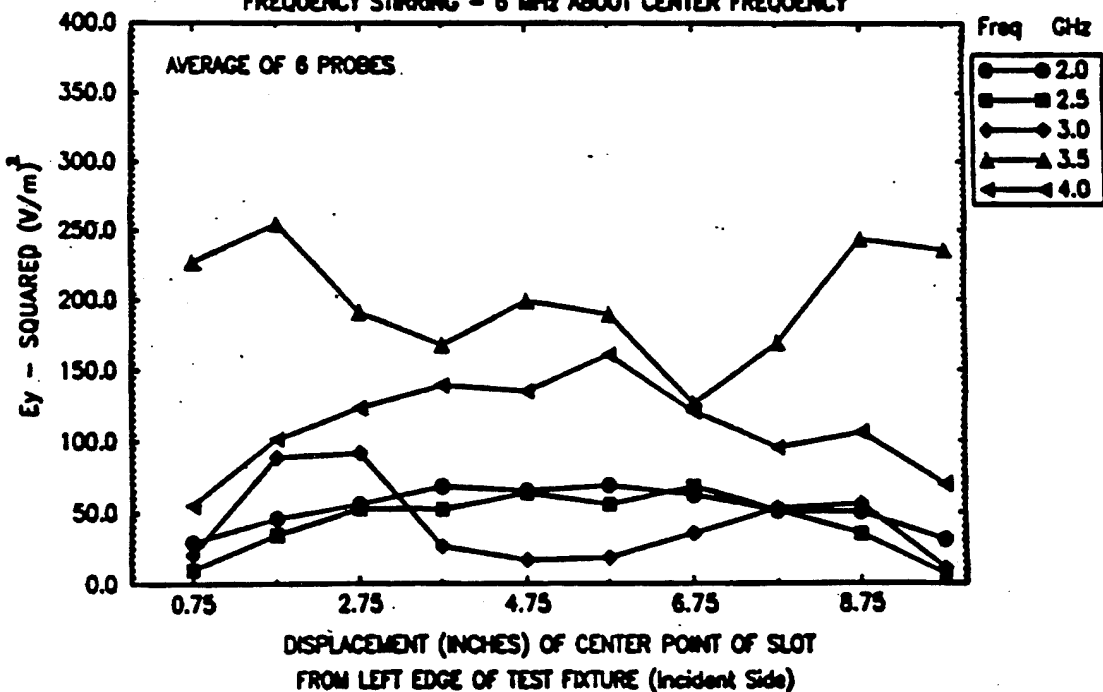
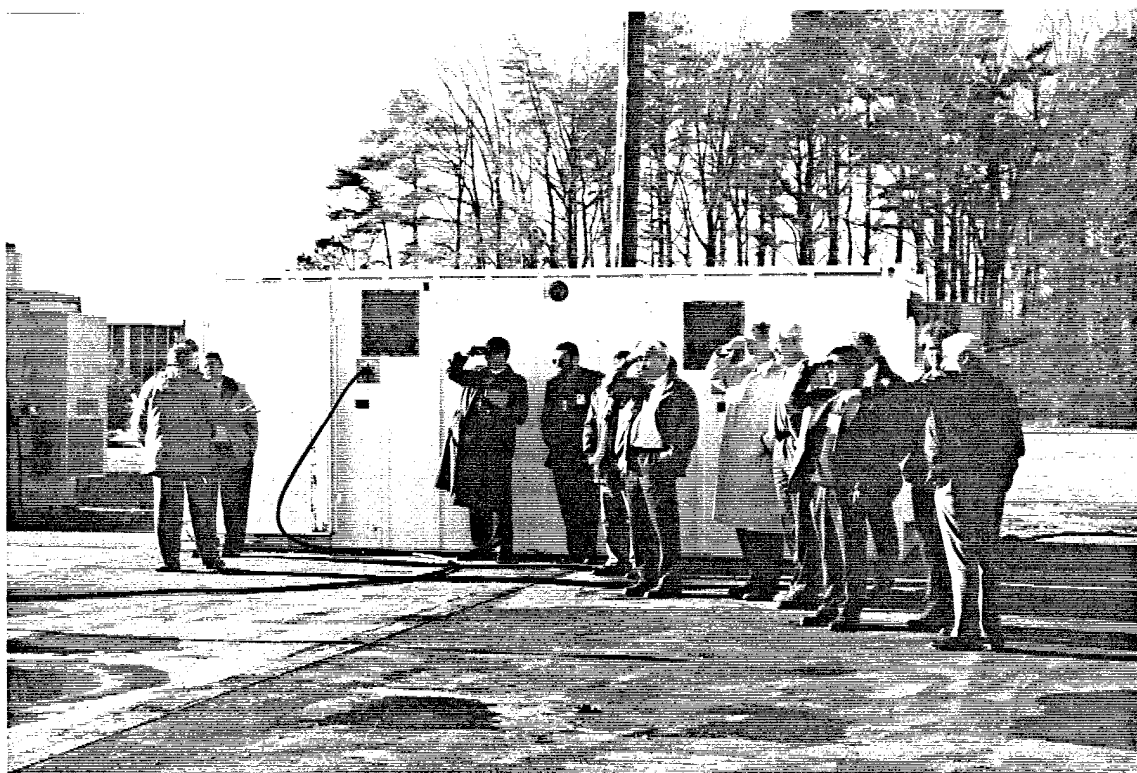


FIGURE 8-B





**MS. DIANE KEMPF
NAVAL AIR WARFARE CENTER AD**



REVERBERATION CHAMBER AND ANECHOIC CHAMBER
OPERATORS GROUP MEETING, 5 - 7 DEC 1995



**EMV Testing of Aircraft:
A Comparison of the Mode-Stirred
and Standard Methods**

Diane R. Kempf
Naval Air Warfare Center AD
Patuxent River, MD



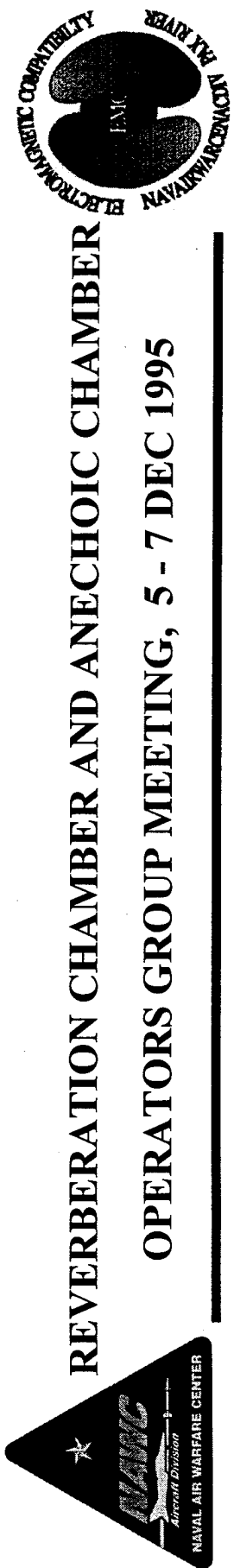
REVERBERATION CHAMBER AND ANECHOIC CHAMBER

OPERATORS GROUP MEETING, 5 - 7 DEC 1995



INTRODUCTION

- Studies performed by Hatfield, Freyer, Crawford, et al, to determine reverb. characteristics of aircraft
- Demonstrated good reverb. characteristics of Boeing 707, 757, Cessna 404, Beech U-21
- Advantages of reverb. chambers for aircraft testing well publicized
- Army had planned aircraft size TEM/reverb. chamber at Ft. Huachuca, AZ
- Still many people don't really understand or are skeptical of:
 - using MSC for box level testing of aircraft equipment
 - using MSC for HERO, EMV testing



INTRODUCTION

- This study performed to demonstrate EMV testing problems using standard methods and improvements obtained using mode-stir techniques
- This study consisted of testing performed on P-3 and E-2C aircraft

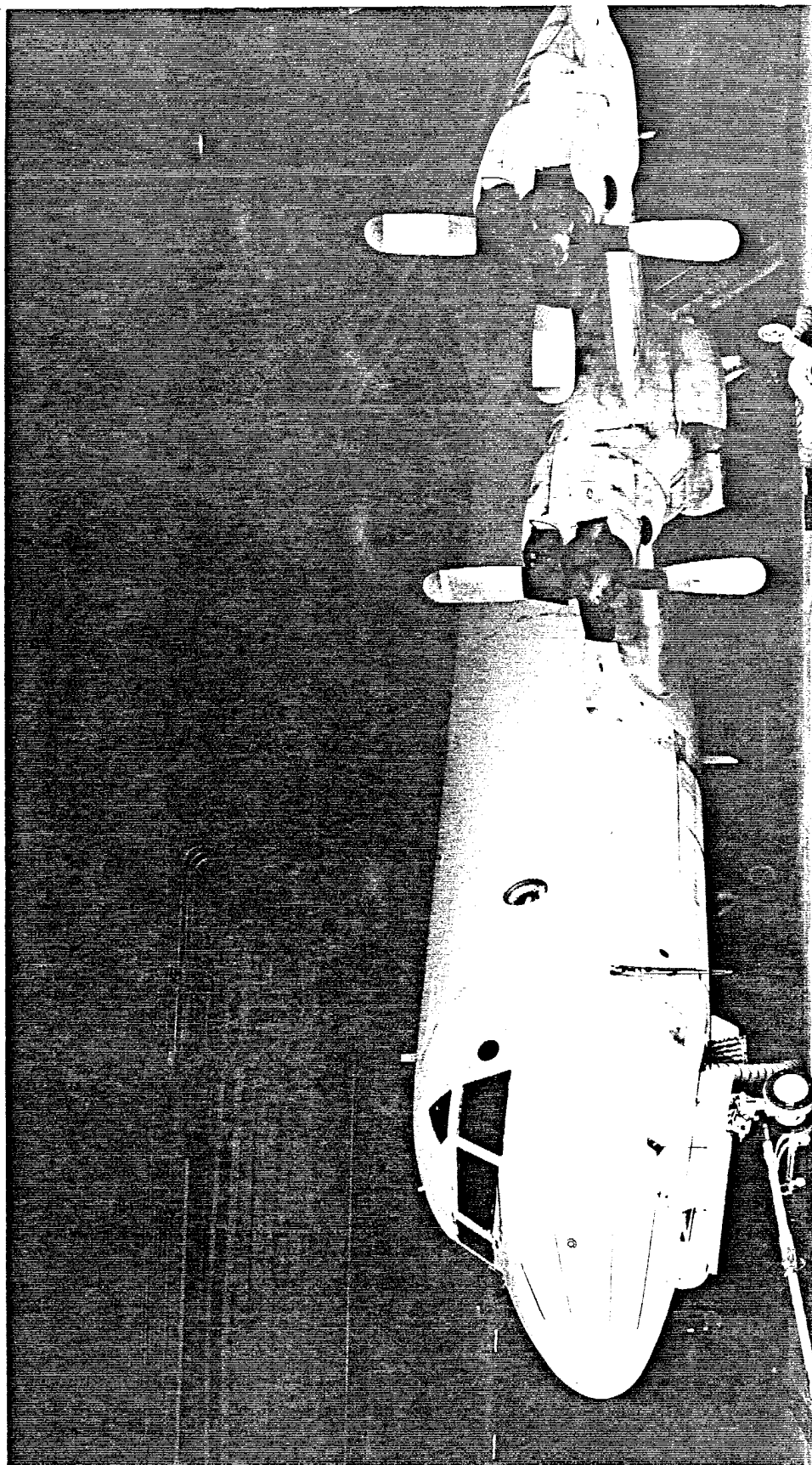


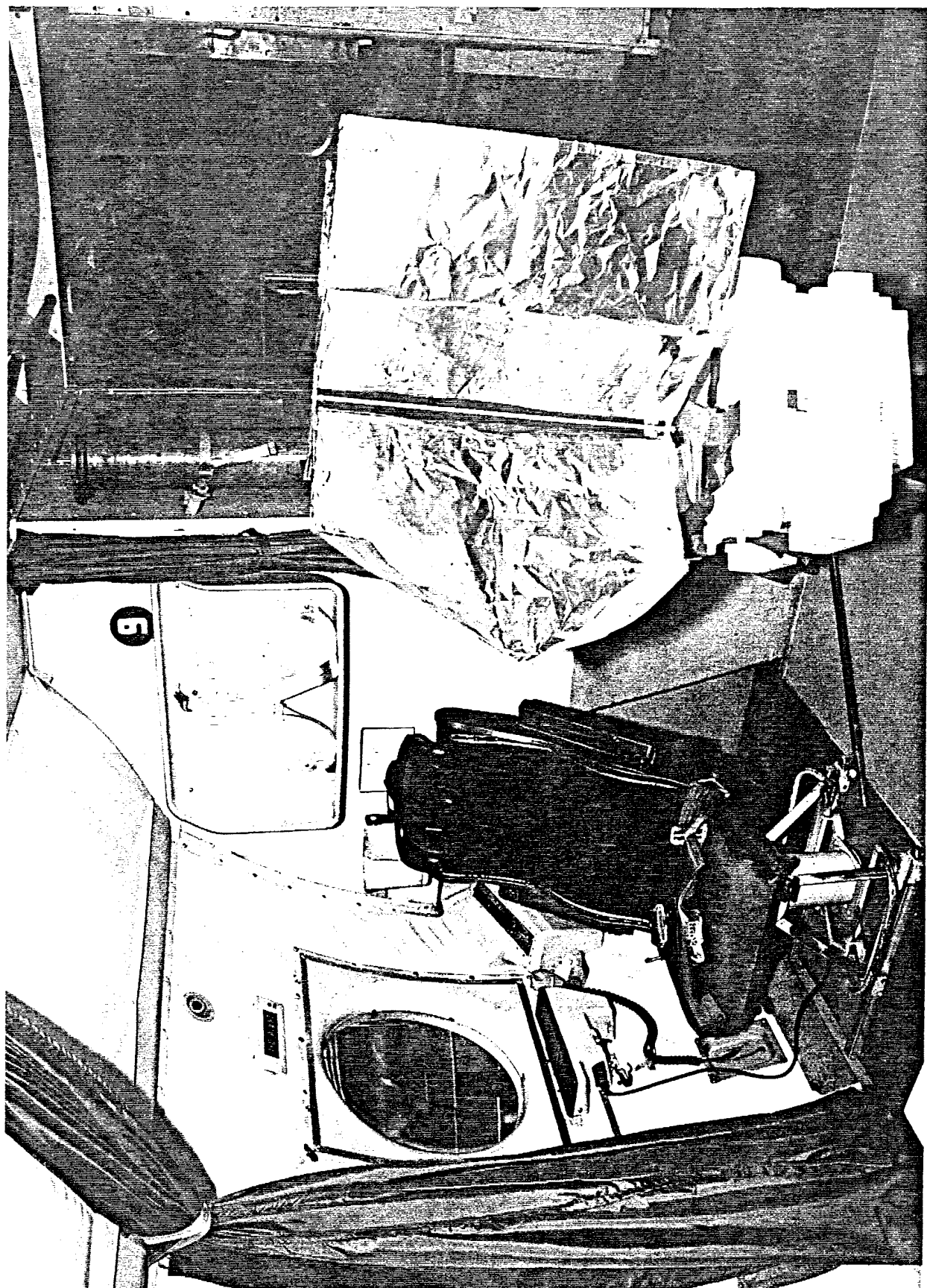
REVERBERATION CHAMBER AND ANECHOIC CHAMBER

OPERATORS GROUP MEETING, 5 - 7 DEC 1995

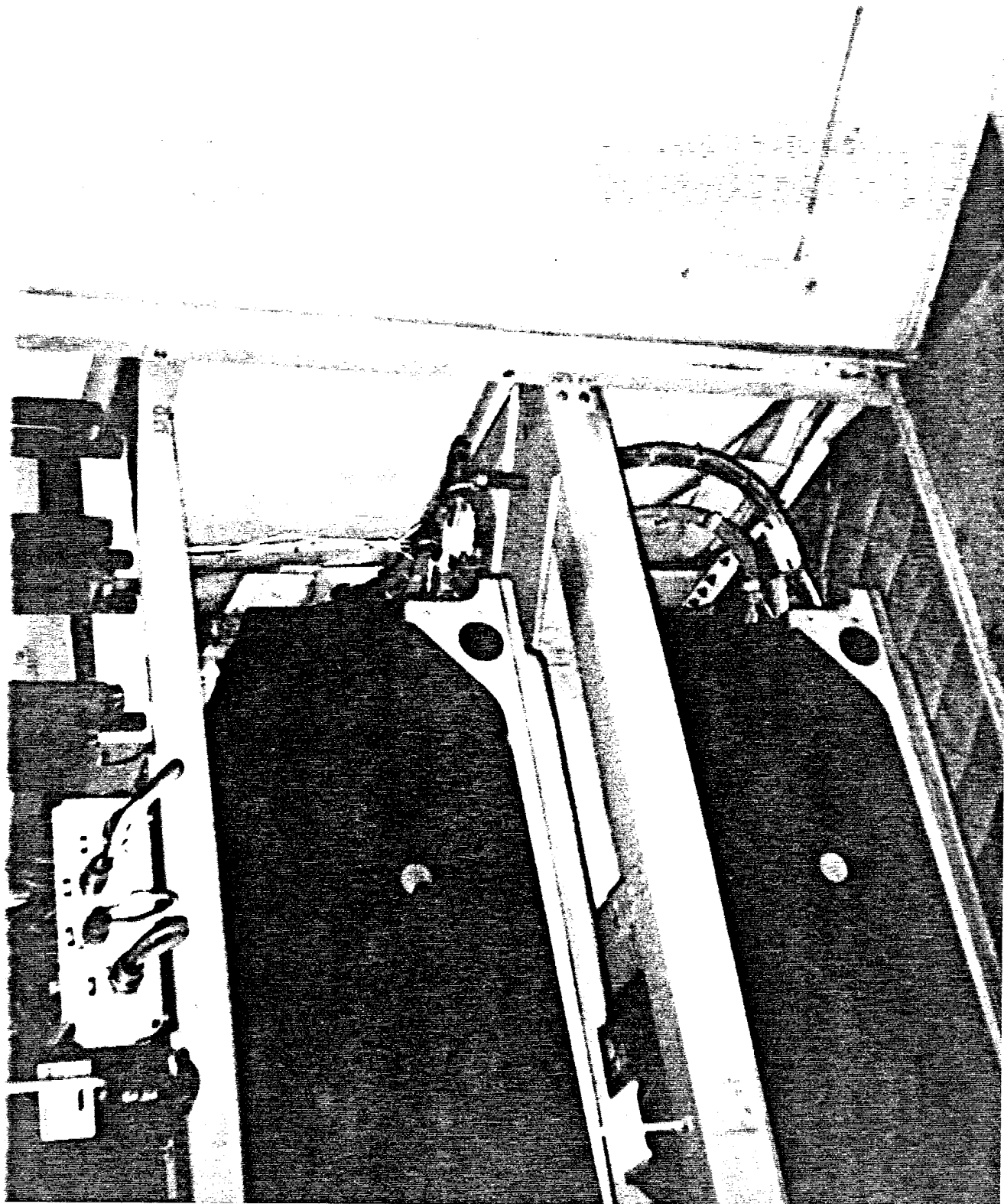
P-3 TESTING OUTLINE

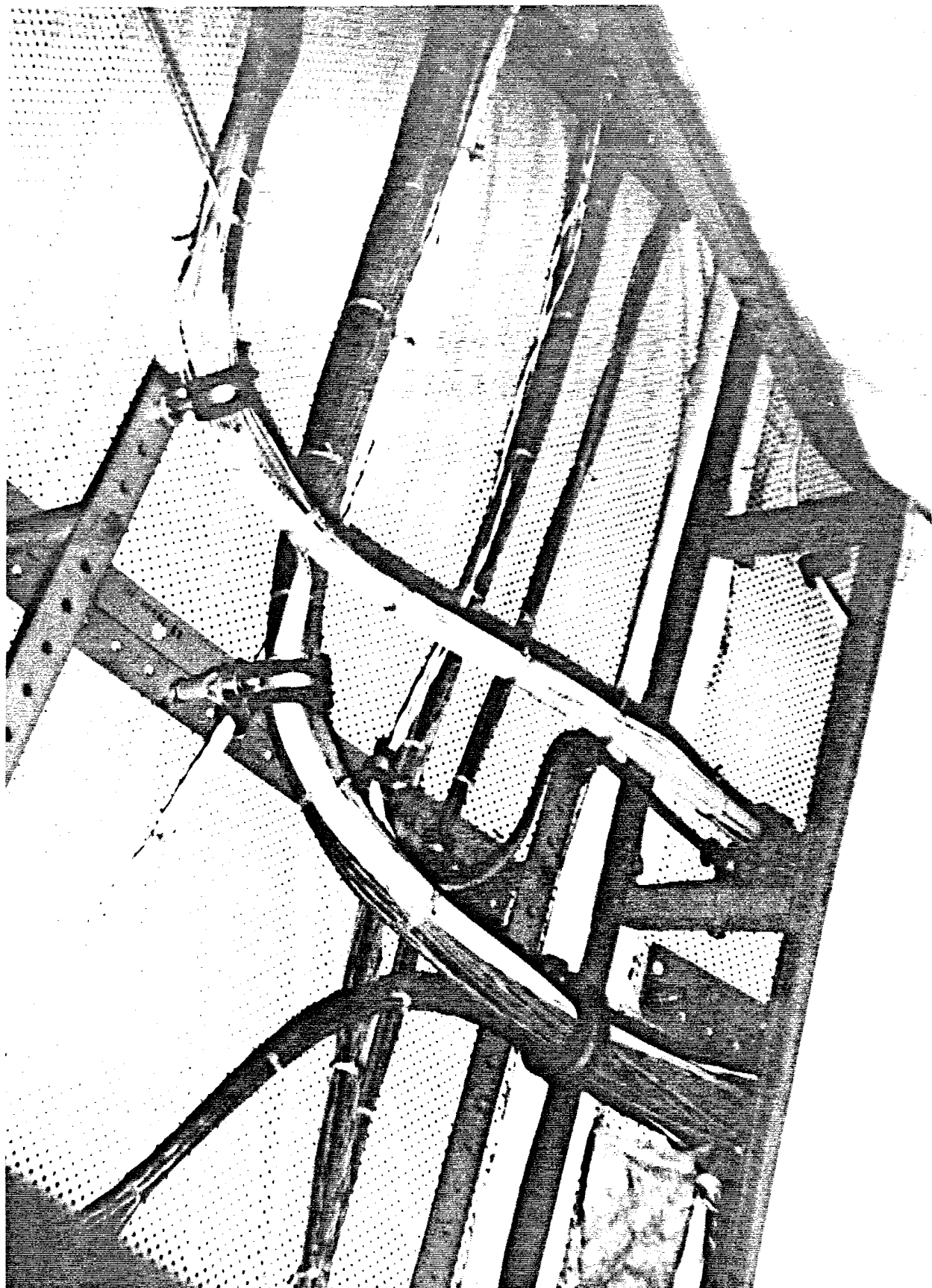
- During EMV testing of the P-3, the CGA was susceptible at 425 MHz
- Repeated test to determine effects of mode-stirring inside aircraft
- Susceptibility was intermittent depending on stirrer position
- Current probe measurements taken on several cables



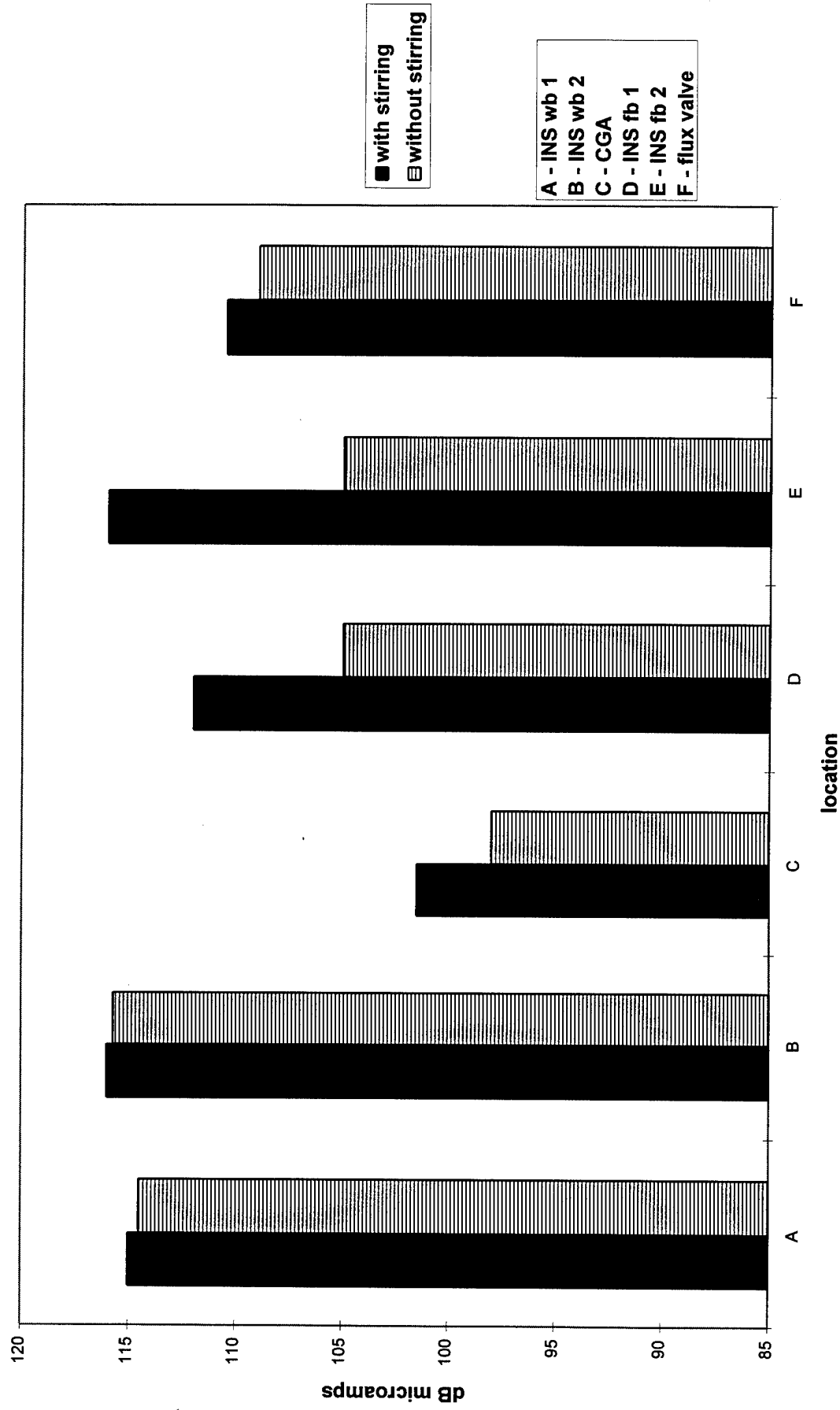








P-3 EMV Induced Currents



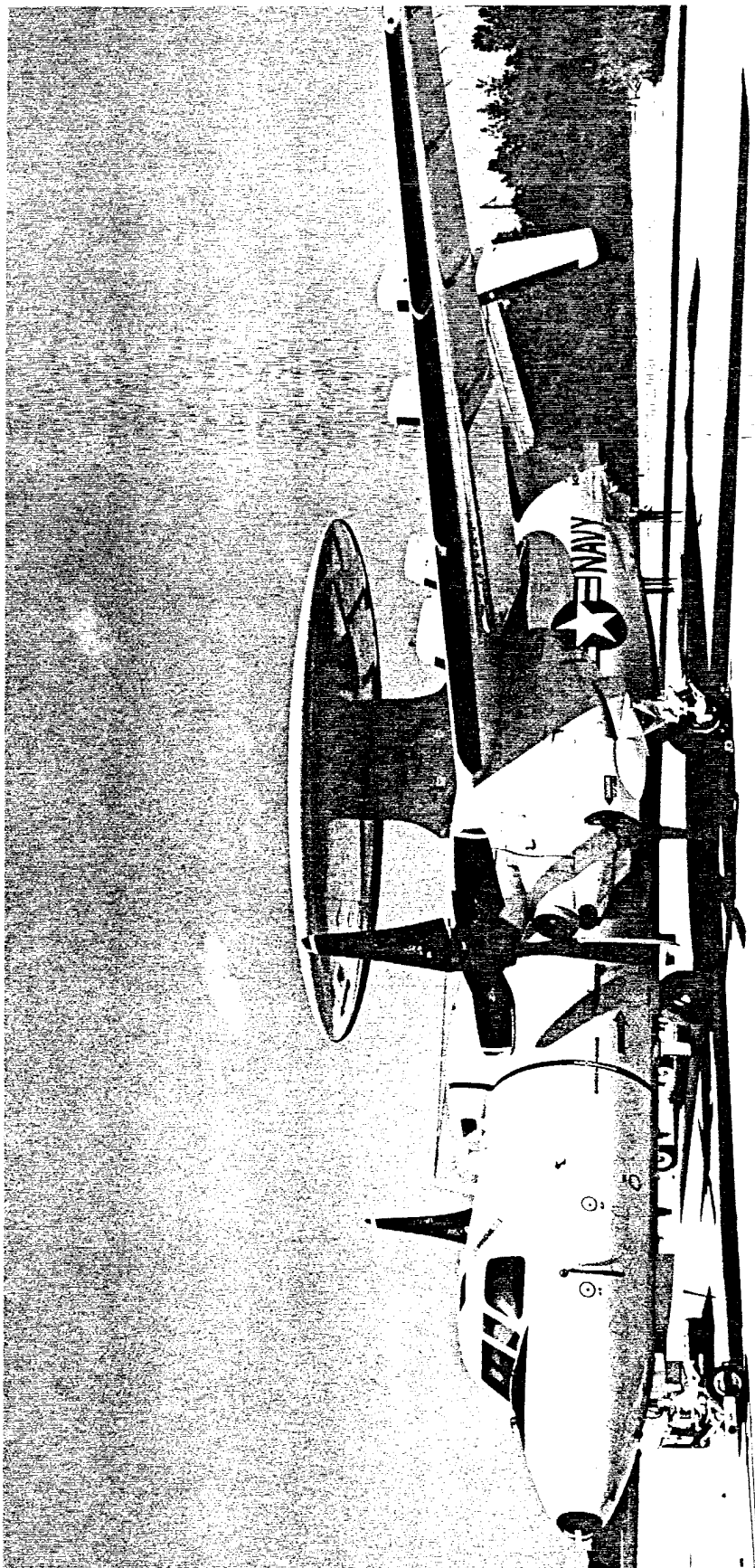


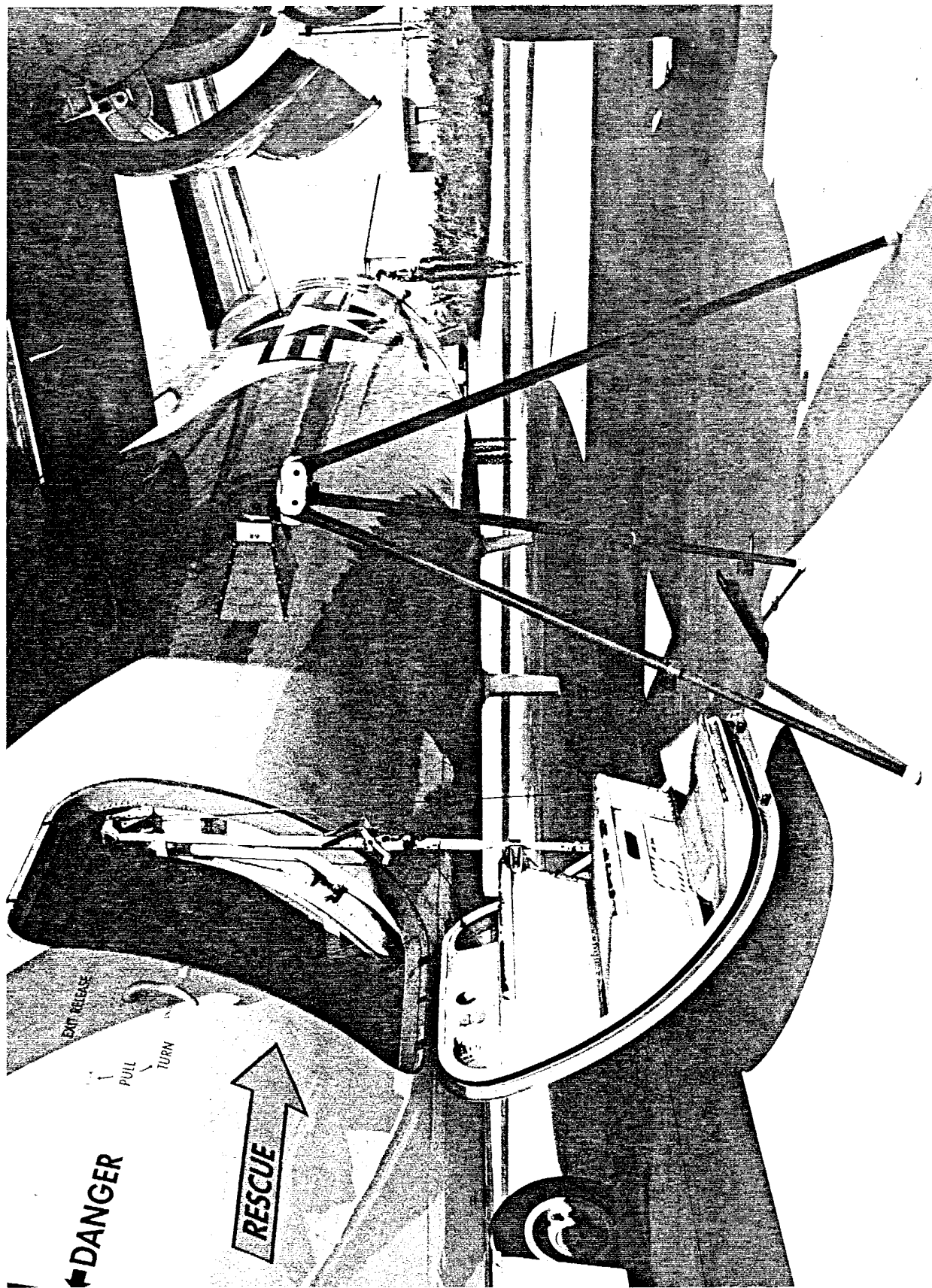
REVERBERATION CHAMBER AND ANECHOIC CHAMBER
OPERATORS GROUP MEETING, 5 - 7 DEC 1995

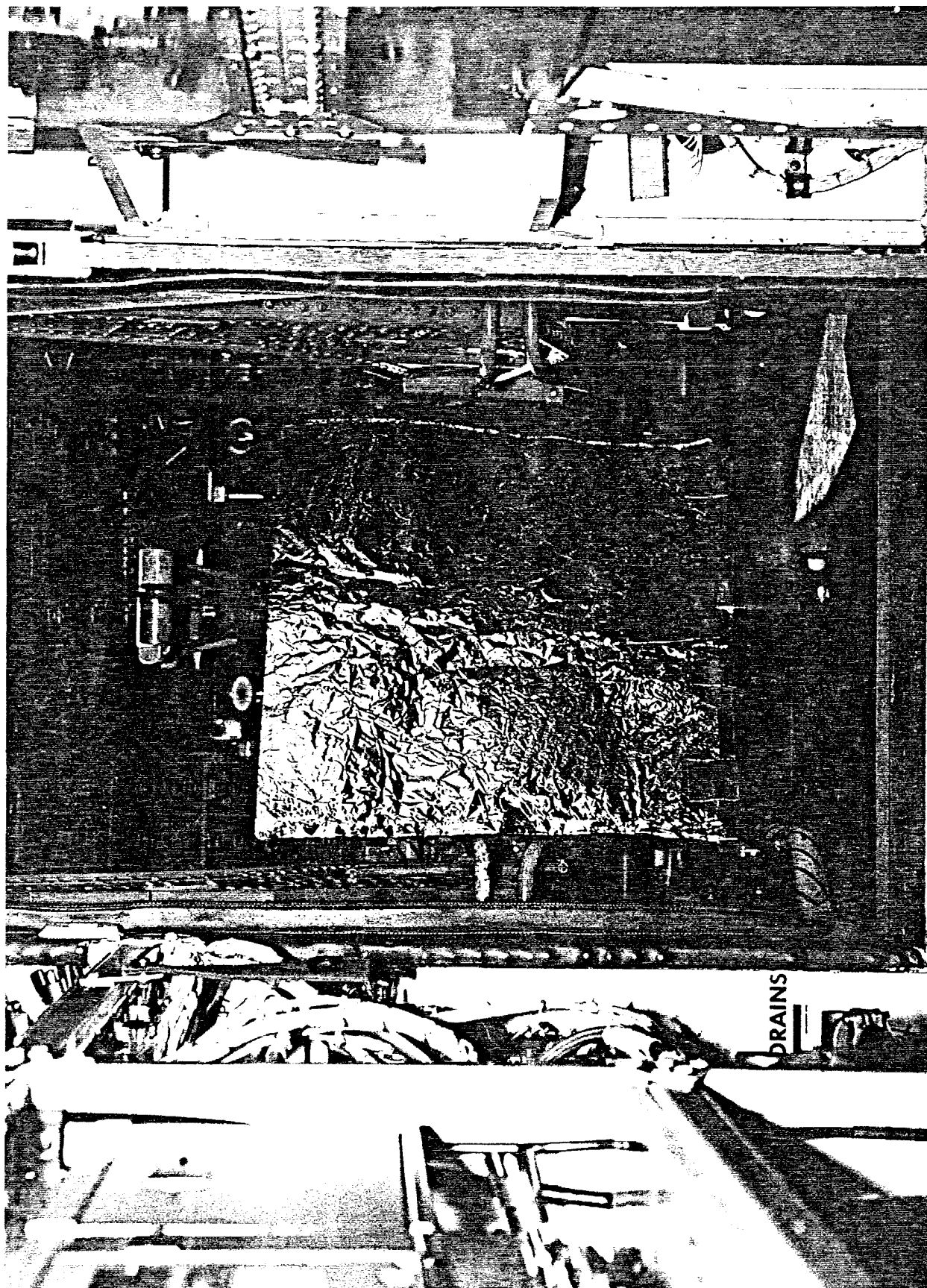


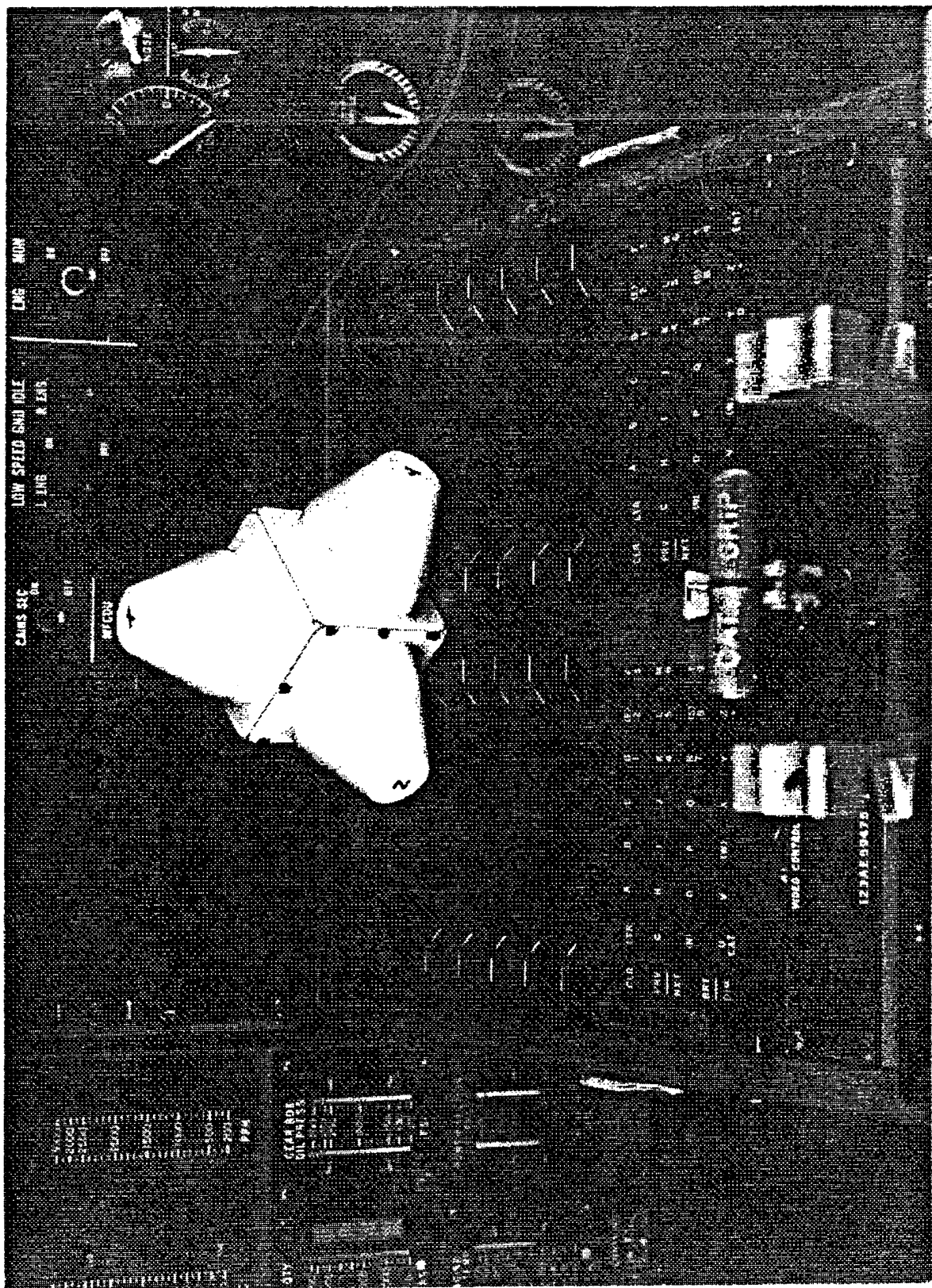
E-2C TESTING OUTLINE

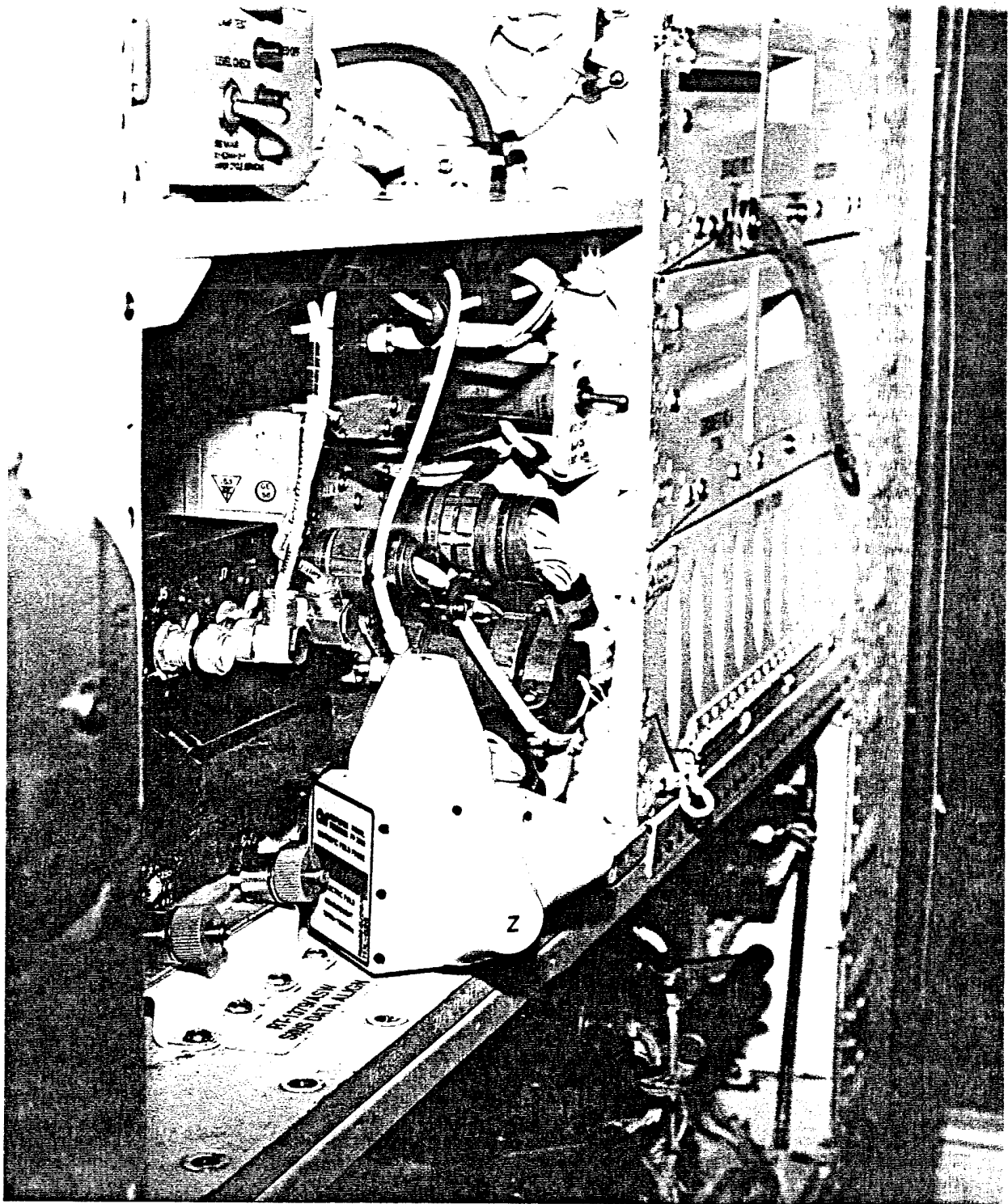
- To compare field uniformity inside aircraft during simulated EMV test with and without mode-stirring
 - 8 field probes set up throughout aircraft
 - 3 mode-stirrers on the aircraft
 - Test frequency range 100 MHz - 10 GHz





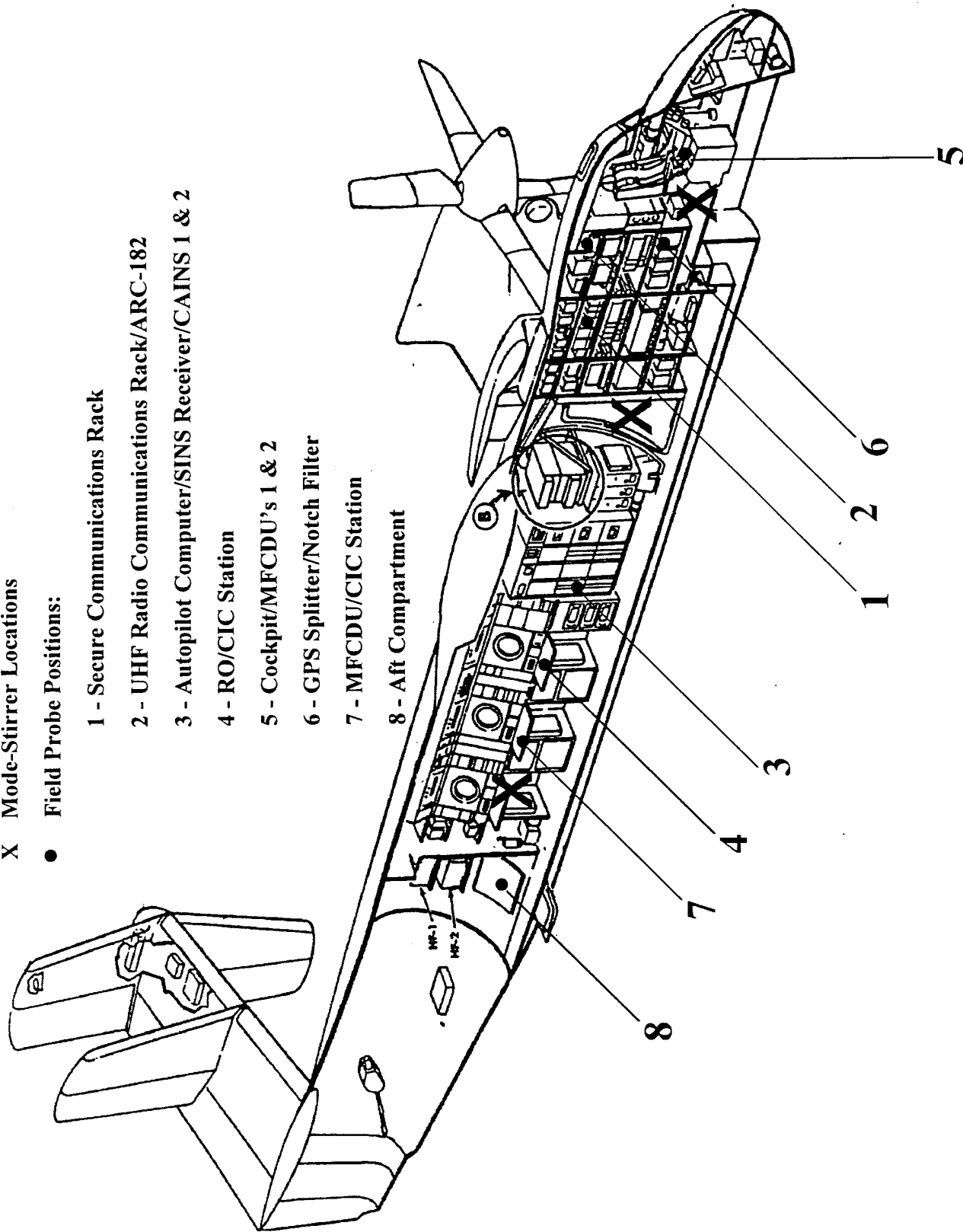




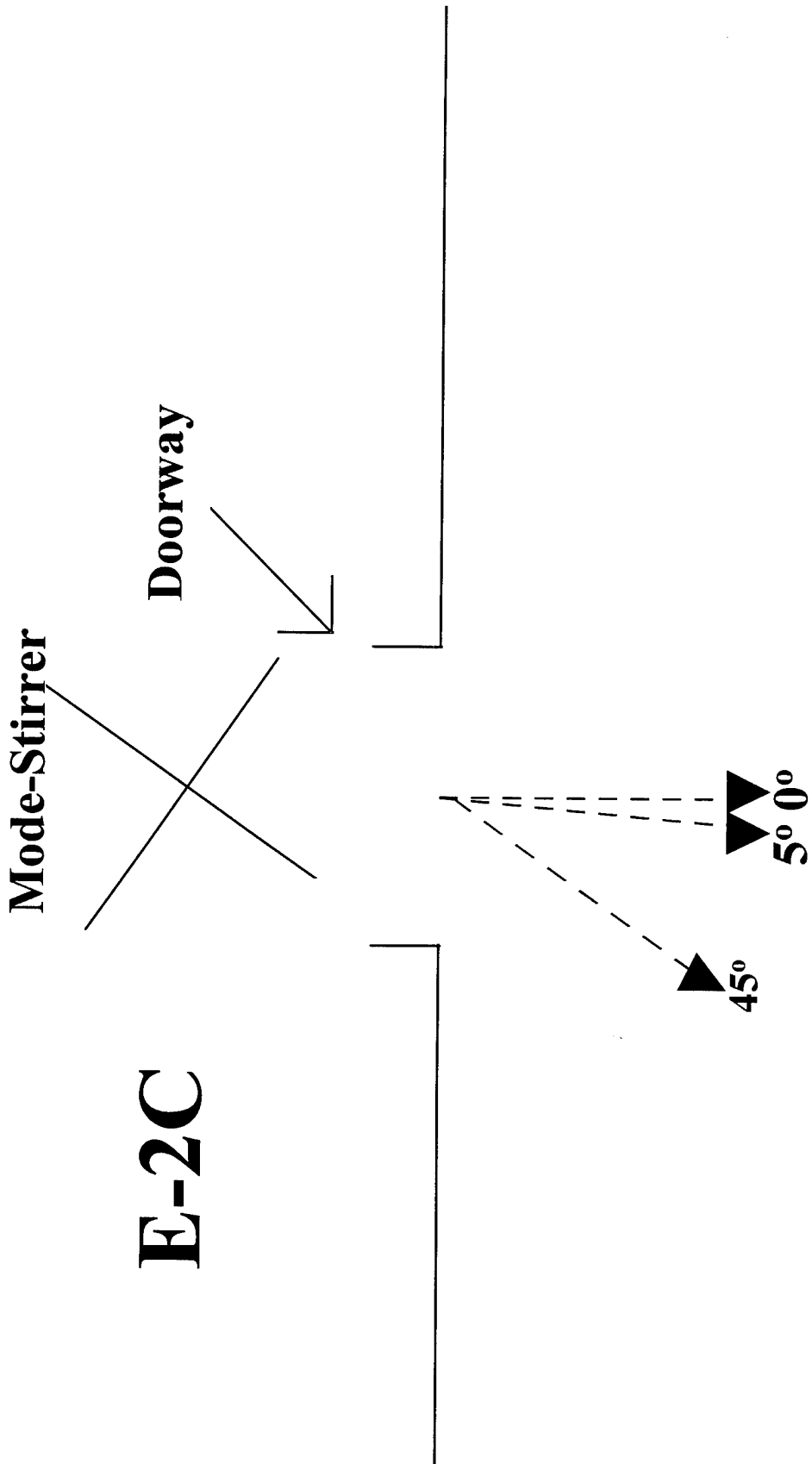


- X Mode-Stirrer Locations
- Field Probe Positions:

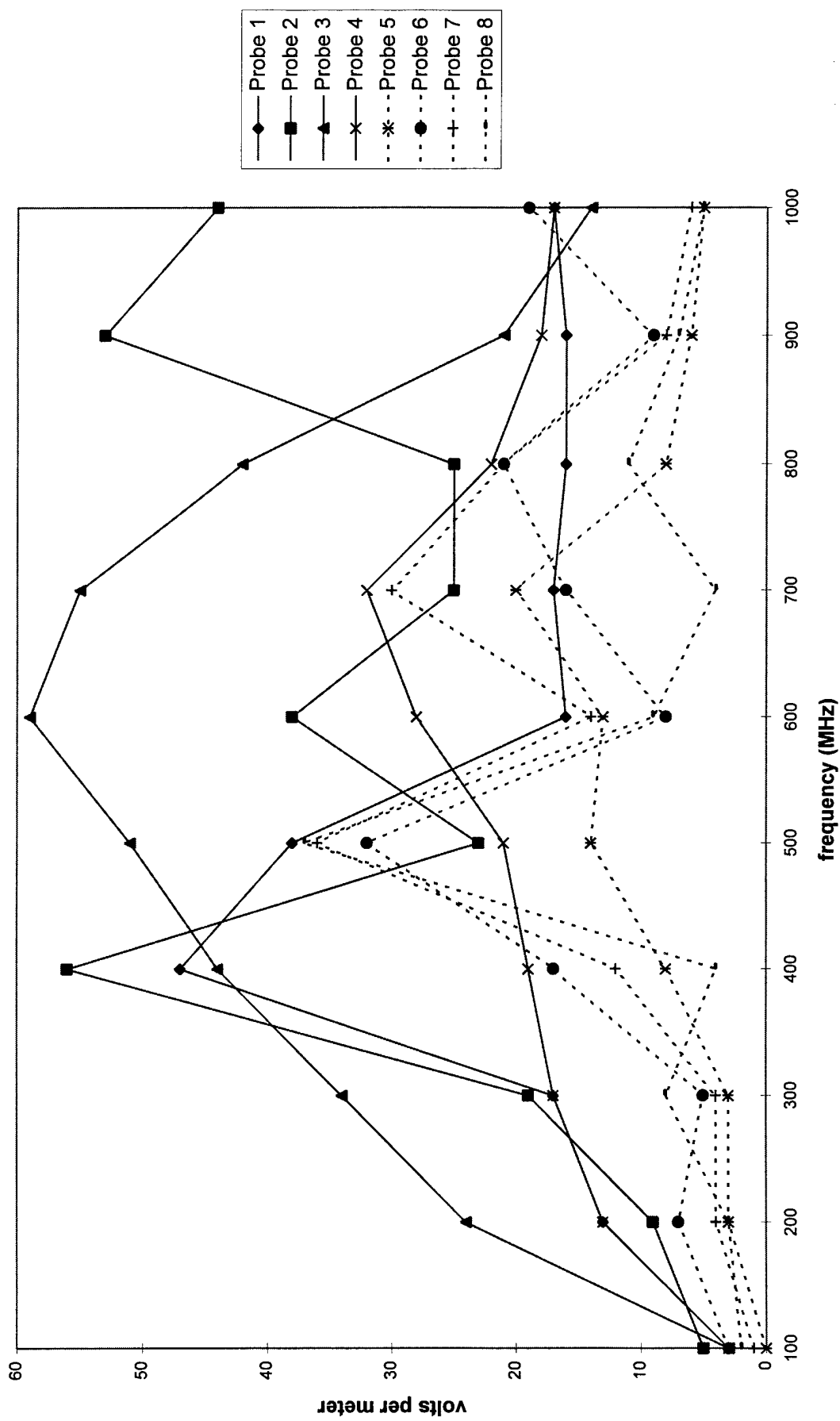
- 1 - Secure Communications Rack
- 2 - UHF Radio Communications Rack/ARC-182
- 3 - Autopilot Computer/SINS Receiver/CAINS 1 & 2
- 4 - RO/CIC Station
- 5 - Cockpit/MFCDU's 1 & 2
- 6 - GPS Splitter/Notch Filter
- 7 - MFCDU/CIC Station
- 8 - Aft Compartment

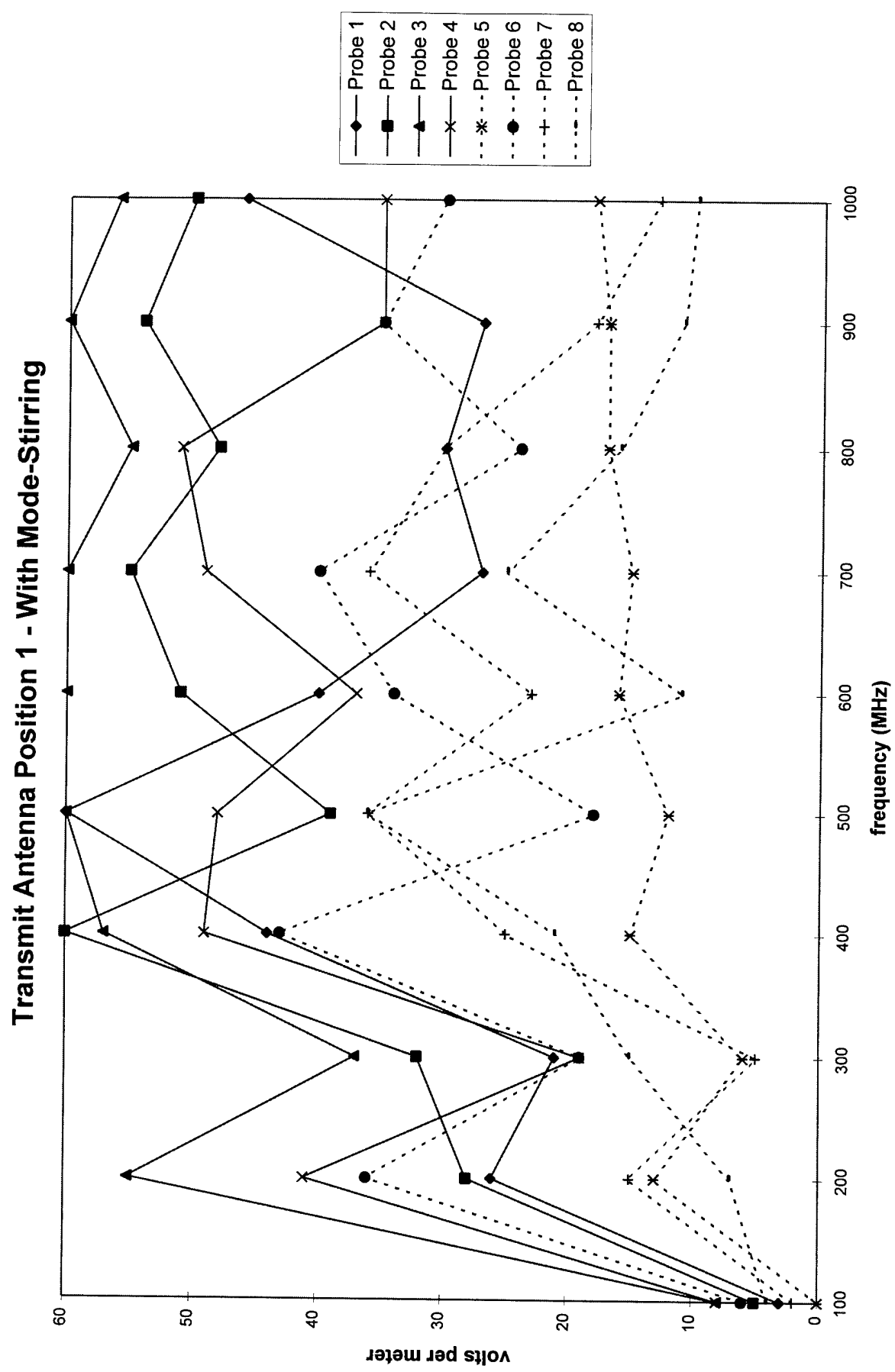


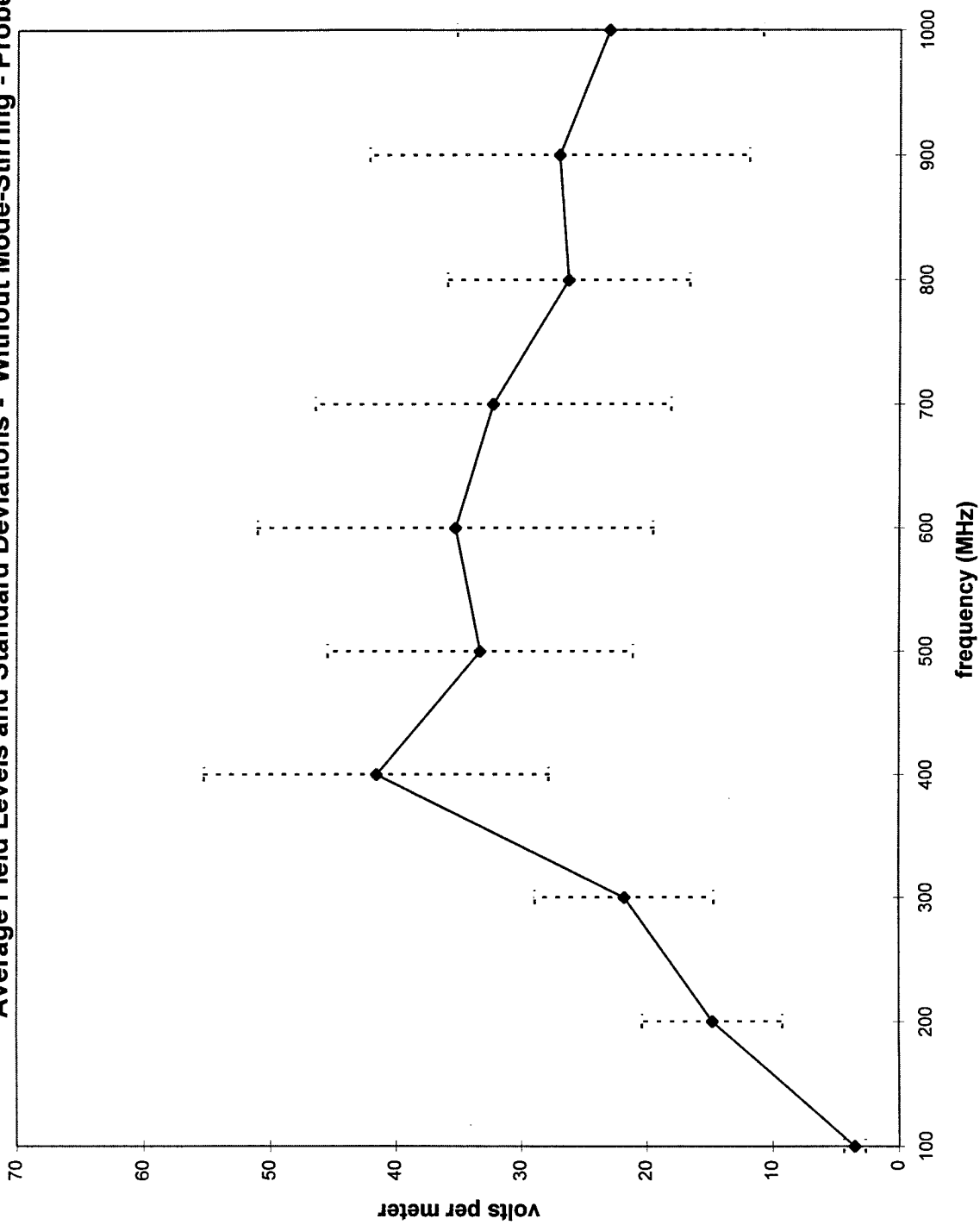
ANTENNA POSITIONS

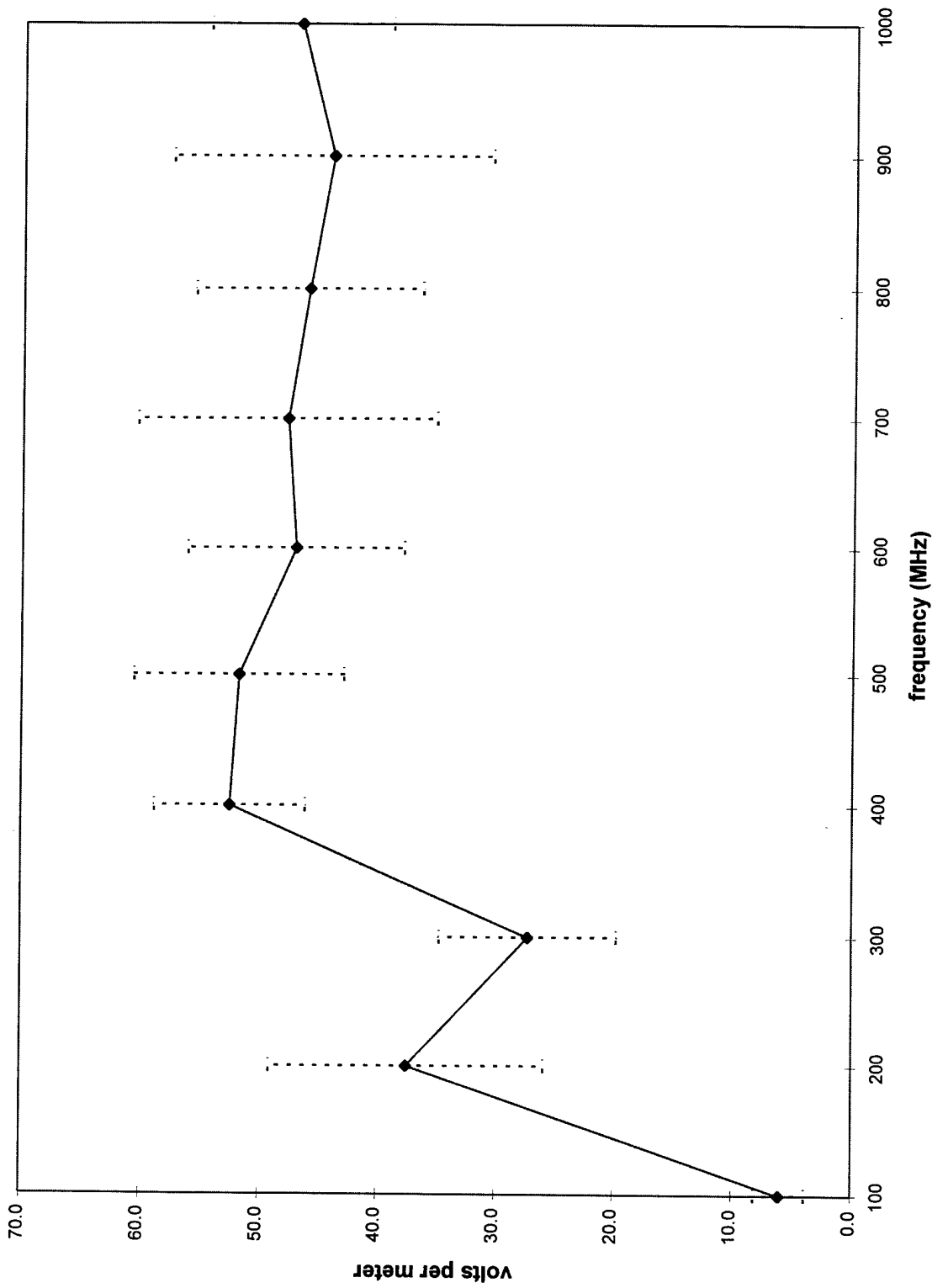


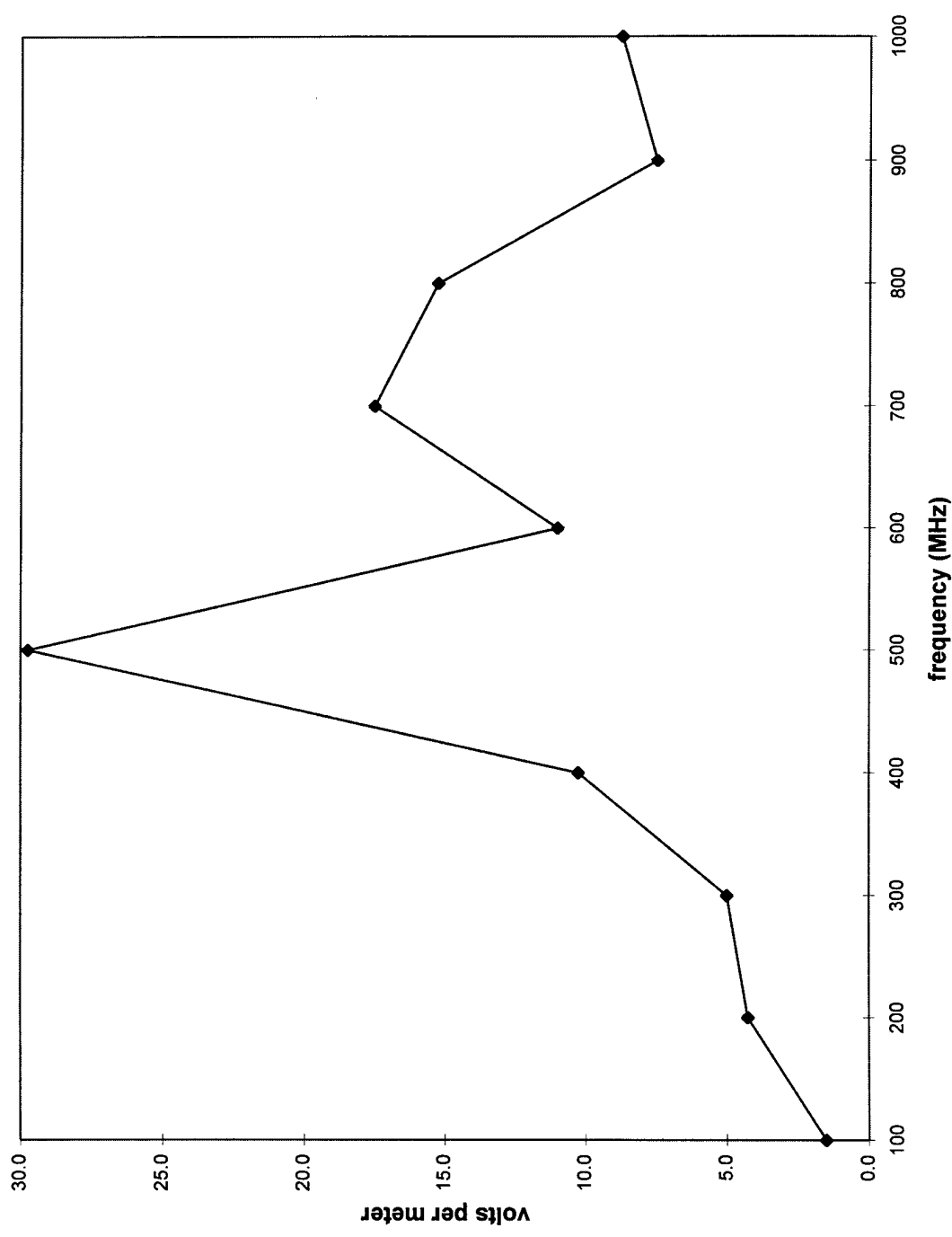
Transmit Antenna Position 1 - Without Mode-Stirring

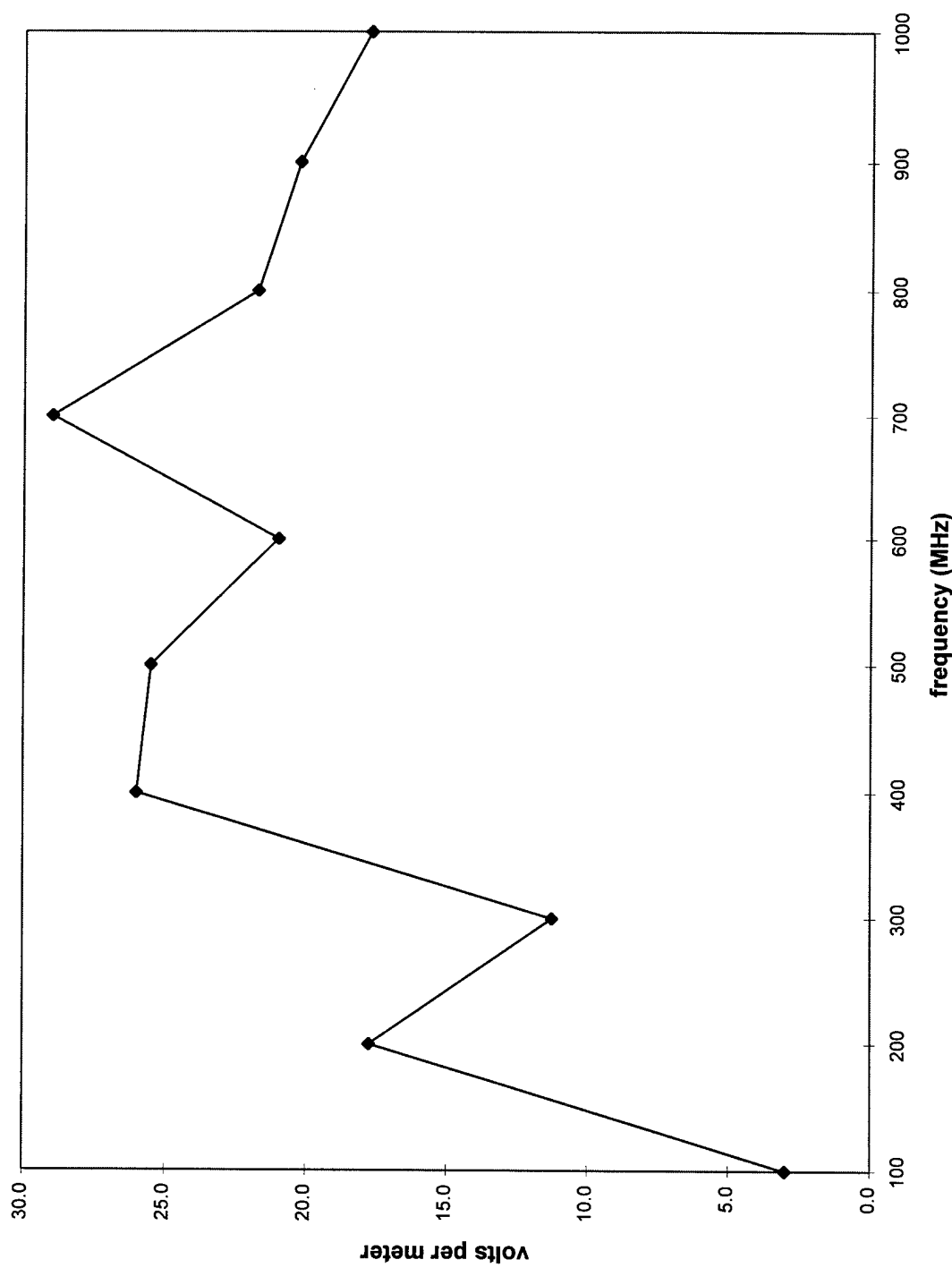


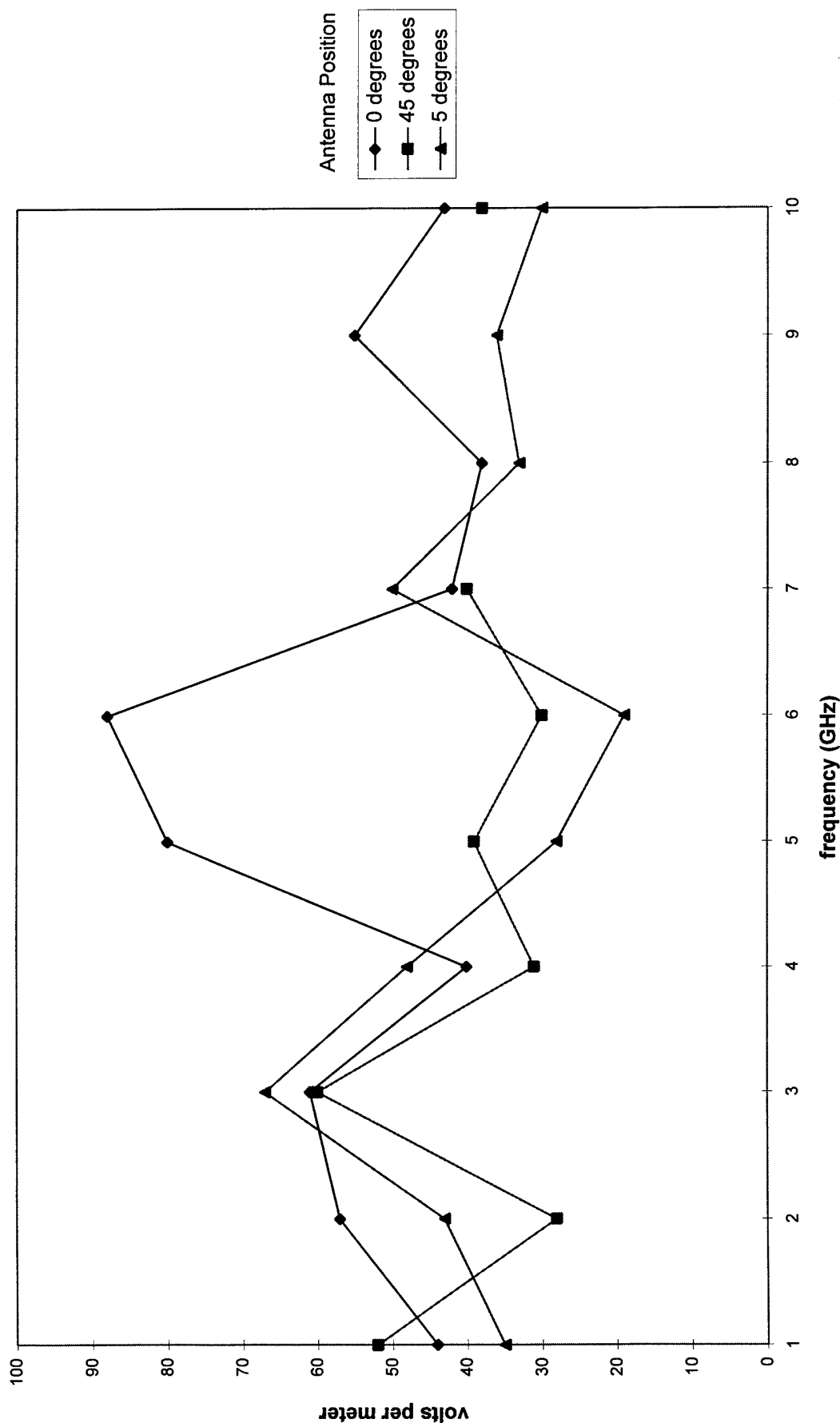


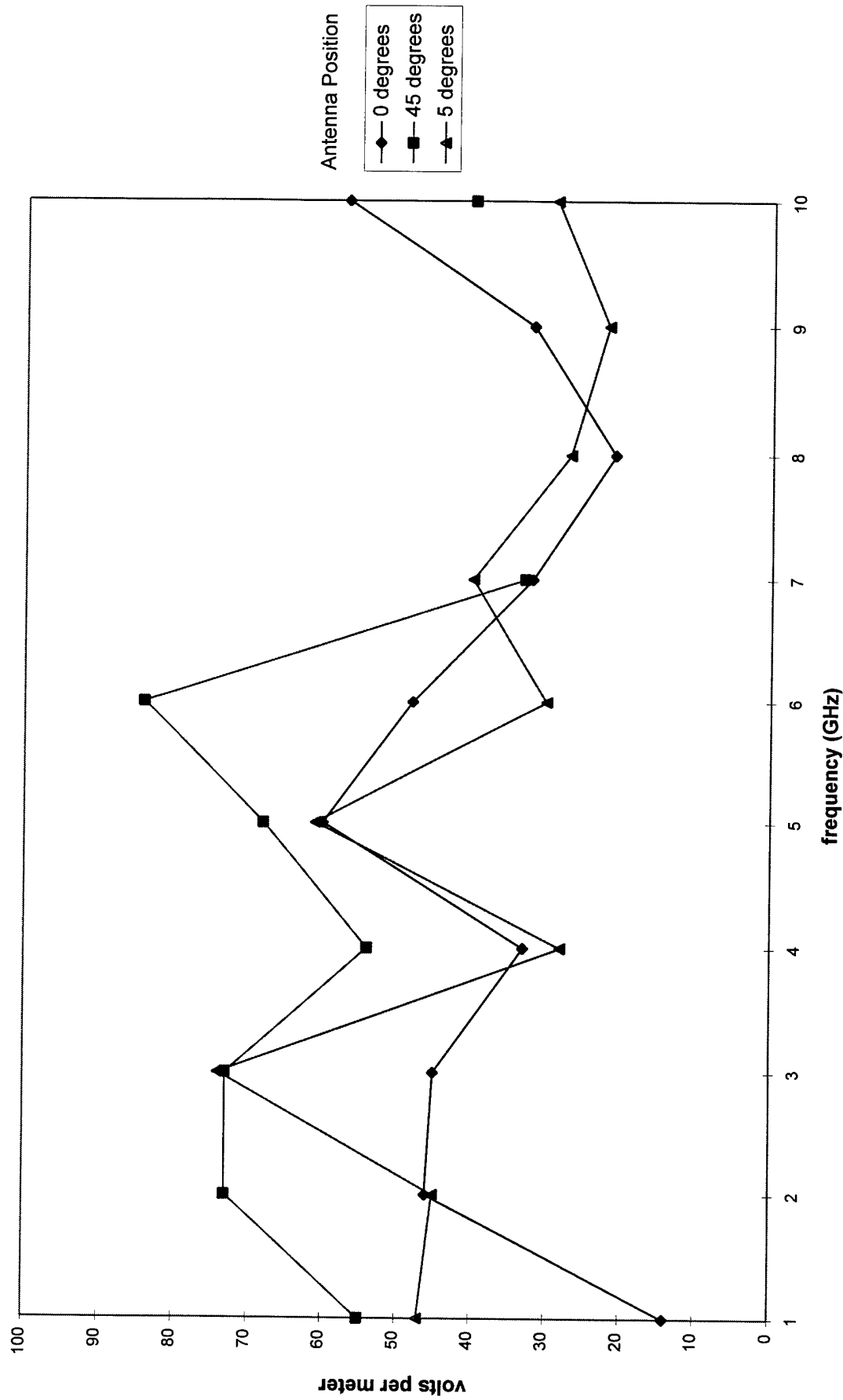
Average Field Levels and Standard Deviations - Without Mode-Stirring - Probes 1 - 4

Average Field Levels and Standard Deviations - With Mode-Stirring - Probes 1 - 4

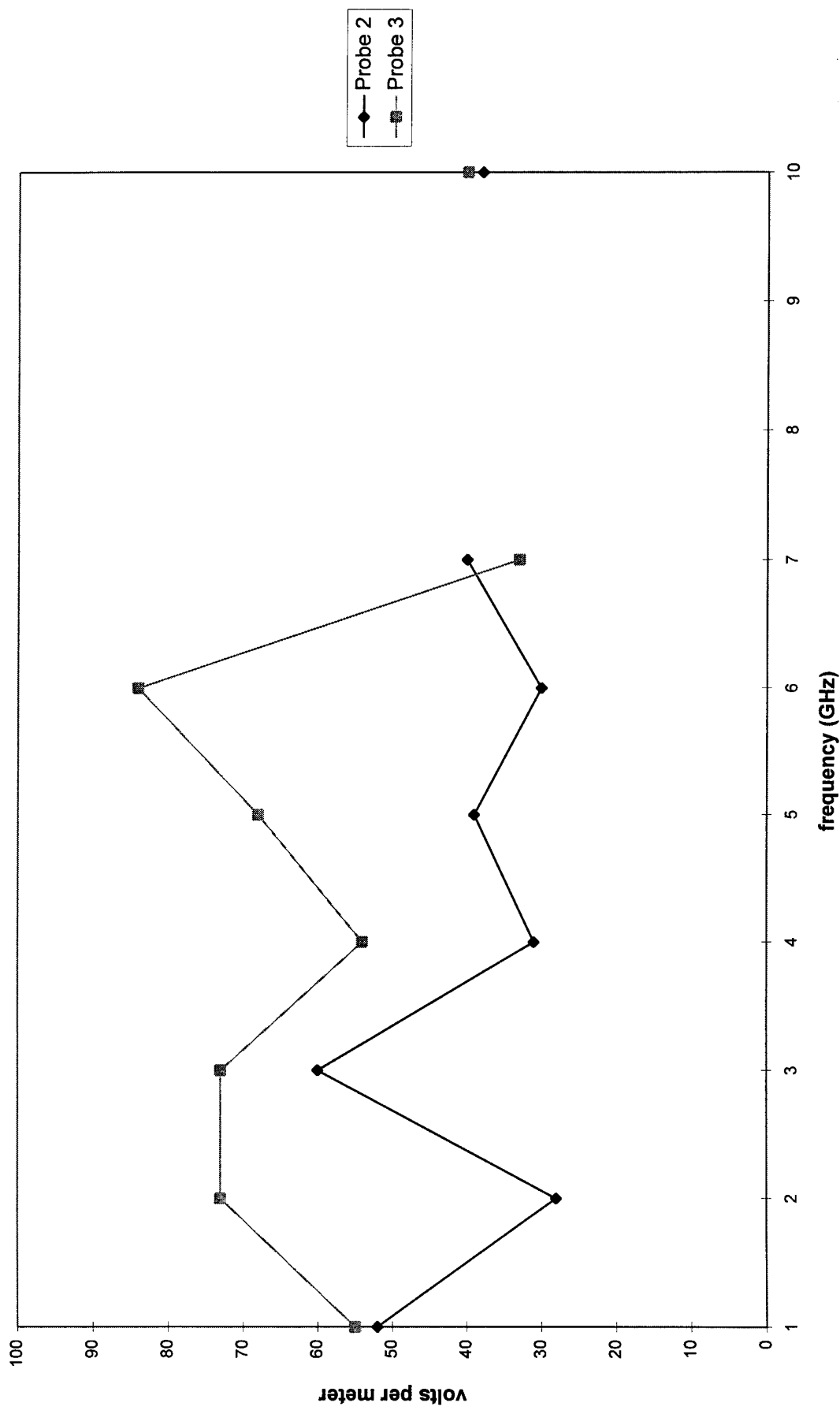
Average Field Levels Without Mode-Stirring - Probes 5-8

Average Field Levels With Mode-Stirring - Probes 5-8

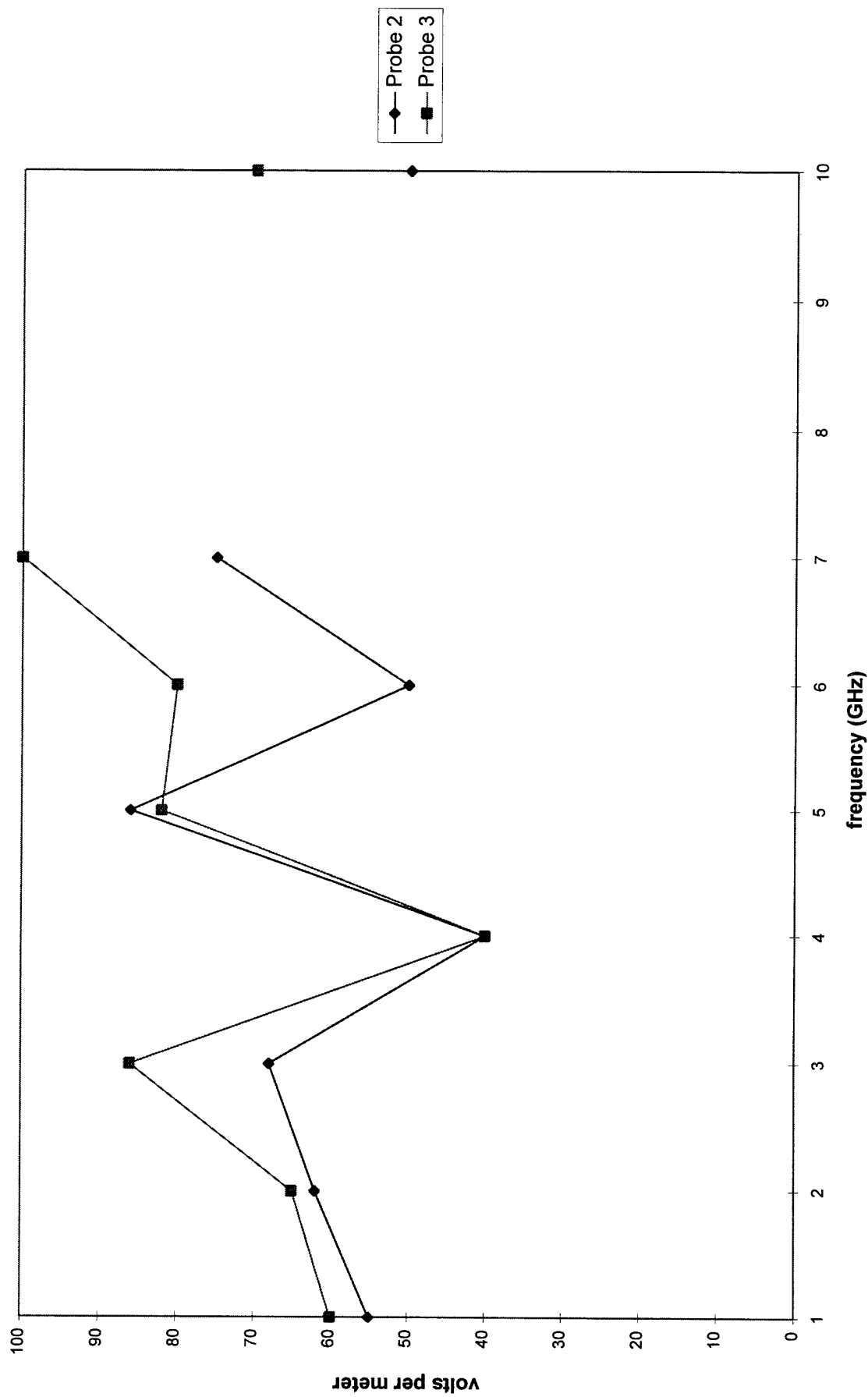
Comparison of 3 Transmit Antenna Positions - Without Mode-Stirring - Probe 2

Comparison of 3 Transmit Antenna Positions - Without Mode-Stirring - Probe 3

Transmit Antenna at 45 Degrees - Without Mode-Stirring - Probes 2 and 3



Transmit Antenna at 45 Degrees - With Mode-Stirring - Probes 2 and 3



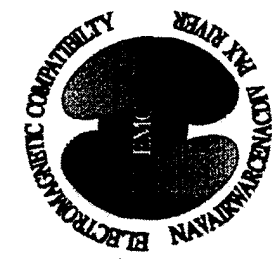


REVERBERATION CHAMBER AND ANECHOIC CHAMBER
OPERATORS GROUP MEETING, 5 - 7 DEC 1995



SUMMARY

- Field levels at individual equipment in an aircraft during standard EMV testing are extremely uncertain
- Significant improvements in field distribution and uniformity when mode-stirring was used
- Even greater field uniformity would be obtained if the aircraft was inside a MSC
- P-3 cable coupling data indicated improved field distribution when mode-stirring was used

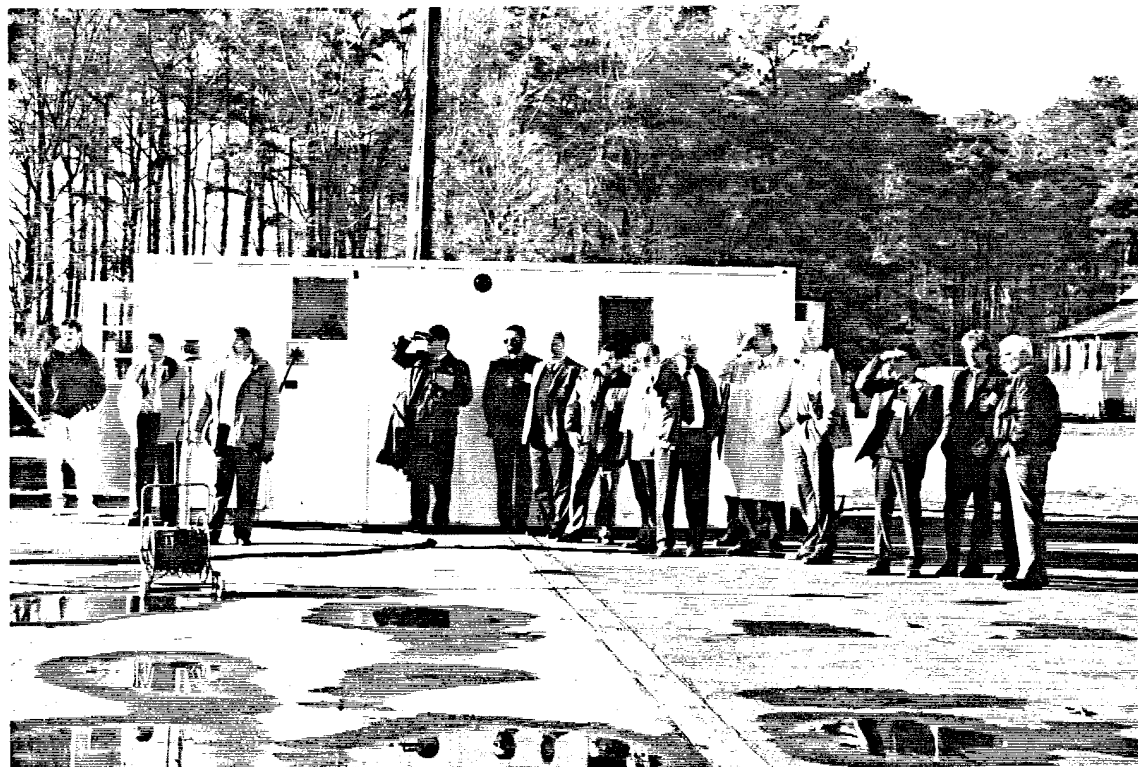


REVERBERATION CHAMBER AND ANECHOIC CHAMBER
OPERATORS GROUP MEETING, 5 - 7 DEC 1995

CONCLUSIONS

- Using standard EMV method, many transmit antenna aspect angles necessary to insure finding all susceptibilities
- Mode-stirring would save time and provide a more thorough test
- Mode-stirring would more accurately simulate real world which is not a static situation
- MSC's should be used for EMV testing of aircraft







NAVAL SEA SYSTEMS COMMAND

NSWC

Naval Surface Warfare Center

DAHLGREN DIVISION



**MR. D. MARK JOHNSON
COMPUTER SCIENCES CORP**



**RF COUPLING MEASUREMENTS ON
PASSENGER AIRCRAFT AVIONICS
EXPOSED TO CAVITY-MODE EXCITATION**

D.M. Johnson
Computer Sciences Corporation
King George, VA 22485

M.O. Hatfield
Naval Surface Warfare Center
Dahlgren, VA 22448

G.J. Freyer
Universal Systems, Inc.
Monument, CO 80132

ABSTRACT

typically instrumented will be presented.

The performance of avionics installed in aircraft which fly through high-intensity electromagnetic environments is an increasingly important issue. The Naval Surface Warfare Center, Dahlgren Division (NSWCDD), in conjunction with the Air Force Phillips Laboratory, has completed the second phase of testing of the electromagnetic reverberation characteristics of a transport aircraft. A part of this testing was the measurement of the radio-frequency (RF) coupling of selected avionics boxes of a decommissioned Boeing 707 aircraft and a simulated avionics box when exposed to cavity-mode excitation. The aircraft avionics boxes were instrumented to measure the RF energy coupling to: 1) an interior component lead and 2) an interior wire leading to the aircraft wiring harness connector plug. The simulated box was instrumented to measure RF coupling to an interior component lead. Tests were conducted on a 707 at Davis Monthan Air Force Base in Tucson, AZ; the tests included excitation of the aircraft within the avionics bay, cockpit and passenger cabin, utilizing mode-stirring techniques. Follow-on tests were and continue to be performed in the Mode-Stirred Chamber (MSC) at the NSWCDD. The aircraft and MSC tests are intended to demonstrate that the RF coupling characteristics of the actual and simulated avionics boxes measured within the MSC constitutes a valid description of the RF coupling characteristics of the same boxes when installed in the aircraft. Test data obtained during testing on the aircraft and in the NSWCDD MSC will be presented. Photographs showing the details of how each box was

1. INTRODUCTION

Mode-stirred chamber (MSC) testing has been suggested as a cost-effective means of obtaining a valid description of the RF coupling characteristics of avionics installed in aircraft which fly through high-intensity electromagnetic environments (EMEs). To demonstrate the applicability of MSC testing, reverberation tests have been performed by Naval Surface Warfare Center, Dahlgren Division (NSWCDD), in conjunction with the Air Force Phillips Laboratory on a decommissioned Boeing 707 aircraft. These tests included RF coupling measurements on selected avionics boxes and a simulated avionics box, when the cockpit, avionics bay and passenger cabin were excited with RF signals and mode-stirring techniques were used. Follow-on tests with these boxes have and continue to be performed at the NSWCDD MSC.

This paper will describe the basic approach used to obtain the data, and present typical data from the aircraft and MSC tests. Data will be presented as received power (dBm) and as coupling transfer function (dBcm²). Received power is the power measured on the points instrumented within the aircraft and simulated avionics boxes (corrected for cable losses) when RF was transmitted into the cavity where the boxes were contained. The RF coupling transfer function is determined by calculating the ratio of received power in mW to power density (mW/cm²) present in the cavity containing the avionics box of interest, measured by an in-band receive antenna.

2. TEST APPROACH

Five boxes from the cockpit instrument panel and avionics bay were extracted for instrumentation prior to testing. For the purposes of this paper, data for the autopilot system amplifier and computer (AP) will be presented. Where relevant, brief comparisons will be made to data obtained on one other avionics box, the radio altimeter indicator (RA).

Two points within each avionics box were selected for monitoring. For the AP, the monitoring points were such that RF coupling to the following could be measured:

- an interior wire leading to the aircraft wiring harness connector plug (channel 1)
- an interior component lead (channel 2)

Figures 1, 2 and 3 show instrumentation implementation for the AP.

Aircraft and MSC data were collected by performing the following:

- RF from 100 MHz to 6 GHz transmitted into an aircraft cavity containing the aircraft box and/or simulated avionics box, or into the MSC
- mechanical mode-stirring was accomplished by rotating a paddle wheel tuner in the test cavity
- RF signals measured with:
 1. an in-band receive antenna
 2. each channel of the instrumented aircraft boxes or simulated avionics box
- all received power data normalized to 0 dBm input and corrected for cable and connector losses

3. AIRCRAFT TEST RESULTS

Figure 4 shows received power

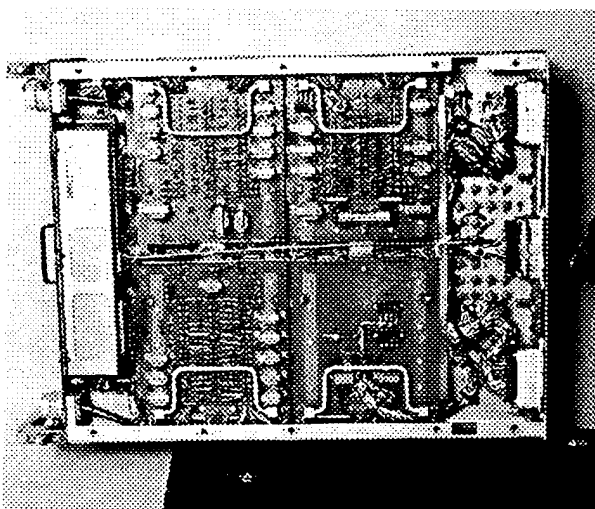


Figure 1. Instrumentation used in AP to monitor point in contact with wiring harness connector plug

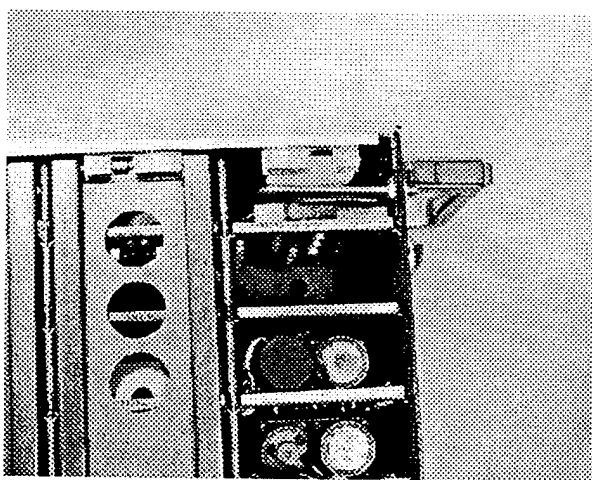


Figure 2. Instrumentation used in AP to monitor circuit component lead

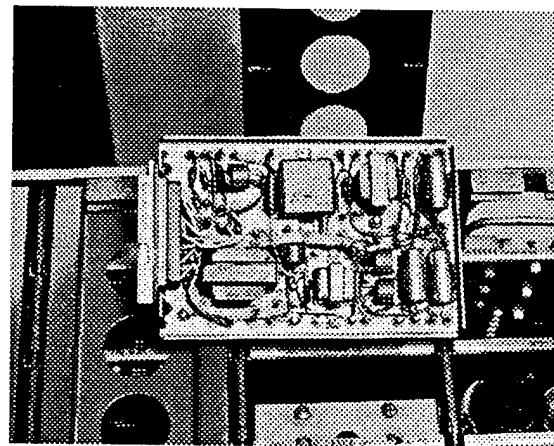


Figure 3. AP circuit card containing components to which an instrumenting probe could be attached

data for channels 1 and 2 of the AP; this is representative of typical measurements made on aircraft avionics when RF was transmitted in the aircraft cavity containing the avionics box of interest.

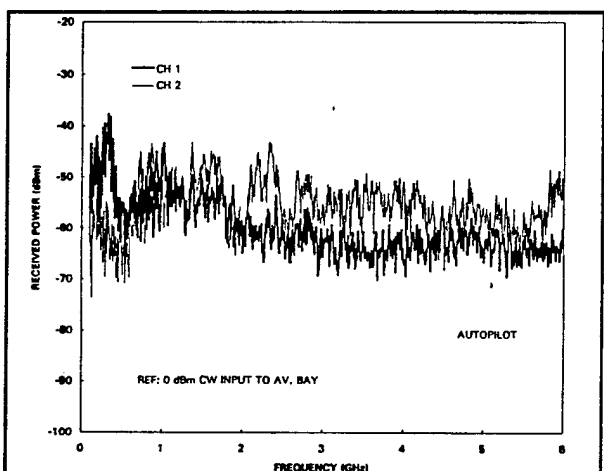


Figure 4. AP ch1 and ch2 response when RF energy was transmitted in avionics bay

Figure 5 shows the power received by an in-band receive antenna positioned in the avionics bay when RF was transmitted into the avionics bay.

The coupling transfer function of the instrumented channels of the aircraft avionics boxes is what is desired to be obtained in these experiments. Received power values are related mathematically to the coupling transfer function by the expression:

$$P_{rec} = PD * \sigma_{rec}$$

where: P_{rec} is the received power in mW

PD is the cavity power density in mW/cm^2

σ is the coupling transfer function, in cm^2 , of the receiver

The transfer functions of the instrumented channels are not known analytically, but can be obtained empirically when the power density inside the cavity of interest is known. The analytic coupling transfer

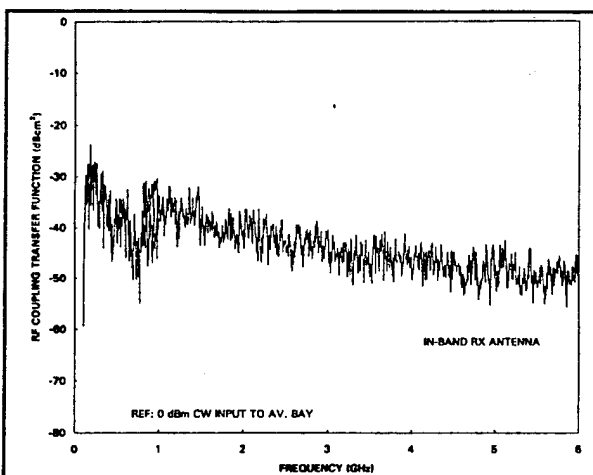


Figure 5. Response of in-band receive antenna when RF energy was transmitted in avionics bay

function of the in-band receive antenna is known, and is equivalent to the effective cross-sectional area of the antenna, discussed in reference 1. The expression for the effective cross-sectional area can be algebraically manipulated to yield an expression for the power density in the cavity of interest:

$$PD = \frac{8 * \pi * P_{rec}}{\lambda^2}$$

where: PD is the cavity power density in mW/cm^2

P_{rec} is the received power in mW

λ is the wavelength in cm of the frequency being transmitted into the cavity

For each instrumented channel of a given aircraft avionics box, such as the AP, the expressions for these coupling transfer functions are unknown in the analytical sense. The coupling transfer functions can be determined empirically using:

- the power density calculated from the in-band antenna received power
- the received power measured on the AP channel of interest

The calculation for the coupling transfer function of each instrumented AP channel is expressed as:

$$CPLG(dB) = 10 \cdot \log \left(\frac{P_{rec}}{PD} \right)$$

where: P_{rec} is the power received, in mW, by an instrumented channel in the avionics box of interest

PD is the power density, in mW/cm^2 , in the cavity containing the AP

Figure 6 shows the RF coupling transfer function of both AP channels, as computed from measurements made during the aircraft tests.

4. MSC RESULTS

Data has been obtained in the NSWCDD MSC for the following variations:

- AP, without wiring harness attached, resting on a dielectric block
- AP, with an unterminated 5-wire simulated wiring harness attached, resting on a dielectric block
- AP, without wiring harness attached, positioned on a ground plane grounded to the MSC floor
- AP, with an unterminated 5-wire simulated wiring harness attached, positioned on a ground plane grounded to the MSC floor

AP results are as follows:

- ch1 and ch2 received power without harness (representative plot), and in-band receive antenna response shown in Figures 7 and 8
- ch1 and ch2 received power with unterminated simulated harness attached (representative

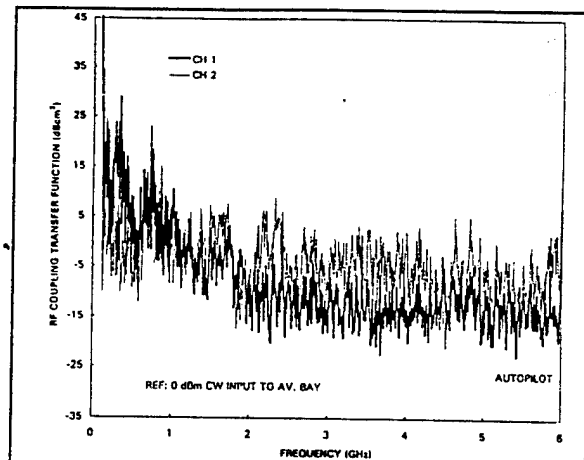


Figure 6. AP ch1 and ch2 coupling transfer function calculated from aircraft test data

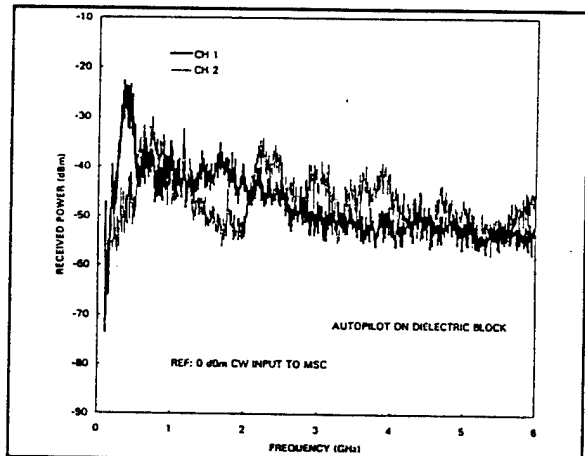


Figure 7. Ch1 and ch2 response of AP w/o harness positioned on dielectric block in MSC

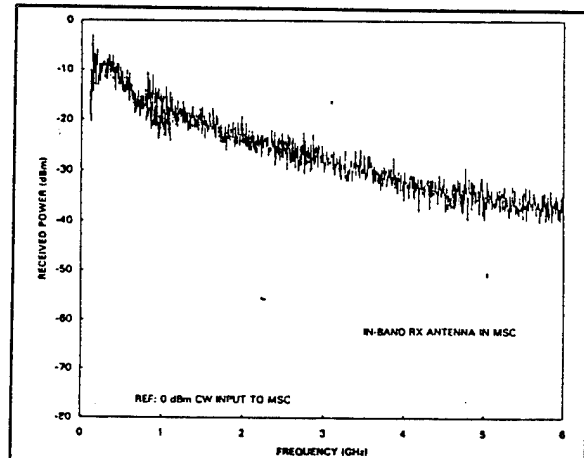


Figure 8. Response of in-band receive antenna in MSC

plot), shown in Figure 9

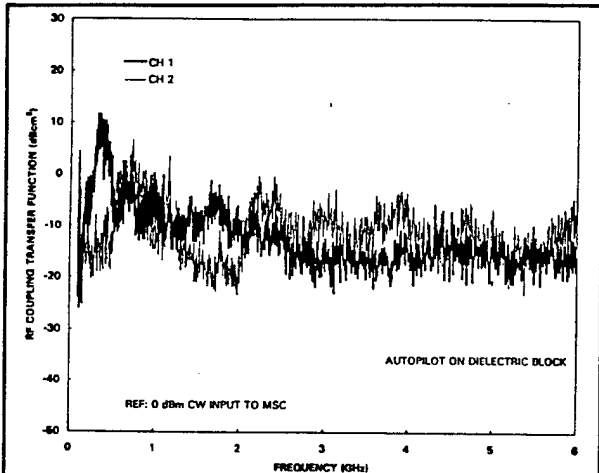


Figure 9. Ch1 and ch2 response of AP w/unterminated simulated wiring harness on dielectric block in MSC

ch1 and ch2 RF coupling transfer functions, AP without harness positioned on dielectric block, shown in Figures 10 and 11

ch1 and ch2 RF coupling transfer functions, AP with unterminated simulated harness on dielectric block, shown in Figures 12 and 13

ch1 and ch2 RF coupling transfer functions, AP without wiring harness on grounded ground plane, shown in Figures 14 and 15

ch1 and ch2 RF coupling transfer functions, AP with unterminated simulated wiring harness on grounded ground plane, shown in Figures 16 and 17

5. SUMMARY

By comparing the RF coupling transfer function of the AP's instrumented channels on the aircraft and in the MSC, the following can be concluded:

- above 2 GHz, the ch1 RF coupling transfer function measured in the

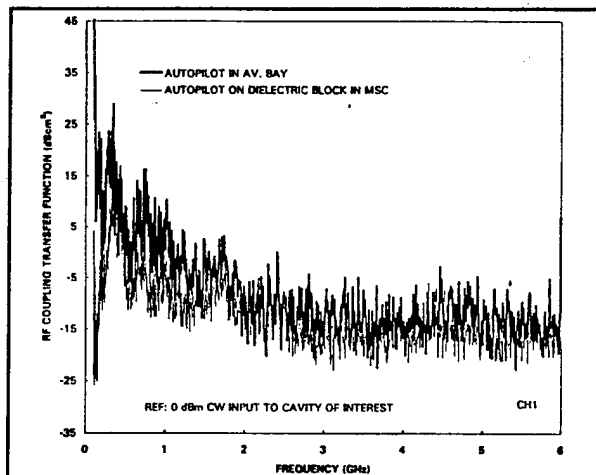


Figure 10. RF coupling transfer function of ch1 AP in avionics bay and AP w/o wiring harness positioned on dielectric block in MSC

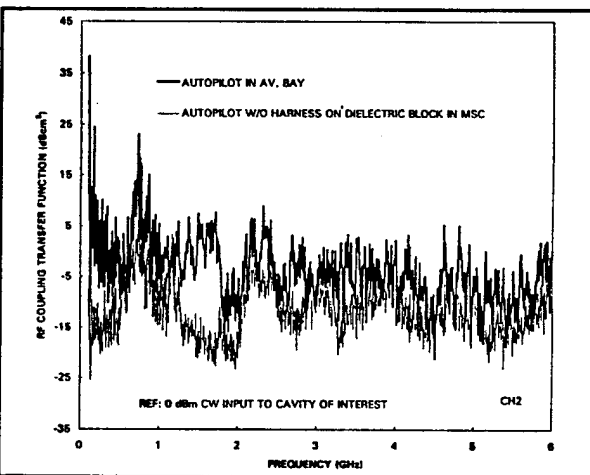


Figure 11. RF coupling transfer function of ch2 of AP in avionics bay and AP w/o wiring harness positioned on dielectric block in MSC

MSC without the wiring harness is an excellent representation of the ch1 RF coupling transfer function measured in the aircraft

when a 5-wire simulated wiring harness is attached, above 1 GHz, the ch1 RF coupling transfer function measured in the MSC is an excellent representation of the ch1 RF coupling transfer function measured on the aircraft above 1 GHz

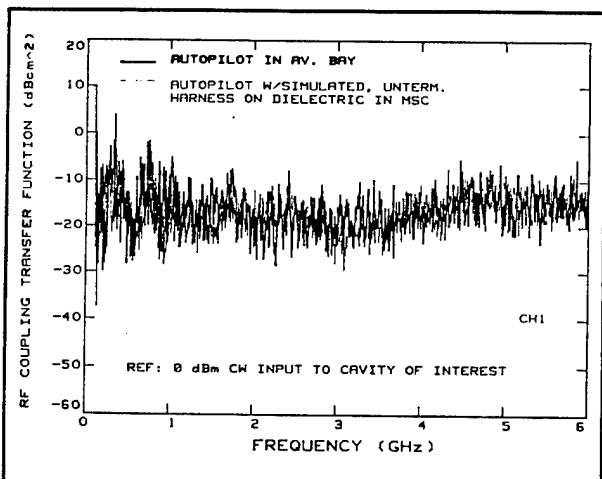


Figure 12. RF coupling transfer function of ch1 of AP in avionics bay and AP w/unterminated simulated wiring harness positioned on dielectric block in MSC

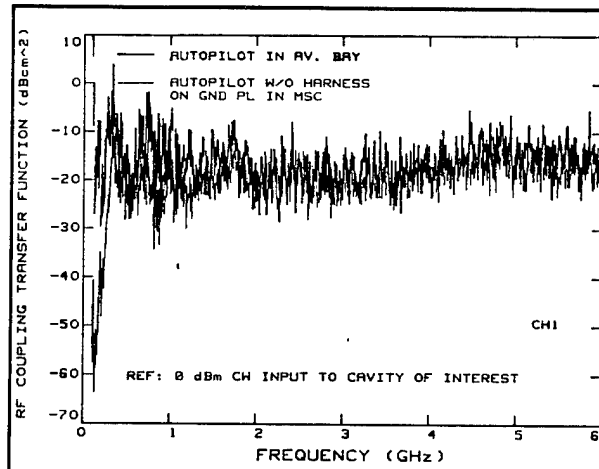


Figure 14. RF coupling transfer function of ch1 of AP in avionics bay and ap w/o wiring harness on grounded ground plane in MSC

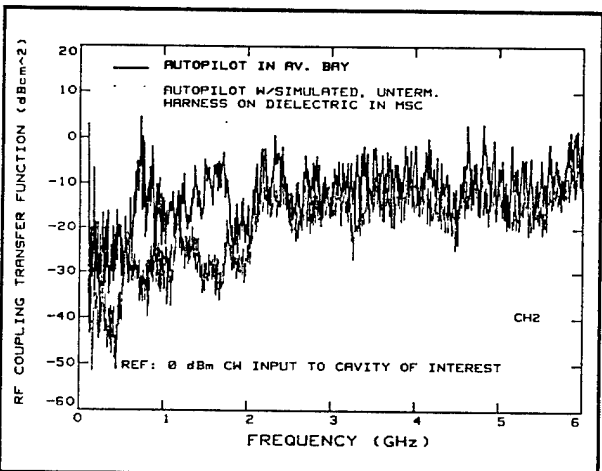


Figure 13. RF coupling transfer function of AP ch2 in avionics bay and AP w/unterminated simulated wiring harness positioned on dielectric block in MSC

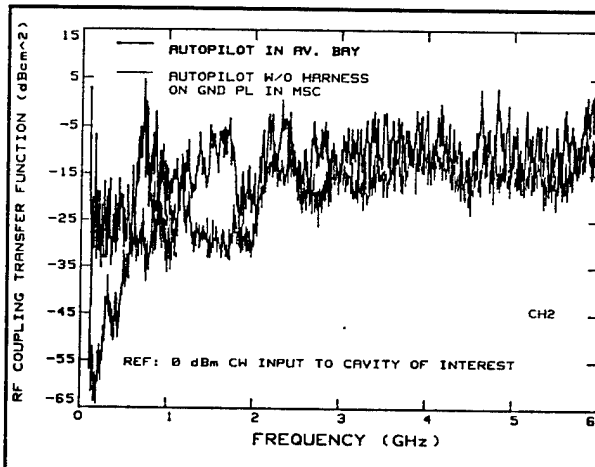


Figure 15. RF coupling transfer function of ch2 of AP in avionics bay and AP w/o wiring harness on grounded ground plane in MSC

above 3 GHz, the ch2 RF coupling transfer function measured in the MSC is a good representation of that measured in the aircraft when a 5-wire simulated harness is attached, above 2 GHz, the ch2 RF coupling transfer function of the AP on a dielectric block measured in the MSC is

an excellent representation of that measured in the aircraft

The effect of wiring harness on measured RF coupling transfer functions of the instrumented AP channels is somewhat different than the effect observed when the radar altimeter indicator (RA) was tested². Measurements of the RF coupling transfer functions of the RA's instrumented channels indicated the following:

the presence of wiring harness yielded the only significant change in the RF coupling transfer functions measured in the MSC

ch1 was influenced more by the presence of wiring harness than ch2

It should be noted that when measurements were made on the RA in the MSC, a section of the RA's associated wiring harness from the aircraft was used. Similar actual lengths of wiring harness from the aircraft were not available for measurements on the AP. It is expected that the RF coupling transfer functions measured on the instrumented channels of the AP in the MSC will more closely match the measurements made on the aircraft when tested with a length of associated wiring harness from the aircraft.

REFERENCES

1. M.L. Crawford and G.H. Koepke, Design, Evaluation, and Use of a Reverberation Chamber for Performing Electromagnetic Susceptibility/Vulnerability Measurements, NBS Technical Note 1092, April 1986.
2. D.M. Johnson, M.O. Hatfield, and G.J. Freyer, RF Coupling Measurements on Passenger Aircraft Avionics and Simulated Avionics Boxes Exposed to Cavity-Mode Excitation, presented at the 7th National Conference on High Power Microwave Technology, Monterey, CA, October 1994.

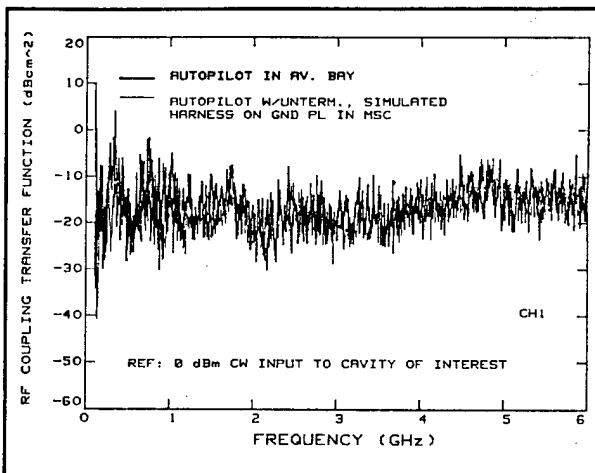


Figure 16. RF coupling transfer function of ch1 of AP in avionics bay and AP w/unterminated simulated harness on grounded ground plane in MSC

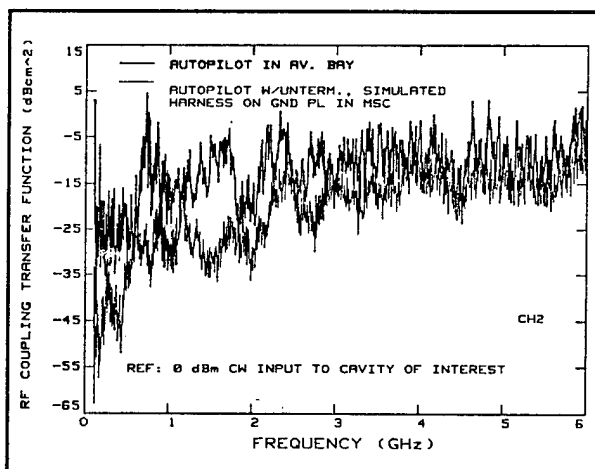


Figure 17. RF coupling transfer function of ch2 of AP in avionics bay and AP w/unterminated simulated wiring harness on grounded ground plane in MSC





MR. RICHARD LARA
U.S. ARMY RESEARCH LABORATORY



RADIATED EMISSIONS TESTS ON BIOMEDICAL TELEMETRY TRANSMITTER DEVICES

RICHARD S. LARA
U.S. ARMY RESEARCH LABORATORY
SURVIVABILITY/LETHALITY ANALYSIS DIRECTORATE
ELECTRONIC WARFARE DIVISION
WHITE SANDS MISSILE RANGE, NM 88002

This paper describes RF radiated emissions tests and power adjustment measurements on biomedical electrocardiogram telemetry transmitters to produce qualifying data and documentation sufficient to certify the devices to FCC Part 15, Paragraph 15.241 acceptance standards. These tests were performed at the U.S. Army electromagnetic analysis facility (EMAF). The facility is a branch of the U.S. Army Research Laboratory, Electronic Warfare Division, located in White Sands Missile Range, New Mexico. It houses four shielded anechoic chambers. The EMAF provides the U.S. Army, Navy, and Air Force with a facility to conduct MIL-STD-461/2 tests and special electromagnetic interference (SEMI), vulnerability assessments on weapon/communication-electronic (CE) systems. SEMI assessments is an out-of-band radio frequency countermeasure (RFCM) technique. This facility can perform electromagnetic interference (EMI) investigations from 100 MHz to 18 GHz, and can produce RF fields up to 200 V/m. The MIL-STD-461/2 test equipment frequency range is from 20 Hz through 40 GHz.

1. INTRODUCTION

1.1 General

The Electronic Warfare Division (EWD) was contracted by a biomedical device manufacturer to conduct a series of radio frequency (RF) radiated emissions tests on some electrocardiogram telemetry transmitters devices.

The objective of the test was to perform RF radiated emission tests and RF power output optimization on the biomedical electrocardiogram telemetry transmitters to produce qualifying data and documentation sufficient to certify the biomedical transmitters to FCC Part 15, Paragraph 15.241 acceptance standards.

FCC acceptance standards state that emissions from the device shall be confined within a 200-kHz band which shall lie wholly within the frequency range of 174 to 216 MHz. The field strength of any emissions radiated within the specified 200-kHz band shall not exceed

1500 microvolt/meter (63.5 dB μ V/m) at 3 meters. The field strength of emissions radiated on any frequency outside of the specified 200-kHz band shall not exceed 150 microvolt/meter (43.5 dB μ V/m) at 3 meters. Figures 1 and 2 are typical wave forms.

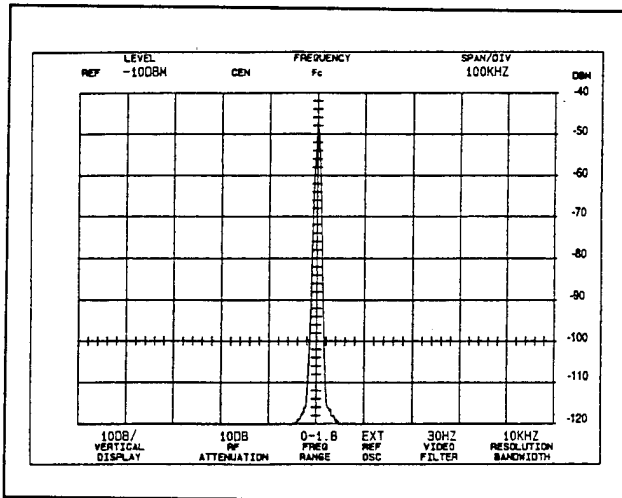


Figure 1. Typical signal of 100-kHz span/div.

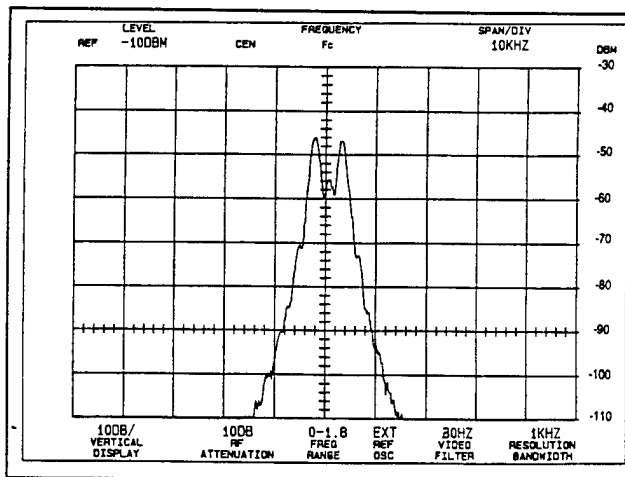


Figure 2. Typical signal at 10-kHz span/div.

1.2 Description of the Devices

The devices are biomedical electrocardiogram telemetry transmitters for in-house monitoring of cardiac patients not in the Intensive Care Unit.

The transmitter units operate in the UHF (ultra high frequency) band at frequencies ranging from 174 to 214 MHz. Leads from the units are attached to the chest area to monitor the patient's heart activity. These leads also become the transmitter antenna elements determining the radiation pattern of the device. A crystal in the unit determines the carrier frequency of each transmitter.

The telemetry devices can be used in a "step-down" unit which are both lower cost and psychologically beneficial to the patient. After a few routine days in the step-down unit, the patient is ready to return home.

1.3 Facility Description

The Electromagnetic Analysis Facility (EMAF), a major U.S. Army Research Laboratory (ARL) facility, was established to perform special electromagnetic interference (SEMI) investigations of selected weapon systems and other communication electronic (CE) equipment, e.g., night vision devices, surveillance systems, laser range finders, etc., to determine whether they are susceptible and/or vulnerable to radio frequency countermeasures (RFCM) in the radio frequency (RF) spectrum from 100 MHz to 18 GHz.

The EMAF consists of four shielded anechoic chambers and the equipment required to perform SEMI investigations. An Antenna Pattern Measurement System (APMS), a Radar Cross Section (RCS) measurement system, and the equipment required to perform MIL-STD-461 susceptibility and radiated emission tests are available. All of these systems and equipment are operated inside shielded enclosures to minimize the possibility of unauthorized signal intercept. The shielded enclosures also isolate the measurements from outside interference sources.

The large chamber nominal reflectivity levels in the quiet zone for various system under test (SUT)-to-antenna separations are shown in Table 1.

The absorber material in the large anechoic chamber is Advanced Electromagnetic (AEMI) type AEP-48. It is capable of dissipating an average power density of 0.5W/in² (77.5 mW/cm² or 540 V/m).

Table 1. Nominal Reflectivity Levels in the Quiet Zone

Frequency	Reflectivity (dB)		
	25 ft	60 ft	90 ft
200 MHz	-32 dB	-13 dB	-10 dB
500 MHz	-54 dB	-23 dB	-18 dB
2000 MHz	<-60 dB	-42 dB	-32 dB
5000 MHz	<-60 dB	-53 dB	-38 dB
8000 MHz	<-60 dB	<-60 dB	-45 dB
10000 MHz	<-60 dB	-58 dB	-49 dB

2.0 DISCUSSION

2.1 Methodology

The biomedical telemetry transmitting device was attached to a subject and activated with the subject assuming both a supine and standing position. The total $|E|$ field (in dB μ V/m) was computed at each of the frequencies of interest in the following manner.

The RF radiated emissions from the device was monitored on an Electro-Metrics Computer Controlled RFI/EMC Receiver Analyzer System model CCS-750. The following steps were taken to calculate the field strengths from these devices. Reference Table 2, the receiver was tuned for maximum signal level and the reading, in **column A**, in dB μ V was recorded. This received signal level was then corrected for cable loss, **column C**, using the cable-loss-versus-frequency table generated at this facility prior to the conduct of these measurements. The radiated $|E|$ field at a given distance was computed by adding the antenna correction factor, **column B**, for a specific frequency. The antenna correction factor was derived mathematically using the frequency and gain of the receive antenna.

With the device operating at center frequency (F_c) MHz, the tuned dipole antenna at vertical polarization and with the subject in a supine position, the measured received signal was 29 dB μ V. The antenna correction factor for this frequency was 13.6 dB, and the cable loss was 1 dB. Thus, the radiated $|E|$ field is computed to be:

$$\begin{aligned}
 |E| &= A + B + C \text{ dB}\mu\text{V} \\
 &= 29 + 13.6 + 1 \text{ dB}\mu\text{V} \\
 &= 43.6 \text{ dB}\mu\text{V}
 \end{aligned}$$

2.2 Test Setup and Procedures

The radiated emissions test and RF power optimization of the biomedical telemetry transmitters were accomplished in the EMAF's large anechoic chamber.

The azimuth positioner with a 10-ft diameter, wooden turntable was placed along the centerline of the chamber with its edge 10-ft from the tips of the absorber material of the target wall. The positioner turntable was covered with 10 in. of absorber material to minimize RF reflections. A styrofoam block was placed on top of the absorber for subject placement. The elevation-over-azimuth positioner is remotely controlled for an azimuth rotation of 0-460-degrees. The floor of the chamber is covered with 52 in. "walk-on" RF absorber material. The absorber material and the azimuth positioner turntable are at the same height, producing a smooth chamber floor surface.

A tuned dipole antenna was placed at 3, 10, and 23.45 meters from the centerpoint of the azimuth positioner along the centerline of the chamber. See Figure 1.

enclosure to prevent outside RF interference. Real-time data collection and data analysis were accomplished in this location.

Three antennas were used to produce the baseline data of the anechoic chamber:

- a. **Biconical** antenna for frequency range of 20 to 200 MHz
- b. **Conical log spiral** antenna for frequency range of 200 to 1000 MHz
- c. **RG 50 standard gain horn (SGH)** antenna for frequency range of 1 to 2.5 GHz

These antennas were placed 3 meters from the center of the azimuth positioner and 1.75 meters above the walk-on material. The frequency swept baseline measurements

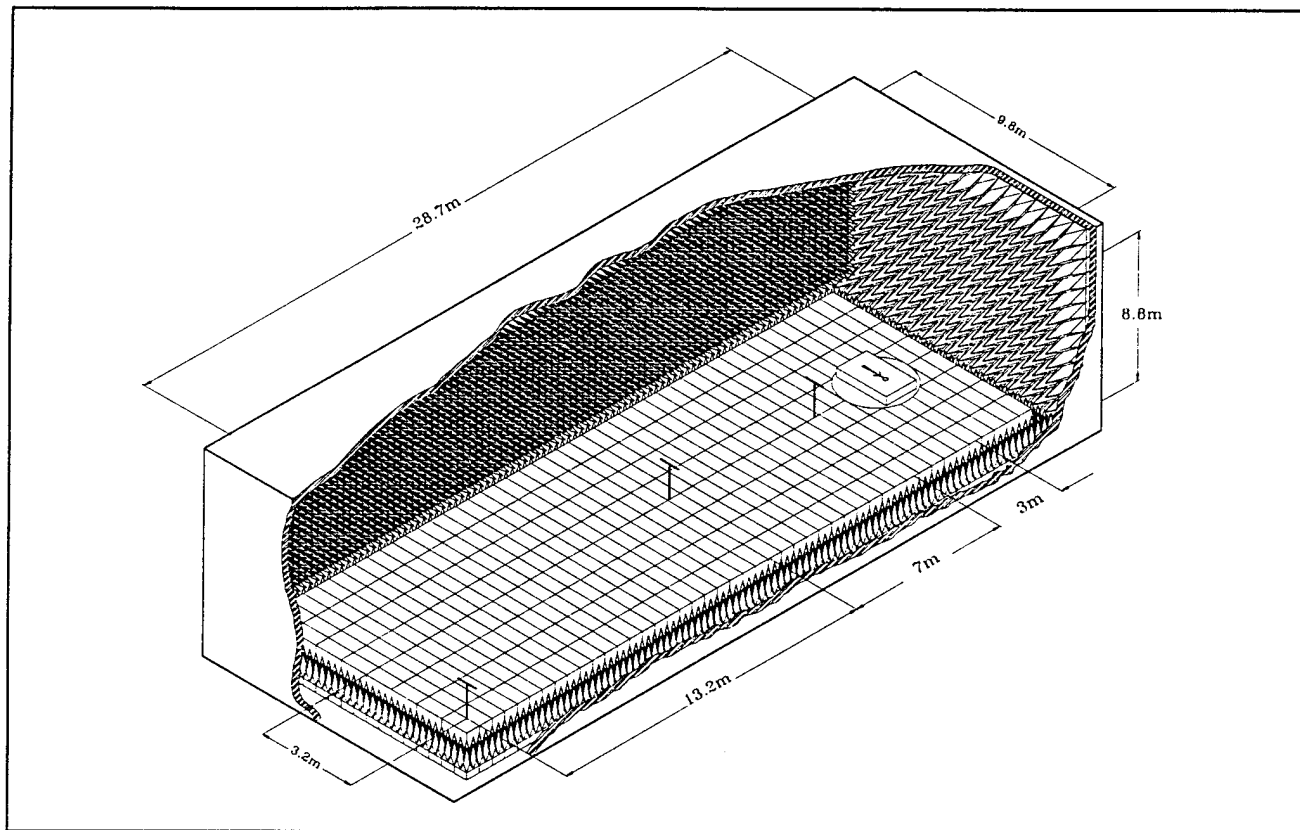


Figure 1. Anechoic chamber test setup.

The cable from the receiving dipole antenna was connected to the CCS-750 computer controlled RFI/EMC receiver analyzer system. The receiver analyzer system, the Tektronix model 494P spectrum analyzer, and other associated electronic equipment were located outside the large anechoic chamber. This area is in an RF-shielded

were performed for both horizontal and vertical polarizations. This baseline data represents the ambient noise level in the RF anechoic chamber in absence of RF emitters. Figures 4 through 8 represent the results of the chamber baseline for frequency ranges of 20 MHz through 2.5 GHz.

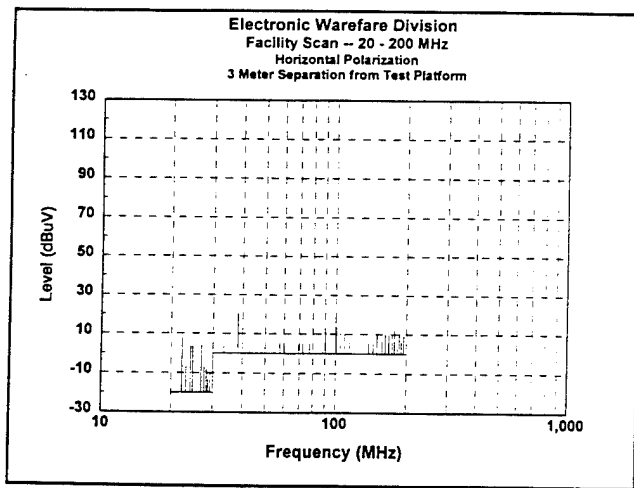


Figure 4. Ambient noise level in the 20 to 200 MHz range, horizontal polarization.

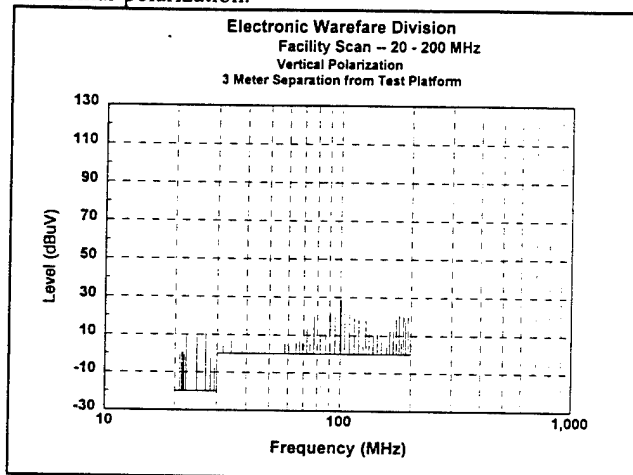


Figure 5. Ambient noise level in the 20 to 200 MHz RF range, vertical polarization.

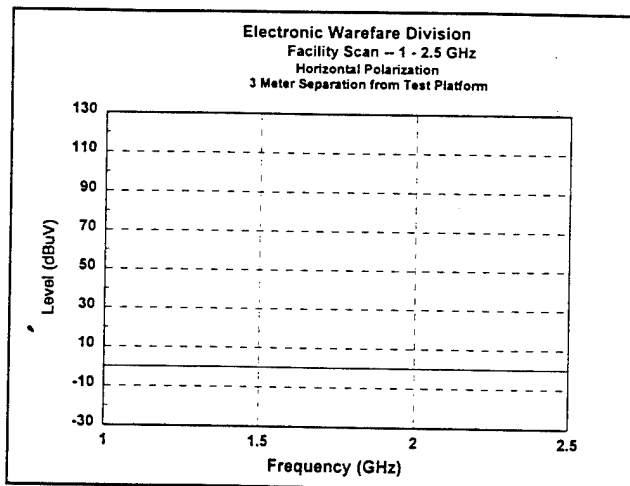


Figure 7. Ambient noise level in the 1 to 2.5 GHz RF range, horizontal polarization.

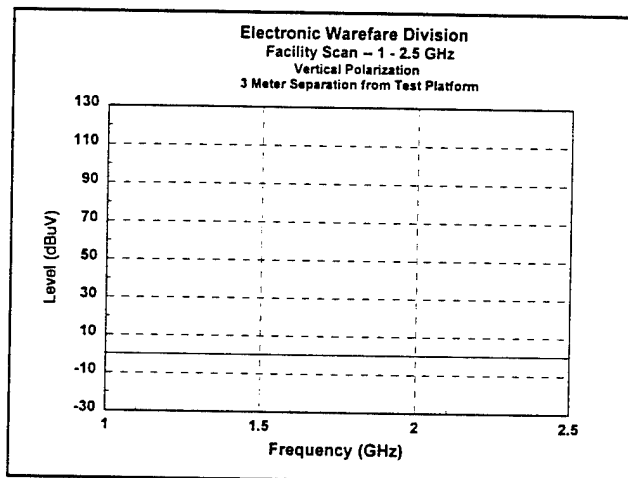


Figure 8. Ambient noise level in the 1 to 2.5 GHz RF range, vertical polarization.

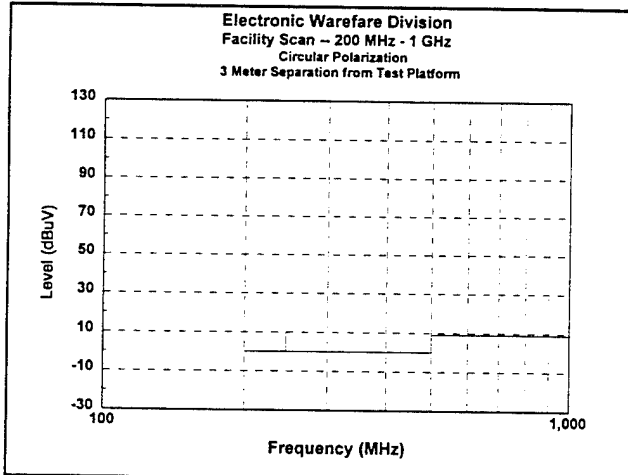


Figure 6. Ambient noise level in the 200 MHz to 1 GHz RF range, circular polarization.

2.2.1 SUT RF Signal Optimization

The telemetry transmitter output power tests were performed with the devices connected to the subject. The subject was placed on the large anechoic chamber's azimuth positioner in either a supine or standing position with the device over the centerpoint of the positioner (see Figure 2). SUT heights were measured to be 44 in. above the walk-on material for the supine position and 59 in. above the walk-on material for the standing position. The same subject was used for all tests. A tuned dipole was placed 3 meters from the device, and the height of the dipole was adjusted to the center line of the device. The antenna was configured for vertical polarization. The positioner was rotated in azimuth to determine the optimum aspect angle for maximum signal received by the dipole. This optimum azimuth angle was found to be 139°. The height of the dipole was then adjusted in increments of approximately 25 cm up to

4 meters above the device centerline. The received signal was recorded for each configuration. The maximum received signal was observed at the dipole height of 68 in. above the walk-on material. Table 2

shows the result of this optimization procedure. A similar method was used for the dipole in horizontal polarization. Table 3 displays the results of this signal optimization procedure.

Table 2. Optimization procedure, vertical polarization.

Test Requirement: FCC Part 15
Antenna:

Test Frequencies: 174–216 MHz
Type: Dipole

Separation Distance: 3 meters
Model: Stoddart 91870-2

Angle of Max Emissions (degrees)	Antenna Height (inches)	Polarization Vert/Hor	Max Emission Measured (dB μ V)	Antenna Factor (dB)	Cable Loss (dB)	Corrected Level (dB μ V/m)	Limit (dB μ V/m)	Deviation from Limit (dB μ V/m)	Subject Position
			A	B	C	A+B+C			
0	44	Vertical	29	13.6	1	43.6	63.5	-19.9	Supine
139	54	Vertical	36	13.6	1	50.6	63.5	-12.9	Supine
139	64	Vertical	36	13.6	1	50.6	63.5	-12.9	Supine
139	68	Vertical	36	13.6	1	50.6	63.5	-12.9	Supine
139	74	Vertical	36	13.6	1	50.6	63.5	-12.9	Supine
139	84	Vertical	35	13.6	1	49.6	63.5	-13.9	Supine
139	94	Vertical	35	13.6	1	49.6	63.5	-13.9	Supine
139	104	Vertical	33	13.6	1	47.6	63.5	-15.9	Supine
139	114	Vertical	33	13.6	1	47.6	63.5	-15.9	Supine
139	124	Vertical	33	13.6	1	47.6	63.5	-15.9	Supine
139	134	Vertical	28	13.6	1	42.6	63.5	-20.9	Supine
139	144	Vertical	26	13.6	1	40.6	63.5	-22.9	Supine
139	154	Vertical	24	13.6	1	38.6	63.5	-24.9	Supine

Table 3. Optimization procedure, horizontal polarization.

Test Requirement: FCC Part 15
Antenna:

Test Frequencies: 174–216 MHz
Type: Dipole

Separation Distance: 3 Meters
Model: Stoddart 91870-2

Angle of Max Emissions (degrees)	Antenna Height (inches)	Polarization Ver/Hor	Max Emission Measured (dB μ V)	Antenna Factor (dB)	Cable Loss (dB)	Corrected Level (dB μ V/m)	Limit (dB μ V/m)	Deviation from Limit (dB μ V/m)	Subject Position
			A	B	C	A+B+C			
139	155	Horiz	22	13.6	1	36.6	63.5	-26.9	Supine
139	145	Horiz	20	13.6	1	34.6	63.5	-28.9	Supine
139	135	Horiz	16	13.6	1	30.6	63.5	-32.9	Supine
139	125	Horiz	20	13.6	1	34.6	63.5	-28.9	Supine
139	115	Horiz	10	13.6	1	24.6	63.5	-38.9	Supine
139	105	Horiz	12	13.6	1	26.6	63.5	-36.9	Supine
139	95	Horiz	18	13.6	1	32.6	63.5	-30.9	Supine
139	85	Horiz	23	13.6	1	37.6	63.5	-25.9	Supine
139	75	Horiz	18	13.6	1	32.6	63.5	-30.9	Supine
139	65	Horiz	22	13.6	1	36.6	63.5	-26.9	Supine
139	59	Horiz	26	13.6	1	40.6	63.5	-22.9	Supine
139	42	Horiz	25	13.6	1	39.6	63.5	-23.9	Supine

The subject with the telemetry device still attached was then placed in a standing position. The tuned dipole was positioned 3 meters from the device, and the procedure outlined earlier was pursued to determine the most sensitive parameters for maximum signal. The dipole height of 59 inches and the azimuth angle of 145° produced the maximum signal for the

horizontal polarization. For vertical polarization, the optimum parameters for the device were; dipole height of 68 in. and 0 degree aspect angle. Table 4 shows the results of this effort.

Table 4. Optimum parameter for maximum signal.

Test Requirement: FCC Part 15
Antenna: Test Frequencies: 174-216 MHz
Type: Dipole Separation Distance: 3 Meters
'Model: Stoddart 91870-2

Angle of Max Emissions (degrees)	Antenna Height (inches)	Polarization Vert/Hor	Max Emission Measured (dB μ V)	Antenna Factor (dB)	Cable Loss (dB)	Corrected Level (dB μ V/m)	Limit (dB μ V/m)	Deviation from Limit (dB μ V/m)	Subject Position
			A	B	C	A+B+C			
0	59	Horiz	25	13.6	1	39.6	63.5	-23.9	Standing
145	59	Horiz	31	13.6	1	45.6	63.5	-17.9	Standing
0	68	Vertical	39	13.6	1	53.6	63.5	-9.9	Standing

The received signal level measurements were performed in compliance with FCC Part 15, with the tuned dipole at the 10 meters separation distance. The most sensitive parameters associated with the two configurations were

obtained using the procedures established earlier and the results are listed in Table 4. This table also lists the results of the measurements performed at the separation distance of 23.45 m.

Table 5. Received signal measurements.

Test Requirement: FCC Part 15.31
Antenna: Test Frequencies: 174-216 MHz
Type: Dipole Separation Distance: 10 Meters
Model: Stoddart 91870-2

Angle of Max Emissions (degrees)	Antenna Height (inches)	Polarization Vert/Hor	Max Emission Measured (dB μ V)	Antenna Factor (dB)	Cable Loss (dB)	Corrected Level (dB μ V/m)	Limit (dB μ V/m)	Deviation from Limit (dB μ V/m)	Subject Position
			A	B	C	A+B+C			
0	46	Vertical	12	13.6	0.8	26.4	53.042	-26.642	Supine
120	46	Vertical	29	13.6	0.8	43.4	53.042	-9.642	Supine
0	122	Vertical	22	13.6	0.8	36.4	53.042	-16.642	Standing
0	135	Horiz	19	13.6	0.8	33.4	53.042	-19.642	Standing
140	135	Horiz	25	13.6	0.8	39.4	53.042	-13.642	Standing
0	156	Horiz	15	13.6	0.8	29.4	53.042	-23.642	Standing
60	156	Horiz	25	13.6	0.8	39.4	53.042	-13.642	Standing
The following tested at 23.45 meters									
0	156	Horiz	15	13.6	0.8	29.4	45.4	-16	Standing
160	156	Horiz	24	13.6	0.8	38.4	45.4	-7	Standing
0	84	Vertical	-3	13.6	0.8	11.4	45.4	-34	Supine
120	84	Vertical	-3	13.6	0.8	11.4	45.4	-34	Supine

2.3 Power Adjustment Measurements

The purpose of the power adjustment measurements was to optimize the devices' RF transmit output power while not exceeding the field strength level of 63.5 dB μ V/m (1500 μ V/m). These measurements were performed with the tuned dipole antenna at a separation distance (SUT to receive antenna) of 3 meters. The receiving antenna height of 68 in. for vertical polarization and an antenna height of 59 in. for horizontal polarization. The subject was in a standing position.

Using the maximum signal receive parameters such as aspect angle, transmitter height, and receive antenna polarization, the power was adjusted on the transmitter devices. The following is a typical method used for these measurements. With the receive dipole

antenna set for vertical polarization and the telemetry transmitter at an azimuth angle of 280°, the transmitter gain was adjusted until a level of 47 dB μ V was recorded at the receiver (Table 6, column A). This level is equivalent to 61.6 dB μ V/m after antenna correction factor (ACF), and cable loss have been taken into consideration.

With the dipole antenna at horizontal polarization and the telemetry transmitter at an azimuth angle of 145°, the transmitter gain was measured to be 44 dB μ V. This level is equivalent to 58.6 dB μ V/m. Note Table 6. This output level was well within the specification of 63.5 dB μ V/m.

The remaining transmitters RF output levels were adjusted using the same procedure.

Table 6. Transmitter power adjustment measurements for the telemetry transmitter.

Test Requirement: FCC Part 15 Test Frequencies: 174-216 MHz Separation Distance: 3 Meters
Antenna: Type: Dipole Model: Stoddart 91870-2

Angle of Max Emissions (degrees)	Antenna Height (inches)	Polarization Vert/Hor	Max Emission Measured (dB μ V)	Antenna Factor (dB)	Cable Loss (dB)	Corrected Level (dB μ V/m)	Limit (dB μ V/m)	Deviation from Limit (dB μ V/m)	Subject Position
			A	B	C	A+B+C			
0	68	Vertical	24	13.6	1	38.6	63.5	-24.9	Standing
280	68	Vertical	32	13.6	1	46.6	63.5	-16.9	Standing
280	68	Vertical	34	13.6	1	48.6	63.5	-14.9	Standing
280	68	Vertical	45	13.6	1	59.6	63.5	-3.9	Standing
280	68	Vertical	47	13.6	1	61.6	63.5	-1.9	Standing
145	59	Horiz	44	13.6	1	58.6	63.5	-4.9	Standing

3.0 SUMMARY AND CONCLUSIONS

A test plan was created to satisfy certain test acceptance criteria for testing the biomedical devices. This plan was implemented and proved effective in fulfilling the FCC Part 15 acceptance test standards. The devices were optimized for maximum RF power output satisfying the technical regulation. We also determine that a motorized antenna positioning fixture for the receive antenna would have reduced some man hours of testing. The EMAF has set in motion efforts to develop specialized instrumentation and techniques for future FCC acceptance standard testing.

The following are the measurements produced using the procedures summarized in this paper.

a) The telemetry transmitters were optimized and were within the field-strength level of 63.5 dB μ V/m (1500 μ V/m) at 3-meters separation distance as specified by FCC Part 15.241.

b) The results obtained at 10 meters also satisfied the field-strength levels using extrapolation techniques specified under FCC Part 15.31.

With the DOD downsizing, the EMAF has become a dual effort facility servicing both industry and Government agencies. The EMAF's primary effort is to perform its assigned mission, then to conduct any other tasks as time permits.





**DR. MAQSOOD MOHD
SVERDRUP TECHNOLOGY**



EMI: A SILENT THREAT TO THE COMBAT CASUALTY CARE MEDICAL ELECTRONIC SYSTEMS

Dr. M.A. Mohd

**Office of the Chief Scientist, USAF Wright
Laboratory Armament Directorate
(Sverdrup Technology)
Eglin AFB, FL**

and

**Major C. L. Linden, Jr.
WRAIR, Division of Surgery
Washington, DC**

Abstract

- High Power Electromagnetic Systems are an Integral Part of Modern Battlefields, and Electromagnetic interference (EMI) is the byproduct of such systems
- This Paper Promotes the Awareness of the Severity of the EM Environment in the Modern Battlefield and Its Impact on Medical Electronics Performance

Abstract (Cont.)

- This Paper Concludes That the Use of High Technology to Minimize the Battlefield Delays and Maximize the Availability of the "Golden Hour" Would Become Ineffective Unless the High Technology Systems Are Designed for Electromagnetic Compatibility (EMC)

EMI: A Silent Threat

- **Upset - a Temporary System Failure During the EMI Event**
- **Burnout - Permanent Damage to the System Due to EMI**
- **Walking Wounded - a System Failure Not Easily Noticeable but Remains Latent Until It Occurs**

Life Threatening Examples in Medical Electronics Systems Due to EMI

- **Pacemakers Stop Functioning Properly During Ambulance Radio Operations**
- **Arrhythmia Monitors, Apnea, and Respiration Monitors Fail to Respond and Alarm Resulting in Fatalities**
- **Microsurgical Drill Runs When the Electrosurgical Unit Is Powered Up**
- **Cellular Phones Cause Malfunction in Incubators, Infusion Pumps, Dialysis Equipment, and Defibrillators**

Life Threatening Examples in Medical Electronics Systems Due to EMI (Cont.)

- Blood Pressure Monitors Malfunction When Paging Transmitter Was Turned On
- Oximeter Shows Healthy Conditions on a Dead Patient Due to Telemetry Transmitter Operation
- Too Many Artifacts on EKG Traces Due to Infusion Pump and Bed Motor Operations

:

:

What is EMC?

- **No Degradation of System Performance and no Effect on Any Other System in the Environment, i.e., the Ability of Systems to Work Together in the Environment**

What is EMI?

- **The Electrical Interference to Other Systems in an Environment, i.e., the Inability of Systems to Work Together in the Environment**

The Challenge of EMC in Combat Casualty Care Systems

- The Modern Battlefield EM Environment is More Dense and Severe, Than the Civilian Settings
- RF Emitters Present in the Combat Area Span a Board Spectrum Range
- The EM Energy Present is Both Impulsive and Continuous; Also, the Near and Farfields Could Be Present in the Environment

The Challenge of EMC in Combat Casualty Care Systems (Cont.)

- **With Limited Resources in a Battlefield the Grounding Scheme and Filtering Requirements Could Be Compromised Resulting in Conductive EMI**
- **To Satisfy Medical Electronics EMC in the Civilian Sector is Challenging Enough, but Satisfying EMC in Combat Casualty Care Medical Electronics Systems is Twice as Difficult**

The Challenge of EMC in Combat Casualty Care Systems (Cont.)

- Unless EMC is Implemented in the Combat Casualty Care Medical Electronics Systems, the Number and Severity of Life Threatening EMI Incidents in the Combat Zone Would be Significantly Higher Than in the Civilian Settings

The Challenge of EMC in Combat Casualty Care Systems (Cont.)

- As Medical Electronic Systems and Devices Continue to Proliferate and Share the Already Crowded Frequency Spectrum, the Burden of Awareness and Knowledge Falls on All Those Engaged in Design, Analysis, Evaluation, Manufacturing, Quality Assurance, and Other Fields Within the Engineering Community

The Challenge of EMC in Combat Casualty Care Systems (Cont.)

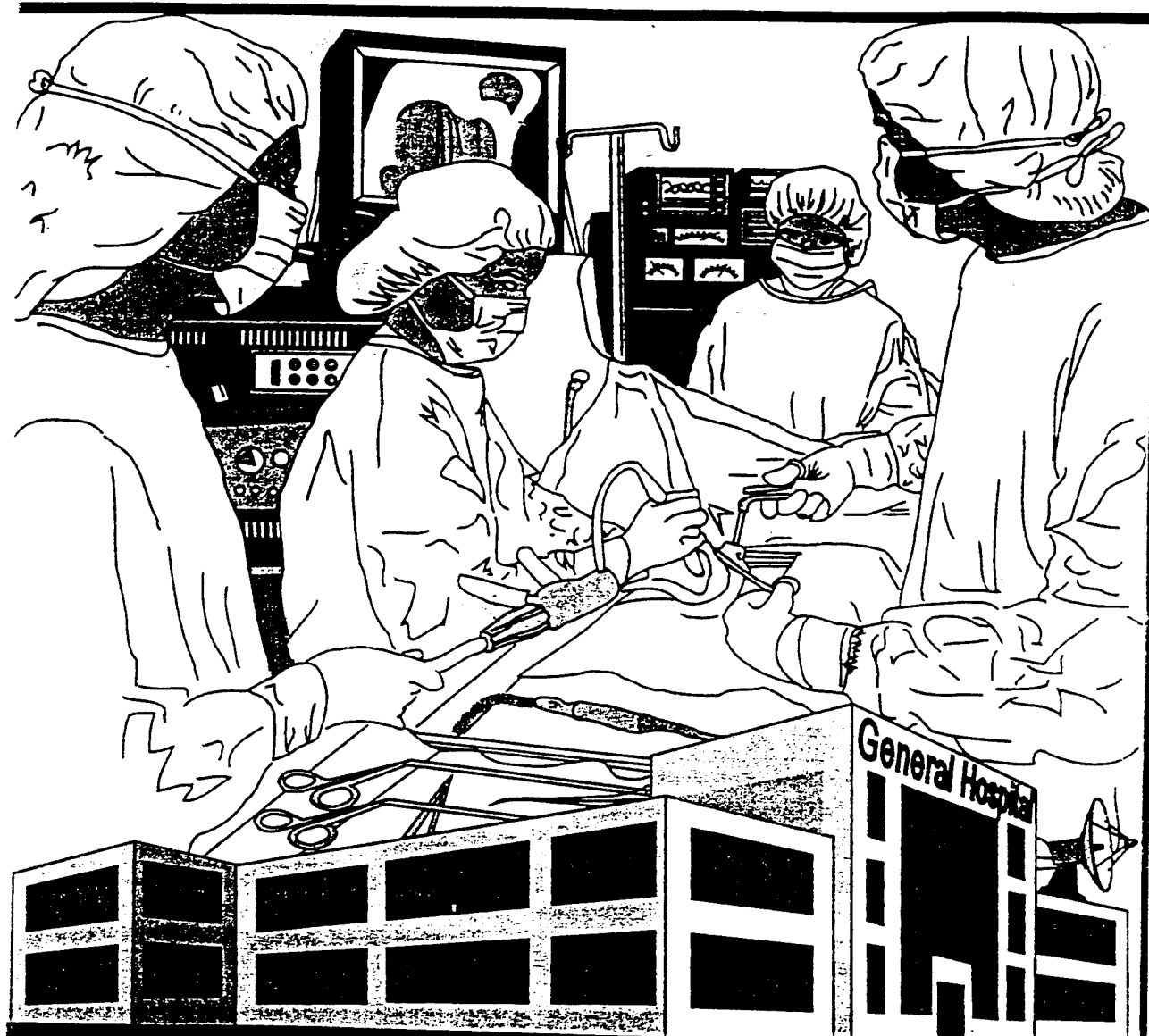
- The EMI and EMC Problems Can be Prevented by:
 - Using Proper System and Circuit Design
 - Choosing the Right Components, and
 - Using Proper Grounding and Shielding Techniques

Conclusion

- The Problem of EMC is Real and the Menace of EMI is Growing With the Pro-
liferation of High Power Electromagnetic
Systems in the Battlefield
- The Advanced Combat Casualty Care
Systems Used to Minimize the Battlefield
Delays and Maximize the Availability of
the "Golden Hour" Would Become
Ineffective Unless These Systems Are
Designed and Tested for EMC

Disclaimer: Views expressed are those of the authors and do not necessarily reflect official U.S. Army or the U.S. Army Medical Department positions, nor does the content change or supersede information in other official publications

AFACCC-151P1



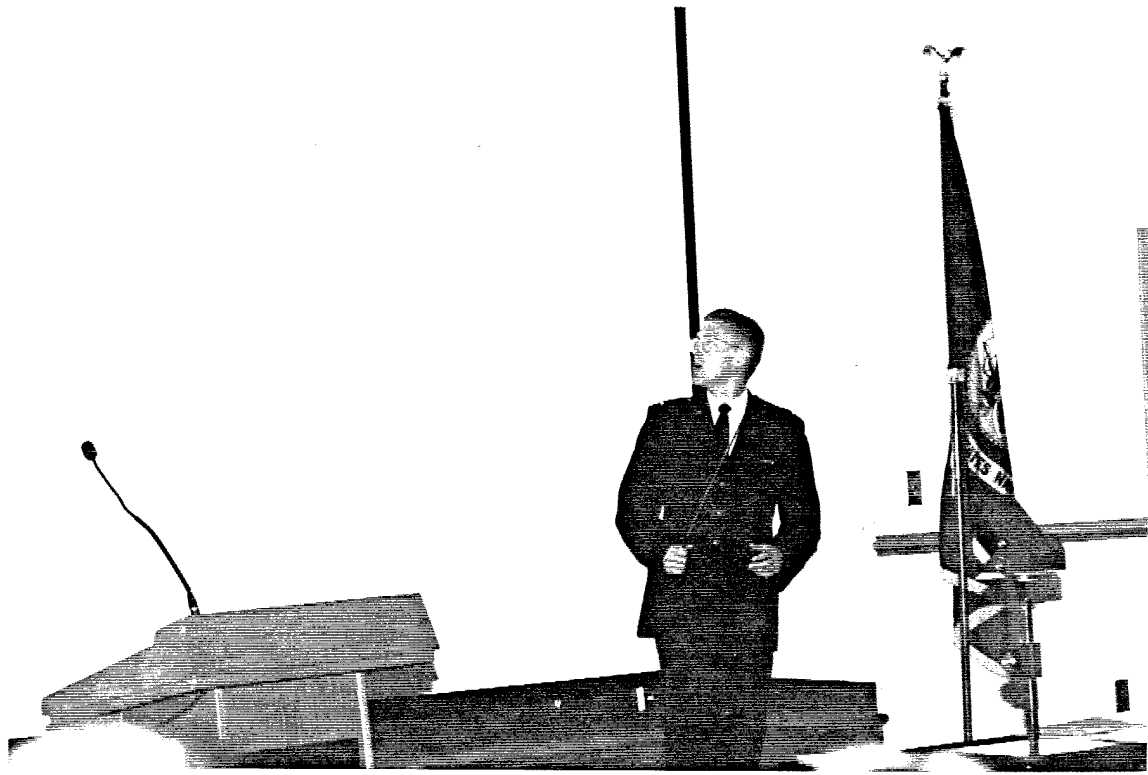
Medical Electronics Ambient EMI Environment in Civilian Settings

Ambient EMI Source	Magnitude	Frequency, or Duration
External RF Fields		
• E-M Field from Radars (CW, Pulsed)	10 to 200 v/m	100 MHz to 18 GHz
• E-M Field from Outside RF Transmitters (CW)	1 to 20 v/m	100 kHz to 1 GHz
Intra-Hospital RF Fields		
• E-M Field from ESU's	Up to 1000 v/m	5 to 1000 MHz
• Diathermy	> 150 Watts	13.5 to 2450 MHz
• Telemetry	> 5 Watts	950 MHz
Power Line Disturbances		
• DM, Slow Variations	+15% - 10%	Up to Several Hours
• DM Drop-Out	100%	Up to Several .5 Cycles
• DM Surge	200%	Up to 1 Cycle
• DM	1 kV	μs to ms
• CM Transient	3 kV	
Lightning Stroke Current	3 kA	1.2 μS/50 μS
ESD (Personnel)	30 Amp at 10 kV	1 μS/20 μS
NMR	16000 Gauss	1 ns/60 ns
		Up to Minutes





**LT. ERIC JOHNSON
PHILLIPS LABORATORY**





REVERBERATION CHAMBERS



EM EVALUATION OF PL'S REVERBERATION CHAMBER

PRESENTED TO

REVERBERATION AND ANECHOIC CHAMBER OPERATORS GROUP

BRIEFER
LT. ERIC JOHNSON

PHILLIPS LABORATORY
ELECTROMAGNETIC EFFECTS DIVISION PL/WSM
5-7 DECEMBER 1995



OVERVIEW

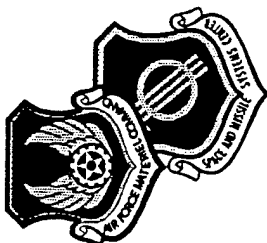
OBJECTIVES

CHAMBER CHARACTERISTICS

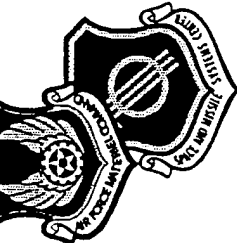
CHAMBER Q

UNIFORMITY TESTS

CONCLUSIONS



OBJECTIVES



CONVERT SCREEN ROOM INTO A REVERBERATION CHAMBER.

AUTOMATE DATA ACQUISITION SYSTEM

ASSESS CHAMBER PARAMETERS AFTER MODIFICATIONS

ENHANCE PL'S EMI/RFI/EMC TESTING CAPABILITIES



REVERBERATION CHAMBER CHARACTERISTICS



CHAMBER LOCATION:

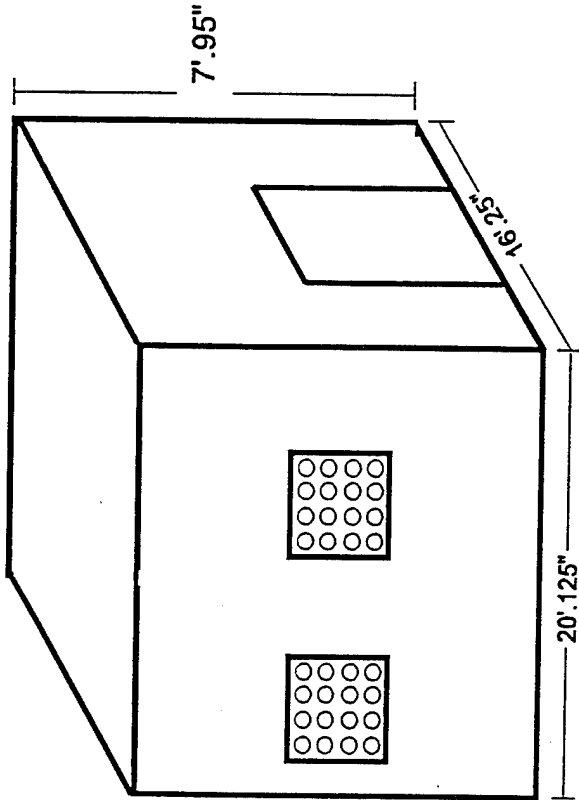
. PL's LESLI TEST FACILITY
KAFB, NM.

CHAMBER DIMENSIONS:

. 20.125' X 16.25' X 7.95'

CHAMBER CONSTRUCTION:

. GALVANIZED STEEL STRUCTURE
1' X 1' ACCESS PANELS





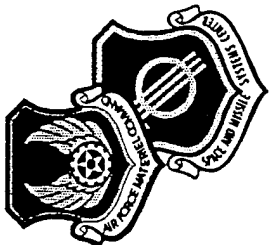
Q MEASUREMENTS

CAVITY RELAXATION TIME METHOD

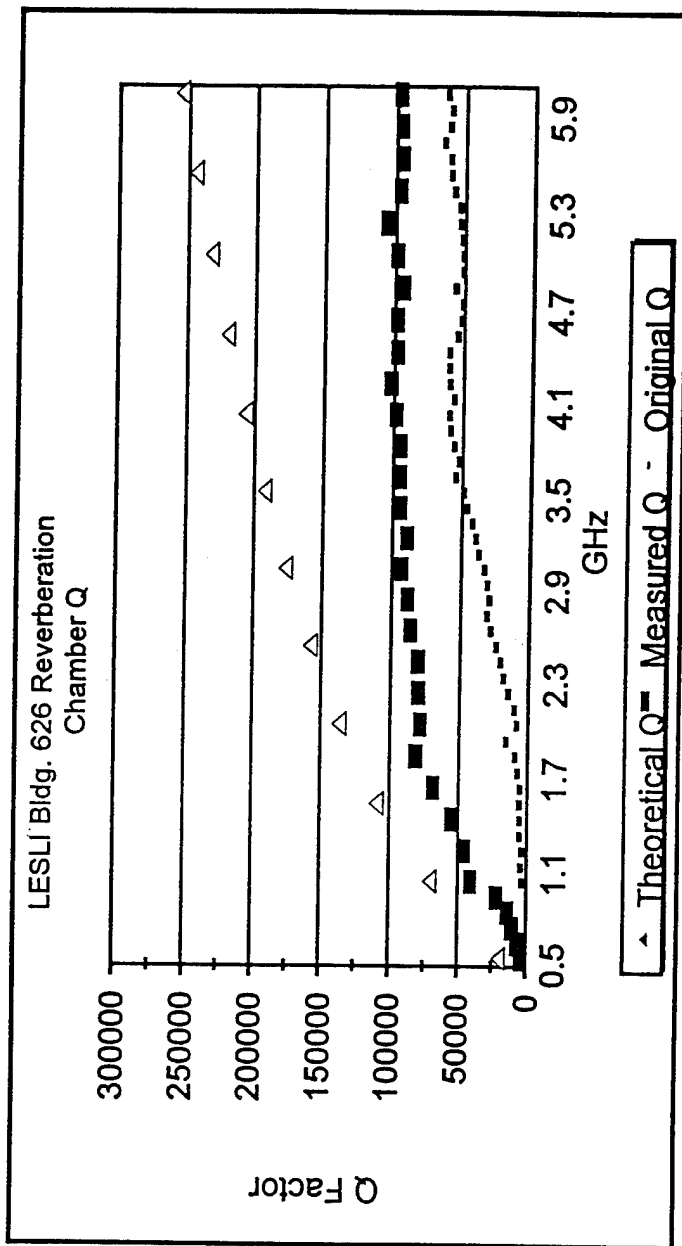
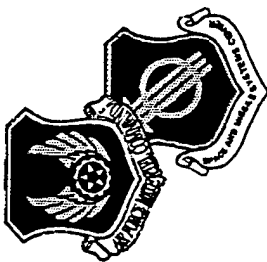
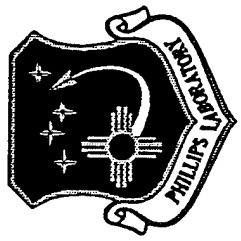
PULSE MODULATED WAVEFORM
90% TO 10% RELAXATION TIME
AVERAGE OF 4000 PULSES

Q MEASUREMENTS PERFORMED BEFORE AND AFTER
MODIFICATIONS.

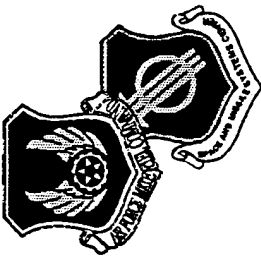
60% IMPROVEMENT ON CHAMBER PERFORMANCE



CHAMBER Q



FIELD UNIFORMITY



FIELD HOMOGENEITY PREDICTION:

BASED ON MEASURED N_Q , MONTE CARLO SIMULATION
AND NOISE BW.

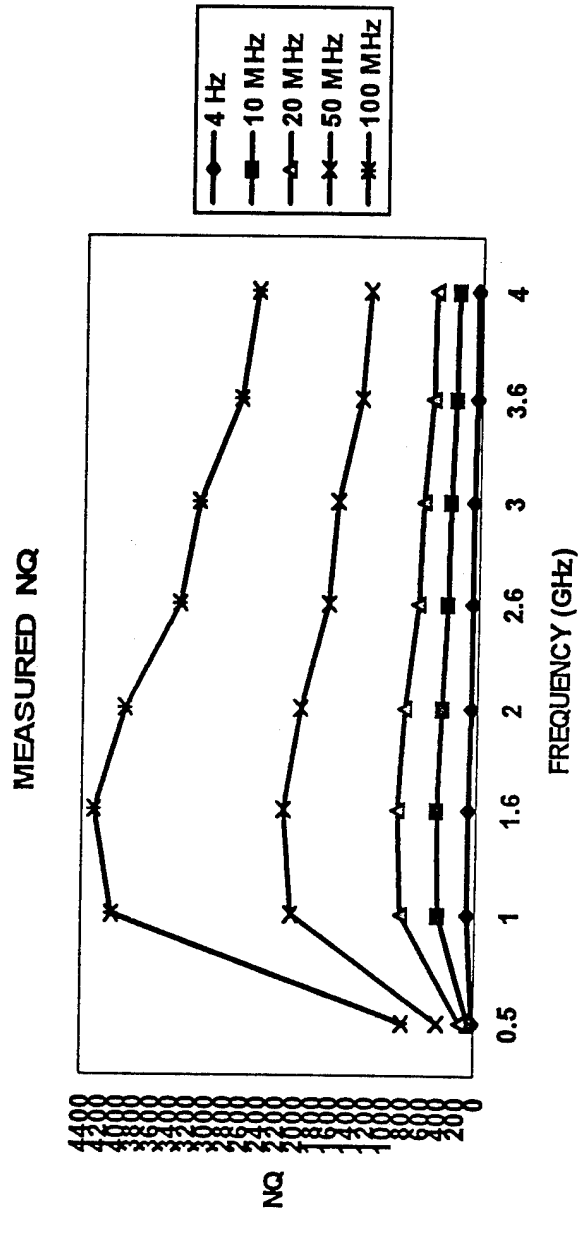
FIELD UNIFORMITY MEASUREMENTS:

- 0.5 - 6 GHz
- 4 NOISE BWs.
- 5 B-DOT SENSORS PLACED AT RANDOM LOCATIONS

MEASURED NQ

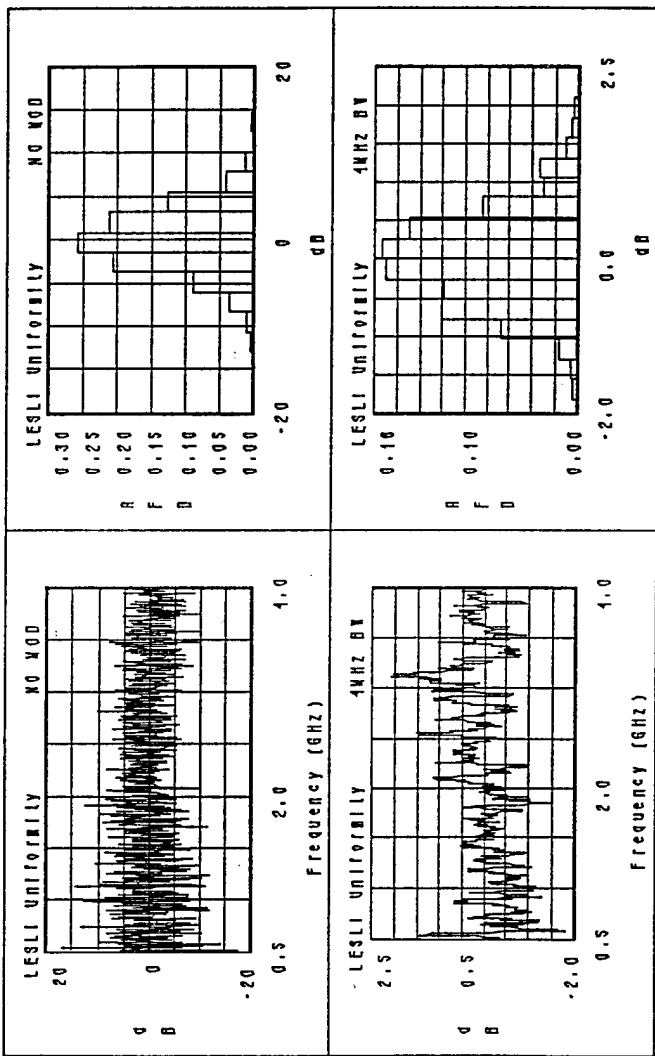
$$BW_Q = f_0 / Q$$

$$NQ = [BW_{BLWGN}] / BW_Q$$



FIELD UNIFORMITY

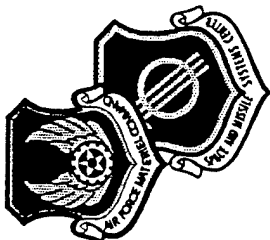
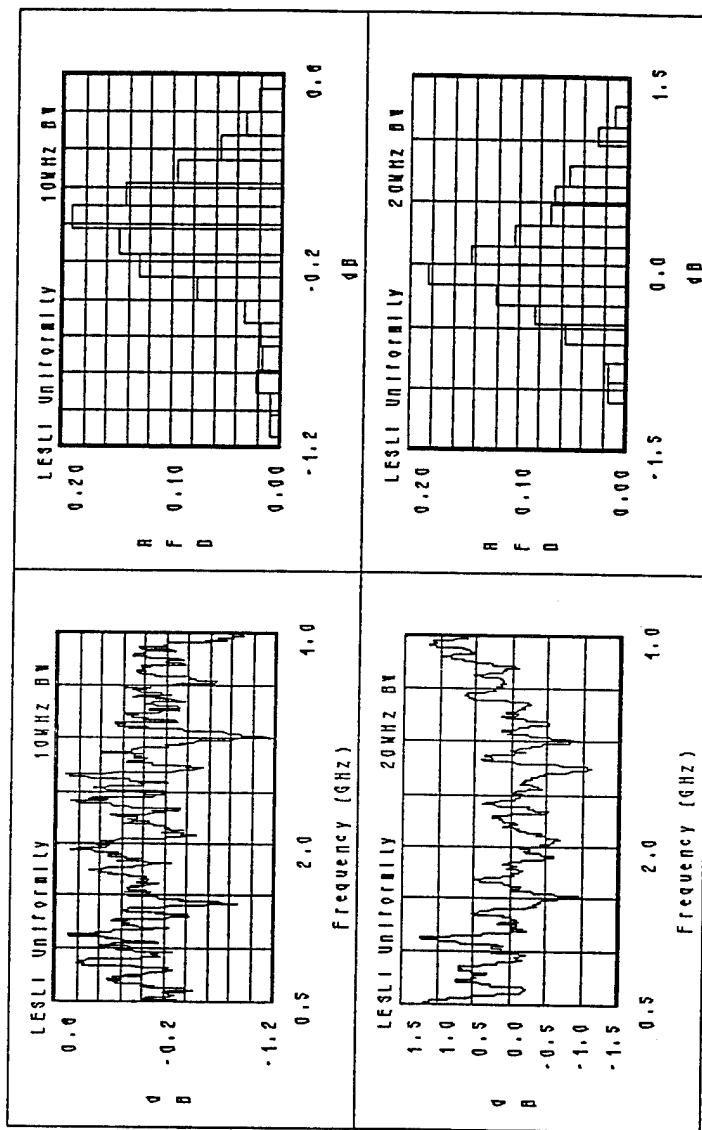
$$\Psi = 10 \log \left\{ (W_{\max}) / (W_{\min}) \right\} = 10 \log \left\{ (Pd_{\max}) / (Pd_{\min}) \right\}.$$



FIELD UNIFORMITY

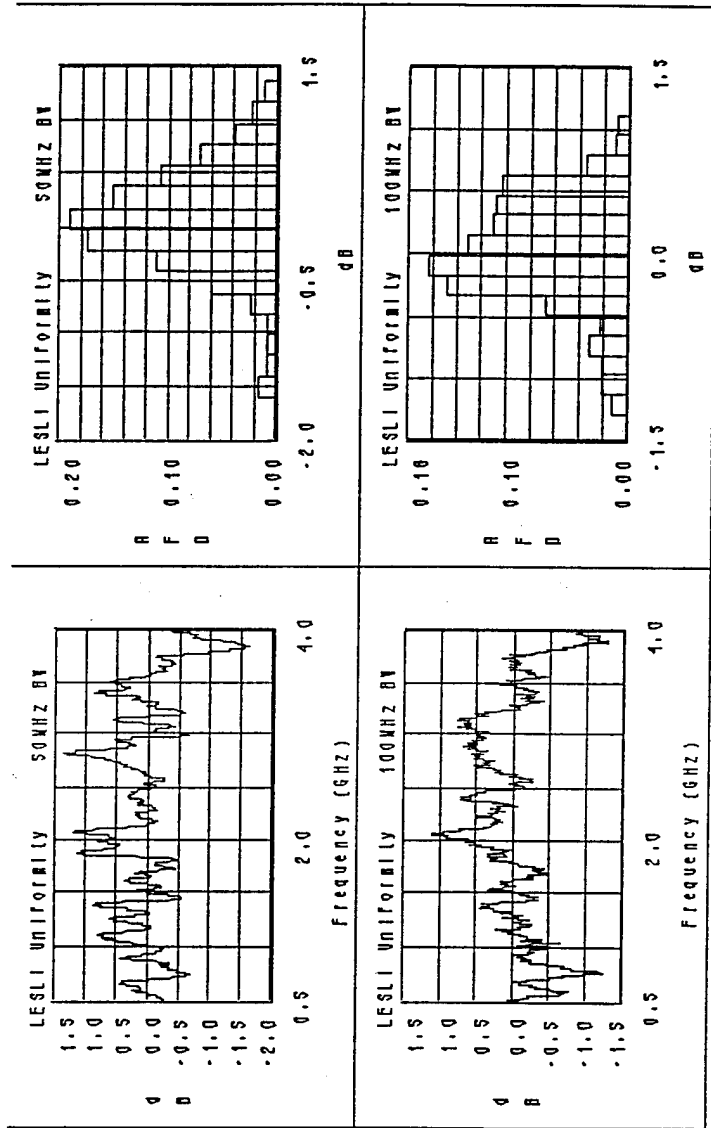


$$\Psi = 10 \log \left\{ (W_{\max}) / (W_{\min}) \right\} = 10 \log \left\{ (Pd_{\max}) / (Pd_{\min}) \right\}.$$



FIELD UNIFORMITY

$$\Psi = 10 \log \left\{ (W_{\max}) / (W_{\min}) \right\} = 10 \log \left\{ (Pd_{\max}) / (Pd_{\min}) \right\}.$$



CONCLUSIONS



WORST CASE RELAXATION TIME = 15.8 μ SEC

MAX PRF = 31.5 KHz with 50% duty cycle

MEASURED Q: 4,000 @ 500 MHz

97,000 @ 6 GHz

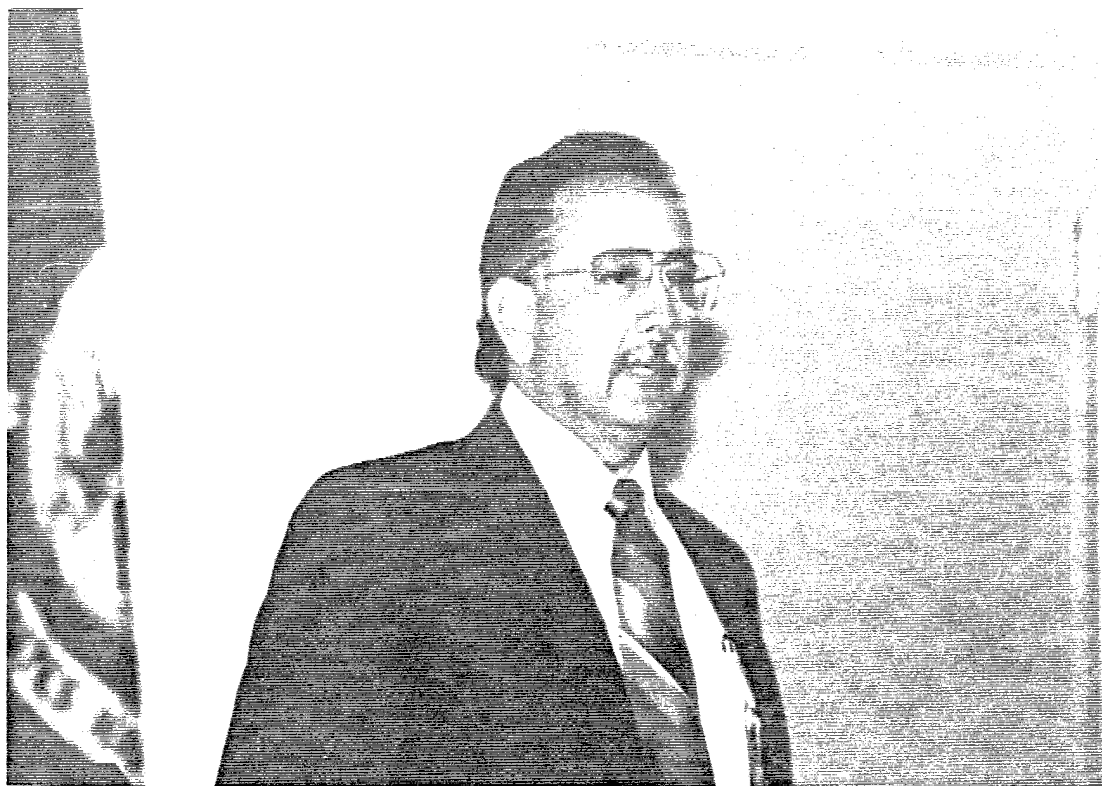
FIELD UNIFORMITY: \pm 2.5 @ 4 MHz noise BW

\pm 1.2 @ 10 MHz noise BW
 \pm 1.0 @ 20 MHz noise BW

\pm 1.5 @ 50 MHz noise BW
 \pm 1.0 @ 100 MHz Noise BW

CHAMBER OFFERS "IDEAL" CHARACTERISTICS FOR THE
 CONDUCT OF EMI/RFI/EMC EXPERIMENTS ON SMALL
 ASSETS

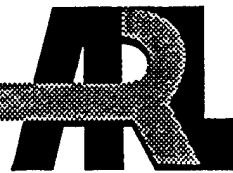




MR. RICHARD LARA
U.S. ARMY RESEARCH LABORATORY



ARMY RESEARCH LABORATORY



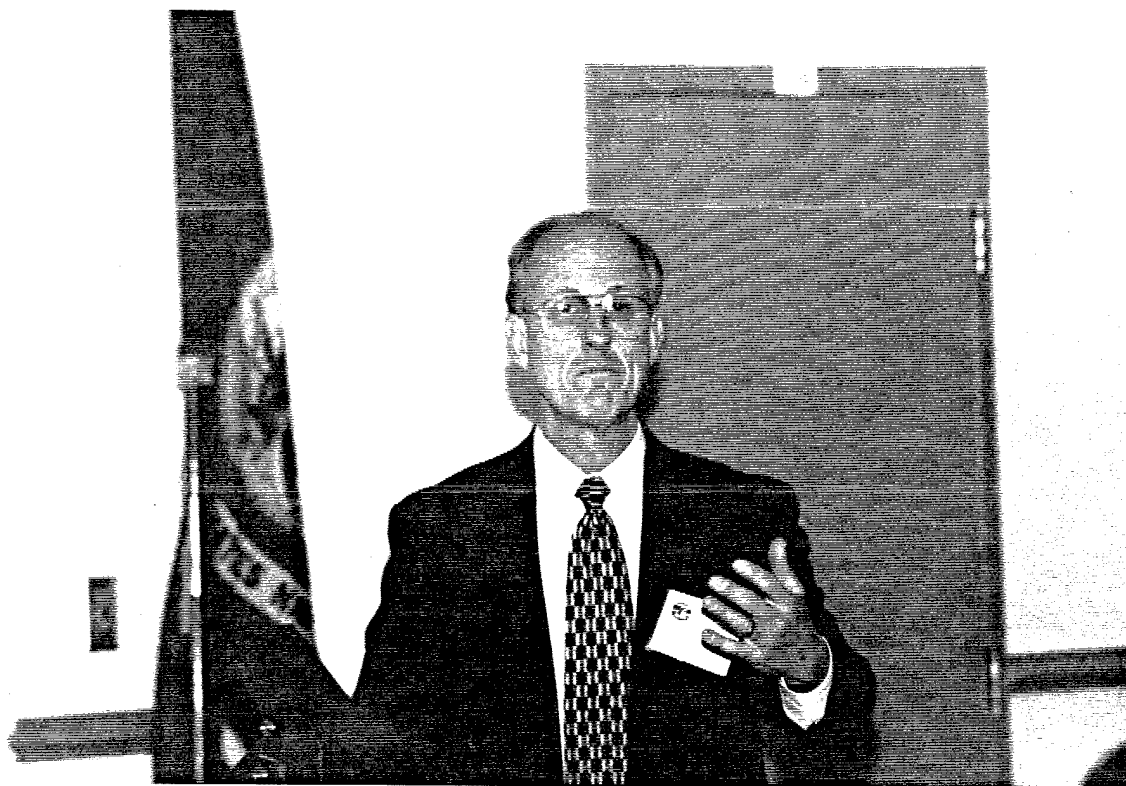
**U.S. ARMY
ELECTROMAGNETIC ANALYSIS FACILITY
WHITE SANDS MISSILE RANGE, N.M.**

**By Richard S. Lara
Electronic Warfare Division**

**Survivability/Lethality Analysis Directorate
Electronic Warfare Division**

NOTE: Due to difficulties encountered in getting permission in time for publication to release this paper with unlimited distribution, it has not been included in these proceedings. Information regarding this subject may be obtained from the author.





**MR. ANTHONY ZANTE
TITAN BETA**



MOBILE MICROWAVE TEST FACILITY

S. Lyons, H. Anamkath, D. Nett, D. Palmer, K. Whitham, A. Zante
 Titan Beta, 6780 Sierra Court, Dublin, CA 94568

INTRODUCTION

As higher power microwave transmitters come into use, both the FAA and the JAA have increased their requirements for aircraft to withstand the effects of transmitted microwave power. One approach for effects testing of aircraft is to test the subsystems at low power that simulates the effect of high power with the appropriate attenuation factors. Another approach is to perform field tests on the entire aircraft to more fully simulate the effects of radiated fields. SAAB Aircraft has taken this second approach and contracted Titan Beta to provide such a system.

A high power microwave test facility (MTF) was provided to SAAB Aircraft for microwave effects testing of aircraft and subsystems. The MTF is transportable constructed within a 40 feet long ISO van that allows it to be moved by truck on the airbase and on roadways throughout the country. This self contained system can be powered by cable or by motor generator. The MTF can be operated outdoors where the five frequency antenna array are directed at the object under test. It can also be operated indoors for testing subsystems and other devices.



FIGURE 1

RF SYSTEMS

The Microwave Test Facility (MTF) operates in five separate frequency bands, L, S, C, X and Ku. The actual frequencies of operation are 1300, 2856, 5710, 9300, 15,000 MHZ. The L, S, and C Band power amplifiers are klystron based and the X and Ku band power amplifiers are magnetrons. The L, S, and C Band systems have a long and short pulse mode of operation, each being 5.85 μ s and 1.85 μ s respectively. The maximum pulse repetition frequency allowable is 1kHz which is available in the short pulse burst mode only. The X Band short and long pulse modes are slightly shorter, and the Ku band has a fixed pulse length of 0.45 μ s and a burst mode repetition rate of up to 2.1 kHz. The peak RF power output from each of the five systems from L band through Ku band is 25, 20, 5, 1, and 0.25 megawatts respectively.

The RF drive system in the MTF for the L, S, and C Bands is generated by three separate RF driver chains, each producing a drive power of about 400 watts. These three chains are driven by a single, synthesized CW microwave source whose frequency is preset by the operator. The L and S Band RF drivers incorporate a solid-state pre-amplifier, attenuator, PIN diode switch and planar triode tube power amplifier stage. The C Band RF driver incorporates all of the above components except that the output power stage is a traveling wave tube amplifier (TWA). The RF output pulse risetimes are a direct function of the PIN diode switches in the RF driver system and are on the order of 100 ns. Since the X and Ku Band microwave power sources are magnetron based, no RF drivers were required.

The high power microwave output from each of the power amplifiers is transmitted through the appropriate waveguide through the outside wall of the mobile trailer. For outdoor operation, each waveguide is then normally routed to the roof of the mobile trailer where it is terminated into its own lensed antenna. Each antenna has the ability to be scanned in elevation and azimuth by remote control. The typical peak field strengths at 15 m available for each band in the outdoor operating mode are 31, 34, 17, 11, and 6.1 kV/m respectively for the L through Ku Bands. Alternatively, the system can be configured for indoor operation where the output transmission waveguides are routed into an anechoic chamber and terminated with the appropriate radiating elements.

MODULATOR

There were 5 different RF sources required for the project.

Independent of the RF source or the pulse width, the source was designed to be on 10 seconds every one minute when commanded. The performance requirement is listed in Table 1.

PARAMETER	RF SOURCE				
FREQ BAND	L	S	C	X	KU
SOURCE FREQ GHz	1.3	2.86	5.71	9.3	15
SHORT PULSE (FWHM) MICROSECOND	1.85	1.85	1.85	1	N/A
SHORT PULSE REP. RATE HZ	1000	1000	1000	1000	N/A
LONG PULSE (FWHM) MICROSECOND	5.85	5.85	5.85	4.5	0.45
LONG PULSE REP. RATE HZ	390	200	160	210	2100
PEAK RF POWER MW	25	20	5	1	0.25
AVERAGE RF POWER KW	57.5	23.4	4.7	0.94	0.238
FIELD STRENGTH PEAK (kV/M)	31	34	17	11	6.1

TABLE 1

MODULATOR SCHEME

For the L, S and C Band RF source one modulator was defined. They had common HVPS to charge the PFN and one thyratron to discharge the . A separate modulator was designed to operate X and Ku Band sources.

MODULATOR FOR L, S AND C BAND RF SOURCES

The modulator was designed to share as many as possible components to operate all the three RF Sources. The basic modulator is a conventional modulator with type E PFN. The control system was designed to assure the connections are properly made for the selected source and all the associated subsystem specific for the source are operating per requirements. The control system also makes sure that each of the source is operating within

the safe region. The major subsystems are described in the following sections.

There are two independent power sources for the modulator. A switching HVPS is used to charge the PFN when operating at the repetition rate of 5 Hz or less. A high voltage three phase transformer with rectifier output and a front end SCR controller is used to provide HV for other modes of operations. This subsystem was designed to provide instant full power on capability for any of the RF Source.

A resonance charge system is used to charge the PFN when high voltage transformer based HVPS is used. Same charging inductor is used independent of the configuration of the PFN or load.

The PFN is conventional type E. Each stage of the PFN had 2 parallel PFN capacitors. For short pulse operation, one of the capacitor from each stage was removed from the PFN. Tuning of each of the coil for short pulse operation vs. long pulse operation as well as L or S Band RF Source vs. C Band RF source was also redefined. The PFN had an end of the line clipper circuit with nonlinear resistor in it.

An ITT F-241 thyratron was used to discharge the PFN in any configuration.

There were two pulse transformer tanks for the system. In one tank there were two separate sockets - one each for L and S Band RF source with one pulse transformer to operate either of the source as well as a resistive load that can be used to trouble shoot modulator. Titan Beta designed a HV switch to enable operator to select the appropriate load from the outside of the tank. The switch also provided setting information to the control system to assure proper connections per selection by the operator .

The second pulse transformer tank had a socket for C Band RF Source.

The operator is expected to make up high voltage connections from the output of the PFN to the appropriate pulse transformer tank. These connections also provide this information to the control system to assure proper connections per selection by the operator.

MODULATOR FOR X AND KU BAND RF SOURCES

The modulator was designed to share as many as possible components to operate all the three RF Sources. The basic modulator is a conventional modulator with type E PFN.

A switching HVPS was used to charge a filter capacitor.

A resonance charge system is used to charge PFN. Due to extreme variation in the PFN capacitance, two different charging inductors

are used - one for the X Band and one for the Ku Band RF Source.

Each of the PFN used is a conventional type E. For the X Band RF source, number of stages of the PFN are changed to change the output pulse width.

An ITT 7322 thyratron was used to discharge the PFN selected.

Each of the RF source had its own pulse transformer. The transformer and additional components were housed in individual enclosed oil tank due to space constrains. The output of the pulse transformer was brought out for connection to the appropriate RF Source.

MECHANICAL SYSTEMS

Antenna Position Control

Each of the five roof-mounted RF antennas can be scanned with position feedback ± 15 degrees azimuth, ± 5 degrees elevation.

Environmental Conditions

The MTF will perform at temperatures from -20 to 30°C , and is designed for long term storage at temperatures from -35 to 40°C . For operator comfort and system component operating requirements, the MTF is equipped with a wall mounted HVAC unit, and interior walls and ceiling are lined with 2" of high R value insulation. The RF tubes are cooled by a closed circuit low conductivity water pumping system inside the trailer transferring waste heat to a water/glycol closed circuit cooling system mounted on the roof of the container.

Dielectric Gas System

A pressurized dielectric gas system controls the pressure in each RF waveguide/antenna circuit to prevent arcing.

Mobility

The MTF is housed in a standard 8' x 40' x 9.5' high cube ISO shipping container modified with the addition of weather proof access doors and cover hatches. The MTF can be moved fully assembled on an air-ride equipped ISO trailer on smooth surfaces. For indoor use, the MTF can be mounted on small wheels and towed by a small forklift. For long distance transport, the antennas and klystrons can be disassembled and packed, and the trailer towed on public roads at highway speeds. It can be also be transported on ocean going container cargo vessels.

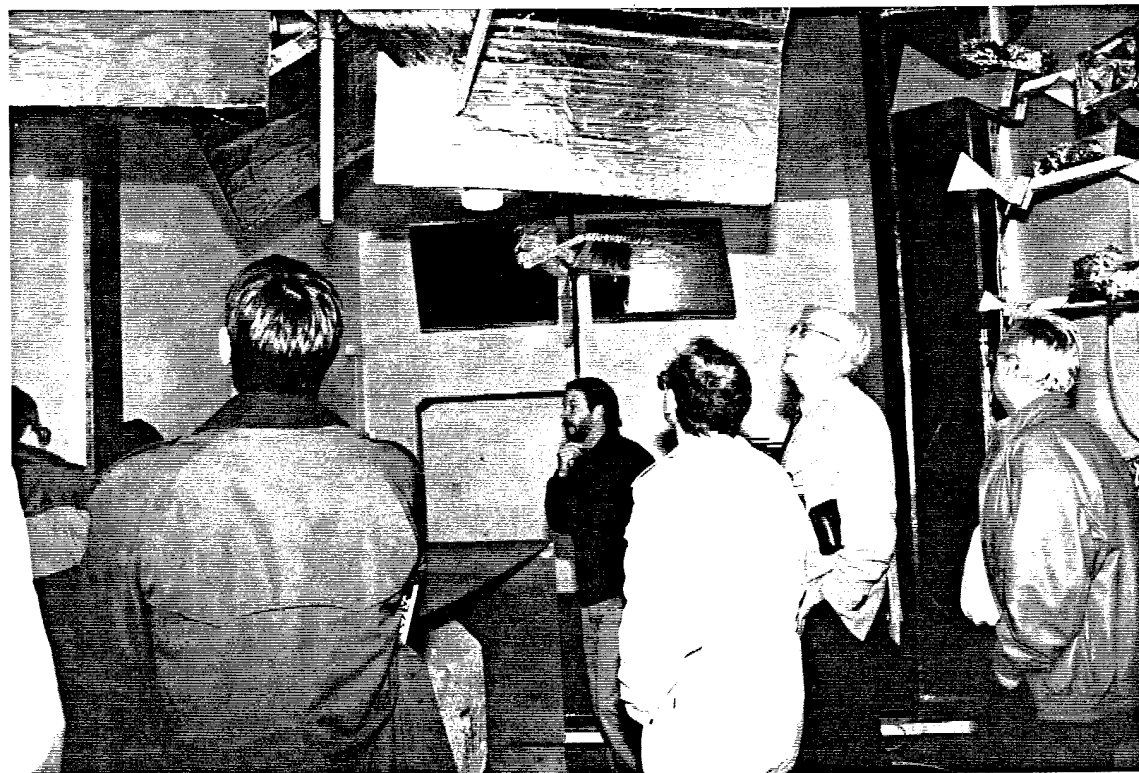
Radiation Shielding

Lead shields are used on each klystron and safety interlocked personnel doors provide for operator safety during operation.

SUMMARY

Titan Beta has provided a mobil, high power, 5 frequency Microwave Test Facility (MTF) to SAAB for high power, high field tests for electro magnetic hardness. The system has been in operation for several years in Sweden.





**REVERBERATION CHAMBER AND ANECHOIC CHAMBER
OPERATORS GROUP MEETING - ATTENDEES
5 - 7 DECEMBER 1995**

MR. POUL ANDERSEN
CHRYSLER CORPORATION
MS-481-47-20
800 CHRSYLER DRIVE
ALBURN HILLS MI 48326-2757
PHONE: 810-576-4644
FAX: 810-576-7045

MR. R. ANDERSON
BRITISH AEROSPACE DEFENCE DYNAMICS
F.P.C. 065, P.O. BOX 5, FILTON,
BRISTOL BS127NQ
ENGLAND
PHONE: 01179318777
FAX: 01179318635

MR. BRUCE ARCHAMBEAULT
SETH CORPORATION
110 SUNRAY DRIVE
JOHNSTOWN, PA 15905
PHONE: 814-255-4417
FAX: 814-255-3417

DR. MATS BACKSTROM
NATIONAL DEFENCE RESEARCH
ESTABLISHMENT
P.O. BOX 1165
S-58111 LINKOPING
SWEDEN
PHONE: +46 13 318430
FAX: +46 13 318170

MR. GAVIN D. BARBER
DEFENCE RESEARCH AGENCY
AVS DEPT Q153 BUILDING
DRA, FARNBOROUGH, HANTS
GU14 6TD
ENGLAND
PHONE: 01252 392501
FAX: 01252 393749

MR. WILLIAM BEAN
WANDEL & GOLTERMANN
410 49TH STREET
VIRGINIA BEACH, VA 23451
PHONE: 804-491-5047
FAX: 84-491-3163

MS. CELESTE M. BELCASTRO
NASA Langley Research Center
MAIL STOP 130
HAMPTON VA 23665-5225
PHONE:
FAX:

MR. BOB BLOCKSIDGE
PHOTONETICS, INC.
401 EDGEWATER PLACE, STE 140
WAKEFIELD, MA 01880
PHONE: 617-245-2333
FAX:

MR. KENNETH BREZINSKI
NAVAL AIR WARFARE CENTER
AIRCRAFT DIVISION (5.1.7.3), MS-3, BLDG 1461
PATUXENT RIVER, MD 20670
PHONE: 301-342-4161 x111 AV 342-4161 x111
FAX: 301-342-4781

MR. CHRIS BROWN
ROME RESEARCH CORP
314 SOUTH JAY STREET
ROME, NY 13440
PHONE: 315-339-0550
FAX: 315-339-0238

MR. CHARLES BUNTING
PHONE:
FAX:

LCDR DON BURNINGHAM
EMBASSY OF AUSTRALIA
1601 MASSACHUSETTS AVE, NW
WASHINGTON, DC 20036
PHONE: 202-797-3338
FAX: 202-797-1838

**REVERBERATION CHAMBER AND ANECHOIC CHAMBER
OPERATORS GROUP MEETING - ATTENDEES
5 - 7 DECEMBER 1995**

MR. FERNANDO CAMARCE
GENERAL MOTORS PROVING GROUND
MAIL CODE: 483-340-111
MILFORD, MI 48380-3726
PHONE: 810-685-5272
FAX:

MR. MIKE CARUSO
LINGREN RF ENCLOSURES INC
400 HIGH GROVE BLVD
GLENDALE HEIGHTS, IL 60139
PHONE: 708-307-7200
FAX:

MR. DONALD E. CLARK
GEORGIA TECH RESEARCH INSTITUTE
SEAL/EEED/ERB/252;347 FERST DR.
ATLANTA GA 30332-0822
PHONE: 404-894-4315
FAX: 404-894-7358

MR. JOHN CLEARY
U.S. AIR FORCE
ROME LABORATORY/ERST
525 BROOKS ROAD
ROME NY 13441-5700
PHONE: 315-330-2841 DSN 587-2841
FAX: 315-330-7083 DSN 587-7083

PROFESSOR PAOLO CORONA
ISTITUTO UNIVERSITARIO NAVALE
(INSTITUTE OF NAVAL UNIVERSITY)
VIA ACTON 38
80133 NAPLES
ITALY
PHONE: +39 81 5513976
FAX: +39 81 5512886

DR. WILLIAM F. CREVIER
JAYCOR
3700 STATE ST, SUITE 300
SANTA BARBARA, CA 93105
PHONE: 805-682-8782
FAX: 805-682-7362

MR. WILHELM V. CSENKI
SAAB-SCANIA AB
SAAB MILITARY AIRCRAFT
S-581 88 LINKOPING
SWEDEN
PHONE: +46 13 183941
FAX: +46 13 182368

MR. R. WAYNE DEVEREUX
VEDA INC.
300 EXPLORATION
LEXINGTON PARK, MD 20653
PHONE: 301-863-4290
FAX: 301-862-2530

MR. CHARLES L. DEVOR
LEHMAN CHAMBERS
5800 CUMBERLAND HIGHWAY
CHAMBERSBURG PA 17201
PHONE: 717-264-2265
FAX: 717-264-9178

MR. TERENCE DONOHOE
HONEYWELL ATSD
M/S AZ75-K26E2
PO BOX 21111
PHOENIX, AZ 85036
PHONE: 602-436-5974
FAX: 602-436-6479

MR. KENNETH L. DUDLEY
NASA Langley Research Center
BLDG 1220, M/S 130
HAMPTON, VA 23681
PHONE: 804-864-1783
FAX: 804-864-4234

MR. DAVID B. ELKINS
U.S. ARMY RTTC
STER-T-E-EM
REDSTONE ARSENAL AL 35898
PHONE: 205-876-3965
FAX: 205-842-9637

**REVERBERATION CHAMBER AND ANECHOIC CHAMBER
OPERATORS GROUP MEETING - ATTENDEES
5 - 7 DECEMBER 1995**

MR. GRANT ERICKSON
BOEING DEFENSE & SPACE
P.O. BOX 3999 M/S 8H-10
SEATTLE, WA 98124
PHONE: 206-773-4251
FAX: 206-773-4173

MR. RICHARD FORD
NRL CODE 5301
4555 OVERLOOK AVE., SE
WASHINGTON, DC 20375-5000
PHONE: 202-767-3440
FAX: 202-767-3658

DR. GUSTAV FREYER
NCEE
20045 CAPELLA DRIVE
MONUMENT, CO 80132
PHONE: (719) 481-8420
FAX: (719) 481-8420

MR. HARRY GAUL
MOTOROLA GSTG
MS H2550
8201 EAST McDOWELL ROAD
SCOTTSDALE, AZ 85252
PHONE: 602-441-5321
FAX:

MS. ROBBIN GOULET
FEDERAL AVIATION ADMINISTRATION-NEW
ENGLAND REGION
BOSTON AIRCRAFT EVALUATION GROUP
12 NEW ENGLAND EXECUTIVE PK
BURLINGTON, MA 01803
PHONE: 617-238-7893
FAX: 617-238-7199

MR. MICHAEL O. HATFIELD
NAVAL SURFACE WARFARE CENTER
DAHlgren DIVISION
CODE F-52
17320 DAHlgren ROAD
DAHlgren, VA 22448
PHONE: 540-653-8594
FAX: 540-663-7494

MR. DAVID L. HERKE
G03, Q153 BUILDING
DEFENCE RESEARCH AGENCY
FARNBOROUGH, HAMPSHIRE
GU14 6TD
ENGLAND
PHONE: 01252 393226
FAX: 01252 393749

MR. C. HOWARTH (W7G)
BRITISH AEROSPACE
MILITARY AIRCRAFT DIVISION
WARTON AERODROME, PRESTON
ENGLAND PR41AX
PHONE: 01772 854391
FAX: 01772 855262

DR. CRAIG JAMES
ROME LABORATORY/ERST
525 BROOKS ROAD
ROME, NY 13441
PHONE: 315-330-2841
FAX:

MR. MICHAEL V. JESSEE
COMPUTER SCIENCES CORPORATION
4485 DANUBE DRIVE, SUITE 14
KING GEORGE, VA 22485
PHONE:
FAX:

LT. ERIC JOHNSON
PHILLIPS LABORATORY (PL/WSM)
3550 ABERDEEN AVE., SE
KIRTLAND AFB, NM 87117
PHONE: 505-846-4608
FAX: 505-846-0566

D. MARK JOHNSON
COMPUTER SCIENCES CORPORATION
4485 DANUBE DRIVE, SUITE 14
KING GEORGE, VA 22485
PHONE: 540-663-8594
FAX: 540-663-7494

**REVERBERATION CHAMBER AND ANECHOIC CHAMBER
OPERATORS GROUP MEETING - ATTENDEES
5 - 7 DECEMBER 1995**

MR. JEFF JONES
FEDERAL AVIATION ADMINISTRATION
AFS-300 AIRCRAFT MAINT. DIV.
800 INDEPENDENCE AVE.
WASHINGTON, DC 20591
PHONE: 202-267-3813
FAX: 202-267-5115

MS. DIANE R. KEMPF
5.1.7.3 M/S 3
NAVAL AIR WARFARE CENTER, AIRCRAFT
DIVISION
PATUXENT RIVER, MD 20670-5304
PHONE: 301-342-4791 x127 DSN 342-4791 x127
FAX:

MR. DON KIRKBRIDE
WESTINGHOUSE ELECTRONIC SYSTEMS
P.O. BOX 746 M/S 504
BALTIMORE, MD 21203
PHONE: 410-993-6432
FAX: 410-993-6618

MR. GALEN KOEPKE
NIST
MS 813.03
325 BROADWAY
BOULDER CO 80303
PHONE: 303-497-5766
FAX: 303-497-6665

MS. SANDRA KOPPEN
NASA LANGLEY RESEARCH CENTER
BLDG 1220, M/S 130
HAMPTON, VA 23681
PHONE: 804-864-6209
FAX:

MR. PETER G. LANDGREN
BOFORS
RUE
S-691 80 KARLSKOGA
SWEDEN
PHONE: 46 586 81428
FAX: 46 586 85789

MR. RICHARD LARA
ARL SLAD EWD
AMSRL-SL-EP
WSMR, NM 88002-5513
PHONE: 505-678-9023
FAX: 505-678-9045

MR. JIM LAW
ROCKWELL-COLLINS
M/S 106-113
400 COLLINS ROAD NE
CEDAR RAPIDS, IA 52498
PHONE: 319-395-1674
FAX: 319-395-3661

MR. BRIAN F. LAWRENCE
LINDGREN RF ENCLOSURES
400 HIGH GROVE BLVD
GLENDALE HEIGHTS, IL 60139
PHONE: 708 307-7200
FAX: 708 307-7571

MR. CARL J. LAZARD
U.S. ARMY RESEARCH LABORATORY
AMSRL-WT-NH
ADELPHI, MD 20783-1197
PHONE: 301-394-3657
FAX: 301-394-3047

DR. JANE M. LEHR
FIORE INDUSTRIES INC.
17 EVERGREEN DRIVE
PLACITAS, NM 87043
PHONE: 505-846-6685
FAX: 505-846-8479

MR. BARRY LOCK
ELECTRICAL/EXPLOSIVES HAZARDS
COMMITTEE
ORDNANCE BOARD
MINISTRY OF DEFENCE
EMPRESS STATE BUILDING
LILLIE ROAD
LONDON SW6 1TR
PHONE: 0171 824 3220
FAX: 0171 824 4357

**REVERBERATION CHAMBER AND ANECHOIC CHAMBER
OPERATORS GROUP MEETING - ATTENDEES
5 - 7 DECEMBER 1995**

MR. WILLIAM P. LUCADO
NAVAL SURFACE WARFARE CENTER
DAHlgren DIVISION
CODE F-52
17320 DAHlgren ROAD
DAHlgren, VA 22448
PHONE: 540-653-8594
FAX: 540-653-7494

MR. OLOF LUNDEN
NATIONAL DEFENCE RESEARCH
ESTABLISHMENT
DEPARTMENT OF SENSOR TECHNOLOGY
P.O. BOX 1165
S-581 LINKOPING
SWEDEN
PHONE: +46 13 31 83 25
FAX: +46 13 31 81 70

MR. CARMEN LUVERA
U.S. AIR FORCE
ROME LABORATORY
RL/ERS
525 BROOKS ROAD
ROME, NY 13441-5700
PHONE: 315-330-3076 DSN 587-3076
FAX: 315-330-7083 DSN 587-7083

MR. JONATHAN MACGAHAN
AMPLIFIER RESEARCH
160 SCHOOL HOUSE ROAD
SOUDERTON, PA 18964-9990
PHONE: 215-723-8181
FAX: 215-723-5688

MR. ERNIE MAGYAR
MAGYAR & ASSOCIATES, INC.
2149 MCGREGOR BLVD, SUITE 14
FT MYERS, FL 33901
PHONE: 941-332-2075
FAX: 941-332-4328

DR. JEREMY G. MANTON
ATTACHE' DEFENCE SCIENCE
EMBASSY OF AUSTRALIA
1601 MASSACHUSETTS AVE., NW
WASHINGTON, DC 20036
PHONE: 202-797-3378
FAX: 202-797-1838

MR. ISMAEL MARTINEZ, JR.
SOUTHWEST RESEARCH INSTITUTE
6220 CULEBRA ROAD
SAN ANTONIO, TX 78228
PHONE: 210-522-3631
FAX: 210-522-3396

MR. ROGER A. MCCONNELL
CKC LABORATORIES
5473A CLOUDS REST
MARIPOSA, CA 95338
PHONE: 209-966-5240
FAX: 209-742-6133

MR. STEELE E. MCGONEGAL
NAVAL AIR WARFARE CENTER, AIRCRAFT
DIVISION
5.1.7.3
PATUXENT RIVER, MD 20670-5304
PHONE: 301-737-1757
FAX: 301-737-1498

MR. LYNN MINER
U.S. AIR FORCE
PHILLIPS LABORATORY
PL/WST
KIRTLAND AFB NM 87117-6008
PHONE: 505-846-4113
FAX: 505-846-0881

DR. MAQSOOD MOHD
SVERDRUP TECHNOLOGY
P.O. BOX 1935
EGLIN AFB, FL 32542
PHONE: 904-729-6115
FAX: 904-729-6377

MR. TRUONG X. NGUYEN
NASA Langley RESEARCH CENTER
BLDG 1220, M/S 130
HAMPTON, VA 23681
PHONE: 804-864-7528
FAX: 804-864-4234

**REVERBERATION CHAMBER AND ANECHOIC CHAMBER
OPERATORS GROUP MEETING - ATTENDEES
5 - 7 DECEMBER 1995**

MR. BE NGUYEN
AMP INC. 106-14
P.O. BOX 3608
HARRISBURG, PA 17105
PHONE: 717-986-7642
FAX:

MR. LARRY POKORNY
AMPLIFIER RESEARCH
160 SCHOOLHOUSE ROAD
SOUDERTON, PA 18964
PHONE: 215-723-8181
FAX: 215-723-5688

MR. JOHN QUINE
ROME RESEARCH CORP.
83 ASHTREE DRIVE
SCHENECTADY NY 12309
PHONE: 518-785-5439, 387-5451
FAX:

MR. BOB RAKOSKI
PHONE:
FAX:

MR. H. DALE REYNOLDS
COMPUTER SCIENCES CORPORATION
AIR FORCE FLIGHT TEST CENTER
P.O. BOX 446, BLDG 1030
EDWARDS CA 93523
PHONE: 805-277-5726
FAX: 805-277-3390

MR. GARY T. ROAN
NAVAL RESEARCH LABORATORY
4555 OVERLOOK AVENUE, SW
CODE 5713
WASHINGTON DC 20375-5000
PHONE: 202-767-6191
FAX: 202-767-6194

MR. VIC SAYER
MCLENNAN SERVO SUPPLIES, LTD.
DOMAN ROAD
CAMBERLEY GU17 7LW
UK
PHONE: 44 1276 26146
FAX: 44 1276 23452

MR. STEPHEN SCEARCE
NASA LaRC
1 SOUTH WRIGHT ST. M/S 130
HAMPTON, VA 23681
PHONE: 804-864-6235
FAX: 804-864-4234

MR. JOE S. SKINNER
VITRO TECHNICAL SERVICES, INC.
PRIMES FACILITY, BLDG 68
PO BOX 1898
EGLIN AFB, FL 32542
PHONE: 904-882-9017 EXT 254
FAX: 904-882-9357

MR. MICHAEL B. SLOCUM
COMPUTER SCIENCES CORPORATION
4485 DANUBE DRIVE SUITE 14
KING GEORGE, VA 22485
PHONE: 540-653-8594
FAX: 540-653-7494

MR. ROBERT B. SMITH
NAVAL AIR WARFARE CENTER
AIRCRAFT DIVISION, DY07, MS 3
48256 SHAW ROAD, BUILDING 1461
PATUXENT RIVER, MD 20670-5304
PHONE:
FAX:

MR. WILLIAM SPERBER
483-340-111
GENERAL MOTORS PROVING GROUND
MILFORD, MI 48380-3726
PHONE: 810-685-5299
FAX: 810-685-5154

MR. S. SRIRAM
SRICO, INC.
664 PETWORTH COURT
POWELL, OH 43065
PHONE: 614-799-0664
FAX: 614-799-2116

**REVERBERATION CHAMBER AND ANECHOIC CHAMBER
OPERATORS GROUP MEETING - ATTENDEES
5 - 7 DECEMBER 1995**

MR. CHARLES E. STEADMAN
DEPARTMENT OF THE AIR FORCE
46TH TEST WING/TSWW
401 W. CHOCTAWHATCHEE AVE. SUITE 265B
EGLIN AFB, FL 32542-5724
PHONE: 904-882-9354 X509 DSN 872-9354 x509
FAX: 904-882-9357 DSN 872-9357

MR. DALE STEFFEN
7655 W. MISSISSIPPI AVE
LAKEWOOD, CO 80226-4332
PHONE: 303-980-0070
FAX: 303-980-0836

MR. JOHN STREETER
ROME RESEARCH CORPORATION
P.O. BOX 138, GERMANY ROAD
VERONA NY 13478-0138
PHONE: (315) 339-0550
FAX:

MR. ED SVEDA
SPECTRUM CONTROL, INC.
8061 AVONIA ROAD
FAIRVIEW, PA 16415
PHONE: 814-474-1571
FAX: 814-474-3110

MR. THOMAS F. TROST
DEPARTMENT OF ELECTRICAL ENGINEERING
TEXAS TECH UNIVERSITY
P.O. BOX 43102
LUBBOCK TX 79413-3102
PHONE: (806) 742-3505
FAX: (806) 742-1245

MR. RAYMOND TUCKER
U.S. AIR FORCE
ROME LABORATORY/ERSS
525 BROOKS ROAD
ROME, NY 13441-4505
PHONE: (315) 330-4217 DSN 587-4217
FAX: (315) 330-7083 DSN 587-7083

MR. STEVEN UHRICH
BOEING COMMERCIAL AIRPLANE CO.
MS 02-58
PO BOX 3707
SEATTLE, WA 98124
PHONE: 206-266-3753
FAX:

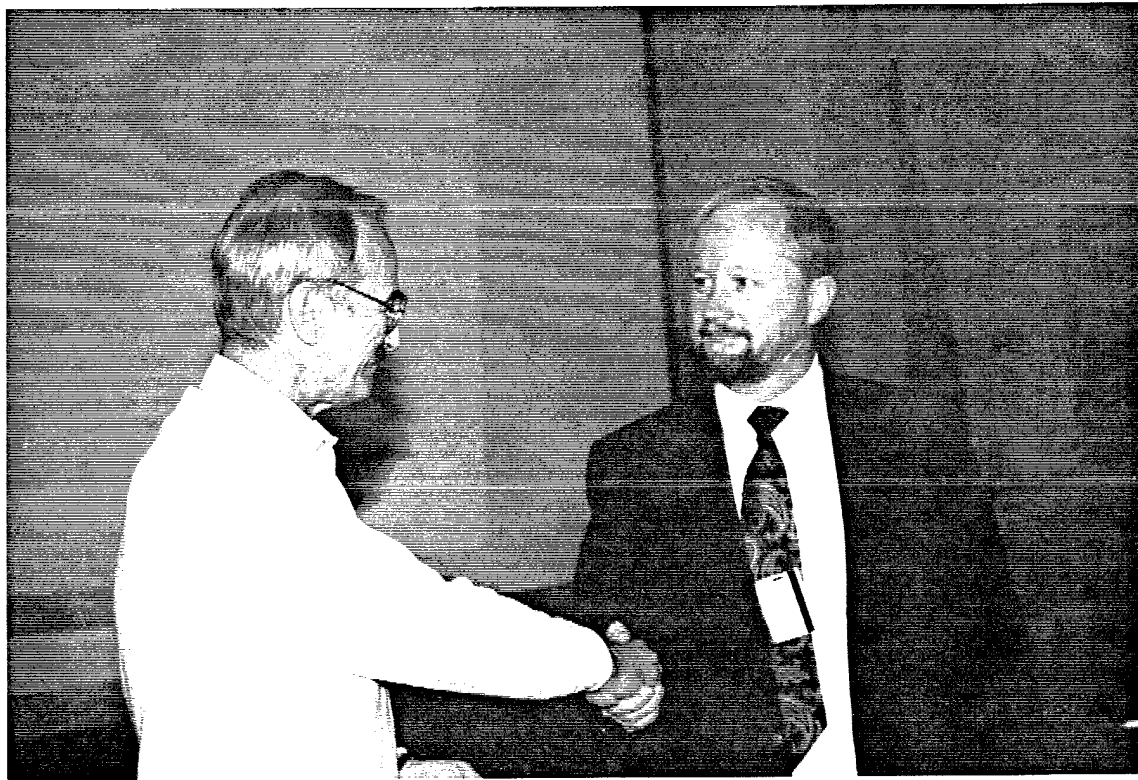
SrA. CHRIS VANZANDT
PHILLIPS LAB/WSM
3550 ABERDEEN AVENUE, SE
KIRTLAND AFB, NM 87117
PHONE: 505-846-6685
FAX: 505-846-0566

MR. CLARK VITEK
CKC LABORATORIES, INC.
5289 NE ELAM YOUNG PKWY, SUITE 6-900
HILLSBORO, OR 97124
PHONE: 503-693-3543
FAX: 503-693-4647

MR. PETE VOURAS
EG&G
16156 DAHLGREN ROAD
DAHLGREN, VA 22448
PHONE: 540-663-9432
FAX: 540-663-0332

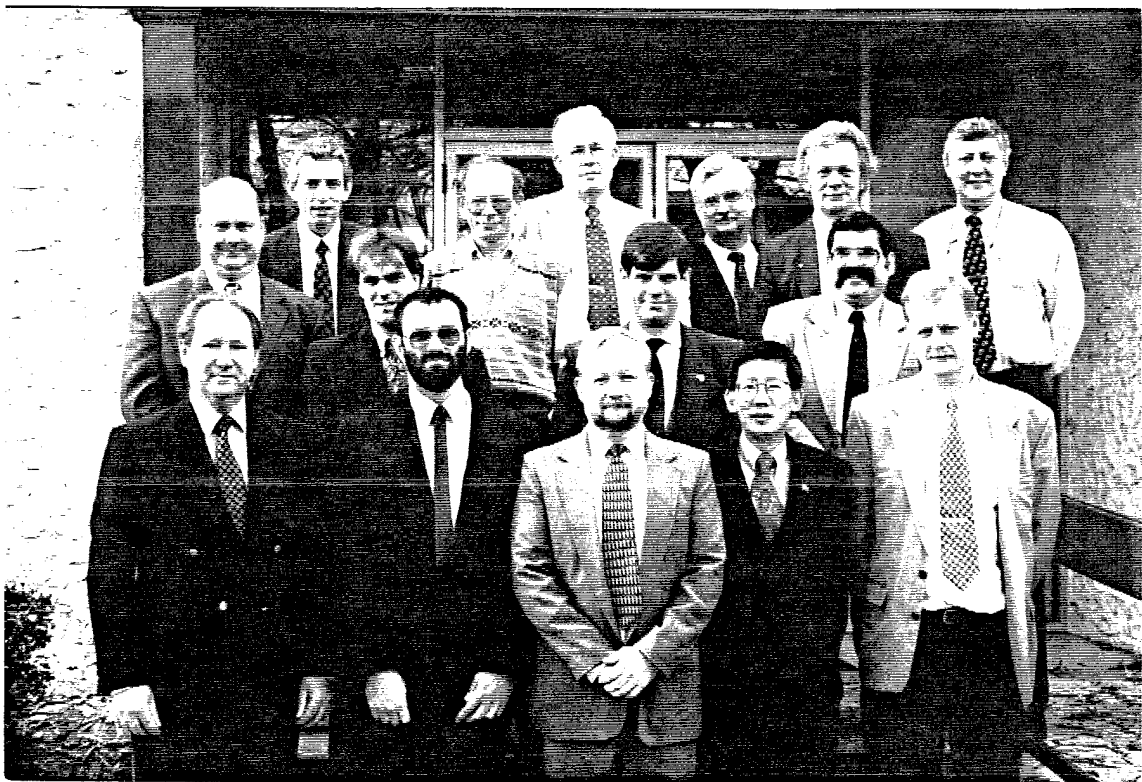
MR. EDWARD YEE
ARMY TECHNOLOGY AND ENGINEERING
AGENCY
491 MONMOUTH ROAD
W. ALLENHURST, NJ 07711
PHONE: 908-532-0799
FAX: 908-532-0456

MR. ANTHONY A. ZANTE
TITAN BETA
6780 SIERRA COURT
DUBLIN, CA 94568
PHONE: 510-828-0555
FAX: 510-828-4054



**MR. LARRY POKORNY OF AMPLIFIER RESEARCH RECEIVES A
PLAQUE IN APPRECIATION FOR SUPPORT OF THE REVERBERATION
CHAMBER DEMONSTRATION AT THE 1995 IEEE EMC SYMPOSIUM**





**THANKS TO ALL AUTHORS AND ATTENDEES
FOR MAKING THIS CONFERENCE A GREAT SUCCESS!**



REPORT DOCUMENTATION PAGE

Form Approved
OMB No. 0704-0188

Public reporting burden for this collection of information is estimated to average 1 hour per response, including the time for reviewing instructions, search existing data sources, gathering and maintaining the data needed, and completing and reviewing the collection of information. Send comments regarding this burden or any other aspect of this collection of information, including suggestions for reducing this burden, to Washington Headquarters Services, Directorate for Information Operations and Reports, 1215 Jefferson Davis Highway, Suite 1204, Arlington, VA 22202-4302, and to the Office of Management and Budget, Paperwork Reduction Project (0704-0188), Washington, DC 20503.

1. AGENCY USE ONLY (Leave blank)			2. REPORT DATE March 1996	3. REPORT TYPE AND DATES COVERED Final, 5 - 7 December 1995
4. TITLE AND SUBTITLE Proceedings of the Reverberation Chamber and Anechoic Chamber Operators Group Meeting, 5 - 7 December 1995			5. FUNDING NUMBERS _____	
6. AUTHOR(s) Michael Hatfield (Editor)				
7. PERFORMING ORGANIZATION NAME(S) AND ADDRESS(ES) Commander Naval Surface Warfare Center, Dahlgren Division (Code F52) 17320 Dahlgren Road Dahlgren, VA 22448-5100			8. PERFORMING ORGANIZATION REPORT NUMBER NSWCDD/MP-96/38	
9. SPONSORING/MONITORING AGENCY NAME(S) AND ADDRESS(ES) _____			10. SPONSORING/MONITORING AGENCY REPORT NUMBER _____	
11. SUPPLEMENTARY NOTES _____				
12a. DISTRIBUTION/AVAILABILITY STATEMENT Approved for public release; distribution is unlimited.			12b. DISTRIBUTION CODE _____	
13. ABSTRACT (Maximum 200 words) <p>This document presents the proceedings of the Anechoic Chamber and Reverberation Chamber Operators Group Meeting, which was held at the Naval Surface Warfare Center Dahlgren Division (NSWCDD) from 5 through 7 December 1995. The meeting was hosted by NSWCDD's Electromagnetic Effects Branch (F52) and was chaired by Michael Hatfield. Topics ranging from "Electromagnetic Compatibility Testing of Electric Cars" to "Radio Frequency (RF) Coupling to Commercial Aircraft Avionics" were presented. The meeting was attended by more than 85 people from both government and industry (including 15 visitors from overseas representing Sweden, Italy, Australia, and the United Kingdom). Also, a workshop on reverberation chambers was held on 4 December 1995 which was attended by 50 people, including 13 overseas visitors.</p>				
14. SUBJECT TERMS Anechoic Chamber, Reverberation Chamber, Electromagnetic Effects			15. NUMBER OF PAGES 462	
			16. PRICE CODE _____	
17. SECURITY CLASSIFICATION OF REPORT UNCLASSIFIED	18. SECURITY CLASSIFICATION OF THIS PAGE UNCLASSIFIED	19. SECURITY CLASSIFICATION OF ABSTRACT UNCLASSIFIED	20. LIMITATION OF ABSTRACT UL	



NAVAL SEA SYSTEMS COMMAND

